VOLCANIC RECORD OF THE WEST ANTARCTIC ICE SHEET IN MARIE BYRD LAND

by
Thomas I. Wilch

Submitted in Partial Fulfillment of the
Requirements of the Degree of
Doctor of Philosophy in Geology
September, 1997

Department of Earth and Environmental Science
New Mexico Institute of Mining and Technology
Socorro, New Mexico, USA

TABLE OF CONTENTS

Part B: Volcanic history of Mt. Petras

Eocene and Oligocene volcanism at Mt. Petras, Marie Byrd Land: implications for middle Cenozoic ice sheet reconstructions in West Antarctica

Part C. Volcanic history of WAIS

Middle to Late Cenozoic volcanic record of the West Antarctic Ice Sheet

LIST OF FIGURES

Part A. Late Quaternary explosive volcanism

Part B: Volcanic history of Mt. Petras

LIST OF TABLES

Part A. Late Quaternary explosive volcanism

Part B: Volcanic history of Mt. Petras

Part C. Volcanic history of WAIS

ABSTRACT

Paleoenvironmental reconstructions and $^{40}Ar/^{39}Ar$ geochronology of the intraglacial Marie Byrd Land volcanic province document cryospheric evolution in West Antarctica since the latest Eocene. This study relies upon detailed field observations of numerous large, polygenetic and smaller, monogenetic volcanoes in Marie Byrd Land, combined with geochemical, petrographic, and extensive $^{40}Ar/^{39}Ar$ geochronology (179 samples) data. Major conclusions of the volcanic record of the West Antarctic ice sheet include:

1. The onset of Marie Byrd Land volcanism in the latest Eocene is recorded by lavas at Mt. Petras, dated to 36.11±0.22 Ma (±2 σ uncertainty). The latest Eocene to early late Miocene interval (36-10 Ma) was characterized by low apparent rates of volcanism. Beginning at 10 Ma, there was a significant apparent increase in volcanicity in Marie Byrd Land. Relatively high rates of volcanism persisted through the Late Neogene and into the Quaternary.

2. The oldest terrestrial indications for glacial ice in West Antarctica are Middle Oligocene (29-27 Ma) tuff cone deposits at Mt. Petras that suggest the presence of a thin, local ice cap or ice and snow on slopes. These deposits overlie an erosional unconformity, with >400 m of topographic relief, suggestive of ongoing erosion in the Oligocene.

3. The first evidence for a widespread West Antarctic Ice Sheet is Late Miocene (9.3-8.2 Ma) glaciovolcanic sequences from across Marie Byrd Land. Interpretations of syn-eruptive paleo-ice-levels suggest that the Late Miocene ice sheet was not significantly higher than the present-day West Antarctic Ice Sheet. Late Miocene subaerial volcanic sequences situated near present-day ice level are consistent with this inference. For the remainder of the Neogene and into the Quaternary, two patterns emerge from the record of syn-eruptive paleo-ice-levels: former WAIS expansions were more extensive at coastal sites than at inland sites, and it appears that the West Antarctic Ice Sheet is in a near maximum configuration that existed at many times but was rarely exceeded.

4. A middle Pleistocene (590±15 ka) ice-sheet high-stand of +550 m is inferred at the coastal volcano, Mt. Murphy, on the basis of late-stage glaciovolcanic tuff cone deposits at Sechrist Peak. Nearly coeval (573±5 ka) inland ice levels the Mt. Berlin (125 km from the coast) were probably no more than 200 m above present-day local ice levels. The extreme thickening of the WAIS at Mt. Murphy may have been driven by sea-level lowering and coastal ice sheet expansion.

5. A ~350 m expansion of the inland West Antarctic Ice Sheet in the Late Wisconsin is inferred at Mt. Takahe (150 km from coast), on the basis of 29±12 ka subglacial to subaerial eruptive sequences at ~350 m above the present-day level of the regional ice sheet. Limits on maximum inland ice-sheet thickening during Late Wisconsinan times are provided by 34±8 ka late-stage parasitic cinder cone deposits on the west flank of Mt. Frakes (located 275 km from coast). These deposits are situated at ~100-150 m above the level of the regional ice sheet, suggesting less extreme inland thickening of the ice sheet.

6. Abundant Late Quaternary (573 ka to 8.5 ka) explosive volcanic eruptions in Marie Byrd Land, capable of widely dispersing volcanic ash onto the ice sheet, occurred at three major felsic alkaline polygenetic volcanoes, Mt. Berlin, Mt. Takahe, and Mt. Siple.

7. Englacial tephra layers exposed in bare ice on the summit ice cap of Mt. Moulton, 30 km from their inferred source at Mt. Berlin, provide a minimum age of 118 ka of the oldest known ice in West Antarctica. This well-dated section of locally derived glacial ice contains a potential "horizontal ice core" record of paleoclimate that dates back to the previous interglacial.

8. Tephra from $^{40}Ar/^{39}Ar$-dated Marie Byrd Land eruptions are correlated by geochemical fingerprinting to ash layers in the 1968 Byrd Station ice core. The 73 ka ice core record contained abundant, 7.5 to 40 ka, coarse ash layers, which were all previously geochemically correlated to Mt. Takahe volcano. Age and geochemical similarities confirm a correlation of the youngest ~7.5 ka tephra layer in the Byrd ice-core to an 8.5±3.4 ka

pyroclastic deposit at Mt. Takahe. Age and geochemical similarities suggest that 20-30 ka tephra layers in the Byrd ice core may correlate to Mt. Berlin rather than Mt. Takahe. These correlations suggest that the $^{40}Ar/^{39}Ar$ chronology of explosive Late Quaternary volcanism in Marie Byrd Land may potentially provide future ice and marine cores with independently dated time horizons.

INTRODUCTION

The goal of this study is to address fundamental questions of Cenozoic global change through the terrestrial volcanic record of the West Antarctic Ice Sheet. These questions focus on issues relating to the behavior, history, and stability of the West Antarctic Ice Sheet in the context of the global climate system. The Marie Byrd Land volcanic province consists of nineteen large, polygenetic volcanoes (2364-4181 m above sea level) and numerous smaller monogenetic volcanoes that are exposed as nunataks in the West Antarctic Ice Sheet. Two aspects of the history of the West Antarctic Ice Sheet are addressed in this analysis of the volcanism in Marie Byrd Land: the record of young explosive volcanism in the West Antarctic Ice Sheet and the record of glaciovolcanic interactions between erupting Marie Byrd Land volcanoes and the West Antarctic Ice Sheet. The former record offers the potential to independently date ice cores, whereas the latter offers the only terrestrial history of the inland West Antarctic Ice Sheet.

The dissertation is subdivided into three independent papers, each of which focuses on specific issues relating to cryospheric evolution in West Antarctica. The first paper (Part A) establishes a precise $^{40}Ar/^{39}Ar$ chronology of Late Quaternary explosive volcanism in West Antarctica is established that offers the potential of an independent chronology of future deep ice and marine core stratigraphies through a critical period of climate history. This paper has two co-authors and is in review at GSA Bulletin. Both co-authors, W.C. McIntosh and N.W. Dunbar, participated in the field work; N.W. Dunbar conducted microprobe analyses of glass and mineral samples; W.C. McIntosh collaborated on $^{40}Ar/^{39}Ar$ analyses.

The second paper (Part B) provides $^{40}Ar/^{39}Ar$ geochronological and lithofacies records of volcanism at Mt. Petras, where 36 Ma lava provides the oldest evidence for volcanism in Marie Byrd Land and 29-27 Ma pyroclastic deposits provide the oldest terrestrial evidence for glacial ice in West Antarctica. This paper on Mt. Petras is in review

at the Bulletin of Volcanology. W.C. McIntosh, a co-author on this paper, collaborated on field work and development of ideas for this study.

The third paper (Part C) is a manuscript in preparation that builds upon the previous papers and merges paleoenvironmental reconstructions and $^{40}Ar/^{39}Ar$ dating results from across the Marie Byrd Land volcanic province into a new comprehensive volcanic record of the West Antarctic Ice Sheet.

Part A: Late Quaternary Volcanic Activity in Marie Byrd Land: Potential $^{40}Ar/^{39}Ar$-dated time horizons in West Antarctic ice and marine cores

ABSTRACT

Late Quaternary volcanic activity at three major alkaline composite volcanoes in Marie Byrd Land, West Antarctica is dominated by explosive eruptions, many capable of depositing ash layers as regional time-stratigraphic horizons in the West Antarctic Ice Sheet and in Southern Ocean marine sediments. A total of twenty eruptions at Mt. Berlin, Mt. Takahe, and Mt. Siple are recorded in welded and non-welded pyroclastic fall deposits and lavas, mostly peralkaline trachyte in composition. The eruptions are precisely dated by the $^{40}Ar/^{39}Ar$ furnace step-heating method to between 573 ka and 8.5 ka.

Englacial tephra layers exposed in bare ice on the summit ice cap of Mt. Moulton, 30 km from their inferred source at Mt. Berlin, provide a minimum age of 118 ka of the oldest known ice in West Antarctica. This well-dated section of locally derived glacial ice contains a potential "horizontal ice core" record of paleoclimate that dates back to the previous interglacial. The coarse grain size and density of the englacial tephra (mean diameters 17-18 mm, densities 540-780 kg/m^3), combined with their distance from source, indicate derivation from highly explosive Plinian eruptions of Mt. Berlin.

Tephra from $^{40}Ar/^{39}Ar$-dated Marie Byrd Land eruptions are identified by geochemical fingerprinting in the 1968 Byrd Station ice core. The 73 ka ice core record contained abundant, 7.5 to 40 ka, coarse ash layers, which were all previously geochemically correlated to Mt. Takahe volcano. We identify a one-to-one geochemical and age correlation of the youngest ~7.5 ka tephra layer in the Byrd ice-core to an 8.5±3.4

ka pyroclastic deposit at Mt. Takahe. We infer that 20-30 ka tephra layers in the Byrd ice core actually were erupted from Mt. Berlin on the basis of age and geochemical similarities. If products of these youngest, as well as older, $^{40}Ar/^{39}Ar$-dated eruptions are identified by geochemical fingerprinting in future ice and marine cores, then they will provide the cores with independently dated time horizons.

INTRODUCTION

The West Antarctic Ice Sheet (WAIS), the world's only remaining marine ice sheet, is considered by many to be inherently unstable and prone to catastrophic collapse and melting (e.g., Hughes, 1973; Mercer, 1978; MacAyeal, 1992; Bindschadler, 1995). A 6 m rise in sea level, equivalent to the volume of water locked up in the WAIS (Drewry et al., 1982), occurred during the ~125 ka isotopic stage 5e interglacial and has been attributed to WAIS collapse (Scherer, 1991). The possibility of catastrophic collapse of the WAIS has stimulated extensive glaciological and geophysical research, including two planned deep ice cores in the West Antarctic Ice Sheet (WAISCORES), one at Siple Dome, near the Ross Ice Shelf and a second at the central ice divide about 200 km east of Byrd Station (Fig.1)(Bindschadler, 1995). One objective of the WAISCORES studies is to determine the basal age of the ice sheet. The 1968 Byrd Station ice core in the WAIS has an inferred basal age of only 73 ka (Hammer et al., 1993). The extensive lateral flow of ice from the ice divide area to Byrd Station may have removed or disturbed much of the basal ice record. Consequently, the 73 ka date of the Byrd core provides only a minimum age of the WAIS. The locations of the future WAISCORES at Siple ice dome and the central ice divide minimize lateral ice-flow problems and will theoretically permit determining the age of the WAIS. On the basis of ice flow models, geophysical data and accumulation histories, Nereson et al. (in press) predicted that both planned WAISCORES could contain climate information dating to the previous interglacial. An age of >125 ka would nullify the hypothesis that the ice sheet collapsed during the last interglacial. The determination of a

basal age using common stratigraphic techniques (sedimentation rates or oxygen isotope correlations) can be complicated by shearing and poor preservation near the base of the ice sheet, as was found in the recent Greenland ice cores (e.g., Dansgaard et al., 1993). In this paper, we document a precise $^{40}Ar/^{39}Ar$ chronology of Late Quaternary explosive volcanism in West Antarctica that can be correlated to tephra layers in the 1968 Byrd ice core. The volcanic record offers the potential of an independent chronology of future WAISCORES and marine core stratigraphies through a critical period of climate history.

Tephra produced by large explosive volcanic eruptions in West Antarctica can be widely dispersed over oceans and ice sheets and trapped within accumulating sediment or snow layers, forming instantaneously deposited time-stratigraphic horizons. These horizons, when dated, can provide independent tests of chronologies based on other methods. In Marie Byrd Land (MBL), West Antarctica, eighteen large alkaline volcanoes (2300-4000 m above sea level) occur as nunataks in or as islands adjacent to the WAIS (Fig. 1). On the basis of geochemical compositions, MBL volcanoes have been interpreted as likely sources of fine-grained ashes recovered from *Eltanin* deep-sea piston cores in the Southern Pacific Ocean (Shane and Froggatt, 1992) and the 1968 Byrd Station ice core in the WAIS (Kyle et al., 1981; Palais et al., 1988).

The 1968 Byrd Station ice core provides the most complete existing record of MBL volcanism. The more than 2000 tephra layers recovered from the ice core were too sparse and too fine (median grain sizes mostly <20 μm) to be directly dated by existing methods (Palais et al., 1988). Available chronology, based in large part on ice-flow models, indicates that the Byrd tephra layers were erupted between 13 and 40 ka, with one isolated layer at 7.5 ka. The tephra layers include fine ash, concentrated in the 14 to 20 ka range and coarse ash (median grain sizes to 60 μm), concentrated in the 20 to 30 ka range. The fine ash and coarse ash layers were interpreted as products of phreatomagmatic and magmatic eruptions, respectively (Palais et al., 1988). Only 24 of the tephra units, one from the 7.5 ka layer and the remainder from the 20-30 ka layers, were geochemically

analyzed and were all correlated to Mt. Takahe, situated about 250 km from the calculated site of tephra deposition (Fig. 1) (Kyle et al., 1981; Palais et al., 1988). The *Eltanin* tephra layers were dated stratigraphically to the Late Quaternary (<60 ka) and correlated geochemically to MBL volcanoes, located more than 1500 km from core sites (Shane and Froggatt, 1992). No specific correlations were made between the *Eltanin* tephra and MBL source volcanoes.

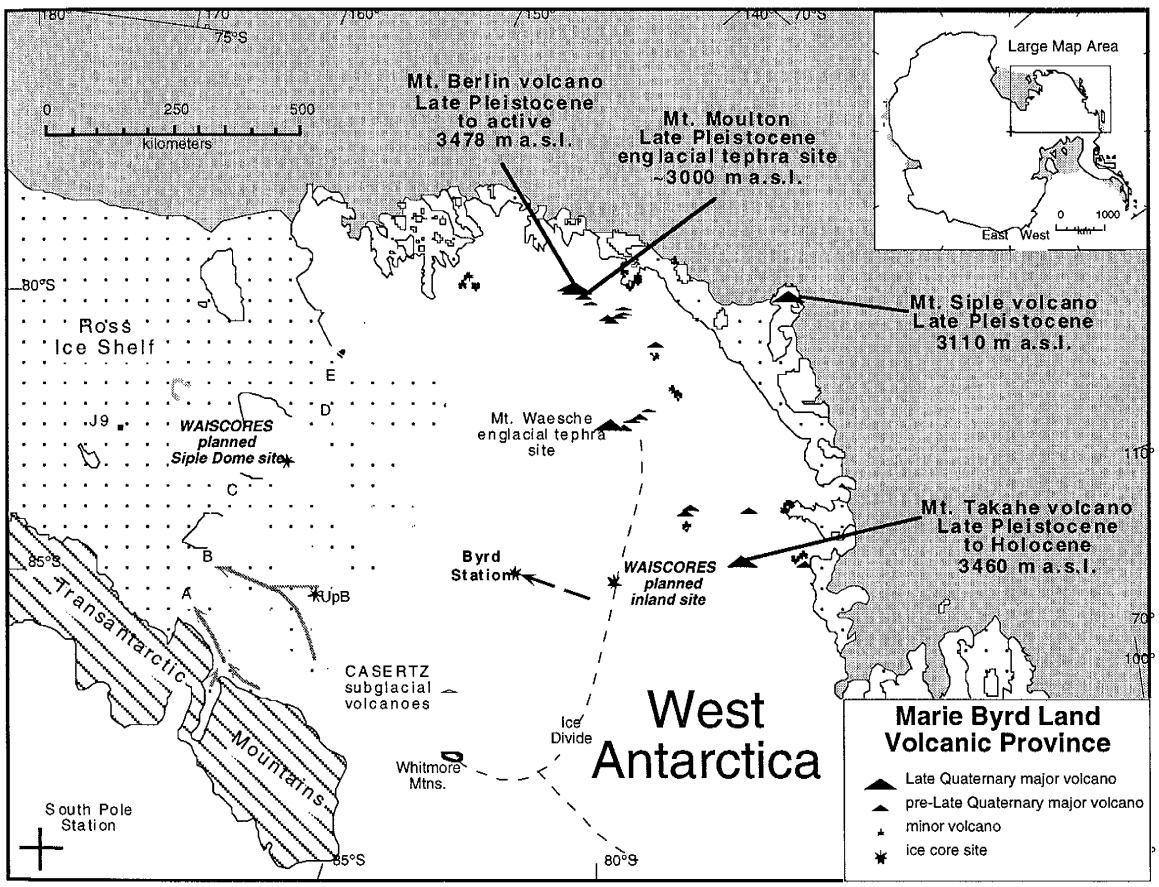

Figure 1. Map of Marie Byrd Land, West Antarctica (Drewry, 1983), showing major volcanoes (triangles) and minor volcanoes (asterisks) and several sites important to research of the West Antarctic Ice Sheet. Volcano study sites are designated by large bold type. The Transantarctic Mountains bisect the continent and form the divide between the mostly terrestrial East Antarctic Ice Sheet and the mostly marine-based WAIS. Five ice streams (A-E) account for about 90% of ice drained from the WAIS (Hughes, 1977). UpB designates the base camp on Ice Stream B. Byrd Station is the 1968 Byrd ice-core drill site. The dashed arrow is the estimated ice-flow vector of 25 ka ice in Byrd ice core. CASERTZ designates the Corridor Aerogeophysics of Southeastern Ross Transect Zone, the area of an inferred active subglacial volcano (Blankenship et al., 1993). J9 is the 1977-79 drill site of the Ross Ice Shelf Project.

There is no previous documentation of widespread explosive Late Quaternary eruptions at source volcanoes in MBL. LeMasurier and Rex (1991) characterize outcrops at the Late Quaternary volcanoes as composed mostly of lavas and noticeably lacking volcanic ash. Four of the MBL volcanoes, Mt. Berlin, Mt. Takahe, Mt. Siple, and Mt. Waesche, were listed as "possibly.. or probably active" by LeMasurier (1990, Fig. B.I.). Previous indications of recent volcanic activity in coastal MBL include steaming ice towers at Mt. Berlin (LeMasurier and Wade, 1968), englacial basaltic tephra layers near Mt. Waesche (Smellie et al., 1990), and trachytic pyroclastic rocks at the summit of Mt. Takahe that were geochemically correlated to tephra layers in the Byrd ice-core (Kyle et al., 1981; Palais et al., 1988). Active subglacial volcanism has also been inferred in southern MBL on the basis of aerogeophysical surveys (Blankenship et al., 1993). Previous attempts at conventional K-Ar dating of exposed coarse-grained summit crater rocks, potential source volcano deposits for ash layers in ice and marine cores, yielded imprecise age estimates of <100 ka (LeMasurier and Rex, 1983; LeMasurier, 1990).

In this paper, we present new field evidence from Mt. Berlin and Mt. Siple that suggest abundant Late Quaternary explosive activity of MBL volcanoes. Field, geochemical and $^{40}Ar/^{39}Ar$ age data chronicle twenty Late Quaternary (573-8.5 ka) trachytic to basanitic eruptions of Mt. Berlin, Mt. Siple, Mt. Takahe. Eruptive units from Mt. Berlin and Mt. Takahe volcanoes are correlated by age and geochemistry to tephra layers in the Byrd Station ice core.

METHODS

Fieldwork and sampling for this study was carried out at Mt. Takahe during the 1985-86 austral summer field season and at Mt. Berlin and Mt. Siple during the 1993-94 field season. Because of ice cover, outcrops at the >3000 m high MBL volcanoes are extremely limited. Most outcrops on Mt. Berlin were sampled and are included in this study. Only samples from the summit crater area of Mt. Takahe and Mt. Siple are included

in this study; the chronology and glaciovolcanic record of mafic outcrops near the bases of Mt. Siple and Mt. Takahe are discussed in Part C of dissertation. In addition, Late Pleistocene tephra samples were obtained from a bare ice area on the summit ice-cap of Mt. Moulton, located 30 km east of Mt. Berlin.

Geochemistry

Previous geochemical analyses reported by Palais et al. (1988) include electron microprobe major-element data from Byrd core coarse ash layers (n=11) and X-ray fluorescence analyses of whole-rock samples from selected outcrops at Mt. Takahe (n=15) and Mt. Berlin (n=2).

Whole-rock powders from Mt. Berlin (n=41) and Mt. Siple (n=2) were analyzed for major and trace elements by X-ray fluorescence (XRF) at the University of Keele and New Mexico Institute of Mining and Technology. Most of the lavas and welded and non-welded pyroclastic fall samples contained abundant microlites and were unsuitable for microprobe analyses.

Obsidian and pumice glass fragments from Mt. Berlin (n=2), Mt. Moulton englacial tephra (n=5) and Mt. Takahe (n=3) and feldspars from four Mt. Moulton englacial tephra samples were analyzed for major elements and F, Cl, and P by electron microprobe at Arizona State University. Major element compositions of a number of glass fragments were determined using an JEOL 8600 electron microprobe at Arizona State University. An accelerating voltage of 15 kV and beam current of 15 nA were used for the analysis. ZAF recalculation procedures were used. In order to minimize volatilization of Na, the beam was enlarged to a diameter of 10 microns, and Na included in the first set of analyzed elements. Analytical error is estimated to be +/- 1%, based on replicate analysis of alkaline glass reference materials KN-18 and KE-12 (Devine et al., 1984).

Samples from Mt. Berlin (n=5) and Mt. Takahe (n=3) were analyzed for trace elements using a Cameca IMS 3f ion microprobe at Arizona State University. A 1-2 nA mass-analyzed primary beam of $^{16}O^-$ was focused to a 10 micron spot. Secondary ion

intensity for trace elements was calibrated against NBS-610, a sodium- and silica-rich glass containing around 500 ppm of 61 trace elements (values used for calibration are mainly from Hollocher et al., 1995). Observed reproducibility of secondary standards suggest that precision of analyses are ±10% .

Microprobe major and trace element data were also obtained from a composite sample of glass shards from 5 tephra layers in the Byrd Station ice core. The tephra layers are from core depths of 1377, 1415, 1457, 1710, and 2006 m. Samples previously analyzed by electron microprobe (Palais et al., 1988) were unavailable for re-analysis.

$^{40}Ar/^{39}Ar$ Dating

Recent advances in $^{40}Ar/^{39}Ar$ geochronology, including laser heating, lower extraction line blanks, and higher resolution mass spectrometers, have led to successes in dating anorthoclase- and sanidine-bearing volcanic rocks as young as Holocene in age (e.g., Hu et al., 1994; van den Bogaard, 1995). Most attempts to date young felsic volcanic rocks have focused on averaging the results of many laser-fusion analyses of single sanidine crystals from the same sample. The principal advantage of the laser method is that contamination by older xenocrysts can be recognized and eliminated from the mean age result (LoBello et al., 1987; Deino and Potts, 1990). The primary disadvantage of the laser method is that small isotopic signal sizes from young samples are near mass spectrometer detection limits, resulting in large analytical uncertainties in isotopic measured ages. In contrast to the laser-fusion method, the more conventional furnace step-heating approach has rarely been used in recent studies of young volcanism. There are two main advantages of the step-heating method: first, large samples can be analyzed, resulting in small analytical uncertainties; and second, the step-heating approach permits assessment of basic assumptions about sample homogeneity and closed system conditions. The disadvantage of the step-heating approach is that problems of xenocrystic contamination cannot be confidently corrected and in the worst case might remain undetected. Given adequately large samples of uncontaminated volcanic alkali feldspar phenocrysts, the

furnace step-heating method potentially results in higher precision and more accurate isotopic measurements and ages than the laser-fusion method. Estimates of accuracy can be obtained by checking the $^{40}Ar/^{39}Ar$ ages with stratigraphy or by comparing them to ages determined by other dating methods.

Samples were dated by $^{40}Ar/^{39}Ar$ methods from Mt. Berlin (n=38), Mt. Takahe (n=6), and Mt. Siple (n=2) volcanoes (Fig. 1). With the exception of ten basanitic to trachytic groundmass concentrates from Mt. Berlin, all of the dated samples are anorthoclase phenocrysts derived from trachytic and phonolitic lavas and pyroclastic rocks. Anorthoclase are high-potassium, anhydrous, low-diffusivity feldspars, ideal for $^{40}Ar/^{39}Ar$ dating. Coarse-grained (0.4-3 mm diameter) anorthoclase crystals were separated from crushed rock samples using standard magnetic, heavy-liquid, and hand-picking techniques and treated for 5-10 minutes with 15% hydrofluoric acid to remove adhering glass. Sample purity of anorthoclase separates was >99%. For the ten aphyric trachyte/phonolite and mafic lava samples from Mt. Berlin, groundmass concentrates (0.4-0.8 mm diameter grain size) were separated magnetically. Mafic samples were treated with 10% hydrochloric acid for five minutes.

Complete analytical methods, data tables, furnace age spectra and laser relative probability spectra are available as Supplemental Data (Appendices 1-5) from the GSA Data Repository. Most samples were irradiated in the D-3 position of the reactor at the Nuclear Science Center, Texas A & M University, College Station, TX for 2 hours (average neutron flux yielded approximately 0.0001 J/hr). The irradiation-induced thermal neutron $^{40}K(n,p)^{40}Ar$ interference reaction was minimized by boron shielding at the Texas A&M reactor. Fish Canyon Tuff sanidine (FCT-1, 27.84 Ma (Deino and Potts, 1990)) was used as a neutron flux monitor. Individual crystals of flux monitors (6 sanidine crystals per monitor position) and seventeen MBL samples (4-10 anorthoclase crystals per sample) were fused with a CO_2 laser. Thirty-seven 50-200 mg samples of anorthoclase were step-heated in a resistance furnace. After laser or furnace heating, argon isotopes were

measured on an Mass Analyzer Products (MAP) 215-50 mass spectrometer at the New Mexico Geochronological Research Laboratory. Typical furnace blanks (including mass spectrometer backgrounds) were 80, 0.2, 0.1, 0.2, 0.6 $x10^{-17}$ moles at masses ^{40}Ar, ^{39}Ar, ^{38}Ar, ^{37}Ar, ^{36}Ar, respectively. The sample ages were corrected for blank, background, mass discrimination, radioactive decay, and interfering reactions. All analytical uncertainties are reported at the 2 sigma confidence level and the decay constants and isotopic abundances used are those suggested by Steiger and Jaeger (1977).

An integrated age and a plateau or mean age were calculated for samples analyzed by furnace step-heating method. The integrated age, equivalent to the K-Ar age of the sample, is a mean of the incremental ages, each weighted by the $\%^{39}Ar$ in each step. The furnace plateau and mean ages and laser mean ages are averages of specified increments weighted by the inverse of variance. The plateau age is defined by three or more contiguous incremental ages that comprise >50% of total ^{39}Ar released and agree within 2 σ (Fleck *et al.*, 1977). Furnace mean ages consist of subjectively selected contiguous incremental ages that are nearly concordant. Laser mean ages include all analyses except those compromised by anomalous blank measurements. There was no definitive evidence for xenocrystic contamination (i.e. anomalously old ages of some crystals relative to others) in laser or furnace data. Uncertainties on plateau and mean ages are calculated using formula in Samson and Alexander (1987). All errors are reported at 2 σ confidence level.

RESULTS

Field Observations

Non-welded and welded trachytic pyroclastic breccias and tuff breccias, composed of pumiceous bombs, obsidian clasts and lithic fragments, were ubiquitous in crater-rim exposures (Fig. 2; Table 1). The lithic fragment components included trachytic lava and hypabyssal clasts, compositionally similar to juvenile pumice and obsidian clasts. Typical

breccia deposits were moderately sorted and crudely to well bedded, with beds mantling topography. Inferred welding processes varied from weak agglutination to load pressure compaction, with fiamme aspect ratios as low as 1:10. Clastic textures are nearly obliterated in agglutinates that were transformed into clastogenic lavas. Clastogenic lavas

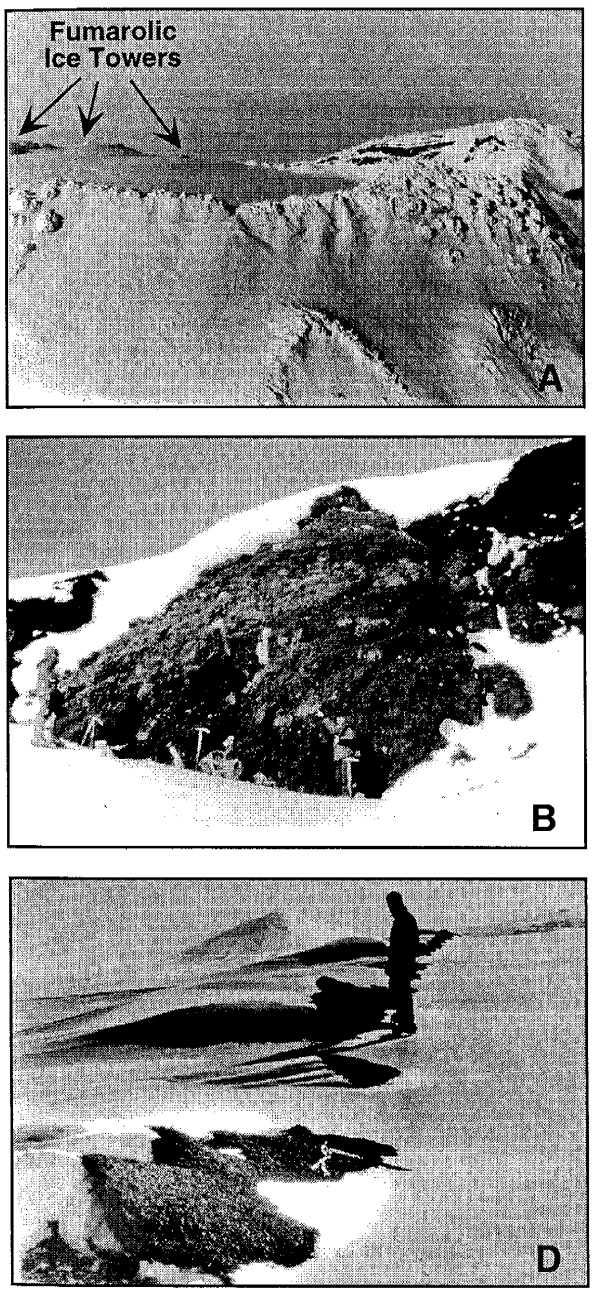

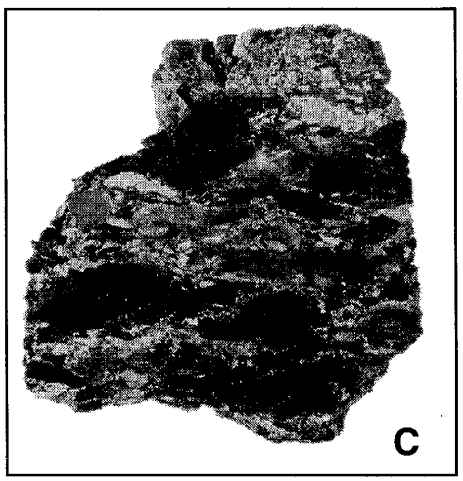

Figure 2. Photographs from Mt. Berlin volcano: a) A view looking west to the 2 km diameter Mt. Berlin summit crater. An 150 m thickness of two welded pyroclastic fall units overlain by thin non-welded deposit are exposed in the crater wall. Several fumarolic ice towers occur on the western rim of the crater ; b) A partly agglutinated pyroclastic fall deposit in summit crater wall of Mt. Berlin contains abundant slightly flattened light-colored pumiceous bombs; c) A 12x12 cm rock slab cut from welded pyroclastic fall deposit at from Merram Peak crater contains flattened pumice and abundant lithic clasts; and d) A view of non-welded englacial tephra layer at Mt. Moulton with Mt. Berlin summit 30 km to the west.

exhibit characteristics of rheomorphism, including recumbent folds. Lithofacies characteristics, such as pumice/lithic content and degree of welding, varied dramatically over short vertical distances but were uniform over lateral distances. Unit thicknesses range from 1 m at Merram Peak crater, to >70 m at the summit crater wall of Mt. Berlin. We interpret these pyroclastic breccias as proximal pyroclastic fall deposits. Welding may have been facilitated by high temperatures and low viscosities of peralkaline magmas (Mahood, 1984). Changes in welding and lithofacies characteristics are attributed to changes in eruption dynamics (column height and eruption rate) rather than changes in magma composition.

Other lithofacies recognized at study sites include: englacial tephra layers, mafic scoria deposits, ash-rich pyroclastic breccia and associated accretionary lapilli-bearing tuff, a distal fiamme-rich tuff, and abundant dense lavas. Several englacial pumiceous tephra layers occur in a stratigraphically coherent horizontal section of bare ice on the summit of Mt. Moulton. We infer that these englacial tephra resulted from explosive eruptions of Mt. Berlin volcano, located 30 km to the west. Two outcrops of mafic scoria and lava deposits on the north flank of Mt. Berlin are attributed to monogenetic cinder cone eruptions. The ash-rich pyroclastic breccia and accretionary lapilli-bearing tuff, which formed part of the youngest sequence in the Mt. Berlin summit crater wall, are attributed to a hydrovolcanic eruptive phase. An isolated outcrop of densely welded(fiamme-rich) tuff on the southeast flank of Mt. Berlin is interpreted as an ignimbrite, one of the rare examples in MBL.

Geochemistry

Major and trace element data from microprobe analyses of Mt. Takahe and Mt. Berlin samples are listed in Table 2 (a complete set of chemical data is available as Supplemental Data (Appendix 6) from the GSA Data Repository). Data from microprobe analyses of eleven glass shards from the Byrd ice core composite sample are included in Appendix 6. Because the sample is a composite of mixed age tephra, analytical data were

TABLE 1. LATE QUATERNARY MARIE BYRD LAND VOLCANOES $^{40}Ar/^{39}Ar$ AGE SUMMARY

Sample	Description type[1]	Sample	Method[2]	n[3]	steps	%^{39}Ar[4]	Age[5] ± 2 s[6] (ka)
Mt. Berlin summit crater trachyte deposits							
WCM93-16	fumarolic ice cave, floor lava	anorth	f p	5	b-f	95.6	**11.5 ± 3.5**
WCM93-25	non-welded pumice fall	anorth	f p	5	b-f	56.4	**15.9 ± 6.2**
WCM93-22	laminated pumice, top of upper welded unit	anorth	l m	8			41 ± 17
			f m	7	f-l	76.9	27.2 ± 1.6
			f m	8	e-l*	95.1	25.5 ± 2.0
			f	2			**26.5 ± 2.1**
WCM93-17	pumiceous rheomorphic tuff, upper welded unit	anorth	f m	9	c-k*	89.9	**24.4 ± 5.0**
WCM93-21	welded fall, below WCM93-22	anorth	f p	9	c-k	85.3	29.6 ± 2.2
			f p	5	g-k	65.4	24.9 ± 3.5
			f	2			**28.3 ± 4.6**
WCM93-23	east side, lower welded unit	anorth	l m	5			30 ± 10
			f p	4	e-h*	58.0	**27.4 ± 4.3**
			f p	4	g-j*	38.3	30.4 ± 7.6
WCM93-19	Summit pumiceous	anorth	f m				highly discordant
WCM93-15	spatter lava with cognate xenoliths	anorth	l m	8			25 ± 14
			f p	9	c-k	79.9	24.4 ± 1.2
			f p	6	d-i	69.5	26.8 ± 3.5
			f	2			**24.7 ± 1.9**
Summit fumarolic cave lava			**f**	**1**			**11.5 ± 3.5**
Summit non-welded fall deposit			**f**	**1**			**15.9 ± 6.2**
Summit crater fall deposits			**f**	**5**			**25.8 ± 1.7**
Mt. Berlin- Merram Peak crater							
WCM93-130	1 m thick pumiceous phonolite fall	anorth	l m	7			170 ± 42
			f p	9	e-m	100.0	**140.7 ± 2.8**
WCM93-123	black/yellow fall (SE)	anorth	l m	8			154 ± 22
WCM93-128	trachyte bomb (WNW)	anorth	f p	5	g-k	72.1	**183.6 ± 2.7**
WCM93-129	pumiceous trachyte fall	anorth	l m	8			197 ± 17
			f p	4	i-l	51.9	**187.1 ± 2.6**
WCM93-133	welded trachyte fall (NE)	anorth	f p	5	h-l	55.7	186.5 ± 1.4
			f p	6	g-l	75.9	182.3 ± 3.0
			f	2			**182.3 ± 3.0**
WCM93-139	welded clastogenic flow	anorth	f p	5	f-j	70.3	**183.8 ± 1.9**
			l m	6			187 ± 34
WCM93-140	welded clastogenic flow	anorth	f p	6	f-k	75.3	**186.1 ± 2.8**
Merram Peak non-welded fall deposit			**f**	**1**			**140.7 ± 2.8**
Merram Peak welded fall deposit			**f**	**5**			**185.0 ± 1.8**

Sample	Description	Sample type[1]	Method[2]	n[3]	steps	%^{39}Ar[4]	Age[5] ± 2 s[6] (ka)
Mt. Berlin- flank trachyte deposits							
WCM93-011	near-vent trachyte lava (NE)	anorth	l m	9			266 ± 30
			f p	6	f-k	73.2	**237.4 ± 3.6**
WCM93-152	welded trachyte ignmibrite (SE)	anorth	l m	6			220 ± 31
			f p	5	f-j	64.6	230.7 ± 2.1
Mt. Berlin- flank deposits mean age			**f**	**2**			**232.4 ± 6.1**
Mt. Berlin- NW flank mafic deposits							
WCM93-001	basanite cinder cone	bas-gms	f p	8	b-i	98.2	250 ± 21
			f p	6	c-h	86.2	236 ± 34
			f	2			**246 ± 22**
WCM93-004	basanite cinder cone	bas-gms	f p	9	b-j	96.7	221 ± 23
			f p	4	c-f	51.3	226 ± 38
			f	2			**222 ± 20**
WCM93-008	hawaiite flow levee	haw-gms	f p	6	a-f	81.2	**221 ± 17**
Mefford Knoll mafic flow mean age			**f**		**3**		**236 ± 19**
Mt. Berlin- Merram Peak (SW) trachyte lava							
WCM93-134	trachyte lava	anorth	l m	7			**410 ± 72**
WCM93-127	foliated trachyte lava	anorth	f m	4	j-m	36.6	**434 ± 18**
WCM93-125	foliated trachyte lava	anorth	f p	9	b-j	88.9	**567.9 ± 5.4**
WCM93-126	clastogenic trachyte lava	anorth	f p	4	c-f	62.5	563 ± 4.7
			f p	8	cc-j	90.6	565.1 ± 6.0
			f	2			**563.8 ± 4.2**
WCM93-137	trachyte lava	anorth	f p	5	b-f	67.9	**575.7 ± 2.6**
WCM93-138	clastogenic trachyte lava	anorth	f m	3	f-h*	30.7	**579 ± 12**
WCM93-135	clastogenic phonolite	anorth	l m	9			616 ± 24
			l m	5			588 ± 48
			f p	5	f-j	61.3	**574.7 ± 4.1**
WCM93-009	trachyte flow levee (NW)	tr-gms	f t	5	all	100.0	**595 ± 36**
Mt. Berlin- SW flank trachyte lava 2			**f**	**1**			**434 ± 18**
Mt. Berlin- SW flank trachyte lava 1			**f**	**6**			**572.6 ± 4.8**
Mt. Berlin- Brandenberger Bluff							
WCM93-014	cinder cone	pt-gms	f m	8		99.0	**2700 ± 50**
WCM93-010	dome lava	ph-gms	f p	5		100.0	**2690 ± 130**
WCM93-037	lava at bluff base	ph-gms	f p	5		100.0	**2830 ± 240**
WCM93-053	clast in hyalotuff	tr-gms	f p	7		100.0	**2684 ± 83**
WCM93-069	clast in hyalotuff	tr-gms	f p	7		100.0	**3500 ± 1000**
WCM93-121	clast in hyalotuff	ph-gms	f p	5		100.0	**2760 ± 120**
WCM93-250	clast in hyalotuff	tr-gms	f p	5		95.3	**2670 ± 120**
Mt. Berlin- Brandenberger Bluff trachyte/phonolite			**f**	**5**			**2717 ± 75**

Sample	Description	Sample type[1]	Method[2]	n[3]	steps	%^{39}Ar[4]	Age[5] ± 2 s[6] (ka)
Mt. Berlin- distal englacial tephra at Mt. Moulton							
WCM93-313	tephra 5, 5 cm thick	anorth	f m	3	k-m*	33.4	13.4 ± 3.8
			f m	2	e-f*	35.1	15.0 ± 1.6
			l m	5			55 ± 52
			f	2			**14.8 ± 1.9**
WCM93-315	tephra 4, 12 cm thick	anorth	f m	3	k-m*	41.3	31.5 ± 4.5
			f p	4	f-i	58.3	**22.6 ± 3.0**
			l m	7			61 ± 26
WCM93-316	tephra 3, 3 cm thick	anorth	f p	3	j-l	57.8	91.1 ± 1.1
			f p	9	d-l	95.6	92.6 ± 1.8
			l m	10			74 ± 18
			f	2			**91.5 ± 1.6**
WCM93-317	tephra 2, 2 cm thick	anorth	f p	6	g-l	82.0	104.6 ± 1.6
			f p	8	d-k	93.6	107.5 ± 2.4
			l m	7			93 ± 34
			f	2			**105.5 ± 3.0**
WCM93-314	tephra 1, 15 cm thick	anorth	f p	6	d-i	87.3	**117.6 ± 3.6**
			l m	7			123 ± 13
			l m	6			111 ± 41
			l m	4			123.5 ± 7.5
			l m	17			123.5 ± 7.3
Mt. Siple summit crater							
WCM93-278	near summit, lava	anorth	f p	5	d-h	63.0	**167.2 ± 2.1**
WCM93-277	crater wall, densely welded fall	anorth	f m	6	d-i	97.3	222.8 ± 4.7
			f p	7	g-m	74.3	224.9 ± 4.2
			f m	7	c-i	81.8	222.2 ± 4.2
			l m	9			170 ± 42
			f	3			**223.6 ± 3.5**
Mt. Takahe summit crater							
W85009	Bucher Rim(S) pumice and obsidian bombs	anorth	f p	6	g-l	70.6	**8.5 ± 3.2**
W85013	Bucher Rim(N) lava beneath welded fall	anorth	f m	9	c-k	94.5	**92.7 ± 7.3**
W85015	Bucher Rim(N), welded fall obsidian	anorth	f p	4	f-i	63.5	**103.2 ± 5.3**
MT85006	9300' outcrop lava	anorth	f p	7	c-i	91.7	**155.2 ± 2.9**
W85022	Bucher rim(S), lava	anorth	f m	5	f-j	77.7	**173.6 ± 3.8**
W85011	Bucher Rim(S), 10 m lava over W85-09	anorth	f m	6	e-j	84.3	**191.2 ± 5.3**

Note: Samples from each site are listed in stratigraphic order from youngest to oldest. [1]Sample type: anorth. = anorthoclase; bas-gms = basanite groundmass; haw-gms = hawaiite groundmass; trach-gms = trachyte groundmass. [2]Method abbreviations: f = furnace step-heating, l= laser fusion, p = plateau age (after Fleck et al., 1977), m = weighted mean age, t = total fusion furnace age, [3]n= the number of apparent ages included in furnace or laser mean age or site mean age calculation. [4]%^{39}Ar = percentage of total ^{39}Ar that is included in mean or plateau age. [5]mean sample ages and unit ages were calculated by weighting by the inverse of variance and are listed in bold type. [6]two-sigma uncertainties of mean sample and unit ages were calculated using method of Samson and Alexander (1987)

TABLE 2. GLASS SHARD AND PUMICE MICROPROBE DATA

WCM93	25	313	315	316	317	314	130	W-9	W-15	W-16
Volcano	Berlin	Moulton	Moulton	Moulton	Moulton	Moulton	Moulton	Takahe	Takahe	Takahe
Rock[1]	trach	trach	trach	trach	trach	trach	trach	trach	trach	trach
Age[2]	16 ka	15 ka	23 ka	92 ka	106 ka	118 ka	141 ka	8.5 ka	103 ka	<8.5 ka
Electron Microprobe Major Element Data (weight %)										
no.	6	5	5	8	6	6	5	6	6	6
SiO_2	60.77 (0.85)	61.76 (0.17)	62.95 (0.44)	63.04 (1.03)	64.39 (0.33)	64.51 (0.61)	63.13 (1.62)	59.54 (0.63)	60.09 (0.44)	60.14 (0.67)
TiO_2	0.45 (0.06)	0.42 (0.02)	0.51 (0.02)	0.45 (0.15)	0.43 (0.01)	0.40 (0.02)	0.40 (0.03)	0.85 (0.03)	0.55 (0.01)	0.57 (0.02)
AL_2O_3	14.73 (0.73)	14.22 (0.14)	14.04 (0.15)	15.12 (1.34)	13.75 (0.18)	14.30 (0.32)	14.15 (0.75)	15.56 (0.24)	14.78 (0.24)	14.37 (0.10)
FeO	8.64 (0.43)	9.10 (0.15)	8.99 (0.11)	7.35 (2.44)	7.97 (0.18)	7.61 (0.36)	8.57 (0.59)	8.15 (0.33)	8.51 (0.19)	9.28 (0.30)
MnO	0.28 (0.04)	0.31 (0.02)	0.31 (0.04)	0.26 (0.12)	0.25 (0.03)	0.21 (0.03)	0.28 (0.06)	0.30 (0.05)	0.32 (0.05)	0.37 (0.03)
MgO	0.04 (0.04)	0.01 (0.01)	0.01 (0.01)	0.02 (0.01)	0.00 (0.00)	0.00 (0.00)	0.01 (0.01)	0.41 (0.07)	0.14 (0.02)	0.03 (0.02)
CaO	1.10 (0.20)	0.94 (0.06)	1.07 (0.05)	1.18 (0.41)	0.97 (0.01)	0.81 (0.04)	0.86 (0.07)	1.87 (0.46)	1.28 (0.19)	1.40 (0.02)
Na_2O	8.91 (1.33)	8.36 (0.41)	7.27 (0.32)	7.09 (0.40)	7.22 (0.25)	7.16 (0.49)	7.69 (2.62)	8.03 (0.29)	9.13 (0.43)	8.61 (0.18)
K_2O	4.43 (0.20)	4.16 (0.11)	4.34 (0.11)	4.92 (1.27)	4.42 (0.11)	4.37 (0.11)	4.10 (0.47)	4.87 (0.23)	4.70 (0.13)	4.74 (0.13)
P_2O_5	0.07 (0.07)	0.07 (0.05)	0.04 (0.05)	0.04 (0.04)	0.07 (0.04)	0.02 (0.02)	0.02 (0.03)	0.11 (0.09)	0.02 (0.03)	0.06 (0.05)
Cl	0.25 (0.03)	0.31 (0.02)	0.22 (0.02)	0.24 (0.09)	0.24 (0.02)	0.28 (0.03)	0.35 (0.01)	0.09 (0.01)	0.18 (0.02)	0.15 (0.02)
F	0.34 (0.04)	0.34 (0.03)	0.26 (0.01)	0.30 (0.10)	0.31 (0.02)	0.34 (0.05)	0.44 (0.05)	0.24 (0.03)	0.32 (0.04)	0.30 (0.04)
P.I.[3]	1.32	1.28	1.19	1.12	1.21	1.15	1.21	1.19	1.36	1.34
Ion Microprobe Trace Element Data (in ppm)										
no.	4	3	3	5	2	3	4	4		
Li	39 (13)	41 (13)	57 (36)	41 (10)	44 (5)	22 (3)	47 (8)	31 (4)		
B	17 (2)	20 (2)	15 (1)	15 (2)	18 (1)	6 (1)	9 (1)	8 (1)		
P	203 (12)	281 (45)	198 (12)	281 (32)	194 (6)	375 (26)	305 (52)	283 (21)		
Rb	153 (12)	168 (9)	141 (14)	180 (36)	182 (4)	93 (7)	163 (28)	138 (8)		
Sr	8 (1)	6 (0)	5 (0)	4 (2)	2 (0)	19 (3)	7 (1)	2 (1)		
Y	124 (17)	142 (9)	110 (6)	122 (7)	143 (3)	60 (5)	97 (2)	98 (4)		
Zr	1495 (145)	1631 (30)	1171 (38)	1282 (36)	1527 (24)	533 (26)	983 (15)	833 (21)		
Nb	253 (17)	300 (10)	207 (3)	206 (12)	254 (23)	100 (3)	185 (10)	166 (5)		
Ba	84 (29)	65 (21)	57 (10)	58 (9)	22 (11)	356 (46)	27 (2)	29 (2)		
La	176 (28)	203 (19)	148 (5)	171 (12)	186 (16)	94 (9)	154 (18)	142 (14)		
Ce	355 (39)	413 (22)	295 (9)	345 (26)	386 (18)	185 (14)	301 (19)	284 (8)		
Nd	133 (20)	147 (15)	117 (3)	149 (39)	141 (11)	71 (11)	115 (6)	113 (8)		
Eu	6 (2)	7 (1)	7 (0)	10 (7)	6 (2)	7 (2)	4 (2)	6 (1)		
Th	25 (3)	29 (2)	18 (2)	25 (10)	28 (0)	9 (2)	17 (4)	15 (3)		
U	10 (1)	10 (0)	7 (1)	20 (27)	6 (2)	2 (1)	4 (0)	2 (0)		

Notes: Geochemical quantitiies in weight % or ppm are data averaged from multiple analyses; quantities in parenthesis are 1 standard deviation uncertainties. [1] rocks classified according to LeBas et al. (1986). [2] ages are $^{40}Ar/^{39}Ar$ mean ages, except age of Mt. Takahe sample W-16, which is inferred from field relationships. [3]P.I.= peralkaline index = molecular $(K_2O + Na_2O)/ Al_2O_3$.

not averaged and one-to-one correlations between tephra layers and source volcano rocks are not possible.

Major element oxide percentages, except % Na_2O, are slightly higher in microprobe data than in XRF data. These differences are attributed to volatilization and loss of sodium during electron microprobe analyses that resulted in lower Na_2O contents (1.85-2.00% lower in microprobe data compared to XRF data) and apparent gains in other oxides. Because of the Na loss problem, it is best to make direct comparisons between major element data obtained by the same technique.

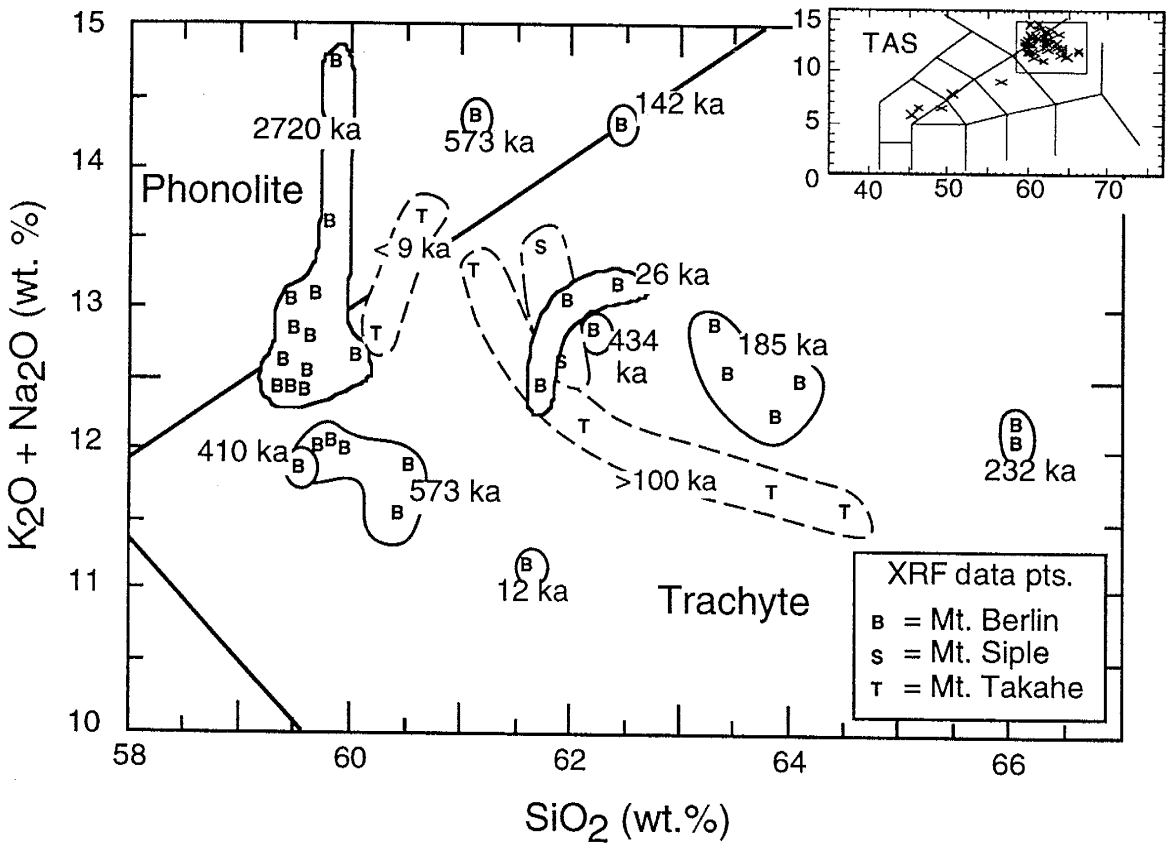

Figure 3. Total alkalis versus silica (TAS) plot of whole-rock XRF data from Mt. Takahe (T), Mt. Siple (S), and Mt. Berlin (B) samples. Same-aged samples are circled. Phonolite and trachyte field boundaries from LeBas et al. (1986). Mt. Takahe data from Palais et al. (1988). In calculating weight percents, major element data was normalized to 100% volatile-free. Inset shows entire TAS plot after LeBas et al. (1986).

Figure 3 shows that whole-rock samples are dominantly trachytes, with minor phonolites. The trachytes are mostly peralkaline, with peralkaline indices (molecular (Na_2O

+ K_2O) /Al_2O_3) as high as 1.48, and include both pantelleritic and comenditic trachytes (LeBas et al., 1986). Although most samples are classified as trachytes, the chemical data cluster into discrete populations which are consistent with the sample ages. Compositions of both Mt. Berlin and Mt. Takahe eruptions have varied with time, although no systematic changes are recognized.

Electron microprobe analyses of alkali feldspar samples from four englacial tephra layers at Mt. Moulton indicate similar Ca-poor (%CaO <0.3) anorthoclase compositions. In thin-section, the anorthoclase feldspars are euhedral, with simple Carlsbad twins and rare tartan twins. We infer that all of the alkali feldspars in the trachytes and phonolites are anorthoclase rather than sanidine.

$^{40}Ar/^{39}Ar$ Geochronology

Mean $^{40}Ar/^{39}Ar$ laser and furnace ages are summarized in Table 1. Representative results (Fig. 4) show single-crystal laser-fusion data with relatively large uncertainties compared to the more precise and reproducible results of the bulk-sample furnace step-heating analyses. The variable, lower precision age determinations of the laser method are attributed to the small ^{40}Ar and ^{36}Ar content in each young crystal and to variability in system blank. Furnace step-heating of multiple anorthoclase crystals (50-200 mg) produced relatively flat age spectra (Fig. 4) yielding plateau or weighted mean ages that are consistent with stratigraphic position and interpreted as geologically meaningful eruption ages. In general, the furnace and laser mean ages overlap at 2σ, but the laser ages have much higher analytical uncertainties (Fig. 5). The mean uncertainty of anorthoclase ages is $\pm$3.6 ka for all furnace-heated samples and $\pm$28 ka for all laser-heated samples. Table 1 shows that the furnace ages are reproducible among different irradiation packages and are consistent with stratigraphy and Figure 6 shows representative age spectra from key study sites.

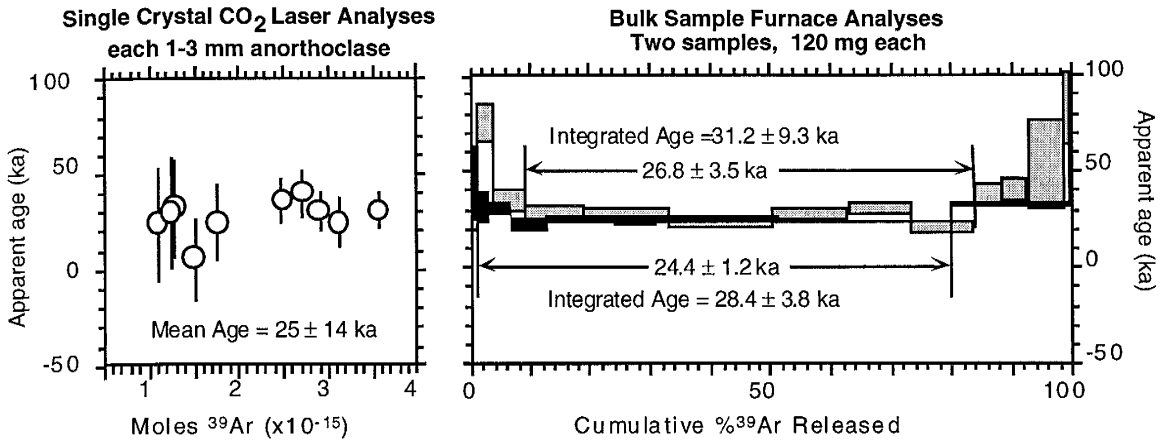

Figure 4. Representative $^{40}Ar/^{39}Ar$ CO_2 laser-fusion ages and age spectra of anorthoclase samples extracted from one Mt. Berlin summit crater wall sample (WCM93-15). Laser data shows ages (± 2 s.d.) of ten individual crystals. Furnace age spectra show incremental step-heated ages of two, multiple-crystal anorthoclase samples.

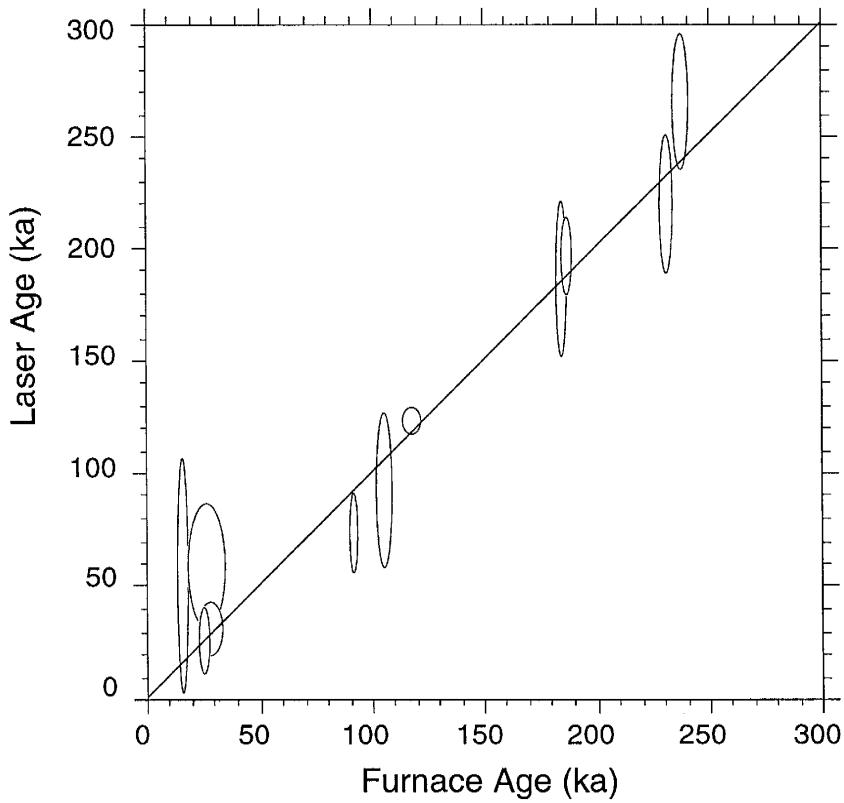

Figure 5. A comparison between replicate sample mean ages obtained by single-crystal laser-fusion and bulk sample furnace step-heating methods. The center of the ellipse is the age intercept, and the width and height correspond to 2 standard deviation uncertainties of furnace and laser mean ages, respectively. Ages are weighted by the inverse of variance and uncertainties are calculated by method of Samson and Alexander (1987).

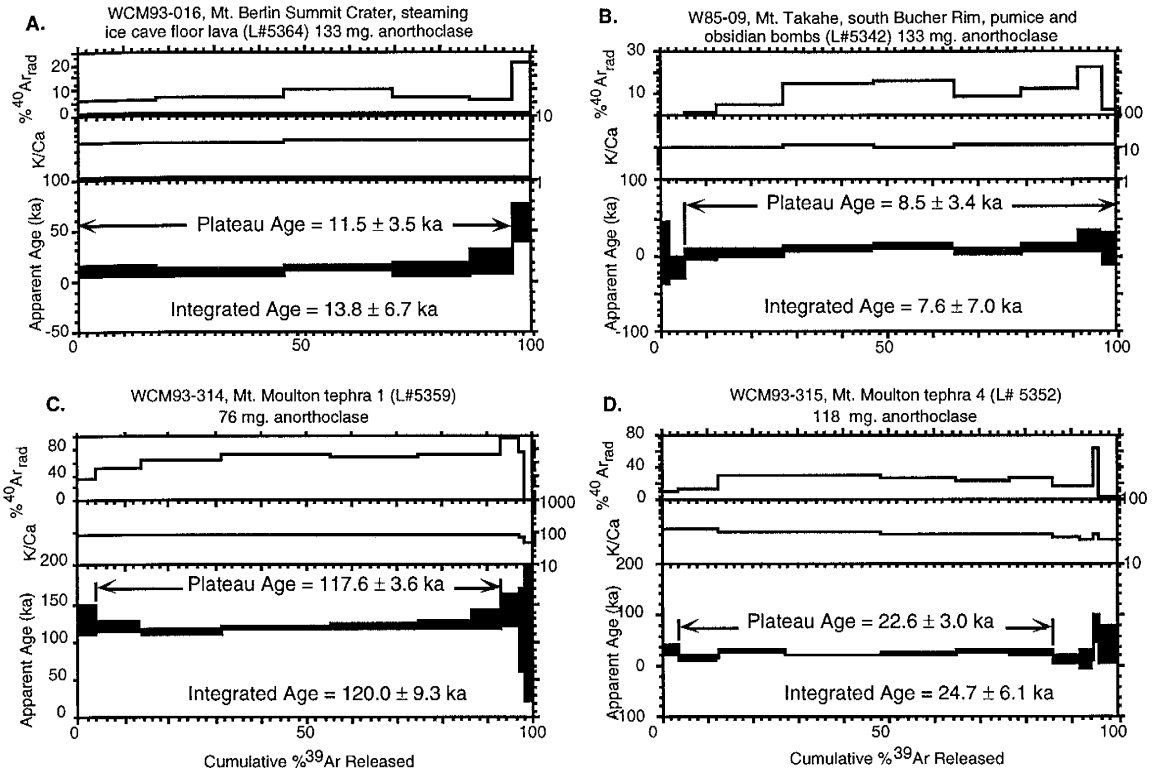

Figure 6. Four representative $^{40}Ar/^{39}Ar$ age spectra of anorthoclase samples. Plots show cumulative $\%^{39}Ar$ released during furnace heating experiment versus apparent age (± 2 s.d.), K/Ca, and radiogenic ^{40}Ar yield. a) Sample WCM93-016 is from a trachyte lava at the floor of fumarolic ice cave on the summit crater rim of Mt. Berlin. b) Sample W85-09 is from the youngest summit crater rim deposit on Mt. Takahe and is correlated to the youngest 7.5 ka tephra in the Byrd Station ice core. c) Sample WCM93-315 was obtained from a distal Mt. Berlin tephra, recovered from the summit ice cap of Mt. Moulton, that has geochemical similarities to the 20-30 ka Byrd Station ice core tephra. d) Sample WCM93-314 also dates an englacial tephra at Mt. Moulton. This age implies that the enclosing summit ice cap is likely as old as the previous interglacial at ~125 ka.

ERUPTION RECORDS

Mt. Berlin

Mt. Berlin, an actively steaming volcano in western MBL with a prominent summit crater and a subsidiary crater at Merram Peak, is the only volcano with documented geothermal activity in West Antarctica (Figs. 1, 2, 7). Mt. Berlin is characterized by a south to southeastward migration of volcanic activity that is perpendicular to the regional westward migration pattern of felsic volcanism as reported by LeMasurier and Rex (1989). Growth of Mt. Berlin occurred in three stages (Fig. 7): first, volcanism was centered at

Brandenberger Bluff (1650 ± m above sea level (a.s.l.)) at 2.7 Ma; second, eruptions from the 3000 m a.s.l. Merram Peak crater occurred from 600 to 140 ka; and third, volcanic activity shifted to the 3478 m a.s.l. summit crater from 26 to 0 ka. The volcanic history is recorded in crater rim and flank deposits on the volcano and in distal tephra exposed in bare

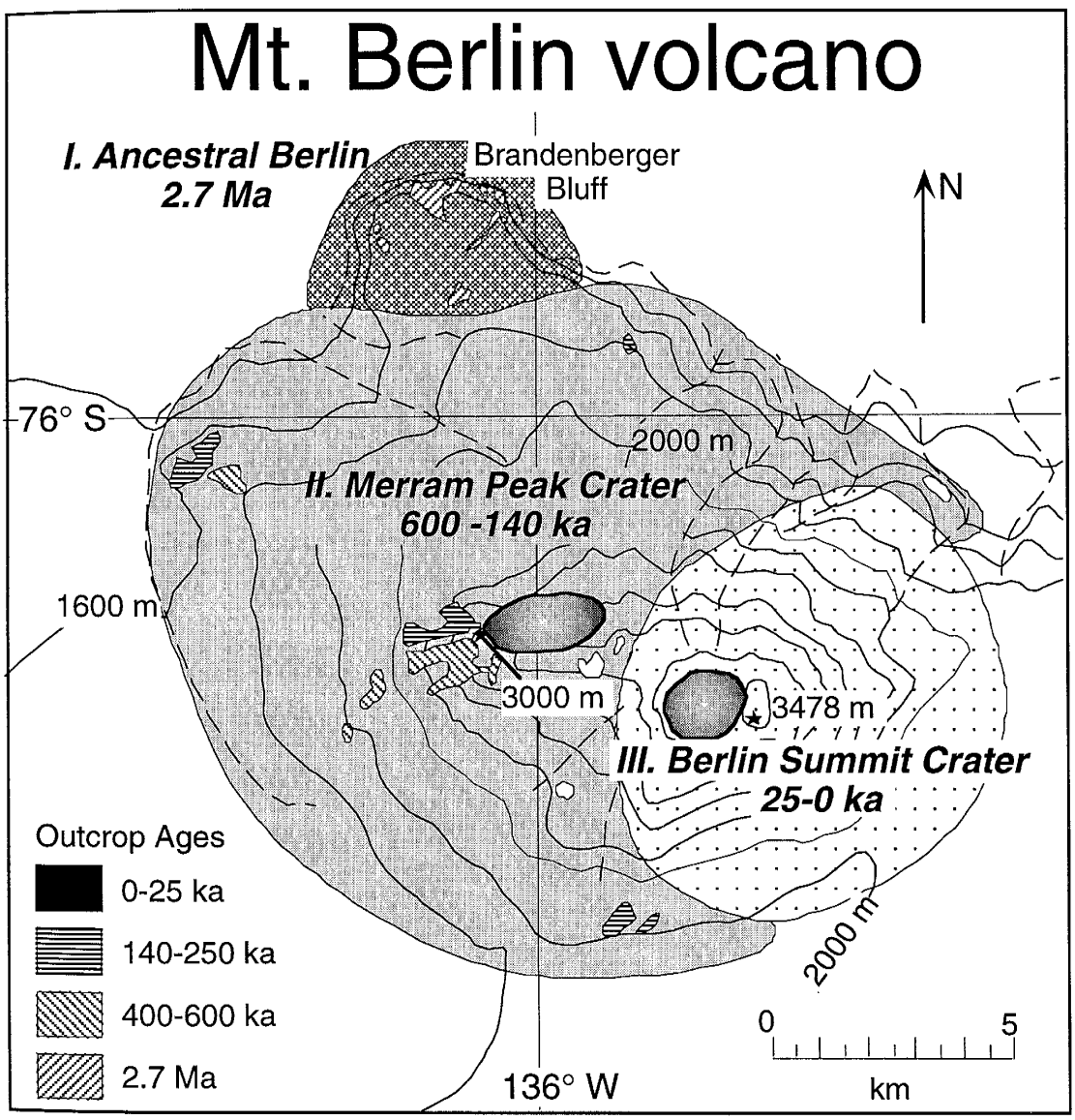

Figure 7. Map showing the distribution and ages of outcrops on Mt. Berlin. Three stages of activity are interpreted from these data, with a southeastward shift in the vent location. Base map is from the Mount Berlin quadrangle, scale 1:250,000. (U.S.G.S., 1973). USGS Reconnaissance Series, Antarctica, U.S. Geological Survey.

ice at the margin of the summit ice cap of Mt. Moulton, located 30 km east of the Mt. Berlin summit. The chronology, geochemistry, and explosivity of Late Quaternary activity at Mt. Berlin are summarized in Figure 8 and discussed below.

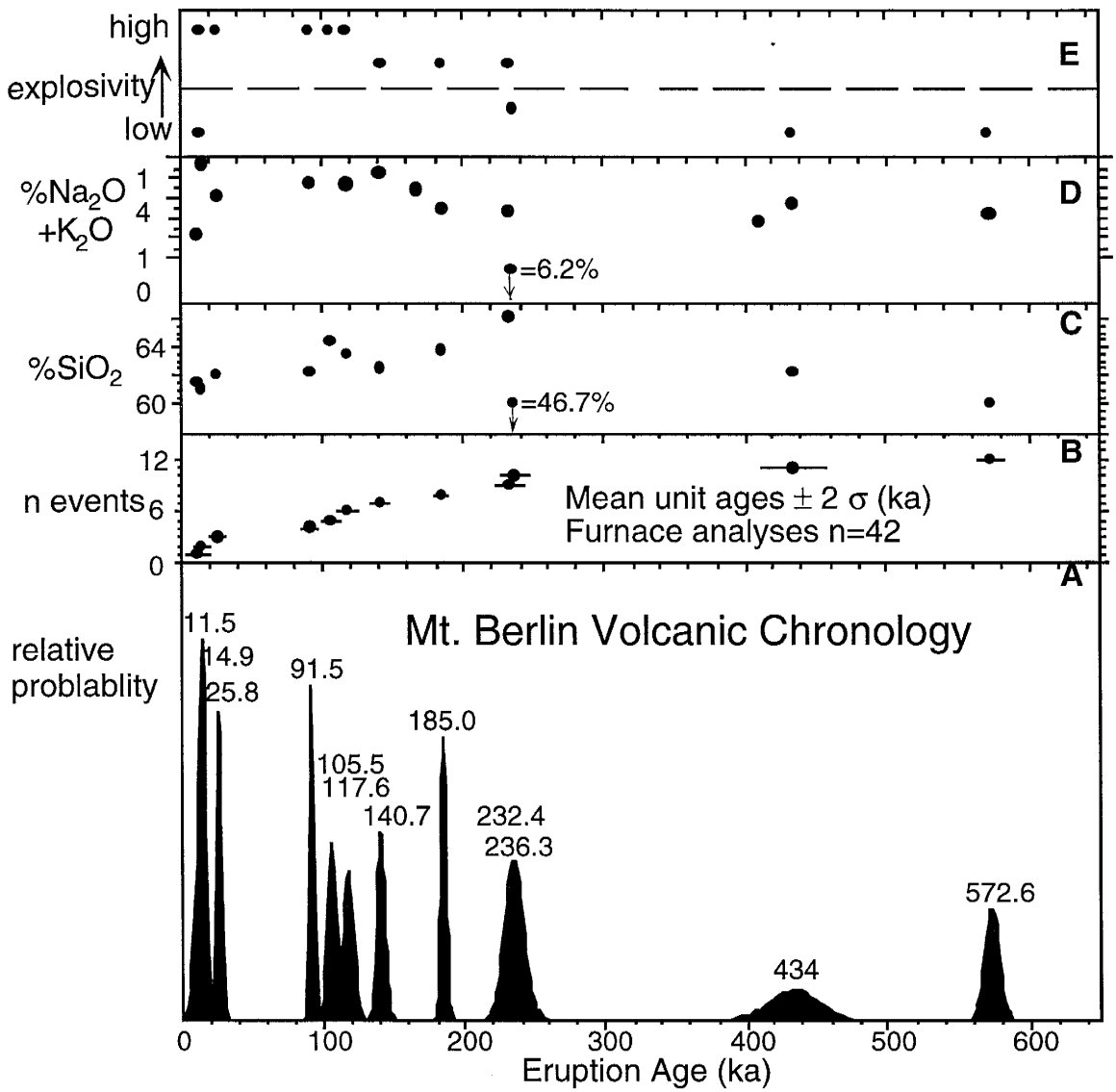

Figure 8. Summary of volcanic activity at Mt. Berlin since 650 ka. A probability distribution plot (a) shows twelve distinct events, based on $^{40}Ar/^{39}Ar$ mean ages (b). Most of the eruptive products were alkalic trachytes (c,d) with SiO_2 contents between 60 and 65% and alkali contents between 11-15%. Major oxides are based on X-ray fluorescence analyses of whole-rock powders. The relative explosivity, shown in (e), is based on the nature of volcanic deposits. Trachytic lavas and mafic cinder cone deposits are classified as effusive (below dashed line), although both deposits may have had explosive phases. Trachytic pyroclastic fall and flow deposits are classified as explosive, with the Mt. Moulton tephra layers associated with the most explosive eruptions.

Stage I. Ancestral volcano. The oldest evidence for volcanic activity at Mt. Berlin is 2.72±0.08 Ma (n= 5) phonolitic/trachytic lava and pyroclastic rocks and 2.70±0.05 Ma (n= 1) phonotephritic cinder cone deposits at and near Brandenberger Bluff on the north side of Mt. Berlin (Supplemental Data; Appendices 1,2, and 6). Trachytic clasts from the Brandenberger Bluff section were previously dated by conventional K-Ar method to 2.2-2.7 Ma (LeMasurier and Rex, 1983), within 2σ uncertainty of the mean $^{40}Ar/^{39}Ar$ age. Brandenberger Bluff is a 300 m thick section composed of steeply dipping (20-30°) fine-grained trachytic/phonolitic lapilli tuff and tuff that overlies a phonolitic lava. Lapilli tuff at the top of the bluff exhibits shallow-dipping planar beds and cross-beds and contains abundant armored lapilli, features indicative of phreatomagmatic base surge eruptions. This section is interpreted as an emergent phreatomagmatic tuff cone, with subaqueously deposited flank deposits and subaerially deposited bluff-top deposits. The highest elevation outcrop (at ~2000 m a.s.l.) associated with the ancestral stage consists of 2.70±0.02 Ma phonotephritic cinder cone deposits. Previous workers interpreted this section as subglacially erupted hyaloclastite, a remnant of a table mountain (LeMasurier and Rex, 1983).

Stage II. Merram Peak crater. The second and apparently most voluminous phase of activity at Mt. Berlin is characterized by growth of the volcano to Merram Peak at 3000 m above sea level and by eruptions from the 2.5 x 1 km diameter Merram Peak crater. The oldest available evidence for activity are dense foliated and clastogenic trachyte lavas located in the vicinity of Merram Peak and dated to 572.6±4.8 ka. Samples from these outcrops were previously dated by the conventional K-Ar method to 620±100 and 630±60 ka (2σ uncertainty; LeMasurier and Rex, 1983). Three subsequent episodes of activity at Merram Peak crater are recorded by proximal deposits west of the crater, including a trachytic lava dated to 434±18 ka, an 18+ m thick, densely to incipiently welded, trachytic pumiceous pyroclastic breccia (Fig. 2c) dated to 185.0±1.8 ka, and a 1 m thick, phonolitic,

non- welded pumice lapilli layer dated to 140.7±2.8 ka. Both of the 185.0 ka and 140.7 ka fall deposits mantle topography.

Flank eruptions also occurred during this interval of volcanism at Merram Peak crater. Groundmass samples from parasitic basanite to hawaiite cinder cone remnants on the northwest flank of Mt. Berlin yield a mean age 236±19 ka. A pyroclastic vent breccia and a near-vent trachyte lava (237.4±3.6 ka) located on the northeast flank and a welded trachytic ignimbrite (230.7±2.1 ka) on the southeast flank are geochemically identical, with a mean age of 232.4±6.1 ka (Fig. 3, Table 1). The ignimbrite contains ~30% fiamme, with typical aspect ratios of 1:10 (h/l). A benmoreite lava (Supplemental Data, Appendix 6) overlies the ignimbrite and signifies a <232 ka effusive eruption. Plagioclase from the benmoreite yielded uninterpretable laser fusion age data.

Stage III. Summit crater. The final and still active phase of Mt. Berlin volcanism was marked by growth of the volcano by more than 400 m to 3478 m above sea level and a southeastward shift of the vent area to the 2 km diameter summit crater (Fig. 2a) . The constructional slopes of the volcano above Merram Peak crater are typically 20-25°. Two prominent welded, trachytic, pyroclastic fall units, totaling more than 150 m in thickness, are exposed in the eastern wall of the summit crater (Fig. 2a). These pyroclastic fall deposits are composed of slightly flattened pumiceous bombs and abundant cognate xenoliths (Fig 2b). We attribute the welding to agglutination with minor load pressure compaction. Recumbent folds seen in one unit suggests that part of the pyroclastic deposit flowed rheomorphically. The ages of the two lower welded units are analytically indistinguishable at 25.8±1.7 ka. These are locally overlain by a >10 m thick sequence of welded and non-welded pyroclastic fall beds. The fall deposits include a 6 m thick lithic- and ash-rich explosion breccia with bomb and lithic clasts to 50 cm diameter and a 2 m thick densely welded obsidian fall. Anorthoclase phenocrysts from the obsidian yielded an age of 15.9±6.2 ka. These crater wall deposits at Mt. Berlin were previously interpreted as lava on the basis of reconnaissance investigations (LeMasurier and Kawachi, 1990).

Five fumarolic ice towers and steaming vents along the summit crater rim attest to ongoing geothermal activity. One ice tower opens into an underlying ice cave system more than 70 m long, with a lava at the cave floor dated to 11.5±3.5 ka (Fig. 6a.). Surface temperatures of the cave floor lava are as high as +12°C.

Distal Mt. Berlin tephra. Glacial ice at the summit of Mt. Moulton volcano, thirty kilometers east of Mt. Berlin (Fig. 1), contains at least 19 non-welded pumice lapilli and ash layers. Five of the layers with the coarsest pumice were sampled in 1993-1994 (Figs. 2 and 9). The 2-15 cm thick coarse tephra layers locally dip steeply 40-45°N, suggesting an upstream ice source at the summit of Mt. Moulton and a downstream impediment to ice flow at the 5.9 Ma Prahl Crag nunatak. The $^{40}Ar/^{39}Ar$ mean ages of the five layers are consistent with stratigraphic order: 14.8±1.9 ka, 22.6±3.0, 91.5±1.6, 105.5±3.0, and 117.6±3.6 (Figs. 6c, 6d, 9, Table 1). The youngest tephra has a trace

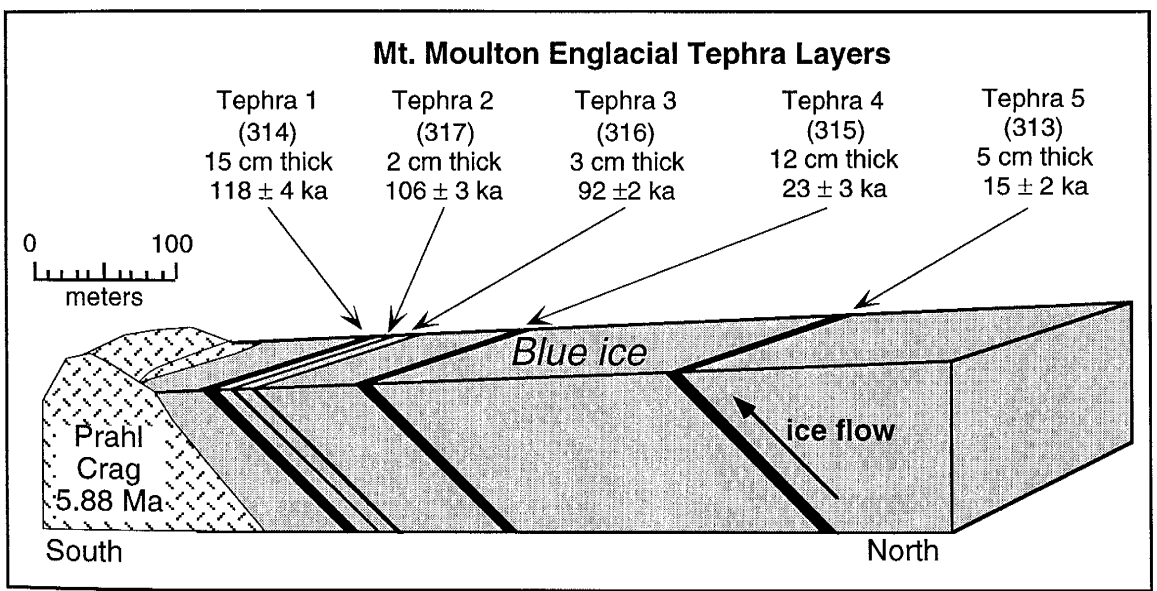

Figure 9. Schematic cartoon showing englacial tephra layers in the summit ice cap of Mt. Moulton, located 30 km east of source at Mt. Berlin. We infer that the tephra layers are exposed at the surface because ice flow from the summit ice cap is deflected upward as it approaches a Late Miocene outcrop obstruction at Prahl Crag.

element composition that is indistinguishable from that of the youngest Mt. Berlin crater wall obsidian, but that is very different from the youngest Mt. Takahe sample (Fig. 10). We infer on the basis of similar trace element trends that all five of the Moulton tephra

layers were derived from Mt. Berlin. The two uppermost tephra layers appear to be co-eruptive with the 15.9±6.2 ka and 25.8±1.7 ka units exposed in the wall of the Mt. Berlin crater (Table 1). Mean ages of the youngest two summit crater and correlative Mt. Moulton units are 14.9±1.9 ka and 25.0±3.1 ka.

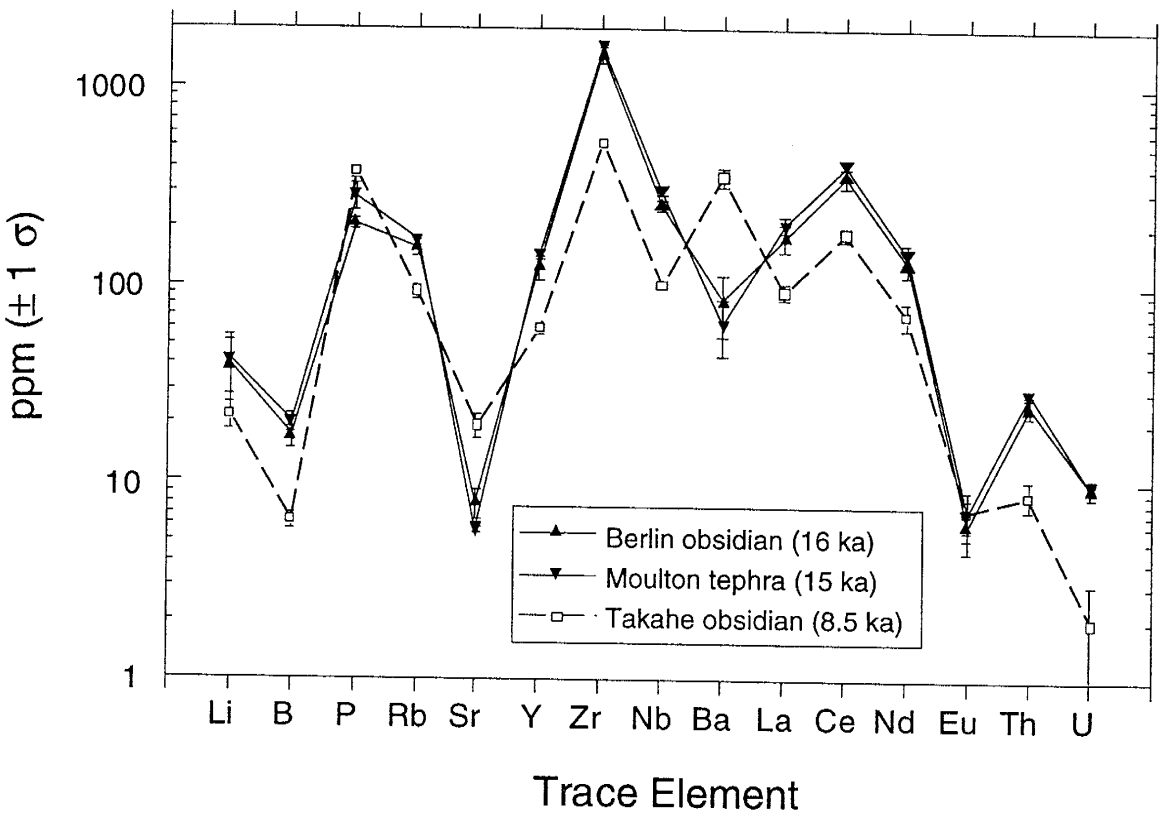

Figure 10. Mean ion microprobe trace element data (± 1 s) of Mt. Berlin sample, WCM93-025; Mt. Moulton englacial tephra, WCM93-313; and Mt. Takahe, W85-09.

The three oldest tephra layers record eruptions that are not represented in Mt. Berlin crater wall outcrops. The distribution and ages of deposits at Mt. Berlin suggest that the volcano grew by more than 400 m during the 141 to 25 ka interval. We speculate the 92-118 ka tephra may be present at Mt. Berlin, buried beneath ice and younger rocks. More detailed fieldwork during the 1996-1997 season delineated a total of 19 tephra layers at Mt. Moulton, including three layers stratigraphically below and presumably older than the 118

ka tephra (Nelia Dunbar, unpublished data). This extensive englacial record of inferred Mt. Berlin eruptions illustrates the fragmentary nature of the record at Mt. Berlin volcano.

Mt. Siple crater rim

Mt. Siple is a 3110 m high, undissected island volcano located along the relatively inaccessible Hobbs Coast (Fig. 1). Because of ice cover, outcrops at the 4-5 km diameter summit caldera and upper slopes of Mt. Siple are extremely limited. The lack of dissection of the coastal volcano combined with the <0.1 Ma age of a satellitic basalt cone near sea level has led to speculation of recent activity of Mt. Siple volcano (LeMasurier and Rex, 1990). Satellite images suggesting active eruption plumes during 1988 were later discounted (Smithsonian Institution, 1988). Previous investigations at Mt. Siple have been limited to coastal satellite centers (LeMasurier and Rex, 1990). In the first visit to the Mt. Siple summit, we sampled the 20+ m thick, moderately to densely welded, pyroclastic fall deposit forming the highest point of the caldera rim. Anorthoclase from the trachytic fall deposit yielded a mean age 223.6±3.5 ka, and a lava sample from a subsidiary vent below the summit crater yielded an age of 167.2±2.1 ka. It is probable that a more complete record of Mt. Siple volcanism is preserved in the shallow marine environment adjacent to the volcano.

Mt. Takahe crater rim

Mt. Takahe is an undissected shield volcano (constructional side slopes 8-12°) with an 8 km diameter ice-filled summit caldera located in eastern MBL, approximately 250 km northeast of the planned WAISCORES drill site on the WAIS ice divide (Fig. 1). Limited exposures at and near the Mt. Takahe caldera rim include a 60 m section of welded and non-welded pyroclastic lapilli deposits, obsidian-bearing bomb-and-block layers, hydrovolcanic tuffs, and lavas (McIntosh et al., 1985). Anorthoclase from a sample of a non-welded obsidian-and-pumice bomb-and-block layer near the top of this sequence has an $^{40}Ar/^{39}Ar$ age of 8.5±3.4 ka (Fig. 6b). This young unit, currently being rapidly eroded, overlies a sequence of lavas and densely welded pyroclastic deposits with ages ranging

from 92.7±7.3 to 191.2±5.3 ka. These older units indicate that Mt. Takahe volcano reached its present elevation by 191 ka, contrary to a previous interpretation (Palais et al., 1988) which suggested that entire volcano construction occurred since <40 ka, the age of the oldest Byrd ice-core tephra layers.

DISCUSSION

Explosivity of MBL eruptions

The dispersive power of volcanic eruptions is largely controlled by height of the eruption column, which can be estimated from lateral changes in deposit thickness and grain size (Carey and Sparks, 1986). Near-vent deposits provide only qualitative measures of eruption explosivity. A wide range of eruption styles, from mildly explosive Strombolian to highly explosive Plinian, could produce the ubiquitous welded and non-welded proximal fall deposits seen at MBL volcanoes. Lavas are associated with non-explosive eruptive episodes, although they do not preclude the possibility of an associated explosive phase.

Although near-vent deposits provide only a qualitative measure of explosivity, the thickness and coarse grain size of englacial tephra layers on Mt. Moulton at a distance of 30 km from their source demonstrate the highly explosive nature of several Mt. Berlin eruptions. Pumice densities and dimensions were measured in four of the tephra layers (Table 3). Mean diameters of the five largest clasts are 17-18 mm in the 25, 92, and 118 ka tephra layers; maximum anorthoclase crystal lengths in these coarser tephra layers are 10 mm. Such limited data do not allow precise reconstructions of eruption conditions but can be used for first-order estimates of eruption column height. Assuming a case of no-wind conditions, the tephra dispersal model of Carey and Sparks (1986) predicts a ~40 km high eruption column for the given density, size and distance from source of coarsest pumice at Mt. Moulton. Assuming a maximum wind speed of 20 m/s (72 km/hr), the same model predicts a ~28 km high eruption column for the given clast parameters. In either case, fine

TABLE 3. MT. MOULTON ENGLACIAL TEPHRA- PUMICE CLAST DATA

WCM 93-	Age (ka)	Diameter (mm) max.	mean*	n	Density (kg/m^3) mean ± 1 σ	% Vesicularity** range	mean	range
313	15	13	9	20	620±150	440-890	76%	66-83%
315	23	25	18	30	780±180	520-114	70%	56-80%
316	92	28	17	30	770±190	480-126	70%	52-82%
314	118	27	18	30	540±100	400-910	79%	65-85%

Notes: Density measurements made following technique by Gay and Smith (1996), a modification of method by Houghton and Wilson (1990).
* average of long, intermediate and short axes of five largest clasts
**based on estimate of DRE density of 2610 kg/m^3

ash from such explosive eruptions would have penetrated the stratosphere and been deposited over large portions of the WAIS and the Southern Pacific Ocean. The close geochemical and geochronological matches between some of the Byrd Station ice core tephra and Mt. Berlin tephra (Table 2, details discussed below) are consistent with these model predictions. A further application of the 28 km high model result predicts that the maximum particle size at a distance of 600 km from vent (distance from Mt. Berlin to Byrd Station) would have been 5 μm. Byrd ice core tephra reached sizes up to 60 μm in diameter, which suggests that the Mt. Berlin eruption intensity or wind speed is underestimated. The dispersive power of Mt. Berlin eruptions can be further evaluated by geochemical and geochronological analyses of englacial tephra layers at Mt. Waesche, which may be correlated to englacial tephra at Mt. Moulton. In the 1996-1997 field season, several coarse ashes at Mt. Waesche (with anorthoclase to 2 mm) were collected and found to be petrographically similar to Mt. Berlin/Mt. Moulton tephra.

Glacial Tephrochronology- Dating ice and marine cores

Ash layers in ice or marine cores can serve as precisely dated time-stratigraphic markers, if they can be geochemically correlated with well-dated source volcanic units.

Tephrochronology correlation studies typically rely on chemical "fingerprinting" of individual tephra units. Grain-discrete analyses of glass fragments, requiring microanalysis techniques, provide the most reliable data. Our preliminary results based on multiple techniques indicate the potential for future correlation of ice core tephra to well-dated source volcano eruptions.

Mt. Berlin was previously rejected as a possible source for Byrd Station ice core tephra because of "significant" geochemical differences between Berlin deposits and Byrd tephra (Palais et al., 1988, p. 313). Instead, all of the Byrd core tephra was correlated to Mt. Takahe, which is situated much closer (350 km) to the calculated Byrd core tephra deposition site than Mt. Berlin (550 km). Palais et al. (1988) recognized that the prevailing winds in central MBL through the troposphere and lower stratosphere, currently out of the west and northwest, favor transport from Mt. Berlin rather than Mt. Takahe. A re-examination of published geochemical data of Palais et al. (1988) suggests that Mt. Berlin is a reasonable source for Byrd core tephra. The major element oxide data of Palais et al. (1988, Table 5) show that, with the exception 0.00% MgO of Mt. Berlin samples, the Mt. Berlin data fall within the range of the Mt. Takahe data. Only the youngest 7.5 ka Byrd ice core tephra layer contained significant weight percent MgO (0.38%), similar to Takahe trachyte samples (0.25-0.65%). All other Byrd ice core tephra layers contain low weight percent MgO (0.02-0.14%).

A comparison of new microprobe data from dated Mt. Berlin and Mt. Takahe samples and Byrd ice-core tephra layers supports the new correlation of 20-30 ka Byrd core samples to Mt. Berlin (Fig. 11). Figure 11 shows that the 20-30 ka Byrd core tephra samples are geochemically similar to the 12-25 ka Mt. Berlin volcano samples, whereas the youngest dated Byrd core sample is geochemically similar to the youngest Mt. Takahe sample. The geochemical affinities between the ice core tephras and source volcanoes are consistent with the new $^{40}Ar/^{39}Ar$ ages (Fig. 12). Although the age of the

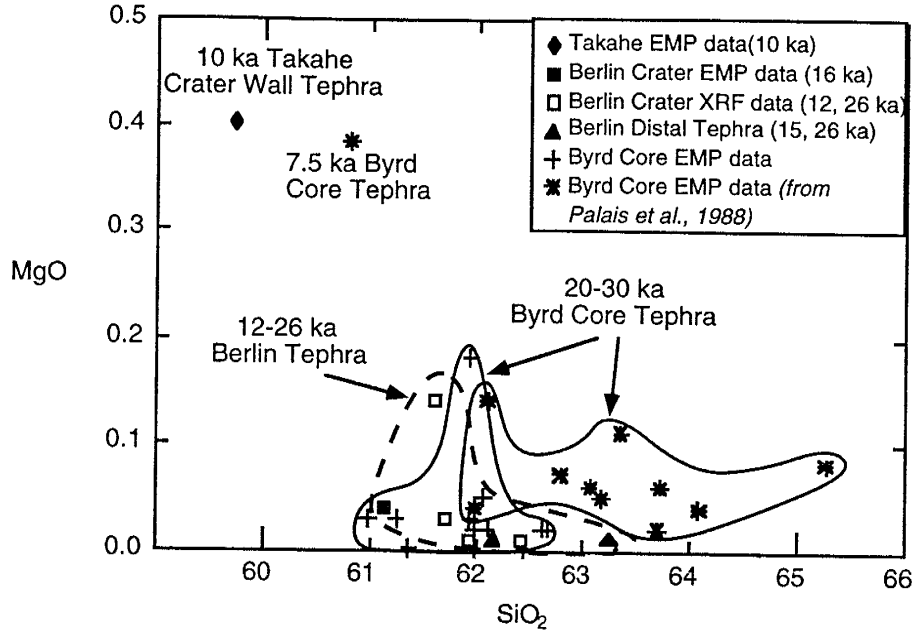

Figure 11. Representative plot of geochemical data from young MBL tephra samples. All data, except XRF data, are based on electron microprobe analyses of glass shards. XRF data are based on x-ray fluorescence analyses of whole-rock samples at the University of Kiele, U.K.

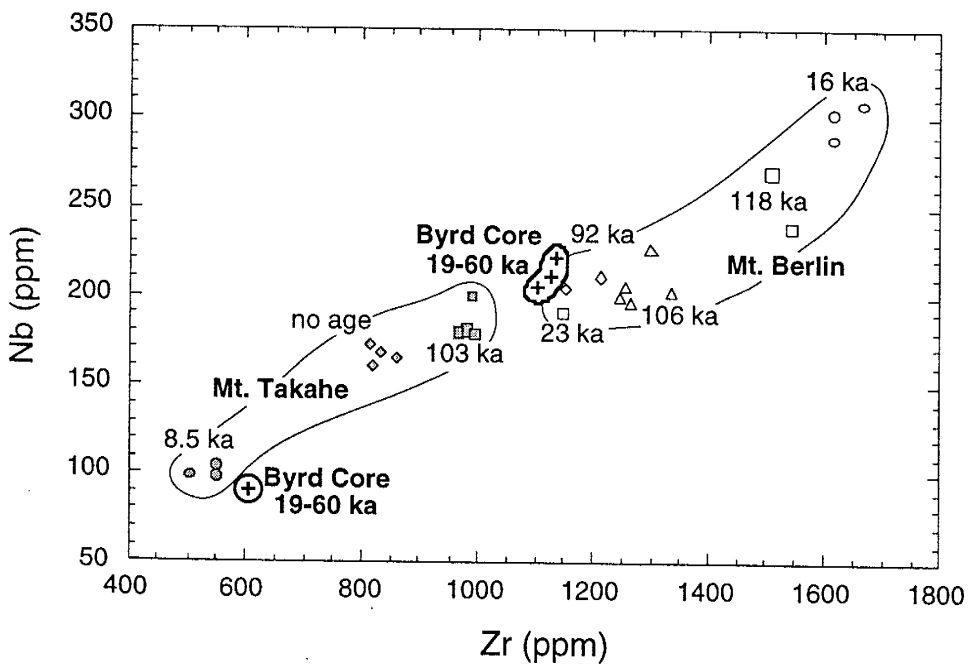

Figure 12. Plot showing niobium (Nb) versus zirconium (Zr), based on individual ion microprobe analyses of volcanic trachytic/phonolitic glass fragments from Mt. Takahe, Mt. Berlin (Mt. Moulton tephra layers), and Byrd core. The 23 ka point is from XRF data. Byrd core data are from individual analyses of a composite sample of five Byrd core tephra layers with model ages between 19 and 60 ka.

base of the Byrd ice core is controversial, the lack of tephra correlative with the older eruptive units at Mt. Berlin is consistent with a basal ice-core age less than 91 ka.

The new correlation of Byrd core tephra to the more distant Mt. Berlin indicates the potential of Mt. Berlin tephrochronology for dating deeper and older ice cores. Preliminary ion microprobe data indicate a unique trace element signature of each of the Mt. Moulton tephra layers and Mt. Takahe crater rim deposits (Table 2, Fig. 13). The Moulton and Takahe trace element data resemble trace element signatures from glass shards in the composite Byrd ice core tephra sample (Fig. 13). If these $^{40}Ar/^{39}Ar$-dated MBL ashes are identified by geochemical fingerprinting in future ice and marine cores, then they will provide the cores with independently dated time horizons.

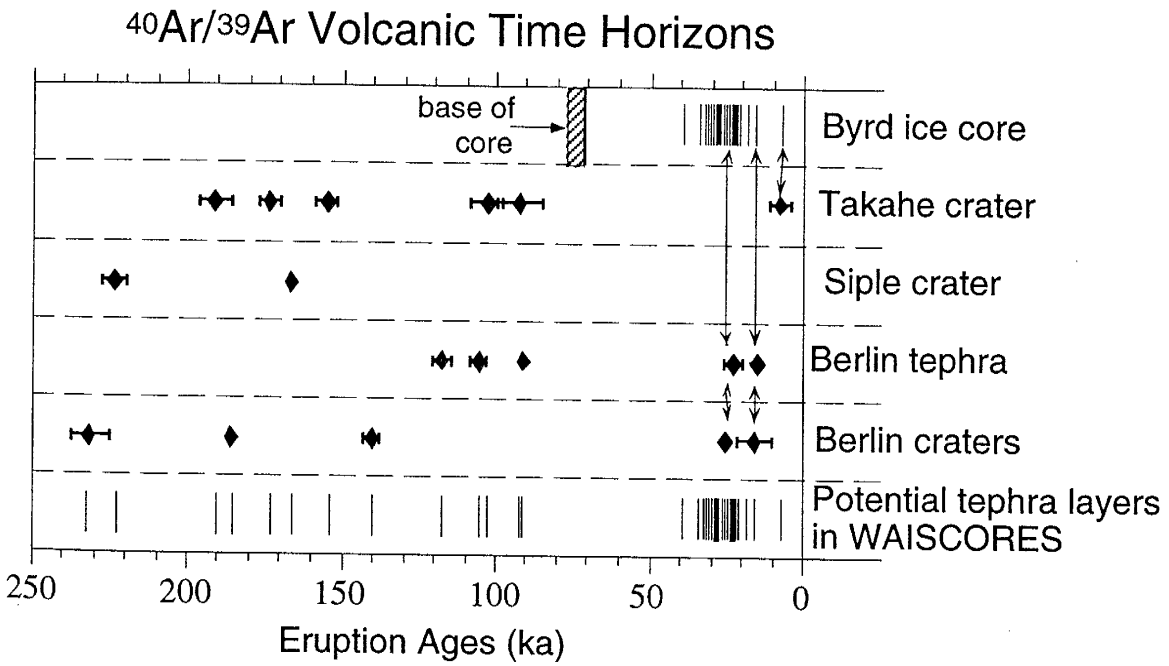

Figure 13. Timeline summarizing tephrochronology in Marie Byrd Land. The black diamonds represent the $^{40}Ar/^{39}Ar$ eruption ages (± 2 s.d.) from Mt. Takahe, Mt. Siple and Mt. Berlin. Most of the eruption ages are mean ages of different and/or replicate samples from each site (see Table 1). The vertical lines at top indicate model ages of coarse tephra layers in the Byrd ice core (Palais et al., 1988). The age of basal ice in the Byrd ice core is estimated at 73 ka based on the Electrical Conductivity Method (Hammer et al., 1994). Double-pointed beaded arrows show correlations among Marie Byrd Land tephra and Byrd ice core tephra layers. Potential Marie Byrd Land tephra time horizons in planned WAISCORES are shown at bottom.

The small number of eruptions identified at the source volcanoes contrasts sharply with the large number of tephra layers in the Byrd ice core. This discrepancy results in part from the poor exposure and burial by subsequent eruptions of source volcano rocks. In addition, the abundant chemically recognized fine ash layers in the Byrd ice core would be overlooked at volcano outcrops and bare-ice area by relatively crude, visual-based sampling techniques.

The oldest ice in West Antarctica?

The Mt. Moulton summit ice cap contains the oldest known ice in West Antarctica. The englacial record of Mt. Berlin eruptions at Mt. Moulton indicates that the interbedded glacial ice is nearly as old as the 125 ka interglacial temperature maximum and has survived more than 100,000 years of climatic fluctuations. An ~390 m stratigraphic thickness of dipping ice and tephra layers is exposed along the horizontal section from the youngest tephra layer (15 ka) to Prahl Crag, including ~30 m stratigraphic thickness of ice between the oldest tephra layer (118 ka) and Prahl Crag (Fig. 9). This well-dated section of glacial ice contains a potential "horizontal ice core" record of paleoclimate that dates back to more than 118 ka. Survival of such ancient West Antarctic ice does not preclude WAIS collapse during or since the ~125 ka interglacial, because temperatures at the high elevation tephra depositional site (3000 m. a.s.l.) would remain below freezing even with dramatic low-elevation temperature increases. In theory, oxygen isotope data from this ~125 ka old ice could test the deglaciation hypothesis (where deglaciation is reflected in relatively higher $\delta^{18}O$ values associated with decreased continentality and warmer local temperatures). The deglaciation hypothesis could be further tested by examining englacial tephra records from Mt. Waesche or other bare-ice areas on the WAIS for evidence of 118 ka Mt. Berlin tephra.

SUMMARY

The $^{40}Ar/^{39}Ar$ chronology of tephra layers and source volcanoes in MBL offers a regional record of Late Quaternary volcanic activity with the following important features:

1) The 8.5-573 ka chronology of twenty, mostly explosive, trachytic eruptions traces the Late Quaternary evolution of Mt. Berlin, Mt. Siple, and Mt. Takahe, three large alkaline composite volcanoes. This record provides a previously unrecognized potential independent chronology for future WAISCORES and marine core records.

2) A detailed history of Mt. Berlin records a three-stage growth and southeastward vent migration. Many Mt. Berlin eruptions have been explosive, capable of depositing ash widely over the WAIS.

3) The youngest trachytic tephra layer in the Byrd ice-core, which was dated by ice-flow models to 7.5 ka, is correlated by age and geochemistry 8.5±3.4 ka tephra layer at Mt. Takahe. Older (13-40 ka) Byrd core tephra layers are not recognized in crater rim exposures at Mt. Takahe.

4) The 19-30 ka tephra layers in the Byrd ice core are similar in age and geochemistry to the 12-26 ka eruptive units at Mt. Berlin. One-to-one correlations between Byrd core tephra and Mt. Berlin deposits are not possible due to the lack of available Byrd core material for geochemical fingerprinting. These Byrd ice core tephra units were previously correlated to Mt. Takahe.

5) The Mt. Moulton summit ice cap contains the oldest known ice in West Antarctica with a minimum age of 118 ka. On a horizontal patch of bare ice at Mt. Moulton, coarse-grained, englacial tephra layers derived from Plinian eruptions of Mt. Berlin delineate five 118 to 15 ka time horizons within an ~390 m stratigraphic thickness of dipping ice and tephra layers. This tephra/ice stratigraphic sequence offers the potential of an easily accessible, stratigraphically coherent, horizontal ice core with a local climate record that can be correlated by stratigraphy and tephrochronology to deep ice and marine core records.

ACKNOWLEDGMENTS

This work was supported by the National Science Foundation (NSF-DPP918806), with additional funding from the New Mexico Geochronological Research Laboratory. We thank U.S. Navy VXE-6 squadron, Antarctic Support Associates, and Ken Borek Air Ltd. for logistical support; mountaineer Tony Teeling for field assistance; Philip Kyle for XRF analyses at the New Mexico Institute of Mining and Technology; John Smellie, British Antarctic Survey for providing XRF data from the University of Keele; Rick Hervig for assistance with microprobe analyses at Arizona State University; Rich Esser, Matt Heizler, and Lisa Peters for assistance with $^{40}Ar/^{39}Ar$ geochronology; and Rich Esser, Matt Heizler, Philip Kyle, and Kurt Panter for comments during preparation of the manuscript;.

REFERENCES

Bindschadler, R.A., 1995, WAIS: The West Antarctic Ice Sheet Initiative: a multi-discplinary study of rapid climate change and future sea level, science and implementation plan, National Science Foundation, p. 75.

Blankenship, D.D., Bell, R.E., Hodge, S.M., Brozena, J.M., Behrendt, J.C., and Finn, C.A., 1993, Active volcanism beneath the West Antarctic ice sheet and implications for ice-sheet stability: Nature, v. 361, p. 526-529.

Carey, S., and Sparks, R.S.J., 1986, Quantitative models for the fall-out and dispersal of tephra from volcanic eruption columns: Bulletin of Volcanology, v. 48, p. 109-125.

Dansgaard, W., Johnsen, S.J., Clausen, H.B., Dahl-Jensen, D., Gundestrup, N.S., Hammer, C.U., Hvidberg, C.S., and Steffensen, J.P., 1993, Evidence for general instability of past climate from a 250-kyr ice-core record: Nature, v. 364, p. 218-220.

Deino, A., and Potts, R., 1990, Single-crystal $^{40}Ar/^{39}Ar$ dating of the Olorgesailie Formation, Southern Kenya Rift: Journal of Geophysical Research, v. 95, p. 8453-8470.

Devine, J.D., Sigurdsson, H., and Davis, A.N., 1984. Estimates of sulfur and chlorine yield to the atmosphere from volcanic eruptions and potential climatic effects. Journal of Geophysical Research, v. 89, p. 6309-6325.

Drewry, D.J., Jordan, S.R., and Jankowski, E., 1982, Measured properties of the Antarctic Ice Sheet: surface configuration, ice thickness, volume, and bedrock characteristics: Annals of Glaciology, v. 3, p. 83-91.

Drewry, J., 1983, Antarctica: Glaciological and Geophysical Folio: Cambridge, Scott Polar Research Institute, University of Cambridge.

Fleck, R.J., Sutter, J.F., and Elliot, D.H., 1977, Interpretation of discordant $^{40}Ar/^{39}Ar$ age spectra of Mesozoic tholeiites from Antarctica: Geochimica Cosmochimica Acta, v. 41, p. 15-32.

Gay, K.R., and Smith, G.A., 1996, Simultaneous phreatomagmatic and magmatic rhyolitic eruptions recorded in the Late Miocene Peralta Tuff, Jemez Mountains, New Mexico, *in* Goff, F., Kues, B.S., Roger, M.A., McFadden, L.D., and Gardener, J.N., eds., New Mexico Geological Society Guidebook, 47th Field Conference, The Jemez Mountains Region, New Mexico Geological Society, Inc., p. 243-250.

Hammer, C.U., Clausen, H.B., and Langway, C.C.J., 1994, Electrical conductivity method (ECM) stratigraphic dating of the Byrd Station ice core, Antarctica: Annals of Glaciology, v. 20, p. 115-120.

Hollocher, K. and Ruiz, J., 1995. Major and trace element determinations on NIST glass standard reference materials 611, 612, 614, and 1834 by inductively coupled plasma- mass spectrometry. Geostatistics Newsletter, v. 19, p. 27-34.

Houghton, B.F., and Wilson, C.J.N., 1989, A vesicularity index for pyroclastic deposits: Bulletin of Volcanology, v. 51, p. 451-462.

Hu, Q., Smith, P.E., Evensen, N.M., and York, D., 1994, Lasing in the Holocene: extending the 40Ar-39Ar laser probe method into the 14C age range: Earth and Planetary Science Letters, v. 123, p. 331-336.

Hughes, T., 1973, Is the West Antarctic Ice Sheet disintegrating?: Journal of Geophysical Research, v. 78, p. 7884-7910.

Hughes, T., 1977, West Antarctic ice streams: Reviews of Geophysics and Space Physics, v. 15, p. 1-46.

Kyle, P.R., Jezek, P.A., Mosley-Thompson, E., and Thompson, L.G., 1981, Tephra layers in the Byrd Station ice core and the Dome C ice core, Antarctica and their climatic importance: Journal of Volcanology and Geothermal Research, v. 11, p. 29-39.

LeBas, M.J., LeMaitre, R.W., Streckeisen, A., and Zanettin, B., 1986, A chemical classification volcanic rocks based on the total alkali-silica diagram: Journal of Petrology, v. 27, p. 745-750.

LeMasurier, W.E., 1990, Marie Byrd Land, *in* LeMasurier, W.E., and Thomson, J.W., eds., Volcanoes of the Antarctic Plate and Southern Oceans, Volume 48: Washington, D.C., AGU, p. 146-163.

LeMasurier, W.E., and Kawachi, Y., 1990, Mount Berlin, *in* LeMasurier, W.E., and Thomson, J.W., eds., Volcanoes of the Antarctic Plate and Southern Oceans, Volume 48: Washington, D.C., AGU, p. 229-233.

LeMasurier, W.E., and Rex, D.C., 1983, Rates of uplift and the scale of ice level instabilities recorded by volcanic rocks in Marie Byrd Land, West Antarctica, *in* Oliver, R.L., James, P.R., and Jago, J.B., eds., Antarctic Earth Sciences: Canberra, Australian Academy of Science, p. 660-673.

LeMasurier, W.E., and Rex, D.C., 1989, Evolution of linear volcanic ranges in Marie Byrd Land, West Antarctica: Journal of Geophysical Research, v. 94, p. 7223-7236.

LeMasurier, W.E., and Rex, D.C., 1990, Mount Siple, *in* LeMasurier, W.E., and Thomson, J.W., eds., Volcanoes of the Antarctic Plate and Southern Oceans, Volume 48: Washington, D.C., AGU, p. 185-188.

LeMasurier, W.E., and Rex, D.R., 1991, The Marie Byrd Land Volcanic Province and its relation to the Cainozoic West Antarctic rift system, *in* Tingey, R.J., ed., The geology of Antarctica: Oxford, Clarendon Press, p. 249-284.

LeMasurier, W.E., and Wade, F.A., 1968, Fumarolic activity in Marie Byrd Land: Science, v. 162, p. 352.

Lo Bello, P., Feraud, G., Hall, C.M., York, D., Lavina, P., and Bernat, M., 1987, $^{40}Ar/^{39}Ar$ step heating and laser fusion dating of a Quaternary volcanic from the Neschers, Massif Central, France: The defeat of xenocrystic contamination: Chemical Geology, v. 66, p. 61-71.

MacAyeal, D., 1992, Irregular oscillations of the West Antarctic ice sheet: Nature, v. 27, p. 321-325.

Mahood, G.A., 1984, Pyroclastic rocks and calderas associated with strongly peralkaline magmatism: Journal of Geophysical Research, v. 89, p. 8540-8552.

McIntosh, W.C., LeMasurier, W.E., Ellerman, P.J., and Dunbar, N.W., 1985, A reinterpretation of glaciovolcanic interaction at Mount Takake and Mount Murphy, Marie Byrd Land, Antarctica: Antarctic Journal of the United States, v. 19, p. 57-59.

Mercer, J.H., 1978, West Antarctic ice sheet and CO_2 greenhouse effect: a threat of disaster: Nature, v. 271, p. 321-325.

Nereson, N.A., Waddington, E.D., Raymond, C.F., and Jacobson, H.P., in press, Predicted age-depth scales for Siple Dome and Inland WAIS ice cores in West Antarctica: Geophysical Research Letters.

Palais, J.M., Kyle, P.R., McIntosh, W.C., and Seward, D., 1988, Magmatic and phreatomagmatic volcanic activity at Mount Takahe, West Antarctica based on tephra layers in the Byrd ice core and field observations at Mt. Takahe: Journal of Volcanology and Geothermal Research, v. 35, p. 295-317.

Samson, S.D., and Alexander, C.E., 1987, Calibration of the interlaboratory $^{40}Ar/^{39}Ar$ dating standard, Mmhb-1: Isotope Geoscience, v. 66, p. 27-34.

Scherer, R.P., 1991, Quaternary and Tertiary microfossils from beneath Ice Stream B: Evidence for a dynamic West Antarctic Ice Sheet history: Palaeogeography, Palaeoclimatology, Palaeoecology, v. 90, p. 395-412.

Shane, P.A.R., and Froggatt, P.C., 1992, Composition of widespread volcanic glass in deep-sea sediments of the Southern Pacific Ocean: an Antarctic source inferred: Bulletin of Volcanology, v. 54, p. 595-601.

Smellie, J.L., McIntosh, W.C., Gamble, J.A., and Panter, K.S., 1990, Preliminary stratigraphy of volcanoes in the Executive Committee Range, central Marie Byrd Land: Antarctic Science, v. 2, p. 353-354.

Smithsonian Institution, 1988, Mt. Siple, Marie Byrd Land: SEAN Bulletin, v. 13(9), p. 6.

Steiger, R.H., and Jaeger, E., 1977, Subcomission on Geochronology: Convention of the use of decay constants in geo- and cosmochronology: Earth and Planetary Science Letters, v. 36, p. 359-362.

U.S. Geological Survey, 1973, Mount Berlin quadrangle, U.S.G.S. Reconnaissance Series, Antarctica, 1:250,000.

van den Bogaard, P., 1995, $^{40}Ar/^{39}Ar$ ages of sanidine phenocrysts from Laacher See Tephra (12,900 yr BP): Chronostratigraphic and petrological significance: Earth and Planetary Science Letters, v. 133, p. 163-174.

Supplemental Data

Appendix I. Summary of $^{40}Ar/^{39}Ar$ Analytical Methods

Sample Preparation. A total of forty-six samples, (35 anorthoclase samples, 4 mafic groundmass samples, 7 trachyte groundmass sample) were dated by the $^{40}Ar/^{39}Ar$ furnace step-heating (n =58 analyses) and single-crystal laser-fusion (n = 20 analyses) methods. Mt. Berlin and Mt. Siple samples were collected during the 1993-1994 field season and Mt. Takahe samples during the 1985-86 field season. The 2-6 kg lava and pyroclastic rock samples were unweathered. Sample preparation and analysis was conducted at the New Mexico Geochronology Research Laboratory at the New Mexico Institute of Mining and Technology, Socorro, NM. Approximately 1 kg of sample was mechanically crushed and sieved to 200-800 μm grain size. Specific preparation techniques for anorthoclase samples and groundmass samples are described below.

Laboratory preparations of anorthoclase dating samples were designed to produce a homogeneous crystal separate free of possible contaminants and suitable for irradiation. Sized samples were passed through a Franz magnetic separator and the non-magnetic fraction, consisting of feldspars (± glass or quartz), was saved for heavy liquid separation. Diluted lithium metatungstate was used to separate non-magnetic fraction into density fractions. The refractive indices of the density fractions were checked with a polarizing microscope and immersion oils. Anorthoclase concentrates (density ~ 2.58 g/cm^3, refractive index ~1.53) were treated in a 15% HF solution for 5 minutes and rinsed several times in deionized water. Non-altered, inclusion-free anorthoclase samples were hand-picked for irradiation under a binocular microscope. Sample purity is estimated at >99%.

In addition to anorthoclase samples, four groundmass concentrates from three mafic deposits and one aphyric trachyte lava were dated. Crushed and sieved samples were rinsed in a 10% HCl solution for 5 minutes and cleaned several times in deionized water. With the aid of a binocular microscope, holocrystalline groundmass concentrates were

and an overall sensitivity of 2.2x 10^{-17} moles Ar/pA. J-factors were determined from the pooled results of 4-6 single crystal analyses from 6 radial positions around the irradiation vessel. The standard deviation of J -factor measurements was generally less than 0.25 % for each position. A blank measurement was made between every four single crystal analyses and the average of each set of bracketing blanks was subtracted from each of the four sample measurements. Typical laser blanks (including mass spectrometer backgrounds) were; 3, 0.1, 0.02, 0.2, 0.15 x10^{-17} moles at masses 40, 39, 38, 37, 36, respectively.

Furnace anorthoclase and groundmass samples were incrementally-heated in 8-12 steps within a double vacuum Mo resistance furnace. Reactive gases were removed during heating for 7 to 10 minutes with a SAES AP-10 getter, and further cleaned following heating for 5 to 7 minutes with a SAES GP-50 getter. The furnace extraction system and mass spectrometer blanks and backgrounds were measured throughout the course of the analyses and were very reproducible. Typical furnace blanks (including mass spectrometer backgrounds) ; 80, 0.2, 0.1, 0.2, 0.6 x10^{-17} moles at masses 40, 39, 38, 37, 36, respectively. The blank measurement made prior to sample analysis was subtracted from the sample measurement. Mass discrimination was measured at several intervals during the course of the analyses. The sample ages were corrected for blank, background, mass discrimination, and interfering reactions. The decay constant and isotopic abundances used in calculations are those suggested by Steiger and Jaeger (1977).

Data Processing. Ages were calculated using MassSpec version 4.27, a Macintosh computer program written in BASIC, by Al Deino of the Berkeley Geochronology Center. Two types of ages were calculated for most samples: an integrated age, and a plateau or mean age. The integrated age, equivalent to the K-Ar age of the sample, is a mean of the incremental ages, each weighted by the $\%^{39}Ar$ in each increment. The plateau and mean ages are means of specified increments weighted by the inverse of variance squared. The plateau age is defined by three or more contiguous

incremental ages that comprise >50% of total ^{39}Ar released and agree within 2 standard deviations (Fleck *et al.*, 1977). Mean ages consist of subjectively selected incremental ages that are nearly concordant. Uncertainties on plateau and mean ages are calculated using formula in Samson and Alexander (1987). All errors are reported at the 2 sigma confidence level.

Notes on Appendices II-V. In the analytical tables (Appendices II and IV) the sample number is followed by the NMGRL irradiation number, sample weight, J-value, and a brief site/sample description. All of the data are blank-corrected. The $^{37}Ar/^{39}Ar$ and K/Ca ratios are corrected for ^{37}Ar decay since irradiation. None of the listed isotope ratios are corrected for interfering reactions. Uncertainties in J-value are not included in age calculations. Listed data are not corrected for interfering reactions.

The age data tables and plots are organized first according to analysis type (furnace or laser and second according to location and third according to age from youngest to oldest. The sample orders for Appendices II-V are listed Table 2.

Appendix I. Table 2. Appendix Sample Lists

Site Name Sample Number	App. II and III # furnace analyses	App. IV and V # laser analyses	Appendices VI Table 1
Mt. Berlin Summit Crater			Mt. Berlin Summit Crater
WCM93-16	1		and Mt. Moulton tephra
WCM93-25	1		WCM93-16
WCM93-22	2	1	WCM93-313
WCM93-17	1		WCM93-315
WCM93-21	2		WCM93-15
WCM93-23	2	1	WCM93-22
WCM93-15	2	1	WCM93-23
			WCM93-316
Mt. Berlin Merram Peak Crater			WCM93-314
WCM93-130	1	1	
WCM93-123		1	Mt. Berlin Merram Peak Crater
WCM93-128	1		WCM93-130
WCM93-129	1		WCM93-128
WCM93-133	2		WCM93-133
WCM93-139	1	1	WCM93-139
WCM93-140	1		WCM93-140
Mt. Berlin- trachytic flank deposits			
			Mt. Berlin- mafic flank deposits
WCM93-011	1	1	WCM93-001
WCM93-152	1	1	WCM93-004
			WCM93-008

Site Name Sample Number	App. II and III # furnace analyses	App. IV and V # laser analyses	Appendices VI Table 1
Mt. Berlin- mafic flank deposits			
WCM93-001	2		Mt. Berlin- trachytic flank deposits
WCM93-004	2		WCM93-151
WCM93-008	1		WCM93-011
			WCM93-152
Mt. Berlin- Merram Peak trachyte lava			
WCM93-127	1		
WCM93-134		1	Mt. Berlin- Merram Peak trachyte lava
WCM93-125	1		WCM93-134
WCM93-126	2		WCM93-127
WCM93-137	1		WCM93-126
WCM93-138	1		WCM93-135
WCM93-135	1	2	WCM93-137
WCM93-009	1		WCM93-138
			WCM93-124
			WCM93-125
			WCM93-009
Mt. Berlin- Brandenberger Bluff			Mt. Berlin- Brandenberger Bluff
WCM93-014	1		WCM93-014
WCM93-010	1		WCM93-010
WCM93-037	1		WCM93-037
WCM93-053	1		WCM93-053
WCM93-069	1		WCM93-069
WCM93-121	1		WCM93-121
WCM93-250	1		WCM93-097
			WCM93-115
Mt. Moulton Englacial Tephra layers- distal Berlin			WCM93-079
WCM93-313	2	1	WCM93-174
WCM93-315	2	1	WCM93-183
WCM93-316	2	1	WCM93-250
WCM93-317	2	1	WCM93-254
WCM93-314	1	3	
			Mt. Siple Summit Crater
Mt. Siple Summit Crater Sample Data			WCM93-278
WCM93-278	1		WCM93-277
WCM93-277	3	1	
Mt. Takahe Summit Crater Sample Data			
W85009	1		
W85013	1		
W85015	1		
MT85006	1		
W85022	1		
W85011	1		

Appendix II. $^{40}Ar/^{39}Ar$ Furnace Age Spectrum Data

Run ID#	Temp °C	$^{40}Ar/^{39}Ar$	$^{37}Ar/^{39}Ar$ x10^{-2}	$^{36}Ar/^{39}Ar$ x10^{-4}	^{39}Ar moles x10^{-15}	K/Ca	Cl/K x10^{-4}	$\%^{40}Ar^*$	$\%^{39}Ar$	Age (ka)	± 2 s.d.
Mt. Berlin summit crater											
WCM93-016, NM-36, 132.9 mg, J=0.0002159											
Mt. Berlin summit crater, lava on ice cave floor											
5364-01B	700	0.4527	13.64	14.79	21.4	3.74	2.70	5.8	17.4	10.1	6.8
5364-01C	800	0.3205	13.27	10.35	34.5	3.84	0.994	7.6	45.4	9.5	4.5
5364-01D	900	0.3151	12.62	9.887	29.2	4.04	1.62	10.3	69.1	12.7	4.3
5364-01E	1000	0.4416	12.31	14.21	21.2	4.15	1.40	7.0	86.3	12.0	7.2
5364-01F	1100	0.8932	12.40	28.82	11.4	4.11	1.12	5.7	95.6	20	12
5364-01G	1200	0.7162	12.25	19.64	5.42	4.16	2.94	20.2	100.0	56	19
integrated age				n=6	123.2	3.96	0.18			**13.8**	**6.7**
plateau age (steps b-f, 95.6% 39Ar)										**11.5**	**3.5**
WCM93-025, NM-36, 130 mg, J=0.0002147											
Mt. Berlin summit crater wall, upper non-welded pumice deposit											
5366-01B	700	1.865	1.890	61.34	3.30	27.0	1.89	2.9	1.66	21	30
5366-01C	800	0.8386	1.247	27.28	10.9	40.9	1.60	4.0	7.16	13	12
5366-01D	900	0.4970	1.270	16.48	21.7	40.2	2.41	2.2	18.1	4.3	5.6
5366-01E	1000	0.3079	1.295	8.486	33.1	39.4	1.32	18.8	34.8	22.4	3.9
5366-01F	1100	0.3314	1.360	9.889	43.0	37.5	2.67	12.1	56.4	15.5	3.1
5366-01G	1200	0.4978	1.424	12.19	35.6	35.8	1.94	27.8	74.3	53.8	4.1
5366-01H	1250	0.5176	1.416	8.806	25.2	36.0	2.00	49.9	87.0	100.0	4.3
5366-01I	1300	0.5402	1.423	10.95	15.5	35.9	2.38	40.3	94.8	84.3	5.1
5366-01J	1350	0.3700	1.419	7.656	8.35	36.0	0.569	39.1	99.0	56	11
5366-01K	1400	0.3724	1.405	2.496	1.90	36.3	1.98	80.4	100.0	116	37
integrated age				n=10	198	37.4	3.86			**41.0**	**5.6**
mean age (steps b-f, 56.4% 39Ar)										**15.9**	**6.2**
WCM93-22, NM-32, 116.8 mg, J=0.0002274											
Mt. Berlin summit crater wall, highly vesicular laminated pumice											
5014-01D	900	0.6154	2.287	18.16	2.99	22.3	3.71	13.0	1.32	33	18
5014-01E	1000	0.5386	2.122	15.15	6.07	24.0	1.81	17.1	4.00	37.9	9.9
5014-01F	1100	0.4980	1.948	14.89	10.4	26.2	1.22	11.9	8.58	24.3	6.1
5014-01G	1250	0.7479	1.933	23.19	23.6	26.4	2.36	8.5	19.0	26.2	5.7
5014-01H	1300	0.3370	1.944	9.229	21.4	26.3	1.88	19.5	28.5	26.9	3.7
5014-01I	1350	0.2318	1.837	5.671	29.5	27.8	1.45	28.2	41.5	26.9	2.5
5014-01J	1425	0.1523	1.672	3.220	26.6	30.5	1.47	38.3	53.2	23.9	2.4
5014-01K	1500	0.1400	1.365	2.491	62.7	37.4	1.47	48.0	80.9	27.5	1.3
5014-01L	1750	0.1586	1.306	3.019	43.2	39.1	1.47	44.3	100.0	28.8	1.6
integrated age				n=9	226	32.4	5.77			**27.3**	**3.0**
plateau age (steps f-k, 76.9% 39Ar)										**26.7**	**1.5**
mean age (steps f-l, 91.4% 39Ar)										**27.2**	**1.6**

Appendix II. $^{40}Ar/^{39}Ar$ Furnace Age Spectrum Data

Run ID#	Temp °C	$^{40}Ar/^{39}Ar$	$^{37}Ar/^{39}Ar$ x10^{-2}	$^{36}Ar/^{39}Ar$ x10^{-4}	^{39}Ar moles x10^{-15}	K/Ca	Cl/K x10^{-4}	$\%^{40}Ar^*$	$\%^{39}Ar$	Age (ka)	± 2 s.d.
WCM93-022, NM-36, 191.1 mg, J=0.0002172											
Mt. Berlin summit crater wall, highly vesicular laminated pumice											
5347-01C	800	0.1903	2.418	4.734	3.60	21.1	2.25	27.3	1.55	20	27
5347-01D	900	0.1228	2.277	3.460	7.72	22.4	1.60	18.0	4.86	9	12
5347-01E	1000	0.1206	2.238	2.369	15.1	22.8	2.23	43.2	11.4	20.4	6.2
5347-01F	1100	0.1507	2.104	3.004	25.1	24.2	1.50	42.0	22.2	24.7	4.2
5347-01G	1200	0.1296	2.047	2.160	35.3	24.9	2.19	51.8	37.3	26.2	2.4
5347-01H	1250	0.1714	2.165	3.797	33.4	23.6	1.85	35.4	51.7	23.7	2.2
5347-01I	1300	1.226	2.346	39.05	41.9	21.7	1.71	6.0	69.7	28.8	7.2
5347-01J	1350	0.1398	2.276	2.490	31.8	22.4	1.75	48.5	83.3	26.5	2.6
5347-01K	1400	0.1613	2.163	2.865	16.4	23.6	1.33	48.4	90.4	30.5	5.2
5347-01L	1500	0.1349	1.828	2.378	10.8	27.9	-0.228	48.8	95.0	25.8	8.7
5347-01M	1750	5.445	2.390	181.6	11.6	21.3	2.19	1.5	100.0	31	32
integrated age				n=11	233	23.3	1.9			**25.7**	**6.4**
mean age (steps e-l, 95.1% 39Ar)										**25.5**	**2.0**
WCM93-017, NM-36, 71.3 mg, J=0.0002141											
Mt. Berlin summit crater wall, green pumiceous rheomorphic tuff											
5360-01C	800	0.5789	0.8702	17.23	5.73	58.6	2.27	12.1	5.60	27	15
5360-01D	900	0.3780	0.9359	9.946	9.58	54.5	1.79	22.4	15.0	32.7	8.7
5360-01E	1000	0.2892	0.9335	6.980	13.1	54.7	1.16	28.9	27.8	32.3	6.7
5360-01F	1100	0.2335	0.9230	6.556	13.2	55.3	1.55	17.2	40.7	15.5	6.3
5360-01G	1200	0.3416	1.141	9.263	14.0	44.7	2.80	20.1	54.3	26.7	6.9
5360-01H	1250	0.2667	1.084	6.851	14.0	47.1	1.99	24.3	68.0	25.2	7.1
5360-01I	1300	0.2442	1.057	6.587	13.5	48.3	0.733	20.5	81.2	19.4	5.3
5360-01J	1350	0.2244	1.047	5.135	6.37	48.7	1.02	32.6	87.4	28	11
5360-01K	1400	0.2446	1.242	5.977	2.53	41.1	1.23	28.1	89.9	27	29
5360-01L	1500	0.2595	0.8563	1.873	1.98	59.6	-1.28	78.8	91.8	79	36
5360-01M	1750	0.6350	1.169	17.83	7.22	43.6	0.963	17.1	98.8	42	12
5360-01N	1750	2.043	0.6789	62.36	1.18	75.1	0.963	9.8	159.8	42	12
integrated age				n=12	102	50.6	9.29			**27.8**	**8.9**
plateau age (steps f-k, 62.1% 39Ar)										**21.7**	**4.4**
mean age (steps c-k, 89.9% 39Ar)										**24.4**	**5.0**

Appendix II. $^{40}Ar/^{39}Ar$ Furnace Age Spectrum Data

Run ID#	Temp °C	$^{40}Ar/^{39}Ar$	$^{37}Ar/^{39}Ar$ $x10^{-2}$	$^{36}Ar/^{39}Ar$ $x10^{-4}$	^{39}Ar moles $x10^{-15}$	K/Ca	Cl/K $x10^{-4}$	$\%^{40}Ar^*$	$\%^{39}Ar$	Age (ka)	± 2 s.d.
WCM93-021, NM-36, 164.7 mg, J=0.0002154											
Mt. Berlin summit crater wall, red welded fall deposit											
5346-01B	700	0.9498	2.030	29.18	1.91	25.1	4.18	9.4	0.90	34	43
5346-01C	800	0.3753	1.831	8.461	3.88	27.9	4.48	33.7	2.73	49	20
5346-01D	900	0.1906	1.775	4.150	8.24	28.7	1.82	36.3	6.63	26.9	9.1
5346-01E	1000	0.1623	1.573	2.898	14.9	32.4	2.45	47.9	13.7	30.1	5.5
5346-01F	1100	0.1660	1.443	3.036	21.6	35.3	1.61	46.5	23.9	30.1	3.8
5346-01G	1200	0.1920	1.508	3.793	31.0	33.8	2.19	42.1	38.5	31.4	3.2
5346-01H	1250	0.2544	1.795	6.021	32.8	28.4	1.34	30.5	54.0	30.1	3.1
5346-01I	1300	0.3308	1.702	8.720	32.9	30.0	2.05	22.4	69.5	28.8	3.5
5346-01J	1350	0.2636	1.514	6.582	24.0	33.7	1.21	26.6	80.9	27.1	4.4
5346-01K	1400	0.2341	1.395	5.907	11.3	36.6	1.90	25.8	86.2	23.4	7.3
5346-01L	1500	0.2175	1.328	6.636	10.3	38.4	1.88	10.2	91.0	8.6	8.0
5346-01M	1750	3.255	1.554	108.0	19.0	32.8	2.19	2.0	100.0	26	20
integrated age				n=12	212	32.3	3.95			**28.2**	**6.5**
plateau age (steps c-k, 85.3% 39Ar)										**29.6**	**2.2**
WCM93-021, NM-36, 114.4 mg, J=0.0002154											
Mt. Berlin summit crater wall, red welded fall deposit											
5346-02A	550	9.171	3.717	286.1	0.377	13.7	4.66	7.8	0.273	279	208
5346-02B	700	0.5675	1.988	7.426	1.56	25.7	2.30	61.6	1.40	136	48
5346-02C	800	0.6796	1.767	17.55	3.67	28.9	3.30	23.9	4.07	63	25
5346-02D	900	0.1951	3.605	3.377	8.44	14.2	2.25	50.2	10.2	38	10
5346-02E	1000	0.2791	2.688	7.074	14.2	19.0	1.91	25.8	20.5	28.0	5.6
5346-02F	1100	0.2683	2.100	6.089	19.5	24.3	1.29	33.5	34.6	34.8	4.7
5346-02G	1200	0.1933	1.999	4.582	31.0	25.5	2.05	30.6	57.2	23.0	3.1
5346-02H	1250	0.4270	1.947	12.37	27.2	26.2	1.69	14.7	76.9	24.5	3.8
5346-02I	1300	0.2699	1.951	6.595	17.4	26.1	1.83	28.3	89.5	29.7	4.5
5346-02J	1350	3.3122	1.623	110.8	9.96	31.4	1.62	1.20	96.7	15	20
5346-02K	1400	0.2372	1.798	6.120	4.51	28.4	2.59	24.3	100	22	18
integrated age				n=11	138	24.8	5.84			**28.2**	**7.7**
plateau age (steps g-k, 65.4% 39Ar)										**24.9**	**3.5**

Appendix II. $^{40}Ar/^{39}Ar$ Furnace Age Spectrum Data

Run ID#	Temp °C	$^{40}Ar/^{39}Ar$	$^{37}Ar/^{39}Ar$ x10^{-2}	$^{36}Ar/^{39}Ar$ x10^{-4}	^{39}Ar moles x10^{-15}	K/Ca	Cl/K x10^{-4}	$\%^{40}Ar^*$	$\%^{39}Ar$	Age (ka)	± 2 s.d.
WCM93-23, NM-32, 120.3 mg, J=0.0002274											
Mt. Berlin summit crater wall, dense flow											
5015-01B	700	4.257	1.624	122.7	3.57	31.4	1.74	14.8	1.51	259	29
5015-01C	800	1.208	1.520	32.21	12.2	33.6	1.47	21.3	6.69	105.4	9.5
5015-01D	900	0.6955	1.326	18.98	21.4	38.5	2.08	19.5	15.8	55.5	5.0
5015-01E	1000	0.4733	1.253	13.68	30.0	40.7	2.07	14.8	28.5	28.6	3.6
5015-01F	1100	0.4983	1.192	14.39	33.9	42.8	1.59	14.8	42.9	30.1	3.4
5015-01G	1250	0.8975	1.296	28.63	50.2	39.4	1.38	5.8	64.1	21.5	5.0
5015-01H	1300	0.8932	1.264	28.29	23.0	40.4	1.07	6.5	73.8	23.7	6.4
5015-01I	1350	0.6731	1.331	20.10	20.5	38.3	2.20	11.9	82.5	32.7	4.9
5015-01J	1425	0.5266	1.216	15.01	5.55	41.9	1.80	15.9	84.9	34	11
5015-01K	1500	0.4638	1.187	13.31	14.2	43.0	2.11	15.4	90.9	29.2	5.2
5015-01L	1750	0.6249	1.280	18.13	21.6	39.9	1.53	14.4	100.0	37.0	5.2
integrated age				n=11	236	39.9	3.6			**38.0**	**5.5**
mean age (steps e-h, 58.0% 39Ar)										**27.4**	**4.3**
WCM93-023, NM-36, 80 mg, J=0.0002147											
Mt. Berlin summit crater wall, dense flow											
5363-01C	800	0.8910	2.286	13.98	9.48	22.3	1.66	53.8	8.47	186	11
5363-01D	900	0.3339	1.836	7.197	14.4	27.8	1.73	36.7	20.9	47.3	5.7
5363-01E	1000	0.2534	1.515	4.613	19.6	33.7	2.03	46.6	37.8	45.6	4.4
5363-01F	1100	0.2844	1.352	4.204	20.9	37.7	1.97	56.6	55.8	62.4	3.9
5363-01G	1200	0.3286	1.427	9.058	15.8	35.8	2.45	18.8	69.4	23.9	5.5
5363-01H	1250	0.3543	1.494	8.773	12.7	34.2	2.24	27.1	80.4	37.2	6.7
5363-01I	1300	0.2884	1.407	6.942	9.64	36.3	3.56	29.2	88.7	32.7	7.8
5363-01J	1350	0.2322	1.310	4.870	6.28	39.0	6.22	38.4	94.1	34	11
5363-01K	1400	0.5155	1.314	13.32	1.44	38.8	4.82	23.8	95.3	48	46
5363-01L	1500	0.3239	1.337	4.781	1.76	38.2	-3.78	56.6	96.9	71	40
5363-01M	1750	3.043	1.686	94.73	3.07	30.3	-0.46	8.0	99.5	95	39
integrated age				n=13	116	33.5	6.9			**56.5**	**9.5**
mean age (steps g-j, 38.3% 39Ar)										**30.4**	**7.6**

Appendix II. $^{40}Ar/^{39}Ar$ Furnace Age Spectrum Data

Run ID#	Temp °C	$^{40}Ar/^{39}Ar$	$^{37}Ar/^{39}Ar$ x10^{-2}	$^{36}Ar/^{39}Ar$ x10^{-4}	^{39}Ar moles x10^{-15}	K/Ca	Cl/K x10^{-4}	$\%^{40}Ar^*$	$\%^{39}Ar$	Age (ka)	± 2 s.d.
WCM93-015, NM-32, 126.8 mg, J=0.0002274											
Mt. Berlin summit crater wall, spatter lava with cognate xenoliths											
5013-01A	550	9.113	1.679	272.3	0.169	30.4	-8.36	11.7	0.06	438	364
5013-01B	700	2.812	1.481	85.70	0.436	34.4	30.3	10.0	0.22	115	146
5013-01C	800	1.096	0.9962	33.44	2.60	51.2	61.4	9.9	1.19	45	39
5013-01D	900	0.5326	0.9310	15.49	5.25	54.8	28.3	14.1	3.13	31	16
5013-01E	1000	0.4049	0.9376	11.16	9.88	54.4	2.95	18.7	6.80	31.0	6.7
5013-01F	1100	0.3819	1.019	11.11	16.1	50.1	2.15	14.2	12.8	22.2	5.6
5013-01G	1250	0.4456	0.9686	12.99	30.5	52.7	1.66	14.0	24.1	25.6	3.8
5013-01H	1300	0.4430	0.9562	12.99	19.0	53.4	2.08	13.4	31.1	24.5	4.1
5013-01I	1350	0.3198	0.9752	8.713	21.0	52.3	1.53	19.7	38.9	25.8	3.6
5013-01J	1425	0.1666	0.9801	3.568	32.9	52.1	2.19	37.1	51.1	25.4	1.9
5013-01K	1500	0.1391	0.9816	2.758	77.7	52.0	1.55	41.8	79.9	23.9	1.0
5013-01L	1750	0.1967	0.9978	3.961	52.3	51.1	1.62	40.8	99.3	32.9	1.4
5013-01M	1750	1.417	1.233	31.64	1.98	41.4	0.168	34.1	100.0	198	34
integrated age				n=13	270	51.9	7.90			**28.4**	**3.8**
plateau age (steps c-k, 79.7% 39Ar)										**24.4**	**1.2**
WCM93-015, NM-36, 117.5 mg, J=0.0002147											
Mt. Berlin summit crater wall, spatter lava with cognate xenoliths											
5344-01B	700	0.7297	1.118	21.19	1.73	45.6	4.64	14.3	1.21	40	43
5344-01C	800	0.3951	1.037	6.899	3.97	49.2	3.93	48.5	3.98	74	18
5344-01D	900	0.2330	0.9897	4.905	7.67	51.6	0.709	38.0	9.33	34	12
5344-01E	1000	0.1841	0.9800	3.808	13.7	52.1	1.86	39.2	18.9	28.0	6.0
5344-01F	1100	0.1953	0.9814	4.204	20.2	52.0	2.59	36.7	33.0	27.5	4.4
5344-01G	1200	0.2243	0.9809	5.644	24.8	52.0	1.75	25.9	50.4	22.4	3.9
5344-01H	1250	0.2221	0.9988	5.135	18.0	51.1	2.06	31.9	62.9	27.3	4.8
5344-01I	1300	0.2262	1.004	4.990	15.1	50.8	2.21	35.1	73.5	30.5	5.2
5344-01J	1350	0.1878	1.000	4.576	14.6	51.0	2.10	28.3	83.7	20.4	4.5
5344-01K	1400	0.2113	0.9917	3.981	6.47	51.4	1.37	44.6	88.2	36	11
5344-01L	1500	0.1928	0.9259	3.067	6.62	55.1	3.41	53.3	92.8	40	11
5344-01M	1750	7.978	0.9123	265.4	8.34	55.9	3.45	1.7	98.6	53	45
5344-01N	1750	1.803	0.9539	53.66	1.95	53.5	3.49	12.1	100.0	84	43
integrated age				n=13	143	51.9	2.54			**31.2**	**9.3**
plateau age (steps d-i, 69.5% 39Ar)										**26.8**	**3.5**

Appendix II. $^{40}Ar/^{39}Ar$ Furnace Age Spectrum Data

Run ID#	Temp °C	$^{40}Ar/^{39}Ar$	$^{37}Ar/^{39}Ar$ x10^{-2}	$^{36}Ar/^{39}Ar$ x10^{-4}	^{39}Ar moles x10^{-15}	K/Ca	Cl/K x10^{-4}	$\%^{40}Ar^*$	$\%^{39}Ar$	Age (ka)	± 2 s.d.
Mt. Berlin Merram Peak crater											
WCM93-130, NM-36, 109 mg, J=0.0002153											
Mt. Berlin, Merram crater (WNW), 1 m thick pumiceous phonolite fall											
5367-01C	800	2.197	0.7312	61.87	3.43	69.8	3.08	16.8	2.58	143	30
5367-01D	900	1.096	0.6029	24.17	7.63	84.6	0.771	34.8	8.34	148	12
5367-01E	1000	0.7402	0.6112	12.74	14.8	83.5	1.58	49.2	19.5	141.3	7.9
5367-01F	1100	0.6030	0.6422	8.062	23.7	79.4	1.93	60.5	37.4	141.7	3.9
5367-01G	1200	0.6031	0.6452	8.342	21.7	79.1	2.62	59.2	53.7	138.5	4.5
5367-01H	1250	0.5466	0.6495	6.143	18.6	78.6	1.84	66.8	67.7	141.9	4.8
5367-01I	1300	0.5701	0.7002	6.841	16.1	72.9	2.42	64.6	79.9	143.0	5.5
5367-01J	1350	0.5371	0.7756	6.152	11.7	65.8	2.92	66.2	88.7	138.1	7.5
5367-01K	1400	0.4581	0.8764	4.597	4.57	58.2	2.82	70.5	92.2	125	16
5367-01L	1500	0.4319	0.6691	2.223	4.58	76.2	2.38	84.9	95.6	142	15
5367-01M	1750	1.395	0.9540	35.71	5.79	53.5	2.02	24.4	100	132	16
5367-01N	1750	5.072	1.418	171.5	0.767	36.0	5.17	0.100		2	110
integrated age				n=11	133	75.8	10.13			**140.5**	**7.6**
plateau age (steps c-m, 100% 39Ar)										**140.7**	**2.8**
WCM93-128, NM-32, 124.3 mg, J=0.0002264											
Mt. Berlin, Merram crater (WNW), in situ trachyte bomb											
5011-01C	800	1.143	1.721	24.11	2.54	29.6	3.65	37.8	0.99	176	28
5011-01D	900	0.7624	1.248	11.38	6.38	40.9	2.05	56.0	3.48	174	11
5011-01E	1000	0.6441	1.214	7.015	12.5	42.0	1.48	67.9	8.35	178.7	6.0
5011-01F	1100	0.6241	1.199	6.316	21.2	42.5	2.11	70.2	16.6	178.9	3.7
5011-01G	1250	0.6589	1.098	7.251	52.8	46.5	2.12	67.6	37.2	181.7	2.4
5011-01H	1300	0.7561	1.047	10.19	37.8	48.7	1.21	60.2	51.9	186.0	3.1
5011-01I	1350	0.7178	0.9814	9.160	41.5	52.0	1.97	62.4	68.1	182.8	2.7
5011-01J	1425	0.6788	0.9356	7.428	19.4	54.5	1.98	67.7	75.7	187.7	3.7
5011-01K	1500	0.7213	0.9489	8.958	33.3	53.8	1.96	63.4	88.7	186.7	3.0
5011-01L	1750	0.8091	1.009	11.55	28.3	50.6	1.28	57.9	99.7	191.4	3.5
integrated age				n=11	257	48.8	9.18			**184.3**	**3.8**
plateau age (steps g-k, 72.1% 39Ar)										**183.6**	**2.7**

Appendix II. $^{40}Ar/^{39}Ar$ Furnace Age Spectrum Data

Run ID#	Temp °C	$^{40}Ar/^{39}Ar$	$^{37}Ar/^{39}Ar$ x10^{-2}	$^{36}Ar/^{39}Ar$ x10^{-4}	^{39}Ar moles x10^{-15}	K/Ca	Cl/K x10^{-4}	%^{40}Ar*	%^{39}Ar	Age (ka)	± 2 s.d.
WCM93-129, NM-32, 125.6 mg, J=0.0002264											
Mt. Berlin, Merram crater (WNW), welded, inflated fall deposit											
5012-01C	800	0.7672	1.546	8.259	3.03	33.0	1.03	68.3	1.18	214	18
5012-01D	900	0.5610	1.297	2.091	6.36	39.3	1.85	89.1	3.67	204.1	8.0
5012-01E	1000	2.118	1.315	55.92	12.2	38.8	1.64	22.0	8.42	191	12
5012-01F	1100	0.5313	1.291	2.423	19.1	39.5	1.72	86.7	15.9	188.0	3.0
5012-01G	1250	0.5703	1.206	3.791	45.1	42.3	1.74	80.5	33.5	187.5	1.9
5012-01H	1300	0.6820	1.196	7.321	37.3	42.7	1.55	68.4	48.1	190.5	2.7
5012-01I	1350	0.5990	1.128	4.951	42.5	45.2	2.37	75.7	64.7	185.2	2.1
5012-01J	1425	0.5793	1.071	4.073	20.7	47.6	1.79	79.3	72.8	187.5	3.1
5012-01K	1500	0.7681	1.054	10.45	40.4	48.4	1.59	59.9	88.6	188.0	2.7
5012-01L	1750	0.8036	1.081	11.40	29.3	47.2	1.38	58.1	100.0	190.8	3.6
integrated age				n=10	256	44.2	4.87			**188.9**	**3.4**
plateau age (steps i-l, 51.9% 39Ar)										**187.1**	**2.6**
WCM93-133, NM-32, 120.2 mg, J=0.0002277											
Mt. Berlin, Merram crater (NE scab), welded fall layer											
5007-01C	800	0.9263	1.593	17.96	3.49	32.0	2.34	42.8	1.40	163	18
5007-01D	900	0.6456	1.363	7.831	8.22	37.4	2.93	64.3	4.70	170.5	8.0
5007-01E	1000	0.5875	1.235	5.442	16.7	41.3	1.13	72.8	11.4	175.5	4.3
5007-01F	1100	0.6389	1.176	7.011	29.5	43.4	1.91	67.7	23.2	177.6	3.0
5007-01G	1250	0.5870	1.173	5.037	52.5	43.5	1.86	74.8	44.3	180.2	1.9
5007-01H	1300	0.5953	1.057	4.847	33.5	48.3	2.39	76.0	57.7	185.8	2.4
5007-01I	1350	0.5693	1.019	3.846	40.5	50.1	1.93	80.1	74.0	187.3	2.2
5007-01J	1425	0.6343	1.026	6.159	18.4	49.7	1.87	71.4	81.3	186.0	3.9
5007-01K	1500	0.5585	0.9852	3.583	29.5	51.8	2.19	81.1	93.2	186.2	2.4
5007-01L	1750	0.7008	0.9387	8.321	17.0	54.4	1.19	65.0	100.0	187.1	4.2
integrated age				n=10	249	46.9	6.96			**182.5**	**3.1**
plateau age (steps h-l, 55.7% 39Ar)										**186.5**	**1.4**
WCM93-133, NM-32, 100.7 mg, J=0.0002277											
Mt. Berlin, Merram crater (NE scab), welded fall layer											
5008-01D	900	0.7128	1.498	13.37	2.26	34.1	2.98	44.7	1.82	131	29
5008-01E	1000	0.5929	1.265	6.949	5.92	40.3	3.18	65.5	6.62	160	10
5008-01F	1100	0.5626	1.148	5.275	11.8	44.4	2.21	72.4	16.2	167.3	5.6
5008-01G	1200	0.5606	1.251	4.009	15.6	40.8	1.89	79.0	28.8	181.9	6.0
5008-01H	1250	0.5544	1.039	3.849	15.8	49.1	1.78	79.6	41.6	181.3	4.9
5008-01I	1300	0.5871	1.005	4.508	15.0	50.8	1.79	77.4	53.7	186.7	5.5
5008-01J	1350	0.6550	1.024	7.359	19.2	49.8	1.41	66.9	69.3	180.0	5.3
5008-01K	1400	0.5318	1.086	3.102	13.7	47.0	2.71	82.9	80.3	181.1	5.9
5008-01L	1500	0.4696	0.9793	0.8019	14.5	52.1	1.67	95.1	92.1	183.2	6.0
5008-01M	1750	3.759	1.475	108.9	9.73	34.6	2.31	14.4	100	223	30
integrated age				n=10	124	46.2	6.588			**182.0**	**8.2**
plateau age (steps g-l, 75.9% 39Ar)										**182.3**	**3.0**

Appendix II. $^{40}Ar/^{39}Ar$ Furnace Age Spectrum Data

Run ID#	Temp °C	$^{40}Ar/^{39}Ar$	$^{37}Ar/^{39}Ar$ x10^{-2}	$^{36}Ar/^{39}Ar$ x10^{-4}	^{39}Ar moles x10^{-15}	K/Ca	Cl/K x10^{-4}	$\%^{40}Ar^*$	$\%^{39}Ar$	Age (ka)	± 2 s.d.
WCM93-139, NM-32, 130 mg, J=0.0002285											
Mt. Berlin, Merram crater (Rainbow Ridge), welded strombolian flow											
5001-01C	800	3.986	2.543	121.8	2.19	20.1	2.83	9.8	0.80	160	39
5001-01D	900	1.074	1.524	22.67	6.24	33.5	3.16	37.7	3.09	167	13
5001-01E	1000	0.9167	1.322	16.44	14.5	38.6	2.15	47.1	8.40	178.1	6.7
5001-01F	1100	0.9334	1.193	16.64	26.6	42.8	1.48	47.4	18.2	182.4	4.7
5001-01G	1250	0.6841	1.132	8.256	61.3	45.1	2.37	64.4	40.6	181.7	2.5
5001-01H	1300	0.5338	1.071	3.057	34.4	47.6	1.60	83.2	53.3	183.0	2.3
5001-01I	1350	0.5099	1.003	2.039	41.1	50.9	1.86	88.3	68.3	185.6	2.0
5001-01J	1425	0.5850	0.9859	4.649	28.1	51.8	0.717	76.6	78.7	184.7	3.2
5001-01K	1500	0.5871	0.9871	4.459	27.4	51.7	1.07	77.7	88.7	188.0	2.9
5001-01L	1750	0.5887	0.9804	4.618	30.8	52.0	2.05	76.9	100	186.7	3.0
integrated age	**total gas age**			n=10	272.5	47.4	10.3			**183.3**	**3.5**
plateau age (steps f-j, 70.3% 39Ar)										**183.8**	**1.9**
WCM93-140, NM-36, 96.4 mg, J=0.0002171											
Mt. Berlin, Merram crater (Rainbow Ridge), welded strombolian flow											
5351-01C	800	6.185	1.001	183.2	1.35	51.0	6.45	12.5	1.03	303	105
5351-01D	900	0.5437	0.9485	-0.007	2.89	53.8	0.807	100	3.21	213	31
5351-01E	1000	0.5436	0.9095	-0.085	6.60	56.1	1.86	101	8.21	214.2	13.1
5351-01F	1100	0.6213	0.9221	5.175	12.1	55.3	1.75	75.5	17.4	183.7	6.7
5351-01G	1200	0.5355	0.8930	2.328	18.6	57.1	1.59	87.2	31.4	183.0	4.8
5351-01H	1250	0.8127	0.8909	11.43	17.8	57.3	1.98	58.5	44.9	186.2	5.9
5351-01I	1300	0.5921	0.8617	3.839	16.9	59.2	1.53	80.9	57.7	187.5	4.5
5351-01J	1350	0.6040	0.8307	4.172	18.3	61.4	1.89	79.7	71.6	188.4	4.9
5351-01K	1400	0.5750	0.8223	3.343	15.8	62.0	1.60	82.9	83.5	186.7	5.6
5351-01L	1500	0.6351	0.8165	3.632	9.33	62.5	1.96	83.2	90.6	206.9	9.4
5351-01M	1750	1.208	0.7943	24.07	12.4	64.2	2.31	41.2	100	194.6	9.9
integrated age				n=11	132	59.3	4.09			**191.5**	**8.0**
plateau age (steps f-k, 75.3% 39Ar)										**186.1**	**2.8**

Appendix II. $^{40}Ar/^{39}Ar$ Furnace Age Spectrum Data

Run ID#	Temp °C	$^{40}Ar/^{39}Ar$	$^{37}Ar/^{39}Ar$ x10^{-2}	$^{36}Ar/^{39}Ar$ x10^{-4}	^{39}Ar moles x10^{-15}	K/Ca	Cl/K x10^{-4}	$\%^{40}Ar^*$	$\%^{39}Ar$	Age (ka)	± 2 s.d.
Mt. Berlin- trachytic flank deposits											
WCM93-011, NM-36, 117.9 mg, J=0.0002169											
Petrel's Crown, trachyte lava											
5345-01C	800	0.7479	2.349	8.579	3.01	21.7	0.492	66.3	2.08	194	25
5345-01D	900	0.6631	2.073	3.256	5.90	24.6	1.22	85.7	5.69	222	13
5345-01E	1000	0.6524	2.038	2.650	9.94	25.0	0.970	88.2	11.8	225.2	7.9
5345-01F	1100	1.8832	2.101	42.99	12.40	24.3	1.82	32.6	19.3	240	14
5345-01G	1200	0.6991	1.967	2.803	14.89	25.9	2.36	88.3	28.4	241.7	6.9
5345-01H	1250	1.8050	1.753	41.51	28.65	29.1	2.91	32.1	45.9	226.9	9.1
5345-01I	1300	0.6760	1.711	2.383	38.81	29.8	2.42	89.7	69.7	237.4	2.9
5345-01J	1350	0.8436	1.733	7.997	19.74	29.4	2.07	72.1	81.7	238.1	6.0
5345-01K	1400	0.5040	1.672	-3.349	5.35	30.5	0.634	120	85.0	236	14
5345-01L	1500	0.8510	1.579	7.601	11.10	32.3	1.55	73.7	91.8	245.6	8.0
5345-01M	1750	4.761	1.673	137.9	13.47	30.5	0.910	14.4	100.0	269	26
integrated age				n=12	164	28.5	4.62			**237**	**10**
mean age (steps f-k, 73.2% 39Ar)										**237.4**	**3.6**
WCM93-152, F5:NM-36, 117.4 mg, J=0.0002126288±0.000002											
Wedemeyer Rock, welded trachyte ignimbrite											
5341-01C	800	1.265	2.207	26.00	1.62	23.1	1.31	39.4	1.1	191	52
5341-01D	900	0.7220	1.779	4.507	4.01	28.7	0.514	81.7	3.9	226	20
5341-01E	1000	0.6812	1.759	3.606	6.38	29.0	3.03	84.5	8.3	221	10
5341-01F	1100	0.6867	1.689	3.303	9.74	30.2	1.42	85.9	15.1	226.4	6.8
5341-01G	1200	0.7039	1.530	3.616	12.7	33.3	1.06	85.0	24.0	229.2	5.7
5341-01H	1250	0.7248	1.398	4.131	16.2	36.5	1.76	83.3	35.2	231.4	4.3
5341-01I	1300	0.7116	1.339	3.697	30.5	38.1	2.31	84.8	56.4	231.4	3.2
5341-01J	1350	0.6823	1.191	2.732	23.8	42.8	1.96	88.3	72.9	231.0	3.4
5341-01K	1400	0.7577	1.147	6.481	8.58	44.5	3.25	74.8	78.9	217	11
5341-01L	1500	0.7120	1.027	2.977	15.0	49.7	1.88	87.7	89.4	239.6	7.3
5341-01M	1750	0.9677	1.155	11.85	14.9	44.2	1.84	63.9	99.7	237.2	7.6
integrated age				n=12	144	39.1	8.46			**230.8**	**7.2**
plateau age (steps f-j, 64.6% 39Ar)										**230.7**	**2.1**

Appendix II. $^{40}Ar/^{39}Ar$ Furnace Age Spectrum Data

Run ID#	Temp °C	$^{40}Ar/^{39}Ar$	$^{37}Ar/^{39}Ar$ x10^{-2}	$^{36}Ar/^{39}Ar$ x10^{-4}	^{39}Ar moles x10^{-15}	K/Ca	Cl/K x10^{-4}	$\%^{40}Ar^*$	$\%^{39}Ar$	Age (ka)	± 2 s.d.
Mt. Berlin- mafic NW flank deposits											
WCM93-01, NM-33, 94.8 mg, J=0.0015007											
Mefford Knoll, basanite cinder cone											
5138-01A	500	50.31	77.03	1675	4.32	0.662	6.06	1.7	1.82	2380	1751
5138-01B	625	0.7069	68.44	22.92	42.9	0.745	0.219	11.6	19.9	222	35
5138-01C	700	0.2965	85.04	9.004	56.3	0.600	0.613	32.2	43.7	259	18
5138-01D	775	0.3387	112.1	11.38	39.6	0.455	0.643	26.1	60.4	239	28
5138-01E	850	0.4246	123.7	14.13	24.4	0.412	1.31	24.0	70.7	276	35
5138-01F	925	0.7655	153.3	26.76	10.3	0.333	2.00	12.0	75.0	250	78
5138-01G	1050	1.728	204.3	61.55	9.96	0.250	4.64	3.8	79.3	180	122
5138-01H	1125	3.561	574.2	132.3	7.67	0.0889	7.60	2.6	82.5	251	222
5138-01I	1200	2.225	1298	107.4	41.5	0.0393	7.76	2.2	100	131	114
integrated age				n=9	237	0.443	0.246			**263**	**86**
plateau age (steps b-i, 98.2% 39Ar)										**250**	**21**
WCM93-01, NM-37, 158.4 mg, J=0.0002214											
Mefford Knoll, basanite cinder cone											
5397-01B	600	9.792	82.48	321.5	3.35	0.619	2.26	3.6	13.8	142	77
5397-01C	700	2.752	87.71	73.88	7.07	0.582	0.772	23.1	42.9	254	23
5397-01D	800	2.816	90.82	80.28	4.41	0.562	0.839	18.2	61.0	205	35
5397-01E	900	4.037	122.3	124.5	2.20	0.417	-1.41	11.2	70.1	180	53
5397-01F	1000	8.294	171.0	255.7	1.05	0.298	5.90	10.5	74.4	348	117
5397-01G	1100	19.97	287.0	661.6	0.860	0.178	16.8	3.2	78.0	257	218
5397-01H	1200	19.58	1065	670.6	5.35	0.048	9.48	3.0	100	234	122
integrated age				n=7	24.3	0.424	0.220			**223**	**68**
plateau age (steps c-h, 86.2% 39Ar)										**236**	**34**
WCM93-04, NM-33, 103.1 mg, J=0.0015007											
Mefford Knoll, basanite breccia with scoria											
5139-01A	500	68.25	27.49	2294	11.4	1.86	0.971	0.7	3.33	1281	2633
5139-01B	625	0.4288	52.20	13.27	61.6	0.977	0.762	17.8	21.4	207	22
5139-01C	700	0.2928	74.47	8.751	63.0	0.685	1.72	31.1	39.8	247	17
5139-01D	775	0.3217	87.36	10.47	48.1	0.584	1.39	24.6	53.9	214	25
5139-01E	850	0.4050	100.2	13.46	30.3	0.509	1.15	20.8	62.7	228	37
5139-01F	925	0.5337	137.6	19.25	18.1	0.371	2.10	13.2	68.0	191	45
5139-01G	1050	0.8863	185.8	33.10	23.4	0.275	3.10	5.7	74.9	137	58
5139-01H	1125	1.477	516.7	60.56	16.6	0.099	7.31	5.7	79.7	228	90
5139-01I	1200	1.423	725.0	65.67	67.9	0.070	5.08	2.8	99.6	108	70
integrated age				n=10	342	0.549	0.550			**229**	**129**
plateau age (steps b-j, 96.7% 39Ar)										**221**	**23**

Appendix II. $^{40}Ar/^{39}Ar$ Furnace Age Spectrum Data

Run ID#	Temp °C	$^{40}Ar/^{39}Ar$	$^{37}Ar/^{39}Ar$ x10^{-2}	$^{36}Ar/^{39}Ar$ x10^{-4}	^{39}Ar moles x10^{-15}	K/Ca	Cl/K x10^{-4}	$\%^{40}Ar^*$	$\%^{39}Ar$	Age (ka)	± 2 s.d.
WCM93-04, NM-37, 124.6 mg, J=0.0002214											
Mefford Knoll, basanite breccia with scoria											
5398-01A	500	413.5	48.25	13985	0.86	1.06	32.2	0.1	2.91	127	2653
5398-01B	600	6.433	53.05	206.2	4.22	0.962	1.59	5.9	17.3	152	52
5398-01C	700	3.281	79.61	95.76	5.83	0.641	2.14	15.6	37.1	205	31
5398-01D	800	2.818	73.26	75.25	4.42	0.696	1.52	23.1	52.2	260	28
5398-01E	900	3.376	101.9	99.51	2.72	0.501	1.59	15.2	61.4	205	45
5398-01F	1000	5.074	147.1	159.6	2.10	0.347	1.63	9.3	68.6	188	58
5398-01G	1100	10.94	244.8	370.3	1.33	0.208	8.87	1.7	73.1	75	122
5398-01H	1200	18.44	634.9	618.2	7.89	0.080	7.65	3.6	100	266	121
integrated age				n=8	29.4	0.503	0.346			**212**	**141**
plateau age (steps c-f, 51.3% 39Ar)										**226**	**38**
WCM93-08, NM-33, 111 mg, J=0.0015007											
Mefford Knoll, hawaiite flow levee											
5140-01A	500	13.05	45.47	439.2	11.1	1.12	2.70	0.8	2.7	275	485
5140-01B	625	0.7302	49.74	23.64	76.4	1.03	2.28	9.6	21.7	189	30
5140-01C	700	0.3810	61.57	11.62	108	0.829	2.18	22.2	48.3	229	17
5140-01D	775	0.5010	72.12	16.05	84.8	0.707	1.74	16.4	69.3	222	20
5140-01E	850	1.049	99.14	35.40	37.5	0.515	2.12	7.5	78.6	212	50
5140-01F	925	1.759	154.0	60.11	10.7	0.331	3.51	5.7	81.2	273	134
5140-01G	1050	2.385	225.3	81.44	8.35	0.226	6.74	6.4	83.3	411	167
5140-01H	1125	2.184	441.9	82.86	57.6	0.115	7.82	3.4	97.5	202	85
5140-01I	1200	5.993	2528	241.5	7.31	0.020	8.60	13.3	99.4	2203	299
5140-01J	1450	7.684	3152	236.9	2.59	0.016	7.08	40.4	100	8573	430
integrated age				n=10	404.1	0.672	0.412			**310**	**60**
plateau age (steps a-f, 81.2% 39Ar)										**221**	**17**

Appendix II. $^{40}Ar/^{39}Ar$ Furnace Age Spectrum Data

Run ID#	Temp °C	$^{40}Ar/^{39}Ar$	$^{37}Ar/^{39}Ar$ x10^{-2}	$^{36}Ar/^{39}Ar$ x10^{-4}	^{39}Ar moles x10^{-15}	K/Ca	Cl/K x10^{-4}	$\%^{40}Ar^*$	$\%^{39}Ar$	Age (ka)	± 2 s.d.
Mt. Berlin- S. Merram Peak deposits											
WCM93-127, NM-32, 40 mg, J=0.0002223											
SE Merram, foliated trachyte lava											
5029-01B	700	32.69	1.625	1064	0.807	31.4	5.90	3.8	1.23	498	281
5029-01C	800	11.75	1.890	370.6	2.28	27.0	-0.15	6.8	4.71	322	94
5029-01D	900	2.649	1.781	51.44	3.85	28.6	0.568	42.7	10.6	453	26
5029-01E	1000	2.321	1.538	38.86	5.36	33.2	4.08	50.6	18.8	471	21
5029-01F	1100	2.560	1.754	43.47	5.95	29.1	1.69	49.9	27.8	512	19
5029-01G	1200	3.634	1.919	78.96	6.87	26.6	1.46	35.8	38.3	522	24
5029-01H	1250	4.633	1.615	115.1	7.14	31.6	0.960	26.6	49.2	494	30
5029-01I	1300	12.26	1.603	371.0	9.30	31.8	3.05	10.6	63.4	520	66
5029-01J	1350	2.653	1.595	53.96	9.72	32.0	0.64	39.9	78.2	425	17
5029-01K	1400	2.229	1.346	38.58	4.15	37.9	3.12	48.9	84.6	437	29
5029-01L	1500	2.786	1.288	56.01	4.71	39.6	2.95	40.6	91.7	454	23
5029-01M	1750	4.035	1.518	100.6	5.42	33.6	0.973	26.3	100.0	426	26
integrated age				n=12	65.6	31.9	3.94			**470**	**35**
mean age (steps j-m, 36.6% 39Ar)										**434**	**18**
WCM93-125, NM-32, 77.6 mg, J=0.0002237											
SE Merram, dense glassy foliated trachyte lava											
5020-01A	550	7.203	19.62	201.6	1.67	2.60	5.33	17.5	1.78	509	52
5020-01B	700	2.451	20.30	36.30	9.88	2.51	1.79	56.9	12.4	562.7	9.6
5020-01C	800	2.325	20.14	31.52	17.5	2.53	1.29	60.6	31.1	569.0	8.4
5020-01D	900	1.850	20.96	15.41	14.5	2.43	1.90	76.3	46.6	569.4	6.3
5020-01E	1000	2.214	20.44	28.03	11.9	2.50	1.98	63.3	59.4	565.5	8.2
5020-01F	1100	4.603	19.35	108.9	10.4	2.64	2.02	30.4	70.5	565	21
5020-01G	1250	8.677	18.40	244.7	9.01	2.77	2.00	16.8	80.1	589	44
5020-01H	1300	6.663	16.25	175.6	4.49	3.14	3.32	22.3	85.0	600	37
5020-01I	1350	4.499	15.84	103.8	3.39	3.22	2.77	32.1	88.6	582	32
5020-01J	1425	4.490	21.02	105.5	1.98	2.43	-0.072	30.9	90.7	560	38
5020-01K	1500	2.422	15.94	37.61	5.14	3.20	1.88	54.6	96.2	534	15
5020-01L	1750	2.887	11.22	63.71	3.55	4.55	2.45	35.1	100.0	409	23
integrated age				n=12	93.4	2.71	0.60			**562**	**18**
plateau age (steps b-j, 88.9% 39Ar)										**567.9**	**5.1**

Appendix II. $^{40}Ar/^{39}Ar$ Furnace Age Spectrum Data

Run ID#	Temp °C	$^{40}Ar/^{39}Ar$	$^{37}Ar/^{39}Ar$ x10^{-2}	$^{36}Ar/^{39}Ar$ x10^{-4}	^{39}Ar moles x10^{-15}	K/Ca	Cl/K x10^{-4}	%^{40}Ar*	%^{39}Ar	Age (ka)	± 2 s.d.
WCM93-126, NM-32, 111.9 mg, J=0.0002264											
SE Merram, foliated trachyte lava											
5009-01A	550	2.360	15.31	36.66	2.51	3.33	3.01	54.6	1.47	526	25
5009-01B	700	1.475	16.72	6.874	2.88	3.05	0.568	87.1	3.17	524	22
5009-01C	800	1.585	16.70	7.537	36.6	3.05	2.05	86.7	24.7	561.4	4.1
5009-01D	900	1.625	15.81	8.463	29.4	3.23	2.21	85.4	42.0	566.4	4.3
5009-01E	1000	1.595	14.27	8.049	21.2	3.58	1.37	85.8	54.5	558.6	4.8
5009-01F	1100	2.293	11.57	30.76	19.0	4.41	1.97	60.7	65.7	568.8	7.9
5009-01G	1250	2.410	10.02	32.07	14.9	5.09	1.42	61.0	74.4	599.9	9.3
5009-01H	1300	2.095	8.851	24.68	7.97	5.76	2.46	65.5	79.1	560	11
5009-01I	1350	2.122	6.609	24.34	9.54	7.72	1.86	66.3	84.8	575	11
5009-01J	1425	1.861	8.595	25.91	2.75	5.94	3.74	59.2	86.4	450	21
5009-01K	1500	1.823	8.419	16.59	14.5	6.06	3.47	73.4	94.9	546.6	6.5
5009-01L	1750	1.686	6.016	15.51	8.69	8.48	1.82	73.1	100	503.2	8.4
integrated age				n=12	170	4.45	1.86			**559.7**	**7.1**
plateau age (steps c-f, 62.5% 39Ar)										**563.0**	**4.7**
WCM93-126, NM-32, 108.5 mg, J=0.0002264											
SE Merram, foliated trachyte lava											
5010-01BB	700	9.517	16.70	281.0	9.31	3.06	1.91	12.9	6.24	501	49
5010-01CC	800	2.091	17.95	24.65	45.3	2.84	1.94	65.8	36.6	562.1	5.8
5010-01DD	900	1.857	18.62	16.55	27.4	2.74	1.91	74.4	54.9	564.5	5.5
5010-01EE	1000	3.408	19.52	68.25	17.6	2.61	1.92	41.3	66.7	574	14
5010-01FF	1100	14.10	21.09	428.1	13.6	2.42	2.45	10.4	75.8	596	68
5010-01GG	1250	21.26	22.30	671.5	12.3	2.29	3.05	6.7	84.0	585	105
5010-01H	1300	7.342	18.71	198.9	6.06	2.73	3.96	20.1	88.1	604	39
5010-01I	1400	3.529	20.57	71.20	4.95	2.48	3.36	40.8	91.4	588	24
5010-01J	1500	2.770	19.93	47.60	8.01	2.56	3.44	49.8	96.8	563	15
5010-01K	1750	2.665	16.34	45.84	4.80	3.12	1.27	49.6	100	540	18
integrated age				n=10	149	2.70	0.269			567	26
plateau age (steps cc-j, 90.6% 39Ar)										**565.1**	**6.0**
mean age (steps cc-ee, 60.5% 39Ar)										**564.1**	**5.7**

Appendix II. $^{40}Ar/^{39}Ar$ Furnace Age Spectrum Data

Run ID#	Temp °C	$^{40}Ar/^{39}Ar$	$^{37}Ar/^{39}Ar$ x10^{-2}	$^{36}Ar/^{39}Ar$ x10^{-4}	^{39}Ar moles x10^{-15}	K/Ca	Cl/K x10^{-4}	$\%^{40}Ar^*$	$\%^{39}Ar$	Age (ka)	± 2 s.d.
WCM93-137, NM-32, 134.2 mg, J=0.0002237											
West Merram, finger, crystal-rich trachyte lava											
5023-01A	550	3.942	18.56	87.25	2.42	2.75	2.91	35.0	1.45	556	32
5023-01B	700	2.131	21.28	24.59	10.6	2.40	2.51	66.6	7.77	573.3	8.6
5023-01C	800	1.766	20.68	12.02	24.2	2.47	2.29	80.8	22.2	575.6	4.9
5023-01D	900	1.693	19.94	9.455	28.3	2.56	1.94	84.4	39.1	576.7	4.0
5023-01E	1000	1.986	19.06	19.56	27.3	2.68	2.22	71.6	55.4	574.3	5.9
5023-01F	1100	1.856	16.93	14.92	23.6	3.01	1.82	76.9	69.5	576.1	5.4
5023-01G	1250	1.970	14.11	17.33	22.2	3.62	1.00	74.5	82.7	592.8	5.7
5023-01H	1300	2.281	13.64	25.70	9.93	3.74	1.71	67.2	88.7	618.4	9.9
5023-01I	1350	2.034	13.28	19.35	5.36	3.84	1.94	72.4	91.9	594	12
5023-01J	1425	1.881	20.47	12.80	1.35	2.49	1.27	80.7	92.7	613	40
5023-01K	1500	2.009	17.20	20.29	7.33	2.97	2.68	70.8	97.0	574.1	8.8
5023-01L	1750	2.802	11.13	49.86	4.95	4.58	2.54	47.7	100.0	539	16
integrated age				n=12	167	2.95	0.70			**579.8**	**7.0**
plateau age (steps b-f, 67.9% 39Ar)										**575.7**	**2.6**
WCM93-138, NM-32, 40 mg, J=0.0002223											
West Merram, base crystal-rich trachyte lava											
5030-01C	800	1.471	7.581	1.627	2.02	6.73	5.07	97.1	3.03	573	50
5030-01D	900	1.571	5.159	2.758	3.95	9.89	2.01	95.1	8.93	599	30
5030-01E	1000	1.510	3.954	-1.213	5.25	12.90	2.58	103	16.8	621	19
5030-01F	1100	1.592	3.734	5.336	6.39	13.66	1.64	90.3	26.4	576	18
5030-01G	1200	1.456	2.742	0.7442	8.12	18.61	1.10	98.6	38.5	576	14
5030-01H	1250	2.412	2.582	32.21	6.80	19.76	1.44	60.6	48.7	586	19
5030-01I	1300	1.706	2.669	-1.642	5.60	19.12	-0.164	103	57.1	704	20
5030-01J	1350	3.019	2.584	50.09	8.69	19.74	1.34	51.0	70.1	618	19
5030-01K	1400	1.117	2.978	-13.90	4.33	17.13	1.64	137	76.6	613	24
5030-01L	1500	1.757	2.292	10.20	10.026	22.26	2.01	82.9	91.6	584	10
5030-01M	1750	4.495	2.184	108.3	5.64	23.36	3.13	28.8	100	520	35
integrated age				n=11	66.8	18.0	5.23			**597**	**20**
mean age (steps f-h, 30.7% 39Ar)										**579**	**12**

Appendix II. $^{40}Ar/^{39}Ar$ Furnace Age Spectrum Data

Run ID#	Temp °C	$^{40}Ar/^{39}Ar$	$^{37}Ar/^{39}Ar$ x10^{-2}	$^{36}Ar/^{39}Ar$ x10^{-4}	^{39}Ar moles x10^{-15}	K/Ca	Cl/K x10^{-4}	$\%^{40}Ar^*$	$\%^{39}Ar$	Age (ka)	± 2 s.d.
WCM93-135, NM-36, 101.5 mg, J=0.0002161											
Kraut Rocks, clastogenic phonolite lava											
5349-01B	700	1.980	0.9045	11.20	0.74	56.4	-2.090	83.3	0.71	643	44
5349-01C	800	1.961	0.8841	14.76	1.88	57.7	-0.401	77.8	2.51	595	29
5349-01D	900	1.602	0.8073	2.981	3.27	63.2	-0.453	94.5	5.66	590	17
5349-01E	1000	1.530	0.7746	0.561	5.62	65.9	0.444	98.9	11.1	590	10
5349-01F	1100	1.515	0.8234	1.362	10.9	62.0	1.02	97.4	21.5	575.0	6.1
5349-01G	1200	1.506	0.8181	1.086	15.0	62.4	2.85	97.9	35.9	574.6	5.5
5349-01H	1250	1.610	0.8144	5.075	11.7	62.6	1.84	90.7	47.2	569.4	7.6
5349-01I	1300	1.544	0.8112	1.827	11.0	62.9	1.14	96.5	57.7	580.8	7.3
5349-01J	1350	1.550	0.7818	2.645	15.3	65.3	1.95	95.0	72.4	573.9	5.3
5349-01K	1400	1.653	0.8025	3.416	3.32	63.6	0.500	93.9	75.6	605	22
5349-01L	1500	1.960	0.7662	16.32	14.11	66.6	2.092	75.4	89.2	576.1	9.2
5349-01M	1750	2.097	0.7468	21.91	11.29	68.3	1.327	69.1	100.0	565	11
integrated age				n=12	104.11	64.2	3.410			**576.9**	**8.8**
plateau age (steps f-j, 61.3% 39Ar)										**574.7**	**4.1**
WCM93-09wr, NM-33, 46.7 mg., J=0.0015007											
Mefford Knoll, aphyric trachyte flow levee											
5141-01B	800	0.6773	4.917	15.67	68.78	10.4	2.01	32.2	28.2	590	23
5141-01C	900	0.7173	5.396	16.22	27.20	9.45	1.88	33.7	39.3	655	38
5141-01D	1000	0.8744	7.981	22.08	22.50	6.39	2.36	26.0	48.5	617	43
5141-01E	1100	1.378	18.57	39.76	56.16	2.75	2.53	15.7	71.5	586	46
5141-01F	1250	1.275	30.27	36.69	69.65	1.69	2.55	16.8	100	578	39
integrated age				n=5	244.3	5.68	3.88			**595**	**36**
plateau age (steps c-f, 71.8% 39Ar)										**611**	**30**

Appendix II. $^{40}Ar/^{39}Ar$ Furnace Age Spectrum Data

Run ID#	Temp °C	$^{40}Ar/^{39}Ar$	$^{37}Ar/^{39}Ar$ x10^{-2}	$^{36}Ar/^{39}Ar$ x10^{-4}	^{39}Ar moles x10^{-15}	K/Ca	Cl/K x10^{-4}	$\%^{40}Ar^*$	$\%^{39}Ar$	Age (ka)	± 2 s.d.
Mt. Berlin- distal englacial tephra layers at Mt. Moulton											
WCM93-313, NM-32, 85.5 mg, J=0.0002285											
Mt. Moulton, Prahl Crag, distal Berlin tephra 5											
5002-12C	800	4.444	1.530	146.3	1.27	33.3	2.40	2.7	0.7	49	68
5002-12D	900	1.851	1.355	58.56	8.86	37.7	1.00	6.5	5.3	50	15
5002-12E	1000	1.161	1.440	36.48	12.7	35.4	1.50	7.2	12.0	34.4	9.5
5002-12F	1100	1.180	1.448	37.61	18.8	35.2	1.76	5.9	22.0	28.6	8.5
5002-12G	1200	0.4876	1.494	14.79	25.0	34.2	1.85	10.6	35.2	21.3	4.5
5002-12H	1250	0.2528	1.407	5.855	20.8	36.3	1.86	31.9	46.2	33.1	3.9
5002-12I	1300	0.2586	1.375	6.012	18.1	37.1	2.33	31.6	55.7	33.5	4.5
5002-12J	1350	0.3063	1.528	8.383	20.7	33.4	1.26	19.4	66.6	24.5	4.1
5002-12K	1400	0.2806	1.505	8.510	16.5	33.9	1.11	10.7	75.4	12.5	5.6
5002-12L	1500	0.1650	1.297	4.906	23.5	39.3	2.00	12.6	87.8	8.6	3.7
5002-12M	1750	0.1399	1.441	3.282	23.2	35.4	1.51	31.3	100.0	18.1	3.4
integrated age				n=11	189	35.7	1.90			**24.5**	**5.9**
mean age (steps e-m, 94.7% 39Ar)										**22.0**	**6.5**
mean age (steps k-m, 33.4% 39Ar)										**13.4**	**3.8**
WCM93-313, NM-36, 183 mg, J=0.0002169											
Mt. Moulton, Prahl Crag, distal Berlin tephra 5											
5358-01B	700	1.480	1.502	47.59	3.64	34.0	0.27	5.1	1.3	29	26
5358-01C	800	0.5611	1.320	16.86	10.5	38.6	1.98	11.3	5.2	24.9	10.5
5358-01D	900	0.3211	1.259	8.871	21.8	40.5	1.28	18.6	13.2	23.4	4.9
5358-01E	1000	0.2106	1.291	5.941	40.5	39.5	1.58	17.0	28.0	14.0	2.7
5358-01F	1100	0.1600	1.347	4.098	55.3	37.9	1.66	24.8	48.3	15.5	1.7
5358-01G	1200	0.2064	1.398	4.868	47.6	36.5	1.82	30.7	65.8	24.7	2.2
5358-01H	1250	0.2087	1.404	4.960	34.5	36.3	1.87	30.2	78.5	24.5	2.8
5358-01I	1300	0.2572	1.451	6.956	24.9	35.2	1.35	20.4	87.6	20.6	4.1
5358-01J	1350	0.4944	1.467	15.42	18.1	34.8	1.73	8.0	94.2	15.5	5.9
5358-01K	1400	0.2586	1.549	6.614	7.04	32.9	0.04	24.8	96.8	25	12
5358-01L	1500	0.8741	2.344	28.15	2.82	21.8	4.51	5.0	97.9	17	32
5358-01M	1750	12.64	1.443	421.5	5.83	35.4	0.87	1.5	100.0	73	77
integrated age				n=12	273	37.1	4.83			**21.2**	**5.7**
mean age (steps c-j, 92.9% 39Ar)										**19.3**	**3.6**
mean age (steps e-f, 35.1% 39Ar)										**15.0**	**1.6**

Appendix II. $^{40}Ar/^{39}Ar$ Furnace Age Spectrum Data

Run ID#	Temp °C	$^{40}Ar/^{39}Ar$	$^{37}Ar/^{39}Ar$ x10^{-2}	$^{36}Ar/^{39}Ar$ x10^{-4}	^{39}Ar moles x10^{-15}	K/Ca	Cl/K x10^{-4}	$\%^{40}Ar^*$	$\%^{39}Ar$	Age (ka)	± 2 s.d.
WCM93-315, NM-32, 104.8 mg, J=0.0002285											
Mt. Moulton, Prahl Crag, distal Berlin tephra 4											
5004-11B	700	12.54	3.019	412.7	0.588	16.9	4.77	2.7	0.3	141	173
5004-11C	800	5.371	1.596	162.2	1.00	32.0	2.98	10.7	0.8	238	101
5004-11D	900	1.966	1.523	61.48	5.21	33.5	3.29	7.6	3.5	62	22
5004-11E	1000	2.806	1.500	36.50	9.60	34.0	3.11	61.6	8.4	712.6	14
5004-11F	1100	1.257	1.456	38.79	15.8	35.1	1.66	8.8	16.6	45.8	9.1
5004-11G	1200	0.7483	1.411	20.77	22.2	36.2	2.52	18.1	28.0	55.7	6.0
5004-11H	1250	0.2480	1.405	3.650	20.0	36.3	1.92	56.9	38.3	58.1	4.7
5004-11I	1300	0.2626	1.395	4.659	19.3	36.6	1.64	47.9	48.3	51.8	4.4
5004-11J	1350	0.1723	1.380	2.346	20.2	37.0	1.67	60.3	58.7	42.8	4.1
5004-11K	1400	0.1934	1.256	4.078	16.3	40.6	1.32	38.1	67.0	30.3	5.4
5004-11L	1500	0.0960	1.101	0.8674	35.5	46.3	1.58	74.0	85.3	29.2	2.4
5004-11M	1750	0.1277	0.950	1.431	28.5	53.7	1.91	67.3	100.0	35.5	3.1
integrated age				n=12	194	40.8	8.70			**77.3**	**6.5**
mean age (steps k-m, 41.3% 39Ar)										**31.5**	**4.5**
WCM93-315, NM-36, 180 mg, J=0.0002170											
Mt. Moulton, Prahl Crag, distal Berlin tephra 4											
5352-01C	800	0.7664	1.518	23.12	8.68	33.6	1.51	11.0	4.0	33	12
5352-01D	900	0.3013	1.480	8.816	17.8	34.5	2.41	13.9	12.2	16.3	4.9
5352-01E	1000	0.2264	1.592	5.339	32.9	32.1	1.65	30.8	27.4	27.3	3.4
5352-01F	1100	0.1774	1.685	4.239	45.0	30.3	1.55	30.0	48.2	20.9	1.9
5352-01G	1200	0.2253	1.761	5.602	35.926	28.97	1.871	27.0	64.8	23.9	2.7
5352-01H	1250	0.2838	1.759	7.304	25.5	29.0	1.61	24.3	76.5	27.1	4.5
5352-01I	1300	0.2575	1.842	6.443	19.8	27.7	1.46	26.5	85.7	26.7	5.8
5352-01J	1350	0.2201	1.976	6.316	13.0	25.8	1.15	15.8	91.7	13.5	6.9
5352-01K	1400	0.2005	2.089	5.701	5.72	24.4	1.95	16.7	94.3	13.1	18
5352-01L	1500	0.2993	1.730	3.877	2.80	29.5	1.85	62.1	95.6	73	28
5352-01M	1750	5.526	2.254	183.4	9.46	22.6	1.24	2.0	100.0	43	36
integrated age				n=11	217	29.7	3.68			**24.7**	**6.1**
plateau age (steps f-i, 58.3% 39Ar)										**22.6**	**3.0**

Appendix II. $^{40}Ar/^{39}Ar$ Furnace Age Spectrum Data

Run ID#	Temp °C	$^{40}Ar/^{39}Ar$	$^{37}Ar/^{39}Ar$ x10^{-2}	$^{36}Ar/^{39}Ar$ x10^{-4}	^{39}Ar moles x10^{-15}	K/Ca	Cl/K x10^{-4}	$\%^{40}Ar^*$	$\%^{39}Ar$	Age (ka)	± 2 s.d.
WCM93-316, NM-32, 132.3 mg, J=0.0002277											
Mt. Moulton, Prahl Crag, distal Berlin tephra 3											
5005-01C	800	3.928	1.241	120.1	1.65	41.1	1.40	9.7	0.6	157	52
5005-01D	900	0.4634	0.8081	7.667	4.56	63.1	1.55	51.2	2.2	97.4	14
5005-01E	1000	0.4346	0.7337	8.100	9.75	69.5	3.04	45.0	5.7	80.4	6.0
5005-01F	1100	0.3442	0.6859	4.220	18.1	74.4	0.86	63.9	12.1	90.3	3.4
5005-01G	1250	0.2908	1.152	2.420	37.8	44.3	1.78	75.6	25.5	90.3	1.7
5005-01H	1300	0.2898	0.6921	2.334	22.9	73.7	2.66	76.3	33.6	90.8	2.7
5005-01I	1350	0.3737	0.6522	4.809	24.3	78.2	2.57	62.0	42.2	95.3	2.9
5005-01J	1425	0.2409	0.6414	0.531	27.0	79.6	2.52	93.6	51.8	92.7	2.3
5005-01K	1500	0.2420	0.7263	0.727	83.2	70.2	1.71	91.3	81.3	90.75	0.93
5005-01L	1750	0.2634	0.9559	1.408	52.6	53.4	1.57	84.4	100.0	91.2	1.3
integrated age				n=10	282	65.4	13.89			**91.5**	**2.4**
plateau age (steps j-l, 57.8% 39Ar)										**91.1**	**1.1**
mean age (steps f-l, 94.3% 39Ar)										**91.1**	**1.1**
WCM93-316, NM-36, 196.1 mg, J=0.0002169											
Mt. Moulton, Prahl Crag, distal Berlin tephra 3											
5361-01C	800	1.571	0.9174	43.79	10.2	55.6	1.64	17.7	3.6	108.4	14
5361-01D	900	0.7859	0.7672	18.49	21.5	66.5	2.93	30.5	10.9	93.8	7.4
5361-01E	1000	0.5365	0.7430	10.09	47.0	68.7	1.90	44.5	27.0	93.3	3.2
5361-01F	1100	0.4204	0.7282	6.265	68.3	70.1	1.83	56.0	50.3	92.3	2.0
5361-01G	1200	0.4352	0.8144	6.820	56.1	62.6	1.73	53.8	69.4	91.6	2.7
5361-01H	1250	0.5727	0.7223	11.18	42.0	70.6	1.67	42.4	83.7	95.1	3.6
5361-01I	1300	0.5719	0.7107	11.35	24.9	71.8	1.36	41.4	92.2	92.7	4.7
5361-01J	1350	0.5422	0.7975	10.63	13.7	64.0	1.12	42.2	96.9	89.5	7.1
5361-01K	1400	0.6198	0.8162	14.36	4.04	62.5	3.17	31.6	98.3	77	21
5361-01L	1500	0.5898	0.8613	9.112	1.96	59.2	2.96	54.4	99.0	126	46
5361-01M	1750	2.928	0.8421	93.55	3.17	60.6	2.44	5.6	100.0	64	34
5361-01N	1750	22.27	0.9862	739.8	0.30	51.7	15.3	1.8	100	158	347
integrated age				n=12	293	67.3	6.2			**93.1**	**5.1**
plateau age (steps d-l, 95.6% 39Ar)										**92.6**	**1.8**

Appendix II. $^{40}Ar/^{39}Ar$ Furnace Age Spectrum Data

Run ID#	Temp °C	$^{40}Ar/^{39}Ar$	$^{37}Ar/^{39}Ar$ x10^{-2}	$^{36}Ar/^{39}Ar$ x10^{-4}	^{39}Ar moles x10^{-15}	K/Ca	Cl/K x10^{-4}	$\%^{40}Ar^*$	$\%^{39}Ar$	Age (ka)	± 2 s.d.
WCM93-317, NM-32, 101.2 mg, J=0.0002277											
Mt. Moulton, Prahl Crag, distal Berlin tephra 2											
5006-01B	700	2.485	1.191	75.12	2.59	42.8	0.15	10.7	1.2	109	31
5006-01C	800	1.698	1.324	49.51	2.12	38.5	1.49	13.9	2.2	97	31
5006-01D	900	0.993	1.128	25.18	5.04	45.2	1.27	25.1	4.6	102.4	14
5006-01E	1000	0.554	1.040	10.70	10.4	49.1	1.84	43.1	9.6	98.1	6.9
5006-01F	1100	0.547	1.006	10.45	17.6	50.7	1.63	43.6	18.0	98.1	4.6
5006-01G	1250	0.355	1.011	3.449	38.7	50.5	1.25	71.5	36.4	104.3	2.0
5006-01H	1300	0.272	0.933	0.378	23.8	54.7	2.01	96.1	47.7	107.3	2.4
5006-01I	1350	0.258	0.910	0.262	28.1	56.0	2.05	97.2	61.0	102.8	2.3
5006-01J	1425	0.284	0.891	1.162	24.4	57.2	2.55	88.1	72.6	102.8	2.3
5006-01K	1500	0.348	0.848	3.115	28.6	60.1	2.10	73.7	86.2	105.4	2.6
5006-01L	1750	0.271	0.834	0.521	29.0	61.2	1.39	94.5	100.0	105.2	1.9
integrated age				n=11	210	54.9	7.22			**103.6**	**3.6**
plateau age (steps g-l, 82.0% 39Ar)										**104.6**	**1.6**
WCM93-317, NM-36, 139 mg, J=0.0002157											
Mt. Moulton, Prahl Crag, distal Berlin tephra 2											
5362-01C	800	1.651	0.8322	43.79	4.00	61.3	1.77	21.6	1.9	139	26
5362-01D	900	0.8396	0.7879	18.19	9.38	64.8	2.26	36.0	6.5	117.6	11
5362-01E	1000	0.5544	0.8168	9.305	23.8	62.5	2.02	50.5	18.0	108.8	5.0
5362-01F	1100	0.4270	0.8140	5.036	42.7	62.7	2.25	65.2	38.7	108.4	2.7
5362-01G	1200	0.4430	0.8535	5.934	39.5	59.8	2.15	60.5	57.8	104.3	2.6
5362-01H	1250	0.4106	0.8122	4.613	33.0	62.8	1.71	66.9	73.8	106.9	3.2
5362-01I	1300	0.4837	0.7830	6.764	22.3	65.2	2.13	58.8	84.6	110.5	4.6
5362-01J	1350	0.4067	0.7533	4.218	16.3	67.7	1.48	69.4	92.5	109.9	5.8
5362-01K	1400	0.4317	0.7490	4.631	6.22	68.1	1.14	68.4	95.5	114.8	14
5362-01L	1500	0.8125	0.9762	23.16	2.20	52.3	6.42	15.8	96.6	50.1	41
5362-01M	1750	0.7992	0.7552	19.77	7.06	67.6	2.30	26.9	100.0	83.9	14
integrated age				n=11	207	63.1	4.5			**107.5**	**5.4**
plateau age (steps d-k, 93.6% 39Ar)										**107.5**	**2.4**
plateau age (steps e-j, 86.0% 39Ar)										**107.2**	**2.4**

Appendix II. $^{40}Ar/^{39}Ar$ Furnace Age Spectrum Data

Run ID#	Temp °C	$^{40}Ar/^{39}Ar$	$^{37}Ar/^{39}Ar$ x10^{-2}	$^{36}Ar/^{39}Ar$ x10^{-4}	^{39}Ar moles x10^{-15}	K/Ca	Cl/K x10^{-4}	$\%^{40}Ar^*$	$\%^{39}Ar$	Age (ka)	± 2 s.d.
WCM93-314, NM-36, 76.3 mg, J=0.0002157											
Mt. Moulton, Prahl Crag, distal Berlin tephra 1											
5359-01C	800	1.028	0.597	23.51	4.21	85.5	1.07	32.4	4.1	130	19
5359-01D	900	0.5762	0.599	9.132	9.78	85.2	1.99	53.2	13.6	119.4	7.5
5359-01E	1000	0.4535	0.572	5.521	18.3	89.2	1.15	64.1	31.5	113.1	4.1
5359-01F	1100	0.4334	0.560	4.421	24.5	91.0	2.28	69.9	55.4	117.9	3.8
5359-01G	1200	0.4457	0.578	4.767	19.7	88.2	2.04	68.5	74.6	118.7	4.3
5359-01H	1250	0.4277	0.562	3.892	11.9	90.7	0.89	73.2	86.2	121.7	6.9
5359-01I	1300	0.4619	0.550	4.494	7.02	92.7	1.94	71.3	93.0	128	12
5359-01J	1350	0.3784	0.592	0.570	3.69	86.2	2.65	95.6	96.6	141	20
5359-01K	1400	0.3869	0.714	3.214	1.42	71.5	1.50	75.5	98.0	114	55
5359-01M	1750	14.90	1.024	492.8	2.04	49.8	0.92	2.3	100.0	134	112
integrated age				n=9	234	88.2	13.1			**120.0**	**9.3**
plateau age (steps d-i, 87.3% 39Ar)										**117.6**	**3.6**

Mt. Siple summit crater

WCM93-278, NM-32, 121.6 mg, J=0.0002178											
Mt. Siple, ridge near summit, crystal rich lava											
5028-01B	700	1.225	5.713	26.45	7.47	8.93	1.25	36.5	3.1	176	11
5028-01C	800	0.7951	5.594	13.03	25.2	9.12	1.90	52.1	13.5	162.8	3.5
5028-01D	900	0.6518	5.386	7.686	30.6	9.47	1.94	65.8	26.1	168.4	2.7
5028-01E	1000	0.6320	5.275	7.235	27.2	9.67	2.56	66.8	37.3	165.8	2.7
5028-01F	1100	0.9048	5.259	16.53	20.2	9.70	1.28	46.4	45.6	165.2	4.6
5028-01G	1250	1.086	5.203	22.33	42.0	9.81	2.66	39.6	62.9	168.8	4.4
5028-01H	1300	1.004	4.786	19.62	33.0	10.7	1.94	42.6	76.5	168.2	4.5
5028-01I	1350	0.8853	4.618	15.30	25.2	11.0	2.71	49.3	86.9	171.6	4.3
5028-01J	1425	1.031	4.976	21.59	3.45	10.3	2.15	38.5	88.3	156	16
5028-01K	1500	2.105	5.067	55.48	13.2	10.1	2.48	22.3	93.7	185	14
5028-01L	1750	1.246	4.686	27.80	15.2	10.9	1.60	34.3	100.0	168.2	7.9
integrated age				n=11	243	9.98	0.69			**168.5**	**5.0**
plateau age (steps d-h, 63.0% 39Ar)										**167.2**	**2.1**

Appendix II. $^{40}Ar/^{39}Ar$ Furnace Age Spectrum Data

Run ID#	Temp °C	$^{40}Ar/^{39}Ar$	$^{37}Ar/^{39}Ar$ x10^{-2}	$^{36}Ar/^{39}Ar$ x10^{-4}	^{39}Ar moles x10^{-15}	K/Ca	Cl/K x10^{-4}	%^{40}Ar*	%^{39}Ar	Age (ka)	± 2 s.d.
WCM93-277, NM-15, 17.3 mg, J=0.0014339											
Mt. Siple, summit crater wall, densely welded fall											
1871-01D	850	0.1523	3.420	1.245	19.9	14.9	1.16	56.5	6.3	223	19
1871-01E	1000	0.1335	3.542	0.6399	87.5	14.4	1.02	63.9	33.9	220.6	4.9
1871-01F	1150	0.1300	3.260	0.4852	58.7	15.6	1.30	66.3	52.4	222.8	6.3
1871-01G	1300	0.1664	3.525	1.637	59.7	14.5	1.36	53.3	71.2	229.5	6.5
1871-01H	1450	0.1881	3.119	2.534	44.4	16.4	1.43	44.5	85.2	216	10
1871-01I	1750	0.4946	2.732	12.82	38.2	18.7	1.22	17.4	97.3	222	19
1871-01J	1750	4.518	2.327	139.6	8.63	21.9	1.59	8.1	100.0	941	156
integrated age				n=7	317	15.7	2.76			**242**	**13**
plateau age (steps d-f, 52.4% 39Ar)										**221.5**	**4.1**
mean age (steps d-i, 97.3% 39Ar)										**222.8**	**4.7**
WCM93-277, NM-36, 96.8 mg, J=0.0002178											
Mt. Siple, summit crater wall, densely welded fall											
5025-01C	800	0.7714	0.8013	5.899	3.00	63.7	2.03	77.5	2.53	235	17
5025-01D	900	0.6670	0.7739	3.112	8.04	65.9	0.944	86.3	9.33	226.0	7.7
5025-01E	1000	0.6247	0.7471	1.555	10.3	68.3	1.58	92.7	18.0	227.5	7.4
5025-01F	1100	0.6246	0.7170	1.312	9.13	71.2	0.940	93.8	25.7	230.3	7.5
5025-01G	1200	0.7305	0.7487	5.086	10.6	68.1	2.19	79.5	34.7	228.2	9.1
5025-01H	1250	0.9002	0.7968	11.28	10.8	64.0	1.94	63.0	43.8	222.8	8.4
5025-01I	1300	1.093	0.7344	17.93	15.2	69.5	2.72	51.6	56.6	221.5	7.8
5025-01J	1350	1.162	0.7398	20.12	17.2	69.0	1.62	48.9	71.2	223.2	7.3
5025-01K	1400	1.050	0.6987	16.01	9.20	73.0	2.08	55.0	78.9	227	10
5025-01L	1500	1.387	0.7456	27.18	11.7	68.4	1.50	42.1	88.8	229	10
5025-01M	1750	2.678	0.7243	70.88	13.2	70.4	0.987	21.8	100.0	229	17
integrated age				n=11	118	68.7	2.87			**226.4**	**9.6**
plateau age (steps g-m, 74.3% 39Ar)										**224.9**	**4.2**

Appendix II. $^{40}Ar/^{39}Ar$ Furnace Age Spectrum Data

Run ID#	Temp °C	$^{40}Ar/^{39}Ar$	$^{37}Ar/^{39}Ar$ x10^{-2}	$^{36}Ar/^{39}Ar$ x10^{-4}	^{39}Ar moles x10^{-15}	K/Ca	Cl/K x10^{-4}	$\%^{40}Ar^*$	$\%^{39}Ar$	Age (ka)	± 2 s.d.
WCM93-277, NM-32, 130.5 mg, J=0.0002178											
Mt. Siple, summit crater wall, densely welded fall											
5026-01B	700	1.819	4.240	41.46	5.04	12.0	1.65	32.8	2.0	234	16
5026-01C	800	1.156	4.064	19.49	21.2	12.6	1.03	50.4	10.3	229.2	5.5
5026-01D	900	1.025	3.864	15.40	29.2	13.2	2.12	55.9	21.7	224.9	3.9
5026-01E	1000	1.047	3.716	16.44	31.3	13.7	2.10	53.9	34.0	221.7	4.2
5026-01F	1100	1.290	3.609	24.98	24.5	14.1	1.63	43.0	43.6	217.6	5.2
5026-01G	1250	2.358	3.946	61.55	41.9	12.9	2.36	23.0	60.0	213	10
5026-01H	1300	2.316	3.857	59.52	30.1	13.2	2.10	24.2	71.8	220	10
5026-01I	1350	2.020	3.677	49.94	30.4	13.9	1.96	27.1	83.8	214.8	8.6
5026-01J	1425	2.051	3.524	52.94	4.79	14.5	4.24	23.9	85.7	192	17
5026-01K	1500	2.270	4.116	56.64	14.9	12.4	2.10	26.4	91.5	236	12
5026-01L	1750	2.709	3.801	71.81	21.7	13.4	2.77	21.8	100.0	232	13
integrated age				n=11	255	13.3	0.758			**221.2**	**8.2**
mean age (steps c-i, 81.8% 39Ar)										**222.2**	**4.2**

Mt. Takahe summit crater

W85-09, G1: NM-36, 118.3 mg, J=0.0002156											
Mt. Takahe, Bucher Rim, south end, lowest unit, pumice & obsidian bombs											
5342-01C	800	1.4424	4.752	48.70	2.34	10.7	1.24	0.5	1.6	3	41
5342-01D	900	0.4021	4.623	15.16	5.40	11.0	2.89	-10.6	5.3	-16.6	15.2
5342-01E	1000	0.3003	4.669	10.11	11.3	10.9	3.45	1.6	13.0	1.9	7.6
5342-01F	1100	0.1736	4.632	5.672	21.2	11.0	1.62	5.4	27.4	3.7	5.5
5342-01G	1200	0.1769	4.607	5.168	28.6	11.1	2.33	15.6	46.9	10.8	4.2
5342-01H	1250	0.1811	4.627	5.242	25.9	11.0	1.96	16.3	64.6	11.4	4.2
5342-01I	1300	0.1779	4.602	5.587	22.1	11.1	2.13	9.0	79.7	6.2	4.7
5342-01J	1350	0.2088	4.567	6.338	17.8	11.2	1.42	11.9	91.8	10	6
5342-01K	1400	0.2322	4.543	6.216	7.26	11.2	2.44	22.30	96.7	20	14
5342-01L	1500	0.876	4.551	29.05	4.79	11.2	2.08	2.40	100	8	22
integrated age				n=10	147	11.1	0.15			**7.6**	**7.0**
plateau age (steps e-l, 94.7% 39Ar)										**8.5**	**3.4**

Appendix II. $^{40}Ar/^{39}Ar$ Furnace Age Spectrum Data

Run ID#	Temp °C	$^{40}Ar/^{39}Ar$	$^{37}Ar/^{39}Ar$ x10^{-2}	$^{36}Ar/^{39}Ar$ x10^{-4}	^{39}Ar moles x10^{-15}	K/Ca	Cl/K x10^{-4}	$\%^{40}Ar^*$	$\%^{39}Ar$	Age (ka)	± 2 s.d.
W85-013, NM-36, 107 mg, J=0.0002168											
Mt. Takahe, Bucher Rim, north end, lava beneath welded fall, peralkaline trachyte											
5379-01C	800	1.329	7.626	38.90	0.774	6.69	1.54	14.0	5.04	72	15
5379-01D	900	0.8676	8.636	23.10	1.39	5.91	2.76	22.1	14.1	74.8	8.3
5379-01E	1000	0.6640	5.021	15.32	2.17	10.2	2.01	32.4	28.2	84.1	6.1
5379-01F	1100	0.5321	4.100	10.32	2.39	12.4	2.00	43.3	43.8	89.9	5.2
5379-01G	1200	0.6830	3.589	14.00	1.80	14.2	1.85	39.8	55.5	106.2	7.5
5379-01H	1250	0.6876	3.627	13.87	1.70	14.1	1.11	40.8	66.6	109.7	6.7
5379-01I	1300	0.5621	5.224	10.78	2.19	9.77	2.05	44.0	80.9	96.8	4.5
5379-01J	1350	0.4041	5.171	6.120	1.64	9.87	1.22	56.2	91.5	88.8	5.6
5379-01K	1400	0.3863	5.656	6.087	0.462	9.02	2.25	54.5	94.5	82	20
5379-01L	1500	0.3519	4.934	4.568	0.113	10.3	3.45	62.7	95.3	86	74
5379-01M	1750	1.632	5.743	46.50	0.726	8.88	2.81	16.1	100.0	103	16
integrated age				n=11	15.37	10.7	2.65			**92.2**	**8.0**
mean age (steps c-k, 94.5% 39Ar)										**92.7**	**7.3**
W85-015, NM-36, 108.2 mg, J=0.0002130											
Mt. Takahe, Bucher rim, north end, trachyte obsidian clast in welded fall, upper unit											
5372-01C	800	3.451	6.750	91.98	0.416	7.56	2.52	21.4	2.6	283	31
5372-01D	900	1.421	7.087	33.29	0.905	7.20	1.06	31.1	8.7	170	12
5372-01E	1000	0.9365	7.382	21.95	1.77	6.91	1.97	31.3	20.5	112.7	7.4
5372-01F	1100	0.7381	7.469	16.63	2.74	6.83	1.78	34.2	38.8	96.8	5.3
5372-01G	1200	0.6439	7.331	13.12	2.69	6.96	2.35	40.6	56.7	100.4	4.7
5372-01H	1250	0.6258	7.006	12.06	2.27	7.28	2.06	43.9	71.8	105.4	5.5
5372-01I	1300	0.6230	6.494	11.80	1.84	7.86	1.44	44.8	84.0	107.3	6.0
5372-01J	1350	0.4746	6.078	8.545	1.26	8.39	1.99	47.7	92.4	87.1	6.9
5372-01K	1400	0.5917	6.512	7.945	0.388	7.84	3.32	61.1	95.0	139	20
5372-01L	1500	0.6666	5.048	14.73	0.287	10.1	4.24	35.2	96.9	90	30
5372-01M	1750	0.9914	5.221	26.50	0.438	9.77	2.38	21.4	99.9	82	19
integrated age				n=11	15.01	7.41	1.12			**111.2**	**8.1**
plateau age (steps f-i, 63.5% 39Ar)										**102.0**	**5.3**

Appendix II. $^{40}Ar/^{39}Ar$ Furnace Age Spectrum Data

Run ID#	Temp °C	$^{40}Ar/^{39}Ar$	$^{37}Ar/^{39}Ar$ x10^{-2}	$^{36}Ar/^{39}Ar$ x10^{-4}	^{39}Ar moles x10^{-15}	K/Ca	Cl/K x10^{-4}	$\%^{40}Ar^*$	$\%^{39}Ar$	Age (ka)	± 2 s.d.
MT85-006, NM-36, 174.3 mg, J=0.0002182											
Mt. Takahe, 9300' outcrop above Benatar?, trachyte lava,											
5357-01C	800	1.675	4.196	42.41	1.06	12.2	1.04	25.4	3.46	167	15
5357-01D	900	0.8306	3.935	14.53	1.93	13.0	1.97	48.6	10.3	159.1	6.2
5357-01E	1000	0.5971	3.690	6.765	3.18	13.8	1.80	67.0	21.5	157.4	3.9
5357-01F	1100	0.6123	3.392	7.470	4.03	15.0	1.86	64.3	35.8	155.1	2.9
5357-01G	1200	0.7711	3.455	12.96	4.95	14.8	1.94	50.7	53.4	153.8	3.7
5357-01H	1250	0.9978	3.782	21.04	6.46	13.5	1.95	38.0	76.3	149.0	4.9
5357-01I	1300	0.8870	3.783	16.66	4.35	13.5	1.48	44.8	91.7	156.6	4.9
5357-01J	1350	0.8283	3.491	11.02	1.22	14.6	0.766	61.0	96.1	198.9	8.9
5357-01K	1400	0.1532	3.404	-9.389	0.207	15.0	0.817	283	96.8	171	48
5357-01L	1500	1.759	3.564	39.83	0.240	14.3	2.10	33.2	97.7	230	34
5357-01M	1750	6.084	3.170	186.5	0.569	16.1	2.28	9.4	100	226	39
integrated age				n=11	28.2	14.0	1.1			**158.8**	**6.2**
plateau age (steps c-i, 91.7% 39Ar)										**155.2**	**2.9**
W85-022, NM-36, 118.2 mg, J=0.0002153											
Mt. Takahe, Bucher rim, south end, >10 m trachyte lava											
5343-01C	800	1.259	2.001	23.29	0.161	25.5	0.385	45.4	1.42	222	61
5343-01D	900	1.201	1.942	24.72	0.357	26.3	3.71	39.3	3.96	183	27
5343-01E	1000	0.6778	1.890	7.215	0.793	27.0	1.81	68.7	9.59	181	13
5343-01F	1100	0.6582	1.828	7.732	1.37	27.9	0.76	65.5	19.3	167.3	8.0
5343-01G	1200	0.5278	1.703	2.766	2.14	30.0	1.87	84.7	34.5	173.5	5.1
5343-01H	1250	0.5494	1.642	3.104	2.13	31.1	1.95	83.5	49.6	178.1	5.5
5343-01I	1300	0.5334	1.645	3.162	2.67	31.0	2.20	82.7	68.6	171.2	4.1
5343-01J	1350	0.4731	1.616	0.740	2.01	31.6	1.88	95.6	82.9	175.7	4.8
5343-01K	1400	0.3134	1.648	-4.827	0.62	31.0	2.19	145.8	87.3	177	16
5343-01L	1500	0.7395	1.773	9.399	0.64	28.8	1.80	62.6	91.9	180	13
5343-01M	1750	6.336	1.630	197.6	1.23	31.3	1.67	7.9	101	194	33
integrated age				n=13	14.1	30.1	4.06			**178**	**10**
mean age (steps f-j, 77.7% 39Ar)										**173.6**	**3.8**

Appendix II. $^{40}Ar/^{39}Ar$ Furnace Age Spectrum Data

Run ID#	Temp °C	$^{40}Ar/^{39}Ar$	$^{37}Ar/^{39}Ar$ x10^{-2}	$^{36}Ar/^{39}Ar$ x10^{-4}	^{39}Ar moles x10^{-15}	K/Ca	Cl/K x10^{-4}	$\%^{40}Ar^*$	$\%^{39}Ar$	Age (ka)	± 2 s.d.
W85-011, NM-36, 112.9 mg, J=0.0002141											
Mt. Takahe, Bucher Rim, south end, 10+ m trachyte lava flow over W85-9 deposits											
5369-01C	800	2.017	1.771	48.63	0.300	28.8	1.62	28.8	1.3	224	32
5369-01D	900	0.9622	1.798	14.60	0.561	28.4	2.49	55.3	4.6	205	18
5369-01E	1000	0.7869	1.771	9.028	1.44	28.8	2.68	66.2	13.2	201.3	6.4
5369-01F	1100	0.7109	1.762	7.126	2.69	29.0	2.32	70.5	29.1	193.5	4.5
5369-01G	1200	0.7808	1.764	10.42	2.81	28.9	1.94	60.7	45.8	183.0	4.8
5369-01H	1250	0.8054	1.753	10.45	2.80	29.1	1.81	61.8	62.4	192.3	5.4
5369-01I	1300	0.7769	1.749	9.885	2.42	29.2	1.67	62.5	76.7	187.5	5.3
5369-01J	1350	0.7174	1.722	7.305	2.01	29.6	1.71	70.1	88.6	194.0	6.0
5369-01K	1400	0.5854	1.734	4.470	0.893	29.4	2.18	77.6	93.9	175	12
5369-01L	1500	0.6774	1.777	6.711	0.345	28.7	3.10	70.9	95.9	185	28
5369-01M	1750	1.138	1.772	20.84	0.505	28.8	1.18	46.0	98.9	202	19
5369-01N	1750	2.169	2.138	76.22	0.106	23.9	4.77	-3.8	99.5	-32	88
integrated age				n=12	16.9	29.0	1.51			**190.1**	**8.0**
mean age (steps e-j, 84.3% 39Ar)										**191.2**	**5.3**

Appendix II. $^{40}Ar/^{39}Ar$ Furnace Age Spectrum Data

Mt. Berlin- Brandenberger Bluff

Run ID#	Temp	$^{40}Ar/^{39}Ar$	$^{37}Ar/^{39}Ar$	$^{36}Ar/^{39}Ar$ x10^{-2}	^{39}Ar moles x10^{-15}	K/Ca	Cl/K x10^{-4}	$\%^{40}Ar^*$	$\%^{39}Ar$	Age (Ma)	± 2 s.d.
WCM93-014, phonotephrite groundmass, NM-33, 79 mg, J=0.0015007											
Mt. Berlin, cinder cone south of Brandenberger Bluff											
5142-01A	500	73.86	0.4693	24.74	2.46	1.087	7.57	1.1	0.8	2.1	2.9
5142-01B	625	2.991	0.4663	0.6814	29.6	1.094	1.74	33.9	10.7	2.742	0.081
5142-01C	700	1.618	0.5641	0.2179	38.3	0.904	1.72	62.9	23.5	2.752	0.039
5142-01D	775	1.430	0.7257	0.1631	34.5	0.703	1.62	70.2	35.0	2.717	0.035
5142-01E	850	1.485	0.7344	0.1810	26.0	0.695	1.68	67.8	43.6	2.725	0.047
5142-01F	925	1.506	0.7328	0.1799	17.5	0.696	2.22	68.4	49.5	2.789	0.061
5142-01G	1050	1.527	0.8119	0.2101	37.2	0.628	2.14	63.4	61.9	2.621	0.039
5142-01H	1125	2.269	1.817	0.4888	100	0.281	3.86	42.5	95.3	2.611	0.057
5142-01I	1200	3.172	6.688	0.9328	13.5	0.0763	5.56	29.3	99.8	2.53	0.13
5142-01J	1450	8.221	7.979	2.5735	0.602	0.0639	6.31	14.9	100.0	3.3	1.3
integrated age					300	0.589	0.37			2.669	0.081
mean age (steps b-i, 99.0% 39Ar)										2.700	0.050

Run ID#	Temp °C	$^{40}Ar/^{39}Ar$	$^{37}Ar/^{39}Ar$ x10^{-2}	$^{36}Ar/^{39}Ar$ x10^{-3}	^{39}Ar moles x10^{-15}	K/Ca	Cl/K x10^{-4}	$\%^{40}Ar^*$	$\%^{39}Ar$	Age (Ma)	± 2 s.d.
WCM93-10, groundmass phonolite, NM-34, 10 mg., J=0.0014461											
Mt. Berlin, Brandenberger Bluff, west end phonolite dome lava											
5237-01B	800	1.578	3.359	1.868	13.6	15.2	1.56	65.2	17.1	2.682	0.045
5237-01C	900	1.532	3.133	1.462	15.5	16.3	2.21	71.9	36.5	2.872	0.046
5237-01D	1000	1.251	2.917	0.610	16.6	17.5	1.36	85.8	57.4	2.796	0.038
5237-01E	1100	1.241	2.741	0.640	14.7	18.6	2.60	84.9	75.8	2.747	0.041
5237-01F	1250	1.179	2.267	0.724	19.2	22.5	2.88	82.0	100.0	2.521	0.031
integrated age				n=5	79.7	18.3	2.82			2.716	0.040
mean age (steps b-f, 100% 39Ar)										2.69	0.13
WCM93-37, groundmass phonolite, NM-34, 25.2 mg., J=0.0014650											
Mt. Berlin, Brandenberger Bluff, east end phonolite lava											
5198-02B	800	16.77	14.21	53.50	32.6	3.59	3.58	5.8	14.6	2.56	0.52
5198-02C	900	18.48	13.95	58.93	47.9	3.66	3.94	5.8	36.1	2.84	0.53
5198-02D	1000	15.30	13.80	48.27	28.2	3.70	2.99	6.8	48.7	2.76	0.38
5198-02E	1100	15.11	13.84	47.53	48.4	3.69	3.37	7.1	70.4	2.84	0.35
5198-02F	1250	15.30	14.27	47.89	66.0	3.57	2.98	7.5	100.0	3.05	0.38
integrated age				n=5	223	3.63	0.06			2.85	0.43
plateau age (steps b-f, 100% 39Ar)										2.83	0.24

Appendix II. $^{40}Ar/^{39}Ar$ Furnace Age Spectrum Data

Run ID#	Temp °C	$^{40}Ar/^{39}Ar$	$^{37}Ar/^{39}Ar$ x10^{-2}	$^{36}Ar/^{39}Ar$ x10^{-3}	^{39}Ar moles x10^{-15}	K/Ca	Cl/K x10^{-4}	$\%^{40}Ar^*$	$\%^{39}Ar$	Age (Ma)	± 2 s.d.
WCM93-53, groundmass trachyte, NM-34, 25.8 mg., J=0.0014650											
Mt. Berlin, Brandenberger Bluff, lava clast in hyalotuff											
5199-02B	800	6.096	8.220	17.11	49.9	6.21	4.34	17.2	26.8	2.77	0.15
5199-02C	900	4.428	9.432	11.47	45.1	5.41	2.00	23.6	51.0	2.76	0.11
5199-02D	1000	3.627	18.68	9.013	17.4	2.73	2.29	27.0	60.3	2.58	0.10
5199-02E	1100	8.517	62.90	25.54	11.2	0.81	2.84	12.0	66.3	2.69	0.21
5199-02F	1250	6.202	42.91	17.63	56.7	1.19	2.78	16.5	96.8	2.70	0.14
5199-02G	1350	5.826	34.15	16.39	5.15	1.49	1.22	17.3	99.5	2.66	0.23
5199-02H	1450	6.678	28.30	19.39	0.875	1.80	-0.29	14.5	100.0	2.56	0.83
integrated age				n=7	186.398	3.69	2.15			2.72	0.14
plateau age (steps b-h, 100% 39Ar)										2.684	0.083
WCM93-69, groundmass trachyte, NM-34, 31.3 mg., J=0.0014650											
Mt. Berlin, Brandenberger Bluff, lava clast in hyalotuff											
5200-02B	800	85.310	14.01	284.5	21.1	3.64	3.46	1.5	10.4	3.3	2.4
5200-02BB	800	161.8	21.06	545.5	2.43	2.42	0.32	0.4	11.6	1.6	4.8
5200-02C	900	72.15	14.80	239.5	30.1	3.45	6.13	1.9	26.5	3.7	2.0
5200-02CC	1000	67.46	22.10	223.3	20.9	2.31	4.18	2.2	36.8	4.0	1.7
5200-02D	1000	55.27	21.66	184.9	3.49	2.36	4.75	1.2	38.5	1.7	1.7
5200-02E	1100	58.42	23.85	193.0	55.5	2.14	4.53	2.4	65.9	3.7	1.6
5200-02EE	1250	47.45	22.38	154.9	69.2	2.28	3.22	3.6	100.0	4.5	1.4
integrated age				n=7	203	2.56	0.62			3.9	1.7
plateau age (steps b-ee, 100% 39Ar)										3.5	1.0
WCM93-121, groundmass phonolite, NM-34, 27.0 mg., J=0.0014650											
Mt. Berlin, Brandenberger Bluff, lava clast in hyalotuff											
5201-02B	800	16.18	14.10	51.18	20.8	3.62	3.05	6.6	8.7	2.81	0.40
5201-02C	900	17.67	11.12	55.96	13.9	4.59	4.63	6.5	14.5	3.02	0.45
5201-02D	1000	20.78	15.73	66.51	49.0	3.24	4.01	5.5	35.0	3.01	0.52
5201-02E	1100	6.650	21.54	19.07	90.7	2.37	3.11	15.5	72.9	2.72	0.14
5201-02F	1250	5.898	17.02	16.48	64.7	3.00	2.06	17.7	100.0	2.75	0.14
integrated age				n=5	239.090	2.96	0.82			2.81	0.26
plateau age (steps b-f, 100% 39Ar)										2.76	0.12

Appendix II. $^{40}Ar/^{39}Ar$ Furnace Age Spectrum Data

Run ID#	Temp °C	$^{40}Ar/^{39}Ar$	$^{37}Ar/^{39}Ar$ x10^{-2}	$^{36}Ar/^{39}Ar$ x10^{-3}	^{39}Ar moles x10^{-15}	K/Ca	Cl/K x10^{-4}	$\%^{40}Ar^*$	$\%^{39}Ar$	Age (Ma)	± 2 s.d.
WCM93-250, groundmass trachyte, NM-34, 25.8 mg., J=0.0014650											
Mt. Berlin, Brandenberger Bluff, lava clast in hyalotuff											
5202-02B	800	7.423	10.61	21.58	33.405	4.81	2.71	14.2	19.0	2.78	0.18
5202-02C	900	6.364	11.46	18.03	9.505	4.45	1.88	16.4	24.4	2.76	0.18
5202-02D	1000	10.06	19.62	30.42	19.686	2.60	2.66	10.8	35.7	2.88	0.25
5202-02E	1100	6.634	27.93	19.17	42.438	1.83	3.20	14.9	59.8	2.61	0.15
5202-02F	1250	4.705	23.18	12.66	62.144	2.20	2.45	20.9	95.3	2.59	0.11
5202-02G	1350	4.223	19.35	10.61	8.335	2.64	2.17	26.1	100.0	2.91	0.18
integrated age				n=6	175.513	2.79	1.24			2.69	0.15
plateau age (steps b-f, 95.3% 39Ar)										2.67	0.12

	Age (Ma)	± 2 s.d.
Compilation of Berlin mean/plateau ages		
WCM93-10 mean age	2.83	0.13
WCM93-37 plateau age	2.68	0.08
WCM93-53 plateau age	2.76	0.12
WCM93-121 plateau age	2.67	0.12
WCM93-250 plateau age	2.69	0.13
mean Brandenberger Bluff age (n=5)	**2.717**	**0.075**

Appendix III.: Age Spectrum Plots of Furnace Step-heating Data

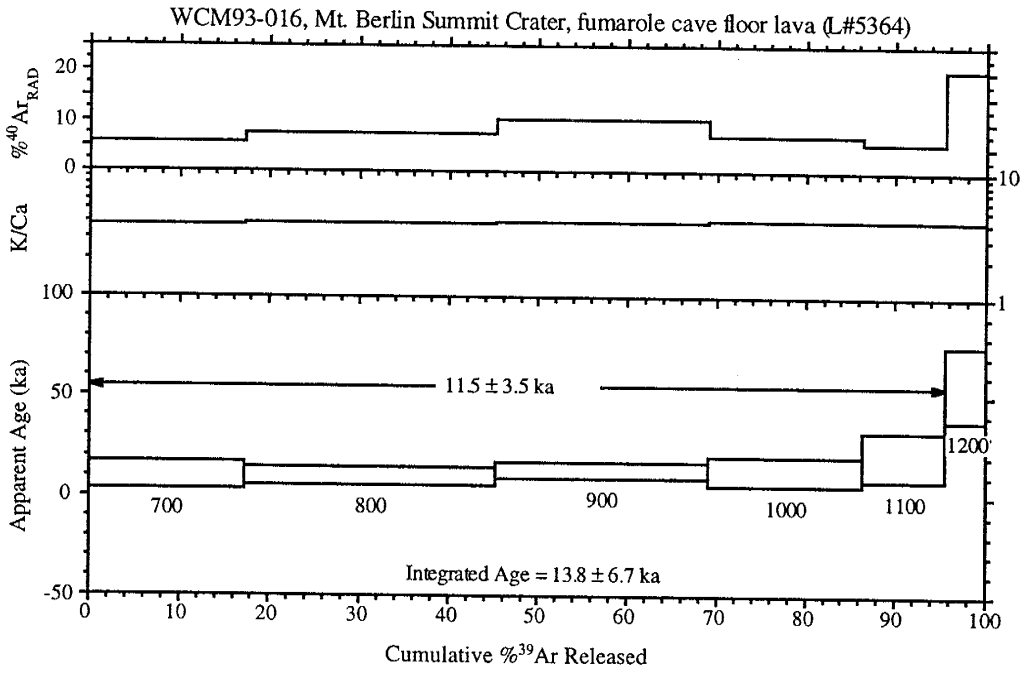

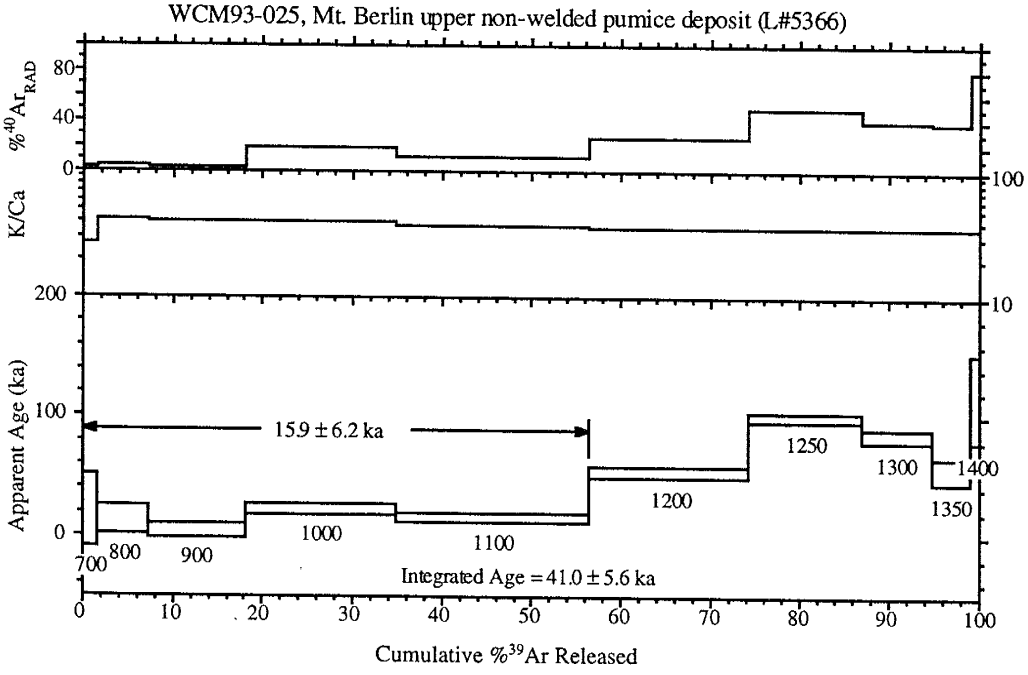

Appendix III.: Age Spectrum Plots of Furnace Step-heating Data

WCM93-22, Mt. Berlin Summit Crater, highly vesicular laminated pumice (L#5014)

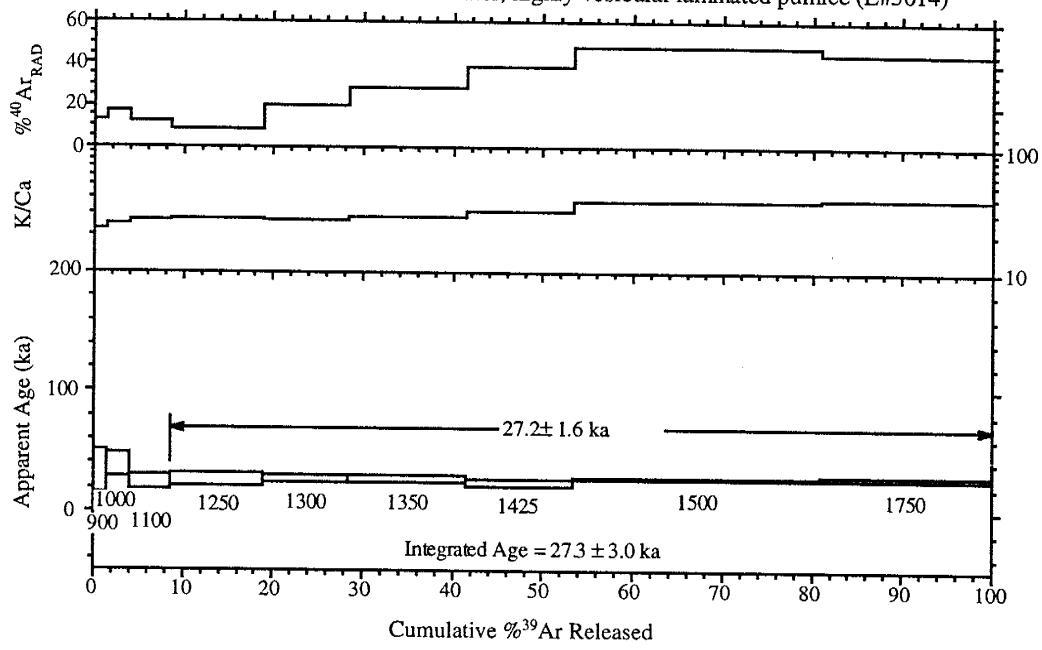

WCM93-22, Mt. Berlin Summit Crater, highly vesicular laminated pumice (L#5347)

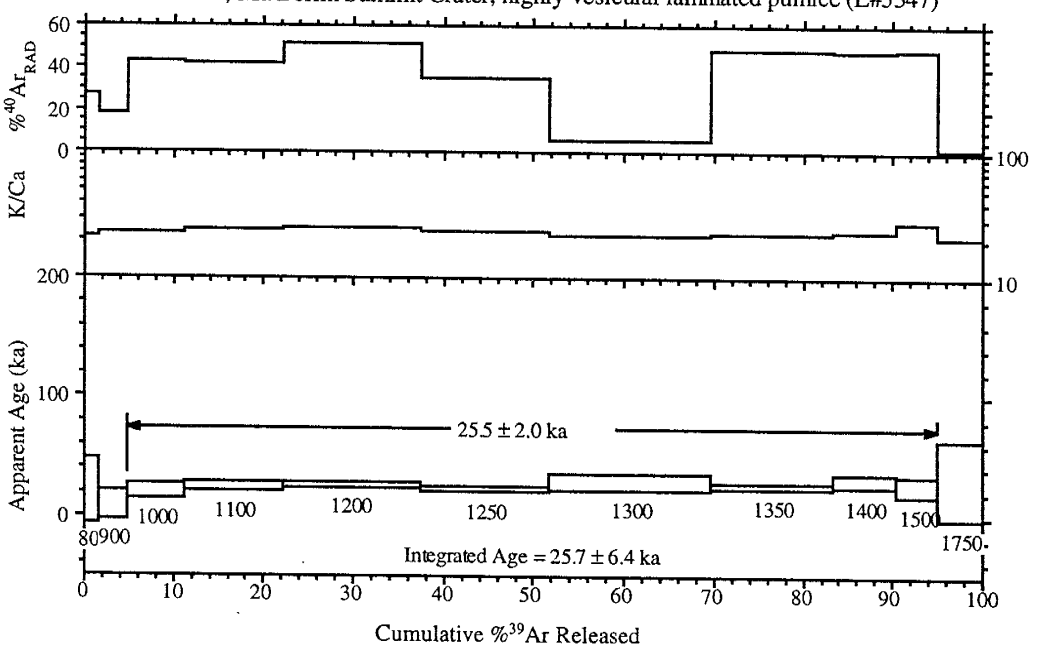

Appendix III.: Age Spectrum Plots of Furnace Step-heating Data

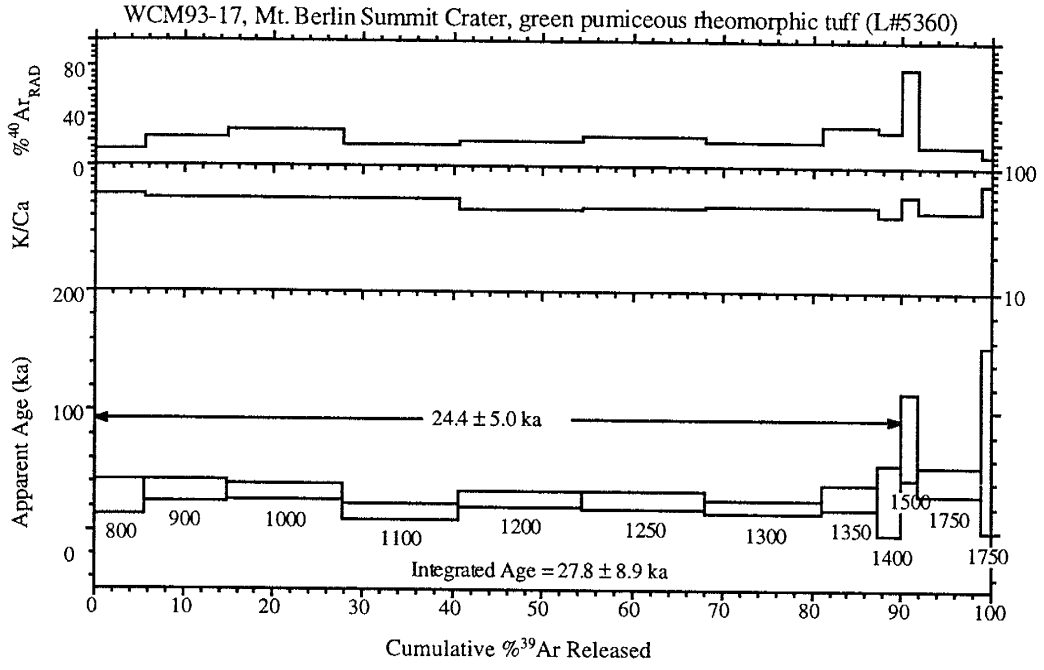

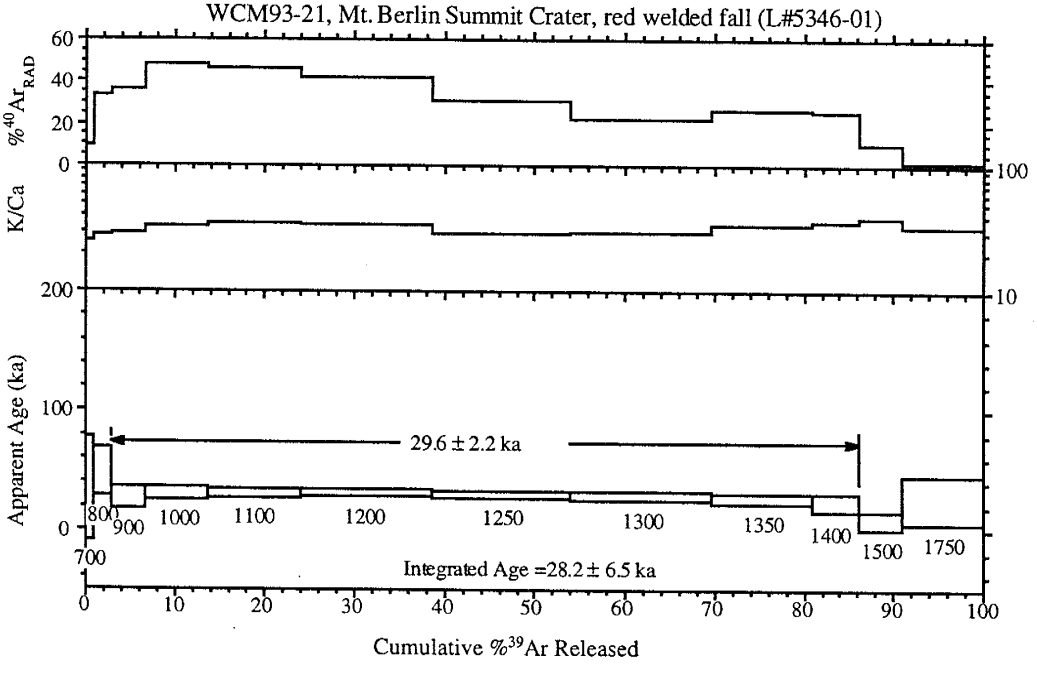

Appendix III.: Age Spectrum Plots of Furnace Step-heating Data

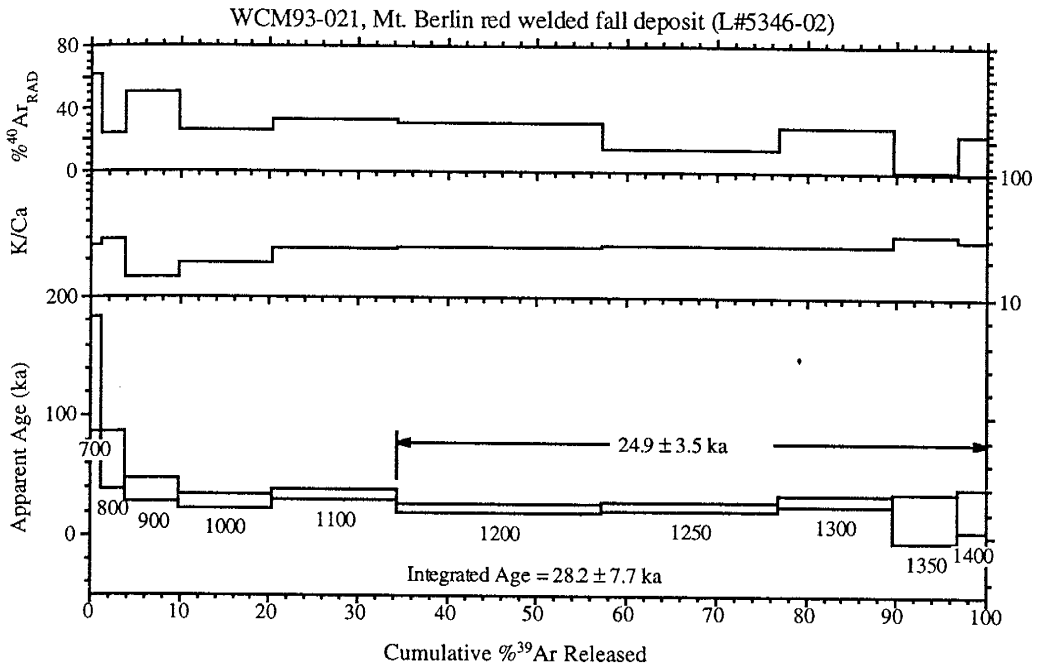

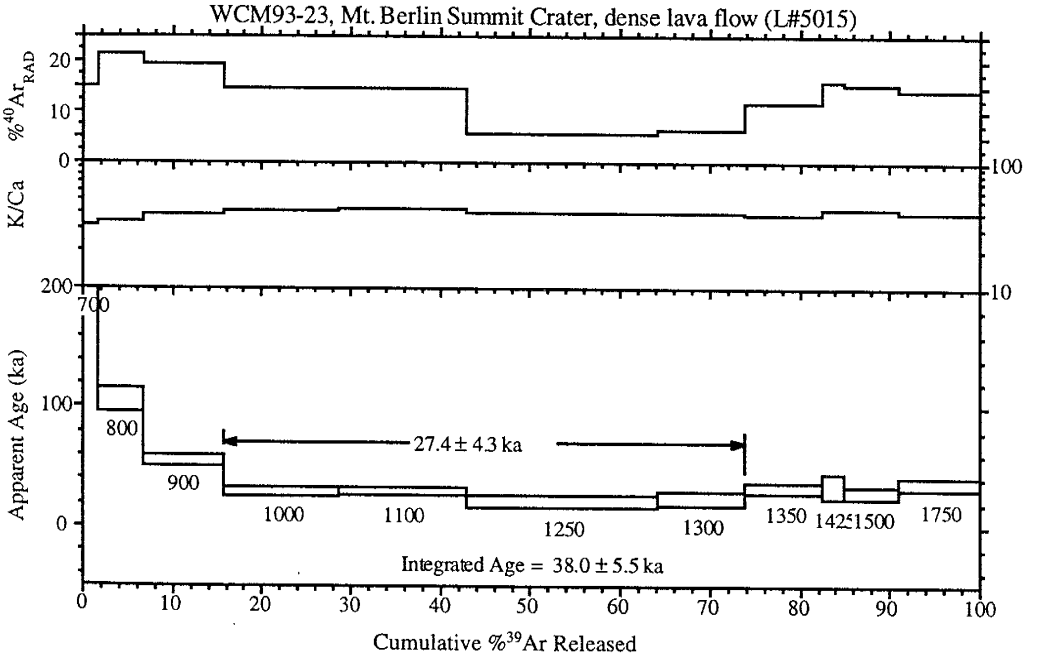

Appendix III.: Age Spectrum Plots of Furnace Step-heating Data

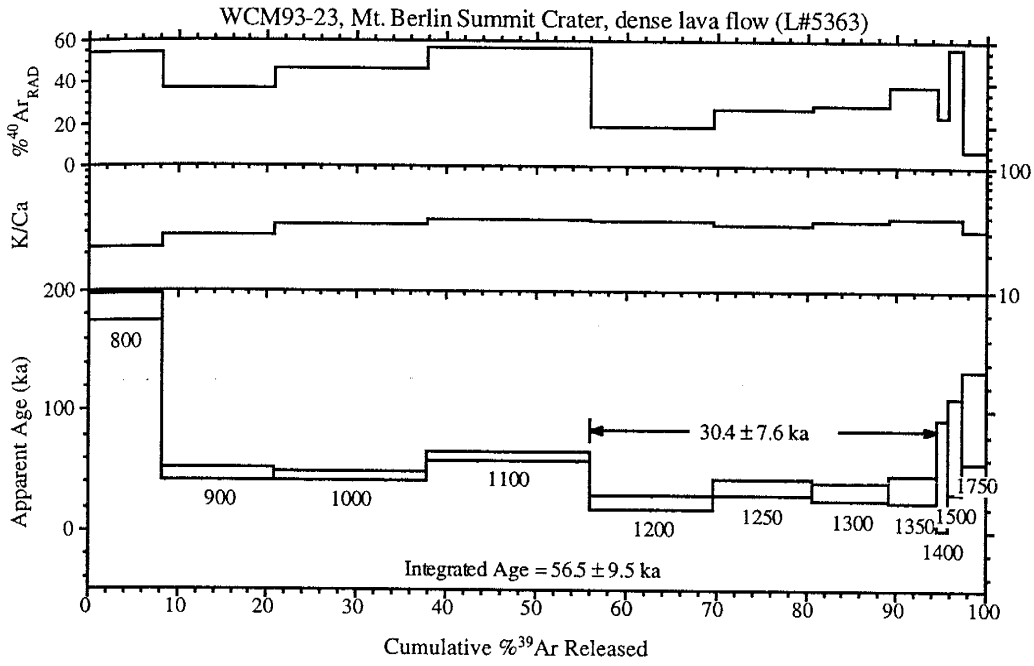

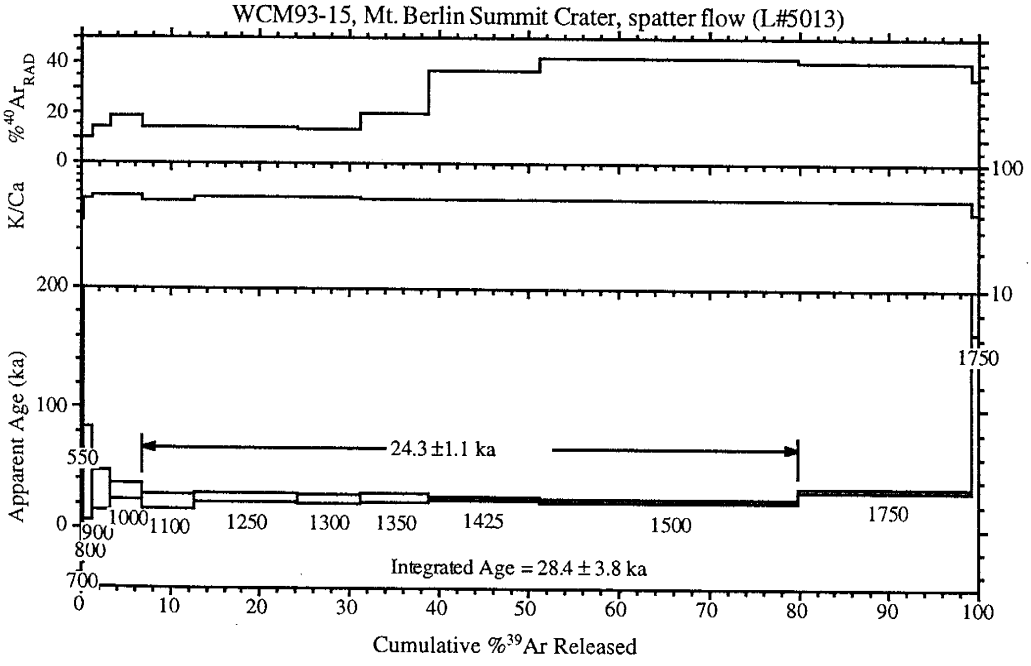

Appendix III.: Age Spectrum Plots of Furnace Step-heating Data

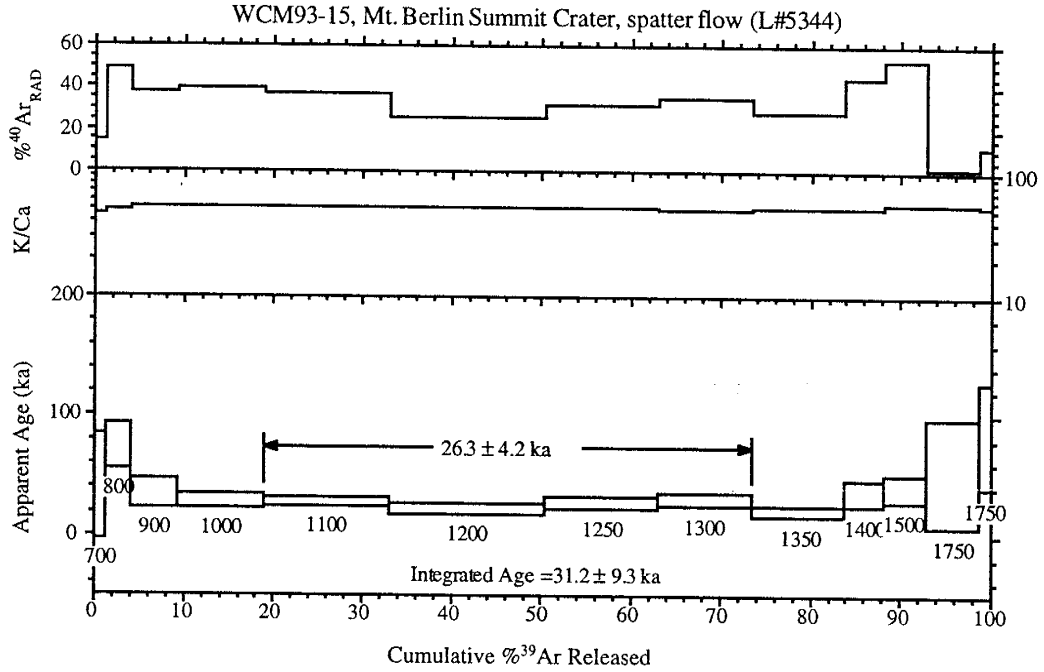

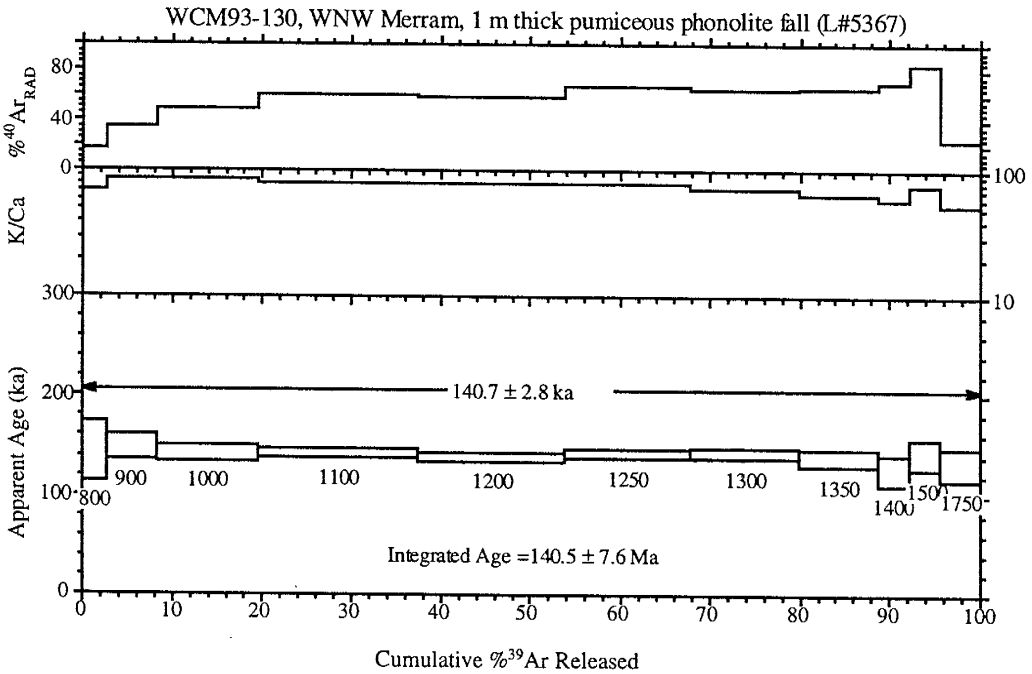

Appendix III.: Age Spectrum Plots of Furnace Step-heating Data

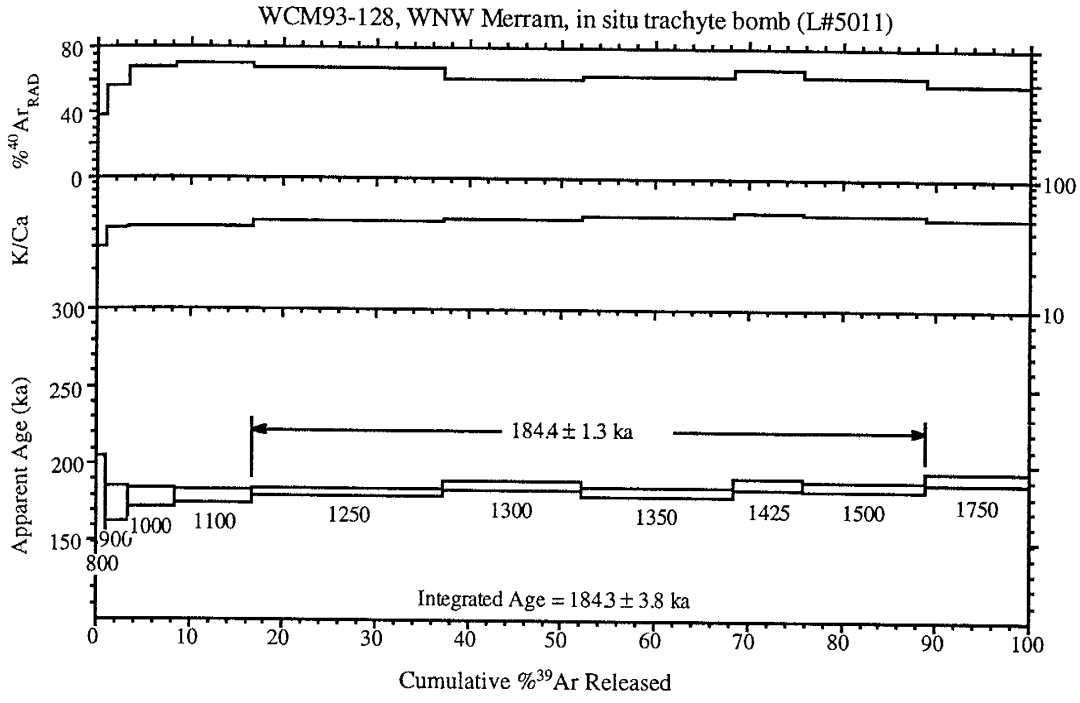

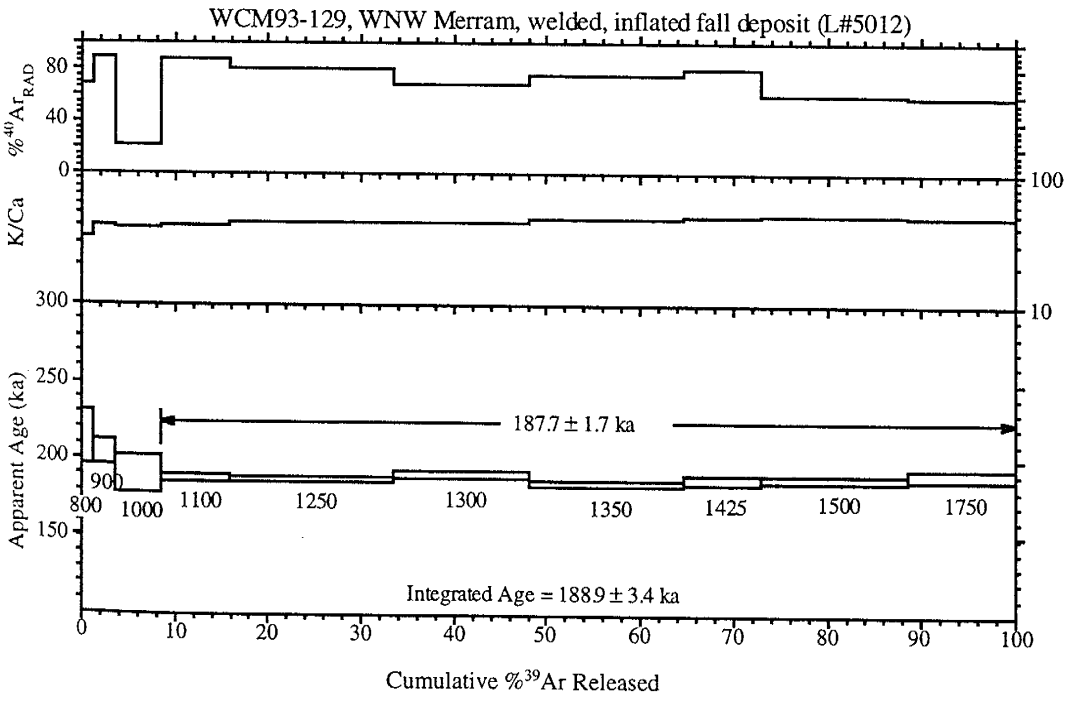

Appendix III.: Age Spectrum Plots of Furnace Step-heating Data

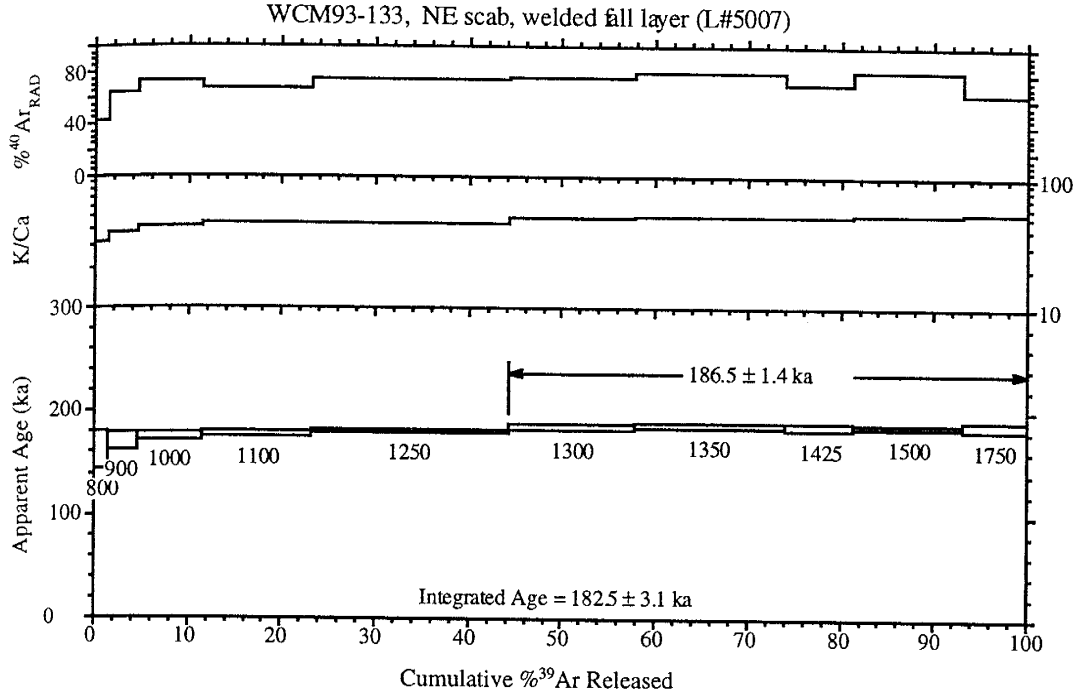

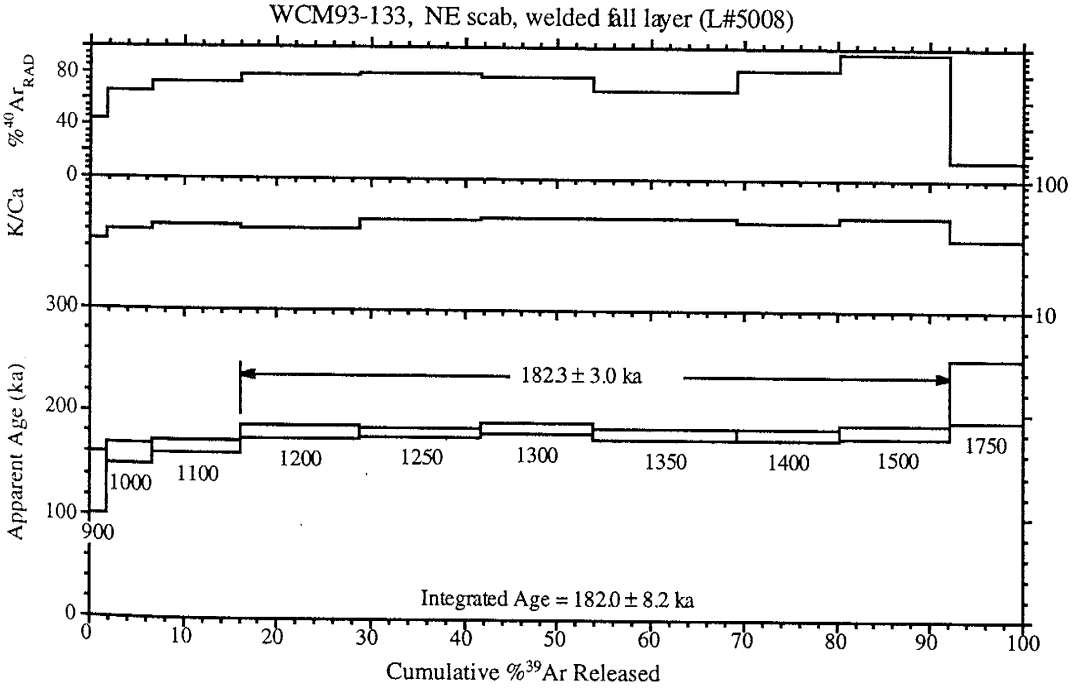

Appendix III.: Age Spectrum Plots of Furnace Step-heating Data

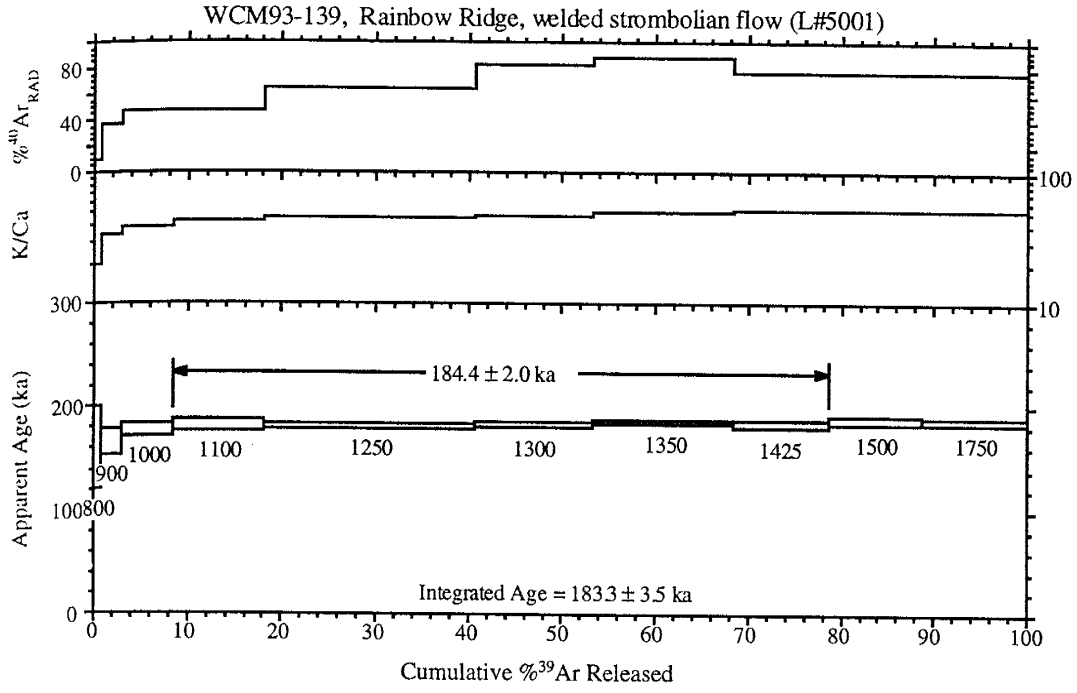

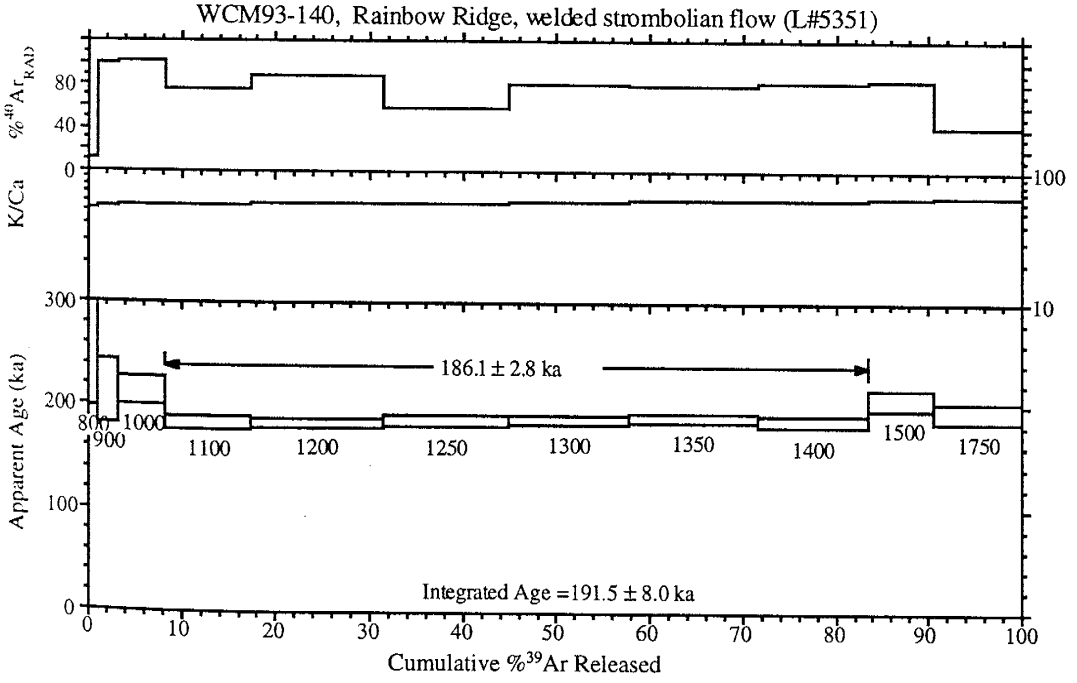

Appendix III.: Age Spectrum Plots of Furnace Step-heating Data

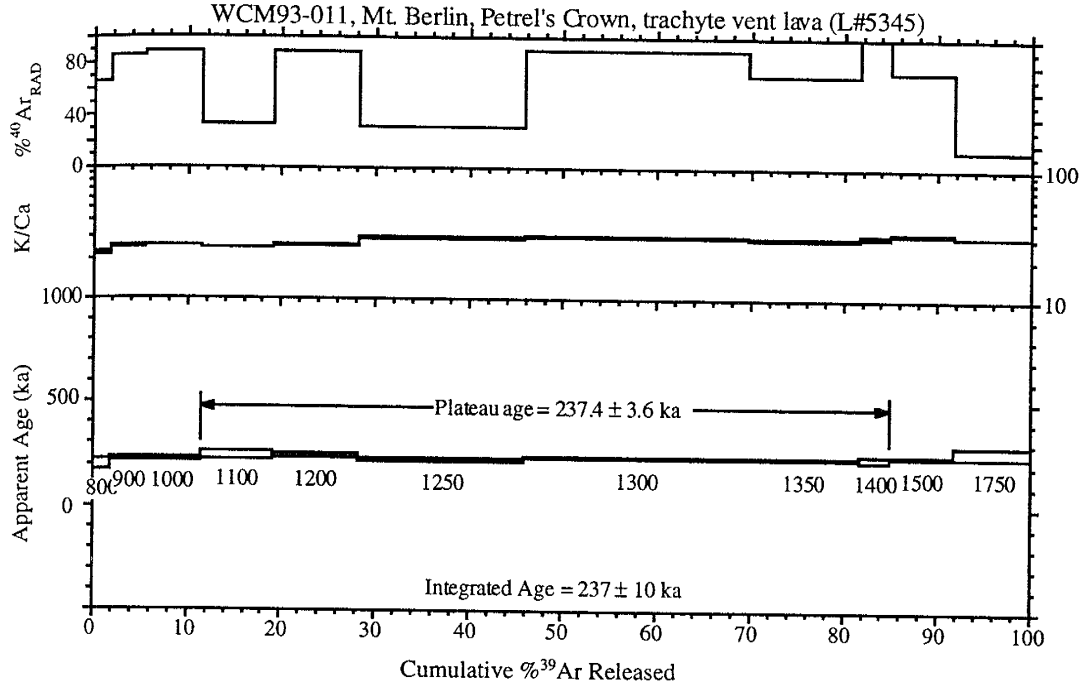

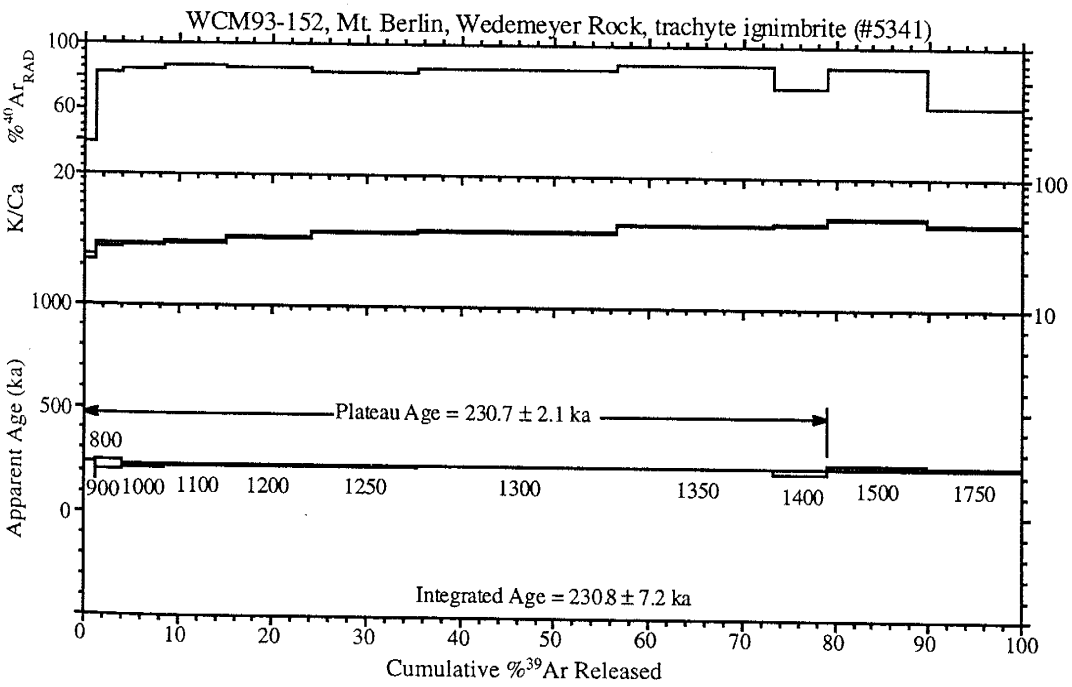

Appendix III.: Age Spectrum Plots of Furnace Step-heating Data

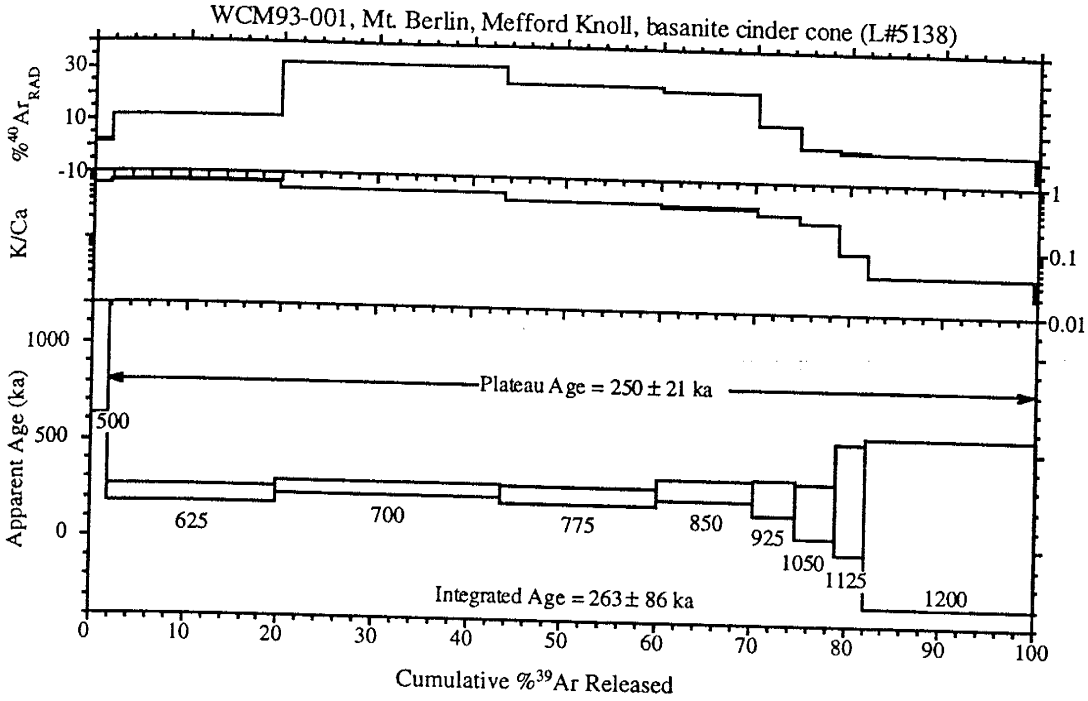

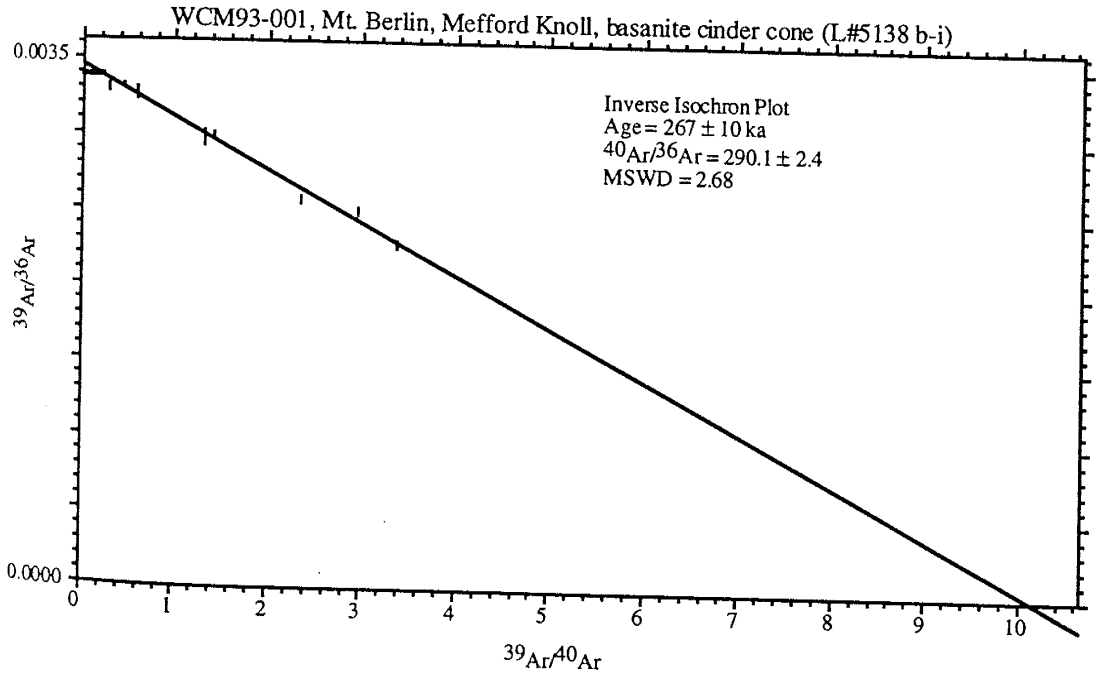

Appendix III.: Age Spectrum Plots of Furnace Step-heating Data

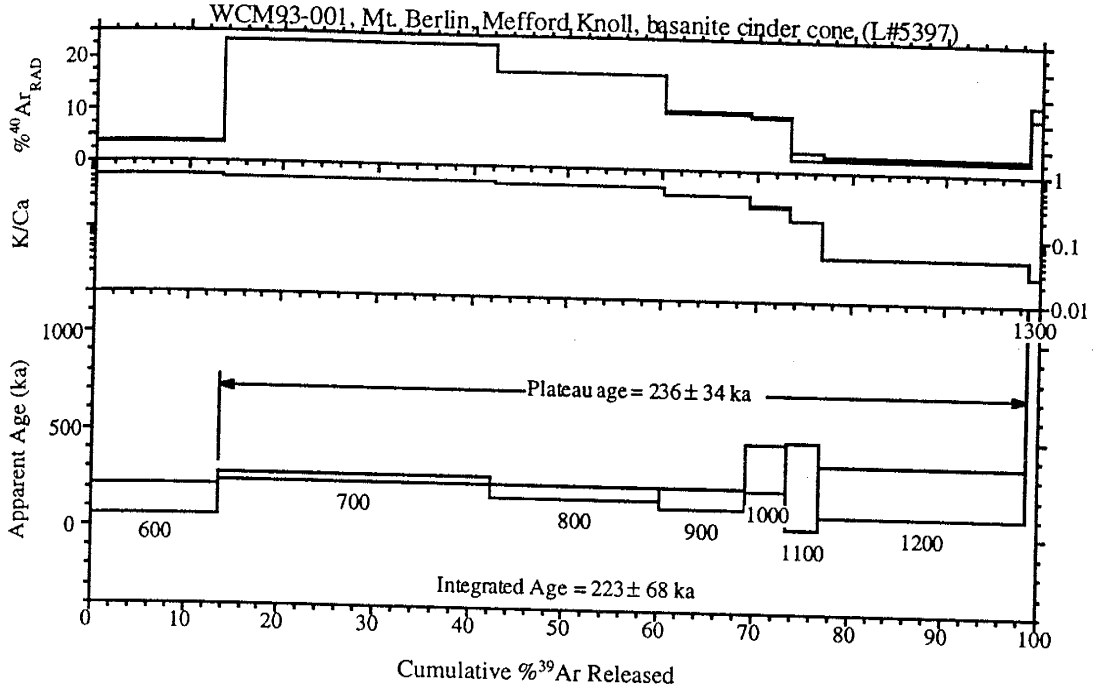

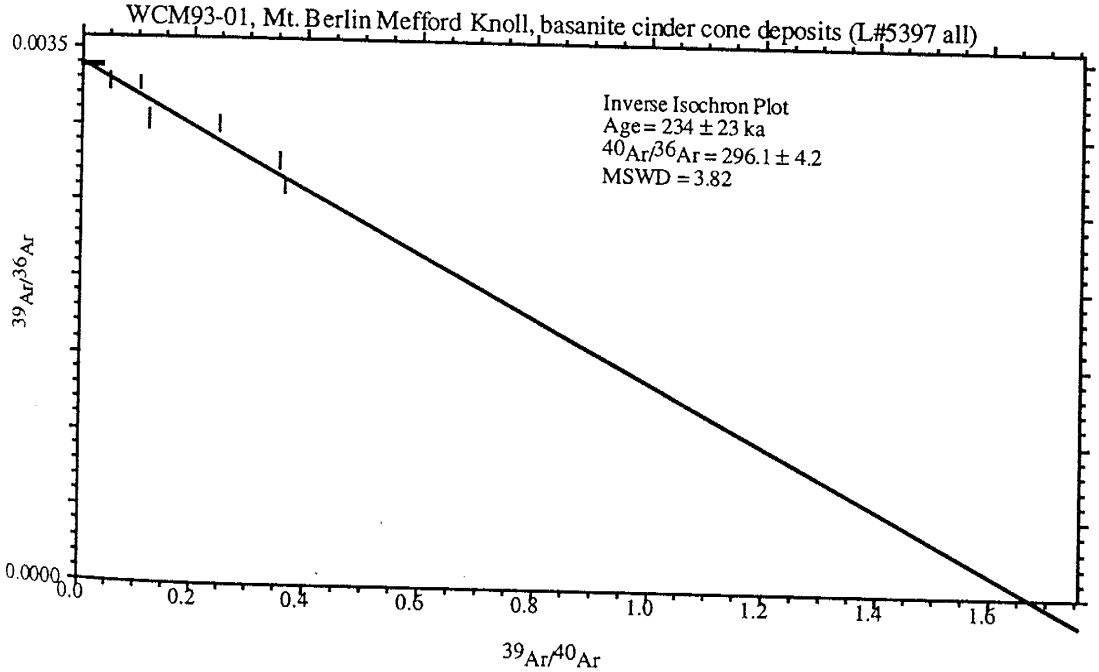

Appendix III.: Age Spectrum Plots of Furnace Step-heating Data

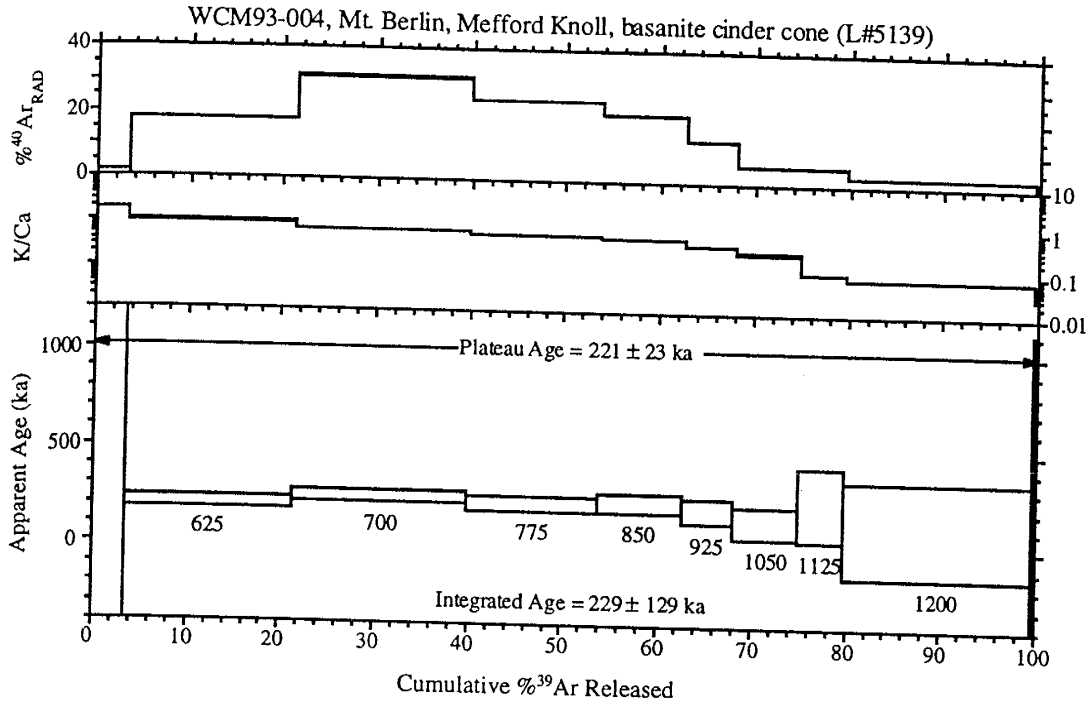

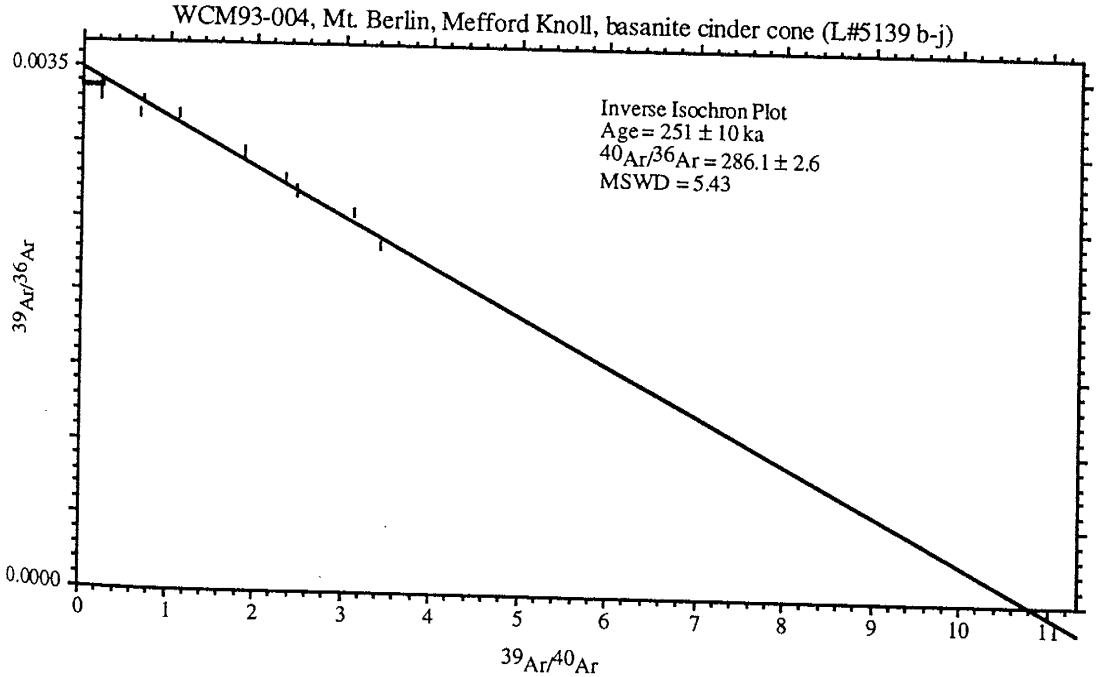

Appendix III.: Age Spectrum Plots of Furnace Step-heating Data

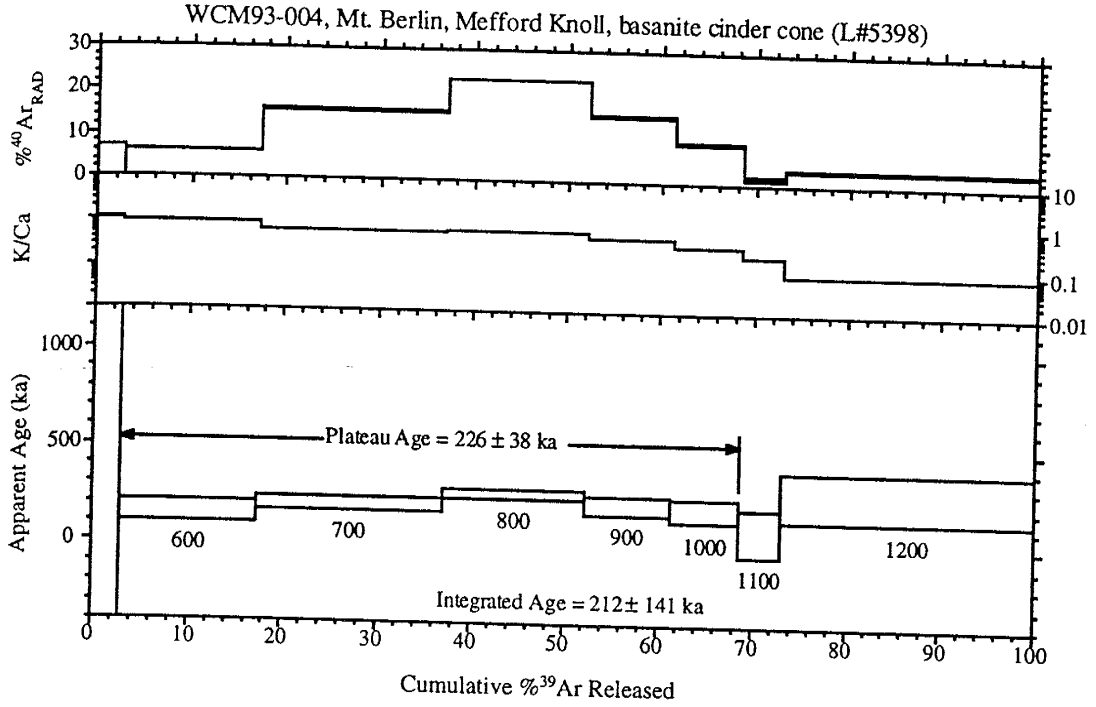

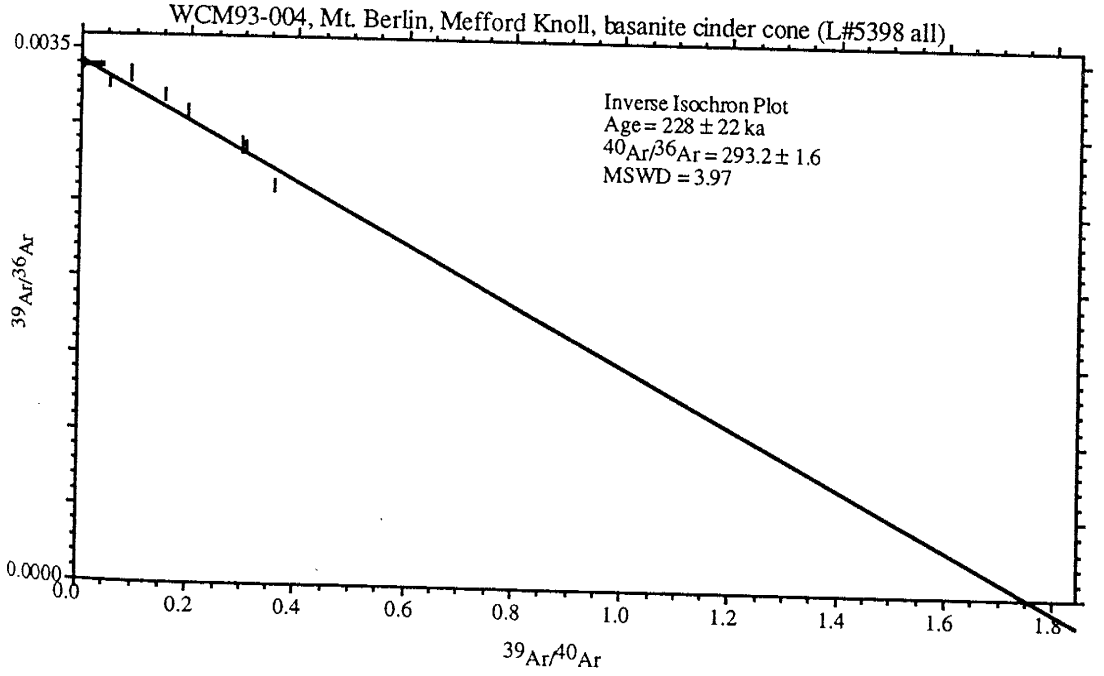

Appendix III.: Age Spectrum Plots of Furnace Step-heating Data

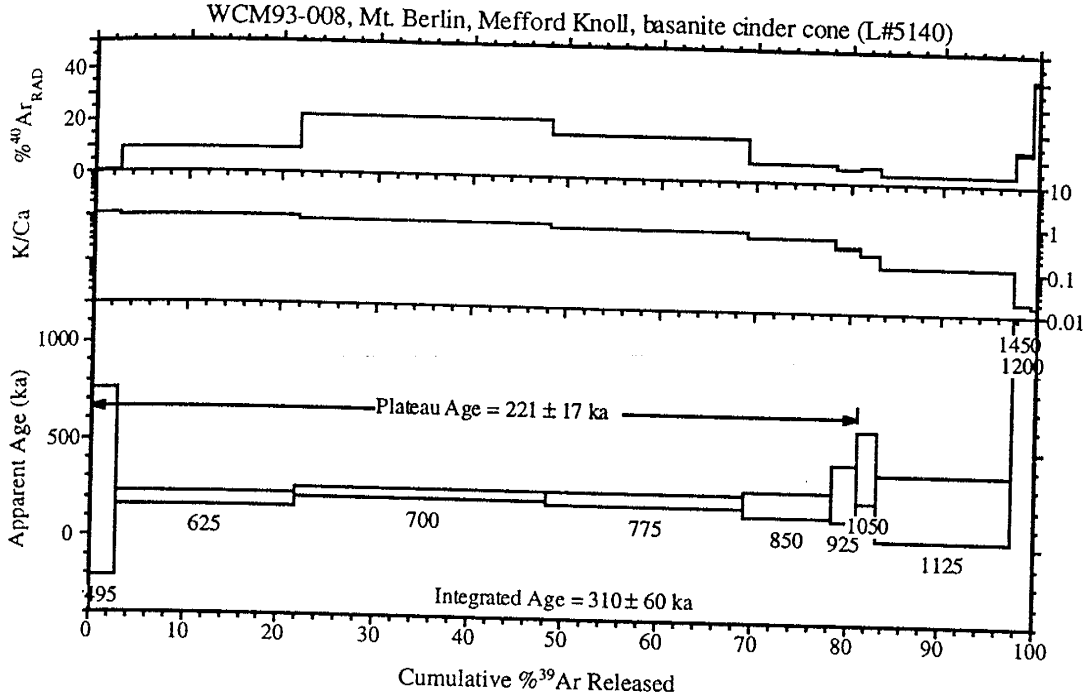

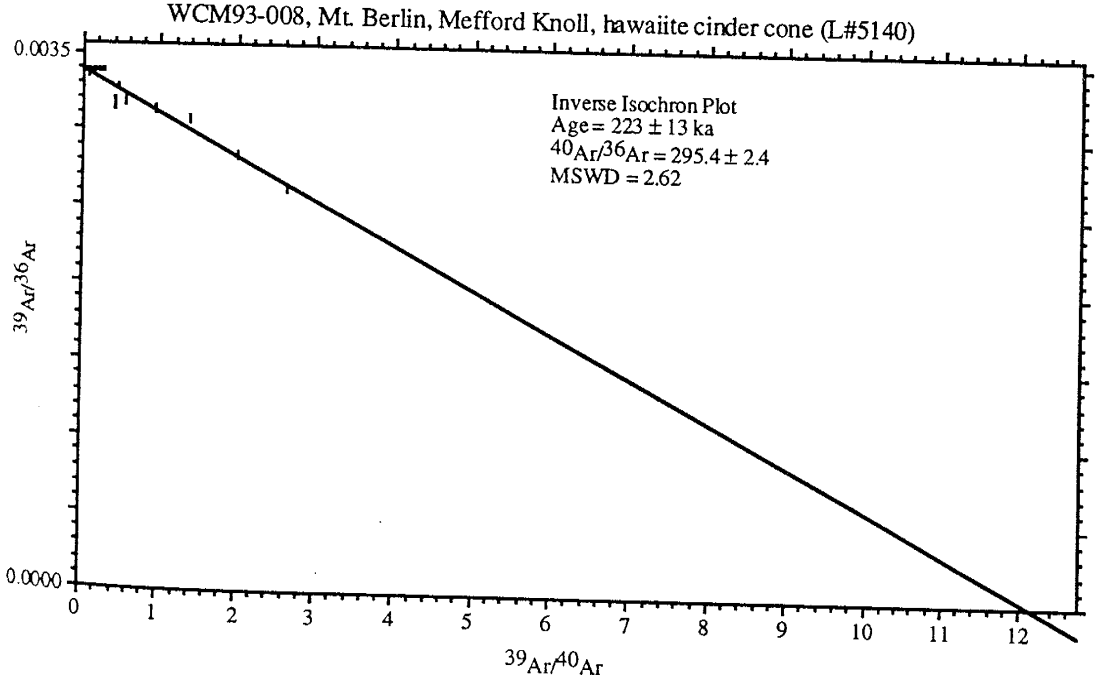

Appendix III.: Age Spectrum Plots of Furnace Step-heating Data

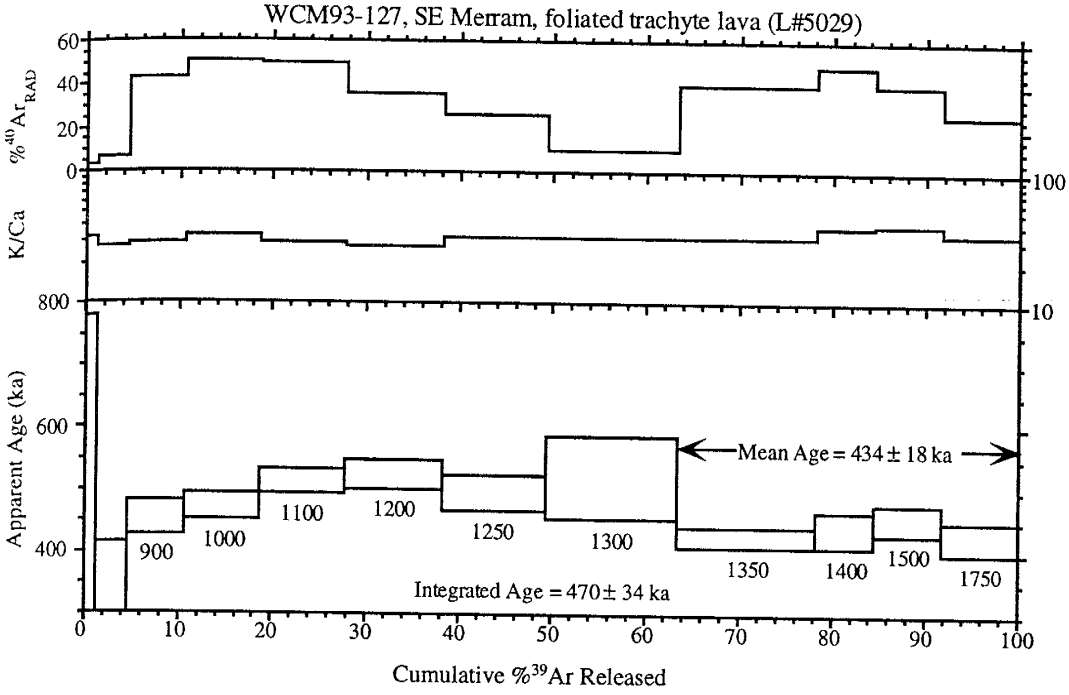

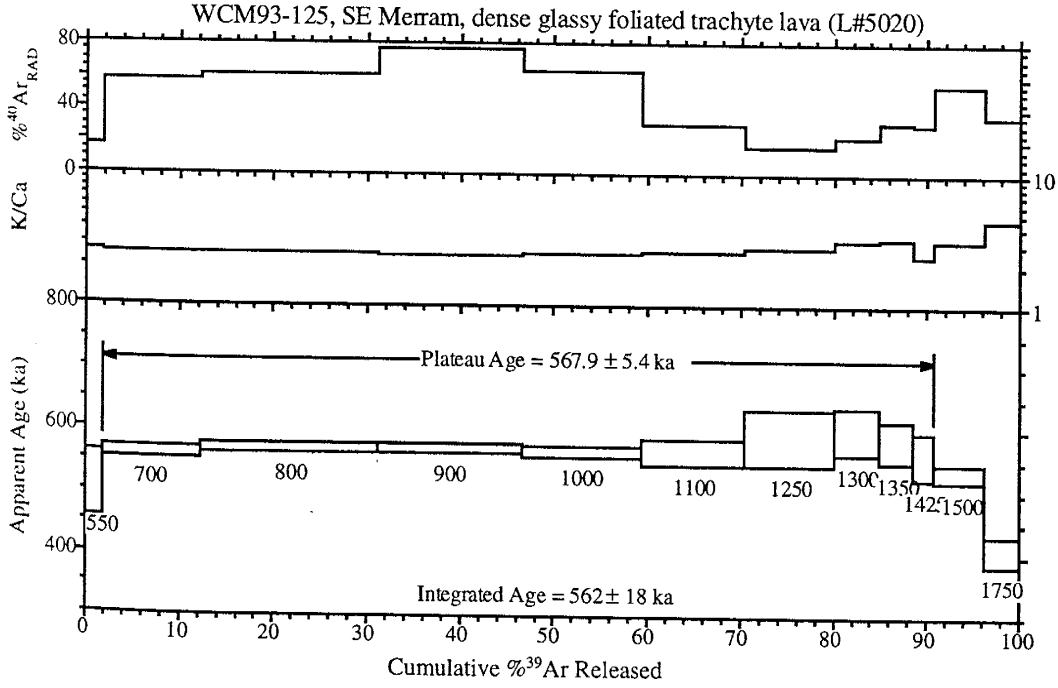

Appendix III.: Age Spectrum Plots of Furnace Step-heating Data

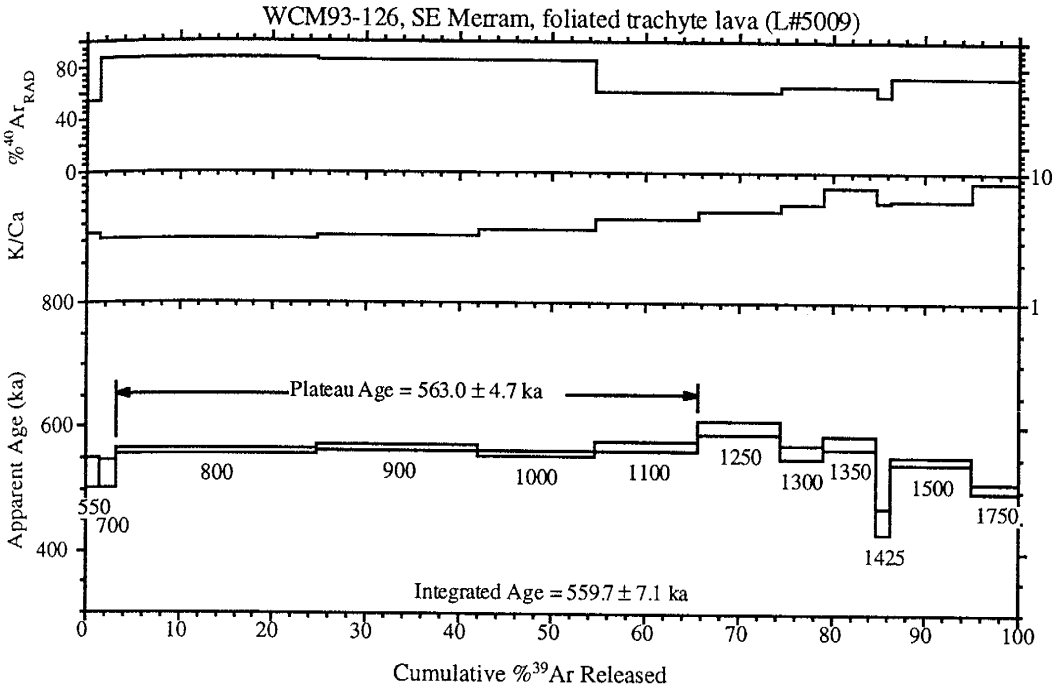

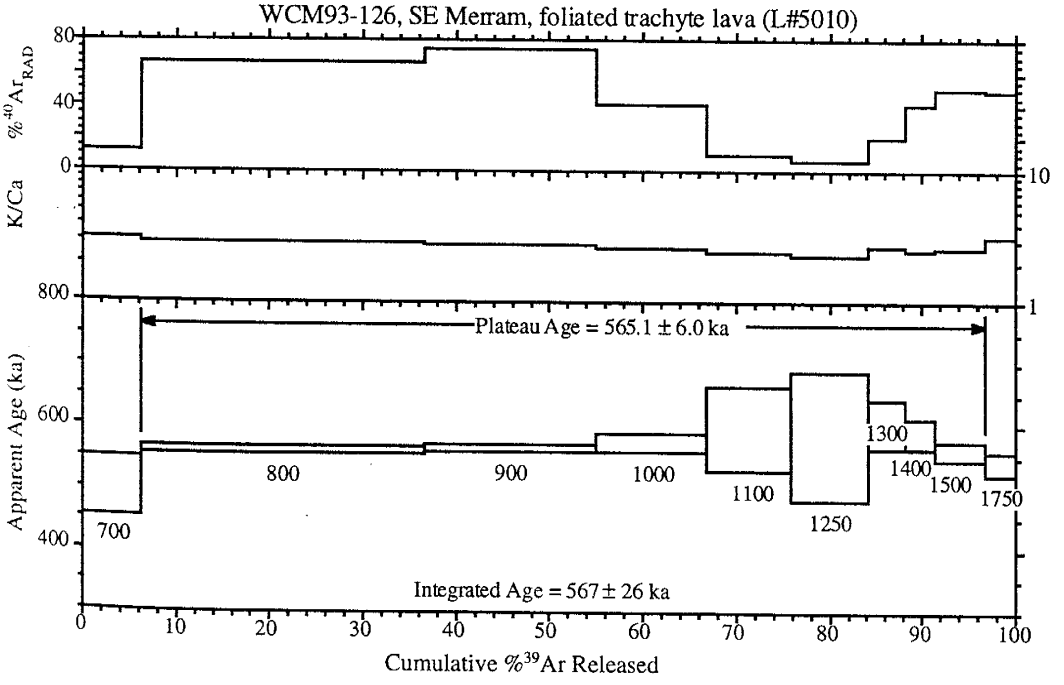

Appendix III.: Age Spectrum Plots of Furnace Step-heating Data

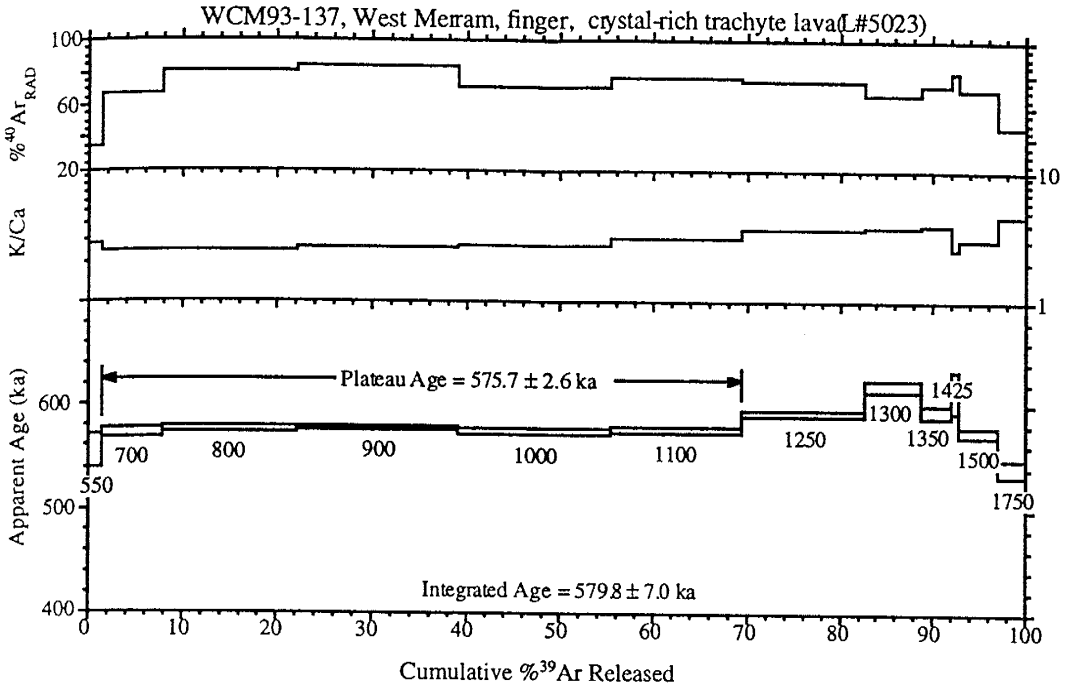

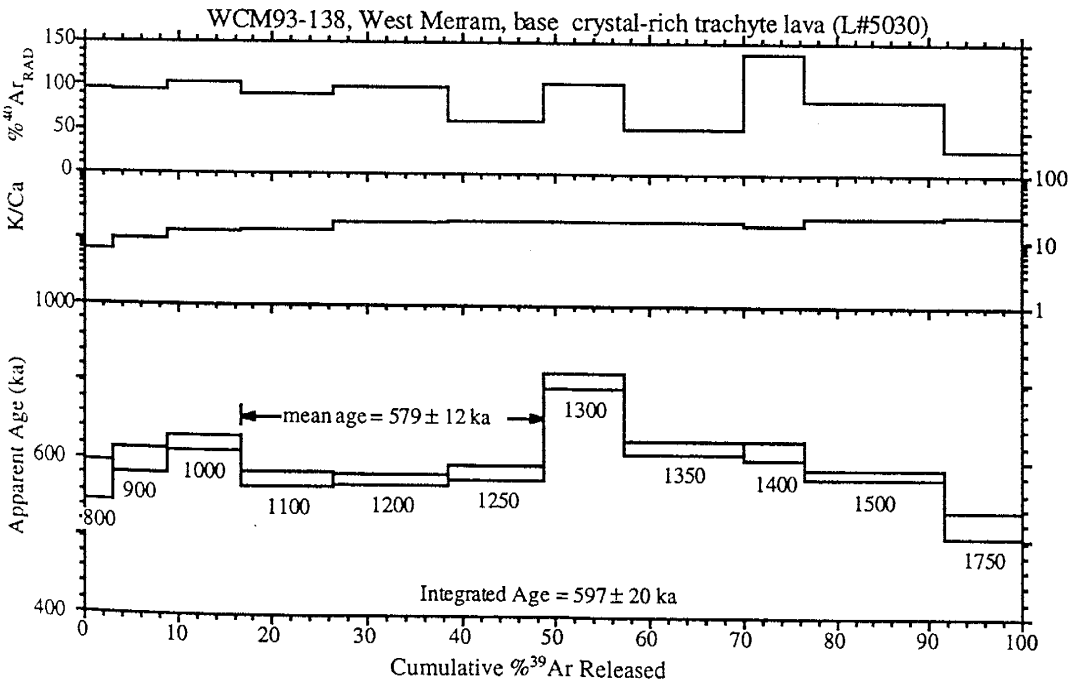

Appendix III.: Age Spectrum Plots of Furnace Step-heating Data

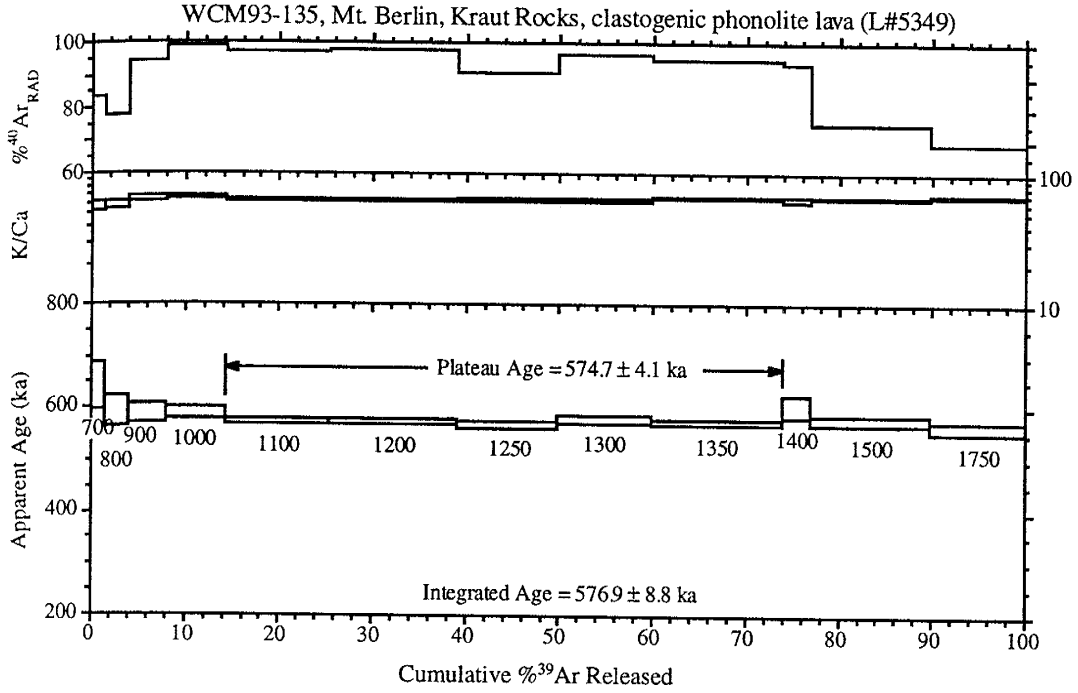

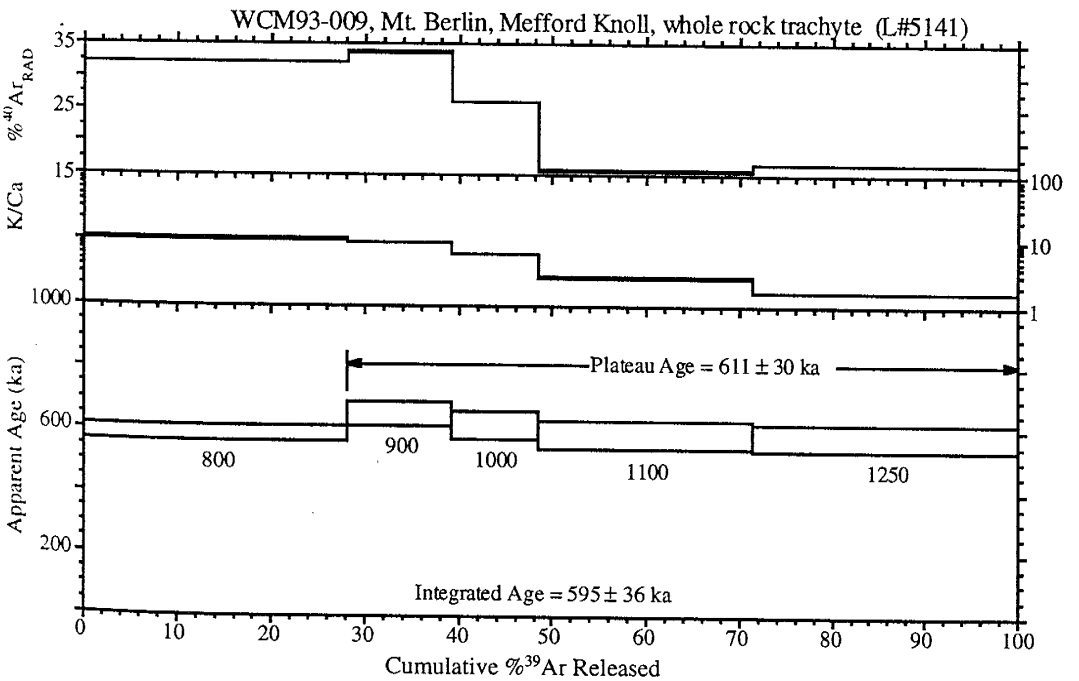

Appendix III.: Age Spectrum Plots of Furnace Step-heating Data

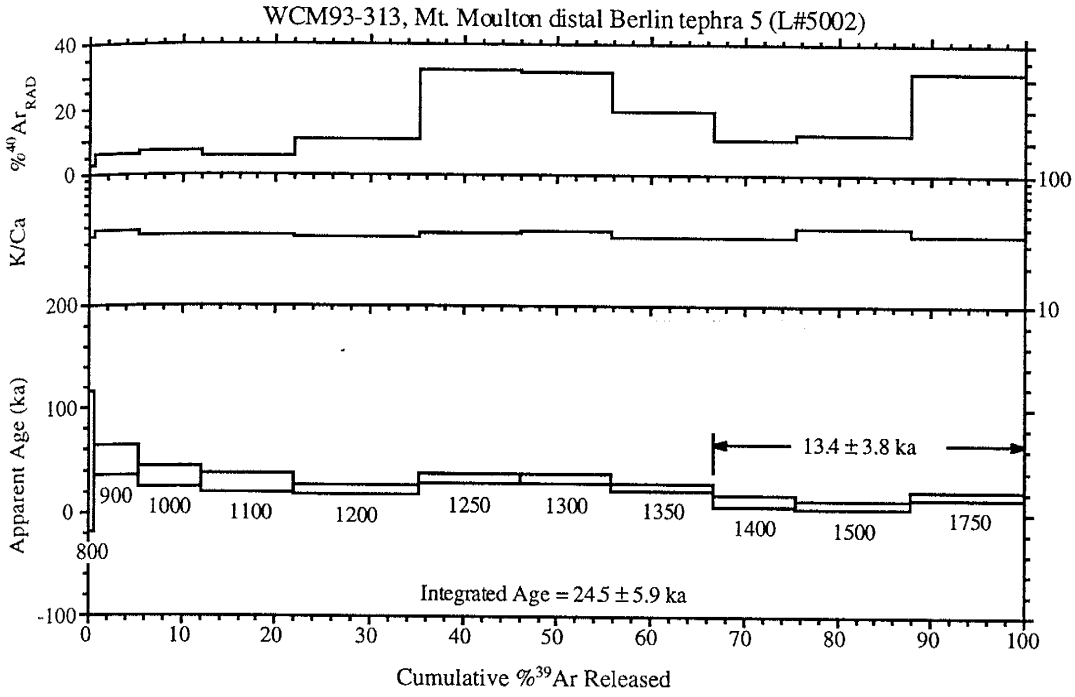

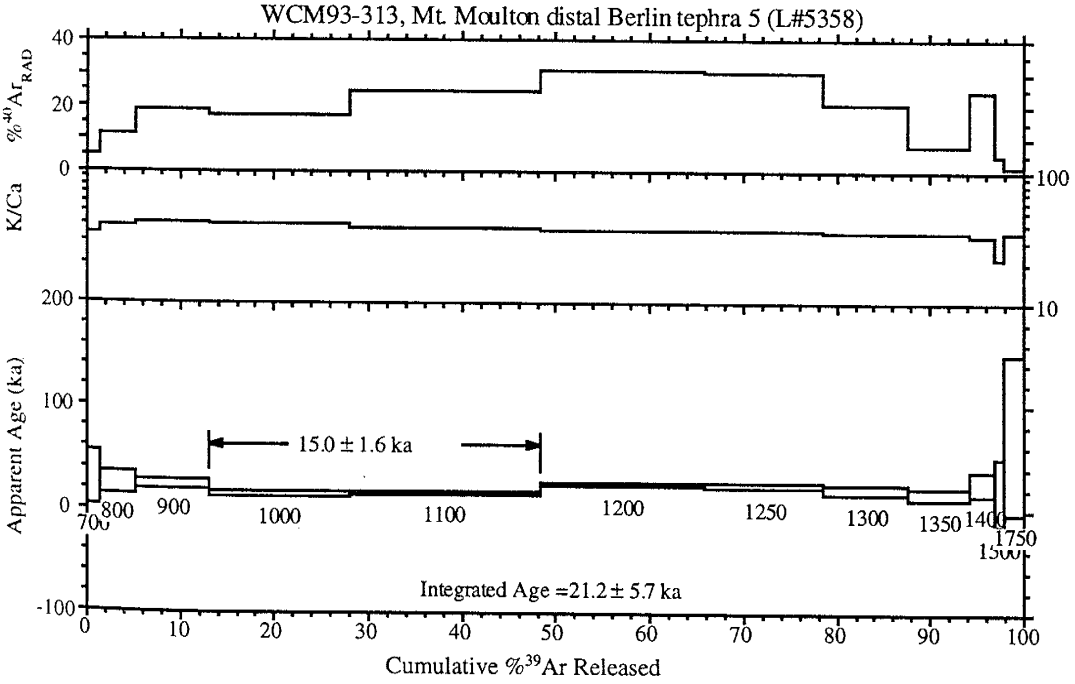

Appendix III.: Age Spectrum Plots of Furnace Step-heating Data

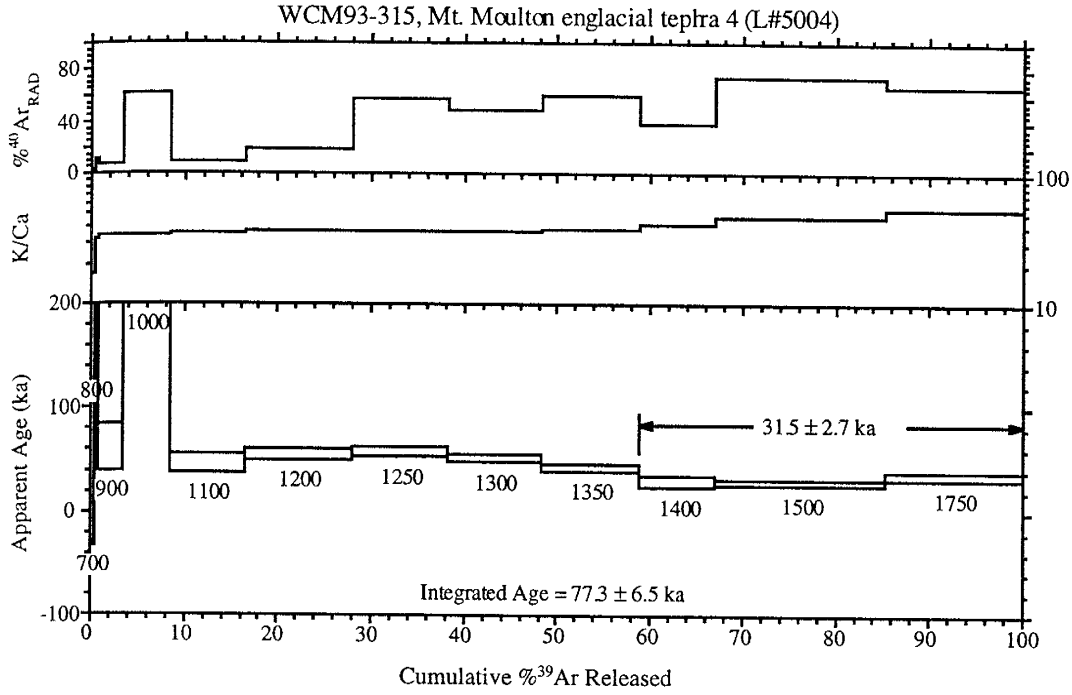

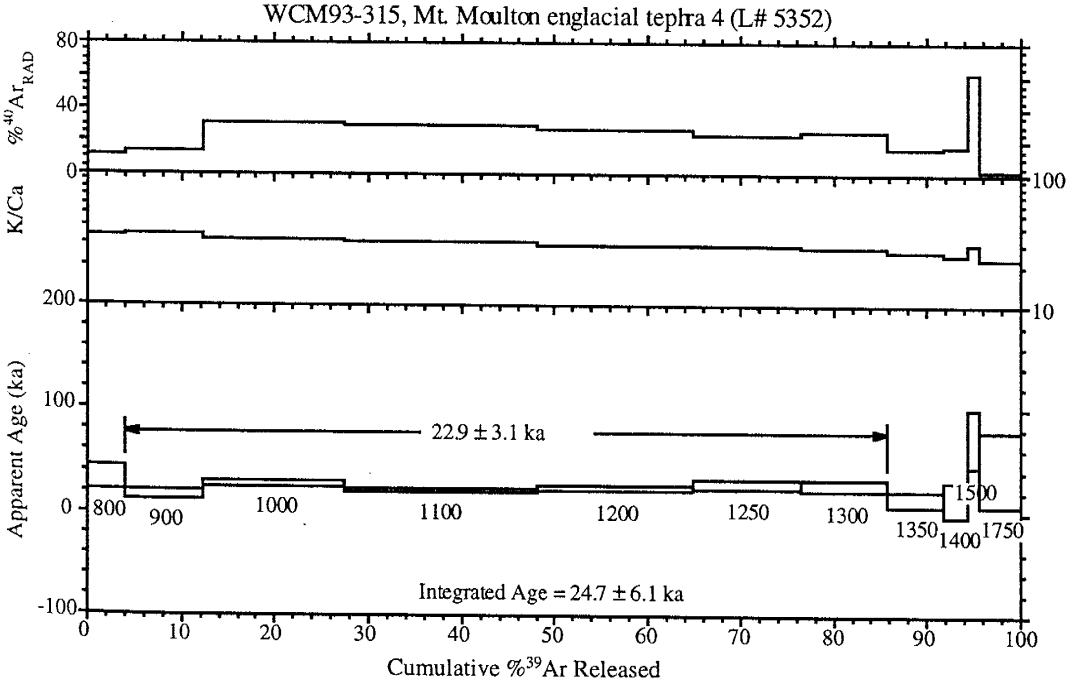

Appendix III.: Age Spectrum Plots of Furnace Step-heating Data

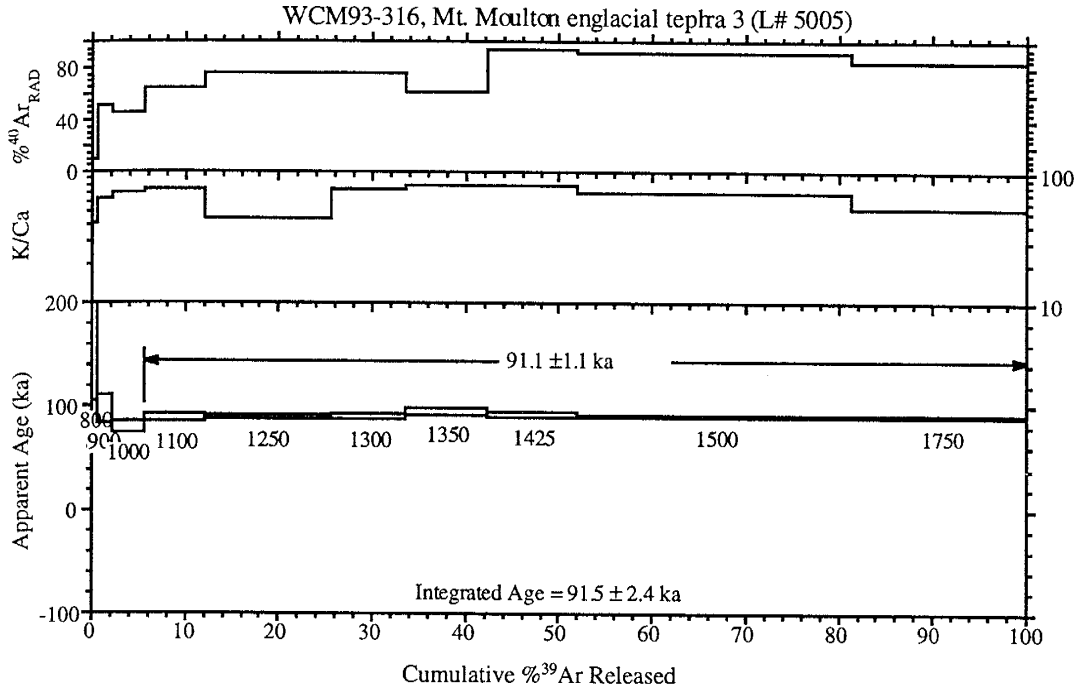

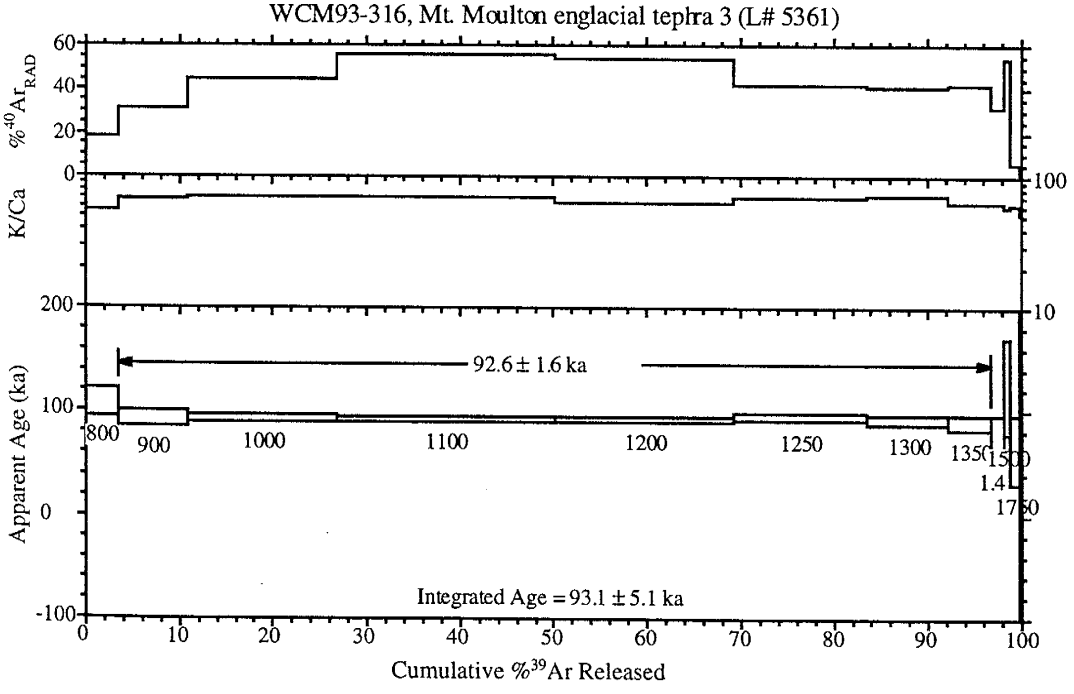

Appendix III.: Age Spectrum Plots of Furnace Step-heating Data

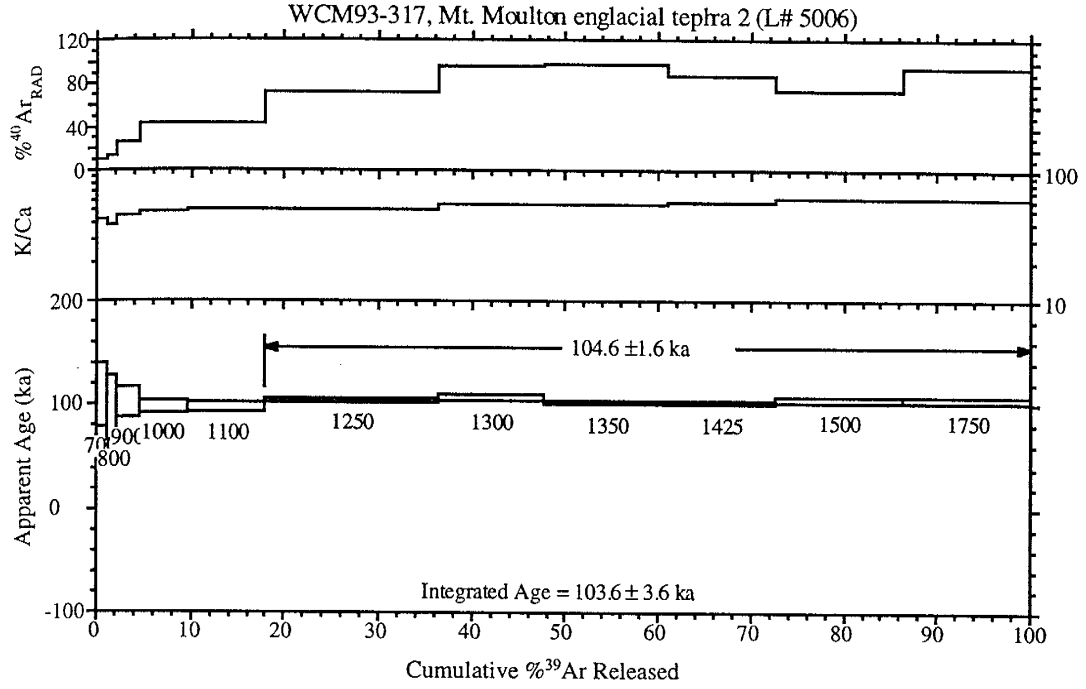

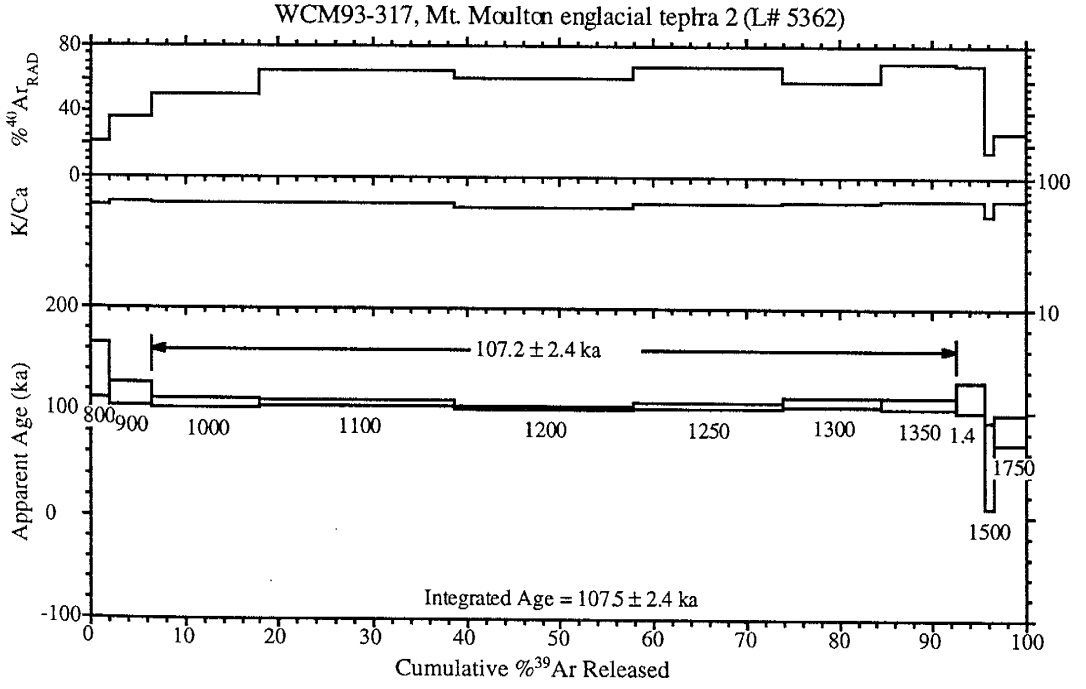

Appendix III.: Age Spectrum Plots of Furnace Step-heating Data

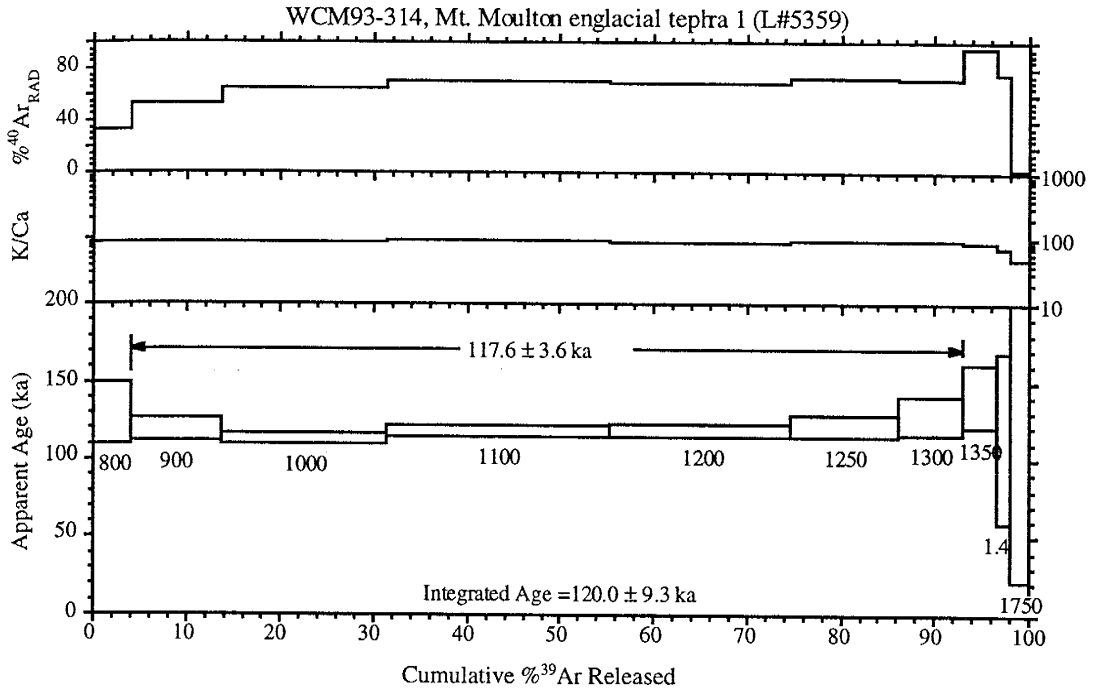

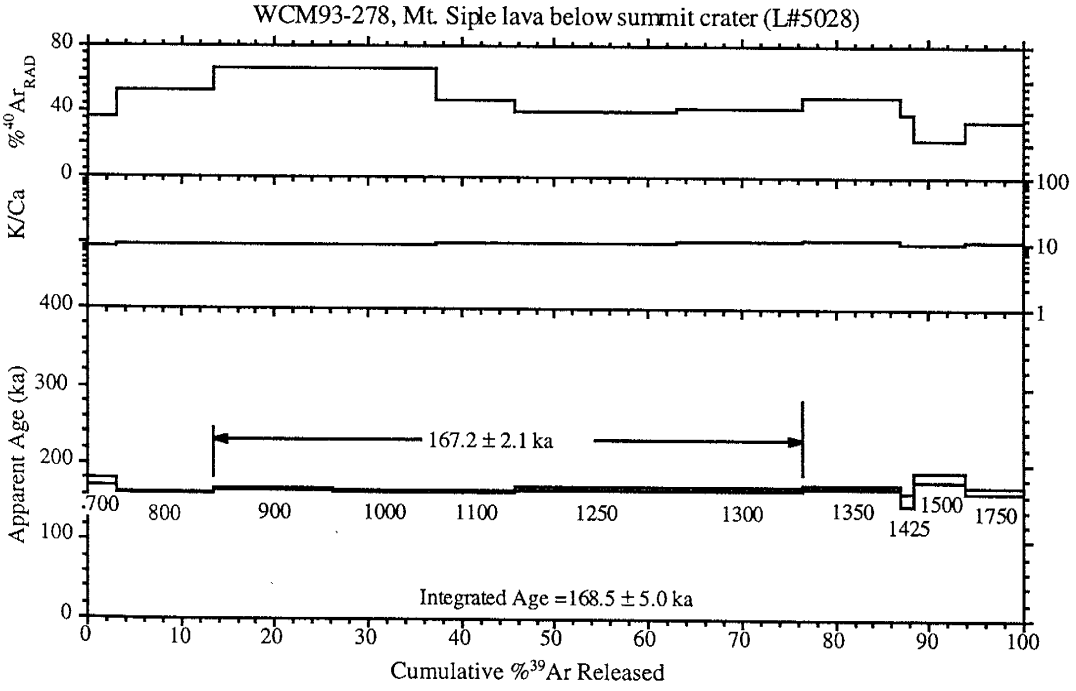

Appendix III.: Age Spectrum Plots of Furnace Step-heating Data

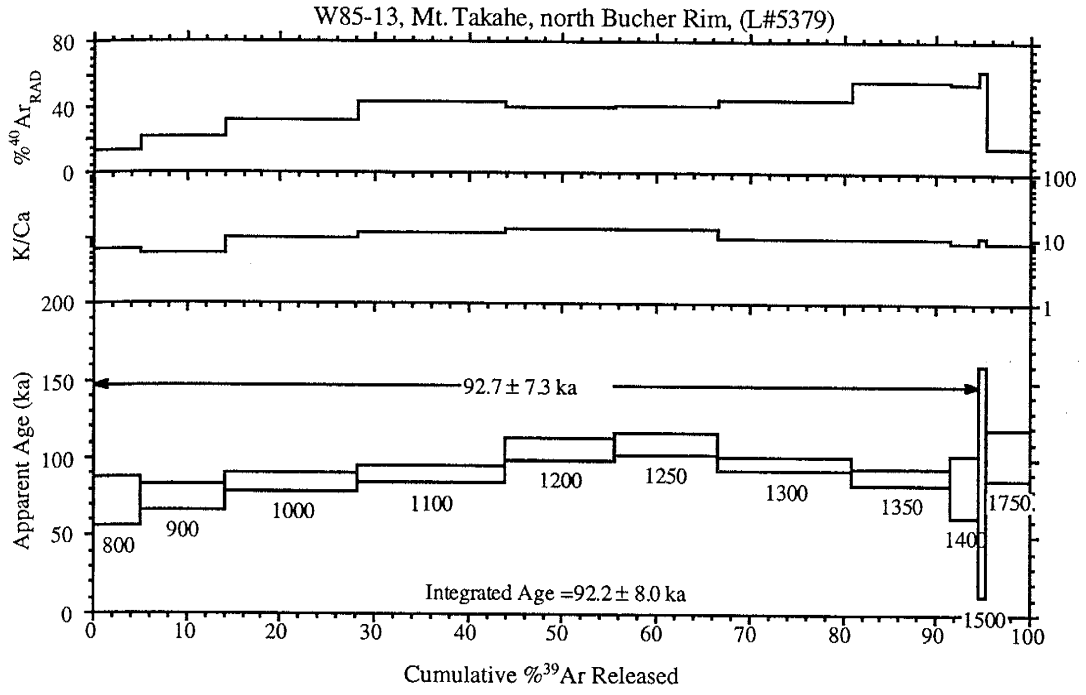

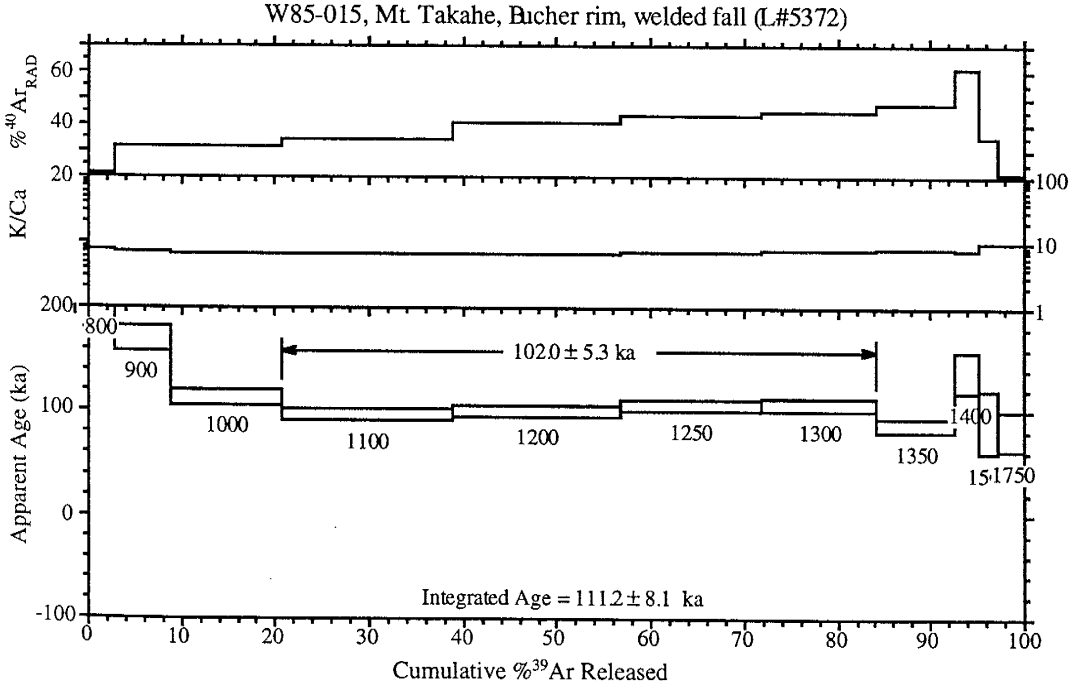

Appendix III.: Age Spectrum Plots of Furnace Step-heating Data

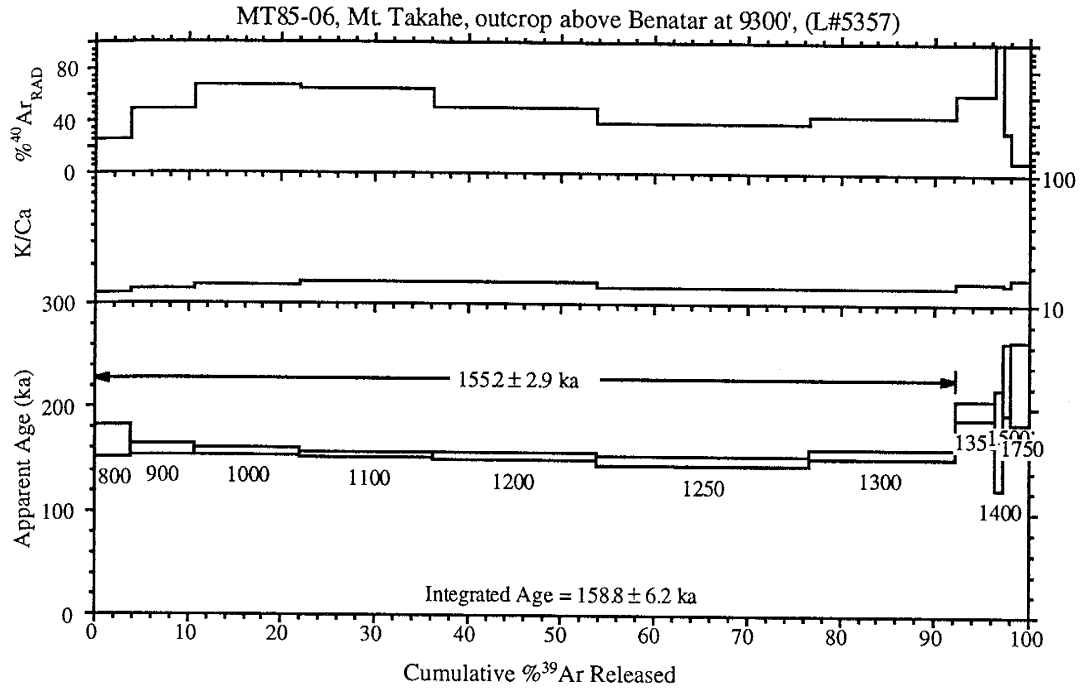

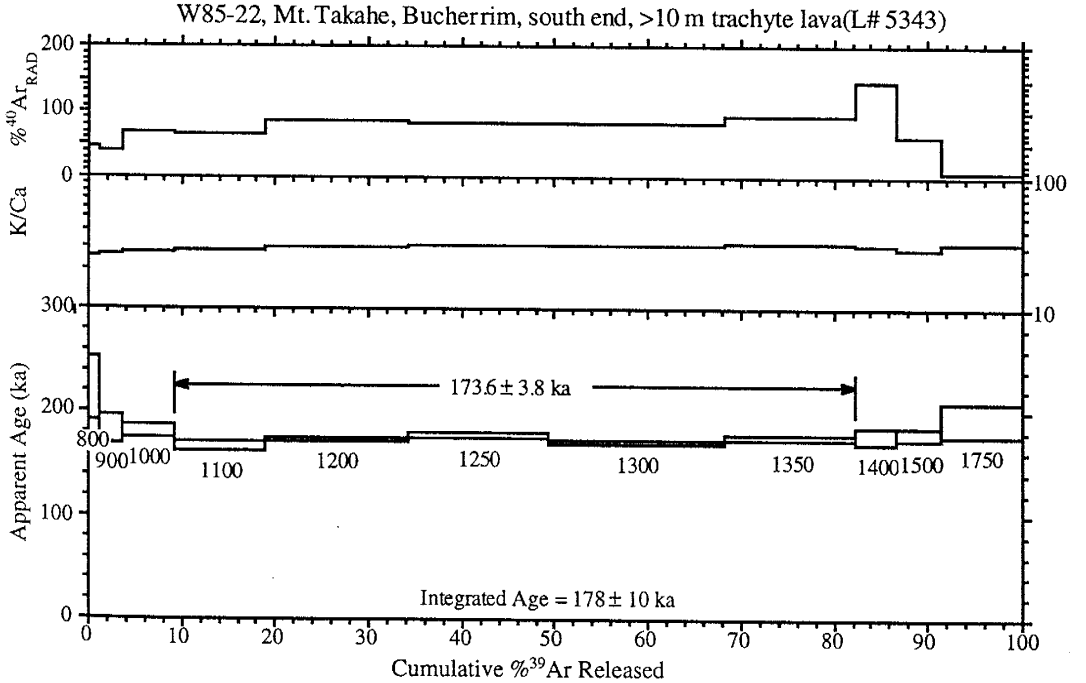

Appendix III.: Age Spectrum Plots of Furnace Step-heating Data

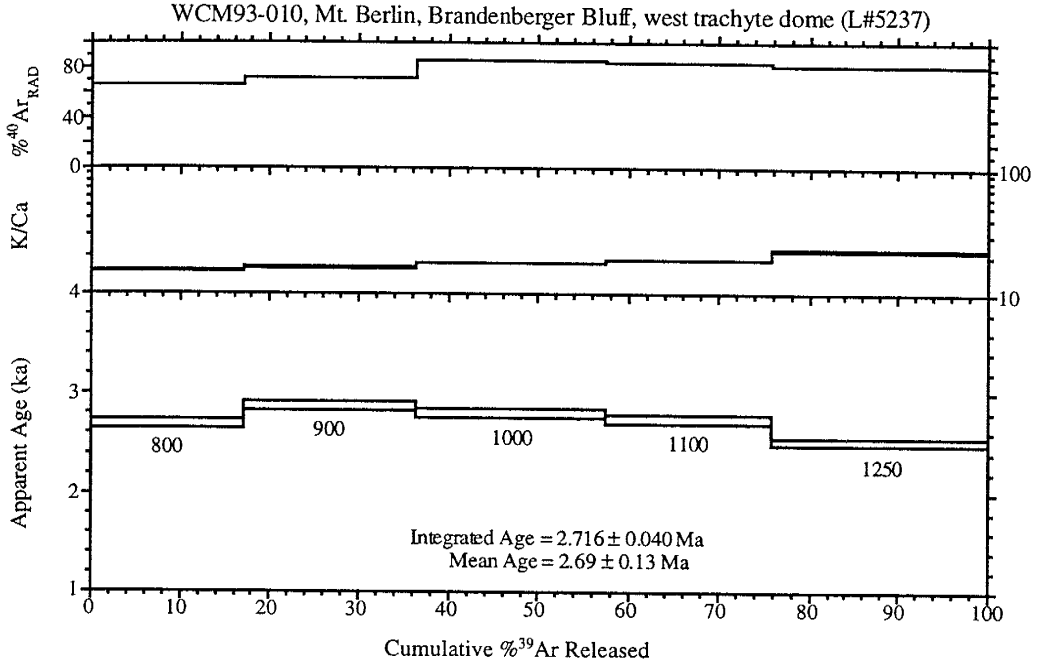

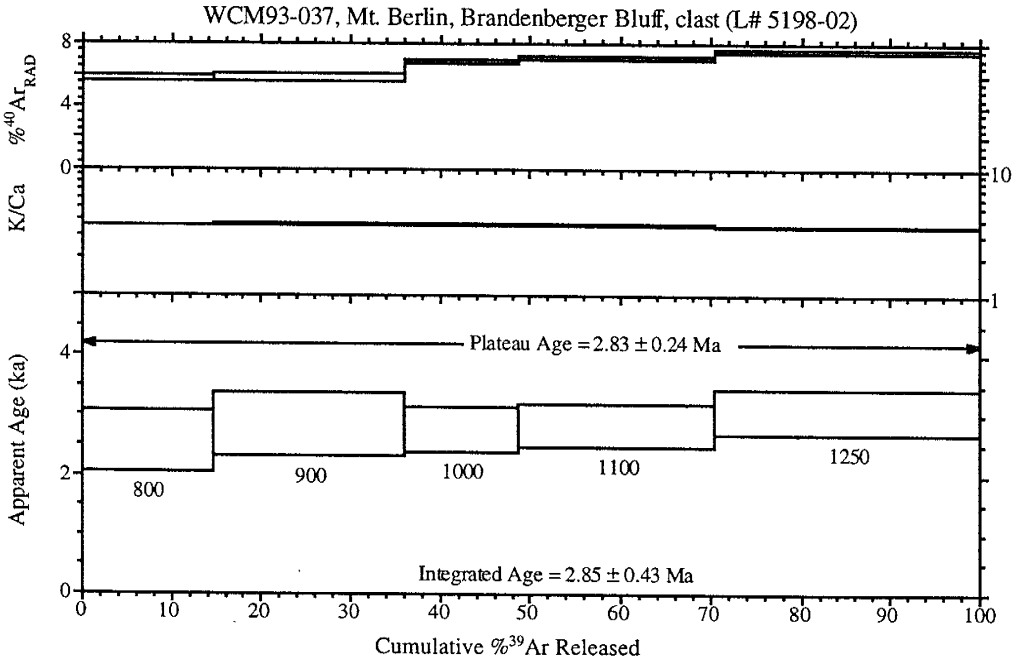

Appendix III.: Age Spectrum Plots of Furnace Step-heating Data

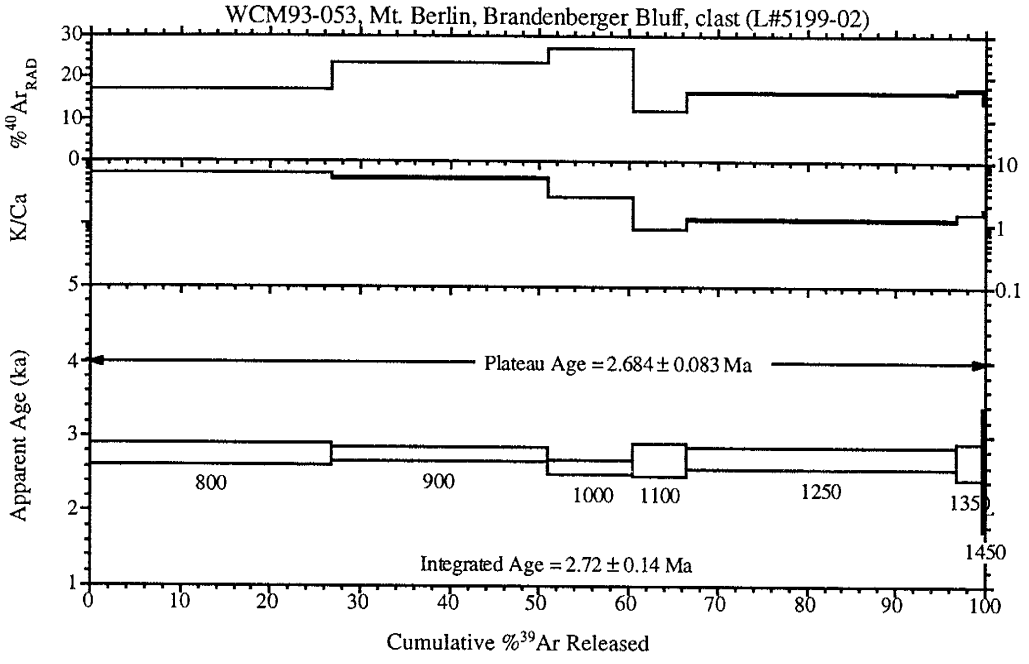

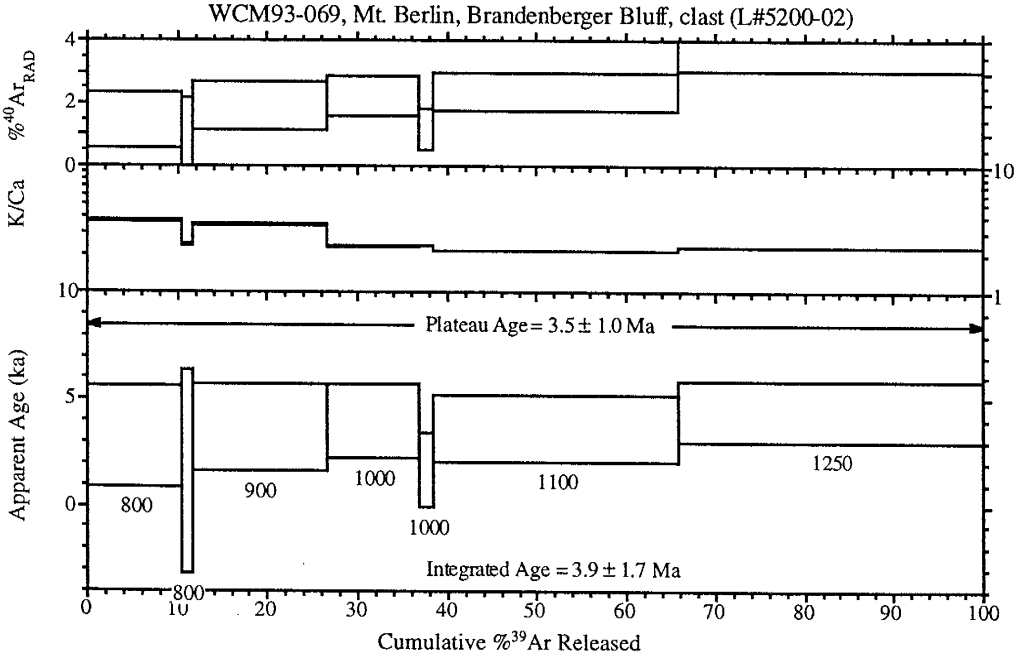

Appendix III.: Age Spectrum Plots of Furnace Step-heating Data

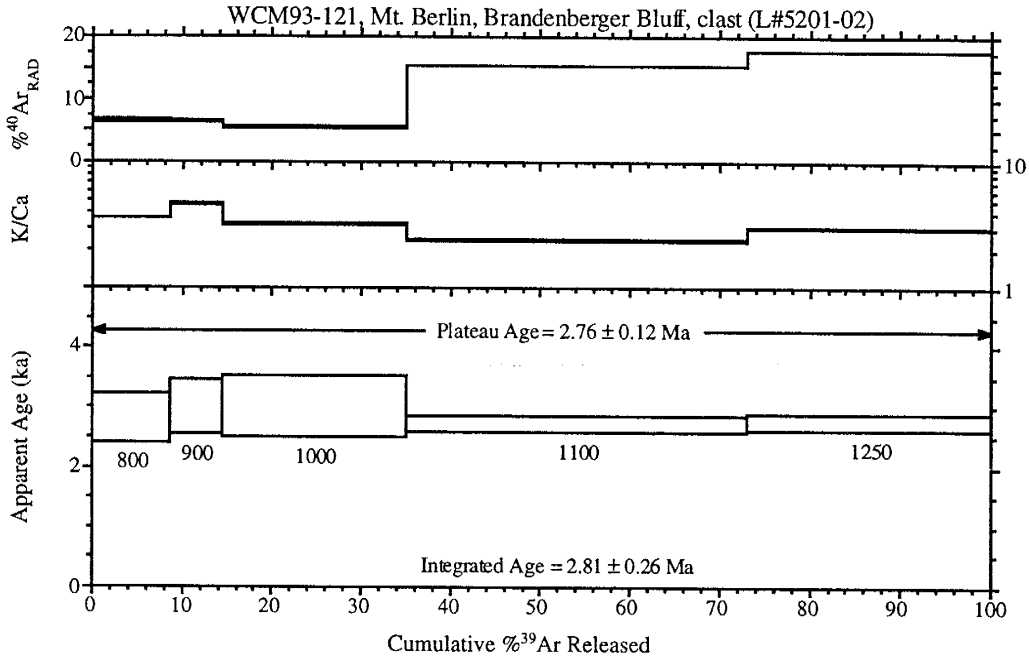

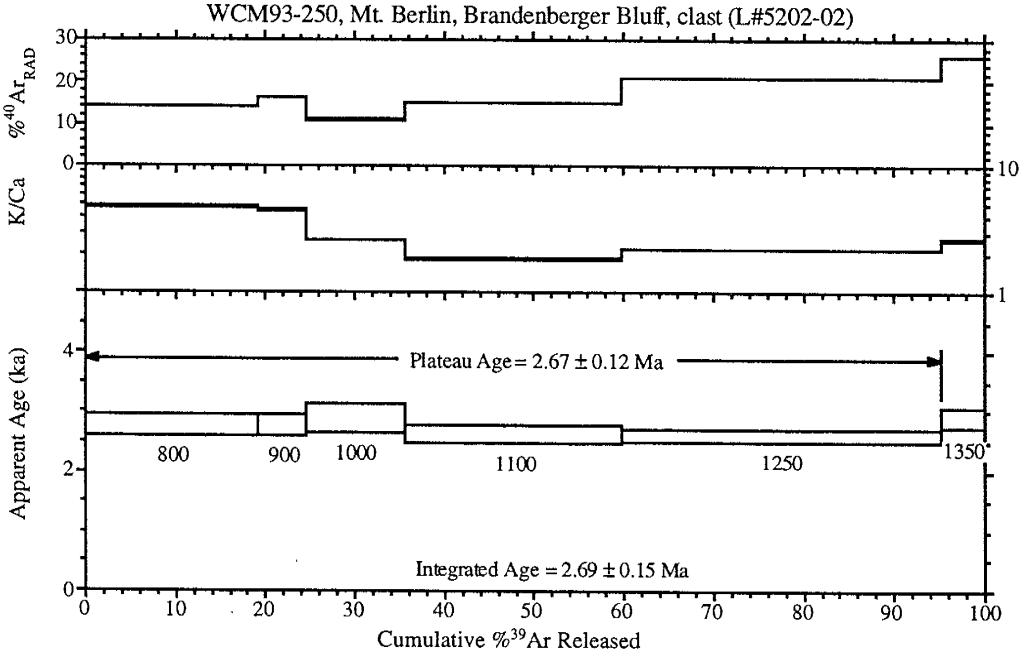

Appendix IV. $^{40}Ar/^{39}Ar$ Laser Data

Run ID#	$^{40}Ar/^{39}Ar$	$^{37}Ar/^{39}Ar$ $x10^{-2}$	$^{36}Ar/^{39}Ar$ $x10^{-4}$	$^{39}Ar_K$ moles $x10^{-15}$	K/Ca	$\%^{40}Ar^*$	Age	± 2 s.d.
Mt. Berlin summit crater								
WCM93-22, NM-32, single crystal, J=0.0002274								
Mt. Berlin, summit crater wall, trachyte welded tuff								
5014-10	0.2540	3.242	7.176	2.58	15.7	17.4	18	15
5014-05	0.4470	3.448	13.33	2.48	14.8	12.4	23	16
5014-02	0.2925	4.221	7.698	2.97	12.1	23.3	28	14
5014-07	0.3015	2.350	6.577	1.28	21.7	36.1	45	32
5014-03	0.2780	1.018	5.505	2.23	50.1	41.7	48	18
5014-08	0.3055	0.421	6.023	2.22	121.1	41.8	52	19
5014-01	0.8694	3.578	24.11	2.92	14.3	18.3	65	15
5014-06	1.395	2.613	39.86	1.81	19.5	15.7	90	23
weighted mean				n=8	33.7	37.4	**41**	**17**
WCM93-23, NM-32, single crystal, J=0.0002274								
Mt. Berlin, summit crater wall, trachyte welded tuff								
5015-05	1.792	1.670	59.59	0.788	30.6	1.8	13	42
5015-04	1.995	1.230	65.24	1.99	41.5	3.4	28	19
5015-09	1.149	1.224	36.49	2.46	41.7	6.2	29	25
5015-01	0.3854	1.188	10.43	3.00	42.9	20.2	32	12
5015-08	2.074	0.9983	66.76	1.50	51.1	4.9	42	40
weighted mean				n=5	41.6	7.3	**30**	**10**
WCM93-15, NM-32, single crystal, J=0.00022742								
Mt. Berlin, summit crater wall, trachyte lava								
5013-09	2.204	1.269	74.32	1.09	40.2	0.4	3	39
5013-07	1.236	0.9576	41.55	1.77	53.3	0.7	4	22
5013-05	0.4008	1.477	12.65	1.29	34.5	6.9	11	28
5013-04	0.9765	1.551	31.77	1.25	32.9	4.0	16	29
5013-10	1.189	1.260	38.64	3.11	40.5	4.1	20	15
5013-01	0.5565	1.216	17.16	1.51	42.0	9.0	20	24
5013-06	0.2614	1.013	7.082	2.48	50.3	20.2	22	14
5013-08	0.5371	0.8236	16.29	3.55	61.9	10.5	23	11
5013-03	0.2826	0.8214	7.254	2.91	62.1	24.3	28	12
5013-02	0.4805	0.8284	12.60	2.73	61.6	22.6	45	13
weighted mean				n=8	48.2	12.5	**25**	**14**
WCM93-15, 22, 23: mean of above three sample analyses (L# 5013, 5014, 5015)								
weighted mean				n=23	41.6	23.4	**31.5**	**7.8**

Appendix IV. $^{40}Ar/^{39}Ar$ Laser Data

Run ID#	$^{40}Ar/^{39}Ar$	$^{37}Ar/^{39}Ar$ $x10^{-2}$	$^{36}Ar/^{39}Ar$ $x10^{-4}$	$^{39}Ar_K$ moles $x10^{-15}$	K/Ca	$\%^{40}Ar^*$	Age	± 2 s.d.
Mt. Berlin Merram Peak crater								
WCM93-130, NM-15, single crystal, J=0.0014444								
WNW Merram, 1 m thick pumiceous phonolite fall								
1299-05	0.1227	0.0750	2.462	2.37	680	14.7	47	90
1299-09	0.1439	0.0833	2.853	1.42	613	19.2	72	146
1299-03	0.2043	0.0328	4.145	1.64	1553	24.4	130	128
1299-02	0.1167	0.0251	1.023	4.39	2036	46.7	142	49
1299-06	0.1673	0.2039	2.384	2.63	250	38.9	169	83
1299-01	0.1861	0.0767	2.969	16.8	665	35.7	173	13
1299-08	0.1667	0.0224	1.825	1.34	2282	48.5	211	161
weighted mean				n=7	1154	793.9	**167**	**21**
WCM93-123, NM-15, single crystal, J=0.0014495								
Mt. Berlin, Merram Crater, SE, black and yellow fall								
1297-03	0.1022	0.3188	1.007	4.16	160	39.8	106	53
1297-05	0.1981	0.5260	3.940	6.49	97	25.3	131	35
1297-02	0.1647	0.0939	2.711	6.38	543	32.0	138	34
1297-01	0.1000	0.7140	0.3956	21.9	71	56.9	149	10
1297-08	0.1297	0.4453	1.305	6.07	115	45.9	156	36
1297-10	0.1656	0.3480	2.017	3.31	147	44.9	194	65
1297-06	0.0961	0.3750	-0.7926	4.53	136	91.4	230	50
1297-04	0.1446	2.6154	0.7069	5.97	20	64.8	245	37
weighted mean				n=8	161	160.9	**154**	**22**
WCM93-129, NM-15, single crystal, J=0.0014498								
Mt. Berlin, Merram Peak, WNW, welded, inflated fall deposit								
1298-08	0.2086	0.1338	4.651	7.20	381	18.8	103	32
1298-09	0.1151	0.1788	1.103	6.10	285	44.0	132	37
1298-07	0.1751	0.2151	2.534	18.8	237	39.1	179	12
1298-03	0.1138	0.6176	0.2607	19.0	83	65.5	195	11
1298-01	0.1473	1.2036	1.408	25.0	42	50.7	195	9
1298-02	0.1777	1.0610	2.378	20.7	48	42.9	200	11
1298-05	0.3264	0.9193	7.242	25.5	55	24.8	212	11
1298-06	0.1266	0.4181	-0.1811	6.35	122	79.2	262	35
1298-04	0.1150	1.4468	-0.6895	6.99	35	90.9	273	30
weighted mean				n=9	143	127	**197**	**17**

Appendix IV. $^{40}Ar/^{39}Ar$ Laser Data

Run ID#	$^{40}Ar/^{39}Ar$	$^{37}Ar/^{39}Ar$ $x10^{-2}$	$^{36}Ar/^{39}Ar$ $x10^{-4}$	$^{39}Ar_K$ moles $x10^{-15}$	K/Ca	$\%^{40}Ar^*$	Age	± 2 s.d.
WCM93-139, NM-32, single crystal, J=0.0002285								
Mt. Berlin, Merram Peak Crater								
5001-08	0.5844	0.7556	8.653	2.76	67.5	56.3	136	19
5001-07	0.5308	0.5142	6.430	2.81	99.2	64.2	141	18
5001-01	0.4831	0.7139	0.9902	4.19	71.5	94.0	187	17
5001-10	0.6582	3.0304	6.313	1.08	16.8	72.0	195	34
5001-04	0.7415	0.7267	6.759	4.32	70.2	73.1	223	14
5001-05	0.5786	0.7882	1.040	2.85	64.7	94.8	226	19
weighted mean				n=6	65.0	26.7	**187**	**34**

Mt. Berlin- trachytic flank deposits

WCM-93-11, NM-34, single crystal, J=0.0014759								
Mt. Berlin, Petrel's Crown, trachytic strombolian vent								
5182-05	0.2010	2.261	4.035	7.57	22.6	41.5	222	35
5182-03	0.1281	1.419	1.373	12.8	36.0	69.0	235	20
5182-09	0.1470	2.234	1.739	5.60	22.8	66.1	258	57
5182-07	0.1314	2.557	1.121	7.19	20.0	76.1	266	39
5182-08	0.1010	1.892	0.02962	7.40	27.0	100	270	40
5182-01	0.1580	1.411	1.448	6.87	36.2	73.5	309	40
5182-02	0.1197	1.993	0.0925	5.11	25.6	98.8	315	51
5182-10	0.1407	2.369	0.5735	8.16	21.5	89.1	334	41
5182-06	0.1421	2.388	0.5907	5.30	21.4	88.9	336	51
weighted mean					25.9	6.2	**266**	**30**
WCM-93-152, NM-34, single crystal, J=0.0014753								
Mt. Berlin, Wedemeyer Rock, trachyte ignimbrite								
5190-02	0.1047	1.241	1.968	4.25	41.1	45.2	126	52
5190-05	0.1120	2.790	1.962	6.25	18.3	50.0	149	39
5190-04	0.1142	0.7881	1.560	8.25	64.7	60.0	182	28
5190-03	0.0873	1.509	0.0865	7.00	33.8	98.2	228	33
5190-01	0.1312	1.158	1.540	13.2	44.1	65.8	230	17
5190-06	0.1124	1.309	0.6846	13.6	39.0	82.7	248	18
weighted mean					40.2	15.1	220	31

Appendix IV. $^{40}Ar/^{39}Ar$ Laser Data

Run ID#	$^{40}Ar/^{39}Ar$	$^{37}Ar/^{39}Ar$ $x10^{-2}$	$^{36}Ar/^{39}Ar$ $x10^{-4}$	$^{39}Ar_K$ moles $x10^{-15}$	K/Ca	$\%^{40}Ar^*$	Age	± 2 s.d.
Mt. Berlin- S. Merram Peak								
WCM-93-134, NM-34, single crystal, J=0.0014753								
Mt. Berlin, Kraut Rocks, trachyte lava								
5186-01	0.2818	2.700	5.113	2.44	18.9	47.0	353	101
5186-02	0.2798	1.180	4.793	2.70	43.2	49.6	369	84
5186-05	0.2471	1.202	3.684	4.30	42.4	56.2	370	53
5186-06	0.3942	2.259	8.393	1.47	22.6	37.5	393	155
5186-03	0.1825	3.008	0.2070	2.10	17.0	97.8	475	110
5186-04	0.2420	2.779	1.707	1.86	18.4	80.0	515	124
5186-09	0.2639	0.445	1.004	2.08	114.6	88.8	624	125
weighted mean					39.6	35.0	**410**	**72**
WCM-93-135, NM-34, single crystal, J=0.0014753								
Mt. Berlin, Kraut Rocks, trachyte lava								
5187-09	0.2176	1.237	0.7518	3.79	41.2	90.1	522	68
5187-07	0.2850	0.9587	2.316	4.45	53.2	76.2	578	61
5187-06	0.2268	0.5783	0.3020	25.4	88.2	96.2	580	11
5187-05	0.3250	3.411	3.307	10.7	15.0	70.7	611	27
5187-10	0.2780	1.265	1.659	13.2	40.3	82.6	612	20
5187-01	0.2582	0.8979	0.9333	11.1	56.8	89.5	615	22
5187-03	0.4225	1.007	6.123	16.9	50.7	57.3	644	17
5187-04	0.3507	1.407	3.624	8.85	36.3	69.7	651	32
5187-02	0.2557	0.6796	0.3013	18.6	75.1	96.6	658	14
weighted mean					50.8	21.6	**616**	**24**
WCM-93-135, NM-34, single crystal, J=0.0014753								
Mt. Berlin, Kraut Rocks, trachyte lava								
5188-09	0.1823	1.482	2.074	4.92	34.4	66.9	325	62
5188-06	0.2247	0.7831	0.3008	7.00	65.2	96.2	575	40
5188-05	0.2643	0.5711	1.468	13.9	89.3	83.7	589	20
5188-07	0.2262	1.037	0.1186	8.84	49.2	98.7	594	33
5188-02	0.2503	1.032	0.8212	17.1	49.4	90.5	603	15
weighted mean					57.5	20.8	**588**	**48**
WCM93-135: mean of above two sample analyses (L# 5187, 5188)							**608**	**22**

Appendix IV. $^{40}Ar/^{39}Ar$ Laser Data

Run ID#	$^{40}Ar/^{39}Ar$	$^{37}Ar/^{39}Ar$ $x10^{-2}$	$^{36}Ar/^{39}Ar$ $x10^{-4}$	$^{39}Ar_K$ moles $x10^{-15}$	K/Ca	$\%^{40}Ar^*$	Age	± 2 s.d.
Mt. Berlin- distal englacial tephra at Mt. Moulton								
WCM93-313, NM-32, single crystal, J=0.0002285								
Mt. Moulton, englacial tephra 5								
5002-02	0.1335	0.6315	4.141	2.01	80.8	8.6	5	24
5002-08	0.1474	0.8605	2.906	2.61	59.3	42.1	26	19
5002-06	0.2992	1.503	5.845	1.09	34.0	42.6	52	43
5002-10	0.1082	5.043	-4.594	1.00	10.1	229	102	38
5002-07	1.4929	9.353	39.85	2.23	5.5	21.6	133	23
weighted mean				n=5	37.9	32.2	**55**	**52**
WCM93-315, NM-32, single crystal, J=0.0002285								
Mt. Moulton, englacial tephra 4								
5004-01B	0.3520	0.6369	8.825	2.42	80.1	26.0	38	15
5004-03	0.3858	0.6523	7.547	0.833	78.2	42.3	67	42
5004-05	0.3746	1.072	7.077	0.793	47.6	44.3	68	47
5004-06	0.9314	0.2053	25.88	1.67	248	17.9	69	23
5004-04	0.5136	1.064	9.373	0.779	48.0	46.2	98	47
5004-02	0.4495	0.4097	5.381	1.10	125	64.7	120	31
5004-07	0.3530	0.1106	1.434	0.548	461	88.0	128	68
weighted mean				n=7	155	152	**61**	**26**
WCM93-316, NM-36, single crystal, J=0.0002176								
Mt. Moulton, englacial tephra 3								
5355-05	0.2742	1.419	5.838	2.16	35.9	37.4	40	14
5355-09	0.3757	1.384	8.455	1.63	36.9	33.7	50	21
5355-04	0.2569	0.8738	3.395	2.77	58.4	61.1	62	12
5355-07	0.2627	0.3993	3.252	3.89	128	63.5	65	8
5355-10	0.2442	0.5500	1.576	3.15	92.8	81.0	78	11
5355-02	0.2772	0.5079	2.195	2.58	100	76.7	83	15
5355-06	0.8278	1.065	20.68	4.26	47.9	26.2	85	8
5355-01	0.6857	1.130	15.81	3.11	45.2	32.0	86	14
5355-03	0.3071	2.764	3.003	2.52	18.5	71.7	86	14
5355-08	0.2797	0.8363	1.978	2.33	61.0	79.3	87	14
weighted mean				n=10	62.5	34.1	**74**	**18**

Appendix IV. $^{40}Ar/^{39}Ar$ Laser Data

Run ID#	$^{40}Ar/^{39}Ar$	$^{37}Ar/^{39}Ar$ $x10^{-2}$	$^{36}Ar/^{39}Ar$ $x10^{-4}$	$^{39}Ar_K$ moles $x10^{-15}$	K/Ca	$\%^{40}Ar^*$	Age	± 2 s.d.
WCM93-317, NM-36, single crystal, J=0.0002165								
Mt. Moulton, englacial tephra 2								
5356-06B	0.2917	0.9162	5.945	1.13	55.7	40.0	46	33
5356-05B	0.3210	0.9523	5.306	1.58	53.6	51.3	64	22
5356-07B	0.3193	2.676	3.398	3.05	19.1	69.1	86	11
5356-03	0.3142	1.014	2.366	2.43	50.3	77.9	96	14
5356-02	0.3413	1.783	3.162	3.58	28.6	73.0	97	10
5356-01	0.4454	1.055	6.406	2.45	48.4	57.6	100	14
5356-04B	0.3242	0.7799	2.185	2.46	65.4	80.2	102	13
weighted mean				n=7	45.9	16.2	**93**	**34**
WCM93-314, NM-32, single crystal, J=0.0002285								
Mt. Moulton, englacial tephra 1								
5003-04	0.3572	0.6185	2.435	1.68	82.5	79.9	118	21
5003-05	0.3776	0.4652	2.946	2.04	109.7	77.0	120	15
5003-03	0.5029	0.5676	6.848	1.44	89.9	59.8	124	23
5003-01	0.3252	0.5652	0.7098	4.37	90.3	93.6	126	8
weighted mean				n=4	93.1	11.6	**123.5**	**7.5**
WCM93-314, NM-36, single crystal, J=0.00021713								
Mt. Moulton, englacial tephra 1								
5354-03	0.3236	0.4638	2.391	3.15	110	78.2	99	13
5354-04	0.3647	0.5835	1.708	3.60	87.4	86.2	123	12
5354-10	0.3610	0.6494	1.535	1.76	78.6	87.5	124	25
5354-05	0.6354	3.7608	10.02	2.68	13.6	53.8	134	16
5354-09	0.3596	0.7121	0.522	1.27	71.6	95.8	135	36
5354-06	0.3487	0.4641	0.144	2.44	110	98.8	135	18
5354-01	0.4694	0.2552	3.934	2.50	200	75.2	138	16
weighted mean				n=7	95.9	56.2	**123**	**13**
WCM93-314, NM-32, single crystal, J=0.0002285								
Mt. Moulton, englacial tephra 1								
5003-04A	0.6159	1.871	14.10	0.525	27.3	32.6	83	80
5003-02B	0.3549	0.9422	4.443	0.706	54.2	63.2	92	54
5003-03A	0.4231	1.259	6.176	0.708	40.5	57.0	99	59
5003-03B	0.3455	0.6006	2.255	0.782	84.9	80.8	115	54
5003-04B	0.3331	0.9879	0.0115	1.59	51.6	100	137	26
5003-02A	0.3871	1.181	0.6707	0.861	43.2	95.1	152	44
weighted mean				n=6	50.3	19.5	**111**	**41**
WCM93-314,mean of above three sample analyses (L# 5003, 5354)								
weighted mean				n=17	79.1	42.6	**123.5**	**7.3**

Appendix IV. $^{40}Ar/^{39}Ar$ Laser Data

Run ID#	$^{40}Ar/^{39}Ar$	$^{37}Ar/^{39}Ar$ $x10^{-2}$	$^{36}Ar/^{39}Ar$ $x10^{-4}$	$^{39}Ar_K$ moles $x10^{-15}$	K/Ca	$\%^{40}Ar^*$	Age	± 2 s.d.
Mt. Siple summit crater								
WCM93-277, NM-15, single crystal, J=0.0014401								
Mt. Siple, summit crater wall, densely welded fall								
1300-09	0.1948	0.1214	5.272	1.40	420	3.6	18	112
1300-04	0.2039	0.1912	5.557	3.36	267	3.9	20	51
1300-05	0.1895	0.2340	3.371	2.43	218	30.6	151	69
1300-01	0.2366	0.3074	4.931	9.48	166	25.0	154	20
1300-08	0.2150	0.1296	3.989	2.35	394	30.4	169	68
1300-03	0.1404	0.1024	1.414	4.62	498	47.5	173	38
1300-07	0.1489	0.0919	1.217	6.11	555	54.4	211	27
1300-10	0.1692	0.1320	1.719	1.83	387	51.1	225	85
1300-02	0.1630	0.1486	0.6647	3.42	343	68.4	289	51
weighted mean				n=9	361	127.2	**170**	**42**

Appendix V.: Relative Probability Plots of Laser-Fusion Data

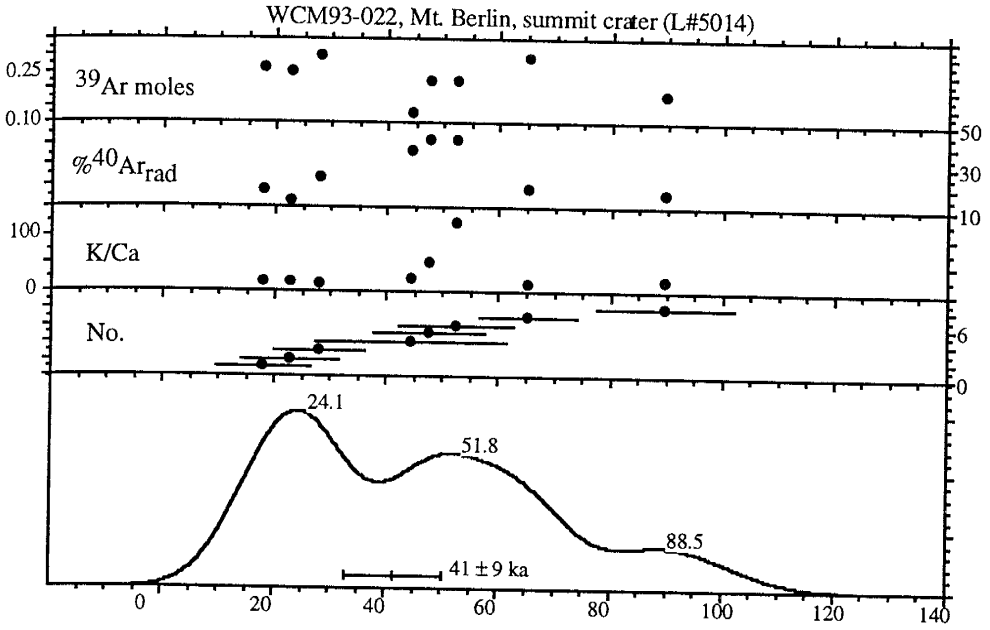

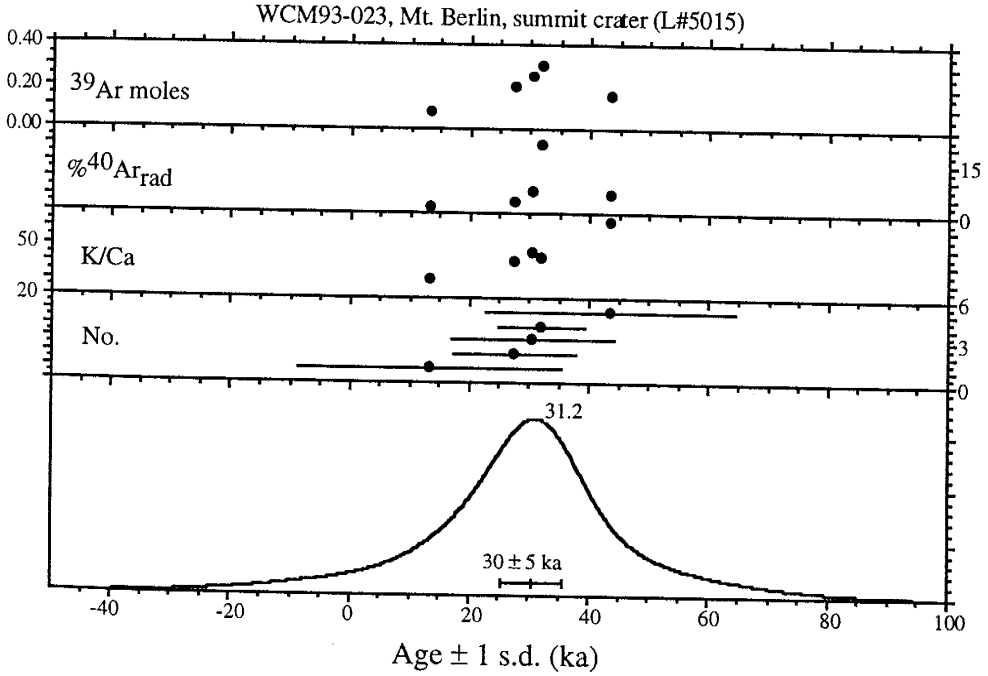

Appendix V.: Relative Probability Plots of Laser-Fusion Data

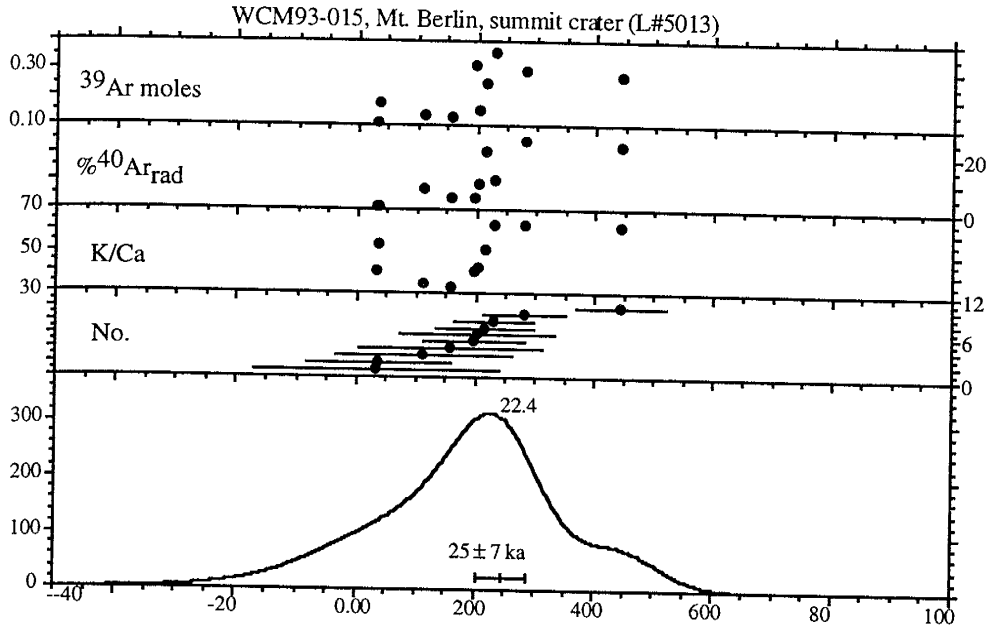

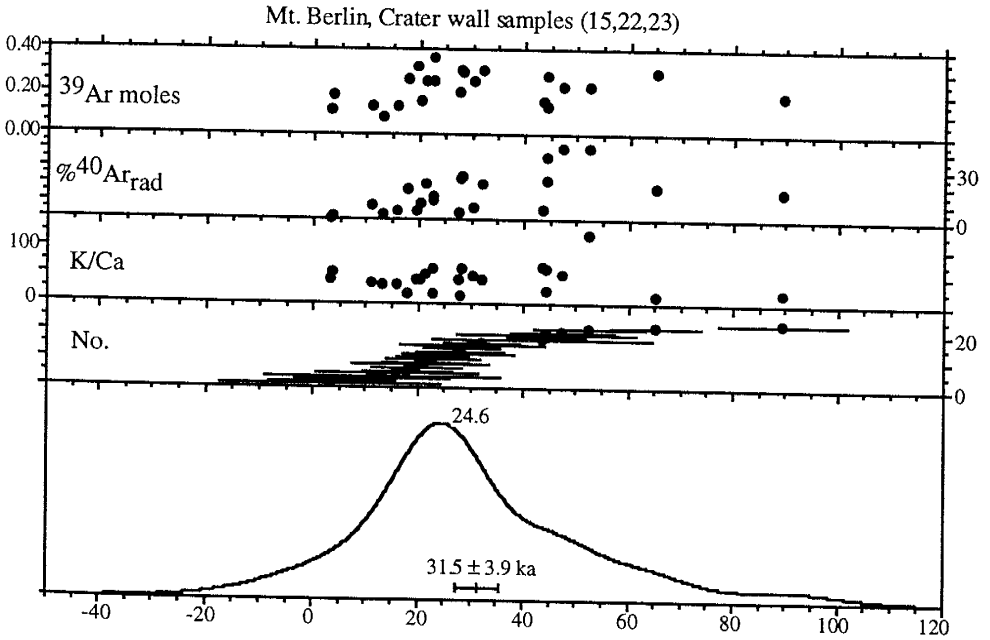

Appendix V.: Relative Probability Plots of Laser-Fusion Data

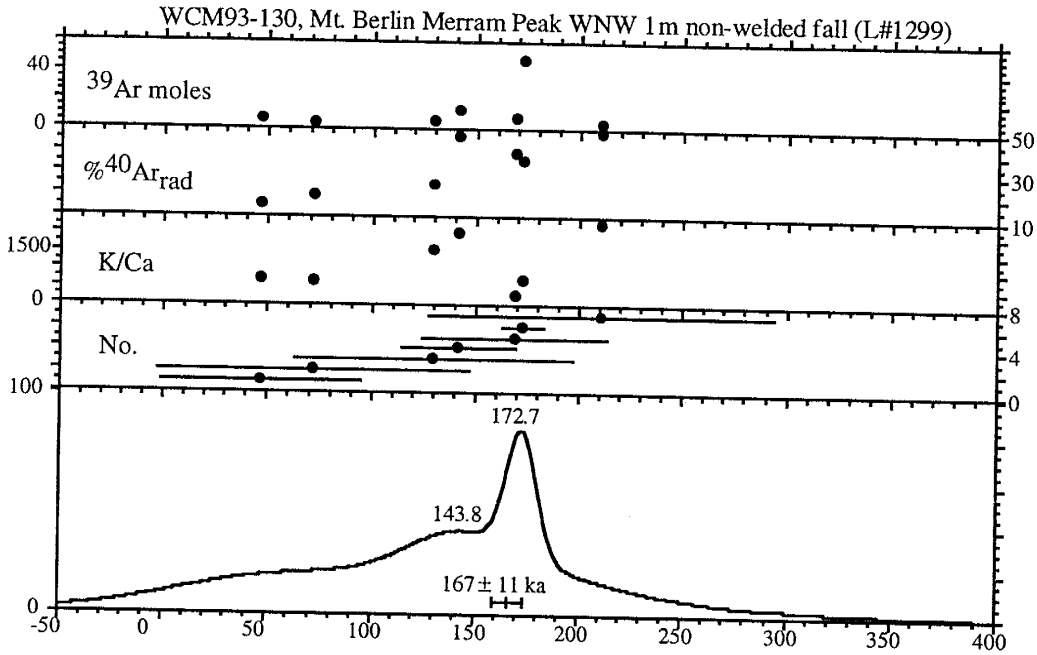

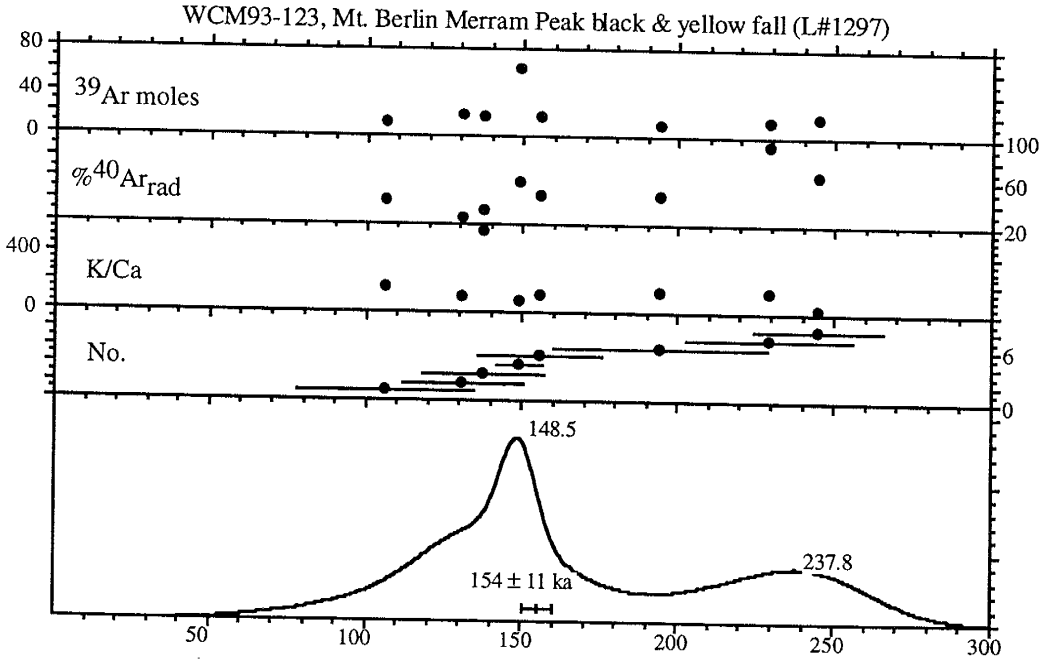

Appendix V.: Relative Probability Plots of Laser-Fusion Data

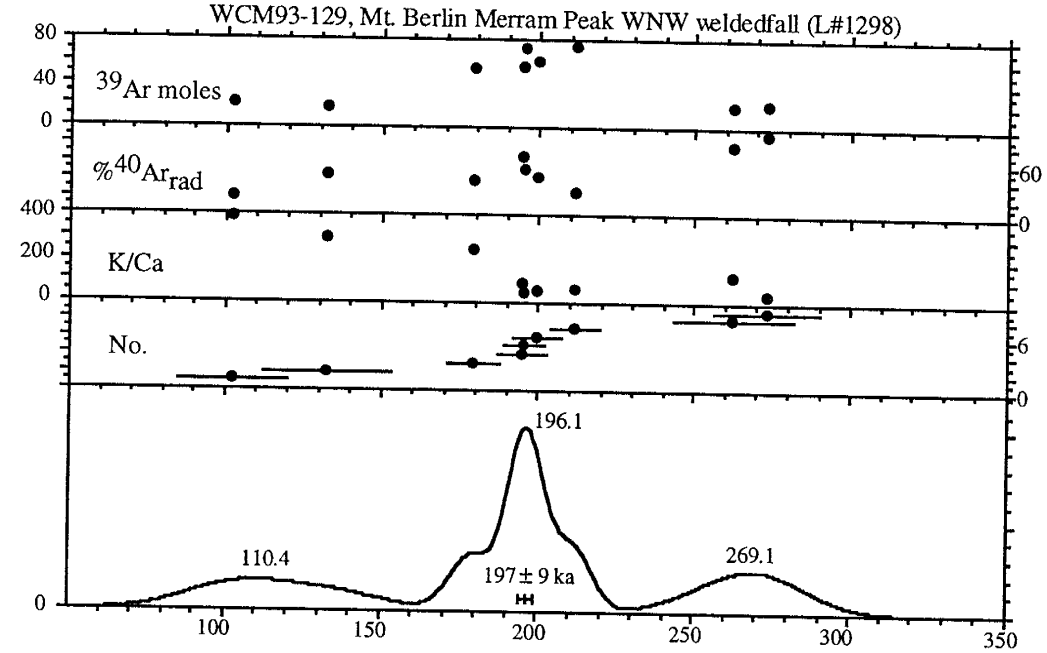

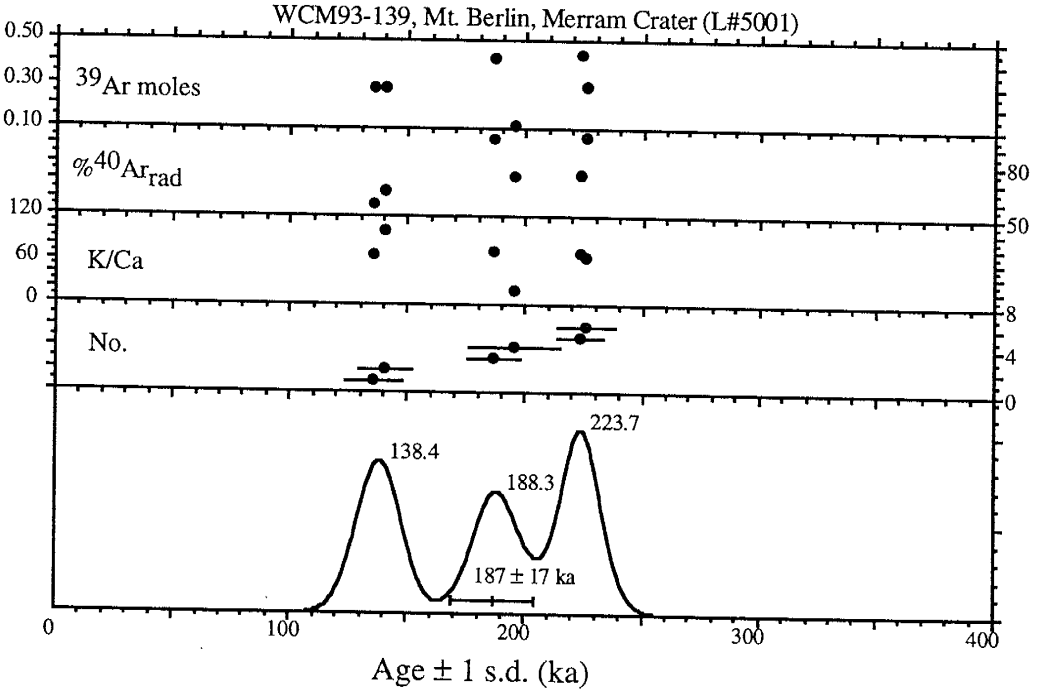

Appendix V.: Relative Probability Plots of Laser-Fusion Data

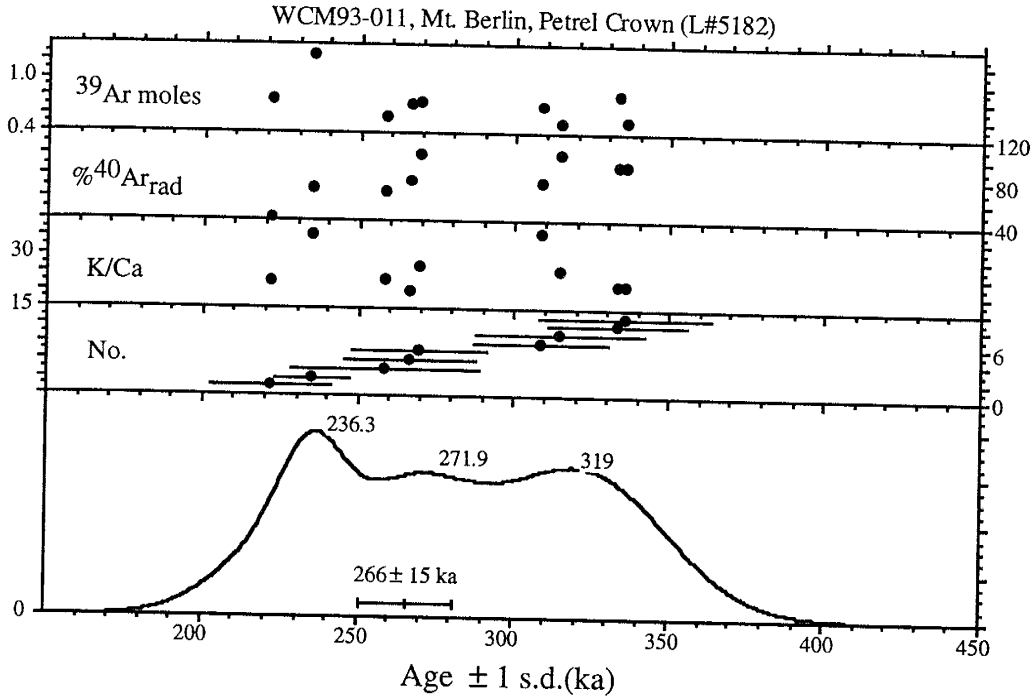

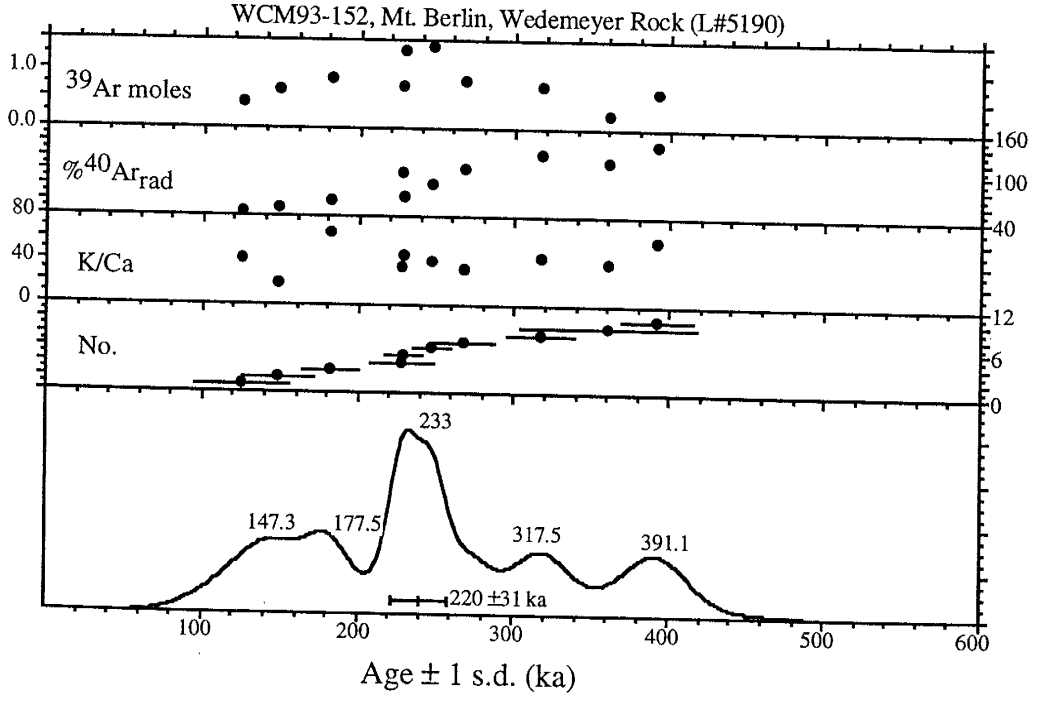

Appendix V.: Relative Probability Plots of Laser-Fusion Data

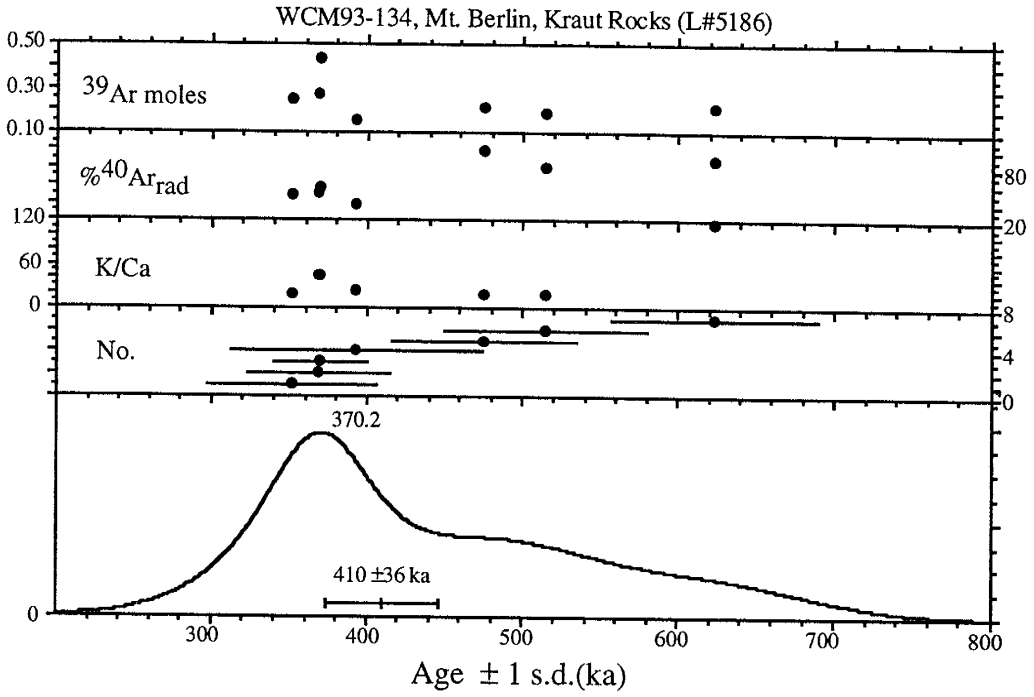

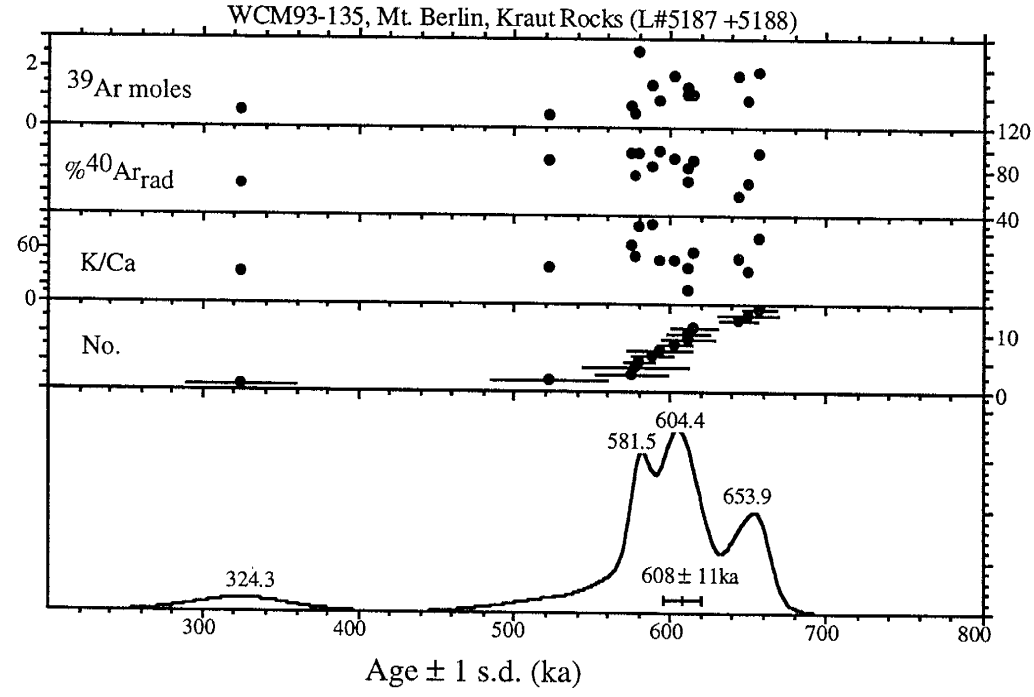

Appendix V.: Relative Probability Plots of Laser-Fusion Data

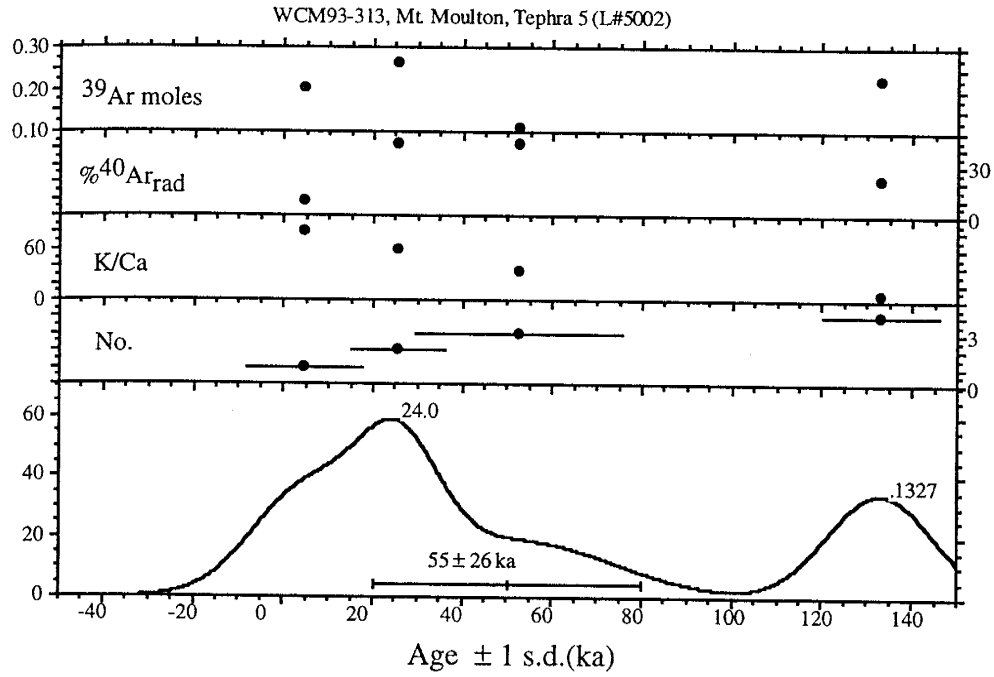

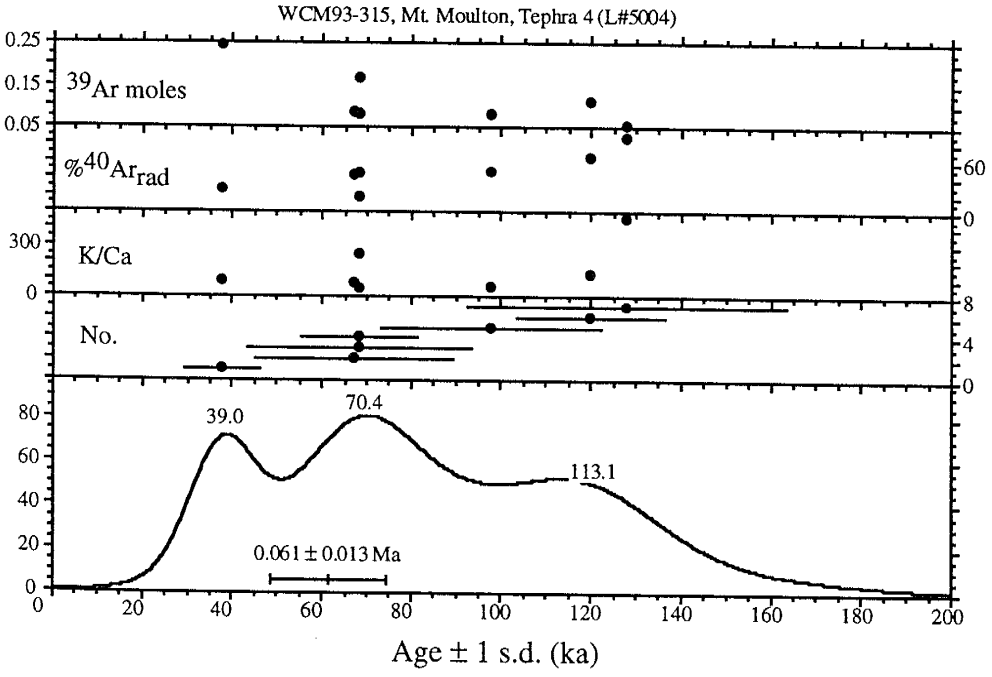

Appendix V.: Relative Probability Plots of Laser-Fusion Data

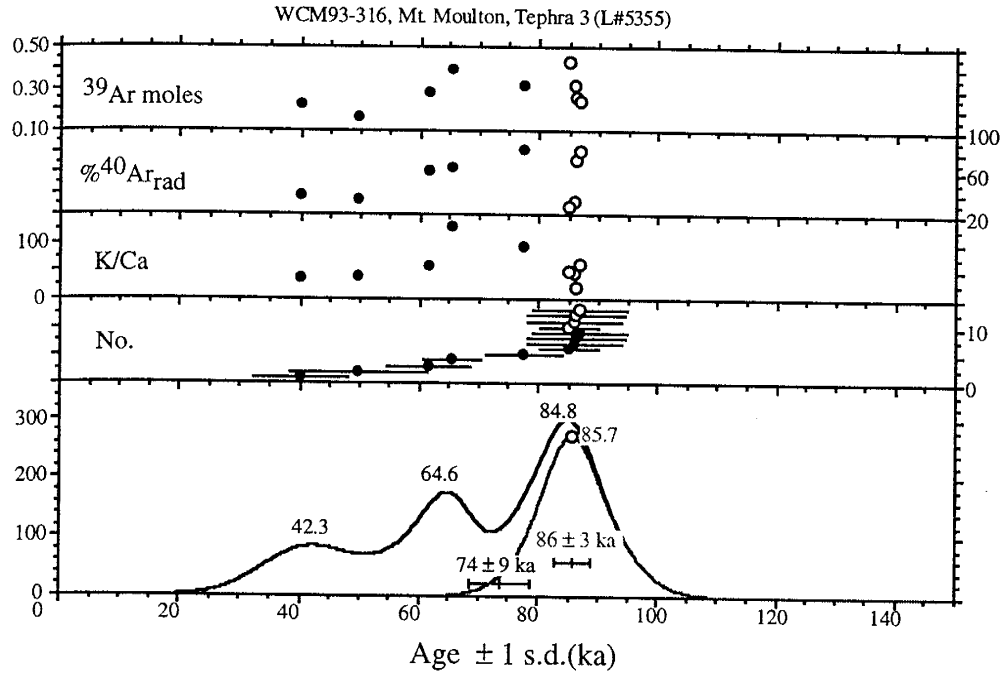

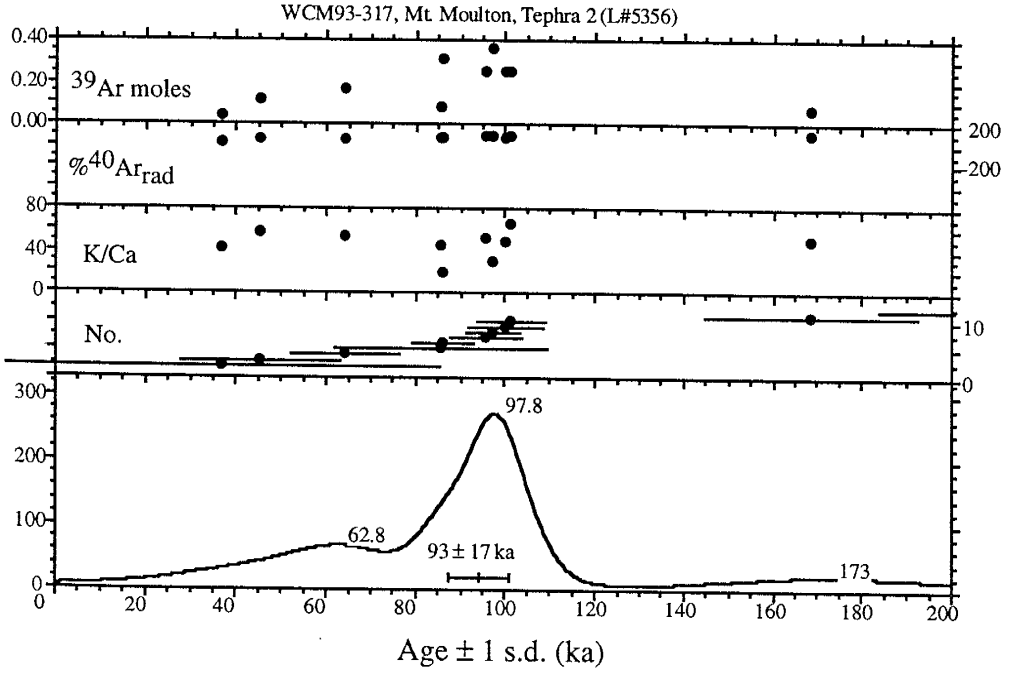

Appendix V.: Relative Probability Plots of Laser-Fusion Data

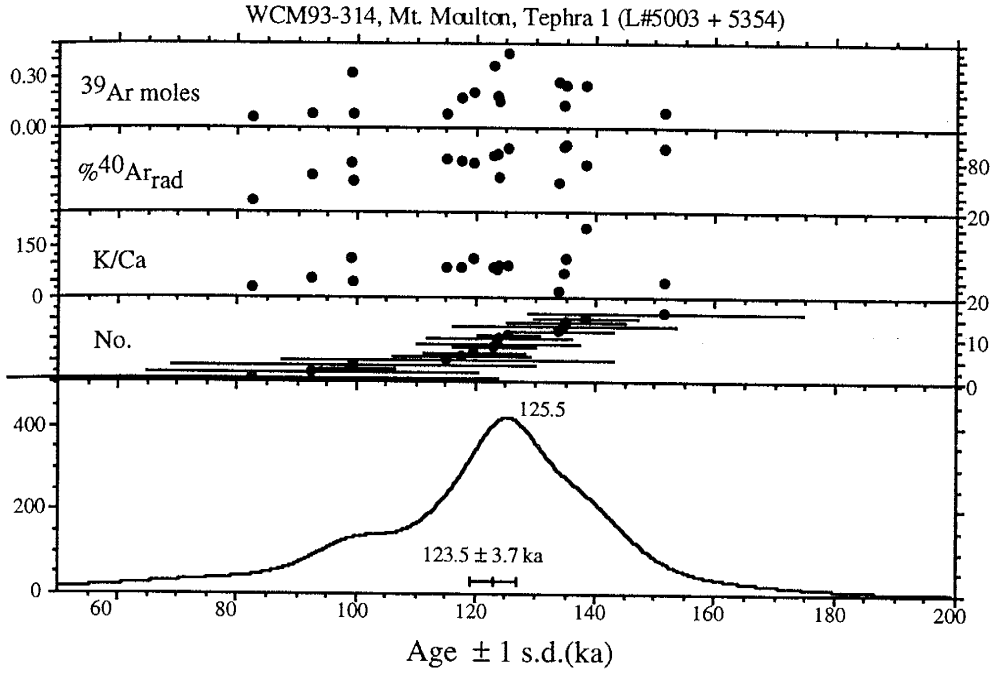

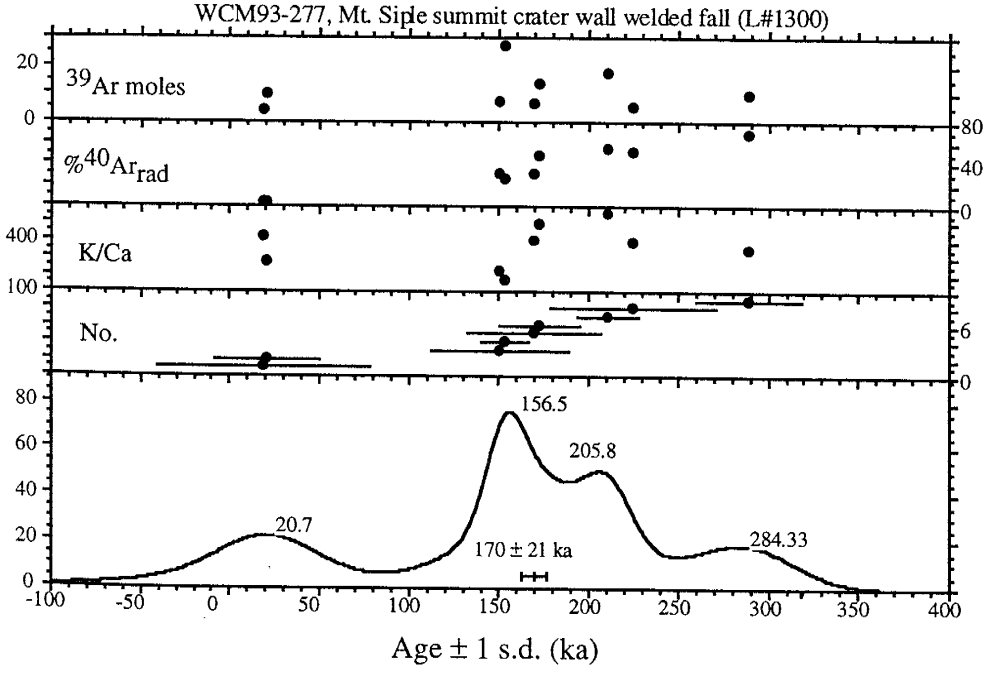

Appendix VI. Table 1. XRF Geochemical Data

WCM93-	16	313	315	15	22	23	316	314	130	128
Volcano	Berlin	Moulton	Moulton	Berlin	Berlin	Berlin	Moulton	Moulton	Berlin	Berlin
Rock Type	trach	phon	trach	trach	trach	trach	trach	trach	phon	trach
Lab.	UK	UK	UK	UK	UK	UK	UK	UK	UK	NM,UK
Age (ka)	12	15	23	26	26	26	92	118	141	185
SiO_2	61.12	60.26	61.20	61.73	60.96	61.72	61.55	63.03	61.66	63.45
TiO_2	0.53	0.44	0.50	0.52	0.61	0.56	0.54	0.41	0.41	0.43
Al_2O_3	15.77	13.58	13.26	13.48	14.40	13.94	13.39	13.55	13.28	14.50
Fe_2O_3	9.03	9.63	9.59	9.65	9.25	9.65	9.36	8.30	9.01	7.57
MnO	0.30	0.30	0.29	0.29	0.31	0.31	0.29	0.24	0.29	0.24
MgO	0.14	0.00	0.00	0.00	0.03	0.00	0.00	0.00	0.00	0.10
CaO	2.05	0.92	1.02	1.12	1.78	1.35	1.10	0.79	0.86	1.18
Na_2O	6.71	10.21	9.26	8.46	7.63	8.41	9.09	9.12	9.65	7.53
K_2O	4.36	4.28	4.48	4.56	4.66	4.59	4.52	4.50	4.43	4.86
P_2O_5	0.10	0.04	0.03	0.04	0.07	0.04	0.04	0.02	0.02	0.04
LOI	0.00	0.16	0.00	0.15	0.11	0.00	0.14	0.44	0.22	0.08
Total	100.09	99.81	99.59	99.99	99.82	100.31	100.02	100.41	99.83	99.94
P.I.	1.00	1.58	1.51	1.40	1.22	1.35	1.48	1.47	1.56	1.22
Cl	56	1237	1001	2111	509	750	1573	1095	1431	0
S	62	455	1060	153	56	93	354	140	112	45
V	0	1	3	0	0	3	0	0	1	1
Cr	2	0	0	0	0	0	0	1	0	7
Ni	5	6	5	6	6	6	5	5	7	4
Cu	9	8	8	8	9	8	11	7	9	4
Zn	180	382	297	280	175	265	336	304	372	219
Ga	32	45	42	41	32	39	44	41	45	36
As										0
Rb	60	150	125	120	70	110	196	151	212	110
Sr	153	7	5	10	12	12	9	3	4	7
Y	64	141	107	104	57	92	160	131	173	79
Zr	510	1591	1147	1102	557	995	2005	1411	1979	761
Nb	86	271	191	184	95	164	296	214	307	119
Mo										7
Ba	1417	38	46	81	465	207	50	14	16	196
La	86	204	132	114	64	126	238	194	245	86
Ce	187	517	368	333	192	301	570	488	588	255
Nd	63	146	122	96	66	88	175	155	175	88
Pb	15	25	19	21	17	19	31	28	33	25
Th	8	36	22	24	10	22	48	31	48	18
U										

Appendix VI. Table 1. XRF Geochemical Data

WCM93-	133	139	140	1	4	8	151	152	11	134
Volcano	Berlin	Berlin	Berlin	Berlin	Berlin	Berlin	Berlin	Berlin	Berlin	Berlin
Rock Type	trach	trach	trach	bas	bas	haw	ben	trach	trach	trach
Lab.	UK	UK	NM,NM	UK	UK	UK	NM	NM	UK,NM	NM
Age (ka)	185	185	185	236	236	236	<232	232	232	410
SiO_2	62.82	62.45	63.39	44.89	45.89	48.77	55.90	65.45	65.56	58.54
TiO_2	0.48	0.44	0.43	3.04	2.90	2.44	1.75	0.33	0.33	0.55
Al_2O_3	14.66	14.58	14.49	15.21	15.55	15.60	15.96	15.19	15.36	15.91
Fe_2O_3	7.85	7.71	7.62	13.93	13.74	12.33	10.46	5.49	5.29	9.32
MnO	0.25	0.25	0.24	0.22	0.22	0.22	0.25	0.16	0.16	0.26
MgO	0.00	0.00	0.33	7.50	6.73	6.11	1.55	0.00	0.05	0.34
CaO	1.37	1.31	1.37	9.53	8.80	8.14	4.46	1.02	0.98	2.47
Na_2O	7.63	8.03	7.30	4.27	4.61	4.63	5.99	6.91	6.92	7.22
K_2O	4.75	4.65	4.82	1.47	1.76	1.84	3.07	5.03	5.14	4.44
P_2O_5	0.03	0.03	0.06	0.78	0.83	0.73	0.77	0.04	0.02	0.21
LOI	0.25	0.83	0.29	0.00	0.00	0.00	0.00	0.00	0.05	0.18
Total	100.10	100.28	100.32	100.34	100.30	100.31	99.57	99.59	99.84	99.45
P.I.	1.21	1.25	1.19	0.57	0.61	0.62	0.83	1.11	1.10	1.05
Cl	156	14414		82	133	123			2	
S	124	1648		57	71	98			46	
V	2	2	0	183	158	110	17	0	1	0
Cr	0	4	5	178	129	140	10	0	11	13
Ni	2	3	0	109	85	85	0	0	0	4
Cu	6	6	0	54	50	44	0	0	4	0
Zn	199	193	211	95	99	103	152	156	169	139
Ga	34	34	37	15	22	21	31	39	38	34
As			0				0	0	0	0
Rb	95	94	99	34	36	35	69	190	194	85
Sr	10	10	9	821	873	755	621	7	6	194
Y	72	73	73	37	37	37	57	82	91	63
Zr	671	669	733	302	330	277	622	967	1075	806
Nb	103	101	119	65	71	54	107	151	154	130
Mo			7				6	12	8	10
Ba	305	240	276	409	459	833	698	29	14	1235
La	95	74		48	45	45			105	
Ce	234	223		105	115	96			281	
Nd	85	78		41	48	39			80	
Pb	35	21		11	13	11	12	39	32	11
Th	18	15	18	6	9	3	14	27	35	18
U							3	9		4

Appendix VI. Table 1. XRF Geochemical Data

WCM93-	127	126	135	137	138	124	125	9	14	10
Volcano	Berlin	Berlin	Berlin	Berlin	Berlin	Berlin	Berlin	Berlin	Berlin	Berlin
Rock Type	trach	trach	phon	trach	trach	trach	trach	trach	phono teph	phono
Lab.	UK	UK	NM	UK	UK	UK	UK	UK	UK,NM2	UK,NM3
Age (ka)	434	573	573	573	573	573	573	573	2700	2720
SiO_2	61.89	59.48	59.71	59.23	58.42	60.13	59.37	60.05	49.58	58.65
TiO_2	0.42	0.52	0.14	0.55	0.56	0.93	0.53	0.63	2.08	0.08
Al_2O_3	15.40	16.56	16.22	16.51	16.28	15.35	16.52	16.75	16.67	19.17
Fe_2O_3	8.02	8.78	7.35	8.87	8.87	9.24	8.75	8.07	13.18	5.01
MnO	0.25	0.27	0.22	0.27	0.27	0.28	0.27	0.25	0.25	0.15
MgO	0.00	0.31	0.02	0.29	0.35	0.52	0.25	0.29	2.80	0.27
CaO	1.54	2.27	0.76	2.31	2.38	2.31	2.26	2.09	6.47	0.72
Na_2O	8.00	7.44	9.43	7.42	7.16	6.84	7.36	6.71	5.65	9.28
K_2O	4.74	4.51	4.57	4.46	4.44	4.59	4.51	5.04	2.07	5.12
P_2O_5	0.04	0.15	0.05	0.17	0.18	0.22	0.16	0.15	1.10	0.02
LOI	0.25	0.09	0.35	0.16	0.79	0.01	0.17	0.00	0.00	1.52
Total	100.53	100.38	98.81	100.24	99.70	100.42	100.14	99.96	99.57	99.98
P.I.	1.19	1.03	1.26	1.03	1.02	1.06	1.03	0.98	0.69	1.09
Cl	6	665		379	338	19	549	167	179	1067
S	112	154		78	49	82	84	74	98	49
V	0	4	0	2	2	1	4	1	14	0
Cr	3	2	11	3	4	0	3	3	4	14
Ni	3	3	6	1	2	5	4	2	5	0
Cu	8	10	0	10	9	9	9	9	18	2
Zn	137	147	332	148	132	145	147	129	131	182
Ga	34	33	53	31	31	31	28	26	24	37
As			6						0	0
Rb	111	88	187	86	83	85	89	74	35	137
Sr	7	181	7	181	198	102	177	73	787	3
Y	71	67	146	67	64	62	66	49	49	77
Zr	817	786	2149	769	717	651	773	554	411	1311
Nb	145	114	348	116	106	100	114	90	80	199
Mo			25						5	8
Ba	151	971	69	919	884	1519	946	969	568	7
La	108	98		98	92	83	104	67	67	145
Ce	245	236		231	227	184	215	162	135	288
Nd	71	64		78	71	64	64	62	57	87
Pb	17	18	27	16	16	19	19	16	6	17
Th	19	17	47	19	17	15	19	12	5	25
U			12						0	5

Appendix VI. Table 1. XRF Geochemical Data

WCM93-	37	53	69	79	97	115	121	174	183	250
Volcano	Berlin	Berlin	Berlin	Berlin	Berlin	Berlin	Berlin	Berlin	Berlin	Berlin
Rock Type	phono	phono	phono	phono	phono	phono	phono	phono	phono	phono
Lab.	NM	NM	NM	NM	NM	NM	NM	NM	NM	NM
Age (ka)	2720	2720	2720	2720	2720	2720	2720	2720	2720	2720
SiO_2	58.18	58.29	58.05	58.30	58.39	58.60	58.52	58.27	58.31	58.52
TiO_2	0.18	0.28	0.30	0.31	0.29	0.25	0.22	0.32	0.31	0.23
Al_2O_3	17.76	17.46	17.24	17.39	17.30	17.58	17.70	17.31	17.44	17.66
Fe_2O_3	6.68	7.78	7.86	7.99	7.82	7.53	7.17	8.13	7.96	7.25
MnO	0.18	0.21	0.22	0.22	0.22	0.21	0.20	0.23	0.22	0.20
MgO	0.06	0.21	0.29	0.14	0.16	0.16	0.21	0.23	0.21	0.08
CaO	1.56	2.03	2.08	2.10	2.05	2.01	1.84	2.14	2.15	1.82
Na_2O	8.32	7.53	7.56	7.70	8.02	7.81	7.93	7.58	7.53	7.52
K_2O	4.88	4.69	4.49	4.64	4.55	4.72	4.86	4.57	4.62	4.79
P_2O_5	0.06	0.07	0.10	0.10	0.10	0.07	0.05	0.11	0.09	0.04
LOI	0.86	1.04	1.59	0.34	0.66	0.54	0.94	0.28	0.33	1.06
Total	98.70	99.60	99.79	99.22	99.57	99.49	99.64	99.17	99.17	99.16
P.I.	1.07	1.00	1.00	1.02	1.05	1.02	1.03	1.01	1.00	0.99
Cl										
S										
V	0	0	0	0	0	0	0	0	0	0
Cr	16	24	25	11	18	14	11	14	14	0
Ni	0	4	3	0	0	0	0	0	0	0
Cu	0	0	0	0	0	0	0	0	0	0
Zn	161	153	150	147	151	153	158	148	150	157
Ga	33	30	28	31	30	31	31	30	30	31
As	0	0	0	0	0	0	0	0	0	0
Rb	87	76	62	78	69	78	78	73	73	74
Sr	44	160	147	126	116	97	74	127	123	82
Y	68	59	56	58	58	62	66	58	57	64
Zr	936	807	785	787	796	834	879	783	786	869
Nb	189	157	153	153	155	162	173	152	152	170
Mo	11	39	12	9	10	6	7	7	6	7
Ba	800	1458	1492	1505	1464	1325	1144	1534	1501	1153
La										
Ce										
Nd										
Pb	7	9	8	8	9	9	10	7	7	7
Th	16	14	14	13	13	14	15	13	12	14
U	4	4	3	3	3	3	4	4	3	4

Appendix VI. Table 1. XRF Geochemical Data

WCM93-	254	277	278
Volcano	Berlin	Siple	Siple
Rock Type	phono	trach	trach
Lab.	UK	UK	UK
Age (ka)	2720	167	224
SiO_2	58.93	61.11	60.98
TiO_2	0.26	0.40	0.59
Al_2O_3	18.13	17.31	17.11
Fe_2O_3	7.43	5.96	5.92
MnO	0.21	0.14	0.12
MgO	0.05	0.14	0.30
CaO	1.87	1.25	1.55
Na_2O	8.05	7.93	6.66
K_2O	4.83	5.32	5.74
P_2O_5	0.04	0.04	0.09
LOI	0.43	0.23	0.92
Total	100.24	99.82	99.99
P.I.	1.02	1.09	1.00
Cl	480	912	471
S	54	49	59
V	0	0	0
Cr	3	3	6
Ni	1	3	0
Cu	7	12	11
Zn	150	144	84
Ga	30	33	29
As			
Rb	76	176	107
Sr	79	9	22
Y	65	79	36
Zr	805	1151	549
Nb	144	186	88
Mo			
Ba	1171	48	260
La	95.00	111	61
Ce	209	253	108
Nd	59	68	39
Pb	16	20	16
Th	13	25	10
U			

Appendix VI- Table 2. Microprobe chemical data from composite Byrd ice core sample

analysis no.	1	2	3	4	5	6	7	8	9	10	11	12
SiO_2	62.32	62.25	62.09	58.05	61.67	60.65	61.72	61.71	61.76	61.67	60.87	61.09
TiO_2	0.47	0.5	0.52	1.22	0.53	0.47	0.48	0.49	0.49	0.47	0.53	0.48
Al_2O_3	14.94	14.86	14.55	16.79	16.01	14.37	14.48	14.7	14.64	14.66	14.51	14.44
FeO	8.66	8.69	8.54	8.11	7.31	9.2	8.66	8.63	8.77	8.72	9.41	9.39
MnO	0.34	0.27	0.35	0.27	0.27	0.43	0.4	0.28	0.35	0.32	0.44	0.35
MgO	0.02	0.02	0	1.09	0.18	0.03	0.05	0	0.02	0.02	0.03	0
CaO	1.13	1.22	1.16	4.03	1.05	1.22	1.15	1.14	1.18	1.19	1.19	1.25
Na_2O	7.19	7.08	7.69	6.69	7.74	8.41	7.92	8.03	7.64	7.87	7.87	8.09
K_2O	4.32	4.53	4.44	3.09	4.7	4.57	4.54	4.52	4.58	4.56	4.47	4.43
P_2O_5	0.07	0	0.07	0.39	0.09	0.09	0.02	0.05	0.02	0.02	0.05	0
Cl	0.19	0.23	0.19	0.07	0.18	0.21	0.2	0.17	0.2	0.21	0.19	0.19
F	0.34	0.34	0.4	0.21	0.27	0.36	0.36	0.29	0.34	0.29	0.43	0.3
Total	100	100	100	100	100	100	100	100	100	100	100	100
Li			23	24					27	23		
B			6	9					11	11		
P			906	193					212	188		
Rb			63	158					153	133		
Sr			369.1	1					1	2.4		
Y			85	123					118	114		
Zr			609	1137					1102	1128		
Nb			91	221					205	211		
Ba			1133	11					8	9		
La			101	164					153	167		
Ce			218	333					335	335		
Nd			98	123					120	123		
Eu			12.2	5.98					4.68	4.56		
Th			10.8	13.4					17.5	17.1		
U			5.9	9.7					4.5	8.5		

Appendix VI. Table 3. Alkali feldspar Electron Microprobe Data

WCM93-	313	314	315	316
no. points	4	4	4	4
SiO_2	65.54 (0.74)	65.65 (0.20)	66.00 (0.19)	65.58 (0.31)
TiO_2	0.03 (0.03)	0.01 (0.01)	0.01 (0.01)	0.03 (0.01)
Al_2O_3	19.72 (0.40)	19.50 (0.13)	19.33 (0.17)	19.60 (0.20)
FeO	0.28 (0.10)	0.36 (0.03)	0.30 (0.06)	0.23 (0.05)
MnO	0.03 (0.03)	0.00 (0.01)	0.00 (0.00)	0.01 (0.02)
MgO	0.00 (0.00)	0.00 (0.00)	0.00 (0.00)	0.00 (0.00)
CaO	0.19 (0.15)	0.05 (0.03)	0.08 (0.03)	0.29 (0.11
Na_2O	8.60 (0.26)	8.64 (0.19)	8.34 (0.20)	8.12 (0.31)
K_2O	5.59 (0.19)	5.73 (0.14)	5.87 (0.11)	6.09 (0.12)
P_2O_5	0.00 (0.00)	0.00 (0.00)	0.03 (0.04)	0.02 (0.03)
Cl	0.00 (0.00)	0.01 (0.01)	0.00 (0.00)	0.00 (0.01)
F	0.03 (0.04)	0.06 (0.03)	0.04 (0.02)	0.03 (0.03)

Values are means of multiple analysis. Numbers in parentheses are 1 standard deviation uncertainties of mean values.

Part B: Eocene and Oligocene Volcanism at Mt. Petras, Marie Byrd Land: Implications for Middle Cenozoic Ice Sheet Reconstructions in West Antarctica

Abstract Evidence for one late Eocene and four middle Oligocene eruptions at Mt. Petras, Marie Byrd Land provides new insights into reconstructions of middle Tertiary ice-sheet configurations, surface topography, and volcanism in West Antarctica. Interpretations of the volcanic record at Mt. Petras based on detailed field lithofacies, petrographic, $^{40}Ar/^{39}Ar$ dating, and geochemical analyses are significantly different from previous interpretations based on reconnaissance studies. A massive, 25 m thick, mugearite lava near the summit of Mt. Petras is $^{40}Ar/^{39}Ar$ dated to 36.11±0.22 Ma (2 σ uncertainty), pushing back the onset of volcanism in the Marie Byrd Land Volcanic Province to latest Eocene time. Middle Oligocene (29-27 Ma) hawaiite volcaniclastic lithofacies at Mt. Petras are interpreted as products of mixed magmatic (strombolian-style) and phreatomagmatic (surtseyan-style) subaerial eruptions. The four hawaiite outcrop areas exhibit characteristics of near-vent tuff-cone environments. The near-vent deposits are located at different elevations and positions on Mt. Petras and suggest four separate eruptive centers, with eruptions dated to between 28.59±0.22 Ma and 27.18±0.23 Ma. The mixed surtseyan and strombolian eruptions imply intermittent contact with external water, which we infer was derived from melting of a thin, local ice cap or ice and snow on slopes. The 29-27 Ma volcanic deposits at Mt. Petras provide the oldest terrestrial evidence for glacial ice in Marie Byrd Land.

The 29-27 Ma tuff cone deposits overlie an erosional unconformity, with >400 m of topographic relief. The relatively high relief pre-volcanic environment is

suggestive of ongoing erosion and is inconsistent with previous interpretations that Mt. Petras was part of a single, regional, low relief, early Cenozoic erosion surface in West Antarctica.

Introduction

The mid-Cenozoic volcanic history at Mt. Petras (75°51'S, 128°38'W), coastal Marie Byrd Land is critical for interpretations of inception of Marie Byrd Land volcanism, early history of the West Antarctic Ice Sheet, and surface uplift of the Marie Byrd Land volcanic highlands (Fig. 1) (LeMasurier 1972a, 1972b; LeMasurier and Rex 1982, 1983; LeMasurier 1990b; LeMasurier et al. 1981;

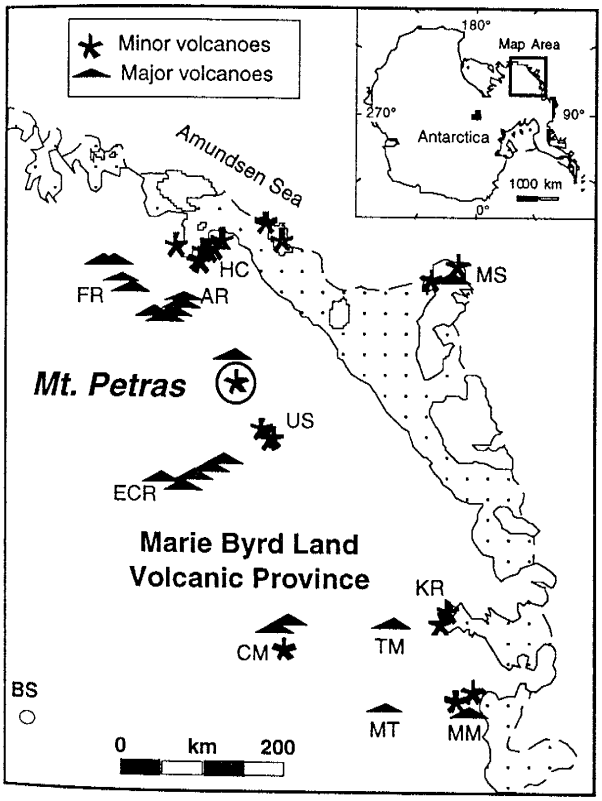

Fig. 1. Map of Marie Byrd Land volcanic province, located in coastal West Antarctica (base map from Drewry, 1983), with inset map of Antarctica continent. Major volcanoes (triangles) include stratovolcanoes and shield volcanoes from 2300 to 4000 m a.s.l. and minor volcanoes (stars) include mostly monogenetic smaller volcanoes (LeMasurier, 1990a). Mt. Petras is designated by an encircled star. Abbreviations: AR = Ames Range; BS = Byrd Station; CM = Crary Mountains; ECR = Executive Committee Range; FR = Flood Range; HC = Hobbs Coast nunataks; KR = Kohler Range; MM = Mount Murphy; MS = Mount Siple; MT = Mount Takahe; TM = Toney Mountains; US = U.S.A.S. Escarpment.

1994). Mt. Petras is a basement nunatak capped by the oldest volcanic rocks in Marie Byrd Land, which have been K-Ar dated to 22-25 Ma (LeMasurier 1990b). The volcanic rocks were previously interpreted as subglacial hyaloclastite erosional remnants of a volcanic table mountain and cited as the first evidence of a thick

regional ice-sheet in West Antarctica (LeMasurier et al. 1981). The volcanic rocks crop out at the summit region of Mt. Petras, where they overlie a bedrock unconformity situated at roughly 2700 m above sea level (LeMasurier et al. 1981). Similar pre-volcanic erosion surfaces in Marie Byrd Land are situated at progressively lower elevations and capped by progressively younger volcanic rocks away from Mt. Petras (LeMasurier and Rex 1983). LeMasurier and Landis (1996) suggested that these remnant surfaces represent relicts of a former regional erosion surface, termed the West Antarctic Erosion Surface (WAES), which was postulated to have formed by continent-wide early Cenozoic marine peneplanation. The elevation differences of these erosion surface remnants have been attributed to progressive domal uplift that accompanied volcanism since middle Cenozoic time (LeMasurier and Rex 1983).

In this paper, we present new data and interpretations on the timing and style of volcanism and on relief on the unconformity at Mt. Petras that differ from previous interpretations and have significant implications for reconstructions of volcanism, glacial history, and surface topography. Our analysis favors subaerial tuff cone eruptions in an ice-contact environment over deep subglacial eruptions. We infer that there is a suggestion of, but no definitive terrestrial evidence for, Oligocene glaciation in Marie Byrd Land. Finally, we suggest that the erosional unconformity at Mt. Petras exhibits relatively high topographic relief (>400 m) that is inconsistent with a model of a single. regional, early Cenozoic low-relief unconformity in Marie Byrd Land.

Geologic setting

In West Antarctica and the Ross Sea region, the relationships between volcanism, intracontinental rifting, and final break-up of Gondwana are not well understood. The break-up of Gondwana was achieved when New Zealand and the

Campbell Plateau separated from West Antarctica prior to 84 Ma (Chron 34; Lawver et al. 1992). Intracontinental rifting is well documented in the Ross Sea region, where the prominent rift-shoulder of the Transantarctic Mountains steps down to the Ross Sea Basin (Cooper and Davey 1985; Cooper et al. 1987, 1991; Fitzgerald 1992). The Ross Sea Basin consists of a series of sediment-filled horst and graben structures attributed to two rifting episodes: early rifting in the Late Cretaceous and late rifting beginning in the Eocene but intensifying in the Late Cenozoic (Cooper and Davey 1985; Cooper et al. 1987, 1991). The intracontinental rift zone is inferred to extend from the Ross Sea to beneath the West Antarctic Ice Sheet (Behrendt et al. 1991, 1996). On the north flank of the rift zone in West Antarctica, alkaline volcanoes of the Marie Byrd Land volcanic province have K-Ar ages as old as to 25 Ma (LeMasurier 1990b). Alkaline volcanoes on both the south and north flanks of the rift are still active today (Kyle 1990; LeMasurier 1990a). The geochemistry of the West Antarctic volcanic rocks suggests a mantle plume source (Behrendt et al. 1992; Kyle et al. 1991; Hole and LeMasurier 1994). High elevation pre-volcanic erosion surfaces in Marie Byrd Land are interpreted as a topographic expression of this plume (LeMasurier and Landis 1996).

Global cooling and the earliest development of the Antarctic Ice Sheet in the earliest Oligocene (ca. 33.7 Ma, time scale from Cande and Kent (1992)) are attributed to thermal isolation of the continent, strengthening of the circum-Antarctic current and the related major reorganization of ocean circulation patterns (Kennett and Barker 1990; Shackleton and Kennett 1975). Early Oligocene glacial diamictites, deposited on continental shelves during ice-sheet expansion, were recovered from drill holes in the Ross Sea and Prydz Bay (Barrett et al. 1987; Hambrey et al. 1991). On the basis of marine data, Kennett and Barker (1990) postulated that the West Antarctic Ice Sheet was fully developed by the Late

Miocene (~8 Ma) and achieved a stable configuration by the Early Pliocene. The pre-Late Pleistocene terrestrial record of the West Antarctic Ice Sheet is largely based on the volcanic record of ice-magma interactions and the presence of rare interbedded tills (LeMasurier 1972a, 1972b; LeMasurier and Rex 1982,1983; LeMasurier et al. 1994). LeMasurier and Rex (1982, 1983) interpreted 22-25 Ma K-Ar dated hyaloclastites at Mt. Petras as the first evidence of a thick, regional ice sheet .

Mt. Petras is glacially dissected nunatak (2867 m a.s.l.), with about 900 m of relief exposed above the level of the West Antarctic Ice Sheet. LeMasurier et al. (1981) reported that a low-relief (<100 m) pre-volcanic unconformity near the summit at ~ 2700 m a.s.l. is eroded into Cretaceous rhyodacite basement rocks, K-Ar dated to 80.8±5.7 Ma (LeMasurier and Wade 1976). Brief reconnaissance field work at the largest volcanic outcrop at Mt. Petras, located on the southwest flank, was the basis for interpretations of the volcanic rocks as 200 m of subhorizontally stratified basaltic hyaloclastite, composed of weakly vesicular clasts, and lacking any significant subaerial component (LeMasurier 1990b). These interpretations of the deposit characteristics together with the observation of interbedded rounded basement clasts led LeMasurier (1990b) to conclude that the volcanic rocks are the remnants of a subglacially erupted table mountain.

Methods

Fieldwork was carried out at Mt. Petras in January, 1994. All known outcrops were examined in detail and a total of 22 samples were collected for geochemical, petrographic and dating analysis (Fig. 2). Outcrop elevations were measured using a hand-held altimeter and elevations were corrected relative to the summit elevation of 2867 m a.s.l., as listed on the U.S.G.S. topographic map.

A sedimentary facies approach was used to characterize volcanic deposits and interpret former eruptive conditions and depositional environments, following recent examples by McPhie et al. (1993), Smellie et al. (1993) and Sohn (1997). Lithofacies at Mt. Petras are based on: 1) rock type (lava or clastic); 2) grain size; 3) sedimentary structures; and 4) clast characteristics (morphology, vesicularity, componentry; after Smellie et al. 1993). Measurements of lithofacies features are based on visual estimates of thin sections and outcrops.

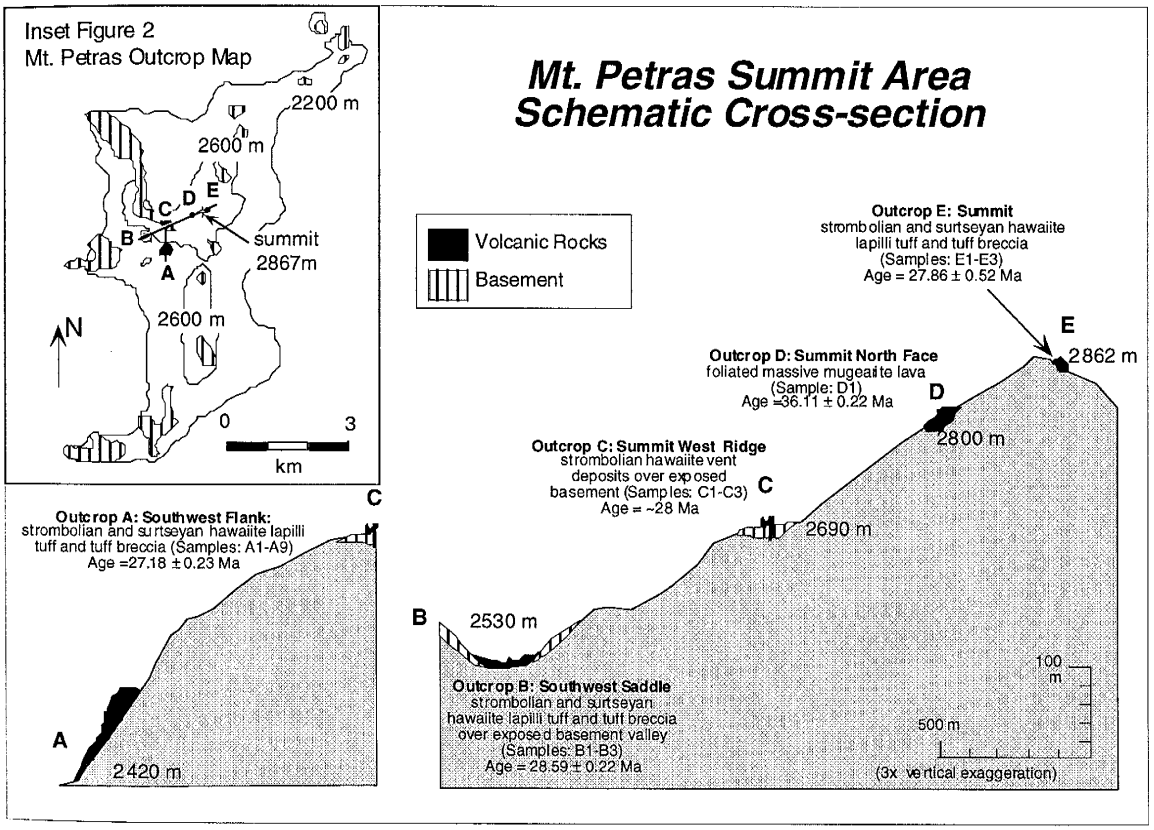

Fig. 2. Schematic cross-section of summit region of Mt. Petras, showing volcanic study sites. Cross-section lines A-C and B-C-D-E are shown on inset topographic map of Mt. Petras outcrops. Most of Petras is covered by snow and ice; basement is shown where it is exposed at surface. Base map is from the McCuddin Mountains quadrangle, scale 1:250,000. (U.S.G.S., 1973). USGS Reconnaissance Series, Antarctica, U.S. Geological Survey.

Six lava and pyroclastic bomb samples were prepared for geochemical and $^{40}Ar/^{39}Ar$ geochronological analyses. The 2-6 kg mafic rock samples were gray to black, slightly vesicular to massive, and unweathered. Major and trace element data on the six samples were obtained by standard X-ray fluorescence methods at the University of Kiele on an ARL8420 spectrometer. Thin sections of lava and bomb samples were analyzed for mineralogy and alteration under a cross-polarizing petrographic microscope. $^{40}Ar/^{39}Ar$ dating sample preparation and analyses were conducted at the New Mexico Geochronology Research Laboratory at the New Mexico Institute of Mining and Technology, Socorro, NM, according to methods described in Appendix I. Six samples were dated, including five holocrystalline groundmass concentrates and one visibly unaltered, aphyric, sideromelane glass concentrate.

Geochemistry and Geochronology Results

Four of the five outcrop groups at Mt. Petras are hawaiite, the fifth is mugearite (Table I; Figs. 2 and 3). The hawaiite samples are blocks and bombs from volcaniclastic rock sequences and cluster into two populations in terms of major and trace element data (Fig. 3, Table I).

One hawaiite population (samples A7, B2, and E1) borders on the hawaiite/basanite boundary and is slightly more sodic and less evolved than the second hawaiite population (sample C1). Previously reported geochemical data (LeMasurier 1990b) are most similar to the less evolved hawaiite population (Fig. 3). In addition to the hawaiites, mugearite lava (sample D1) crops out just north of the summit and a chemically identical mugearite xenolith clast (sample A2) was sampled in the hawaiite volcaniclastic deposits. The mugearite lava is more evolved chemically (Fig. 3) than the hawaiites. The three distinct chemical populations suggest at least three separate eruptions.

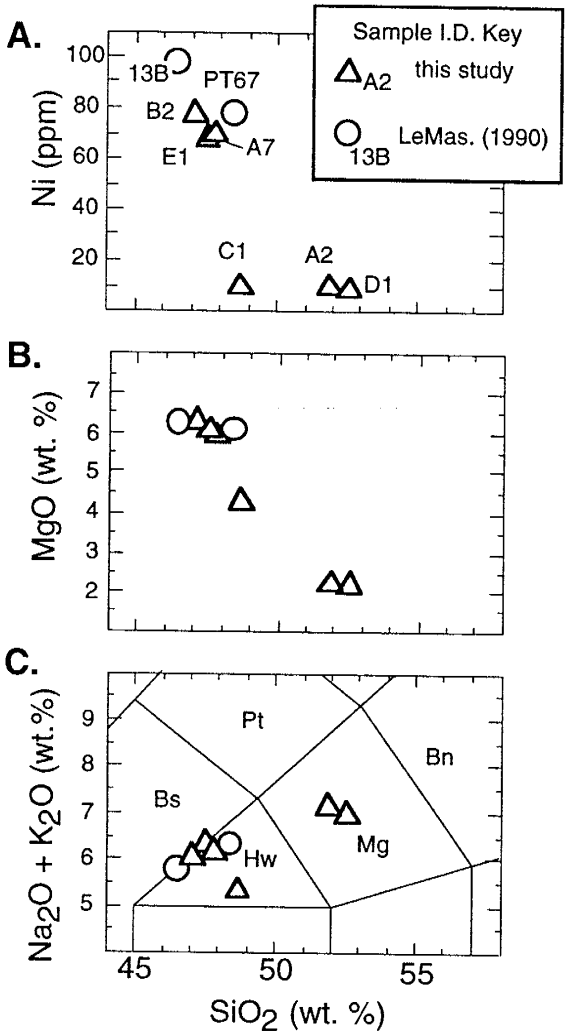

Fig. 3 a-c. Geochemical plots of major and trace elements versus silica (SiO_2), based on XRF analyses. All major element oxides are weight percents, normalized to 100% water-free. Plots include **a** Nickel (Ni) versus silica (sample numbers shown), **b** Magnesium (MgO) versus silica; 3c.), and **c** Total alkalis (Na_2O+K_2O) versus silica, with classification boundaries of LeBas et al. (1986). Abbreviations: Bn = benmoreite; Bs = basanite; Hw = hawaiite; Mg = mugearite; Pt = phonotephrite. See Fig. 2 for sample outcrop locations. Sample A2 is a dense mugearite xenolith clast in hawaiite lapilli tuff.

Table 1 X-Ray fluourescence geochemical data

Sample	A2	D1	A7	E1	C1	B2
F#	323	332	329	333	337	343
Comp.	mugearite	mugearite	hawaiite	hawaiite	hawaiite	hawaiite
SiO_2	50.84	51.24	47.02	47.30	47.23	45.87
TiO_2	1.90	1.94	2.61	2.68	3.11	2.64
Al_2O_3	14.59	14.33	16.09	16.21	14.84	15.73
Fe_2O_3	15.47	15.60	12.62	12.92	15.88	13.00
MnO	0.22	0.23	0.21	0.21	0.20	0.21
MgO	2.20	2.13	5.78	6.02	4.15	6.11
CaO	6.07	5.54	8.42	8.38	6.93	8.46
Na_2O	4.83	4.55	4.35	4.46	3.54	4.33
K_2O	2.18	2.21	1.71	1.83	1.63	1.58
P_2O_5	1.32	1.31	0.80	0.80	1.07	0.78
LOI	0.03	0.49	0.27	0.00	1.03	1.09
Total	99.65	99.57	99.89	100.56	99.62	99.80
Ba	814	882	521	487	485	510
Ce	148	162	122	130	116	122
Cl	159	60	214	268	158	241
Cr			137	133		143
Cu	29	26	45	46	31	44
Ga	27	29	22	20	26	19
La	67	64	64	64	60	73
Nb	65	62	86	87	57	85
Nd	64	73	47	51	64	51
Ni	9	8	69	69	9	77
Pb	13	13	11	13	9	12
Rb	41	45	40	53	53	27
S	128	51	98	335	647	275
Sr	426	414	809	783	604	788
Th	10	10	10	10	9	10
V	22	17	159	155	193	162
Y	67	69	37	37	54	37
Zn	169	169	104	108	188	108
Zr	474	461	380	382	372	380

I.D. number designates to outcrop and sample number. F# is field sample number. Rock type classification from LeBas *et al.* (1986.).

The $^{40}Ar/^{39}Ar$ age data are summarized in Table II and shown in age spectra in Fig. 4. The samples were highly radiogenic (70-97% radiogenic ^{40}Ar), with fairly uniform K/Ca distributions. Only one sample met the plateau criteria of Fleck et al. (1977); three other samples contained one step that lies slightly outside the 95% confidence interval. Four of the six Mt. Petras sample ages are considered

reliable; the age spectrum and isotope correlation ages of each of these samples agree within 2 σ (Table II, Fig. 4). Two hawaiite samples (A7 and E1; Figs. 4a, 4d) yielded descending age spectra, which may reflect recoil redistribution of reactor-produced ^{39}Ar during irradiation (Turner and Cadogen, 1974). Apparent ages from 600 to 1100°C steps comprise more than 50% of the cumulative ^{39}Ar released and are nearly concordant at 2 σ. The weighted means of these ages are interpreted as the best estimates of the eruption ages of each sample. One hawaiite

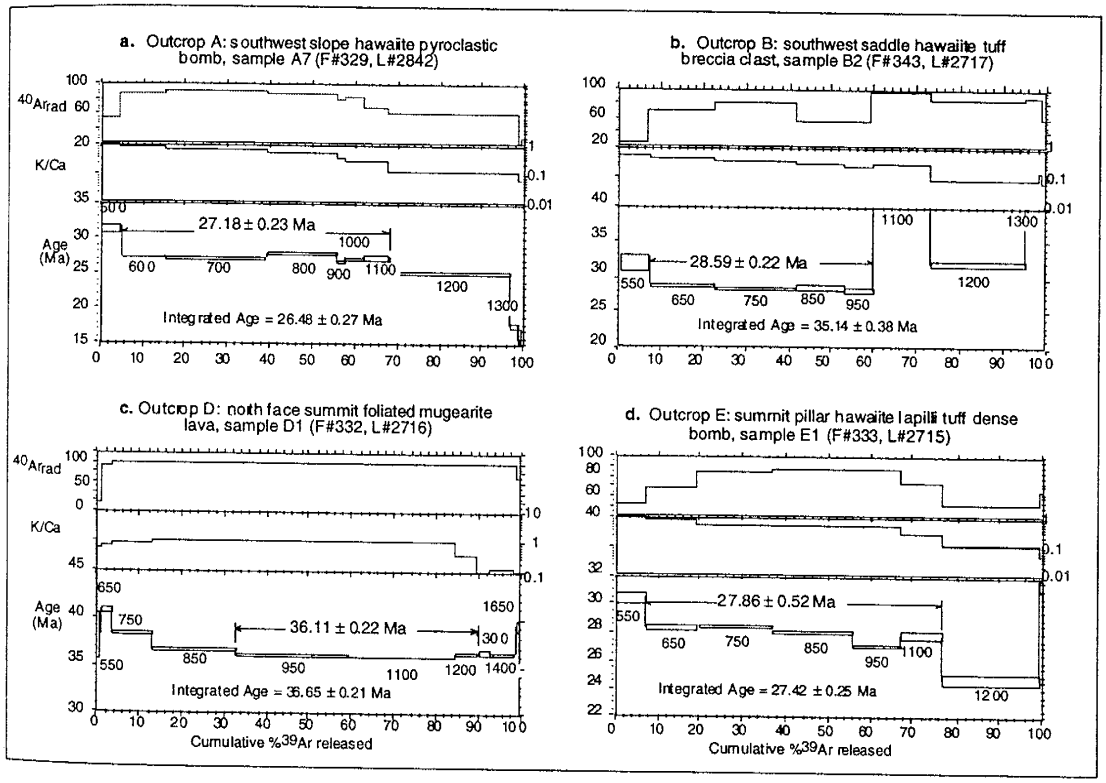

Fig. 4 a-d. $^{40}Ar/^{39}Ar$ age spectra of groundmass samples from four Mt. Petras outcrops. Plots show percentage of cumulative ^{39}Ar versus apparent age, K/Ca, and % radiogenic ^{40}Ar. Each box represents a heating step at listed furnace temperatures (°C): the height shows ±2σ analytical uncertainty on apparent age and ±1σ uncertainty on K/Ca and % radiogenic ^{40}Ar; the width designated the relative proportion of K-derived ^{39}Ar in that step. Variations in K/Ca are expected in multiple phase groundmass samples and reflect changes in gas composition during heating experiment.

Table 2 Summary of $^{40}Ar/^{39}Ar$ Age Data

Outcrop	Sample # (F#)	Description	Total Fusion Data		Isotope Correlation Data					Age Spectrum Plateau Data		
			Age ± 2σ (Ma)[1]	$\%^{40}Ar_{rad}$	Age ± 2σ (Ma)[2]	$^{40}Ar/^{36}Ar \pm 2\sigma$	MSWD	steps (°C)	$\%^{39}Ar$	Age ± 2σ (Ma)[3]	$\%^{39}Ar$	$\%^{40}Ar_r$
A. southwest flank	A2 (323)	mugearite lava xenolith	38.90 ± 0.30	93.9	no data					36.2 ± 0.51	36.0	96.7
A. southwest flank	A7 (329)	dense hawaiite bomb interior	26.48 ± 0.27	77.6	27.2 ± 0.72	295.6 ± 8.6	8.26	600-1200	63.2	27.2 ± 0.23*	63.2	87.2
B. southwest saddle	B2 (343)	aphyric hawaiite lava, 2 m thick	35.14 ± 0.38	72.4	28.6 ± 0.74	296.6 ± 3.0	3.11	650-950	52.5	28.6 ± 0.22	52.5	68.0
C. summit west ridge	C1 (337)	aphyric glassy hawaiite lava, rare xenoliths	27.90 ± 0.38	76.5	no data					highly discordant		
D. summit north face	D1 (332)	massive mugearite lava	36.65 ± 0.21	97.4	36 ± 0.86	385 ± 43	1.28	950-1200	66.2	36.1 ± 0.22*	57.4	99.3
E. summit	E1 (333)	dense hawaiite bomb interior	27.42 ± 0.25	72.1	27.5 ± 0.69	315.9 ± 7.4	53.7	650-1100	69.3	27.9 ± 0.52*	69.3	81.0

Reliable sample age estimates in boxes. F# is field sample number. [1]Total fusion age and uncertainty are weighted by $\%^{39}Ar$ in each step. $\%^{40}Ar_{rad}$ is the percent radiogenic in all heating steps or selected plateau steps. [2]Isochron age does not assume atmospheric value for $^{40}Ar/^{36}Ar$. [3]Plateau age and uncertainty are weighted by inverse of varia selected, contiguous incremental ages. *Sample did not meet plateau criteria of Fleck et al. (1977), because one step lies slightly outside the 95% confidence interval. MSW mean standard weighted deviation, calculation follows York (1969). Analytical tables in attached appendix, following methods section.

sample (B2, Fig. 4b) produced a well-defined age spectrum plateau that is 7.5 Ma younger than the total fusion age. The older incremental ages, concentrated in the higher temperature steps, are associated with an increase in percent radiogenic ^{40}Ar composition spectrum, suggesting contamination by an older xenocryst or xenolith, possibly partially degassed Cretaceous rhyodacite.

The mugearite lava sample (D1; Fig. 4c) also produced a descending age spectrum, possibly suggestive of ^{39}Ar recoil or minor contamination by an older xenocrystic material. The close agreement of the total fusion, isotope correlation, and plateau ages indicates that the recoil or contamination did not have a significant effect on the age of the sample. The isotope correlation analysis of this sample produced an anomalously high non-radiogenic $^{40}Ar/^{36}Ar$ ratio (385±43 compared to modern atmospheric value of 295.5), which is attributed to imprecision arising from an experimental artifact and is interpreted as imprecise and unreliable. The anomalously high trapped $^{40}Ar/^{36}Ar$ composition does not change the isotope correlation age.

The ages cluster into two groups: ~36 Ma mugearite and 29-27 Ma hawaiite (Table II). The best age for mugearite lava is 36.11±0.22 Ma (Fig. 4b); the mugearite xenolith age agrees within uncertainty but the age spectrum is more discordant. The three reliable hawaiite ages (Table II, Fig. 4a, 4b, 4d) are derived from samples that appear chemically indistinguishable on the basis of XRF major element and limited trace element data. These three ages ($\pm 2\ \sigma$ uncertainties) do not overlap and these samples are tentatively interpreted to represent three chronologically distinct eruptions. The 27.18±0.23 Ma $^{40}Ar/^{39}Ar$ age of the southwest flank outcrop is concordant with the 26.0±1.0 Ma conventional K-Ar age of the same outcrop but is older than two other K-Ar dates, 23.6±1.0 Ma and 23 ± 1 Ma, of the same outcrop (K-Ar ages from LeMasurier and Rex 1982, 1983; ages corrected for decay constants of Steiger and Jaeger (1979) following

Dalrymple (1979)). The hawaiite glass sample (C1) has a unique geochemical signature (Table I) and produced a discordant spectrum, which may reflect recoil redistribution of ^{39}Ar during irradiation of the glassy sample. The total fusion age, 27.90±0.38 Ma, of the sample lies within the 27-29 Ma interval of hawaiite volcanism and is considered the best age estimate for that outcrop. The $^{40}Ar/^{39}Ar$ age data combined with XRF geochemical data suggest a total of five eruptions: mugearite lava extrusion at 36 Ma and four volcaniclastic eruptions between 29 and 27 Ma. Our interpretations of $^{40}Ar/^{39}Ar$ age data indicate that Mt. Petras volcanism occurred in the latest Eocene (36 Ma) and middle Oligocene (29-27 Ma) times, making it the oldest known volcanism in Marie Byrd Land.

Lithofacies Results

Rocks from the five Mt. Petras outcrops are subdivided into two broad lithofacies categories: coherent lava and volcaniclastic rocks (after McPhie et al. 1993). The coherent lava consists of one outcrop of 36 Ma massive mugearite lava (Lithofacies Lm); the volcaniclastic rocks comprise four outcrops (14 samples) of 27-29 Ma hawaiite (Fig. 2). The volcaniclastic rock lithofacies are given pyroclastic rock facies names, because they are composed largely of vesiculated juvenile clasts, formed by explosive fragmentation processes. Two end-member lithofacies types characterize most pyroclastic deposits: welded tuff breccia (Lithofacies TBw) and palagonitized lapilli tuff (Lithofacies LT). These two types are closely associated in small and large outcrops.

Massive lava: (Lithofacies Lm): description and interpretation

An aphyric, holocrystalline mugearite lava, $^{40}Ar/^{39}Ar$-dated to 36.11±0.11 Ma, crops out on the slope just north between 2797 and 2822 m above sea level. This lava is massive throughout the 25 m thick section and exhibits strong horizontal foliation. We interpret this outcrop as the dense interior of a lava flow.

The original volume of this lava is unknown, but the presence of 36 Ma mugearite xenoliths in the 29-27 Ma hawaiite volcaniclastic deposits more than one kilometer from *in situ* mugearite lava suggests that it was more extensive than the small outcrop that is currently exposed.

Welded tuff breccia (Lithofacies TBw): description and interpretation

The TBw lithofacies consists of crudely stratified, steeply dipping (>50°), incipiently to densely welded sandy gravel breccias, composed of large, vesicular glassy bombs (up to 1 m in length) in a yellow cindery sandy gravel matrix. The bombs are fusiform and some have distinct reddened edges. Minor amounts of non-welded tuff breccia containing pyroclastic bombs are associated with the TBw deposits. The matrix material of the TBw deposits is moderately palagonitized, moderately to well sorted, clast-supported, highly vesicular, subangular vitriclastic lapilli tuff (Table III). Matrix grains typically have fluidal or cuspate morphologies and show signs of welding such as flattening of vesicles and sintered margins (Fig. 5). Rare xenolith clasts are typically glass-coated. At one locality, a densely welded breccia shows sign of post-depositional flowage.

The TBw deposits are interpreted as primary ballistic fall deposits that resulted from dry, magmatic, strombolian-type eruptive phases. The depositional environment is interpreted to be subaerial on the basis of red, deuteric oxidation of some bomb surfaces (Walker and Croasdale 1972) and welding. The welding and large sizes (to 1 m in length) bombs suggest that these are near-vent deposits. Wide ranges in vesicularity and shape of vitric clasts are common in strombolian deposits and can result from pyroclast or cognate wall rock recycling or lava stagnation in a vent pond prior to eruption (see summary by Houghton and Hackett 1984). The relative scarcity of the TBw lithofacies compared to LT lithofacies (described below) is also consistent with intermittent, mildly explosive strombolian style eruptions.

Table 3 Volcaniclastic rock petrographic data

Sample I.D. (F#)	Deposit Characterisics					Components						Lithofacies sample (deposit)
						sideromelane (palagonite)		tachylite		holo. haw.	lithic, crystal, other	
	grain-size	bedding	sorting	grain-support	clast morphology	%	vesic range %	%	vesic range %	%	% (type)	
Outcrop A: southwest flank												
A1 (322)	muddy sandy gravel	planar contorted	mod.	clast	cuspate, fluidal, armored lap	60	30-80	40	0-80			LTs, LTa
A3 (325)	sandy gravel	crude planar	mod.	clast	fluidal, cuspate	45	30-80	45	0-80	10		LTs (TBw)
A4 (326)	gravel	planar	mod.	clast	fluidal, blocky	60	0-90	35	5-30	5	tr.	LTs
A5 (327)	sand and gravel	crude planar	mod.	clast	fluidal, armored lap	70	0-85	30	0-85		tr.	LTs, LTa
A6 (328)	sandy gravel	planar	poor	clast	fluidal, cuspate, armored lap	80	10-75	15	0-80		5 (bsmt.)	LTs, LTa
A8 (330)	sand	planar, lensoid	well	clast	blocky, cuspate	55	0-20	10	0-30	30	5 (crystal)	Ts
A9 (331)	muddy sandy gravel	planar	mod.	clast	fluidal, blocky	60	30-80	20	0-50	20		LTs
Outcrop B: southwest saddle												
B1 (341)	sandy gravel	contorted	mod.	clast	blocky	30	0-50	15	0-30	55	tr.	LTs
B3 (344)	sandy gravel	massive	mod.	clast	fluidal, cuspate, blocky	0		90	0-90	10	tr.	LTm
Outcrop C. summit west ridge												
C1 (337)	gravel	crude planar	well	clast	welded, fluidal, cuspate	70	25-70	30	25-70		tr.	L (TBw)
C2 (338)	muddy sandy gravel	crude planar	mod.	clast	fluidal, cuspate	60	15-70	20	15-70	15	5 (bsmt.)	LTs (TBw)
C3 (339)	muddy sandy gravel	massive	poor	clast	blocky, fluidal	60	0-75	15	10-65	5	20 (f.g., juv., bsmt.)	LTm
Outcrop E: summit												
E2 (335)	muddy gravel	planar	poor	matrix	fluidal, blocky, armored lap.	60	40-80	5	50-70	20	15 (f.g., juv.)	LTs, LTa
E3 (336)	muddy sandy gravel	planar	mod.	mix	fluidal, blocky	20	0-75	20	10-90	40	20 (f.g., juv.)	LTs

Notes: Outcrop localites (italics) are shown in Figure 2.

F# is field sample number. Bedding from field observations.

Component analysis based on visual estimates of thin-sections.

Abbreviations: mod. = moderate; tr. = trace; bsmt. = basement; f.g. = fine-grained; juv. = juvenile.

Facies code abbreviations: LT = lapilli tuff; L = lapillistone; TB = tuff breccia;

s = stratified; a = armored; w = welded; m = massive.

Lapilli Tuff (Lithofacies LTs, LTm, LTa): description and interpretation

The LT lithofacies dominates the volcaniclastic rock outcrops at Mt. Petras and is subdivided into three types: stratified lapilli tuff (LTs), massive lapilli tuff (LTm), and armored lapilli tuff (LTa) (facies code after Sohn 1997). Clast components in the LT deposits include palagonitized and fresh sideromelane glass, tachylite glass, holocrystalline hawaiite lava, plagioclase and olivine crystal fragments, mugearite xenoliths, and rhyodacite xenoliths (Table III). Sideromelane and tachylite glass typically comprises more than 75% of clasts, contains fine - grained microphenocrysts (<500 μm) of plagioclase, olivine and clinopyroxene and exhibits a wide range of vesicularity from 0 to 90% (Fig. 5). Clast morphologies include fluidal and cuspate glass shards and blocky glass and lithic fragments. Fluidal grains have smooth, rounded or spiny margins and are highly vesiculated (>50%) and commonly broken (Fig. 5c). Cuspate shards have angular intersecting concave grain boundaries formed by fragmentation of thin vesicle walls. Blocky grains are subangular to subrounded and are poorly vesiculated (0-30%). A thin veneer of very fine ash particles (typically 100 μm thick) coats some but not all blocky coarse ash and fine lapilli grains in armored lapilli tuff units (LTa). These ash coatings have non-uniform thicknesses (50-350 μm) and appear to consist of fine-grained (~5 μm diameter) glass and crystal fragments (Fig. 5d).. Some lithic grains are coated by a layer of coherent glass.

Both the LTm and LTs lithofacies contain rare (0-5 %) out-sized lithic clasts and pyroclasts. The lithic clasts are subangular to subrounded, basement and mugearite lithologies, up to 10 cm in diameter, and sometimes coated with hawaiite lava. No signs of glacial molding or polish were observed on any of the lithic

clasts. Intact and broken pyroclastic bombs and blocks occur as outsized clasts up to 30 cm in length in some deposits.

Overall, the deposits are moderately sorted, clast-supported, and either massive (LTm) or planar bedded (LTs and LTa). Bedding planes typically dip steeply (20-90°). The beds can be traced continuously across smaller outcrops (<15 m diameter), but are discontinuous and pinch out in larger outcrops. Contacts between the LT lithofacies and the TBw lithofacies appear conformable. At one outcrop, a lobe of coherent lava was brecciated into massive lapilli tuff (LTm). The LT deposits are moderately palagonitized
and cemented weakly by secondary smectite, calcite, and/or zeolite minerals.

Several features of the LT lithofacies are consistent with both "dry" magmatic and "wet" phreatomagmatic eruptive phases. Diagnostic features of magmatic eruptions are fusiform pyroclastic bombs, lava-coated and glass-coated lithic clasts, and scoriaceous and fluidal droplet lapilli and ash grains. Similar out-sized bombs at Ilchonbong tuff cone, South Korea were attributed to periodic, dry strombolian eruptions in between hydromagmatic explosions (Sohn and Chough 1992). The lack of bomb and block sags indicates either sluggish eruptions of the pyroclasts or slight reworking on steep slopes. The lava-coated and lava-free, subangular to subrounded lithic clasts are interpreted as xenoliths eroded and crudely milled during magmatic and phreatomagmatic eruptions, respectively. The fluidal droplet morphologies of lapilli clasts are formed by surface tension and are indicative of subaerial strombolian eruptions (Walker and Croasdale 1972). An analogue for the inferred mixed magmatic/phreatomagmatic eruption at Mt. Petras is the 1963-67 eruption of Surtsey volcano, Iceland, which was a emergent tuff cone dominated by continuous uprush and jetting of tephra, steam, and water, with intermittent strombolian explosions (Thorarinsson et al., 1964). The type "surtseyan" eruption characterizes one style of phreatomagmatic eruptions, where

interactions between vesiculating magma and a wet slurry of sediments drive the eruption (Kokelaar, 1986).

Lithofacies features indicative of phreatomagmatic eruptions include: clasts that are heterogeneous in composition, morphology and vesicularity (Wohletz 1983, Kokelaar 1986; Houghton and Schmincke 1989, Houghton and Wilson, 1989), well-developed but often contorted planar bedding (Wohletz, 1983; Sohn, 1997), induration and palagonitization (Wohletz 1983), and armored lapilli beds (Waters and Fisher 1971) (Table III). The lithofacies characteristics are interpreted to result from a combination of strombolian style magmatic explosivity and surtseyan style bulk-interaction steam explosivity (Kokelaar, 1986). The predominance of coarse grained clasts (lapilli) in the Mt. Petras deposits favors less energetic surtseyan style eruptions rather than highly energetic "taalian" style surges (see summary discussion in Wohletz and Heiken 1992). The low percentage of lithic clasts (<10%) suggests that the fragmentation depth was relatively shallow (Sohn 1997). Some reworking of beds is inferred from discontinuous nature of beds in large outcrops. Changes in bedding and grain-size characteristics (*e.g.* ash-rich massive beds versus lapilli-rich planar beds) are attributed to variations in water:magma mixing ratios, and geologic and hydrologic conditions (Sohn 1997). Possible eruption recycling of clasts is suggested by uneven mud-coating on some clasts in the LTa deposits and the mixture of fluidal and blocky clasts (Houghton and Smith 1993). Other explanations for the heterogeneous assortment of poorly and highly vesiculated tachylite, sideromelane and holocrystalline clasts include hydromagmatic interactions between highly vesiculated magma and wet poorly vesiculated tephra, partially degassed magma, and/or wall-rock in the vent (Houghton and Hackett 1984; Kokelaar 1986). The absence of traction bedforms such as cross-bedding favors deposition from pyroclastic fall over surge processes.

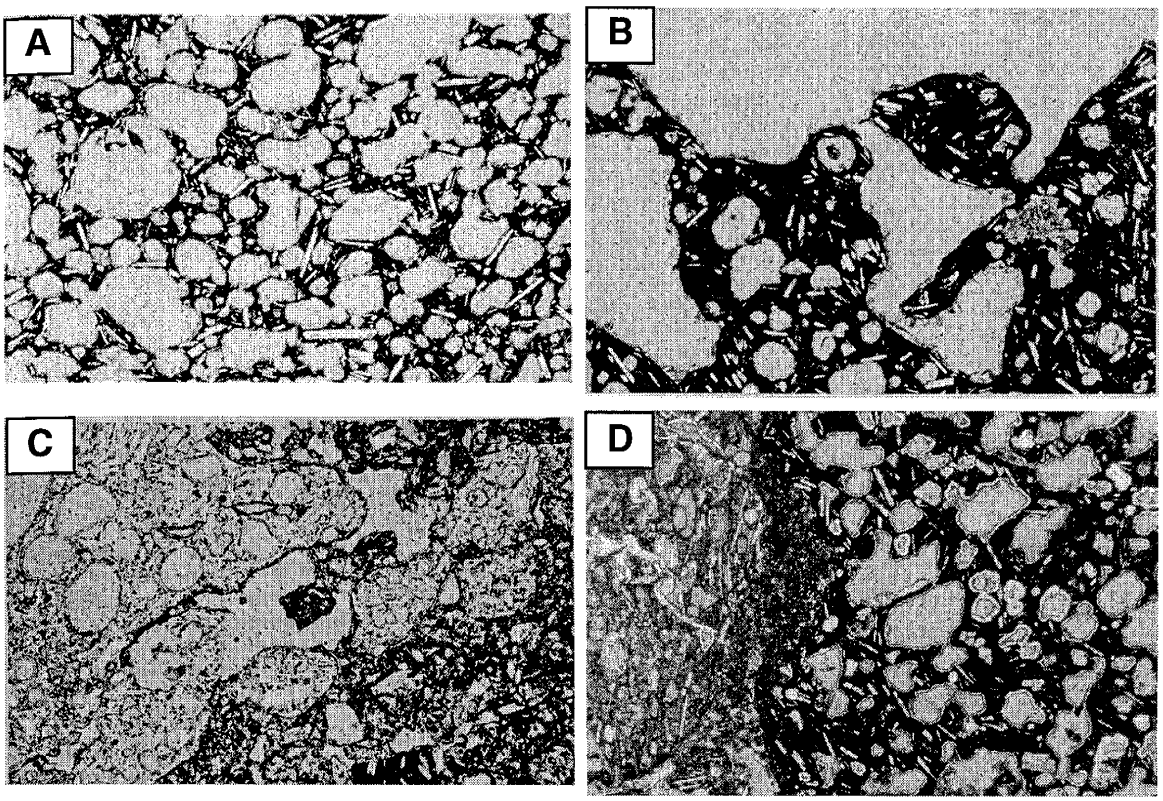

Fig. 5 a-d. Photomicrographs of Mt. Petras hawaiite samples; thin section area covered in each photograph is 2.8 x 2.0 mm. **a** Highly vesicular tachylite glass pyroclast from summit outcrop (sample E3). Vesicles are beginning to coalesce. Contact between siderомelane and tachylite pyroclasts appears molded and interlocking. **b** Margin of fragile fluidal tachylite pyroclast from southwest flank outcrop (sample A3). Vesicularity is moderate to weak. **c** Fluidal, moderately to highly vesicular sideromelane pyroclast (light colored on left) and tachylite pyroclasts from summit outcrop (sample E2). **d** Vesicular tachylite pyroclast coated by layer of fine ash, with thickness up to 350 mm (Lithofacies LTa). Adjacent grain is a vesicular sideromelane pyroclast.

The LT lithofacies are interpreted as products of wet surtseyan-style eruptive phases, dominated by tephra finger jets and pyroclastic fall processes. A subaerial depositional environment is inferred on the basis of interbedded, welded pyroclastic deposits (TBw). A subaqueous eruption in a cupola of steam as described by Kokelaar (1986) could explain the highly vesiculated tachylite pyroclasts but not the degree of welding and deuteric oxidation of some pyroclasts. The combination of intrusive lava and wet sediments (LTm) at one outcrop is suggestive of a near-vent surtseyan tuff cone setting (Kokelaar 1986; Sohn 1997). The limited exposures do not allow reconstruction of volcano morphology, except to state the steep-dipping lapilli tuff strata are also consistent with near-vent tuff cone facies rather than tuff ring facies (Sohn 1997). Oversteepened beds (>45° for wet, mud-rich sediments) are attributed to post-depositional collapse phenomena (see discussion by Sohn 1997). This interpretation is consistent with a model by Sohn (1997) that suggested the morphology of phreatomagmatic volcanoes, tuff cone or tuff ring, is controlled largely by the dominant depositional process and that tuff cones result from fall deposition and tuff rings result largely from surge deposition.

Pyroclastic lithofacies associations

Stratigraphic relationships among pyroclastic lithofacies and the inferred eruption histories of the four hawaiite outcrops are summarized in Table 4 and shown by example in Figure 5. All of the pyroclastic lithofacies are interpreted as products of explosive eruptions, ranging from wet, surtseyan to dry, strombolian in style. Figure 6 shows vertical lithofacies variations in a >40 m high stratigraphic section located on the southwest flank outcrop A (Fig. 2, pt. A), from which

Table 4 Outcrop descriptions and interpretations (locations shown in Fig. 2)

Location	Elevation (m)	Age ± 2σ	Lithofacies
Outcrop A: southwest flank	**2422-2517 m**	**27.18±0.23 Ma**	**TBw, LTs, LTa, LTm**
Description:	Most extensive exposures at Mt. Petras consist of two outcrops. The smaller outcrop is about 10 x 50 m in size and is the lowest *in situ* outcrop at Mt. Petras. It consists of slightly convoluted LTs and LTm lithofacies dipping 30° N that contain numerous out-sized juvenile pyroclastic bombs and lava-coated mugearite xenoliths. The larger outcrop is at least 100 x100 m in map area and includes a >40 m high stratigraphic section (Fig. 6). Stratigraphic section is described in text.		
Interpretation:	Near-vent primary pyroclastic fall and reworked fall tuff cone deposits. Eruption style progressed through four stages: 1) surtseyan with intermittent strombolian; 2) wet surtseyan; 3) dry strombolian; and 4) surtseyan with intermittent strombolian.		
Outcrop B: southwest saddle	**2532-2537 m**	**28.59±0.22 Ma**	**TBw, LTs, LTm**
Description:	Isolated outcrops with no apparent stratigraphic situated in a bedrock saddle. Lithofacies include vertically foliated welded tuff breccia, intrusive lava brecciating into a massive lapilli tuff slurry, stratified lapilli tuff with outsized pyroclastic bombs.		
Interpretation:	Tuff cone vent deposits with surtseyan and strombolian facies.		
Outcrop C: summit west ridge	**2682-2692 m**	**27.90±0.38 Ma (?)**	**TBw, LTm**
Description:	A 10 x 20 m outcrop that overlies bedrock and consists of two steeply dipping units. A densely welded tuff breccia flanked by massive lapilli tuff, overlying bedrock.		
Interpretation:	Tuff cone vent facies. Eruption style progressed from wet surtseyan to dry strombolian.		
Outcrop D: summit north face	**2797-2822 m**	**36.11±0.22 Ma**	**Lm**
Description:	Massive mugearite lava exposed in 25 m thick section on slope just north of summit. Lava is horizontally foliated, holocrystalline, and aphyric.		
Interpretation:	Product of effusive eruption. No associated pyroclastic rocks or autoclastic breccias exposed.		
Outcrop E: summit	**2852-2862 m**	**27.86±0.52 Ma**	**LTs**
Description:	An approximately 10 m high outcrop, located 200 m west of the true summit, consists of near vertically oriented, interbedded fine and coarse lapilli tuff. Fluidal droplet lapilli pyroclasts common.		
Interpretation:	Near-vent (?) tuff and cinder cone deposits. Mixed strombolian and surtseyan eruption.		

alternating eruption styles can be inferred. The stratigraphic section can be divided into two parts: the lower 15 m of the section is characterized by well bedded, finer grained lapilli tuffs with up to 10% lithic clasts (LTm, LTs and LTa lithofacies); and the upper 25 m is characterized by coarser grained lapilli tuff (LTs) and welded and non-welded tuff breccia (TBw) with oxidized pyroclastic bombs to 1 m in length. The relative abundance of juvenile material (i.e. intact and fragmented vitric clasts) increases up section and is higher in the upper section compared to the lower section. Overall, the pyroclastic rocks are well-bedded, with northward dipping beds that steepen up section, oriented nearly vertical in places.

Vertical lithofacies changes are characterized by alternating surtseyan (LTa, LTs, LTm) and strombolian lithofacies (TBw and some LTs), indicative of fluctuations of external water during eruptions (Fig. 6). The conformable contacts throughout the outcrop suggest a single eruption or series of eruptions without significant time hiatuses (i.e. no time for erosion). In many cases, eruptive sequences progressed from wet surtseyan to a dry strombolian conditions. All of the Mt. Petras outcrops exhibit characteristics of near-vent, subaerial tuff cone setting, including steeply dipping, contorted, and discontinuous planar beds, large pyroclastic bombs (to 1 m), welding and deuteric oxidation, and brecciating intrusive hawaiite.

Lateral lithofacies changes in the Mt. Petras outcrops are difficult to observe because of the limited extent of most outcrops. In general, beds appeared to be continuous across the 5-15 m strike length of most outcrops. However, in lower section of the southwest flank outcrop, LT beds cannot be traced laterally more than 10 m. The LT bed contacts in this section do not appear to be erosive. The lateral discontinuity of beds suggests that the clasts were remobilized by mass flow processes on the steep side-slopes, as was observed in Korean tuff cones (Sohn, 1997). The TBw beds at the base of the upper section are continuous across the

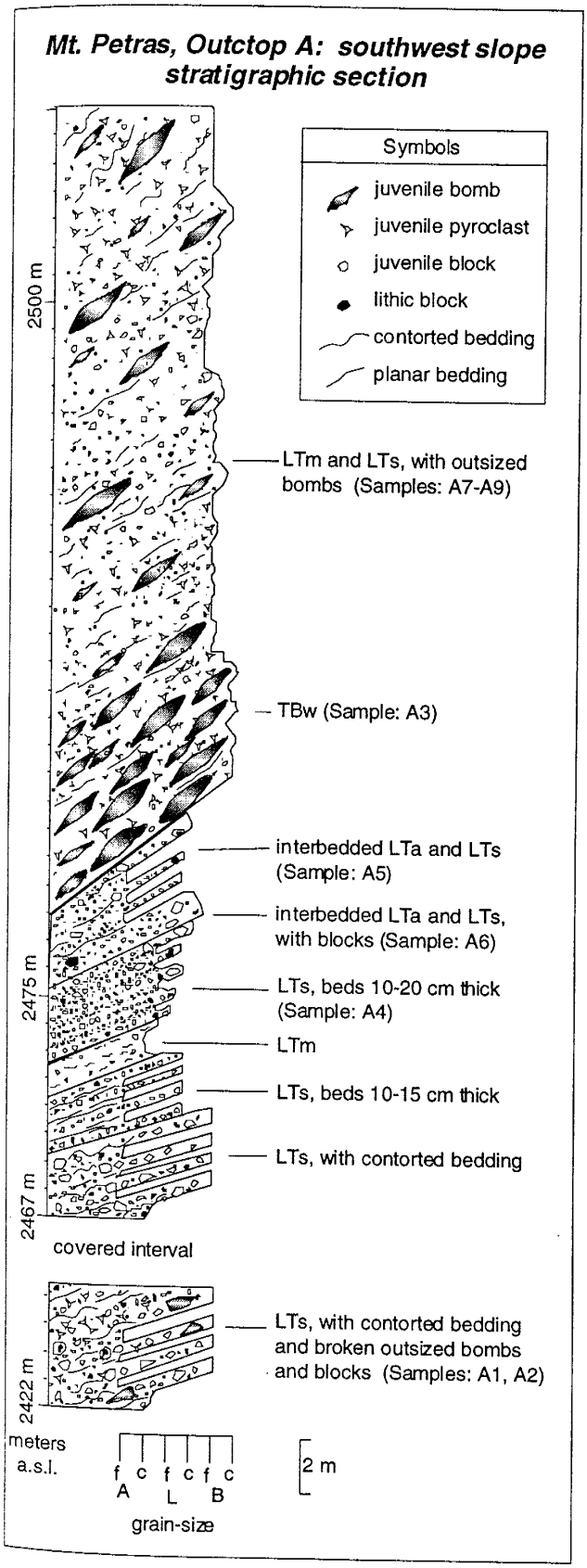

Fig. 6. Outcrop log of 40 meter thick stratigraphic section located on the southwest flank (see Fig. 2, outcrop A for location). Beds dip steeply into the slope (to north). Lithic clasts shown with black clasts. Bombs are pillow shaped, juvenile clasts are white clasts. Grain-size abbreviations: A = ash; L = lapilli; B = block or bomb; c = coarse; f = fine. Lithofacies abbreviations: L= lapilli, T=tuff, B=breccia, , a= armored, m=massive, s=stratified, w=welded.

entire outcrop and thicken slightly along strike. The continuity of TBw beds is attributed to the welding at time of emplacement.

Discussion

Pre-volcanic erosion surface

Hawaiite pyroclastic rocks situated in the southwest saddle at 2690 m. a.s.l. (Fig. 2, pt. A) and the summit west ridge at 2530 m. a.s.l. (Fig. 2, pt. C) overlie bedrock, indicating a minimum of 160 m of vertical relief on the pre-hawaiite unconformity (Fig. 2). The position of 29-27 Ma *in situ* hawaiite rocks down to elevations of 2422 m a.s.l. extends the minimum vertical relief on the pre-hawaiite unconformity to 270 m. Finally, the presence of the 36 Ma mugearite lava at elevations up to 2822 m a.s.l. further extends the minimum vertical relief on the pre-hawaiite unconformity to 400 m. The relatively high relief on the unconformity is consistent with an environment of active erosion. The interval of erosion covers 50 Ma and is bracketed by the underlying ~80 Ma rhyodacite and the ~29 Ma hawaiite.

The new measurement of >400 m relief on the unconformity at Mt. Petras is inconsistent with a previous estimate of < 100 m based on reconnaissance observations made from a helicopter (LeMasurier 1990b). The previously reported low relief on the unconformity at Mt. Petras was used to support the hypothesis of the West Antarctic erosion surface (WAES) as a single Early Cenozoic erosion surface (LeMasurier and Landis, 1996). Elsewhere in Marie Byrd Land, pre-volcanic erosion surfaces are reported as being flat (<100 m of relief) and overlain by mostly Late Miocene and Pliocene volcanic rocks (LeMasurier and Landis 1996). By definition, the age of each unconformity is the age of the overlying volcanic rocks. There is no evidence to support a model of a single, low-relief, Early Cenozoic WAES, nor is there evidence for a postulated Early Cenozoic

marine planation of West Antarctica. On the contrary, exposed rocks at Mt. Petras suggest an environment of active, possibly early Oligocene, erosion. The fact that the volcanic outcrops at Mt. Petras are preserved as erosional remnants suggests that there has been abundant post-volcanic erosion.

At present, the only data on surface uplift at Mt. Petras are the maximum limits based on ages and elevations of subaerially erupted rocks. The maximum amount of surface uplift at Mt. Petras is 2522 m since 27 Ma, constrained by the age and elevation of the lowest *in situ* subaerially erupted rocks at the southwest flank outcrop site. Similar maximum limits on surface uplift can be established for other subaerial eruption sites in Marie Byrd Land; such limits do not document actual uplift but place limits on the maximum possible uplift since the eruption age. There are no data to support a previous model of progressive domal uplift of coastal Marie Byrd Land since middle Cenozoic times coincident with volcanism (LeMasurier and Rex, 1983).

Eruption History at Mt. Petras

Five eruptions at Mt. Petras are identified on the bases of $^{40}Ar/^{39}Ar$ ages, geochemistry, lithofacies analysis, and field relations. The first stage of volcanism occurred at 36.11±0.22 Ma with an apparently dry extrusion of massive mugearite lava. The second stage of eruptions includes four hawaiite pyroclastic events between 29 and 27 Ma. These events were initiated with surtseyan and strombolian eruptions in the southwest saddle area at 28.59±0.22 Ma. The next eruptions occurred at 27.90±0.38 Ma (?) and 27.86±0.52 Ma, with deposition of surtseyan and strombolian lapilli tuff and welded pyroclastic rocks at the summit west ridge and summit areas (outcrops C and E, respectively). The final phase of volcanism was deposition of 27.18±0.23 Ma tuff cone material on the southwest flank (outcrop A). All the hawaiite outcrops are interpreted as vent complexes or near-

vent lithofacies that resulted from subaerial surtseyan and strombolian eruptions (Fig. 2).

Our interpretations do not support previous field interpretations of the volcanic rocks as subglacial hyaloclastite erosional remnants of a volcanic table mountain or the existence of a thick regional ice-sheet in West Antarctica during Oligocene times (LeMasurier et al. 1981). Our study suggests limited syneruptive glacial ice as indicated by lithofacies associations, ages and outcrop distributions (discussed below).

Eruptive and depositional environment at Mt. Petras

All of the 29-27 Ma pyroclastic outcrops are derived in part from surtseyan eruptions, that require interaction between magma and water (ice) or wet sediments. In broad terms, there are three possible environments for water-magma interactions: subterranean (groundwater) environment; deep subaqueous (subglacial) environment, and shallow subaqueous (subglacial) to subaerial environment.

Interaction with deep-seated groundwater is ruled out because of the low number of basement clasts, lack of a maar crater, and the abundance of highly vesiculated pyroclasts in all of the deposits (Wohletz 1983, Leat and Thompson 1987; Houghton and Schmincke 1989; Sohn 1997). The inclusion of rare rhyodacite and mugearite lithic clasts in the pyroclastic deposits suggest limited interaction with groundwater at a shallow depth. Such limited interaction is supported by the presence of basement lithic clasts coated by juvenile glass in some deposits (Houghton and Schmincke 1989).

An alternative model for the origin of the Mt. Petras outcrops is that the eruptions ejected material directly into a relatively deep subaqueous environment, with no contact with open-air. This alternative requires that the assumed subaerial eruption features formed in cupola of steam and tephra as is envisioned to have occurred at submarine volcano Surtla, Iceland (Kokelaar 1986). Grab-samples

from the submarine volcanic edifice at Surtla include deuterically oxidized (reddened) and agglutinated pyroclasts and one deformed, 22-cm-long spatter bomb. The cupola model cannot be disproved, but it is not preferred for the following reasons: the lack of glacial, lacustrine, or marine sedimentary deposits mixed in with or underlying the volcanic outcrops, the lack tractional sedimentary structures common in subaqueous environments, and the very extensive zone of bomb welding in deposits at the southwest flank outcrop A.

We conclude that a shallow subaqueous to subaerial environment best explains the observations. Three possible types of shallow subaqueous environments are evaluated below:

1) Sea water. The suggestion by LeMasurier and Landis (1996) that the erosion surface formed by early Cenozoic marine planation would be consistent with a sea water source for phreatomagmatic interaction. Although sea water has been an important source of water in many tuff cone eruptions, it seems unlikely at Mt. Petras given the lack of marine fossils or clays, lack of tractional bedforms as seen elsewhere (Thorarinsson 1964; Kokelaar and Durant 1983; Cas et al. 1989), and the requirement for >400 m of sea level variation in <2 Ma.

2) Surface water (stream or lake). Stream and lake water are considered unlikely sources of external water because of the lack of fluvatile and lacustrine sediments as lithic clasts in the volcanic deposits and as preserved deposits on the landscape. Furthermore, both lake and stream interactions require fairly complicated paleohydrologic settings: four perched shallow lakes at different elevations or a stream dropping >400 m over just a few kilometers.

3) Glacial meltwater. The deposits at Mt. Petras are similar to the uppermost deposits of volcanic table mountain sequences, associated with eruptions that have emerged above water level in confined englacial lakes (Jones 1969, Skilling 1994). Volcanic table mountains are glacial-volcanic edifices that grow in

several stages: beginning with effusion of pillow lavas under high confining pressures, followed by hydromagmatic explosions of fine tuffs under low confining pressures, and culminating in mildly explosive and effusive subaerial cinder cone/lava eruptions with an associated subaqueous flow foot delta forming where lava enters englacial lake (Jones 1969). Recent models of englacial volcanism show the same basic progression of eruptive conditions and lithofacies as in the table mountain models but include reworking of deposits as an additional important process and differentiate eruptions in thick-ice/ponded-water environments to thin-ice/flowing-water environments (Skilling 1994; Smellie and Skilling 1994; Smellie and Hole, in press). Mt. Petras outcrops differ from table mountain and other englacial volcanic sequences in that they show no signs of deep-water:magma interactions, such as poorly vesiculated pillow lavas and hyaloclastite breccias. Only vesiculated surtseyan and strombolian tuffs occur where volcanic rocks are exposed in contact with basement rocks. The surtseyan style eruptions at Mt. Petras are consistent with eruptions through very shallow water.

Subaerial eruption of highly vesiculated magma through shallow englacial lakes, possibly associated with a small ice cap or a veneer of slope ice, is consistent with many features of the Mt. Petras outcrops including: the heterogeneous clast populations, the lack of fossil-bearing sediments, the lack of wave re-working, the outcrop elevation variations and geographic distribution of the outcrops, the possibility of fluctuating waters during individual eruptions. When volcanoes erupt through a glacier or ice sheet, two common components are glacial unconformities and glacially striated or molded clasts. However, at Mt. Petras, there is no evidence for pre-volcanic glacial deposits. Our preferred explanation for the Mt. Petras outcrops is that they result from hydromagmatic interactions with a thin veneer of ice. A thin-ice environment is consistent with the lack of glacial deposits

and with the apparently random distribution of the volcanic centers on the landscape. The fluctuations between dry and wet eruptive conditions can be explained by meltwater draining and refilling shallow englacial ice chambers.

Summary

The volcanic history at Mt. Petras offers new data and interpretations of mid-Cenozoic volcanism, glaciation, and landscape evolution in Marie Byrd Land, West Antarctica. Five eruptions are inferred from $^{40}Ar/^{39}Ar$ dating, XRF geochemistry and field analyses. Onset of volcanism in Marie Byrd Land occurred at 36.11±0.11 Ma, with the eruption of massive mugearite lava near the summit of Mt. Petras. Four pyroclastic eruptions of hawaiite composition rocks occurred between 29 and 27 Ma, characterized by mixed surtseyan and strombolian style eruptions. These subaerial eruptions involved intermittent interaction with water derived from a thin, local ice cap or snow and ice on the slopes of a relatively high relief (>400 m) bedrock nunatak. The 29-27 Ma pyroclastic deposits at Mt. Petras provide the oldest terrestrial evidence for glacial ice in Marie Byrd Land but offer no evidence for a thick, continental ice sheet at that time.

Acknowledgments

This work was supported by the National Science Foundation (NSF-DPP918806), with additional funding from the New Mexico Geochronological Research Laboratory. We thank U.S. Navy VXE-6 squadron, Antarctic Support Associates, and Ken Borek Air Ltd. for logistical support; Nelia Dunbar and Tony Teeling for field assistance; John Smellie, British Antarctic Survey, for providing XRF data from the University of Keele, and Nelia Dunbar and Kurt Panter for useful criticism of manuscript.

References

Barrett PJ, Elston DP, Harwood DM, McKelvey BC, Webb PN (1987) Mid-Cenozoic record of glaciation and sea-level change on the margin of the Victoria Land basin, Antarctica. Geology 15: 634-637

Behrendt JC, LeMasurier WE, Cooper AW (1992) The West Antarctic rift system-a propagating rift "captured" by a mantle plume? In: Yoshida Y (ed) Recent progress in antarctic earth science. Terra Scientific Publishing Company, Tokyo, pp 315-322

Behrendt JC, LeMasurier WE, Cooper AK, Tessensohn F, Trehu A, Damaske D (1991) Geophysical studies of the West Antarctic rift system. Tectonics 10: 1257-1273

Behrendt JC, Saltus R, Damaske D, McCafferty A, Finn CA, Blankenship DD, Bell RE (1996) Patterns of late Cenozoic volcanic and tectonic activity in the West Antarctic rift system revealed by aeromagnetic data. Tectonics 15: 660-676

Cande SC, Kent DV (1992) A new geomagnetic polarity time scale for the Late Cretaceous and Cenozoic. Journal of Geophysical Research 97: 13,917-13,952

Cas RAF, Landis CA, Fordyce RE (1989) A monogenetic, Surtla-type, Surtseyan volcano from the Eocene-Oligocene Waiareka-Deborah volcanics, Otago, New Zealand: a model. Bull Volcanol 51: 281-298

Cooper AK, Davey FJ (1985) Episodic rifting of Phanerozoic rocks in the Victoria Land Basin, Western Ross Sea, Antarctica. Science 229: 1085-1087

Cooper AK, Davey FJ, Behrendt JC (1987) Seismic stratigraphy and structure of the Victoria Land Basin, western Ross Sea, Antarctica. In: Cooper AK, Davey FJ (eds) The Antarctic continental margin: geology and geophysics

of the western Ross Sea, Earth Science Series. Circum-Pacific Council for Energy and Mineral Resources, Houston, Texas, pp 27-65

Cooper AK, Davey FJ, Hinz K (1991) Crustal extension and origin of sedimentary basins beneath the Ross Sea and Ross Ice Shelf, Antarctica. In: Thomson MRA, Crame JA, Thomson JW (eds) Geological evolution of Antarctica. Cambridge University Press, Cambridge, England, pp 299-304

Dalrymple GB (1979) Critical tables for conversion of K-Ar ages from old to new decay constants. Geology 7: 558-560

Deino A, Potts R (1990) Single-crystal 40Ar/39Ar dating of the Olorgesailie Formation, Southern Kenya Rift. J Geophys Res 95: 8453-8470

Drewry J (1983) Antarctica: Glaciological and Geophysical Folio . Scott Polar Research Institute, University of Cambridge, Cambridge

Fitzgerald PG (1992) The Transantarctic Mountains of southern Victoria Land: the application of apatite fission track analysis to a rift shoulder uplift. Tectonics 11: 634-662

Fleck RJ, Sutter JF, Elliot DH (1977) Interpretation of discordant $^{40}Ar/^{39}Ar$ age spectra of Mesozoic tholeiites from Antarctica. Geochim Cosmochim Acta 41: 15-32

Hambrey MJ, Larsen B, Ehrmann WU (1991) The glacial record from the Prydz Bay continental shelf, east Antarctica. In: Barron J, Larsen B et al. (eds) Ocean Drilling Program, 119, Scientific Results, College Station, Texas, pp 77-132

Hole MJ, LeMasurier WE (1994) Tectonic controls on the geochemical composition of Cenozoic mafic alkaline volcanic rocks from West Antarctica. Contrib Min Pet 117: 187-202

Houghton BF, Hackett WR (1984) Strombolian and phreatomagmatic deposits of Ohakune craters, Ruapehu, New Zealand: a complex interaction between

external water and rising basaltic magma. J Volcanolo Geotherm Res 21: 207-231

Houghton BF, Schmincke HU (1989) Rothenberg scoria cone, East Eifel: a complex strombolian and phreatomagmatic volcano. Bull Volcanol 51: 28-48

Houghton BF, Smith RT (1993) Recycling of magmatic clasts during explosive eruptions: estimating the true juvenile content of phreatomagmatic volcanic deposits. Bull Volcanol 55: 414-420

Houghton BF, Wilson CJN (1989) A vesicularity index for pyroclastic deposits. Bull Volcanol 51: 451-462

Jones JG (1969) Intraglacial volcanoes of the Laugarvatn Region, south-west Iceland, I. Q J Geol Soc London 124: 197-211

Kennett JP, Barker PF (1990) Latest Cretaceous to Cenozoic climate and oceanographic developments in the Weddell Sea, Antarctica: an ocean-drilling perspective. In: Barker PF, Kennett JP et al. (eds) Proceedings of the Ocean Drilling Program, scientific results, Vol. 113. U.S. Government Printing Office, Washington, pp 937-958

Kokelaar BP, Durant GP (1983) The submarine eruption and erosion of Surtla (Surtsey), Iceland. J Volcanol and Geotherm Res 19: 239-246

Kokelaar BP (1986) Magma-water interactions in subaqueous and emergent basaltic volcanism. Bull Volcanol 48: 275-289

Kyle PR (1990) McMurdo Volcanic Group- western Ross Embayment. In: LeMasurier WE, Thomson JW (eds) Volcanoes of the Antarctic Plate and Southern Oceans. AGU, Washington, D.C., pp 19-25

Kyle PR, McIntosh WC, Panter KS, Smellie JL (1991) Is volcanism in Marie Byrd Land related to a mantle plume? Sixth International Symposium on

Antarctic Earth Sciences , 337. National Institute of Polar Research, Saitama, Japan

Lawver LA, Royer J-Y, Sandwell DT, Scotese CR (1991) Crustal development: Gondwana break-up, Evolution of the Antarctic continental margins. In: Thomson MRA, Crame JA, Thomson JW (eds) Geological evolution of Antarctica. Cambridge University Press, Cambridge, England, pp 533-540

Leat PT, Thompson RN (1988) Miocene hydrovolcanism in NW Colorado, USA, fuelled by explosive mixing of basic magma and wet unconsolidated sediment. Bull Volcanol 50: 229-243

LeBas MJ, LeMaitre RW, Streckeisen A, Zanettin B (1986) A chemical classification volcanic rocks based on the total alkali-silica diagram. J Pet 27: 745-750

LeMasurier WE (1972) Volcanic record of Antarctic glacial history: Implications with regard to Cenozoic sea levels. In: Price RJ, Sugden DE (eds) Polar Geomorphology, Special Publication 4. Institute of British Geographers, London, pp 59-74

LeMasurier WE (1972) Volcanic record of Cenozoic glacial history in Marie Byrd Land. In: Adie RJ (ed) Antarctic Geology and Geophysics. Universitetsforlaget, Oslo, pp 251-260

LeMasurier WE (1990) Marie Byrd Land. In: LeMasurier WE, Thomson JW (eds) Volcanoes of the Antarctic Plate and Southern Oceans. AGU, Washington, D.C., pp 146-163

LeMasurier WE (1990) Miocene-Oligocene centers, Mount Petras and USAS Escarpment. : LeMasurier WE, Thomson JW (eds) Volcanoes of the Antarctic Plate and Southern Oceans. AGU, Washington, D.C., pp 239-243

LeMasurier WE, Harwood DM, Rex DC (1994) Geology of Mount Murphy Volcano: An 8-m.y. history of interaction between a rift volcano and the West Antarctic ice sheet. Geo Soc Am Bull 106: 265-280

LeMasurier WE, Landis CA (1996) Mantle-plume activity recorded by low-relief erosion surfaces in West Antarctica and New Zealand. Geo Soc Am Bull 108: 1450-1466

LeMasurier WE, McIntosh WC, Rex DC (1981) Mid-Tertiary glacial history recorded at Mt. Petras, Marie Byrd Land. Antarct J U.S. 16: 19-21

LeMasurier WE, Rex DC (1982) Volcanic record of Cenozoic glacial history in Marie Byrd Land and western Ellsworth Land: Revised chronology and evaluation of tectonic factors. In: Craddock C (ed) Antarctic Geoscience. University of Wisconsin Press, Madison, pp 725-734

LeMasurier WE, Rex DC (1983) Rates of uplift and the scale of ice level instabilities recorded by volcanic rocks in Marie Byrd Land, West Antarctica. In: Oliver RL, James PR, Jago JB (eds) Antarctic Earth Sciences. Australian Academy of Science, Canberra, pp 660-673

LeMasurier WE, Wade FA (1976) Volcanic history in Marie Byrd Land: implications with regard to southern hemisphere tectonic reconstructions. In: Gonzalez-Ferran O (ed) Proceedings of the International Symposium on Andean and Antarctic Volcanology Problems. IAVCEI, Rome, pp 398-424

McPhie J, Doyle M, Allen R (1993) Volcanic textures: a guide to the interpretation of textures in volcanic rocks. Centre for Ore Deposit and Exploration Studies, University of Tasmania, Hobart, Tasmania, p 198

Samson SD, Alexander CE (1987) Calibration of the interlaboratory 40Ar/39Ar dating standard, Mmhb-1. Isot Geosci 66: 27-34

Shackleton NJ, Kennett JP (1975) Paleotemperature history of the Cenozoic and the initiation of Antarctic glaciation: oxygen and carbon isotope analyses in

DSDP Sites 277, 279, and 281. In: Kennett JP, Houtz RE et al.(eds) Initial Reports of the Deep Sea Drilling Project 29. U.S. Government Printer, Washington D.C., pp 743-755

Skilling IP (1994) Evolution of an englacial volcano: Brown Bluff, Antarctica. Bull Volcanol 56: 573-591

Smellie JL, Hole MJ (in press) Products and processes in Pliocene-Recent, subaqueous to emergent volcanism in the Antarctic Peninsula: example of englacial Surtseyan volcano construction. Bull Volcanol 59

Smellie JL, Hole MJ, Nell PAR (1993) Late Miocene valley-confined subglacial volcanism in northern Alexander Island, Antarctic Peninsula. Bull Volcanol 55: 273-288

Smellie JL, Skilling IP (1994) Products of subglacial volcanic eruptions under different ice thicknesses two examples form Antarctica. Sed Geol 91: 115-129

Sohn YK (1997) Hydrovolcanic processes forming basaltic tuff rings and cones on Cheju Island, Korea. Geo Soc Am Bull 108: 1199-1211

Sohn YK, Chough SK (1992) The Ilchulbong tuff cone, Cheju Island, South, Korea: depositional processes and evolution of an emergent Surtseyan-type tuff cone. Sedimentology 39: 523-544

Steiger RH, Jaeger E (1977) Subcommission on Geochronology: Convention of the use of decay constants in geo- and cosmochronology. Earth Planet Sci Lett 36: 359-362

Thorarinsson S, Einarsson T, Sigvaldason G, Elisson G (1964) The submarine eruption off the Vestmann Islands 1963-1964: A preliminary report. Bull Volcanol 27: 435-445

Turner G, Cadogan PH (1974) Possible effects of 39Ar recoil in 40Ar/39Ar dating. Geochim Cosmochim Acta, Supplement 5 2: 1601-1615

Walker GPL, Croasdale R (1972) Characteristics of some basaltic pyroclastics. Bull Volcanol 35: 303-317

Waters AC, Fisher RV (1971) Base surges and their deposits: Capelinhos and Taal volcanoes. J Geophys Res 76: 5596-5614

Wohletz K, Heiken G (1992) Volcanology and geothermal energy. University of California Press, Oxford, England, p 432

Wohletz KH (1983) Mechanisms of hydrovolcanic pyroclast formation: grain-size, scanning electron microscopy, and experimental studies. J Volcanol and Geotherm Res 16: 31-63

Appendix B.I.-$^{40}Ar/^{39}Ar$ Dating Methods

Unaltered homogeneous groundmass concentrates (200-800 μm grain size) were separated from crushed bulk samples using standard sieving, magnetic, weak HCl acid treatment, and hand-picking methods. Approximately 50 mg of each sample were placed in machined Al discs and sealed in an evacuated quartz tube along with interlaboratory neutron flux standard Fish Canyon Tuff sanidine (FCT-1 with an age of 27.84 Ma (Deino and Potts 1990) relative to Mmhb-1 age of 520.4 (Samson and Alexander 1987)). Samples were irradiated in the L67 position of the Ford Nuclear Reactor at the University of Michigan for 10 hours (neutron flux yields approximately 0.015 J/hr). Following irradiation, the flux monitor crystals were placed in holes drilled in a copper planchet and fused by a CO_2 laser in an argon extraction system under ultra-high vacuum conditions. J-factors were determined from the pooled results of 4-6 single crystal analyses from 6 radial positions around the irradiation vessel.

The irradiated groundmass samples were incrementally-heated in 8-11 steps within a double vacuum Mo resistance furnace. Argon isotopic compositions were determined with a MAP 215-50 mass spectrometer operated in electron multiplier mode with an overall sensitivity of 2.2×10^{-17} moles Ar/pA. The sample ages were corrected for blank, background, mass discrimination, and interfering reactions. Typical furnace blanks (including mass spectrometer backgrounds) were 24, 0.2, 0.04, 0.2, 0.1 x 10^{-16} moles at masses 40, 39, 38, 37, and 36, respectively. Mass discrimination measured prior to sample analyses yielded a mean value 1.0071 ± 0.0017. The decay constant and isotopic abundances used in calculations are those suggested by Steiger and Jaeger (1977).

Two techniques to assess $^{40}Ar/^{39}Ar$ incremental heating data are the age spectrum method and the isotope correlation (inverse isochron) method. These

methods differ in their treatment of the non-radiogenic $^{40}Ar/^{36}Ar$ content of the sample: the age spectrum method assumes a modern atmospheric composition of non-radiogenic $^{40}Ar/^{36}Ar$ equal to 295.5; the isotope correlation method calculates the non-radiogenic $^{40}Ar/^{36}Ar$ composition from a linear regression of isotope ratios. Samples with uniform, highly radiogenic compositions, such as the Mt. Petras samples, are not well suited for isotope correlation analysis, because the determination of the trapped non-radiogenic $^{40}Ar/^{36}Ar$ component is imprecise, possibly inaccurate, and does not strongly influence the calculated age. In this study, the age spectrum ages are interpreted as eruption ages of the samples.

Appendix B.II.-$^{40}Ar/^{39}Ar$ Analytical Data

Run ID#	Temp °C	$^{40}Ar/^{39}Ar$	$^{37}Ar/^{39}Ar$	$^{36}Ar/^{39}Ar$ x10^{-3}	$^{39}Ar_k$moles x10^{-15}	K/Ca	Cl/K x10^{-2}	$\%^{40}Ar^*$	$\%^{39}Ar$	Age± 2 σ	(Ma)
WCM93-323, whole rock mugearite, 52.5 mg, NM-30, J=0.0015107											
Mt. Petras, main outcrop, lava clast											
2841-01A	500	263.4	0.6694	840.8	3.51	0.762	3.45	5.7	1.0	40.3	8.7
2841-01B	600	41.00	0.7896	89.51	9.22	0.646	1.14	35.6	3.5	39.4	1.1
2841-01C	700	17.30	0.7132	10.73	30.7	0.715	0.191	81.9	12.0	38.20	0.30
2841-01D	800	14.38	0.5489	2.899	49.5	0.930	0.077	94.2	25.7	36.56	0.19
2841-01E	900	13.61	0.4554	0.8935	80.3	1.12	0.090	98.2	48.0	36.05	0.15
2841-01F	1000	14.08	0.4971	0.4603	76.1	1.03	0.577	99.1	69.1	37.68	0.18
2841-01G	1100	18.60	0.7883	0.8889	43.0	0.647	0.141	98.8	81.0	49.42	0.19
2841-01H	1200	15.33	3.017	1.682	44.7	0.169	1.985	98.1	93.4	40.63	0.17
2841-01I	1300	13.44	2.365	1.491	20.5	0.216	0.907	97.9	99.1	35.57	0.17
2841-01J	1450	14.77	2.374	5.823	2.32	0.215	0.674	89.4	99.7	35.70	0.52
2841-01K	1750	16.45	2.671	12.51	1.02	0.191	1.142	78.6	100.0	35.0	1.0
integrated age				**n=11**	**361**	**0.790**				**38.90**	**0.30**
mean age (steps d-e, 36.0% ^{39}Ar)										**36.24**	**0.51**
WCM93-329, whole rock hawaiite, 53.3 mg, NM-30, J=0.0015102											
Mt. Petras, main outcrop, pyroclastic bomb from upper surface											
2842-01A	500	20.75	0.538	31.24	11.0	0.948	8.81	55.6	5.0	31.17	0.59
2842-01B	600	11.62	0.730	5.310	23.4	0.699	5.63	86.8	15.8	27.28	0.19
2842-01C	700	10.89	0.933	3.206	51.1	0.547	3.34	91.8	39.2	27.04	0.15
2842-01D	800	11.36	1.222	4.099	36.0	0.417	2.74	90.0	55.8	27.66	0.26
2842-01E	900	12.41	1.783	9.165	4.81	0.286	3.45	79.1	58.0	26.58	0.39
2842-01F	1000	11.95	1.935	6.939	8.85	0.264	2.72	83.9	62.0	27.15	0.23
2842-01G	1100	14.77	2.325	16.43	13.5	0.219	3.42	68.2	68.2	27.27	0.31
2842-01H	1200	14.57	4.906	19.30	62.4	0.104	4.93	63.3	96.8	25.03	0.27
2842-01I	1300	10.44	4.388	14.49	4.44	0.116	1.90	62.0	98.9	17.62	0.39
2842-01J	1450	27.30	8.961	74.94	1.43	0.057	0.624	21.3	99.5	15.9	1.4
2842-01K	1750	16.09	8.720	40.58	1.03	0.059	0.221	29.5	100.0	13.0	1.6
integrated age				**n=11**	**218**	**0.383**				**26.48**	**0.27**
mean age (steps b-g, 63.2% ^{39}Ar)										**27.18**	**0.23**
WCM93-332, whole rock mugearite, 33.2 mg, NM-30, J=0.0016419											
Mt. Petras, near summit pillar, foliated aphyric lava											
2716-01A	550	77.00	0.833	216.7	2.63	0.613	3.31	16.9	1.1	38.1	2.6
2716-01B	650	15.06	0.694	3.942	6.69	0.736	0.291	92.5	3.9	40.79	0.30
2716-01C	750	13.34	0.589	0.8874	22.2	0.866	0.088	98.2	13.2	38.41	0.18
2716-01D	850	12.65	0.524	0.4937	46.0	0.974	0.062	99.0	32.5	36.72	0.15
2716-01E	950	12.39	0.473	0.2931	63.4	1.08	0.084	99.4	59.1	36.14	0.15
2716-01F	1100	12.32	0.487	0.2708	61.0	1.05	0.313	99.5	84.7	35.96	0.17
2716-01G	1200	12.64	1.285	1.153	12.4	0.397	1.39	97.9	89.9	36.34	0.23
2716-01H	1300	12.95	4.764	2.979	7.02	0.107	2.50	95.9	92.9	36.51	0.34
2716-01I	1400	12.85	3.752	2.514	14.0	0.136	2.21	96.3	98.7	36.38	0.22
2716-01J	1650	18.64	4.408	18.79	2.99	0.116	1.72	71.9	100.0	39.40	0.66
integrated age				**n=10**	**238**	**0.884**				**36.65**	**0.21**
plateau age (steps e-g, 57.4% ^{39}Ar)										**36.11**	**0.22**
WCM93-333, whole rock hawaiite, 34.1 mg, NM-30, J=0.0016163											
Mt. Petras, summit pillar, hawaiitic lapilli tuff											
2715-01A	551	19.88	0.535	31.74	14.5	0.954	6.85	52.9	7.3	30.43	0.45
2715-01B	650	14.52	0.753	16.19	24.1	0.678	5.64	67.3	19.4	28.27	0.26
2715-01C	750	11.70	1.057	6.671	35.2	0.483	5.16	83.7	37.2	28.35	0.16
2715-01D	850	11.06	1.164	4.947	37.6	0.438	4.72	87.4	56.2	28.00	0.16
2715-01E	950	10.70	1.201	4.839	21.9	0.425	4.49	87.3	67.2	27.07	0.16
2715-01F	1100	13.04	1.888	12.09	18.6	0.270	4.41	73.5	76.6	27.78	0.31
2715-01G	1200	16.60	4.564	28.47	45.6	0.112	4.98	51.3	99.6	24.73	0.33
2715-01H	1300	16.77	10.644	21.92	0.843	0.048	2.70	66.1	100.0	32.3	1.3
integrated age				**n=8**	**199**	**0.419**				**27.42**	**0.25**
mean age (steps b-f, 69.3% ^{39}Ar)										**27.86**	**0.52**

Run ID#	Temp	$^{40}Ar/^{39}Ar$	$^{37}Ar/^{39}Ar$	$^{36}Ar/^{39}Ar$	$^{39}Ar_k$moles	K/Ca	Cl/K	$\%^{40}Ar^*$	$\%^{39}Ar$	Age±	
2 σ	°C			x10^{-3}	x10^{-15}		x10^{-2}			(Ma)	
WCM93-337, whole rock hawaiite, 25.7 mg, NM-30, J=0.0016297											
Mt. Petras, lower pillar, hawaiitic tuff breccia over basement											
2714-01A	550	31.26	1.070	59.13	26.4	0.477	0.321	44.3	26.1	40.29	0.66
2714-01B	650	9.950	1.256	7.454	15.1	0.406	0.410	78.6	41.0	22.87	0.25
2714-01C	750	12.37	1.297	3.426	16.1	0.393	0.774	92.4	56.9	33.34	0.24
2714-01D	850	11.75	1.426	4.007	16.5	0.358	0.887	90.7	73.2	31.07	0.19
2714-01E	950	6.563	1.894	3.961	9.56	0.269	1.50	84.0	82.7	16.17	0.33
2714-01F	1100	3.892	3.169	2.263	12.7	0.161	6.70	88.5	95.3	10.12	0.24
2714-01G	1200	3.823	7.023	2.307	3.10	0.073	3.67	95.7	98.3	10.78	0.60
2714-01H	1300	9.379	9.215	1.603	1.69	0.055	2.87	102.3	100.0	28.16	0.97
integrated age				**n=8**	**102**	**0.355**				**27.90**	**0.38**
WCM93-343, whole rock hawaiite, 33.2 mg, NM-30, J=0.0016422											
Mt. Petras, North Ridge saddle, hawaiitic tuff breccia in basement valley											
2717-01A	550	42.98	1.069	109.0	8.55	0.477	4.85	25.2	7.3	31.81	1.27
2717-01B	650	14.22	1.246	15.30	17.8	0.409	1.59	68.7	22.6	28.74	0.25
2717-01C	750	12.12	1.425	8.512	22.0	0.358	1.19	80.0	41.5	28.53	0.19
2717-01D	850	17.72	1.965	27.36	13.4	0.260	1.56	55.1	53.0	28.73	0.38
2717-01E	950	17.40	2.345	27.09	7.98	0.218	1.86	54.9	59.8	28.14	0.53
2717-01F	1100	20.82	2.086	5.054	15.6	0.245	6.33	93.5	73.2	56.85	0.29
2717-01G	1200	13.06	6.368	9.063	25.7	0.080	3.81	83.1	95.2	32.01	0.20
2717-01H	1300	23.29	5.843	11.32	3.32	0.087	0.83	87.5	98.1	59.60	0.59
2717-01I	1400	29.72	3.397	12.70	1.64	0.150	0.53	88.2	99.5	76.2	1.5
2717-01J	1650	42.40	8.071	60.42	0.61	0.063	1.94	59.3	100.0	73.4	2.3
integrated age				**n=10**	**117**	**0.265**				**35.14**	**0.38**
plateau age (steps b-e, 52.5% ^{39}Ar)										**28.59**	**0.22**

Part C: Middle to Late Cenozoic Volcanic Record of the West Antarctic Ice Sheet

ABSTRACT

Paleoenvironmental reconstructions and $^{40}Ar/^{39}Ar$ geochronology of nineteen large polygenetic volcanoes and numerous smaller monogenetic volcanoes in Marie Byrd Land, West Antarctica provide proxy "dipstick" records of changing ice levels of the West Antarctic Ice Sheet since the latest Eocene. Interpretations of eruptive and depositional environments are based on lithofacies studies and indicate whether the volcanoes erupted below, near, or above the level of the ice sheet. An enriched conceptual model of glaciovolcanism in Marie Byrd Land is developed to differentiate volcanic records of local ice levels from records of West Antarctic Ice Sheet levels. The model builds upon the traditional Icelandic table mountain model but addresses several complicating features of the glaciovolcanic environment of Marie Byrd Land. Specific complications include: ice-level feedback effects caused by obstructions to ice-flow, changes in ice level in coastal regions caused by rises or falls of sea level, glaciovolcanic interactions with slope ice, volcanism on interfluves between regions fast-flowing ice, and uncertainties about post-volcanic uplift.

A new detailed $^{40}Ar/^{39}Ar$ chronology of volcanism and proxy ice-level changes, based on dating analyses of 177 samples, offers improvements in precision and accuracy over the previous K/Ar chronology. There is a significant revision of the chronology of

some volcanoes, by rejecting imprecise K/Ar ages in favor of precise, stratigraphically controlled $^{40}Ar/^{39}Ar$ ages. In addition, late Pleistocene samples (to 29±12 ka) were dated at high levels of precision from sequences that were previously undatable by the K/Ar method.

The Eocene to Pleistocene volcanic history provides a proxy record of ice level changes in West Antarctica, with the following major conclusions: 1) the first indications for ice in West Antarctica are the early Oligocene (29-27 Ma) emergent tuff sequences at Mt. Petras, where limited local syn-eruptive glaciation is inferred; 2) the first evidence for a widespread West Antarctic Ice Sheet is Late Miocene (~9.3 Ma) glaciovolcanic sequences from across Marie Byrd Land; 3) paleo-ice-level expansions of the WAIS were more extensive at coastal sites than at inland sites; 4) the West Antarctic Ice Sheet is in a near maximum configuration that existed at several times since 9.3 Ma but was rarely exceeded; and 5) two significant expansions of the West Antarctic Ice Sheet above its present-day level occurred at 590±15 ka, when ice levels were 550 m higher at the coastal volcano, Mt. Murphy, and at 29±12 ka, when ice levels were ~350 m higher at the inland volcano, Mt. Takahe.

INTRODUCTION

There is intense scientific interest in the history, dynamics, and future of the West Antarctic Ice Sheet (WAIS), chiefly because it is the world's only remaining marine ice sheet and is considered by many to be inherently unstable and prone to catastrophic collapse and melting (e.g. Hollin, 1962; Hughes, 1973; Mercer, 1978; MacAyeal, 1992; Bindschadler, 1995). If the WAIS were to collapse, global sea level would rise by 6 m. The stability of the WAIS is a function of some balance between external controls of sea level and climate and internal controls of marine ice-sheet and ice-stream dynamics (Alley and Whillans, 1991; MacAyeal, 1992; Bentley, 1997). One method of assessing the significance of controlling factors is to compare records of past ice-sheet configurations to

records of paleoclimate. Mapping and dating of glacial deposits in the Dry Valleys area near McMurdo Sound have led to a detailed record of Late Wisconsinan expansions of the WAIS (Denton et al., 1989). The record of the pre-Late Wisconsinan WAIS is poorly known due to the lack of exposed glacial deposits. In Marie Byrd Land (hereafter, MBL), West Antarctica, numerous large middle to late Cenozoic volcanoes preserve records of syn-eruptive interactions with ice that can be used to infer paleo-ice-levels of the WAIS (Fig. 1)(LeMasurier, 1972a, 1972b). The premise of this volcanological approach is that when volcanoes erupt below, at, or above the level of an ice sheet, the resulting rocks exhibit specific textural features and structures that are diagnostic of their eruptive environments. Subglacially erupted rocks imply higher paleo-ice-levels relative to the present-day level; subaerially erupted rocks imply lower relative paleo-ice-levels. Thus, records of the age, elevation, and eruptive environment of volcanic rocks provide snapshot views of the syn-eruptive level of the ice sheet.

Volcanism and glaciation have been active geological forces in MBL since middle Cenozoic time. About 50 middle to late Cenozoic alkaline volcanic centers, including nineteen large, polygenetic volcanoes (2364-4181 m above sea level), are exposed as nunataks in the WAIS (Fig. 1). LeMasurier (1972a, 1972b) and LeMasurier and Rex (1982, 1983) reconstructed a volcanic record of glaciation in West Antarctica, based on regional reconnaissance field work and K/Ar geochronology. Recent studies by LeMasurier et al. (1994) and Wilch and McIntosh (Part B of the dissertation) have presented more detailed accounts of glaciovolcanic interactions at Mt. Murphy and Mt. Petras, respectively.

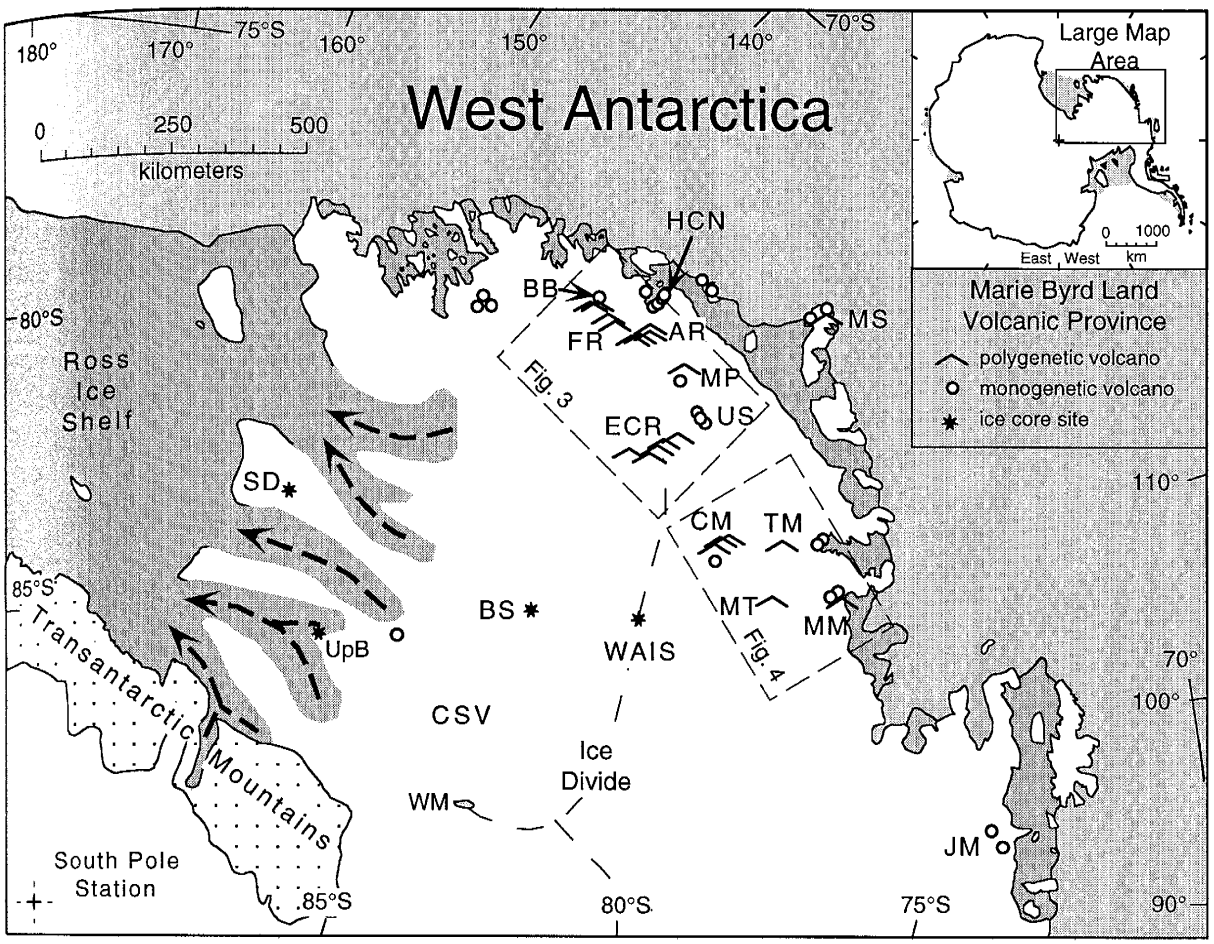

Figure 1. Map of Marie Byrd Land, West Antarctica (Drewry, 1983), showing polygenetic volcanoes (white triangles), minor volcanoes (asterisks), and several sites important to research of the West Antarctic Ice Sheet (WAIS). The Transantarctic Mountains bisect the continent and form the divide between the mostly terrestrial East Antarctic Ice Sheet and the mostly marine-based WAIS. Ice streams (arrows) account for about 90% of ice drained from the WAIS (Hughes, 1977). Volcano abbreviations: AR = Ames Range; BB = Brandenberger Bluff, CM = Crary Mountains; ECR = Executive Committee Range; FR = Flood Range; HCN=Hobbs Coast Nunataks; JM = Jones Mountains; MM = Mt. Murphy; MP = Mt. Petras; MS = Mt. Siple; MS = Mt. Siple; MT = Mt. Takahe; TM = Toney Mountain, and US = U.S.A.S. Escarpment. Drill sites (circles): BS = the 1968 Byrd ice-core drill site; CSV = CASERTZ subglacial volcano (Corridor Aerogeophysics of Southeastern Ross Transect Zone), inferred to be active by Blankenship et al. (1993); SD = planned WAISCORES drill site at Siple Dome; UpB = the base camp on Ice Stream B; WAIS = planned WAISCORES drill site at central ice divide. Other abbreviations: WM = Whitmore Mountains.

In this paper, we develop a new regional synthesis of glaciovolcanism in MBL through time, based on systematic re-examination and $^{40}Ar/^{39}Ar$ geochronology of many MBL volcanoes. The organization of the paper is intended to facilitate understanding of a subject that is both broad and complex. First, relevant background on the glacial and geologic history in West Antarctica is presented. Second, advances in understanding are summarized and a new conceptual model of glaciovolcanism is introduced. Third, methods and results are presented, including field studies, $^{40}Ar/^{39}Ar$ geochronology, volcanic lithofacies, and paleoenvironmental reconstructions of specific MBL volcanoes. Finally, the paleoenvironmental reconstructions and the $^{40}Ar/^{39}Ar$ dating results are merged, yielding a new comprehensive volcanic record of the WAIS.

BACKGROUND

Antarctic cryosphere evolution

The Antarctic cryosphere is dominated by two ice sheets, the massive, mostly land-based East Antarctic Ice Sheet (27 x 10^6 km^3) and the relatively small, mostly marine-based West Antarctic Ice Sheet (3 x 10^6 km^3) (Drewry, 1983). The earliest development of the Antarctic cryosphere is attributed to a global cooling event in the earliest Oligocene, ca. 33.7-33.4 Ma (time scale from Cande and Kent, 1992; Kennett (1995) provides a summary). Inception of a full-scale East Antarctic Ice Sheet is attributed to a middle Miocene climatic deterioration at about 14 Ma (e.g., Kennett, 1977; Savin et al., 1975; Shackleton and Kennett, 1975, Denton et al., 1993). A long-standing debate (e.g., Webb and Harwood, 1991; Clapperton and Sugden, 1991; Denton et al., 1993; Wilson, 1995) over whether the East Antarctic Ice Sheet has been stable or highly dynamic during much of the Neogene appears be resolved in favor of stability. Neogene diatoms that were used to date the evidence for a dynamic ice sheet have been shown to be present only in the upper few centimeters of critical glacial deposits (Stroeven et al., 1996). The same diatoms have

been shown to be common windblown sediments in Antarctica today (Kellogg and Kellogg, 1996; Burckle 1996).

The development and stability of the WAIS are also debated, chiefly because the history of the WAIS is poorly known, being based on very limited marine and terrestrial data. According to interpretations of marine data by Kennett and Barker (1990), the WAIS fully developed in the Late Miocene (~10-8 Ma) and achieved a relatively stable configuration by the early Pliocene (5 Ma). Others (e.g., Scherer, 1991; LeMasurier et al., 1994) have suggested that the WAIS has never achieved a stable configuration, but has fluctuated between full-bodied and disintegrated configurations for its entire history.

West Antarctic lithosphere evolution

Large-scale asymmetric intracontinental rifting of the nearly stationary Antarctic plate formed the Ross Sea basin and deep marine basins beneath the WAIS, as well as generated regional volcanism (Cooper and Davey 1985; Cooper et al. 1987, 1991; Kyle, 1990). The Ross Sea Basin consists of a series of sediment-filled horst and graben structures attributed to two rifting episodes: early rifting in the Late Cretaceous and late rifting that began in the Eocene and intensified in the late Cenozoic (Cooper and Davey 1985; Cooper et al. 1987, 1991). The intracontinental rift zone is inferred to extend from the Ross Sea to beneath the West Antarctic Ice Sheet (Behrendt et al., 1991, 1996). Middle to late Cenozoic alkaline volcanoes are exposed on both the south flank of the rift zone in the Transantarctic Mountains and the north flank in MBL (Kyle, 1990; LeMasurier and Rex, 1989).

The MBL volcanic province consists of nineteen large, intracontinental rift, polygenetic alkaline volcanoes and numerous isolated monogenetic volcanic centers. LeMasurier and Rex (1991) described the volcanoes as "highly alkaline, bimodal, sodic, and dominated by basaltic rocks". The geochemistry of the volcanic rocks suggests a mantle plume source (Behrendt et al. 1992; Kyle et al. 1991; Hole and LeMasurier 1994;

Hart et al., 1997). High-elevation, pre-volcanic erosion surfaces in MBL are interpreted as a topographic expression of this plume (LeMasurier and Landis 1996). Several of the felsic shield volcanoes are aligned in linear chains, with ages that suggest systematic migration of felsic volcanism away from the center of the volcanic province (LeMasurier and Rex, 1991). The migration patterns are attributed to reactivation of relict N-S and E-W fractures by regional crustal doming (LeMasurier and Rex, 1989, 1991; Panter et al., 1994).

LeMasurier (1972a, 1972b) recognized a pattern of stratigraphic relationships among most large MBL volcanoes that is characterized by a mafic "basal succession" overlain by a felsic shield volcano. Late stage parasitic cinder cones and tuff cones are situated on the shield flanks. The basal succession consists of subglacial to subaerial, basaltic lava flows and volcaniclastic rocks that overlie a flat pre-Cenozoic basement. The basal succession includes many reported hyaloclastite deposits that were interpreted as erupted in subglacial environments (LeMasurier, 1972a, 1972b; LeMasurier and Rex, 1982, 1983).

LeMasurier (1972a; 1972b) first recognized that the volcanic record of subglacial eruptions in MBL affords a proxy record of former ice-sheet high-stands. Several glaciovolcanic reconstructions of the WAIS were postulated on the basis of reconnaissance field studies and conventional K/Ar dating (LeMasurier, 1972a; 1972b; LeMasurier and Rex, 1982, 1983). These reconstructions relied on the Icelandic table mountain model as an analogue for all sites and on the recognition of abundant subglacial hyaloclastites to infer higher paleo-ice-levels since middle Tertiary times (LeMasurier, 1972a, 1972b; LeMasurier and Rex, 1982, 1983). The reported abundance of subglacial hyaloclastite deposits contrasts sharply with the lack of subglacial pillow lavas (e.g., LeMasurier, 1972a). This disparity was attributed to the tendency of microlite-rich melts to form hyaloclastites rather than coherent pillow lavas (LeMasurier, 1976).

A NEW UNDERSTANDING OF GLACIOVOLCANISM IN WEST ANTARCTICA

Our glaciovolcanic reconstruction benefits from a number of methodological advances, including in-depth field studies, field and laboratory lithofacies analysis and interpretations, $^{40}Ar/^{39}Ar$ geochronology, and a conceptual framework. Fieldwork for this study was focused on detailed lithofacies analysis of sites that are critical for the glaciovolcanic history, including Mt. Takahe, Mt. Murphy, the Crary Mountains, and monogenetic volcanoes in central and western MBL (Hobbs Coast Nunataks and Mt. Petras) (Fig. 1). Paleoenvironmental reconstructions evolved from a conceptual model of glaciovolcanism that differentiates volcanic records of local ice level changes from records of regional ice-sheet changes. An integral part of our paleoenvironmental reconstructions is a chronologic framework based on extensive $^{40}Ar/^{39}Ar$ dating of rocks from numerous isolated outcrops and some shield-building stratigraphic sequences.

$^{40}Ar/^{39}Ar$ geochronology

The $^{40}Ar/^{39}Ar$ method offers three important advantages over the conventional K/Ar method (McDougall and Harrison, 1988). First, $^{40}Ar/^{39}Ar$ ages are consistently more precise than the K/Ar ages. The increased precision can be attributed to a variety of factors, including higher resolution mass spectrometers, analysis of single aliquots of small samples, and analysis of plateau or mean ages by the furnace step-heating age-spectrum method and single-crystal laser-fusion method. Increased precision allows assessing eruption rates of individual volcanic centers and identifying inaccurate ages in stratigraphic sequences. In many cases, rocks from the same outcrops yield $^{40}Ar/^{39}Ar$ ages that are an order magnitude more precise than K/Ar ages.

Second, recent technical innovations, including laser heating, lower extraction line blanks, and higher resolution mass spectrometers, allow precise and accurate $^{40}Ar/^{39}Ar$ dating of volcanic rocks as young as 0.010 Ma (e.g., Wilch et al. (Part A); Hu et al.,

1994; van den Bogaard, 1995; Chen et al., 1996). Most studies have focused on laser dating of sanidine or anorthoclase feldspars from felsic rocks (e.g., Hu et al., 1994; van den Bogaard, 1995; Chen et al., 1996), although young mafic groundmass samples have been dated successfully (e.g., this study; Heizler et al., in review). The K/Ar method has elsewhere been successfully used to date young mafic and intermediate rocks to relatively high levels of precision (2 s.d. uncertainty of ± ~20%) (Singer et al., 1997). However, such precise results have not been obtained from conventional K/Ar analyses of young MBL rocks, where the argon signal has been reported as not detectable, yielding maximum age constraints of <0.1 Ma (e.g., LeMasurier and Rex, 1991).

Third, perhaps the most important advance of the $^{40}Ar/^{39}Ar$ dating method over conventional K/Ar methods is that it provides several ways to identify inaccurate ages. In theory, $^{40}Ar/^{39}Ar$ furnace step-heating analyses of a single homogeneous volcanic rock sample should produce a concordant age spectrum. Discordant apparent ages suggest that a sample inhomogeneous as a result of excess or loss of argon or contamination by older xenocrysts. In some cases, discordant ages (and sample inhomogeneities) are isolated to one part of the age spectrum and interpretation can be made of the sample age. In other cases, discordant age spectra are uninterpretable and the results are rejected. Sample inhomogeneities are also revealed in isotope correlation plots (i.e., inverse isochrons) and again, in the special cases (e.g., excess argon contamination), age corrections can be justified. The K/Ar method provides no means to readily recognize erroneous ages; as a result, very wide ranges of K/Ar ages have been reported for some MBL volcanic outcrops (e.g., Eocene to late Miocene ages of Turtle Peak in LeMasurier, 1972; LeMasurier and Rex, 1982; LeMasurier et al., 1994).

Lithofacies Analysis

Recent field-based lithofacies studies have led to major advances in understanding glaciovolcanic and hydrovolcanic processes (e.g., Smellie et al., 1993; Skilling, 1994;

Smellie and Skilling, 1994; Smellie and Hole, in press; Sohn and Chough, 1992; Sohn, 1996). The lithofacies approach requires detailed field work and cannot be effectively applied in reconnaissance studies. In typical lithofacies analysis, paleoenvironmental interpretations are built upon non-genetic descriptions of rock units and their relationships to one another. For example, non-genetic volcanic lithofacies designations are typically based on rock type (lava or clastic), grain size, sedimentary structures and clast characteristics (morphology, vesicularity, componentry) (McPhie et al., 1993). In volcanological studies, partly genetic lithofacies designations that define the original clast-forming mechanism, such as pyroclastic or autoclastic, are commonly used (e.g., Sohn and Chough, 1992, 1993, 1994 1996). Depositional processes and environments are interpreted by comparison of features of lithofacies and lithofacies assemblages to modern analogues.

In the case of MBL studies, volcanic lithofacies analysis has resulted in significant changes in the interpretations of many specific outcrops that have direct implications for paleo-ice-levels (see Part B of dissertation). Many of these changes result in part from clear definitions of terminology that are required for detailed lithofacies analyses. For example, in previous reconnaissance studies (LeMasurier 1972a, 1972b; LeMasurier and Rex, 1982, 1983), the term hyaloclastite was broadly defined as a fracture-bounded, glassy, fragmental rock, and also included most palagontized or altered fragmental rock. Hyaloclastites were interpreted as indications of subglacial environments and higher paleo-ice-levels. This broad definition of hyaloclastite has two major weaknesses. First, the definition does not differentiate clasts produced by passive granulation in a subaqueous setting from those produced by hydromagmatic explosivity in an emergent to subaerial environment. Second, palagonite is a product of hydration and alteration of quenched sideromelane glass and is common in a variety of hydrovolcanic environments from deep subaqueous to emergent and subaerial (e.g., Fisher and Schmincke, 1984). Palagonitized deposits have also been identified in dry, strombolian subaerial volcanoes, where they are

attributed to post-eruptive alteration by steam or surface water (Houghton and Schmincke, 1984; McIntosh and Gamble, 1981; LeMasurier et al., 1994). The broad usage of the term hyaloclastite in previous studies led to an overestimation of the number of subglacial volcanic deposits and higher-than-present paleo-ice-levels. Many previously reported hyaloclastites are re-interpreted in this paper as pyroclastic rocks derived from emergent to subaerial eruptions.

An enriched conceptual model of glaciovolcanism in West Antarctica

The ultimate objective in developing a conceptual model of glaciovolcanism is to provide a framework for evaluating volcanic proxy records of past fluctuations of the WAIS. Previous records of glaciovolcanism in MBL relied heavily on the table mountain analogue, typically interpreting all subglacial to subaerial volcanic transitions as "dipstick" measures of WAIS levels. Our new conceptual model addresses the complexities of the glaciovolcanic environment of West Antarctica, in order to differentiate records of local ice level from those of the WAIS level. The conceptual model is presented in Figure 2 (A-E) with specific themes highlighted below. Site examples listed in Figure 2 are described in detail in the results section.

Old models- table mountain analogues. The ancient subglacial to subaerial table mountains, or tuyas (Mathews, 1947), of British Columbia, Iceland and Antarctica (Jones, 1969, 1970; Allen et al., 1982; Wörner and Vierick, 1987, Skilling 1994; Smellie and Skilling, 1994; Smellie and Hole, 1997) are obvious potential analogues for volcanic sequences in MBL. Elements of the table mountain model, particularly the character of deposits relative to local syn-eruptive ice level, can be broadly applied to MBL deposits. However, the classic monogenetic, basaltic table mountains of Iceland and British Columbia provide only a starting point for interpretations of MBL sequences, many of which are polygenetic, felsic, and largely concealed beneath local and regional ice.

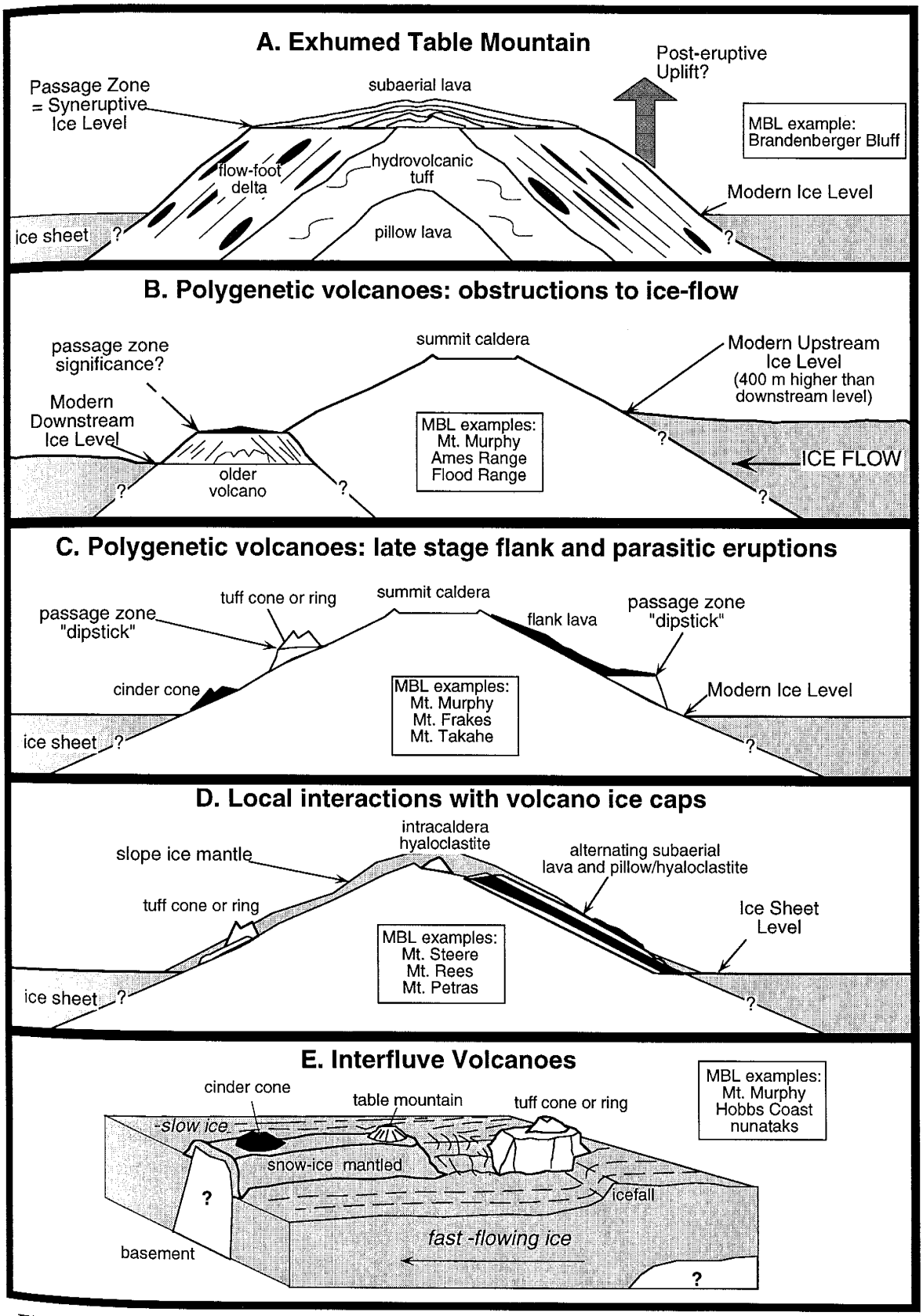

Figure 2. Cartoon sketches illustrating different aspects of the conceptual model of glaciovolcanism. Details explained in text.

Table mountains (Fig. 2a) are characterized by three stages of growth from a subglacial to subaerial environment, each with distinct lithofacies assemblages (Jones, 1970). The first stage is characterized by effusion of pillow lava and hyaloclastite breccia into a melted subglacial chamber, where the confining pressure is high enough to suppress volatile-driven explosive eruptions. As the pillow pile builds, continued thermal erosion results in collapse of the subglacial ceiling and formation of an intraglacial lake. Confining pressures decrease as the pillow pile and the vent level build to higher levels and effusion is superseded by second stage hydromagmatic explosive eruptions, that result in the deposition of glassy tuff by pyroclastic fall and resedimentation processes. The third stage occurs when the vent emerges above lake level or is sealed from infiltrating lake water. This stage is characterized by subaerial effusive and mildly explosive eruptions of lava flows and cinders. Flow-foot breccias, composed of coherent and detached pillow lavas and hyaloclastite, are deposited as subaerial lava flows enter water and tumble down the steep (up to 30°) volcaniclastic pile. Jones and Nelson (1970) termed the horizontal transition from subaerial lavas to subaqueous flow-foot breccias the "passage zone". The elevation of the passage zone records changes in ice levels or intraglacial lake levels but also records uplift or subsidence of the volcanic pile (Jones and Nelson, 1970). Ideally, preserved table mountains with passage zones provide "dipstick" measurements of minimum paleo-ice-levels.

Recent studies of table mountain sequences on the Antarctic Peninsula provide more detailed interpretations of their processes and deposits (Skilling, 1994, Smellie and Skilling, 1994; Smellie and Hole, 1997). These process-oriented studies are based on lithofacies analysis and interpretations of paleoenvironments in relation to local ice conditions. Surtseyan tuff cones are used as analogues for the emergent (second) stage of table mountain growth and abundant remobilized turbidite and mass flow deposits are recognized on the subaqueous slopes of emergent englacial volcanoes. Skilling (1994) and Smellie and Hole (1997) suggested that sudden draining of the englacial lakes is common

in some cases and can result in deposition of subaerial lavas on slopes far below ice-level. In such cases, the "passage zone" from subaqueous to subaerial depositional environments forms parallel to the depositional slope. Volcanic-induced draining of englacial lakes beneath temperate or small ice caps is well known from studies of Grímsvötn volcano and jökulhlaups in Iceland (e.g. Gudmundsson and Björnsson, 1991) and Deception Island near the Antarctic Peninsula (Baker et al., 1969). The glacial hydrology associated with eruptions beneath relatively small, temperate ice caps has been studied extensively in Iceland (Björnsson, 1988) but the validity of Icelandic ice cap models to the WAIS environments has not been addressed.

Much of the volcanism in the WAIS is more complicated than is predicted by the early table mountain models (e.g., Jones, 1969) and the more recent models (e.g. Skilling, 1994).

The uplift caveat. One complication of the volcanic record of the WAIS is that all paleo-ice-level elevations are relative to modern elevations and do not account for possible uplift or subsidence of volcanic centers (Fig 2a). This uplift caveat is problematic in many terrestrial ice-sheet reconstructions, particularly those reconstructions of older (pre-Pleistocene) glaciations (e.g. Wilch et al., 1993). LeMasurier and Landis (1996) suggested that progressively higher elevations of the pre-volcanic basement unconformity and older volcanoes toward the center of the MBL volcanic province are a surface expression of regional domal uplift that has been ongoing since inception of volcanism in middle Tertiary times. We interpret the pre-volcanic unconformity as a time-transgressive erosion surface that appears to be very flat in some places (e.g. Bowyer Butte) and quite rugged in other places (e.g. Mt. Petras exhibits 400 m of relief; and Mt. Murphy exhibits 900 m of relief, McIntosh et al., 1991). Although the trend of higher unconformities and older volcanoes toward the center of the volcanic province is real, there are no constraints on either the timing or the amount of (basement) surface uplift at any location. In the absence of geologic constraints on uplift, we propose tentative paleo-ice-level elevations

that assume no uplift. The impact of this assumption is diminished by the fact that much of our WAIS reconstruction relies on the latter part of the volcanic history of MBL (since 9 Ma).

Volcanoes as ice flow obstructions. A major complicating factor of large polygenetic volcanoes is that they are obstructions to regional ice flow and produce higher ice levels upstream and lower ice levels downstream (Fig. 2b). An example of the ice-damming effect is the coastal volcano, Mt. Murphy, where upstream ice levels are 400 m higher than downstream ice levels. Many of the volcanoes of Marie Byrd Land have coalesced to form linear ranges. The Flood Range in western Marie Byrd forms a >60-km-long barrier to ice flow, with upstream ice levels 400-800 m higher than downstream ice levels(cf. Fig. 3). Because polygenetic volcanoes can be long-lived, their effect on ice-flow patterns can change with time. Consequently, interpretations of exposed glaciovolcanic sequences on the downstream sides of volcanic obstructions require careful consideration. Not all MBL volcanoes produce ice-damming effects: ice sheet elevations surrounding some inland volcanoes (e.g., Mt. Takahe) are consistent, irrespective of regional ice flow patterns.

Early versus late stage eruptions. Interpretations of early shield-building sequences can be complicated by issues related to changing ice-flow patterns and ice-sheet levels during volcano construction. The lower shield areas of many of the volcanoes in MBL are buried by ice, so problems relating to ice damming can be often ignored. In other cases where rocks are exposed at the base of polygenetic volcanoes, paleo-ice-level interpretations must account for the ice-damming effect.

Late stage shield-building flank eruptions or parasitic eruptions that occur on pre-existing shields provide less complicated paleo-ice-level indicators (Fig. 2c). Presumably ice-damming effects produced by the pre-existing shield had a similar effect on local ice-flow patterns and elevations as they do today. Subglacial to subaerial sequences preserved

in flank deposits (e.g. Mt. Takahe) provide reliable "dipstick" records of paleo-ice-levels that can used in glaciological models. Conversely, the lowest elevations of subaerially erupted parasitic volcanoes (e.g., English Rocks at Mt. Frakes) provide limits on the maximum elevation of the syn-eruptive ice sheet at those locations.

Volcanic interactions with slope ice. The volcanoes of MBL are mantled in snow and ice of variable thickness ranging from no ice at the limited volcanic outcrops to probably >100 m in local glaciers and ice-filled calderas. This mantle of snow and ice provides ample opportunities for glaciovolcanic interactions above the level of the ice sheet (Fig. 2d). The possibility that glaciovolcanic sequences resulted from interactions with slope ice rather than the regional ice sheet must be evaluated at each site.

There are many non-Antarctic examples where historical lavas have been observed overriding ice, cutting open channels into ice, and tunneling into ice on the flanks of volcanoes (see summary review by Major and Newhall, 1989). In these cases, the lavas were quenched and generally fragmented where they came into contact with ice. Presumably, these lava-slope ice interactions produced dipping "passage zones" from subglacial to subaerial depositional environments.

Models of eruptions beneath valley-confined glaciers provide possible analogues for the type of sequences produced on volcanoes with a moderately thick ice mantle (to 100 m). Eruptions beneath valley-confined glaciers have been inferred from volcanic sequences in Iceland (Walker and Blake, 1966) and Alexander Island, Antarctica (Smellie et al., 1993). The Icelandic sequence consists of pillow lava, hyaloclastite breccia and minor tillite, representing a single subglacial eruptive phase (Walker and Blake, 1966). The Alexander Island deposits consist of stacked sequences of tillite, pillow lava and hyaloclastite breccia, and remobilized phreatomagmatic tuff, representing multiple eruptive phases (Smellie et al., 1993). In the Alexander Island example, the eruption was not subglacial but occurred in an emergent environment and alternated between explosive

hydromagmatic and effusive phases (Smellie et al., 1993). In both Icelandic and Alexander Island sequences, deposition in thermally excavated subglacial tunnels is inferred, with the resulting post-glacial landform being a volcanogenic "esker".

Explosive hydrovolcanic eruptions on volcano slopes may have an associated pillow lava phase and produce dipping passage zones (Smellie et al., 1993) or they may simply produce monogenetic tuff cones/rings, without an effusive pillow lava phase. Mixed hydromagmatic-fall and base-surge deposits are documented in both tuff cone and lower relief tuff ring sequences in non-glacial environments (e.g., Wohletz and Sheridan, 1983). Sohn (1996) outlined several factors that control the hydromagmatic eruption styles, depositional processes and character of the deposits, including the water-magma mixing ratio, ground-water flow patterns, and aquifer characteristics. Sohn (1996) suggested that base-surge eruptions are typically associated with deeper explosions in weak substrates, where water has only limited access to the vent. Such environments may have been common on the slopes of active Antarctic volcanoes.

Volcanoes on interfluves between glaciers and ice streams. Small volcanoes perched on interfluves between areas of faster flowing ice may exhibit records of changing local ice levels that give false impressions of the magnitude and elevations of regional ice level variations (Fig. 2e). Regional growth of the ice sheet may not cause higher ice levels at these nunataks if the local ice streams compensate by discharging ice at a greater rate. Records of higher local ice levels on the interfluves may indicate times of higher regional ice levels, if it can be shown that the passage zones lie above the level of the regional ice sheet. Records of unchanged ice levels are more difficult to interpret and may be associated with times of higher, similar, or lower regional ice levels relative to today. Uncertainites about the timing of down-cutting of the adjacent drainages weaken interpretations of regional paleo-ice-level in all cases.

Inland versus coastal thickening of ice sheet. Ice sheets flow outward under their own weight (Hughes, 1987). Inland thickening by snow accumulation will result in outward expansion and thickening in coastal regions (e.g. Paterson, 1981; Hughes, 1987). Lateral expansion of the grounding line will effectively raise ice sheet levels more dramatically at coastal site than at inland sites. Marine ice sheets drained by ice streams, such as the WAIS, are a special case. The ice stream profile may be maintained in coastal regions regardless of inland ice level changes (Hughes, 1987).

Sea-levels changes can further complicate ice flow at the margins of marine-based ice sheets. Sea-level rises can buoyantly lift and destabilize grounded ice margins, which may result in accelerated ice flow. Sea-level falls will result in expansion of grounded ice. Such sea-level changes may have affected local ice levels at coastal volcanoes (Mt. Murphy) and at interfluve volcanoes adjacent to glaciers draining in the sea (e.g., the Hobbs Coast nunataks).

METHODS AND RESULTS

Field Studies

Detailed field observations and sampling were carried out at Mt. Takahe in 1984-85 (W.C. McIntosh only), Mt. Murphy and U.S.A.S. Escarpment in 1990-91(W.C. McIntosh only), the Crary Mountains in 1992-93 (both authors), and Mt. Berlin, Mt. Moulton, Mt. Bursey, Mt. Andrus, Mt. Siple, Mt. Flint, Reynolds Ridge, Mt. Petras, and several nunataks near Hobbs Coast in 1993-94 (both authors) (Figs. 3 and 4). During the course of these field studies more than 1000 samples were collected for laboratory analysis. At most sites, outcrop elevations were measured using a hand-held altimeter and elevations were corrected relative to the spot elevations listed on the U.S.G.S.

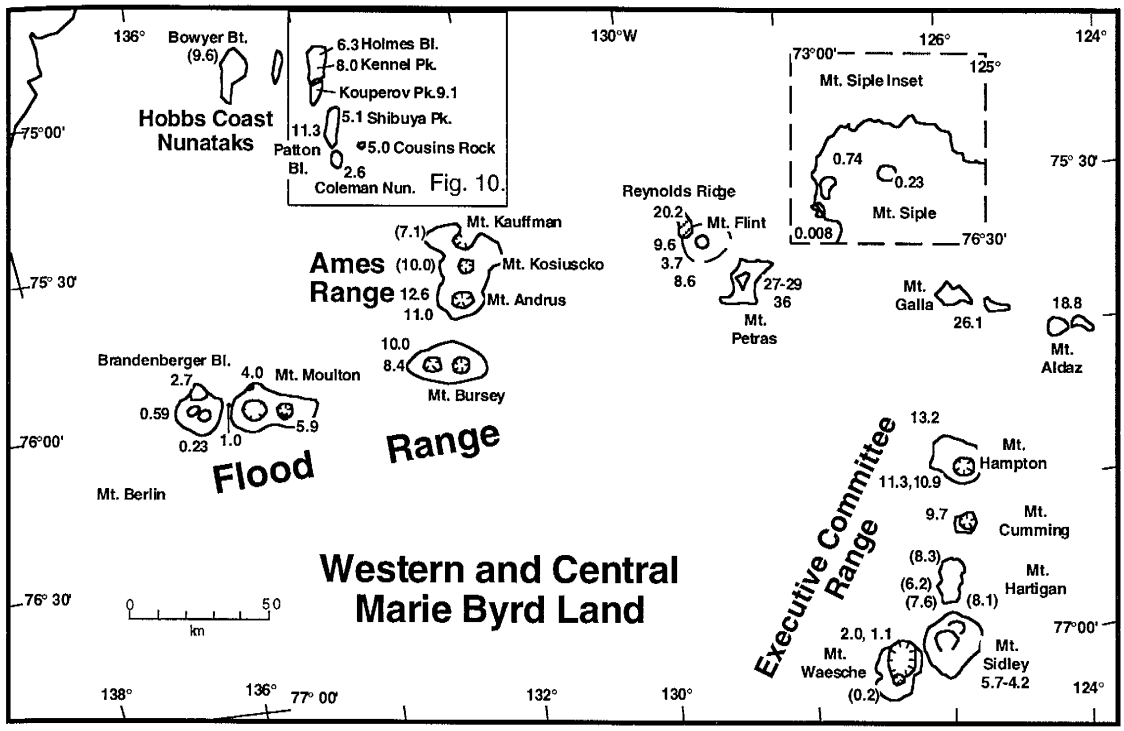

Figure 3. Map of volcanoes of western and central Marie Byrd Land, showing outlines of volcanoes and ages of volcanoes. Ages in parentheses indicate K/Ar ages from LeMasurier and Thomson (1990). Executive Committee Range $^{40}Ar/^{39}Ar$ ages from Panter et al., 1994. All other ages are $^{40}Ar/^{39}Ar$ ages from this study (Table 1). Areas in boxes are inset maps (dashed line) or are shown in separate figures as larger maps (solid line).

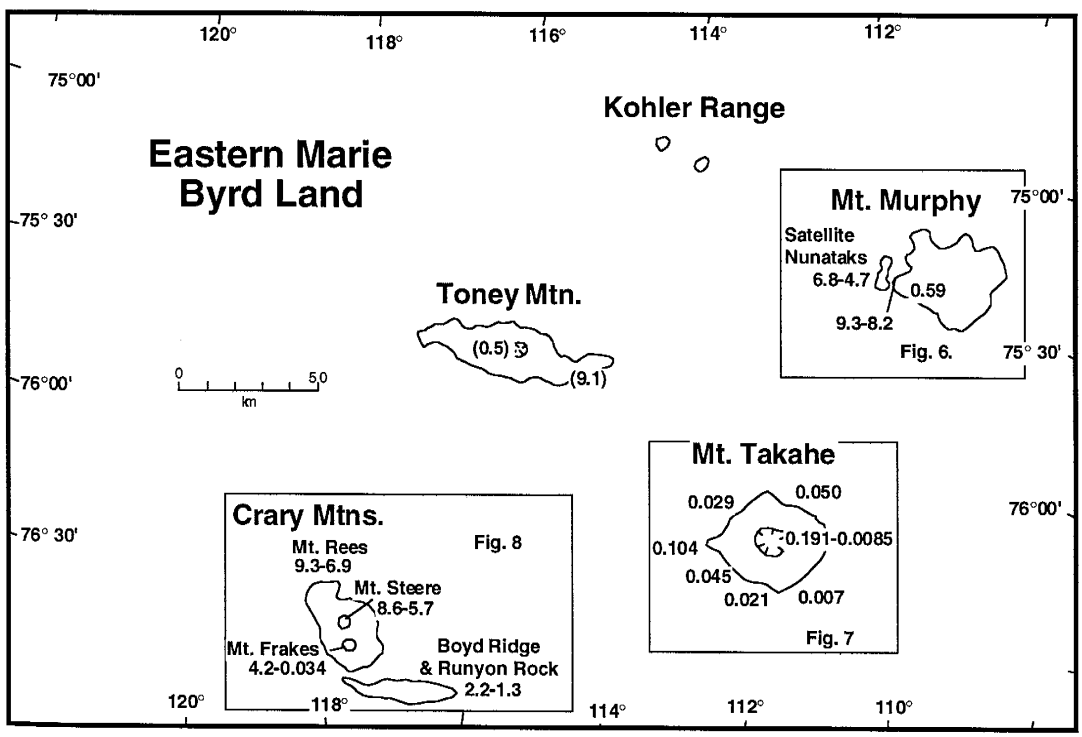

Figure 4. Map of volcanoes of eastern Marie Byrd Land, showing outlines of volcanoes and ages of volcanoes. Ages in parentheses indicate K/Ar ages from LeMasurier and Thomson (1990). All other ages are $^{40}Ar/^{39}Ar$ ages from this study (Table 1). Areas in boxes are shown in separate figures as larger maps (solid line).

Reconnaissance Series, Antarctica, 1:250,000 scale topographic quadrangle maps. Some outcrop elevations are estimated from the topographic maps. Most sites with previously reported glaciovolcanic records were re-examined for this study.

In this paper, we introduce new field data and interpretations and $^{40}Ar/^{39}Ar$ geochronology data from studies in the Crary Mountains (1993-94) and central and western Marie Byrd Land (1992-93). The extensive $^{40}Ar/^{39}Ar$ geochronology includes many new ages for samples collected during the 1984-85 and 1990-91 field seasons at Mt. Takahe and Mt. Murphy. Descriptions of the geology at Mt. Murphy and Mt. Takahe are derived mostly from publications by McIntosh et al. (1985, 1991) and LeMasurier et al. (1994).

$^{40}Ar/^{39}Ar$ Geochronology Results

$^{40}Ar/^{39}Ar$ dating sample preparation and analyses were conducted at the New Mexico Geochronology Research Laboratory at the New Mexico Institute of Mining and Technology, Socorro, NM, according to methods described in appendices of Parts A and B of dissertation. Fish Canyon Tuff sanidine (FC-1, 27.84 Ma (Deino and Potts, 1990)) was used as a neutron-flux monitor. The sample ages were corrected for blank, background, mass discrimination, radioactive decay, and interfering reactions. All analytical uncertainties are reported at the 2 σ confidence level and the decay constants and isotopic abundances used are those suggested by Steiger and Jaeger (1977). All mafic and intermediate groundmass samples and plagioclase samples, as well as young (<0.6 Ma) potassium feldspar (inferred to be anorthoclase) phenocryst samples, were analyzed by the furnace incremental heating method; older anorthoclase phenocryst samples were analyzed by CO_2 laser-fusion method.

Table 1 summarizes the dating results, and more complete data included in Appendix I (Pages C-86 to C-143). Dating efforts concentrated on sites of detailed fieldwork: Crary Mountains (61 samples); Hobbs Coast nunataks (22 samples); Mt. Petras

(6 samples; summarized in Part B); Mt. Murphy (14 samples); Mt. Berlin (38 samples; summarized in Part A); Mt. Takahe (14 samples, including 6 crater rim samples described in Part A of dissertation). Fewer samples were analyzed from Mt. Andrus, Mt. Flint, Mt. Moulton, and Mt. Bursey, because of the limited number of sites visited at these volcanoes. A total of 177 samples were dated. Major and trace element data based on standard X-ray fluorescence analyses were obtained at the University of Kiele and New Mexico Tech for most dating samples (Appendix II, Pages C-144 to C-160). Thin sections of lava and bomb samples were analyzed for mineralogy and alteration under a cross-polarizing petrographic microscope.

The age results were interpreted according to the following guidelines. Single-crystal laser-fusion ages and errors were calculated according to the method of Samson and Alexander (1987). Very few laser-fusion ages of anorthoclase crystals from the same sample differed by more than their 2 σ analytical errors. These rare discordant ages are attributed to xenocrysts (older ages), contaminants such as low potassium plagioclase (low-precision older or younger ages), or alteration (typically low-precision younger ages). For most furnace step-heating results, plateau ages (after Fleck et al., 1977) or "selected mean ages" were interpreted as the best estimates of the eruption ages. Selected mean ages represent the weighted mean of near-plateau segments of age spectra ,where typically one step lies slightly outside of 2 σ uncertainty. In a few cases, isotope correlation ages provide the best eruption age estimates for samples yielding discordant age spectra, high trapped $^{40}Ar/^{36}Ar$ content, and a low MSWD (mean standard weighted deviation) value. Several samples were analyzed in duplicate and the ages for these were averaged according to Samson and Alexander (1987). All plagioclase analyses were accompanied by analyses of groundmass from the same samples.

Table 1. $^{40}Ar/^{39}Ar$ Dating Results: Marie Byrd Land Volcanic Province

I.D.	Outcrop	Rock type	sam (meth)	Irrad.# Lab #	Total Fusion Age ± 2 s.d. (Ma)	Isochron Age ± 2 s.d. (Ma)	$^{40}Ar/^{36}Ar$ ± 2 s.d.	MSWD	steps	%^{39}Ar	Mean (Plateau) Age ± 2 s.d. (Ma)	steps (type)	%^{39}Ar	Geology notes
Mt. Murphy (1990-91 Field Season)														
WM 90														
69	Sechrist Peak	basn	gms (F)	nm-17 1860	0.66 ± 0.15	0.599 ± 0.086	294 ± 15	0.97	C-E	66	0.587 ± 0.043	C-E (N)	66	west flank
139	Sechrist Peak	basn	gms (F)	nm-17 1866	0.60 ± 0.18	0.601 ± 0.028	292.9 ± 3.6	1.27	B-I	96.4	0.592 ± 0.040	B-I (N)	96.4	dense intrusive interior
									mean age (n=2)		**0.590 ± 0.015**			
34	main shield basal section	trach	gms (F)	RD79 604	8.15	no isochron					**8.22 ± 0.04**	C-I (N)	90.0	trachyte lava dome, 50 m thick (1980-~2130')
37		basn	gms (F)	nm-1 704	8.86 ± 0.37	8.584 ± 0.090	301.6 ± 4.6	47.6	E-H	58	8.80 ± 0.20	D-G (N)	79.9	thin (subaerial?) lava, 1820'
			gms (F)	nm-1 61	9.65 ± 0.16	8.717 ± 0.066	304.5 ± 3.0	21.7	D-H	81.5	8.86 ± 0.15	D-H (SM)	81.5	" "
									mean age (n=2)		**8.84 ± 0.13**			
39		basn	gms (F)	nm-1 63	9.21 ± 0.21	9.180 ± 0.051	246.9 ± 7.8	63.9	C-G	89.3	9.03 ± 0.12	B-G (SM)	92	lava assoc. w/hyaloclastite 1320'
			gms (F)	nm-1 705	9.48 ± 0.26	9.225 ± 0.055	300.1 ± 3.8	0.816	B-E	85.3	9.26 ± 0.14	B-D (N)	85.3	" "
									mean age (n=2)		**9.13 ± 0.24**			
33		basn	gms (F)	nm-1 703	9.57 ± 0.34	9.376 ± 0.089	296.8 ± 4.0	3.8	A-F	98.9	9.39 ± 0.12	A-F (N)	98.9	1.5 m lava (striated) 1210'
			gms (F)	nm-1 62	9.09 ± 0.13	9.180 ± 0.120	278.1 ± 17	0.45	C-E	58.3	9.070 ± 0.090	C-E (N)	58.3	" "
									mean age (n=2)		**9.19 ± 0.32**			
50		basn	gms (F)	nm-1 707	9.31 ± 0.21	9.306 ± 0.049	299.2 ± 2.8	25.5	B-G	87.0	9.35 ± 0.13	B-G (SM)	87	pillow 15' above tillite, lower than 1210'
			gms (F)	nm-1 706	9.13 ± 0.18	9.272 ± 0.054	301.1 ± 3.4	12.0	B-E	78.0	9.32 ± 0.13	B-E (SM)	78	" "
									mean age (n=2)		**9.335 ± 0.097**			
99	Hedin Nunatak	basn	gms (F)	RD84	6.23	**6.20 ± 0.24**	305.2 ± 6.4	0.5	ALL	100.0	no plateau			subaerial lava, upper tuya (MB51.29B)
110	Hedin Nunatak	basn	gms (F)	nm-17	12.0 ± 5.00	**6.50 ± 0.12**	310 ± 0.9	3.69	ALL	100	highly discordant			MB51-13, lowest tindar
47	Icefall Nunatak	basn	gms (F)	nm-17 1859	6.46 ± 0.25	6.43 ± 0.11	300.6 ± 5.2	1.96	B-F	58.8	**6.52 ± 0.13**	B-F (N)	58.8	high subaerial lava
48	Icefall Nunatak	basn	gms (F)	nm-17 1853	11.3 ± 4.60	**6.80 ± 0.20**	301.9 ± 2.4	2.58	A-H	95.7	7.10 ± 0.25	E-H (N)	51.9	lobe in low hyaloclastite
94	Turtle Peak	basn	gms (F)	nm-17 1857	5.17 ± 0.58	4.588 ± 0.091	299.7 ± 2.2	0.933	C-H	96.6	**4.70 ± 0.15**	C-H (N)	96.6	v. vesicular pahoehoe top
92	Turtle Peak	basn	gms (F)	nm-17 1861	5.69 ± 0.22	5.71 ± 0.10	289.5 ± 5.6	29.3	B-H	90.9	**5.65 ± 0.23**	B-H (SM)	90.9	top pillow
87	Turtle Peak	basn	gms (F)	nm-43 6064	16.8 ± 2.80	**5.95 ± 0.6**	316.3 ± 3.8	1.87	B-I	99.5	9.36 ± 0.60	D-F (SM)	64.7	angular clast in lower flow-foot breccia

Table 1. $^{40}Ar/^{39}Ar$ Dating Results: Marie Byrd Land Volcanic Province

I.D.	Outcrop	Rock type	sam (meth)	Irrad.# Lab #	Total Fusion Age ± 2 s.d. (Ma)	Isochron Age ± 2 s.d. (Ma)	$^{40}Ar/^{36}Ar$ ± 2 s.d.	MSWD	steps	$\%^{39}Ar$	Mean (Plateau) Age ± 2 s.d. (Ma)	steps (type)	$\%^{39}Ar$	Geology notes
Mt. Takahe (1984-85,1990-91 Field Seasons) (see Part A of dissertation for summit crater data)														
MT 85-1	Gill Bluff	trach	gms (F)	nm-37 5386	-0.01 ± 0.10	no isochron					0.022 ± 0.026	C-G (N)	85.0	pillow interior, passage zone sequence
MT 85-2	Gill Bluff	trach	gms (F)	nm-37 5387	0.006 ± 0.047	no isochron					0.028 ± 0.014	C-I (N)	92.1	lava, passage zone sequence
W85-85	Gill Bluff	trach	gms (F)	nm-36 5340	0.063 ± 0.04	no isochron					0.034 ± 0.018	C-G (N)	86.7	pillow interior, passage zone sequence
											mean age (n=3)	**0.029 ± 0.012**		
W85-31	Moll Spur	trach	gms (F)	nm-37 5392	-0.07 ± 0.19	no isochron					**0.021 ± 0.040**	A-I (SM)	100	lava, passage zone sequence
MT 85-10	Oeschger Bluff	basn	gms (F)	nm-37 5391	0.009 ± 0.04	no isochron					**0.007 ± 0.013**	C-G (N)	80.1	pahoehoe lava
MT 85-3	Roper Point	basn	gms (F)	nm-37 5388	0.104 ± 0.10	no isochron					**0.104 ± 0.028**	B-F (N)	77.2	lava
W85-35	Stauffer Bluff	trach	gms (F)	nm-36 5339	0.05 ± 0.11	no isochron					**0.050 ± 0.029**	B-F (SM)	75.9	pillow lava, passage zone sequence
MT 85-9	Steuri Glacer	trach	gms (F)	nm-37 5368	0.086 ± 0.01	no isochron					**0.045 ± 0.007**	D-F (SM)	55.7	lava
Mt. Rees, Crary Mountains														
TW 92-														
174	Trabucco Cliff	trach	ano (L)	nm-4 235							**8.943 ± 0.057**	8		lava flow top of section
175		trach	ano (L)	nm-4 234							**8.948 ± 0.058**	9		lava flow top of section
6		trach	ano (L)	nm-21 2152							**8.975 ± 0.068**	10		massive flow, above 3
15		trach	ano (L)	nm-4 236							**9.007 ± 0.044**	8		lava flow middle of section
1		haw	gms (F)	nm-13 1421	9.42 ± 0.17	7.958 ± 0.080	351.0 ± 4.2	253.0	ALL	100.0	**9.13 ± 0.53**	ALL (SM)	100	lobe hyaloclastite
36	Tasch Ridge	phono	ano (L)	nm-21 2154							**7.521 ± 0.059**	10		phonolite dike
41		mug	gms (F)	nm-21 2538	9.20 ± 0.14	8.42 0.24	305.5 28	5.05	B-E	49.9	**8.50 ± 0.16**	B-E (SM)	49.9	hyaloclastite lobes
38		basn	gms (F)	nm-13 1534	8.239 ± 0.046	8.118 ± 0.058	313.0 ± 9.0	154.2	D-I	96.3	**8.21 ± 0.13**	D-I (SM)	96.3	7315' pillow hyaloclastite
34		mug*	gms (F)	nm-13 1424	8.422 ± 0.053	8.038 ± 0.058	347.3 ± 9.4	13.2	B-G	84.1	**8.230 ± 0.087**	B-G (SM)	84.1	7430' intrusive hyaloclastite
31		mug	gms (F)	nm-13 1418	9.130 ± 0.064	8.904 ± 0.056	309.5 ± 2.8	554.1	ALL	100.0	**8.98 ± 0.28**	ALL (SM)	100	6050' pillow lobe interior
28		ben*	gms (F)	nm-13 1417	9.232 ± 0.079	8.752 ± .057 9.059 .071	324.1 ± 2.6 298.0 6.2	100.5 0.976	ALL B-D	100 54.1	**9.075 ± 0.064**	AB-AD	54.1	5960' spatter-fed lava
23		ben	gms (F)	nm-13 1416	8.943 ± 0.056	8.846 ± 0.010	309.2 ± 1.8	39.1	A-H	88.6	**8.91 ± 0.12**	ALL (SM)	100	5705' pillow lobe
59		basn	gms (F)	nm-13 1420	9.44 ± 0.38	9.034 ± 0.063 8.06 0.38	302.5 ± 1.8 352.0 19.8	20.0 11.6	ALL E-G	100 65,0	**9.34 ± 0.24**	E-G (SM)	65	5390' lava flow

Table 1. $^{40}Ar/^{39}Ar$ Dating Results: Marie Byrd Land Volcanic Province

I.D.	Outcrop	Rock type	sam (meth)	Irrad.# Lab #	Total Fusion Age ± 2 s.d. (Ma)	Isochron Age ± 2 s.d. (Ma)	$^{40}Ar/^{36}Ar$ ± 2 s.d.	MSWD	steps	%^{39}Ar	Mean (Plateau) Age ± 2 s.d. (Ma)	steps (type)	%^{39}Ar	Geology notes
117	southwest of Tasch Pk.	basn*	gms (F)	nm-13 1402	6.78 ± 0.18	6.915 ± 0.050	286.3 ± 1.8	96.9	B-G	94.5	**6.82 ± 0.26**	B-G (SM)	94.5	lava flow
114	southwest of Tasch Pk.	basn*	gms (F)	nm-13 1401	6.72 ± 0.14	7.099 ± 0.062	283.5 ± 2.4	35.6	B-G	99.3	**6.92 ± 0.21**	B-G (SM)	99.3	lava flow
112	north end	trach	gms (F)	nm-21 2486	12.517 ± 0.077	NO ISOCRHON					**9.02 ± 0.19**	C-F (SM)	51.5	lava flow, striae (240)
109	north end	trach	gms (F)	nm-21 2487	8.761 ± 0.097	8.763 ± 0.058	282.4 ± 5.4	5.52	C-M	94.1	**8.699 ± 0.075**	C-M (SM)	94.1	lava flow, striae (328)
Mt. Steere, Crary Mountains														
TW 92-118	west side	phono	ano (L)	nm-21 2165							**7.547 ± 0.054**	9		flow banded lava, striated
95	Steere moraine	mug	gms (F)	nm-21 2493	6.832 ± 0.065	5.72 ± 0.11	303.3 ± 45	0.27	C-E	60.6	**5.735 ± 0.042**	C-E	60.6	flow banded lava
64	interior Steere	phono	gms (F)	nm-13 1535	8.053 ± 0.044	8.033 ± 0.051 8.033 0.053	301.1 ± 2.6 301.1 3.8	18.4 22.1	ALL B-I	100 98.9	**8.058 ± 0.076**	B-I (SM)	98.9	dike
53	interior Steere	trach	ano (L)	nm-21 2156							**8.235 ± 0.083**	10		lava flow dome
93	interior Steere	rhyo	ano (L)	nm-21 2160							**8.246 ± 0.080**	9		dike
63	interior Steere	trach	ano (L)	nm-21 2157							**8.271 ± 0.076**	10		dike, 145, 67E salt and pepper dike
51	interior Steere	trach	ano (L)	nm-21 2155							**8.325 ± 0.061**	9		lava flow, exposed plug
107	N. Steere arete	trach*	ano (L)	nm-21 2162							**8.342 ± 0.061**	8		dike, 7915'
104	N. Steere arete	trach*	ano (L)	nm-21 2161							**8.350 ± 0.083**	8		flow banded lava, 7475'
108	N. Steere arete	trach*	ano (L)	nm-21 2164							**8.368 ± 0.056**	10		flow banded lava, 7915'
91	East Side	trach	ano (L)	nm-21 2159							**8.457 ± 0.089**	8		flow banded lava
181	SE Side	phono	ano (L)	nm-21 2173							**7.91 ± 0.20**	5		dike, fine grained
182	SE Side	rhyo	ano (L)	nm-21 2196							**8.523 ± 0.060**	10		flow banded lava
183	SE Side	rhyo	ano (L)	nm-21 2197							**8.523 ± 0.058**	10		flow banded lava
178	SE Side	trach	ano (L)	nm-4 238							**8.552 ± 0.043**	8		flow banded lava
169	Lie Cliff SE ridge	basn	gms (F)	nm-13 1415	6.257 ± 0.065	5.928 ± 0.013	341.4 ± 2.7	1132	a-g	80.5	**6.41 ± 0.43**	B-D (SM)	76	5950' lava flow
165	Lie Cliff SE ridge	bas	gms (F)	nm-13 1414	7.42 ± 0.14	7.38 ± 0.10	296.5 ± 18.2	4.39	B-E	65.3	**7.378 ± 0.072**	B-E (SM)	65.3	5695' lava, same as 162 but fresher
162	Lie Cliff SE ridge	bas	gms (F)	nm-17 1883	6.650 ± 0.090	6.699 0.025	266.8 103	5.3	B-E	60.7	**6.695 ± 0.048**	B-E	60.7	lava flow
80	Lie Cliff	trach	ano (L)	nm-21 2158							**7.818 ± 0.056**	9		dike, 1.5 m wide
85	Lie Cliff	haw	gms (F)	nm-13 1412	8.50 ± 0.14	8.65 ± 0.09	267.9 ± 5.8	84.6	B-G	90.5	**8.38 ± 0.33**	B-G (SM)	90.5	5350' lava flow
82	Lie Cliff	mug	gms (F)	nm-13 1411	9.02 ± 0.11	8.06 ± 0.07	329.8 ± 9.4	213.9	CC-G	82.1	**8.28 ± 0.21**	CC-G (SM)	82.1	5250' hyaloclastite lobe
79	Lie Cliff	mug	gms (F)	nm-21 2095	8.410 ± 0.062	8.432 0.076	296.9 2.0	2.34	C-E	93.1	**8.435 ± 0.061**	C-E	93.1	
86	Lie Cliff	haw	gms (F)	nm-13 1413	8.62 ± 0.27	8.16 ± 0.13	302.8 ± 2.8	5.6	B-G	93.4	**8.52 ± 0.23**	B-G (SM)	93.4	5110' lava flow

Table 1. $^{40}Ar/^{39}Ar$ Dating Results: Marie Byrd Land Volcanic Province

I.D.	Outcrop	Rock type	sam (meth)	Irrad.# Lab #	Total Fusion Age ± 2 s.d. (Ma)	Isochron Age ± 2 s.d. (Ma)	$^{40}Ar/^{36}Ar$ ± 2 s.d.	MSWD	steps	$\%^{39}Ar$	Mean (Plateau) Age ± 2 s.d. (Ma)	steps (type)	$\%^{39}Ar$	Geology notes
TW 92-														
89	Lie Cliff NW ridge	phono	ano (L)	nm-21 2172							**7.676 ± 0.061**	10		dike, intrudes entire section
193	Lie Cliff NW ridge	mug	gms (F)	nm-13 1406	8.410 ± 0.100	8.019 ± 0.011	311.9 ± 1.0	28.2	a-g	64.7	**8.19 0.18**	B-G (SM)	83.4	5900' feeder dike, lava
192	Lie Cliff NW ridge	phono	ano (L)	nm-21 2174							**8.222 ± 0.065**	10		feeder dike, lava
194	Lie Cliff NW ridge	haw*	gms (F)	nm-13 1407	8.47 ± 0.10	8.018 ± 0.053	313.4 ± 2.2	5.98	C-G	98.6	**8.19 ± 0.22**	C-G (SM)	98.6	5750' glassy breccia
189	Lie Cliff NW ridge	haw	gms (F)	nm-13 1404	8.93 ± 0.27	7.844 ± 0.076	309.5 ± 1.8	19.4	ALL	100.0	**8.45 ± 0.46**	ALL (SM)	100	5730' glassy lava
190	Lie Cliff NW ridge	haw	gms (F)	nm-13 1405	9.17 ± 0.35	7.057 ± 0.070	319.6 ± 1.8	12.6	ALL	100.0	**8.27 ± 0.64**	ALL (SM)	100	5720' pillow lava
186	Lie Cliff NW ridge	haw	gms (F)	nm-13 1403	8.93 ± 0.39	8.42 ± 0.13	294.8 ± 2.8	0.196	F-H	61.5	**8.40 ± 0.11**	F-H	61.5	5400' subaerial lava
Mt. Frakes, Crary Mountains														
145	Morrison Rocks	bas	gms (F)	nm-13 1398	2.001 ± 0.073	1.975 ± 0.027	256.6 ± 5.2	145.0	C-H	98.5	**1.81 ± 0.10**	C-H (SM)	98.5	subaerial lava
142	Morrison Rocks	bas	gms (F)	nm-13 1397	2.02 ± 0.11	1.887 ± 0.084	287.6 ± 20	12.1	C-E	59.9	**1.815 ± 0.051**	C-E (SM)	59.9	subaerial lava
128	Morrison Rocks	haw	gms (F)	nm-13 1395	2.48 ± 0.11	2.428 ± 0.042	313.9 ± 8.4	7.34	D-G	67.4	**2.517 ± 0.057**	D-G (SM)	67.4	subaerial lava
125	Morrison Rocks	haw	gms (F)	nm-13 1394	2.68 ± 0.27	2.607 ± 0.065	293.0 ± 2.4	1.70	D-I	52.3	**2.535 ± 0.093**	D-I (SM)	52.3	subaerial lava
130	Morrison Rocks	bas	gms (F)	nm-13 1396	3.782 ± 0.087	3.886 ± 0.041	293.4 ± 6.8	1.37	E-H	51.5	**3.876 ± 0.034**	E-H	51.5	subaerial lava
122	Morrison Rocks	phono	ano (L)	nm-4 237							**4.170 ± 0.045**	8		lava flow
121	Morrison Rocks	phono	ano (L)	nm-21 2188							**4.183 ± 0.036**	5		lava flow
127	Morrison Rocks	phono	ano (L)	nm-21 2173							**4.251 ± 0.032**	9		lava flow
151	English Rock	basn	gms (F)	nm-39 5621	0.158 ± 0.039	0.035 ± 0.019	293.7 ± 4.7	0.1	B-F	78.4	0.032 ± 0.010	B-F	78.4	parasitic cone
			gms (F)	nm-13 1391	0.122 ± 0.049	0.024 ± 0.012	302.3 ± 9.2	0.5	B-G	86.1	0.035 ± 0.010	B-G	86.1	" "
									mean age (n=2)		**0.0335 ± 0.0077**			
157	English Rock	basn	gms (F)	nm-17 1877	0.78 ± 0.11	±	300.6 ± 58	53.5	CC-G	93.4	0.826 ± 0.079	CC-G (SM)	93.4	parasitic cone
			gms (F)	nm-13 1392	0.858 ± 0.072	0.920 ± 0.015	268.6 ± 4.0	10.5	D-H	91.8	0.851 ± 0.036	D-H (SM)	91.8	" "
									mean age (n=2)		**0.847 ± 0.038**			
159	English Rock	basn	gms (F)	nm-13 1393	1.624 ± 0.039	1.625 ± 0.024	280.6 ± 12.4	7.36	D-G	71.9	**1.598 ± 0.021**	D-G (SM)	71.9	parasitic cone

Table 1. $^{40}Ar/^{39}Ar$ Dating Results: Marie Byrd Land Volcanic Province

I.D.	Outcrop	Rock type	sam (meth)	Irrad.# Lab #	Total Fusion Age ± 2 s.d. (Ma)	Isochron Age ± 2 s.d. (Ma)	$^{40}Ar/^{36}Ar$ ± 2 s.d.	MSWD	steps	%^{39}Ar	Mean (Plateau) Age ± 2 s.d. (Ma)	steps (type)	%^{39}Ar	Geology notes
Boyd Ridge, Crary Mountains														
139	E. Boyd Ridge	ph-tph	gms (F)	nm-13 1409	1.295 ± 0.040	1.283 ± 0.056	294.1 ± 6.4	0.342	E-G	74.4	**1.272 ± 0.027**	E-G	74.4	subaerial lava
			plg (F)	nm-21 2962	1.68 ± 0.54	0.950 ± 0.072	298.2 ± 8.6	4.32	C-F	48.4	0.96 ± 0.15	C-F (SM)	48.4	" "
			plg (F)	nm-21 2963	5.50 ± 0.28	0.941 ± 0.063	343.9 ± 5.4	5.91	A-E	39.2	1.029 ± 0.093	C-E (SM)	36.9	" "
135	W. Runyon Rock	haw	gms (F)	nm-13 1400	2.63 ± 0.026	2.21 ± 0.19	300.2 1 2.8	3.43	ALL	100	2.41 ± 0.19	A-C	78.5	juvenile clast from hyalo-
			gms (F)	nm-13 1408	2.86 ± 0.37	1.97 ± 0.30	303.0 ± 3.2	4.55	B-F	97.6	2.67 ± 0.39	B-F (SM)	97.6	clastite
									mean age (n=2)		**2.24 ± 0.45**			
134	N.E. Runyon Rock	phono	ano (L)	nm-21 2189							**2.019 ± 0.049**	10		debris flow below 135
Hobbs Coast Nunataks														
WM 93														
199	Coleman (south)	basn	gms (F)	nm-33 5152	2.43 ± 0.30	2.614 ± 0.07	291.5 ± 3.2	2.15	C-I	83.2	**2.54 ± 0.08**	C-I	83.2	dense lava, below upper surge deposit
185	Coleman (south)	basn	gms (F)	nm-33 5146	3.27 ± 0.98	2.7 ± 0.94	295 ± 6.0	0.45	B-E	59.7	**2.60 ± 0.28**	B-E	59.7	lava, SW moat
184	Coleman (south)	basn	gms (F)	nm-33 5144	2.56 ± 0.43	2.7 ± 0.29	295.7 ± 4.0	0.064	B-E	61.1	**2.66 ± 0.13**	B-E	61.1	lava, SW moat
192	Coleman (south)	basn	gms (F)	nm-33 5149	2.72 ± 0.70	2.670 ± 0.520	295.0 ± 4.2	0.4	B-F	68.5	**2.61 ± 0.20**	B-F	68.5	lava, SW moat
190	Coleman (south)	basn	gms (F)	nm-33 5148	3.91 ± 0.65	3.2 ± 0.28	296.9 ± 2.6	8.06	A-G	98.9	3.340 ± 0.290	C-F (SM)	46.0	lava, base of upper lava
195	Coleman (south)	basn	gms (F)	nm-33 5150	51.4 ± 8.3									weathered & vesicular bomb
198	Coleman (south)	basn	gms (F)	nm-33 5151	8.12 ± 0.85	5.04 ± 0.57 5.82 2.2	310.4 ± 3.2 304.2 17.4	10.8 9.42	ALL D-F	100 41.1	7.28 ± 0.79	D-F (SM)	41.1	dense bomb
188	Coleman (south)	basn	gms (F)	nm-33 5147	2.58 ± 0.34	1.71 ± 0.55 2.68 1.23	314.2 ± 15 292.7 29	1.79 0.68	B-F D	B- 66.1 46.1	**2.46 ± 0.14**	B-F	66.1	basal lava flow SW moat
208	Coleman (north)	basn	gms (F)	nm-33 5132	2.60 ± 0.30	2.59 ± 0.10	293.4 ± 4.8	11.0	B-F	100 66.8	**2.55 ± 0.13**	B-F (SM)	66.8	clast w/in scoriaceous dike
207	Coleman (north)	basn	gms (F)	nm-33 5155	2.74 ± 0.34	2.83 ± 0.17	280.3 ± 11.0	3.8	C-G	53.1	**2.59 ± 0.11**	C-G (SM)	53.1	dike intruding lapilli tuff
205	Coleman (north)	basn	gms (F)	nm-33 5154	3.70 ± 1.00	2.35 ± 0.74	297.8 ± 4.0	0.4	B-H	78.5	**2.75 ± 0.31**	B-H	78.5	dike intruding lapilli tuff
202	Colemen (north)	basn	gms (F)	nm-33 5153	2.69 ± 0.47	2.89 ± 0.37	294.3 ± 4.8	3.9	B-E	51.1	**2.81 ± 0.27**	B-E	51.1	dike intruding lapilli tuff
218	Cousins Rock	ph-tph	gms (F)	nm-33 5133	4.79 ± 0.21	4.85 ± 0.12	296.2 ± 4.2	5.3	C-H	87.0	**4.87 ± 0.11**	C-H	87.0	dense bomb interior
219	Cousins Rock	ph-tph	gms (F)	nm-33 5134	4.91 ± 0.12	4.871 ± 0.081	312.3 ± 15.4	1.3	C-E	56.9	**4.956 ± 0.049**	C-E	56.9	lava
307	Patton Bluff	bas	gms (F)	nm-33 5162	10.73 ± 0.55	11.049 ± 0.074	291 ± 2.4	94.9	ALL	100	**11.32 ± 0.25**	D-G (SM)	46.2	lava, 15 m thick
221	Shibuya scab	haw	gms (F)	nm-33 5135	4.98 ± 0.40	5.05 ± 0.15	293.7 ± 2.4	7.54	A-H		**5.06 ± 0.16**	C-E	53.4	dense bom interior
223	Shibuya	haw*	gms (F)	nm-33 5136	9.14 ± 0.77	5.12 ± 0.44	297.4 ± 5.8	3.46	C-G	72.3	**5.26 ± 0.24**	C-G (SM)	72.3	lava crusts

Table 1. $^{40}Ar/^{39}Ar$ Dating Results: Marie Byrd Land Volcanic Province

I.D.	Outcrop	Rock type	sam (meth)	Irrad.# Lab #	Total Fusion Age ± 2 s.d. (Ma)	Isochron Age ± 2 s.d. (Ma)	$^{40}Ar/^{36}Ar$ ± 2 s.d.	MSWD	steps	%^{39}Ar	Mean (Plateau) Age ± 2 s.d. (Ma)	steps (type)	%^{39}Ar	Geology notes
229	Shibuya	haw	gms (F)	nm-33 5137	4.36 ± 0.20	4.78 ± 0.28	313.1 ± 9.0	4.39	C-F	56.9	**4.75 ± 0.12**	C-F (SM)	56.9	dike
303	Kouperov Pk	bas	gms (F)	nm-34 5212	13.1 ± 2.8	**9.09 ± 0.49**	301.1 ± 2.0	1.54	A-J	99.6	9.96 ± 0.60	F-J (SM)	53.0	lava at south end over u.c.
		plg (F)	nm-34 5213	9.39 ± 0.54	9.18 ± 0.056 9.216 0.053	314.9 ± 6.2 310.3 5.4	34.5 31.5	B-I A-I	99.6 100	9.55 ± 0.420	B-I (SM)	99.6	" "
304	Kouperov Pk	bas	gms (F)	nm-34 5214	11.3 ± 3.3	**9.16 ± 0.75** 9.00 0.46	298.9 ± 5.6 299.3 3.4	1.29 1.81	D-I ALL	77.9 100	9.60 ± 0.44	D-I	77.9	lava
		plg (F)	nm-34 5215	8.84 ± 0.67	8.725 ± 0.094 8.948 0.075	307.5 ± 7.2 300.1 4.2	18.9 63.1	D-H ALL	59.8 100	8.95 ± 0.39	D-H (SM)	59.8	" "
299	Kennel Pk	haw	gms (F)	nm-34 5238	8.61 ± 0.67	no iscochron					**7.99 ± 0.89**	B-H (SM)	95.8	pillow lobe interior
292	Holmes Bluff	basn	gms (F)	nm-33 5160	6.13 ± 0.25	6.31 ± 0.13	294.2 ± 5.0	0.95	B-F	85.6	**6.28 ± 0.08**	B-F	85.6	lava
Mt. Siple														
WM 93 **270**	mid-flank	bas	gms (F)	nm-34 5210	0.76 ± 0.16	0.722 ± 0.029 0.730 0.019	297.5 ± 4.8 295.0 2.2	3.00 9.43	B-G ALL	88.6 100	**0.736 ± 0.036**	B-H	97.8	lithic clasts in lapilli tuff
		plg (F)	nm-34 5211	1.04 ± 0.57	no iscochron					1.09 ± 0.60	A-I (SM)	100	" "
275	Doom cliff	haw	gms (F)	nm-33 5156	0.23 ± 0.36	0.048 ± 0.02	296.7 ± 3.6	3.02	ALL	100	**0.008 ± 0.088**	A-E	51.2	lithic clasts in lapilli tuff
		gms (F)	nm-37 5399	-0.03 ± 0.40	0.031 ± 0.064	291.8 ± 6.6		B-E	57.6	-0.041 ± 0.076	B-E (SM)	57.6	" "
Shepard Island														
255	Mathewson Pt.	basn	gms (F)	nm-34 5204	0.43 ± 0.14	0.454 ± 0.062	297.5 ± 6.0	1.38	B-E	74.4	**0.475 ± 0.049**	B-E	74.4	lava flow interior,
		plg (F)	nm-34 5205	0.47 ± 0.66	no isochron					0.62 ± 0.97	A-J	100	ponded flows in tuff cone
258	Mathewson Pt.	basn	gms (F)	nm-34 5206	0.999 ± 0.67	0.432 ± 0.16	297.8 ± 2.8	0.470	B-G	68.5	**0.55 ± 0.14**	B-G	68.5	lava clast from within tuff beds
		plg (F)	nm-34 5207	0.29 ± 0.56	0.222 ± 0.007	304.5 ± 2.4	223	B-E	97.1	0.31 ± 0.33	B-E	99.4	" "
265	Mt. Petinos	haw	gms (F)	nm-34 5208	0.55 ± 0.25	0.338 ± 0.099	298.6 ± 4.2	0.195	A-E	63.3	**0.40 ± 0.09**	A-E	63.3	lithic clast in tuff beds
		plg (F)	nm-34 5209	1.88 ± 0.91	no isochron					no plateau			" "
Ames and Flood Ranges														
308	Mt. Andrus, eroded cinder cone	basn	gms (F)	nm-33 5163	9.1 ± 0.23	9.167 ± 0.042	294 ± 2.0	2.4	ALL	100	**9.163 ± 0.063**	c-f	61.8	lava, strombolian cone
309	Mt. Andrus, Lind Ridge	trach	ano (L)	nm-33 5197							**12.552 ± 0.062**	10		stromb lava, massive
311	Mt. Andrus, Lind Ridge	trach	ano (L)	nm-34 5225							**11.045 ± 0.082**	10		pumiceous lava
312	Mt. Andrus, Lind Ridge	trach	ano (L)	nm-34 5226							**11.04 ± 0.19**	6		pumiceous lava
156	Mt. Bursey, Starbuck crater	trach	ano (L)	nm-34 5191							**8.447 ± 0.056**	10		lava

Table 1. $^{40}Ar/^{39}Ar$ Dating Results: Marie Byrd Land Volcanic Province

I.D.	Outcrop	Rock type	sam (meth)	Irrad.# Lab #	Total Fusion Age ± 2 s.d. (Ma)	Isochron Age ± 2 s.d. (Ma)	$^{40}Ar/^{36}Ar$ ± 2 s.d.	MSWD	steps	%^{39}Ar	Mean (Plateau) Age ± 2 s.d. (Ma)	steps (type)	%^{39}Ar	Geology notes
160	Mt. Bursey, Koerner Bluff	phono	ano (L)	nm-34 5193							**9.951 ± 0.060**	10		fresh lava
161	Mt. Bursey, Koerner Bluff	haw	gms (F)	nm-33 5145	9.73 ± 0.24	10.083 ± 0.075	287.7 ± 2.2	60.3	C-H	100	**9.99 ± 0.34**	C-H (SM)	90?	dense bomb interior
146	Mt. Moulton, Gawne	haw	gms (F)	nm-37 5402	2.20 ± 1.50	1.05 ± 0.18	296.6 ± 2.8	0.567	A-H	77.7	1.11 ± 0.15	A-H	77.7	bomb interior
	Nunatak		gms (F)	nm-33 5143	0.99 ± 0.79	1.07 ± 0.12	292.8 ± 2.0	1.38	A-I		0.99 ± 0.10	B-E (SM)	44.7	" "
									mean age (n=2)		**1.03 ± 0.14**			
318	Mt. Moulton, Prahl Crag	rhyo	ano (L)	nm-34 5227							**5.874 ± 0.046**	9		obsidian welded fall
345	Mt. Moulton, Edward's spur	phono	ano (L)	nm-34 5228							**3.98 ± 0.14**	10		platy lava
Mt. Flint														
WM 93 279	south rim	bas	gms (F)	nm-33 5157	9.28 ± 0.35	9.62 ± 0.06	289 ± 2.2	25.9	ALL	100	**9.55 ± 0.20**	B-F (SM)	66.4	stromb lava
281	south rim	bas	gms (F)	nm-33 5158	3.680 ± 0.200	3.740 ± 0.050	290.6 ± 3.4	1.81	B-H	100.0	**3.700 ± 0.063**	B-G	56.1	stromb.
284	lower cone	basn	gms (F)	nm-33 5159	9.52 ± 0.53	8.65 ± 0.26	293.4 ± 4.4	1.68	F-H	50.9	**8.55 ± 0.24**	F-H	50.9	lava
288	Reynolds Ridge	trach	ano (L)	nm-34 5194							**20.192 ± 0.096**	10		hypabbyssal lava
291	Reynolds Ridge	trach	ano (L)	nm-34 5195							**20.22 ± 0.12**	10		lava, 20-25% fsp
USAS Escarpment														
90-181	Mt. Aldaz	bsn	gms (F)	RD84 35	22.0 ± 2.7	**18.8 ± 1.4**	321.3 1.4	3.78	A-J	98.5	19.37 ± 0.53	B-F (SM)	66.4	stromb lava
MB7 0.1	Mt. Galla	bsn	gms (F)	RD84	30.70 ± 0.68	**26.06 ± 0.21**	335.9 ± 4.0	34.20	ALL	100.0	highly discordant	B-G	56.1	stromb lava

Note: I.D. refers to field sample number. Boxes around numbers indicate stratigraphic sequences. Samples in stratigraphic sequences are listed from youngest to oldest.

Rock Type determined by XRF (TAS classification after LeBas et al., 1986) in most cases, except those marked by astericks which are based on field estimates.

Rock type abbreviations: bas = basalt; ben = benmoreite; bsn = basanite; haw = hawaiite; mug = mugearite; phono = phonolite; ph-tph = phonotephrite; rhyo = rhyolite; trach = trachyte.

Sam = sample type, abbreviations include gms = groundmass, ano = anorthoclase, and plag = plagioclase. (meth) = heating method, (F) = furnace and ((L) = laser

Steps (meth) indicate sequence of furnace heating steps or number of laser fusion analyses included in mean age and (meth) indicate method of mean age calculation with: (N)= natural plateau (after Fleck et al. (1977); (SM) = selected mean age.

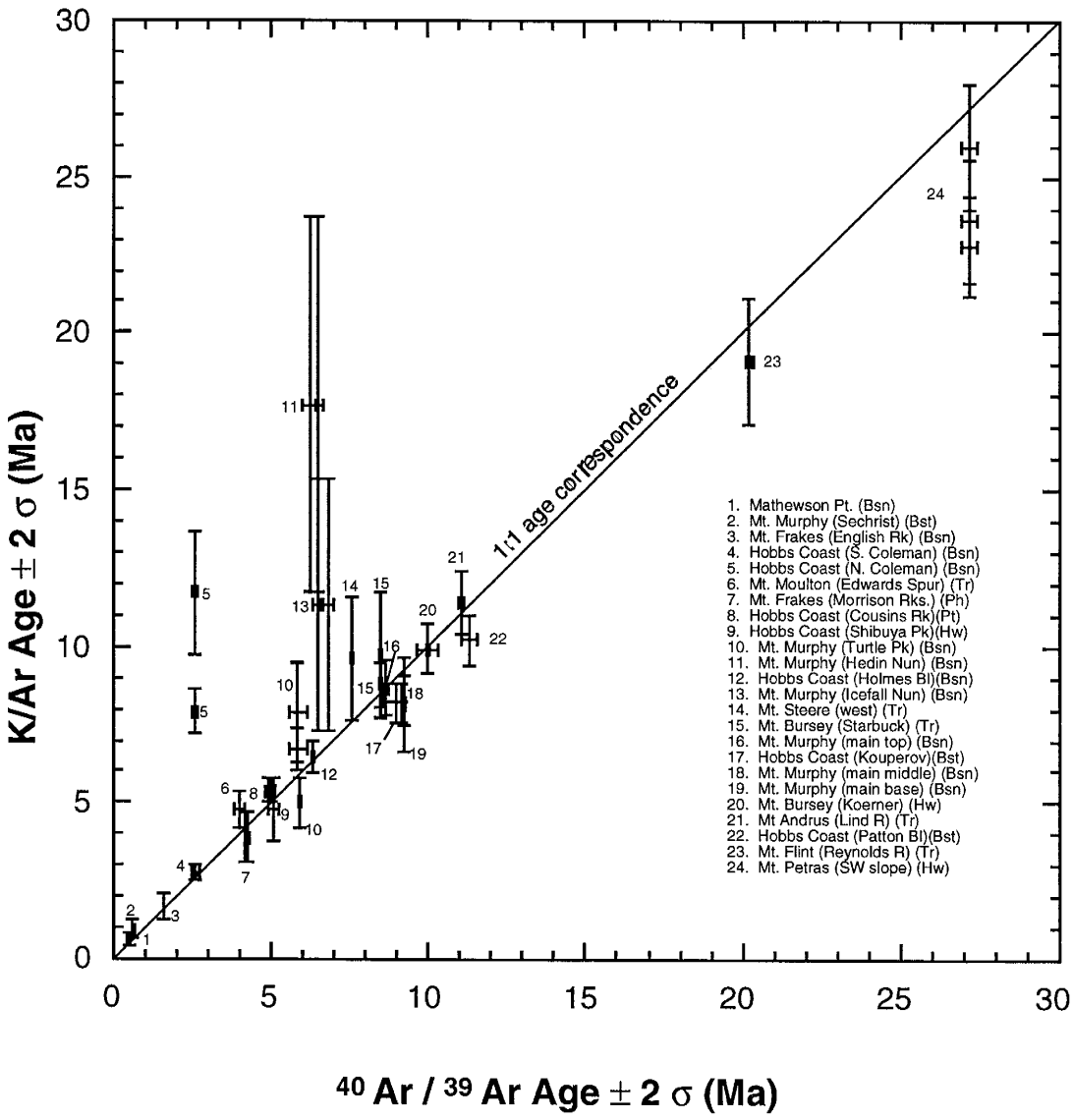

Figure 5. Plot of $^{40}Ar/^{39}Ar$ ages versus K/Ar ages of selected samples from the same outcrops, showing higher precision of $^{40}Ar/^{39}Ar$ results. Only sites with nearly concordant or concordant ages are included in this plot. The K/Ar ages are from LeMasurier and Rex (1983) and Hart et al. (1997), with reported uncertainties assumed to be ±1 σ. All of the ages were corrected for decay constants suggested by Steiger and Jaeger (1977). The ages from LeMasurier and Rex (1983) were corrected for decay constants suggested by Steiger and Jaeger (1977), according to method of Dalrymple (1979). Several of the ages from LeMasurier and Rex (1983) were cited by Hart et al. (1997), but 1977 decay constant values were not applied to these ages.

The improved precision of the $^{40}Ar/^{39}Ar$ geochronology over the previous K/Ar chronology is shown in Fig. 5. The most striking differences in levels of precision are between $^{40}Ar/^{39}Ar$ single-crystal laser-fusion ages and K/Ar ages of felsic samples from the same sites (those in Fig. 5): $^{40}Ar/^{39}Ar$ laser-fusion results yielded an average analytical precision of ±0.7%, whereas K/Ar results yielded an average analytical precision of ±16%. Levels of analytical precision of ages of mafic and intermediate groundmass samples also differ significantly: averaging ±3% for $^{40}Ar/^{39}Ar$ ages and ±14% for K/Ar ages. Apparent ages obtained by $^{40}Ar/^{39}Ar$ and K/Ar methods commonly differ by more than 1 m.y. but in most cases overlap at ±2 σ uncertainty level. In some cases, the ages differ by several million years, and do not overlap at 2 σ uncertainty.

Application of the furnace step-heating age-spectrum method, combined with high-precision ages from stratigraphically controlled sequences, make it possible to identify inaccurate ages. Approximately 10% of the analytical data, mostly from Crary Mountains samples, were rejected because the spectra were uninterpretable. Several glassy mafic and intermediate pillow-lava samples from stratigraphic sections at Mt. Steere and Mt. Rees in Crary Mountains yielded highly discordant age spectra with total-fusion ages that disagreed with stratigraphic order. In these sequences, high precision and reproducible single-crystal laser-fusion ages from analysis of intercalated felsic lavas or dikes provide stratigraphic control.

Significantly different $^{40}Ar/^{39}Ar$ and K/Ar chronologies of Coleman Nunatak, Hobbs Coast have implications for petrologic models as well as the glaciovolcanic history of MBL. A wide range of previous K/Ar ages, 11.7 to 2.5 Ma, was interpreted as an indication of long-lived volcanism at Coleman Nunatak (LeMasurier and Rex, 1983; Hart et al., 1997). Detailed sampling (n=12) and high precision $^{40}Ar/^{39}Ar$ ages suggest that the volcanism was monogenetic and occurred at 2.6 Ma. In a 75 m thick sequence of lavas and

tuffs at the south end of Coleman Nunatak, five samples from different stratigraphic levels yielded concordant $^{40}Ar/^{39}Ar$ ages of 2.56±0.08 Ma. Three glassy pyroclastic bomb and block samples collected from tuff units between 2.56 Ma lava flows yielded much older ages that were rejected because the age spectra are discordant and violate stratigraphic order. Two samples from the lava and tuff sequence were previously dated by the K/Ar method, which yielded much older ages of 11.7±2.0 Ma and 7.90±0.72 Ma (Hart et al., 1997). Eruption of the 2.56 Ma lava and tuff sequence was apparently coeval with eruption of a tuff cone sequence at the north end of Coleman Nunatak, $^{40}Ar/^{39}Ar$-dated to 2.60±0.12 Ma (n=4). K/Ar ages from the north end of Coleman Nunatak range from 2.5 to 3.2 Ma (LeMasurier and Rex, 1983; Hart et al., 1997) and overlap the $^{40}Ar/^{39}Ar$ ages of that site. Hart et al. (1997) developed a complicated petrologic model to explain the lack of chemical and isotopic changes at Coleman Nunatak over such a long K/Ar time interval (8 Ma). The $^{40}Ar/^{39}Ar$ ages combined with the geochemical data of Hart et al. (1997) suggest that Coleman Nunatak is a chemically homogeneous, monogenetic volcano.

Dating results from satellite nunataks just west of Mt. Murphy provide additional examples of significant differences between $^{40}Ar/^{39}Ar$ and K/Ar ages. Initial K/Ar dating of Turtle Peak resulted in apparent ages ranging from middle Eocene to middle Miocene (LeMasurier, 1972b; LeMasurier and Rex, 1982). More recent K/Ar ages of Turtle Peak are 6.70±0.64 Ma and 7.9±1.6 Ma for rocks from the base of the section and 9.8±3.0 Ma for rocks situated 100 m above the base (LeMasurier et al., 1994). In contrast, the $^{40}Ar/^{39}Ar$ ages of Turtle Peak are significantly younger and more consistent with stratigraphy: 5.95±0.60 Ma for the basal section, 5.65±0.23 Ma for the middle section, and 4.70±0.15 Ma for uppermost section. K/Ar ages of Hedin Nunatak and Icefall Nunatak are 17.7±6.0 Ma and 11.3±4.0 Ma, respectively, whereas $^{40}Ar/^{39}Ar$ ages are much younger at 6.50±0.12 and 6.20±0.24 Ma for Hedin Nunatak and 6.80±0.10 Ma and 6.52±0.08 for Icefall Nunatak. K/Ar dating of these nunataks has been difficult due to low radiogenic yields and secondary alteration (LeMasurier et al., 1994). Both of these

problems are common in glassy basaltic rocks. In fact, additional samples from the satellite nunataks of Mt. Murphy were analyzed by the $^{40}Ar/^{39}Ar$ dating method but yielded highly discordant, uninterpretable age spectra with much older total fusion ages; these results were rejected.

Finally, the $^{40}Ar/^{39}Ar$ method can be used to date very young rocks (100-10 ka), thus permitting establishing chronologies through the critical Wisconsinan glacial cycle. High precision dating of anorthoclase samples was discussed extensively in Part A of dissertation. Very young ages (104±28 ka to 7 ±13 ka) were obtained by $^{40}Ar/^{39}Ar$ analysis of groundmass samples from Mt. Frakes and Mt. Takahe. The level of precision is variable for young groundmass samples (ranging from ±7 to ±29 ka) and appears to be, in part, a function of analytical blank stability. Analytical blanks are measured between every four sample analyses (on average) and are subtracted from sample measurements. Unstable blanks during sample analyses can have profound effects on the calculated samples ages, easily changing it by several thousands of years. High blanks are common in analyses of glassy rocks and it appears that the blank signals may be driven up by water that is released from glass during heating. Despite these caveats, fairly high levels of precision and reproducibility were obtained from several samples, including two separate analyses of a basanite groundmass sample from the base of Mt. Frakes, which yielded plateau ages of 32 ±10 ka and 35 ±10 ka.

More consistent age results were obtained by $^{40}Ar/^{39}Ar$ dating of groundmass samples from older Pleistocene rocks. Early to late Pleistocene ages (100 ka to 1 Ma) were obtained by analysis of groundmass samples from Mt. Berlin, Mt. Frakes, Mt. Murphy, Mt. Siple, Mt. Takahe, and Shepard Island. As an example, two groundmass samples from Sechrist Peak at Mt. Murphy yielded ages of 587±43 ka and 592±40 ka (Table 1). The K/Ar age of this site is 940±280 ka, which lies outside of ±2 σ uncertainty of the $^{40}Ar/^{39}Ar$ ages (LeMasurier et al., 1994). In general, the $^{40}Ar/^{39}Ar$ ages of recent

volcanism differ significantly from previous K/Ar ages of the same sites and offer a more refined and reliable chronology of middle to late Pleistocene eruptions in MBL.

Marie Byrd Land Volcanic Lithofacies

Lithofacies features were evaluated in outcrops, hand-samples and thin-sections. Definitions of volcanic and lithofacies terminology generally follow suggestions by Fisher and Schmincke (1984) and McPhie et al. (1993). The previous broad usage of the term hyaloclastite (e.g., LeMasurier, 1972a, 1972b), is refined and the terms hyalotuff and hyaloclastite are used instead. Hyalotuffs and hyaloclastites are differentiated based on grain morphometry, following recommendations by Honnerez and Kirst (1975) and Skilling (1994) and Smellie and Skilling (1994). Hyaloclastites are characterized by angular, blocky, poorly vesiculated vitriclasts that commonly exhibit a jigsaw-fit arrangement and hyalotuffs are characterized by highly vesiculated vitriclasts with broken vesicle walls (Skilling, 1994; Smellie and Skilling, 1994). In this study hyalotuffs and hyaloclastites are differentiated based on estimated clast vesicularity (hyaloclastite <25%; hyalotuff>25%), following Skilling (1994). No particular fragmentation method is implied by the two terms, although empirical observations suggest that hyaloclastites are typically formed by cooling-contraction granulation processes (sensu Kokelaar, 1986), and hyalotuffs by explosive hydromagmatic interactions. The MBL lithofacies are subdivided into four classes: coherent lavas, autoclastic deposits, pyroclastic deposits, and sedimentary deposits.

Coherent lava is the most common lithofacies of MBL volcanoes. MBL lavas include a wide range of alkaline to peralkaline compositions from basanite to trachyte and phonolite, and rare rhyolites. For this study, coherent lava lithofacies are subdivided into dominant "dry" and subordinate "wet" end-members, based on presence or absence of features characteristic of interactions with water. The "dry" lava lithofacies includes lavas with reddened, brecciated bases and pahoehoe tops that are interpreted to result from

subaerial lava effusion, without recognizable water interaction. Many inferred subaerial lavas appear to be clastogenic, i.e. derived from agglutinated pyroclastic spatter. Two "wet" lava lithofacies, pillow lava and hackly, jointed lava, are interpreted as water-cooled and generally associated with underwater depositional environments (see e.g. Fuller, 1933 Moore, 1975; Tribble, 1991, Walker, 1992). Two variations of pillow lava lithofacies are recognized: compound pillowed flows that form either nested sets with minor interpillow hyaloclastite breccia, and distinct lobes with abundant (>10%) interpillow hyaloclastite breccia. Pillow lavas are common at the Crary Mountains, Mt. Murphy, and Mt. Takahe, but are very rare elsewhere in Marie Byrd Land. The hackly, jointed lava lithofacies includes slightly glassy, compound and simple flows and intrusive bodies, with irregular to hackly jointing and rare crude pillow structures. Some of these jointed lavas resemble "para-pillows" of Icelandic flow-foot delta sequences (Jones, 1970), which Walker (1992) suggested form when thin, subaqueous lavas flow too fast down steep underwater slopes to develop pillow (or tube) structures or are cut off from their sources. We interpret these jointed lavas and intrusive rocks as water-cooled (Skilling, 1994), although a subaqueous origin cannot be inferred in all cases . In rare cases, lava apophyses locally deform bedding and exhibit hackly jointing. These apophyses are interpreted as dikes or incursive flows that intruded wet volcaniclastic sediments. Many lavas, particularly felsic lavas, lack diagnostic features of subaerial or subaqueous environments. Unless these lavas are be associated with other subaqueous deposits, they have been tentatively interpreted as subaerial lavas.

Autoclastic deposits are formed by mechanical granulation while lava flows. Like coherent lavas, autoclastic deposits of MBL are subdivided into two end-member categories: dry, subaerial lava-flow breccias and wet, hyaloclastite breccias. Both types of breccia deposits are easily identified by their close association with coherent lava facies. Subaerial lava-flow breccias are ubiquitous in MBL and are recognized by welding textures and reddening caused by deuteric oxidation. Exposures of hyaloclastite breccias are much

less common in MBL and are recognized by blocky, curviplanar, quenched vitriclasts, and association with pillow lavas. In MBL, many autoclastic deposits exhibit characteristics between these dry and wet end members and must be evaluated in relation to local stratigraphy to determine the depositional environment.

Hyaloclastite breccias are not strictly autoclastic deposits because they are formed wholly or in part by a process called cooling-contraction granulation when water comes in contact with lava (Carlisle, 1963; Kokelaar, 1986). Several MBL hyaloclastite breccias are well stratified, suggesting they were locally redeposited on underwater slopes by sediment gravity flow or fluvial processes. In some cases, it appears that the hyaloclastites and parent pillow lavas were moving down slope together and pillow lobes or fingers were injected up into the hyaloclastite breccia (see similar example by Bergh and Sigvaldason, 1991) .

Pyroclastic deposits are also common in MBL sequences and are dominated by two types: pyroclastic-fall and base-surge deposits. Pyroclastic-fall deposits are products of magmatic and hydromagmatic explosions and typically form crudely to well-stratified deposits that mantle topography. A magmatic origin is inferred where pyroclasts are well-sorted and exhibit uniform, moderate to high vesicularity and angular to fluidal shapes. Reddening by deuteric oxidation and welding are common features and are interpreted as indications of close proximity to a subaerial vent (Walker and Croasdale, 1973). A hydromagmatic origin is inferred by relatively poor sorting, fine grain sizes, variable vesicularity, armored lapilli, predominance of sideromelane glass (in basalts), and blocky forms (Wohletz, 1983, Fisher and Schmincke, 1984). In MBL, base-surge deposits were previously unrecognized in late-stage flank deposits and in smaller monogenetic volcanoes. The MBL base-surge deposits were identified by comparison to base-surge deposits described elsewhere (e.g. Fisher and Schmincke, 1984) and typically form moderate to poorly sorted, planar, cross-stratified, or massive beds that thicken and thin laterally. Individual clasts in base-surge deposits resemble those in hydromagmatic-fall deposits,

except that they are often much more rounded due to turbulent lateral transport. Both base surge and hydromagmatic-fall deposits in MBL consist mostly of hyalotuffs. These hyalotuffs commonly include signs of wet, hydromagmatic origin, such as armored (i.e. ash-coated) lapilli and bedding plane sags caused by ballistic impacts. Surge and fall deposits are commonly interbedded. In western and central MBL, many fall and surge deposits contain clasts that exhibit a continuum of characteristics from hydromagmatic explosivity (blocky shapes, a wide range of vesicularity) to magmatic explosivity (fluidal to cuspate shapes, high vesicularity).

Sedimentary deposits are rare in MBL and include deposits formed by glacial, mass-flow, and fluvial processes. Sedimentary deposits are characterized by their heterogeneous rock types, subrounded clast shapes, sedimentary structures, and stratigraphic context. Despite the intraglacial setting of the MBL volcanic province, interbedded glacial tills/tillites and glacial-erosional unconformities are rare.

Paleoenvironmental Reconstructions: Polygenetic Volcanoes

There are nineteen large polygenetic volcanoes in MBL including, thirteen in western and central MBL (Fig 3) and six in eastern MBL (Fig. 4). $^{40}Ar/^{39}Ar$ ages of the polygenetic volcanoes range from 20.20±0.08 Ma (±2 s.d. uncertainty) at Mt. Flint (Table 1) to 8.5±3.4 ka at Mt. Takahe (see Part A, dissertation). Mt. Berlin is an active volcano, with several steaming fumarolic ice towers on the periphery of the summit caldera. Most of the polygenetic volcanoes are poorly exposed due to snow and ice cover and lack of dissection. The degree of dissection does not appear to be controlled by the age of volcanoes: middle to late Miocene volcanoes in the Ames and Flood Ranges are undissected, whereas Mt. Murphy and Mt. Steere, late Miocene volcanoes in eastern MBL, are deeply eroded. Dissection at Mt. Murphy and Mt. Steere is expressed in deep cirques and wide valleys that probably resulted from localized headward erosion rather than by ice-sheet overriding.

Polygenetic volcanoes located in western and central MBL are poorly exposed but generally suggest that syn-eruptive ice levels were not much higher than ice levels of today (Fig. 3). The rare exposures are dominated by felsic lavas and welded pyroclastic deposits. An extreme example of the lack of exposure is Mt. Moulton in the Flood Range, a 35 km x 15 km volcano with 1500 m vertical relief above the ice-sheet surface but only two small outcrops. An exception is Mt. Sidley in the Executive Committee Range, where mostly felsic lava and pyroclastic rocks are well exposed in the 6-km-diameter caldera amphitheater (Panter et al., 1994). Evidence for glaciovolcanic interactions is recognized at only two central MBL volcanoes, Mt. Siple and Mt. Sidley. Mt. Siple, a nearshore island volcano with a summit caldera elevation of 3110 m a.s.l., is isolated from the WAIS by floating ice shelves (Figs. 1,3). Hydrovolcanic tuff deposits cropping out at low elevations on the northern, seaward flanks are interpreted as products of magma interaction with local slope ice, although magma-seawater interactions of deposits at the sea shore cannot be precluded (e.g. Fig. 2e). Mt. Sidley, the highest volcano in MBL at 4181 m a.s.l. is located at the inland ice divide (Figs. 1,3). Mixed hyaloclastite and epiclastic deposits exposed in the caldera wall were interpreted to result from "limited glaciovolcanic interaction" ca. 5.5 Ma (Panter et al., 1994) that likely occurred in the ice-filled caldera and above the level of the WAIS (Panter, pers. comm.).

In contrast to the limited record from western and central MBL polygenetic volcanoes, the six large polygenetic volcanoes of eastern MBL contain abundant evidence for glaciovolcanic interactions and changing ice levels (Fig. 4). Mt. Murphy, Mt. Rees, and Mt. Steere all exhibit evidence for fluctuating ice levels in the late Miocene. Mt. Murphy also shows signs of changing ice levels in the Pliocene and Pleistocene. Lower flank volcanic deposits at Mt. Takahe, an undissected late Pleistocene shield volcano, provide a record of changing ice level during Wisconsinan time. late Wisconsinan subaerial volcanic deposits near the level of the WAIS at Mt. Frakes, an undissected Plio-Pleistocene shield volcano in the Crary Mountains, afford upper limits on ice expansion

during the last glacial maximum. All six of the polygenetic volcanoes in eastern MBL expose felsic rocks on their upper flanks.

Four of the eastern MBL volcanoes, Mt. Murphy, Mt. Takahe, Mt. Rees and Mt. Steere, exhibit a wide diversity of lithofacies and stratigraphic relationships that exemplify key elements of the conceptual model of glaciovolcanism (Fig. 2). The complexity at these volcanoes is attributed to their geographic positions on the ice sheet and as well as their long eruptive histories during periods of fluctuating regional and local ice. Detailed descriptions (below) of glaciovolcanic sequences along a transect from Mt. Murphy (at coast), through Mt. Takahe (150 km inland from coast), to the Crary Mountains (Mt. Rees, Mt. Steere, and Mt. Frakes; 250 km inland from coast) illustrate important differences in character of volcanic deposits and nature of ice level changes at inland versus coastal sites on the ice sheet.

Mt. Murphy. Mt. Murphy is a complex polygenetic coastal volcano with the most extensive glaciovolcanic record of all volcanoes in MBL (Fig. 6). Because of its location, Mt. Murphy forms both an obstruction to ice flow (Fig. 2b) and can be considered a large interfluve volcano (Fig. 2e). The inland ice level is at ~800 m a.s.l. and the coastal ice level is at ~200 m a.s.l. The ice sheet drains around Mt. Murphy through the Pope and Haynes Glaciers. The most extensive rock exposures and evidence for glaciovolcanic interactions at Mt. Murphy are on the western flanks and in satellite nunataks that stand out as interfluves in the Pope Glacier. LeMasurier et al. (1994) used volcanic sequences at the lower southwest flank of the Mt. Murphy shield, at Sechrist Peak and at three satellite nunataks as evidence for higher paleo-ice-levels during Miocene to Pleistocene times. We dated 14 samples from these sequences by the $^{40}Ar/^{39}Ar$ method and offer a significantly revised chronology of inferred higher ice levels compared to the previous K/Ar chronology of LeMasurier et al. (1994).

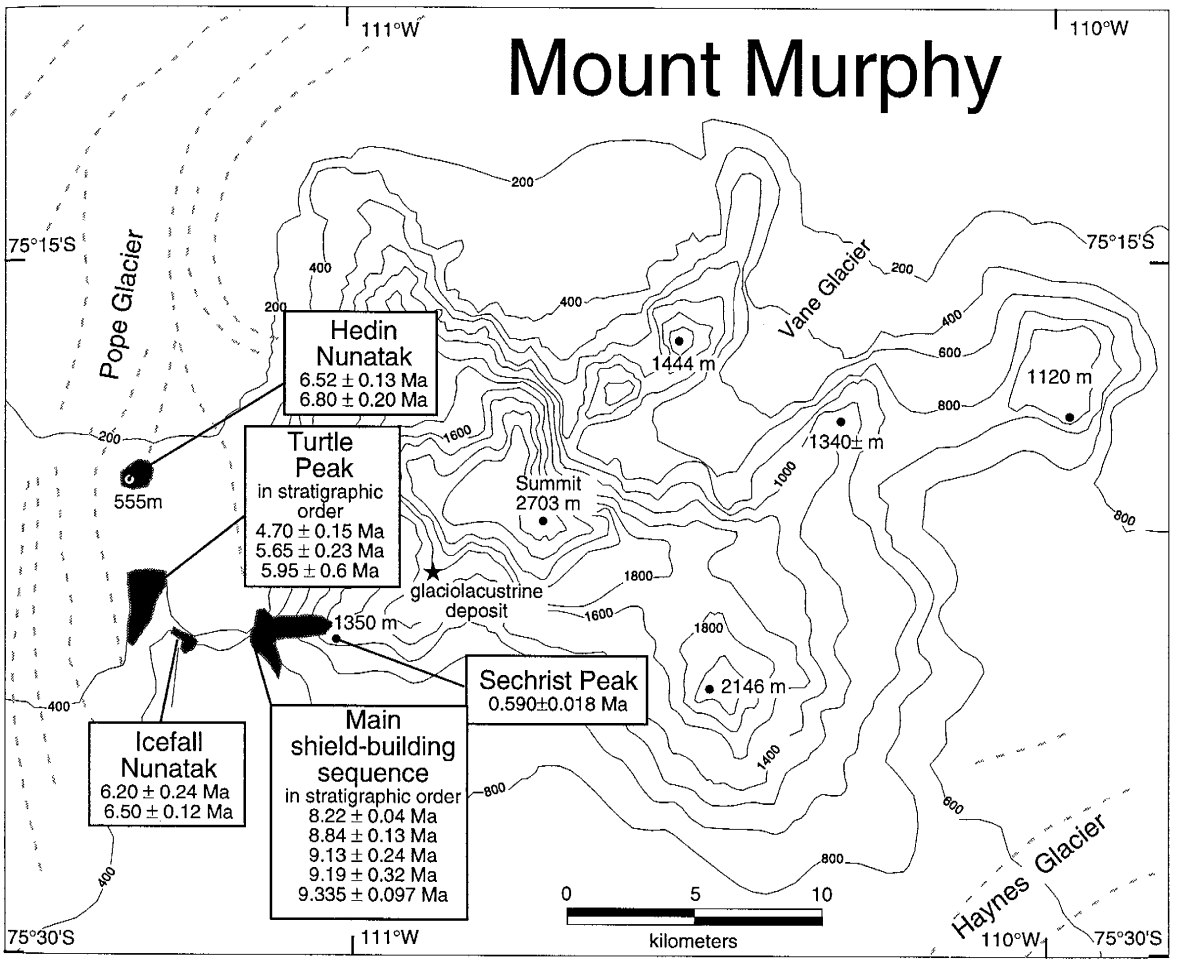

Figure 6. Topographic map of Mt. Murphy volcano showing rock exposures described by LeMasurier et al. (1994) and new $^{40}Ar/^{39}Ar$ dates. Ice flow around Mt. Murphy is quite complex. Base map is the Mount Murphy quadrangle (1972), scale 1:250,000 USGS Reconnaissance Series, Antarctica, U.S. Geological Survey.

A stratigraphic section at the base of the main shield of Mt. Murphy exemplifies the complex interactions between growing polygenetic volcanoes and an active ice sheet. The section consists of late Miocene pillow lava and hyaloclastite breccia with intercalated palagonitized Strombolian tuff up to 300 m above present ice level (LeMasurier et al.,

1994). The alternation between pillow lava and Strombolian tuff was interpreted to represent rapid ice-level variations in the late Miocene, with ice high stands up to 300 m above today's ice level (LeMasurier et al., 1994). A 5 m thick striated-clast-bearing heterolithic tillite is sandwiched between overlying pillow and hyaloclastite deposits and underlying striated basalt lava near the base of the volcano (LeMasurier et al., 1994). Additional striated lava surfaces and tillites are exposed in the middle and upper sections of the sequence (McIntosh et al., 1991). Three K/Ar ages reported from this sequence violate stratigraphic order but have large overlapping uncertainties (LeMasurier et al., 1994). New $^{40}Ar/^{39}Ar$ ages of this sequence are generally consistent with stratigraphy and suggest that the alternations between subaqeuous and subaerial eruptions occurred mostly between 9.34 and 8.84 Ma (Table 1, Fig. 6).

Pleistocene-aged mixed hydrovolcanic and strombolian deposits, situated at 1200 m above sea level m at Sechrist Peak, were interpreted as products of emergent tuff cone eruptions at 940±280 ka (LeMasurier et al., 1994). The emergent eruptions were attributed to interaction between magma and an expanded WAIS at 0.94 Ma and imply that ice sheet was 600 m above its present level at that time. Two $^{40}Ar/^{39}Ar$ ages are significantly younger and more precise than the K/Ar age and pinpoint the ice-sheet high-stand at 590 ± 15 ka.

Three "interfluve" nunataks located just west of Mt. Murphy (Icefall Nunatak, Hedin Nunatak, and Turtle Peak) are composed, in part, of pillow lava and hyaloclastite breccia, suggesting higher syn-eruptive local relative ice levels (McIntosh et al., 1991; LeMasurier et al., 1994). These nunatak have been re-dated by the $^{40}Ar/^{39}Ar$ method to latest Miocene-Pliocene (6.80-4.70 Ma), as was discussed in $^{40}Ar/^{39}Ar$ Geochronology Results section. LeMasurier et al. (1994) described these sequences as table-mountain remnants; McIntosh et al. (1991) interpreted these sequences as multi-story table-mountain sequences that exhibit multiple passage zones at 250 m to 400 m above present local ice level. The elevations of the uppermost passage zones appear to be consistent with the

present level of the regional ice sheet. However, uncertainties associated with the coastal interfluve setting preclude establishing absolute WAIS paleo-ice-level elevations. These uncertainties include the timing of volcanism relative to erosion on interfluves and the effects of changes in sea level on local ice levels. The satellite nunataks are conservatively re-interpreted as indications of the presence of an active late Miocene ice-sheet, without specific implications for paleo-ice-levels.

In addition to the glaciovolcanic records of ice levels, a small outcrop of laminated conglomeratic mudstone perched on the flanks at 1000 meters above the volcano base has been interpreted as a glaciolacustrine deposit formed at a time of very high ice-sheet levels (LeMasurier et al. 1994). The deposit contains a mixed age (24 and 3.5 Ma) assemblage of recycled microfossils including fragmented marine diatoms, silicoflagellates and radiolaria (LeMasurier et al. 1994). The microfossils were interpreted as originating in open marine basins of West Antarctica during ice-free intervals and being glacially transported by the WAIS during later ice sheet expansions (LeMasurier et al. 1994). LeMasurier et al. (1994) assigned a minimum age for the deposit of late Pliocene, the age of the youngest recycled marine diatoms, recovered from the mudstone. One interpretation of the biostratigraphic ages of the marine microfossils that they date several ice-free intervals in West Antarctica and cyclic glaciation and deglaciation through the Neogene (LeMasurier et al., 1994). We prefer an alternative interpretation: that the microfossils are windblown, without implications for the age of the deposit or the deglaciation of West Antarctica. A windblown origin has been demonstrated for similar microfossil assemblages elsewhere in Antarctica (Kellogg and Kellogg, 1996; Burckle, 1996; Stroeven and Prentice, 1997).

Mt. Takahe. Mt. Takahe is an undissected shield volcano with an 8 km diameter ice-filled summit caldera located in eastern MBL, approximately 150 km from the coast (Fig. 1, 7). Mt. Takahe exemplifies a polygenetic volcano that does not produce an ice-damming effect (Fig. 2c). Rock exposures at Mt. Takahe are extremely limited (<1% of

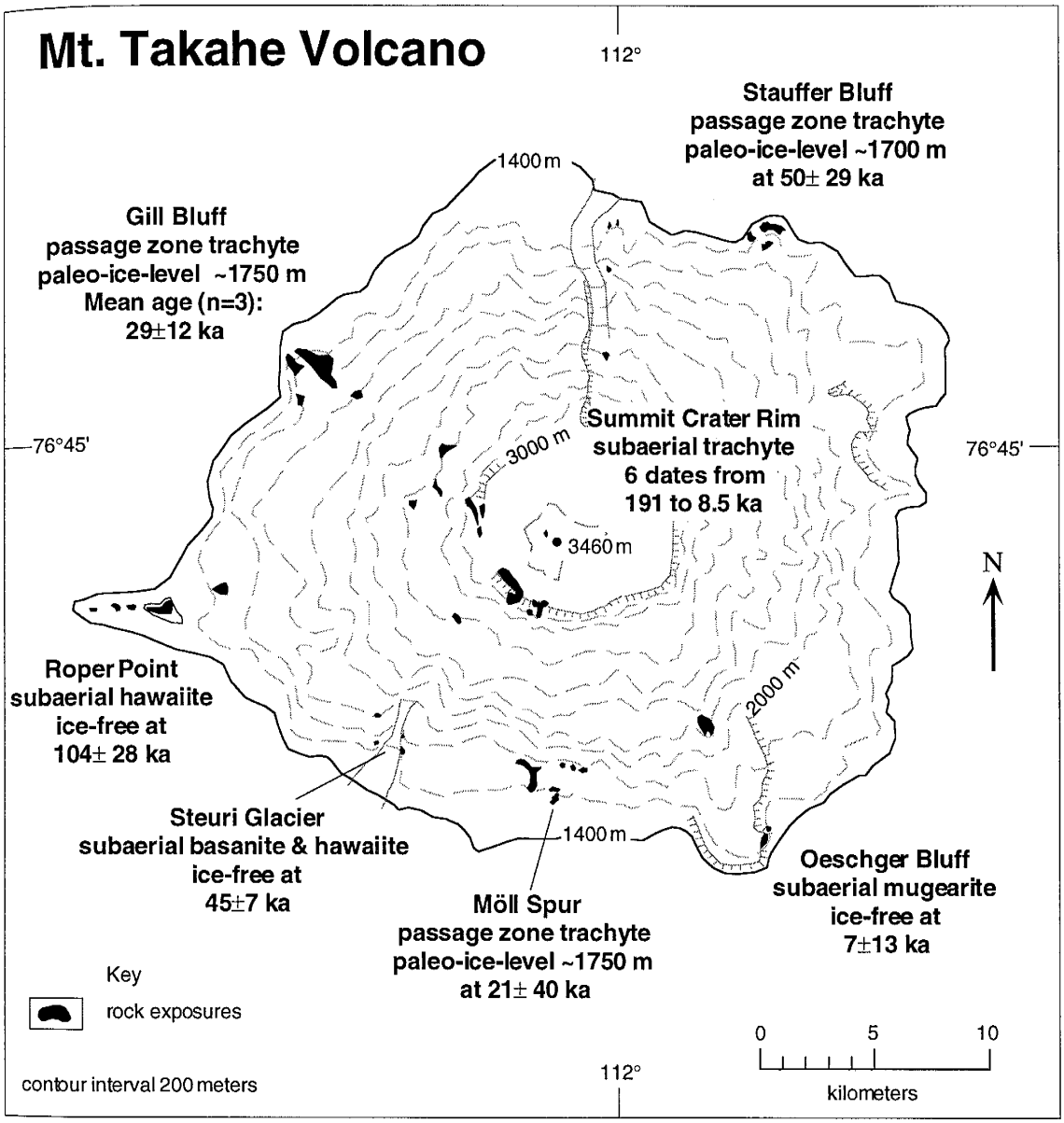

Figure 7. Outcrop map of Mt. Takahe volcano showing limited rock exposures, moraines, and preliminary $^{40}Ar/^{39}Ar$ dates. The $^{40}Ar/^{39}Ar$ ages from the summit crater deposits are included in Wilch et al. (Part A, dissertation). The $^{40}Ar/^{39}Ar$ ages of the lower flank outcrops are preliminary and based on analyses of bulk groundmass samples at the New Mexico Geochronological Research Laboratory; dating of mineral separates from these rocks will improve the age precision. and resolution of eruptive history. Passage zones at Gill Bluff, Moll Spur, and Stauffer Bluff mark transitions from subglacial to subaerial eruptive environments. Paleo-ice-levels, eruptive environments, and moraine locations from Palais et al. (1988); rock types from McIntosh et al. (1985), Palais et al. (1988), and LeMasurier and Rex, (1990). Previous K-Ar ages of same outcrops all <100,000 years except Stauffer Bluff, which was dated to 310,000±90,000 years (LeMasurier and Rex, 1990). Base map is the Mount Takahe quadrangle (1972), scale 1:250,000 USGS Reconnaissance Series, Antarctica, U.S. Geological Survey.

exposed volcano) and consist of a 60 m thick stratigraphic section on the caldera rim and nine outcrops on the lower flanks, situated as high as 400 m above present ice level (Fig. 7 Map). Rocks from several locations were previously dated to <100 ka by the conventional K-Ar method (LeMasurier and Rex, 1990) but have been re-dated by the $^{40}Ar/^{39}Ar$ method to between 191 and 7 ka. The caldera rim chronology, with $^{40}Ar/^{39}Ar$ ages extending to 191.2±5.3 ka, suggests that Mt. Takahe volcano had reached its present elevation by 191 ka (Part A of dissertation). The lower flank deposits represent late stage shield-building flank eruptions and parasitic vent eruptions and therefore provide ideal sites for paleo-ice-level "dipstick" measurements (Fig. 2c).

Three trachytic subglacial to subaerial volcanic passage zone sequences are situated about 300 to 400 m above the present ice sheet level at Stauffer Bluff, Gill Bluff and Möll Spur (Fig. 7)(McIntosh et al., 1985). The inferred subglacial deposits consist of pillow lava and hyaloclastite breccia that form flow-foot delta sequences (McIntosh et al., 1985). Above the passage zones, subaerial deposits consist of reddened lavas at Gill Bluff and Moll Spur and hydrovolcanic tuff at Stauffer Bluff. Groundmass trachyte samples from these outcrops yield $^{40}Ar/^{39}Ar$ ages ranging from 21±40 ka to 50±29 ka. Three samples from Gill Bluff provide the most precise ages (34±18 ka; 28± 14 ka; 22±26 ka), with a weighted mean of 29± 12 ka. Future $^{40}Ar/^{39}Ar$ dating efforts will focus on separating anorthoclase from these samples in order to improve the level of precision. The implication of the field and $^{40}Ar/^{39}Ar$ age data is that at one or more times since ~80 ka ice levels at Mt. Takahe were 300-400 m higher than they are at present.

All other outcrops on the lower flanks consist of basanite to trachyte lava flows and pyroclastic tuffs erupted under subaerial conditions (McIntosh et al., 1985). $^{40}Ar/^{39}Ar$ analyses of bulk groundmass samples from three outcrops yielded ages of 104 ± 28 ka, 45± 7 ka, and 7 ± 13 ka. The 104 ka at Roper Point rocks crop out down to the level of the ice sheet, whereas the 45 ka rocks at Steuri Glacier and 7 ka rocks at Oeschger Bluff are situated ~ 200 m and ~100 m above the ice sheet level, respectively (Fig. 7). These age

and elevation data of subaerially erupted rocks provide upper elevation limits on syn-eruptive ice levels.

The ages of the Gill Bluff passage zone suggests that at least one significant ice-sheet high-stand occurred in the late Wisconsin. The duration of the late Wisconsinan high stand is limited to between 45 ±7 ka and 7±13 ka, the ages of the lower elevation subaerial deposits at Steuri Glacier and Oeschger Bluff. The relatively low-precision age of Stauffer Bluff 50±29 ka does not permit determining whether the passage zone at that site represents a distinct earlier glaciation.

Crary Mountains: Mt. Rees, Mt. Steere and Mt. Frakes. The Crary Mountains consist primarily of three large coalesced volcanoes, aligned from NNW to SSE: Mt. Rees, Mt. Steere, and Mt. Frakes (Fig. 8). Southeast of these main volcanoes is Boyd Ridge, an east-west oriented, lower relief ridge with very limited rock exposures. The degree of dissection of the volcanoes increases to the north, with deep cirques cut into the east side of Mt. Steere and Mt. Rees. On the basis of reconnaissance field work and four K/Ar ages, the Crary Mountains were characterized as late Miocene to early Pliocene shield volcanoes composed of bimodal alkaline lava and hyaloclastite (LeMasurier and Thomson, 1990). Detailed field work combined with $^{40}Ar/^{39}Ar$ dating of 62 samples provides a more comprehensive record of volcanism in the Crary Mountains (Table 1, Fig. 8).

Mt. Rees is an elongate, eroded late Miocene (mostly 9-8 Ma) polygenetic volcano with a summit elevation of 2709 m (Fig. 8.). Thick stratigraphic sequences at Trabucco Cliff (Fig. 8,9a and 9b) and Tasch Peak (Fig. 10) consist mostly of mafic to intermediate volcanic rocks with subordinate interlayered felsic lavas. The mafic to intermediate rock outcrops are characterized by two alternating lithofacies: 1) unbrecciated lavas with oxidized bases and, 2) palagonitized glassy

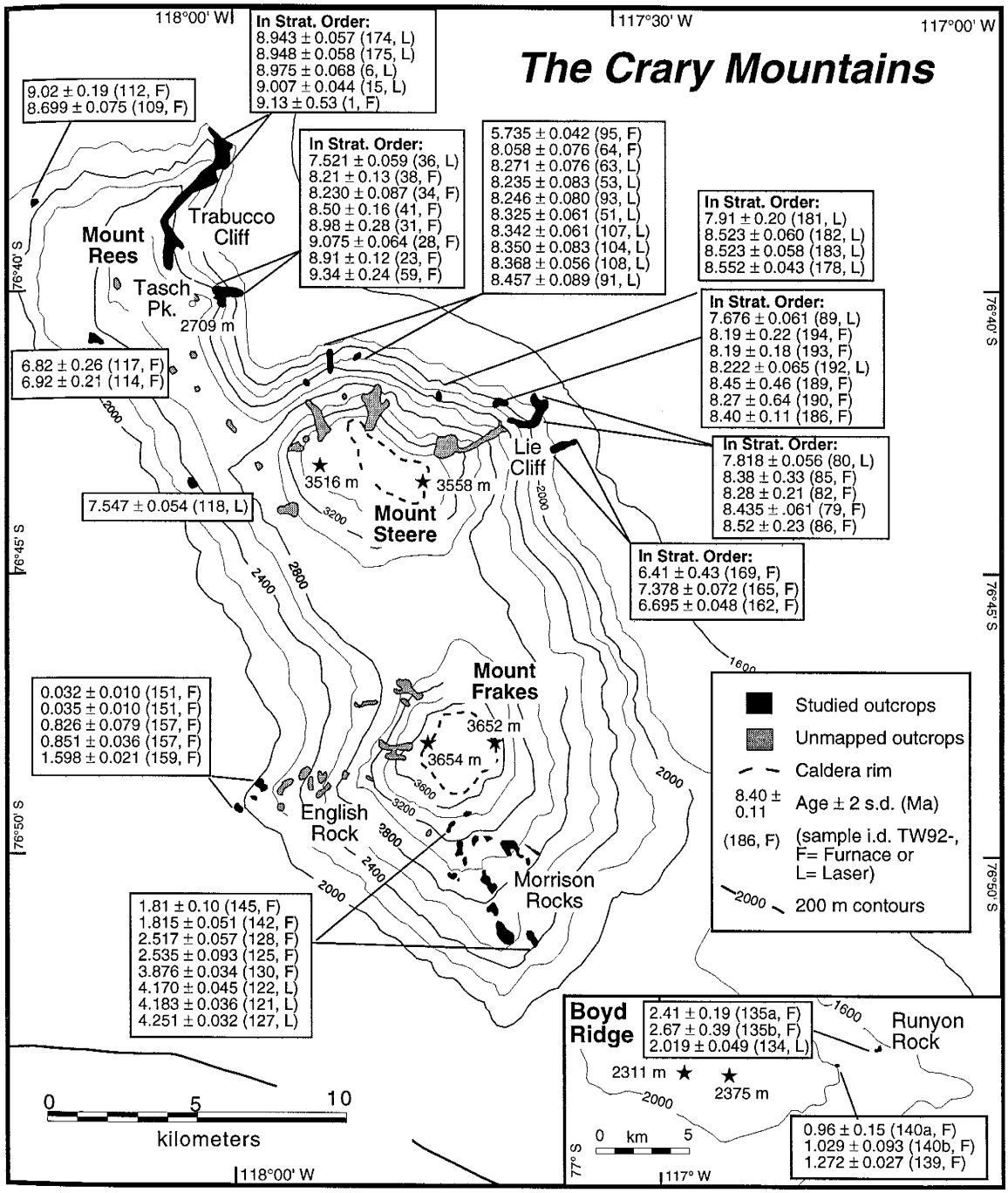

Figure 8. Sketch map and $^{40}Ar/^{39}Ar$ chronology of Crary Mountains. $^{40}Ar/^{39}Ar$ ages at Mt. Rees and at Lie Cliff area of Mt. Steere are from alternating lithofacies sequences and are in stratigraphic order. $^{40}Ar/^{39}Ar$ ages at other Mt. Steere sites and at Mt. Frakes and Boyd Ridge are from isolated outcrops and are listed from youngest to oldest. Base map is the Crary Mountains quadrangle (1973), scale 1:250,000 U.S.G.S. Reconnaissance Series, Antarctica, United States Geological Survey. Stars indicate elevation localities from U.S.G.S. base map.

hyaloclastite breccias and pillow lavas. In places, oxidized clastogenic lava comprises the dry lithofacies. The $^{40}Ar/^{39}Ar$ ages at several levels in the Trabucco Cliff sequence agree with stratigraphic order (from 9.13±0.53 to 8.94±0.06 Ma) but are analytically indistinguishable from one another (Fig. 9a.). A short interval of eruptions is consistent with the lack of unconformities in the sections. No tillites or glacially striated surfaces (typically associated with wet-based glaciations) were observed within the subglacial volcanic sequences. At Tasch Peak ridge, the $^{40}Ar/^{39}Ar$ ages from several levels are mostly in stratigraphic order and range from 9.34±0.24 to 8.21±0.13 Ma. The mostly intermediate to mafic, alternating lavas and hyaloclastite breccias are cut by a trachytic dike, dated to 7.52±0.06 Ma. The alternating "wet" and "dry" lithofacies sequences at Trabucco Cliff and Tasch Peak ridge are inferred to represent fluctuations between subaerial and subglacial depositional environments.

Mt. Steere is a late Miocene (9-6 Ma) polygenetic volcano with an intact summit caldera at 3558 meters above sea level. Mt. Steere is deeply dissected by cirques, which expose felsic flow-banded lavas and breccias, cut by numerous felsic to mafic dikes on the north and northeast sides and basanite lavas and breccias with subordinate trachyte lava on the east side at Lie Cliff. Samples, all obtained from the lowest 800 m of the volcano, yielded $^{40}Ar/^{39}Ar$ ages from 8.55±0.04 Ma to 5.74± 0.04 Ma. Lie Cliff and adjacent ridge exposures to the north and south contain basal Mt. Steere exposures, which are dominated by basanite deposits near the base and trachytic lavas near the top. Basanite rocks at Lie Cliff and adjacent ridge outcrops resemble the glaciovolcanic sequences at Mt. Rees, with alternating "wet" and "dry" lithofacies and no syn-eruptive tillites or striated surfaces. The volcanic sequences in Lie Cliff and an adjacent ridge to the north were erupted over a short interval, with eruptions that cannot be differentiated by $^{40}Ar/^{39}Ar$ dating, with overlapping ages ranging from 8.52±0.23 Ma to 8.19± 0.18 Ma.

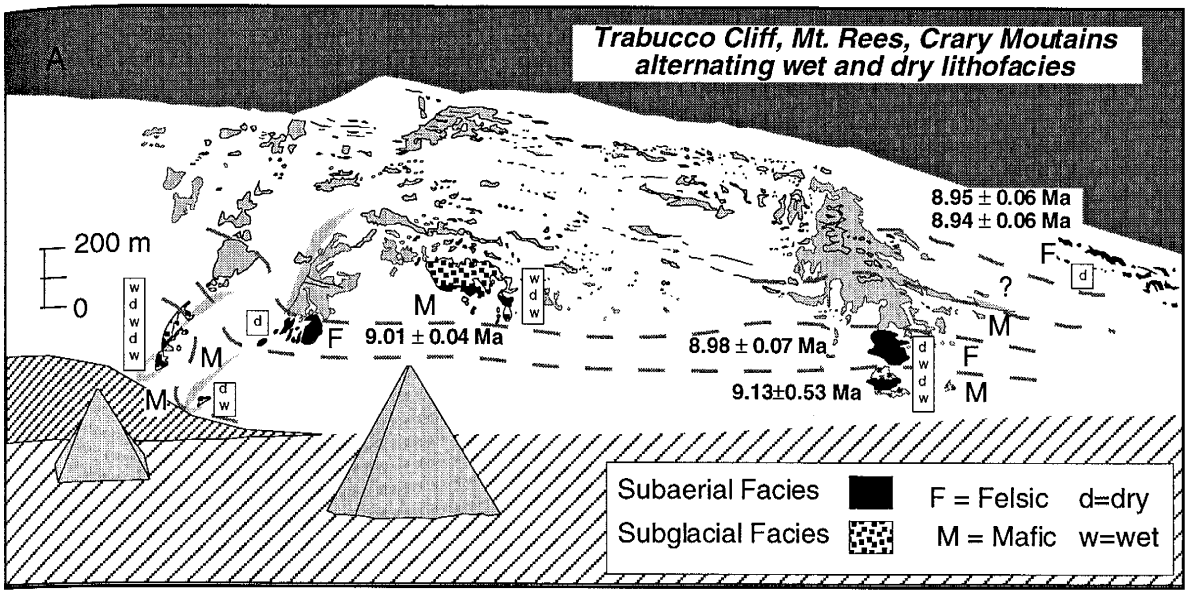

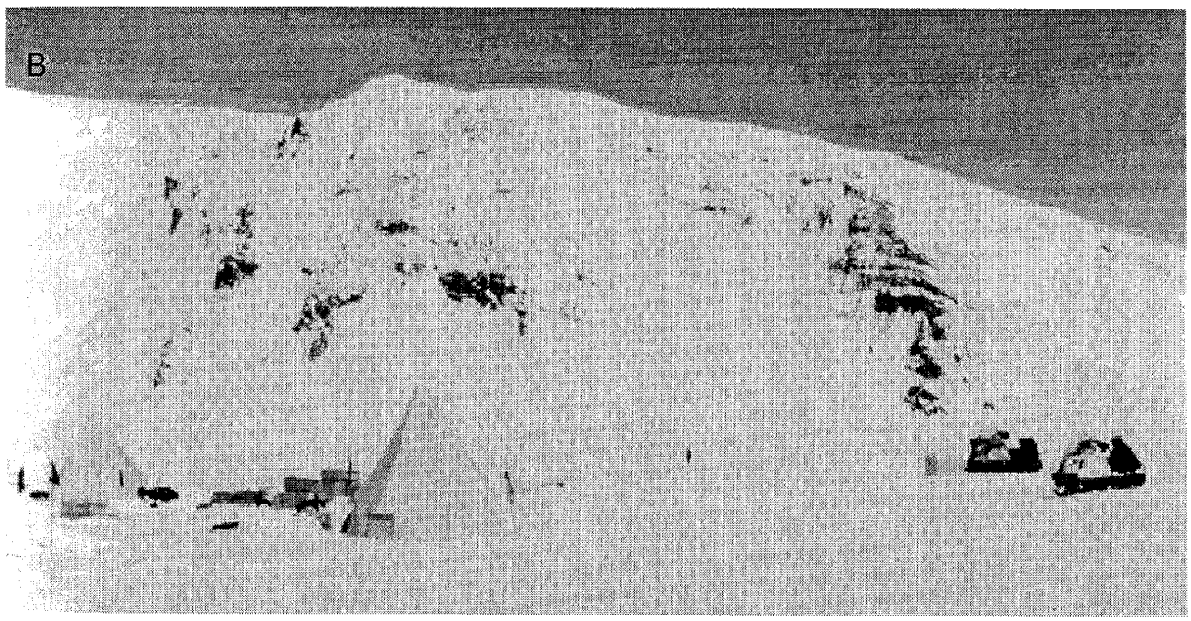

Figure 9. Sketch (a) and photograph (b)) of Trabucco Cliff outcrops at Mt. Rees, Crary Mountains, showing alternating "wet" and "dry" lithofacies and compositions, and $^{40}Ar/^{39}Ar$ ages. In boxes, w and d denote wet and dry lithofacies, respectively.

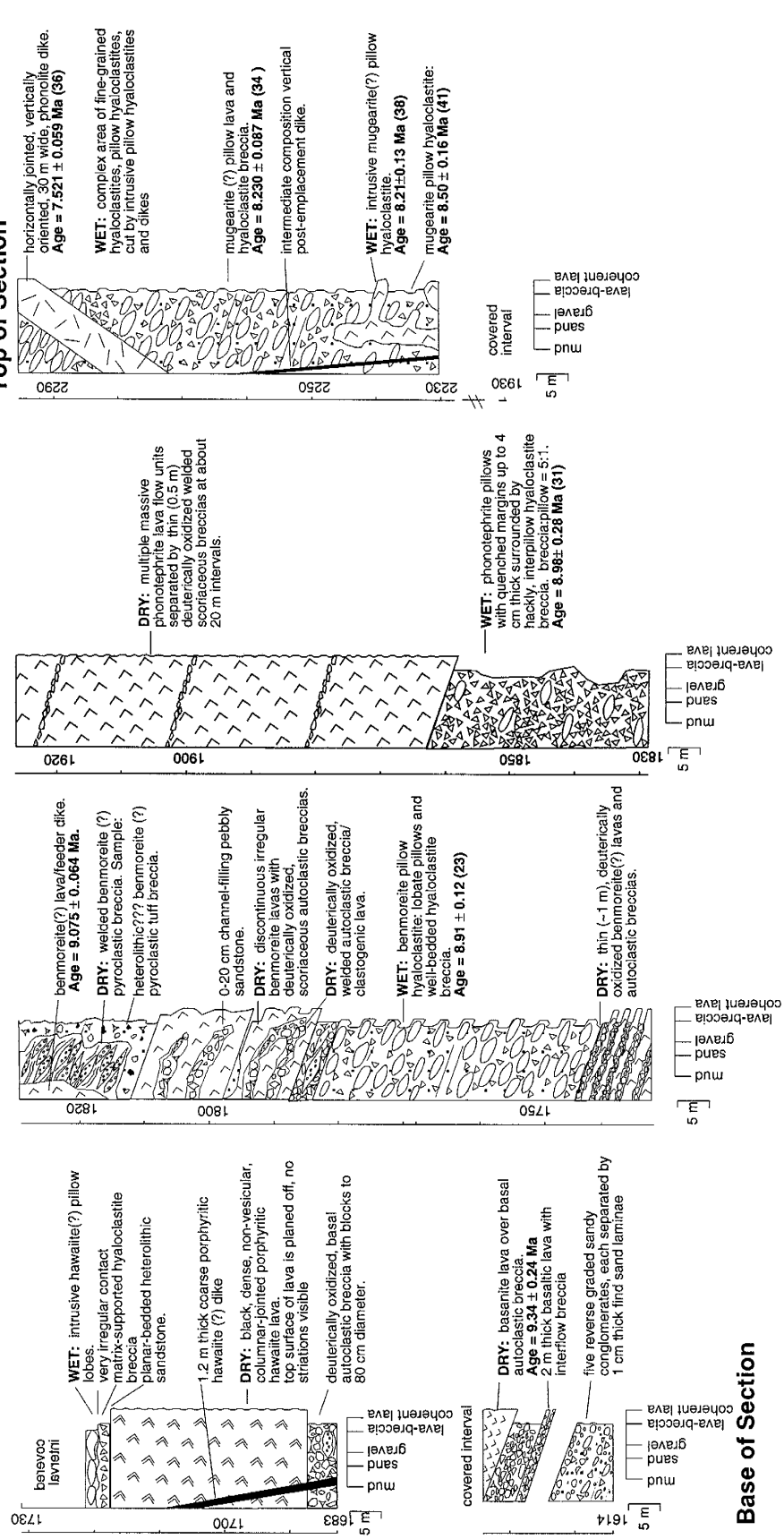

Figure 10. Stratigraphic section of Tasch Ridge, Mt. Rees, Crary Mountains, showing alternating wet and dry lithofacies and $^{40}Ar/^{39}Ar$ ages.

These mafic and intermediate eruptions occurred concurrently with trachyte, phonolite and rhyolite eruptions. A second interval of alternating subglacial and subaerial eruptions between 7.38±0.07 Ma and 6.41±0.43 Ma is recorded in ridge outcrops located just southeast of Lie Cliff.

The alternating wet and dry lithofacies at Mt. Rees and Mt. Steere are difficult to interpret in terms of changing ice sheet levels and are tentatively interpreted as products of interactions between lavas and local slope ice or snow. The indistinguishable, high precision $^{40}Ar/^{39}Ar$ ages in many parts of the sequences indicate that they accumulated over short time intervals. The multi-story alternating lithofacies comprise slope-forming constructional sequences that lack interbedded glacial deposits and glacial unconformities. The passage zones from subglacial to subaerial lithofacies are not horizontal but are dipping along with the alternating lithofacies. Skilling (1994) and Smellie and Hole (1997) suggested that sloping passage zones can form after drainage of an intraglacial lake. However, at Mt. Rees and Mt. Steere, there is no evidence for ponded or flowing water. The up-sequence transition from wet to dry lithofacies can be explained by lavas interacting with slope ice and snow to form pillows and hyaloclastites until they build above the level of slope ice and form dry lavas. The up-sequence transition from dry to wet lithofacies is more difficult to interpret and may have resulted from lava flowing through open channels or tunnels in the ice. The lack of glacial tills and unconformities suggests that the ice was thin or cold-based. We suggest that these interaction occurred on the slopes of the growing Mt. Steere and Mt. Rees volcanoes above the level of the ice sheet. The Alexander Island model of alternating lithofacies produced during valley-confined subglacial volcanism provides an analogue for these Crary Mountain sequences (Fig. 2d).

In contrast to Mt. Steere, the Pliocene to latest Pleistocene (4.25±0.03 Ma to 33.5±7.4 ka) Mount Frakes shield volcano is completely undissected and

exposed rocks consist entirely of subaerially erupted phonolite, hawaiite and basanite (Fig. Crary Map). The absence of glaciovolcanic sequences at Mt. Frakes may simply reflect the lack of dissection. Like Mt. Takahe, Mt. Frakes has lower flank, late-stage parasitic vents that provide "dipstick" measures of paleo-ice-levels (Fig. 2c). Late-stage basanite and hawaiite cinder cone deposits crop on the south side of Mt. Frakes at Morrison Rocks and on the western side of Mt. Frakes at English Rock. The youngest cinder cone deposits at English Rock, dated to 33.5± 7.4 ka, are situated ~150 m above the level of the ice sheet. These deposits limit syn-eruptive ice-sheet expansion to <150 m above the present ice level.

Paleoenvironmental Reconstructions: Monogenetic volcanoes

Several small, Oligocene to Pliocene, eroded, monogenetic basaltic volcanoes located mostly in the Hobbs Coast region (Fig. 11) and McCuddin Mountains (Fig. 3) exhibit evidence for glaciovolcanic interactions. Most of these sites were previously interpreted as subglacial hyaloclastites, comprising the interior remnants of table mountains and implying thicker former ice sheet conditions (LeMasurier, 1990). Detailed re-examination of many sites led to identification of a greater diversity of paleoenvironments, including abundant emergent and subaerial environments and rare subglacial environments. In general our interpretations differ significantly from previous interpretations and suggest lower or unchanged local paleo-ice levels relative to today. The regional significance of the paleo-ice-levels is complicated by the fact that many of these volcanoes are located on glacial interfluves as depicted in Figure 2e.

Evidence for subglacial environments is limited to a few monogenetic volcanoes in the Hobbs Coast region, and includes molded or striated pre-volcanic unconformities, glacial till, and pillow lava and hyaloclastite breccias (Fig. 11). Pre-volcanic erosional

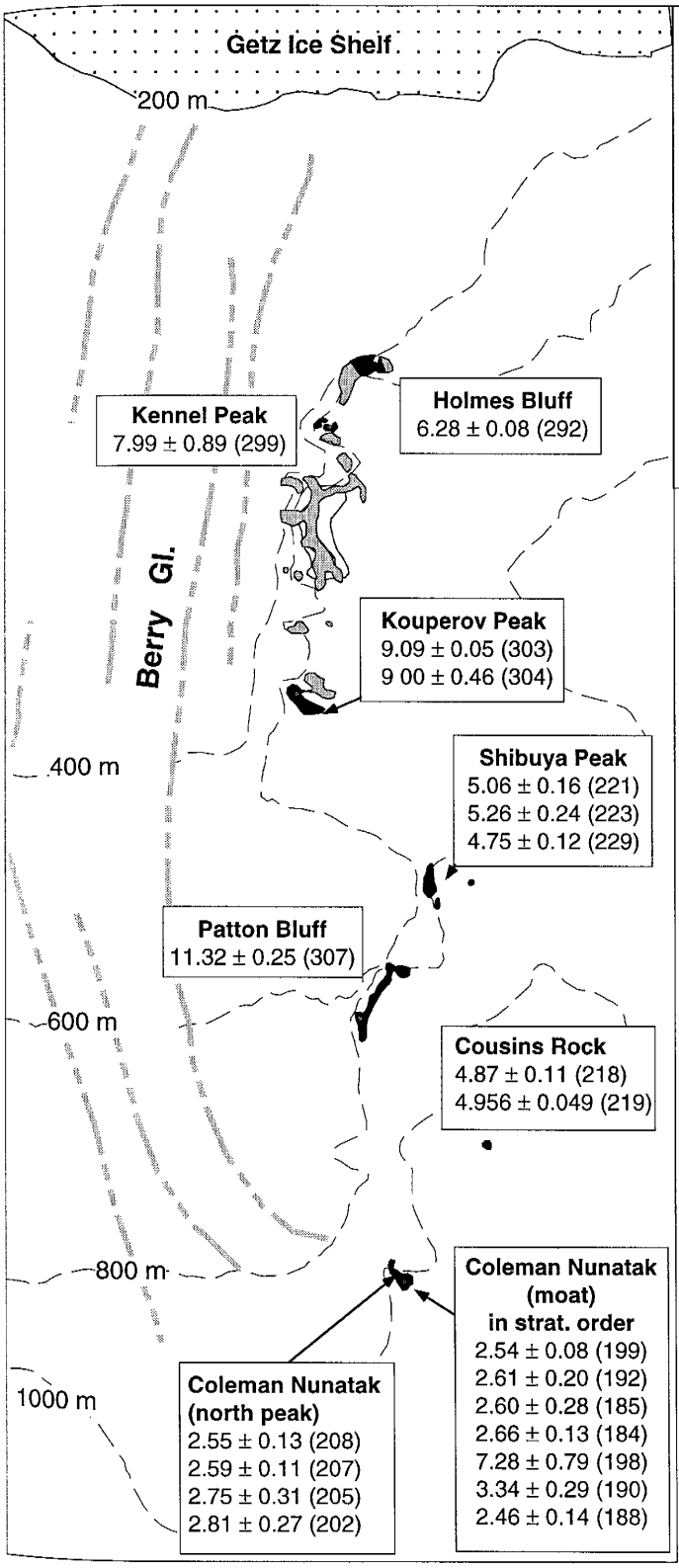

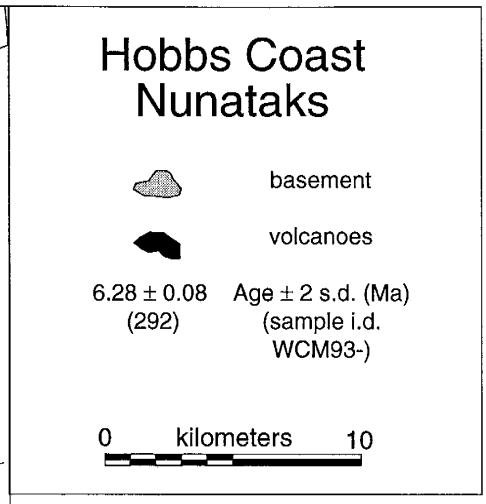

Figure 11. Map of Hobbs Coast nunataks, showing basement rock, volcanic centers and $^{40}Ar/^{39}Ar$ ages. Base map is Hobbs Coast quadrangle, scale 1:250,000, U.S.G.S. Reconnaisance Series, Antarctica.

unconformities that have molded and/or striated surfaces underlie late Miocene volcanic deposits at Bowyer Butte, Holmes Bluff, and Kennel Peak. At Bowyer Butte (not visited in this study), striated granodiorite basement rocks are overlain by a 5 meter thick deposit of reported hyaloclastite and a <100 m thick basalt lava flow (LeMasurier et al., 1979). At Holmes Bluff, a ~55 m thick, columnar-jointed, late Miocene valley-filling lava flow with a 1.3 m thick basal breccia overlies a 1.5 m thick palagonitized strombolian lapilli tuff and a partially molded basement unconformity. The upper surface of the basement unconformity exhibits areas of weathered, irregular vertical joint blocks and areas of surface molding but no striations. This surface is tentatively interpreted as weathered glacial unconformity. In a previously undescribed rock exposure at Kennel Peak, a <1 m thick diamict is sandwiched between underlying molded granitic basement rocks and overlying hawaiitic pillow lavas and interpillow hyaloclastite breccia. The exposure is in a deep wind moat on the east side of Kennel Peak and the pre-volcanic unconformity is situated approximately 75 m lower than the level of the local ice surface. The diamict is a weakly cemented, poorly sorted, bouldery gravelly mud. Boulder clasts are subangular and appear to be composed of local bedrock; gravel clasts are subrounded to subangular, molded and faceted and are composed of plutonic and metamorphic basement lithologies and pebble and laminated mudstone clasts. This diamict is interpreted to be a thin, patchy basal till that overlies a glacially molded bedrock surface.

The overlying volcanic sequence at Kennel Peak comprises the only exposed pillow lava/hyaloclastite breccia sequence in the western MBL. The 100+ m thick section consists of very crudely bedded, steeply dipping (15-30°) late Miocene (7.99 ± 0.89 Ma) pillow lavas and interpillow hyaloclastite breccia. The pillow sequence is interrupted by an unconformity, which is overlain by a planar stratified, crudely graded pebble hyaloclastite. The pillow lavas and hyaloclastites are inferred to have been deposited in a subglacial chamber onto thin basal till and glacially molded bedrock. The vesicularity and steep dips of the interbedded pillow lava and hyaloclastite, and the presence of similar age subaerial

lava flows elsewhere at Kennel Peak (LeMasurier et al., 1990) suggest that the deposits form part of a subaqueous flow-foot delta sequence, possibly associated with subaerial lava effusion. The pillow lava and hyaloclastite sequence extend only ~25 m above today's ice surface, suggesting that the syn-eruptive local paleo-ice-level was only slightly higher than today's ice level. As with other glacial interfluve volcanoes in MBL, translation of local late Miocene paleo-ice-levels at Kennel Peak to regional syn-eruptive paleo-ice-levels is difficult.

There are several monogenetic volcanic centers in western and central MBL that are interpreted as the products of emergent hydromagmatic to subaerial explosive eruptions, including Mt. Petras, Brandenberger Bluff (Mt. Berlin), Cousins Rock, Shibuya Peak, Coleman Nunatak, and Holmes Bluff. Evidence for hydromagmatic explosivity includes clast populations with variable vesicularity and blocky shapes; palagonitized or altered glassy hyalotuff; planar, massive, and cross stratified beds; armored lapilli; soft-sediment deformation structures; pyroclastic bombs and blocks; and bedding plane sags. The eruptions produced hydrovolcanic base surge or fall deposits that are locally interbedded or closely associated with subaerially erupted strombolian deposits, characterized by abundant oxidized highly vesicular tachylite, fluidal and cuspate lapilli, droplet grains, welded bombs and lapilli, and lavas with oxidized and welded breccias. The Shibuya Peak hyalotuff section includes abundant rounded and molded basement clast, suggesting eruption through a debris layer at the base of a glacier. Many of the monogenetic volcanoes are situated on glacier interfluves and must be interpreted cautiously. Detailed descriptions of Mt. Petras were presented in Part B of dissertation and two additional detailed descriptions of emergent hydromagmatic volcanoes (Brandenberger Bluff and Coleman Nunatak) are described below.

Brandenberger Bluff. At Brandenberger Bluff, located on the north side of Mt. Berlin, a ~350 m thick Pliocene (2.71±0.08 Ma) lava and volcaniclastic sequence exhibits evidence for subglacial, emergent and subaerial paleoenvironments. The north-facing bluff

section is about 250 m thick and 1 km wide and is composed of steeply dipping (20-30°), well stratified, fine-grained trachytic/phonolitic hyalotuff that overlies a highly jointed and brecciated, aphyric glassy trachyte/phonolite lava. Sohn (1995) described a very similar trachyte lava at the base of a subaqueous tuff cone sequence in Korea. The bluff face deposits include thick sections of cyclic packages of normally graded, lapilli-dominated hyalotuff and massive fine hyalotuff and areas of large slide blocks (10's m diameter) that are interpreted as intraglacial turbidites and collapse breccias, respectively. Throughout the bluff section both pumice lapilli and blocky, aphyric, glassy lapilli are common. Lapilli-dominated hyalotuff at the top of the bluff exhibits shallow-dipping planar beds and cross-beds and contains abundant armored lapilli, interpreted as subaerial hydrovolcanic base-surge deposits. The margins of the bluff top surface include areas of intense soft-sediment deformation. This sequence is interpreted as an intraglacial emergent tuff cone, a felsic variation of the basaltic table mountain, composed of subaqueously deposited lava and tuff flank deposits and subaerially deposited bluff-top deposits. The abundant deformation may have developed as supporting ice walls collapsed. The basal lava and several clasts from within the tuff cone sequences were dated by the $^{40}Ar/^{39}Ar$ method, with a mean age of 2.71±0.08 Ma (presented in Part A of dissertation). Phonotephritic cinder cone deposits, located up slope and about 100 m elevation above the top of Brandenberger Bluff, yield an identical age of 2.70±0.05 (also in Part A of dissertation). These phonotephrite deposits indicate complete emergence above ice level.

The passage zone from subaqueous to subaerial depositional environments is situated near the top of Brandenberger Bluff, at ~1650 m a.s.l. and approximately 250 m above the level of the ice sheet on the north side of Mt. Berlin. Currently, ice flow is obstructed by Mt. Berlin and the elevation of the ice sheet on the upstream (south) side of Mt. Berlin is at about 1800-2000 m a.s.l., as is depicted in Fig. 2b. In middle Pliocene time when the Brandenberger Bluff tuff cone emerged above ice level, the Mt. Berlin edifice did not exist and there was probably no local obstruction to ice flow. In the absence

of Mt. Berlin, local ice elevations at Brandenberger Bluff would be at ~1800 m a.s.l. Remarkably, the exposed passage zone at Brandenberger Bluff may actually record a lower late Pliocene WAIS level, because of changes in ice-flow patterns after its eruption.

Coleman Nunatak. Coleman Nunatak is an example of a monogenetic volcano where there is abundant evidence for hydromagmatic volcanism. The basaltic nunatak is approximately 1x3 km in size and has gently undulating top surface just above the level of the ice sheet, with a small peak at the north end and a ~75 m deep, 1 km long wind moat at the south end .

Volcaniclastic deposits in a wind moat exposure at Coleman Nunatak are dominated by alternating packages of poorly sorted, crudely stratified to massive, thick beds (~1 m) of coarse hyalotuff (lapillistone), and well-stratified, moderately sorted, thin beds (0.5-5 cm) of medium hyalotuff (lapilli tuff) (Fig. 12). Individual beds can be traced for only short distances (<4 m) whereas bed packages are traceable for > 50 m. The beds are typically plane parallel, with rare low angle cross stratification and crude normal and reverse grading. Smaller clasts (<1 cm) tend to be subrounded, highly vesicular tachylite, whereas larger clasts tend to be subangular, poorly vesicular holocrystalline basanite. Mud-coated lapilli clasts and reddened, breadcrust-textured pyroclastic bombs (to 25 cm) associated with bedding plane sags occur locally. The alternating units interfinger with scoriaceous lapillistone and tuff breccia that contains reddened pyroclastic bombs. The combination of scoriaceous pyroclastic lithofacies and well bedded lapilli tuff with armored lapilli and asymmetric bedding plane sags suggest these deposits were formed by mixed hydromagmatic and magmatic fragmentation processes. The discontinuous, erosive, massive, planar, and cross-stratified beds are suggestive of base-surge deposits (Fisher and Schmincke, 1984). A 40x60 m area of mega-breccia is situated near the base of the eastern moat section. The mega-breccias are composed of up to 5 m diameter blocks of lithified, well bedded palagonitized hyalotuff. Lapilli clasts in the hyalotuff blocks resemble the dominant finely vesicular scoria lapilli of the upper and lower tuff units.

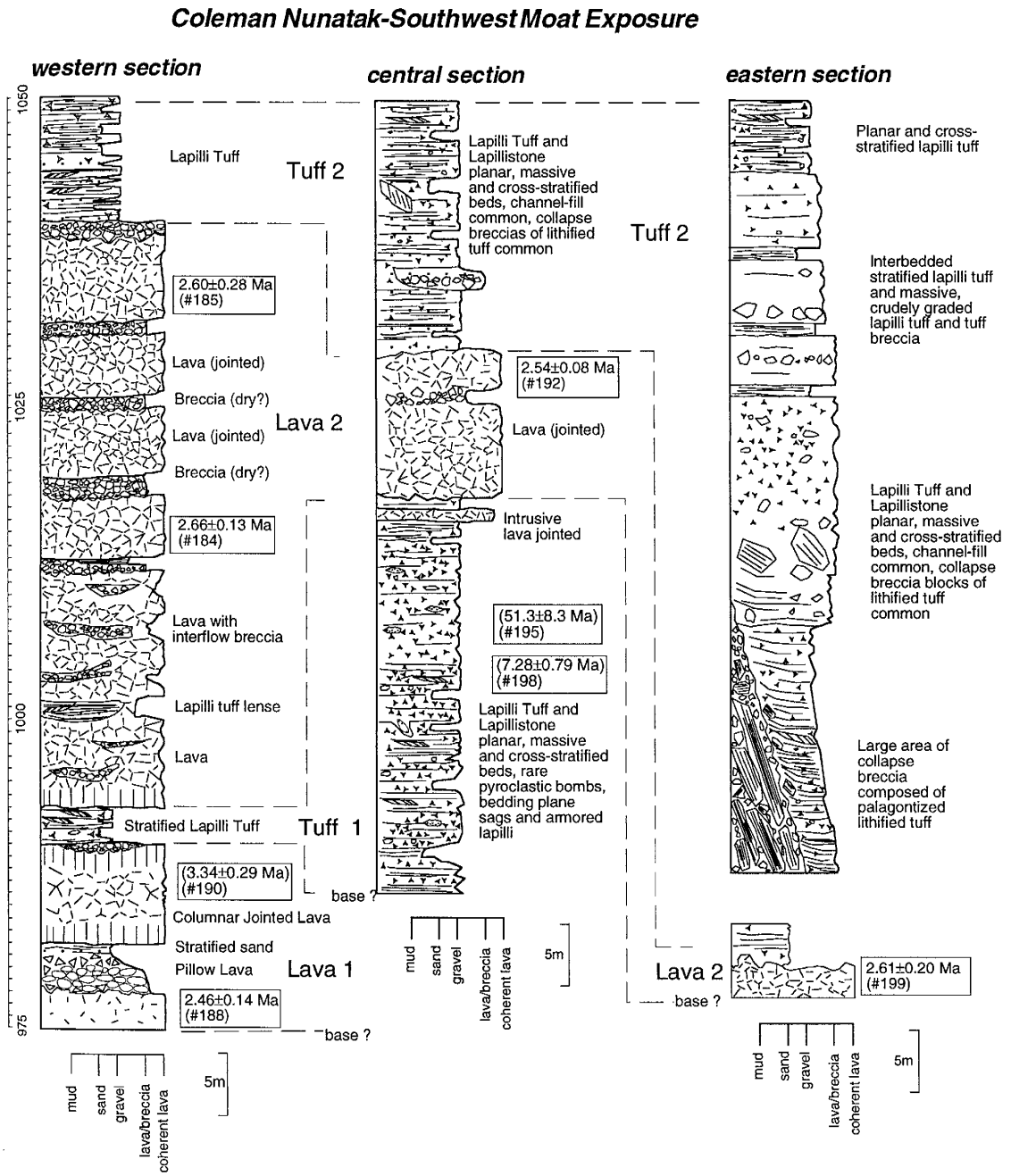

Figure 12. Volcanic stratigraphy in three moat sections at south end of Coleman Nunatak, Hobbs Coast. $^{40}Ar/^{39}Ar$ ages (±2 s.d.) are in boxes; rejected ages are in parentheses. Stratigraphy described in text. Comparison of ages to previous K/Ar ages is described in $^{40}Ar/^{39}Ar$ Geochronology section.

The hydrovolcanic tuff and strombolian units are intercalated with compound lava flows that are slightly glassy, and highly jointed. The top of the lowest lava flow grades into pillow lava and hyaloclastite breccia. The minor pillow lava, hyaloclastite breccia and glassy textures all suggest subaqueous depositional environments. The combination of base-surge deposits and minor subaqueous lavas is indicative of an emergent intraglacial environment, where interaction with meltwater controlled the explosive hydromagmatic eruption style, and modified the lava flows slightly. As was suggested for Brandenberger Bluff, the large-scale collapse breccias may have developed as supporting ice walls collapsed.

A prominent steeply southward dipping angular unconformity separates subhorizontally stratified to deformed hyalotuff below it from steeply dipping massive to deformed hyalotuff above it. Several irregular intrusive lava apophyses cut across the pyroclastic rock exposures and are loci of soft sediment deformation. The stratified hyalotuff resembles stratified sequences in the moat section, described above. This section is interpreted as an eroded tuff cone vent, dominated by base-surge deposits at lower levels, that are cut by a "vent-funnel" unconformity and overlain by vent-slurry hyalotuff (as in Kokelaar, 1983). In summary, detailed field and dating analyses suggest that Coleman Nunatak is an emergent 2.6 Ma monogenetic tuff cone that formed when local ice was at a similar level as it is today. The glacier interfluve location precludes establishing WAIS elevations.

PALEO-ICE-LEVELS OF THE WEST ANTARCTIC ICE SHEET

A synthesis of paleoenvironmental reconstructions and high precision $^{40}Ar/^{39}Ar$ age data provides a proxy record of paleo-ice-levels of the WAIS since latest Eocene times (Table 2, Fig. 13). Table 2 summarizes data pertinent for paleo-ice-level determinations. The regional ice levels listed in Table 2 account for complications discussed in the

Table 2. Volcanic Records of Paleo-Ice-Levels in West Antarctica

Volcano/ Area	Diagnostic Lithofacies	Paleo-environment	Paleo-Ice-Level Relative to Local	Regional	Distance from (km)	Age ±2 s.d.	Reference
Mt. Takahe, Oeschger Bl.	lava	subaerial, late stage cone	200	< +200	150	0.007 ± 0.006	this study
Mt. Takahe, Gill Bluff	scoriaceous lava/pillow	subglacial to subaerial, late-stage flank	350	350	150	0.029 ± 0.012	this study
Mt. Frakes, English Rock	scoriaceous tuff	subaerial, late stage cone	150	< + 150	275	0.034 ± 0.008	this study
Mt. Takahe, Moll Spur	scoriaceous lava/pillow	subglacial to subaerial, late-stage flank	350	350	150	0.039 ± 0.014	this study
Mt. Takahe, Steuri Glacier	scoriaceous tuff	subaerial, late stage flank	50	< + 50	150	0.045 ± 0.008	this study
Mt. Takahe, Stauffer Bl.	hyalotuff/pillow lava	subglacial to emergent late-stage flank	350	350	150	0.050 ± 0.015	this study
Mt. Takahe, Roper Pt.	scoriaceous tuff	subaerial, late stage cone	50	< + 50	150	0.104 ± 0.028	this study
Mt.Waesche	scoriaceous tuff, lava	subaerial, shield-building	0	same or lower	310	(0.2 ±. 0.4)	L&T (1990)
Mt. Berlin, Wedemeyer Rock	ignimbrite	subaerial, late stage flank(?)	50	< + 50	125	0.232 ± 0.006	Part A
Mt. Berlin, Mefford Knoll	scoriaceous tuff	subaerial, late stage cone	200	< +200 (?)	125	0.236 ± 0.019	Part A
Mt. Berlin, Kraut Rocks	lava	subaerial, shield-building	200	< +200 (?)	125	0.434 ± 0.018	Part A
Mt. Berlin, Kraut Rocks	lava	subaerial, shield-building	200	< +200 (?)	125	0.573 ± 0.005	Part A
Mt. Murphy, Sechrist Peak	hyalotuff	emergent, late-stage cone	550	550	30	0.590 ± 0.015	this study, L(1994)
Mt. Frakes, English Rock	scoriaceous tuff	subaerial, late-stage cone	250	< +250	275	0.851 ± 0.036	this study
Mt. Moulton, Gawne Nunatak	scoriaceous tuff	subaerial, late-stage cone	200	< +200	125	1.11 ± 0.15	this study
Boyd Ridge	scoriaceous tuff	subaerial, late-stage cone	200	< +200	275	1.32 ± 0.01	this study
Mt. Frakes, English Rock	scoriaceous tuff	subaerial, late-stage cone	350	< +350	275	1.60 ± 0.02	this study
Boyd Ridge, Runyon Rokc	hyalotuff-hyaloclastite	subglacial-emergent, isolated monogenetic(?)	50	50	280	2.02 ± 0.05	this study
Hobbs Coast, Coleman Nunatak	hyalotuff, lava	emergent-subaerial, interfluve	0	same?	75	2.57 ± 0.07	this study
Mt. Berlin, Brandenberger Bluff	hyalotuff, jointed lava	subglacial to emergent, exhumed table mountain	300	<-50	125	2.77 ± 0.02	Part A, this study
Mt. Flint	scoriaceous tuff	subaerial, late stage cone	100	< +100	100	3.70 ± 0.06	this study
Mt. Moulton, Edwards Sp.	lava	subaerial, shield-building	100	< +100	125	3.98 ± 0.14	this study
Mt. Murphy, Turtle Peak	scoriaceous tuff/ pillow lava	subglacial to emergent, interfluve	200	same (?)	30	4.59 ± 0.04	this study
Mt. Sidley	lava, tuff	subaerial, shield-building	0		300	4.60 ± 0.02	this study

Table 2. Volcanic Records of Paleo-Ice-Levels in West Antarctica

Volcano/ Area	Diagnostic Lithofacies	Paleo-environment	Paleo-Ice-Level Relative to Local	Regional	Distance from (km)	Age ±2 s.d.	Reference
Hobbs Coast, Shibuya Peak	hyalotuff	emergent-subaerial, interfluve	0	same (?)	60	4.92 ± 0.29	this study
Hobbs Coast, Cousins Rock	hyalotuff, scoriaceous tuff	emergent-subaerial, interfluve	0	same (?)	70	4.94 ± 0.08	this study
Mt. Murphy, Turtle Peak	scoriaceous tuff/ pillow lava	subglacial to emergent, interfluve	200	same (?)	30	5.65 ± 0.11	this study
Mt. Murphy, Turtle Peak	scoriaceous tuff/ pillow lava	subglacial to emergent, interfluve	200	same (?)	30	5.84 ± 0.29	this study
Mt. Murphy, Hedin Nunatak	scoriaceous tuff/ pillow lava	subglacial to emergent, interfluve	200	same (?)	30	6.20 ± 0.24	this study
Hobbs Coast, Holmes Bluff	scoriaceous tuff	subaerial, interfluve	0	same (?)	40	6.30 ± 0.08	this study
Mt. Hartigan	lava	subaerial, shield-building	100	< +100	200	6.40 ± 0.80	this study
Mt. Murphy, Icefall Nunatak	scoriaceous tuff/ pillow lava	subglacial to emergent, interfluve	200	same (?)	30	6.47 ± 0.08	this study
Mt. Murphy, Hedin Nunatak	scoriaceous tuff/ pillow lava	subglacial to emergent, interfluve	200	same (?)	30	6.50 ± 0.12	this study
Mt. Murphy, Icefall Nunatak	scoriaceous tuff/ pillow lava	subglacial to emergent, interfluve	200	same (?)	30	6.80 ± 0.10	this study
Mt. Kauffman	lava	subaerial, shield-building	400	<+400	90	(7.6 ± 0.6)	L&T (1990)
Hobbs Coast, Kennel Pk	pillow/hyaloclastite/ tillite	subglacial-subaerial(?), interfluve	25	25(?)	45	7.99 ± 0.89	this study
Mt. Steere, Lie Cliff (oldest)	hyaloclastite-pillow/subaerial lava	subglacial/subaerial, slope-ice	0	same or lower	250	8.19 ± 0.19	this study
Mt. Rees, Tasch Ridge (youngest)	hyaloclastite-pillow/subaerial lava	subglacial/subaerial, slope-ice	0	same or lower	250	8.21 ± 0.13	this study
Mt. Murphy, main shield (top)	pillow/hyaloclastite, scoriaceous tuff	subglacial- subaerial, shield-building	300	same?	30	8.22 ± 0.02	this study
Mt. Hartigan	lava	subaerial, shield-building	250	< +250	200	(8.36 ± 0.82)	L&T (1990)
Mt. Bursey, Starbuck Cr.	scoriaceous tuff	subaerial, late- stage cone	50	< +50	140	8.45 ± 0.06	this study
Mt. Hartigan	lava	subaerial, shield-building	200	< +200	200	(8.5 ± 0.66)	L&T (1990)
Mt. Steere, Lie Cliff (oldest)	hyaloclastite-pillow/subaerial lava	subglacial/subaerial, slope-ice	0	same or lower	250	8.52 ± 0.11	this study
Mt. Flint	scoriaceous tuff	subaerial, late- stage cone	100	< +100	90	8.55 ± 0.24	this study
Mt. Kosciusko	lava	subaerial, shield-building	200	< +200	110	8.66 ± 0.35	L&T (1990)
Mt. Murphy, main shield (near top)	pillow/ hyaloclastite, scoriaceous tuff	subglacial/subaerial, shield-building	300	< +300	30	8.84 ± 0.13	this study
Mt. Rees, Trabucco Cliff (youngest)	hyaloclastite-pillow/subaerial lava	subglacial/subaerial, slope-ice	0	same or lower	250	8.94 ± 0.06	this study

Table 2. Volcanic Records of Paleo-Ice-Levels in West Antarctica

Volcano/ Area	Diagnostic Lithofacies	Paleo-environment	Paleo-Ice-Level Relative to Local	Paleo-Ice-Level Relative to Regional	Distance from (km)	Age ±2 s.d.	Reference
Mt. Rees, Trabucco Cliff (oldest)	hyaloclastite-pillow/subaerial lava	subglacial/subaerial, slope-ice	0	same or lower	250	9.13 ± 0.53	this study
Mt. Andrus, near Lind	scoriaceous tuff	subaerial, late- stage cone	250	< +250		9.16 ± 0.06	this study
Mt. Murphy, main shield (base)	pillow/ hyaloclastite, scoriaceous tuff	subglacial/subaerial, shield-building	300	< +300	110 30	9.34 ± 0.10	this study
Mt. Rees, Tasch Ridge (oldest)	hyaloclastite-pillow/subaerial lava	subglacial/subaerial, slope-ice	0	same or lower	250	9.34 ± 0.24	this study
Mt. Flint	cinder cone	subaerial, late-stage flank	300	< +300		9.55 ± 0.20	this study
Hobbs Coast, Bowyer Bt.	lava, hyaloclastite	subglacial-subaerial(?), interfluve	200	< +200	90 25	(9.56 ± 0.9)	L&T (1990)
Mt. Bursey, Koerner Bl.	lava	subaerial, shield-building	400	< +400		9.95 ± 0.06	this study
Mt. Cumming	lava	subaerial, shield-building	200	< +200	140 250	(10 ± 1)	L&T (1990)
Mt. Kosciusko	lava	subaerial, shield-building	200	< +200		(10 ± 0.8)	L&T (1990)
Mt. Hampton	lava	subaerial, shield-building	200	< +200	110 210	(10.1 ± 1.6)	L&T (1990)
Mt. Andrus, Lind Ridge	clastogenic lava	subaerial, shield-building	200	< +200		11.05 ± 0.08	this study
Hobbs Coast, Patton B.	hyalotuff, lava	emergent-subaerial, interfluve	0	0	110 65	11.32 ± 0.25	this study
Mt. Hampton	lava	subaerial, shield-building	200	< +200	210	(13.7 ± 1)	L&T (1990)
Mt. Whitney	lava	subaerial, shield-building	200	< +200	210	(13.7 ± 1)	L&T (1990)
U.S.A.S. Escarp., Mt. Aldaz	scoriaceous tuff	subaerial, isolated monogenetic	0	same or lower	175	18.80 ± 1.40	this study
Mt. Flint, Reynolds R.	lava	subaerial, shield-building	0	same or lower	90	20.20 ± 0.08	this study
U.S.A.S. Escarp., Mt Galla	hyalotuff	emergent, slope ice (?)	0	same (?)	175	26.06 ± 0.21	this study
Mt. Petras, southwest slope	hyalotuff	emergent, slope ice	325	n.d.	170	27.18 ± 0.23	this study
Mt. Petras,summit	hyalotuff	emergent, slope ice	750	n.d.	170	27.86 ± 0.52	this study
Mt. Petras, summit west ridge	hyalotuff	emergent, slope ice	580	n.d.	170	27.90 ± 0.38	this study
Mt. Petras, southwest saddle	hyalotuff	emergent, slope ice	430	n.d.	170	28.59 ± 0.22	this study
Mt. Petras, summit north face	lava	subaerial, isolated monogenetic	740	n.d.	170	36.11 ± 0.22	Part B

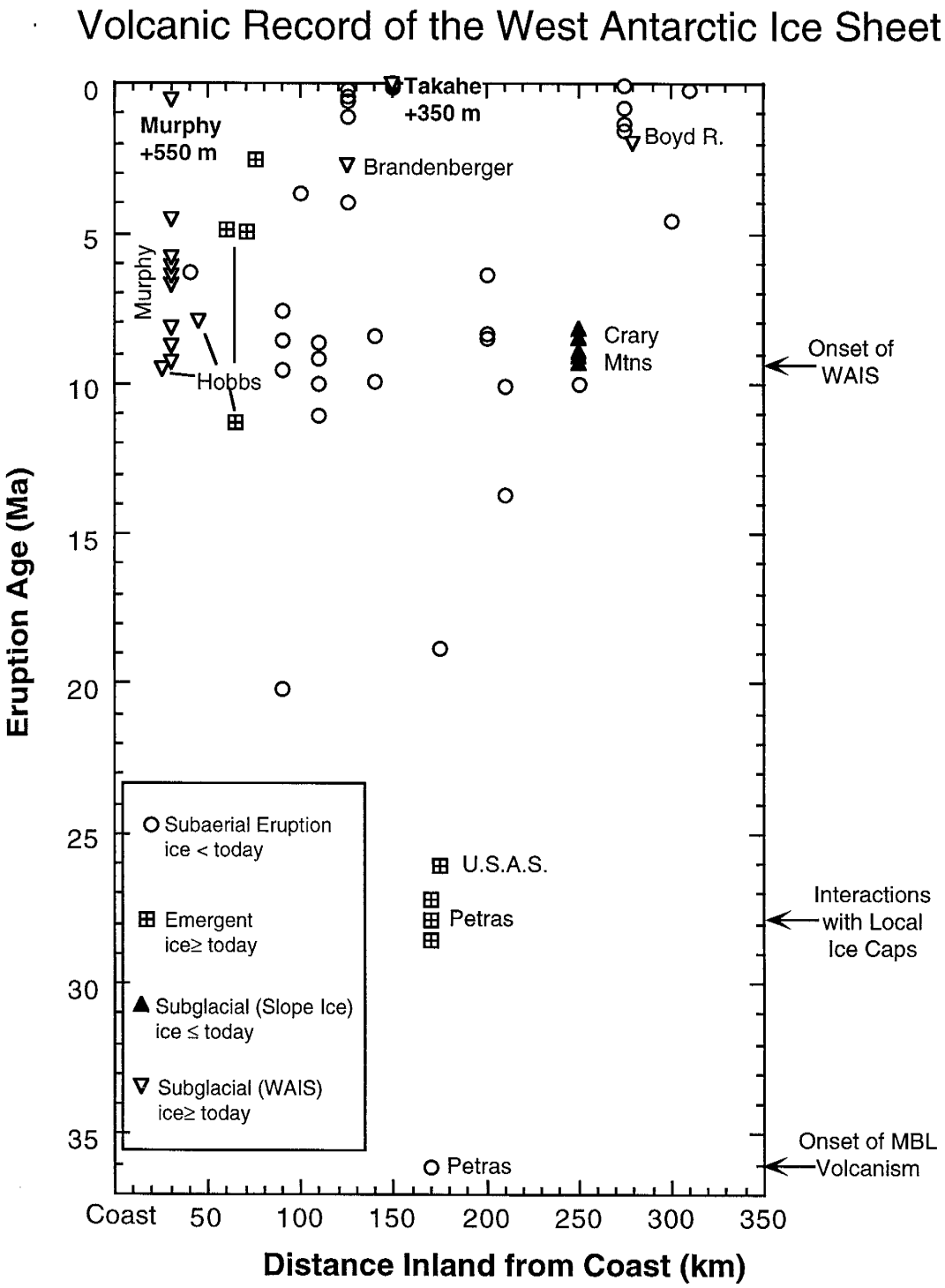

Figure 13. Plot of eruption ages versus distance of volcano from the coast. Emergent and subglacial eruptions imply ice-magma interactions and ice-sheet presence. Elevations of syn-eruptive high-stands are in meters above the regional ice sheet. Most subglacial eruptions occurred at or above the level of the present-day ice sheet.

conceptual model of glaciovolcanism. A summary of the volcanic record of the WAIS is presented below:

Latest Eocene to Middle Miocene (36-18 Ma)

The record of MBL volcanism suggests at most very limited interaction with water or ice between 36 and 18 Ma and offers no evidence for a regional ice sheet during this interval. The earliest known volcanism in MBL occurred in the late Eocene (36.11 ± 0.22 Ma), when massive lava was erupted at Mt. Petras (Fig. 3). Mid-Oligocene (29-27 Ma) surtseyan and strombolian deposits at Mt. Petras provide the first terrestrial evidence for glacial ice in Marie Byrd Land. These eroded tuff cone deposits are inferred to be products of intermittent contact of magma with external water, probably derived from melting of a thin, local ice cap or ice and snow on slopes (Part B of dissertation). In a small outcrop situated at the level of the ice sheet near Mt. Galla, a 26.06±0.42 Ma hyalotuff provides an additional suggestion of local late Oligocene glaciation. At Reynolds Ridge on the north end of Mt. Flint, a 20.20±0.08 Ma subaerial trachyte lava is situated at the level of the ice sheet, suggesting lower syn-eruptive ice-levels in the early Miocene. Palagonitized strombolian tuff-breccia deposits at Mt. Aldaz (18.8±1.4 Ma) provide further indications of lower-than-present syn-eruptive ice levels in the early Miocene.

The suggestion in the Mt. Petras volcanic record for no ice in the latest Eocene (36 Ma) followed by limited ice presence beginning in the late Oligocene (29-27 Ma) is consistent with marine isotopic inferences of a major global climate cooling event at the Eocene/Oligocene boundary, ca 33.7 Ma (Kennett, 1977; Kennett and Barker, 1990). The no-ice inference for the Eocene does not preclude an ice sheet or ice below the level of the exposed subaerial lava. There is abundant evidence in marine records for Oligocene glaciation in East Antarctica but the extent and character of the glacial systems are not well established (see summaries by Barrett, 1996; Kennett, 1995). Numerous glacial diamictites dated to ~30.5-22 Ma were recovered from the CIROS-1 core sequences on the

continental margin of east Antarctica in the Ross Sea (Barrett et al., 1989). Late Oligocene glacial diamictites were also recovered from drill holes in Prydz Bay, on the east Antarctica margin of the southern Indian Ocean (Hambrey, 1990). Overall, marine records indicate a dynamic East Antarctic glacial system after 30 Ma, when local ice caps and possibly large-scale ice sheets fluctuated in response to climatic events (see Barrett, 1996, Kennett, 1995 for references). Ice-sheet modeling suggests that if the relatively stable, land-based East Antarctic Ice Sheet is in a dynamic mode of growth and decay, then the less-stable marine-based WAIS will behave dynamically (e.g., Hughes, 1973; Huybrechts, 1993). Such a dynamic system, characterized by alternations between cold glacial and cool temperate interglacial climates (e.g., Barrett, 1989) is consistent with the glaciovolcanic record during this interval.

Middle Miocene (ca. 18-10 Ma)

The record of middle Miocene volcanism in MBL is extremely fragmentary, with no evidence for volcanism from 18 to 13 Ma and only limited evidence from ~13-10 Ma. Several polygenetic volcanoes in the Ames and Executive Committee Ranges were apparently formed during this interval, all of which are interpreted as consisting of subaerially erupted, mostly felsic lavas and pyroclastic rocks (Table 2, Fig. 3). Many of the outcrops are situated near the level of the WAIS and suggest that syn-eruptive WAIS levels were similar to or lower than they are today (Table 2, e.g., Mt. Andrus, Mt. Hampton, Mt. Whitney). A small outcrop of palagonitized hyalotuff at Patton Bluff in the Hobbs Coast nunataks suggests limited hydrovolcanic interactions at 11.32±0.25 Ma.

Preceding this interval of limited volcanism, the global climate system underwent a dramatic transition at ~14.8-14.0 Ma from relative warmth of the early Miocene to cold climates of the late Neogene, culminating in the development of a relatively stable East Antarctic Ice Sheet by ~14.2 Ma (Flower and Kennett, 1993, p. 877, 1994; Savin et al., 1975, Shackleton and Kennett, 1975; Kennett, 1977; Miller et al., 1985). Climatic

deterioration is supported by marine oxygen and carbon isotope data, global sea level changes, and glacial geomorphic interpretations (Flower and Kennett, 1993, p. 877, 1994; Savin et al., 1975, Shackleton and Kennett, 1975; Kennett, 1977; Miller et al., 1987; Denton et al., 1993). Sediment records near East Antarctica show a sharp increase in ice-rafted detritus beginning at 14.2 Ma that has persisted until today (Kennett and Barker, 1990). By contrast, there is no evidence for significant ice-rafted detritus near West Antarctica in middle Miocene time (Kennett and Barker, 1990). The absence of the WAIS during this interval is consist with the lack of evidence for significantly higher ice levels between 18 and 10 Ma.

Late Miocene to Middle Pleistocene (10-1 Ma)

Late Miocene (10-8 Ma). The late Miocene interval from 10 to 8 Ma marks an apparent acceleration in polygenetic volcanism in MBL and provides the first substantial evidence for the a widespread WAIS. Late Miocene (9-8 Ma) glaciovolcanic sequences are exposed at the inland Crary Mountains (Mt. Steere and Mt. Rees), at Kennel Peak and Bowyer Butte near the Hobbs Coast, and at coastal Mt. Murphy volcano. The Mt. Murphy main shield sequence records fluctuating syn-eruptive (mostly 9.34±0.10 to 8.84±0.13 Ma) paleo-ice-levels up to 300 m higher than today's local ice level. Relatively low-elevation striated glacial unconformities and interbedded tillites record fluctuating ice flow across the growing volcano during this interval.

Interpretations of WAIS paleo-ice-levels from the main shield outcrops at Mt. Murphy are complicated by two factors. First, the main shield sequences are located on the west side of Mt. Murphy, where ice is currently descending from high upstream levels at ~800 m a.s.l. to low downstream levels of ~200 m a.s.l. The elevations of these sequences (up to ~800 m a.s.l.) are about the same as the elevation of the regional ice sheet on the upstream side. Therefore, these outcrops may record fluctuations of an ice sheet that was smaller than today's ice sheet. Second, because Mt. Murphy is at the coast where

glaciers are feeding into the Getz Ice Shelf, the local ice configurations may be very responsive to changes in sea level. Third, the coastal position of Mt. Murphy may facilitate draining of englacial lakes formed by volcanism and passage zone sequences may be much lower than the paleo-ice-level. By this scenario, the main shield sequences provides evidence for higher late Miocene ice levels. In summary, the complex setting of Mt. Murphy precludes making interpretations about regional paleo-ice-levels based solely on the main shield sequence.

Coeval glaciovolcanic sequences at Mt. Rees and Mt. Steere in the Crary Mountains (9.34±0.24 to 8.19±0.19 Ma) apparently resulted from slope-ice interactions and imply that abundant local slope extended to near or below the level of the modern ice sheet. The Mt. Rees and Mt. Steere reconstructions support interpretations of Mt. Murphy that suggested lower or unchanged syn-eruptive WAIS levels in the late Miocene.

Monogenetic volcanoes at Bowyer Butte (9.56±0.90 Ma; K/Ar from LeMasurier and Thomson, 1990) and Kennel Peak (7.99±0.89 Ma) provide indications of late Miocene paleo-ice-levels that were 50-200 m higher than today's local ice levels. Interpretations of regional ice-level changes from these local ice-level is complicated by the fact that both sites are situated on interfluves between glaciers that are descending steeply from inland areas to the Getz Ice Shelf. A further complication is that both volcanoes are situated along prominent linear scarps, almost certainly related to faults of unknown age (LeMasurier and Landis, 1996). The pillow lava, hyaloclastite breccia, tillite and striated basement rocks do provide additional evidence for widespread glaciation in West Antarctica in the late Miocene.

During this interval of abundant glaciovolcanism, late-stage cinder cones and subaerial lava were erupted at Mt. Flint (9.55±0.20 and 8.55±0.24 Ma), Mt. Bursey (8.45±0.046 Ma) and Mt. Andrus (9.16±0.06 Ma), and Kouperov Peak (9.11±0.42 Ma). These subaerially erupted deposits provide upper elevation limits on late Miocene paleo-ice-

levels ranging from <50 to ≤300 m above present ice level (Table 2). Poorly exposed, subaerially erupted shield-building sequences in the Executive Committee Range (Mt. Cumming (10.0±1.0 Ma), Mt. Hartigan (8.66±0.66 Ma)) and Ames Range (Mt. Kosciusko (8.66±0.35 Ma)) provide local limits on syn-eruptive paleo-ice-levels at < 200-250 m above present local ice level (all ages by K/Ar method from LeMasurier and Thomson (1990)).

In summary, the record of 10 to 8 Ma volcanism in MBL provides substantial evidence for a widespread glaciation of West Antarctica by 9 Ma. The possibility of higher or lower ice levels during this interval cannot be verified by the volcanic record. Marine data from the Weddell Sea also implies that development of a large-scale WAIS occurred ca. 10-8 Ma. Significant glacial erosion in West Antarctica during this interval is indicated by increased deposition of hemipelagic sediments and ice-rated detritus and rapid deposition of turbidite sequences (Kennett and Barker, 1990; Kennett, 1995). The marine sediment record "suggests considerable climatic/cryospheric instability in the source area" during this interval (Kennett and Barker, 1990, p. 956).

The coincidence of increased volcanism and widespread glaciation in West Antarctica at 10-8 Ma may reflect a cause-and-effect relationship. Sigvaldason et al. (1992) suggested that "vigorous crustal movements" in response to isostatic changes caused by "glacier deloading" may have caused higher rates of late Quaternary volcanism in Iceland. McGuire (pers. comm., 1997) recognized increased late Quaternary volcanicity in coastal and island volcanoes in the Mediterrean during periods of rapid sea level change, and he suggested that rapidly changing sea level can cause edifice slope failure and consequent decompressive expulsion of magma stored at shallow depths. Kennett and Barker (1990) described the early WAIS (10-6 Ma) as quite dynamic with frequent growth and decay cycles. Regional isostatic crustal readjustments and sea-level changes during the latest Miocene may have caused the apparent increase in volcanism after 10 Ma. Although such

an association is highly speculative, the coincidence of inception of a full-bodied but dynamic WAIS and increased volcanism in Marie Byrd Land is compelling.

Latest Miocene- Middle Pleistocene (ca. 8-1 Ma) This interval is characterized by continued polygenetic volcanism, late-stage flank eruptions on older volcanoes, and isolated monogenetic volcanism. Monogenetic volcanism at Brandenberger Bluff north of Mt. Berlin, at the satellite nunataks of Mt. Murphy and at several nunataks near the Hobbs Coast provides abundant evidence for glaciovolcanism between 6.8 and 2.6 Ma. Passage zones in table mountain sequences at Turtle Peak, Hedin Nunatak, Icefall Nunatak, and Brandenberger Bluff record local syn-eruptive paleo-ice-level elevations up to 350 m above today's local ice-level. The nunataks at Mt. Murphy are situated on interfluves at about the same elevation as the main shield outcrops described in the previous section. Extracting accurate WAIS syn-eruptive paleo-ice-level elevations from these local ice levels is not possible because small changes in WAIS elevations or local erosion or fault displacement at the interfluve margins could have dramatic effects on local ice level at the interfluve. In addition, ice flow in these localities may have been strongly affected by sea level or by ice-damming effects of Mt. Murphy.

Brandenberger Bluff (2.72 Ma) also has a passage zone at 350 m above local ice level. However, it is on the lee side of Mt. Berlin, a younger volcano which forms a major obstruction to ice flow. The elevation of the WAIS upstream of Mt. Berlin is at ~1800 m, about 50 m higher than the passage zone at Brandenberger Bluff, implying a reduced WAIS at 2.72 Ma. However, it is possible that the regional ice configuration and elevations prior to growth of Mt. Berlin were different from today's configuration.

In the Hobbs Coast nunataks, emergent hydrovolcanism was common during this time interval, with subaerial eruptions of fall and base surge hyalotuffs at Cousins Rock (4.94±0.08 Ma), Shibuya Peak (4.90±0.29 Ma), and Coleman Nunatak (2.57±0.07 Ma).

The Shibuya Peak hyalotuff contains abundant molded, well-rounded boulders, possibly resulting from eruption through a glacial-debris layer.

Taken together the volcanic records at these sites imply that syn-eruptive paleo-ice-levels were similar to today's WAIS level at several locations during the 8-1 Ma interval. This may indicate that the WAIS configuration through this interval was relatively stable. Alternatively, the volcanic record may only document ice-sheet high-stands, and records of lower paleo-ice-levels may be currently concealed beneath the ice. Interpretations of other proxy records of late Neogene climate and cryospheric evolution in Antarctica have led to divergent views about the stability of the Antarctic Ice Sheet through this interval. On the basis of interpretations of glaciogenic Sirius Group diamictites dated by microfossils, Webb and Harwood (1991) postulated that the East Antarctic Ice Sheet was highly unstable during the Early Pliocene, when global temperatures and sea levels were higher than today. They suggested that climate warming caused complete deglaciation of West Antarctica and major deglaciation of East Antarctica, reducing the Antarctic Ice Sheet to one-third its present volume. The deglaciation hypotheses depends upon the mid-Pliocene age of the deposits, which has recently been challenged by a number of workers (Burckle and Potter, 1996; Kellogg and Kellogg, 1996; Stroeven and Prentice, 1997; Barrett, 1997). The alternative view-point, presented in Sugden et al. (1993), advocates persistent, stable polar climate and landscape systems in East Antarctica since the middle Miocene cooling event at 14 Ma. These arguments are based on a wide range of geomorphological and marine data, and ice-sheet modeling (Sugden et al., 1993). The stability hypothesis does not explicitly address the WAIS, but it follows that stability in East Antarctica is a prerequisite for stability in West Antarctica. Kennett (1995) suggested that a "semi-permanent" WAIS was established by ~5 Ma, on the basis consistent appearance of ice-rafted detritus and an end of turbidite deposition at 4.8 Ma. Marine records in the Ross Sea document numerous WAIS advances onto and retreats from the continental shelf, but there no evidence for collapse of WAIS (see reviews by Kennett, 1995; Barrett, 1997). WAIS advances onto the

continental shelf would probably be accompanied by inland ice-sheet thickening, but there is no supporting evidence for higher inland ice levels in the 8-1 Ma glaciovolcanic record of MBL.

Middle Pleistocene to Holocene (1-0 Ma)

The record of Quaternary volcanism offers strong evidence for two significant ice-sheet expansion events (Fig. 14). A middle Pleistocene (590±15 ka) ice-sheet high-stand of +550 m is inferred at Mt. Murphy, on the basis of late-stage tuff cone eruptions at Sechrist Peak. At about the same time (573±5 ka), shield-building eruptions of subaerial lava occurred at Kraut Rocks, on the west flank of Mt. Berlin. These lavas imply that syn-

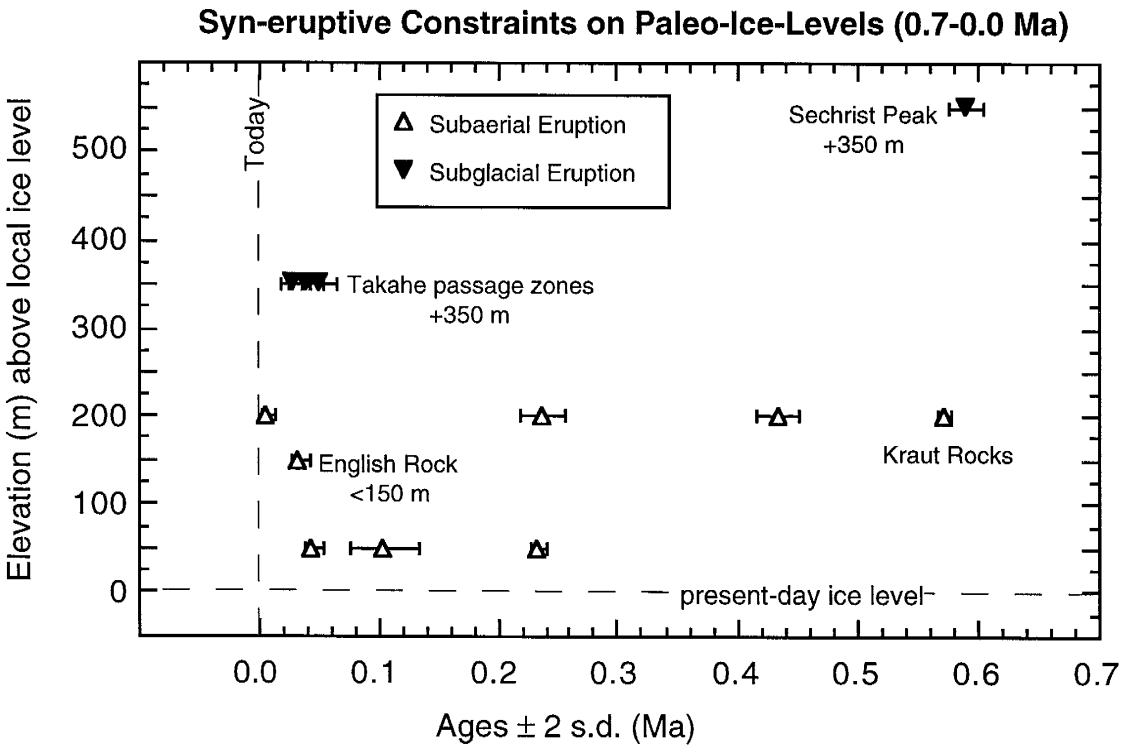

Figure 14. Plot of ages and elevations of 0.7 to 0.0 Ma deposits relative to present-day local ice level. Cross-reference with Table 2. A low-precision K/Ar age from Mt. Waesche is not included on this plot.

eruptive local ice was at a lower elevation than the lavas. The lowest elevation lava (~1850 m. a.s.l.) is situated about 200 m higher than local ice levels but about 200 lower than the upstream level of the WAIS, in an area where present-day ice is descending from high upstream levels of about 2000 m a.s.l. to much lower downstream levels of about 1400 m a.s.l. Although it is difficult to place an absolute elevation on the regional paleo-ice-level, it is probable that syn-eruptive ice-sheet thickening at Kraut Rocks was much less extreme than at Sechrist Peak. The marine oxygen isotope record suggests significant global-ice build-up occurred at ~0.6 Ma (isotopic stage 16) (e.g., Raymo et al., 1989). The extreme thickening of the WAIS at Mt. Murphy may have been driven by sea-level lowering and coastal ice sheet expansion.

A late Wisconsinan ice-sheet high stand is inferred at Mt. Takahe, on the basis of 29±12 ka passage zone sequences at Gill Bluff situated at ~350 m above the present-day level of the regional ice sheet (Fig. 14). Two other passage zone sequences at Mt. Takahe, Stauffer Bluff (50±29 ka) and Moll Spur (21±40 ka), offer corroborating evidence for late Wisconsinan paleo-ice-levels at ~350 m higher then the present-day ice level. Limits on the duration of a late Wisconsin ice-sheet high stand at Mt. Takahe are provided lower elevation subaerial deposits at Oeschger Bluff (7±13 ka) and Steuri Glacier (45±7 ka). Late-stage parasitic cinder cone deposits at English Rock, Mt. Frakes offer another constraint on inland ice-sheet thickening during the late Wisconsin. These 34±7 ka cinder cones are situated at ~100-150 m above the level of the regional ice sheet, and limit syn-eruptive ice-sheet expansion to <150 m. The English Rock constraint on uplift may indicate either that the inland WAIS during the late Wisconsinan expansion recorded at . The youngest cinder cone deposits at English Rock, dated to 33.5± 7.4 ka, are situated ~150 m above the level of the ice sheet. These

The late Wisconsinan (ca. 25-14 ka) history of the WAIS has been studied extensively but remains a subject of debate. The configuration of the WAIS during this last glacial cycle has bearing on several fundamental issues, including the importance of the

WAIS to the global sea level mass budget during late Wisconsin time, the relationship between the WAIS and the global climate system, and the current stability of the WAIS. Mutually exclusive hypotheses have been proposed for and against expansion of the WAIS in both coastal and interior regions of West Antarctica. Continental shelf records and glacial geologic data from in and near McMurdo Sound have been interpreted by many workers as evidence for late Wisconsin expansions of the Antarctic Ice Sheet across the continental shelf and into the mouth of ice-free valleys (e.g., Thomas & Bentley, 1978; Kellogg et al., 1979, Kellogg and Kellogg, 1987; Stuiver et al., 1981; Denton et al., 1989; Anderson, 1991). The CLIMAP reconstruction of the Antarctic Ice Sheet at 18 ka took into account ice-sheet expansions and concluded that ice-sheet growth during late Wisconsinan times caused lowering of global sea level by 24 m, of which 16 m was attributed to the WAIS (Stuiver et al., 1981). In a study of raised beaches in the McMurdo Sound area, Colhoun *et al.* (1992) argued that ice in the Ross Sea was less extensive and thinner than previously suggested and concluded that the Antarctic Ice Sheet had a negligible effect on late Wisconsinan global sea level, lowering it by only 0.5 to 2.5 m.

Late Wisconsinan inland ice levels of the WAIS are also debated. On the basis of changes in total gas content in the Byrd Station ice core, Raynaud and Whillans (1982) suggested that the WAIS at Byrd Station was 200-250 lower at the last glacial maximum than it is at present. Subsequent thickening of the inland ice sheet during the Holocene to its present configuration has been attributed to increased precipitation (Jouzel et al., 1989). In contrast, glacial geologic records (Karlen and Melander, 1978; Denton et al., 1992; Borns et al., 1996) from West Antarctica offer evidence for higher inland paleo-ice-levels, but these records were not well dated.

The passage zone "dipstick" records at Mt. Takahe offer the first well-dated geologic evidence for higher inland WAIS levels during late Wisconsinan times. The possibility that the WAIS was significantly larger in the late Wisconsin suggests that it had

a significant effect on the global sea level budget at the last glacial maximum and on the subsequent rise in sea level.

CONCLUSIONS

Paleoenvironmental reconstructions and $^{40}Ar/^{39}Ar$ geochronology of the intraglacial Marie Byrd Land volcanic province document cryospheric evolution in West Antarctica since the latest Eocene. Major conclusions of the volcanic record of the WAIS include:

1. The onset of Marie Byrd Land volcanism in the latest Eocene is recorded by lavas at Mt. Petras, dated to 36.11±0.22 Ma (±2 σ uncertainty). The latest Eocene to Early late Miocene interval (36-10 Ma) was characterized by low apparent rates of volcanism. Beginning at 10 Ma, there was a significant apparent increase in volcanicity in Marie Byrd Land. Relatively high rates of volcanism persisted through the late Neogene and into the Quaternary.

2. The oldest terrestrial indications for glacial ice in West Antarctica are middle Oligocene (29-27 Ma) tuff cone deposits at Mt. Petras that suggest the presence of a thin, local ice cap or ice and snow on slopes. The implication of limited local glaciation in West Antarctica at that time agrees with interpretations suggesting active glacial systems in East Antarctica.

3. The first evidence for a widespread West Antarctic Ice Sheet is late Miocene (9.3-8.2 Ma) glaciovolcanic sequences from across Marie Byrd Land. The onset of increased glaciovolcanism in Mare Byrd Land coincides with the first occurrences of abundant ice-rafted detritus at 10-8 Ma (Kennett, 1995). Determinations of absolute elevations of syn-eruptive WAIS levels are not possible but the sequences tentatively indicate that the late Miocene ice sheet was not significantly higher than the present-day West Antarctic Ice Sheet. late Miocene subaerial volcanic sequences situated near present-day ice level are consistent with this inference. Two patterns emerge from the record of

syn-eruptive paleo-ice-levels since 10 Ma : former WAIS expansions were more extensive at coastal sites than at inland sites, and it appears that the West Antarctic Ice Sheet is in a near maximum configuration that existed at many times but was rarely exceeded.

4. A middle Pleistocene ice-sheet high stand of +550 m is inferred at the coastal volcano, Mt. Murphy, on the basis of late-stage 590±15 ka tuff cone deposits at Sechrist Peak. Nearly coeval (573±5 ka) inland ice levels at Mt. Berlin (125 km from the coast) were probably no more than 200 m above present-day local ice levels. The extreme thickening of the WAIS at Mt. Murphy may have been driven by sea-level lowering and coastal ice sheet expansion. This ice-sheet high stand may correspond to global ice expansion (and eustatic lowering) at isotopic stage 16 in the marine record.

5. A ~350 m expansion of the inland West Antarctic Ice Sheet in the late Wisconsin is inferred at Mt. Takahe (150 km from coast), on the basis of 29±12 ka subglacial to subaerial eruptive sequences at ~350 m above the present-day level of the regional ice sheet. Limits on maximum inland ice-sheet thickening during late Wisconsinan times are provided by 34±8 ka late-stage parasitic cinder cone deposits on the west flank of Mt. Frakes (located 275 km from coast). These deposits are situated at ~100-150 m above the level of the regional ice sheet, suggesting less extreme inland thickening of the ice sheet. An expanded ice-sheet during the late Wisconsin suggests that the WAIS had a considerable impact on subsequent global sea level rise into the Holocene.

ACKNOWLEDGMENTS

This work was supported by the National Science Foundation (NSF-DPP918806), with additional funding from the New Mexico Geochronological Research Laboratory. We thank U.S. Navy VXE-6 squadron, Antarctic Support Associates, and Ken Borek Air Ltd. for logistical support; mountaineer Tony Teeling for field assistance; Philip Kyle for XRF analyses at the New Mexico Institute of Mining and Technology; John Smellie, British

Antarctic Survey for providing XRF data from the University of Keele; Rich Esser, Matt Heizler, and Lisa Peters for assistance with $^{40}Ar/^{39}Ar$ geochronology.

REFERENCES

Allen, C. C., Jercinovic, M. J., and Allen, J. S. B., 1982, Subglacial volcanism in north-central British Columbia and Iceland: Journal of Geology, v. 90, p. 699-715.

Alley, R. B., and Whillans, I. M., 1991, Changes in the West Antarctic Ice Sheet: Science, v. 254, p. 959-963.

Anderson, J. B., 1991, Marine record of Late Quaternary glacial-interglacial fluctuations in the Ross Sea and evidence for rapid, episodic sea level change due to marine ice sheet collapse, *in* Bindschadler, R. A., ed., West Antarctic Ice Sheet Initiative: Antarctic Research Series, Vol. 56, NASA, p. 231-263.

Baker, P. E., Davies, T. G., and Roobol, M. J., 1969, Volcanic activity at Deception Island in 1967 and 1969: Nature, v. 224, p. 553-560.

Barrett, P. J., Hambrey, M. J., Harwood, D. M., Pyne, A. R., and Webb, P. N., 1989, Synthesis, *in* Barrett, P. J., ed., Antarctic Cenozoic history from CIROS-1 drillhole, McMurdo Sound: Wellington, DSIR Publishing, p. 241-251.

Barrett, P., J., 1996, Antarctic palaeoenvironment through Cenozoic times- A review: Terra Antarctica, v. 3, p. 103-119.

Behrendt, J. C., LeMasurier, W. E., Cooper, A. K., Tessensohn, F., Trehu, A., and Damaske, D., 1991, Geophysical studies of the West Antarctic rift system: Tectonics, v. 10, no. 6, p. 1257-1273.

Behrendt, J. C., LeMasurier, W., and Cooper, A. W., 1992, The West Antarctic rift system- a propagating rift "captured" by a mantle plume?, *in* Yoshida, Y., ed., Recent progress in antarctic earth science: Tokyo, Terra Scientific Publishing Company, p. 315-322.

Behrendt, J. C., Saltus, R., Damaske, D., McCafferty, A., Finn, C. A., Blankenship, D. D., and Bell, R. E., 1996, Patterns of late Cenozoic volcanic and tectonic activity in the West Antarctic rift system revealed by aeromagnetic data: Tectonics, v. 15, p. 660-676.

Bentley, C. R., 1997, Rapid sea-level rise soon from West Antarctic ice sheet collapse?: Science, v. 275, p. 1077-1078.

Bergh, S. G., and Sigvaldason, G. E., 1991, Pleistocene mass-flow deposits of basaltic hyaloclastite on a shallow submarine shelf, South Iceland: Bulletin of Volcanology, v. 53, p. 597-611.

Bindschadler, R. A., 1995, WAIS: The West Antarctic Ice Sheet Initiative: a multi-discplinary study of rapid climate change and future sea level, science and implementation plan, National Science Foundation, p. 75.

Bjornsson, H., 1988, Hydrology of ice caps in volcanic regions: Reykjavik, Societas Scientarium Islandica, University of Iceland, 139 p.

Blankenship, D. D., Bell, R. E., Hodge, S. M., Brozena, J. M., Behrendt, J. C., and Finn, C. A., 1993, Active volcanism beneath the West Antarctic ice sheet and implications for ice-sheet stability: Nature, v. 361, p. 526-529.

Borns, H., Dorion, C., Calkin, P. E., Wiles, G. C., and Barclay, D., 1996, Evidence for thicker ice in interior West Antarctica, *in* Third annual WAIS workshop, Sterling, VA.

Burckle, L. H., and Potter, N., Jr., 1996, Pliocene-Pleistocene diatoms in Paleozoic and Mesozoic sedimentary and igneous rocks from Antarctica: A Sirius problem solved: Geology, v. 24, p. 235-238.

Cande, S. C., and Kent, D. V., 1992, A new geomagnetic polarity time scale for the Late Cretaceous and Cenozoic: Journal of Geophysical Research, v. 97, p. 13,917-13,952.

Carlisle, D., 1963, Pillow breccias and their aquagene tuffs. Quadra Island, British Columbia: Journal of Geology, v. 71, p. 48-71.

Chen, Y., Smith, P. E., Evenssen, N. M., York, D., and Lajoie, K. R., 1996, The edge of time: dating young volcanic ash layers with the ^{40}Ar-^{39}Ar laser probe: Science, v. 274, p. 1176-1178.

Clapperton, C. M., and Sugden, D. E., 1990, Late Cenozoic glacial history of the Ross Embayment, Antarctica: Quaternary Science Reviews, v. 9, p. 253-272.

Colhoun, E. A., Mabin, M. C. G., Adamson, D. A., and Kirk, R. M., 1992, Antarctic ice volume and contribution to sea-level fall at 20,000 yrs B.P. from raised beaches: Nature, v. 358, p. 316-319.

Cooper, A. K., and Davey, F. J., 1985, Episodic rifting of phanerozoic rocks in the Victoria Land Basin, Western Ross Sea, Antarctica: Science, v. 229, p. 1085-1087.

Cooper, A. K., Davey, F. J., and Behrendt, J. C., 1987, Seismic stratigraphy and structure of the Victoria Land Basin, western Ross Sea, Antarctica, *in* Cooper, A. K., and Davey, F. J., eds., The Antarctic continental margin: geology and geophysics of the western Ross Sea, Earth Science Series: Houston, Texas, Circum-Pacific Council for Energy and Mineral Resources, p. 27-65.

Cooper, A. K., Davey, F. J., and Hinz, K., 1991, Crustal extension and origin of sedimentary basins beneath the Ross Sea and Ross Ice Shelf, Antarctica, *in* Thomson, M. R. A., Crame, J. A., and Thomson, J. W., eds., Geological evolution of Antarctica: Cambridge, England, Cambridge University Press, p. 299-304.

Dalrymple, G. B., 1979, Critical tables for conversion of K-Ar ages from old to new decay constants: Geology, v. 7, p. 558-560.

Deino, A., and Potts, R., 1990, Single-crystal $^{40}Ar/^{39}Ar$ dating of the Olorgesailie Formation, Southern Kenya Rift: Journal of Geophysical Research, v. 95, p. 8453-8470.

Denton, G. H., Bockheim, J. G., Rutford, R. H., and Andersen, B. G., 1992, Glacial history of the Ellsworth Mountains, West Antarctica, *in* Webers, G. F., Craddock, C., and Splettstoesser, J. F., eds., Geology and paleontology of the Ellsworth Mountains, West Antarctica: Boulder, Colorado, Geological Society of America Memoir 170, p. 423-432.

Denton, G. H., Bockheim, J. G., Wilson, S. C., and Stuiver, M., 1989, Late Wisconsin and Early Holocene Glacial History, Inner Ross Embayment, Antarctica: Quaternary Research, v. 31, p. 1-32.

Denton, G. H., Sugden, D. E., Marchant, D. R., Hall, B. L., and Wilch, T. I., 1993, East Antarctic Ice Sheet sensitivity to Pliocene climatic change from a dry valleys perspective: Geografiska Annaler, v. 75A, p. 155-204.

Drewry, J., 1983, Antarctica: Glaciological and Geophysical Folio: Cambridge, Scott Polar Research Institute, University of Cambridge.

Fisher, R. V., and Schmincke, H., 1984, Pyroclastic rocks: Berlin, Springer-Verlag, 472 p.

Fleck, R. J., Sutter, J. F., and Elliot, D. H., 1977, Interpretation of discordant $^{40}Ar/^{39}Ar$ age spectra of Mesozoic tholeiites from Antarctica: Geochimica Cosmochimica Acta, v. 41, p. 15-32.

Flower, B. P., and Kennett, J. P., 1993, Middle Miocene ocean-climate transition: High resolution oxygen and carbon isotopic records from Deep Sea Drilling Project site 488A, southwest Pacific: Palaeoceanography, v. 8, p. 811-843.

Flower, B. P., and Kennett, J. P., 1994, The middle Miocene climatic transition: East Antarctic ice sheet development, deep ocean circulation and global carbon cycling: Palaeogeography, Palaeoclimatology, Palaeoecology, v. 108, p. 537-555.

Fuller, R. E., 1931, The aqueous chilling of basaltic lava on the Columbia River Plateau: American Journal of Science, v. 21, p. 281-300.

Gudmundsson, M. T., and Björnsson, H., 1991, Eruptions in Grimsvotn, Vatnajokull, Iceland, 1934-1991: Jökull, v. 41, p. 21-45.

Hambrey, M. J., Larsen, B., and Ehrmann, W. U., 1991, The glacial record from the Prydz Bay continental shelf, east Antarctica, *in* Barron, J., Larsen, B., and al., e., eds., Ocean Drilling Program, 119, Scientific Results: College Station, Texas, p. 77-132.

Hart, S. R., Blusztajn, J., and Craddock, C., 1995, Cenozoic volcanism in Antarctica: Jones Mountains and Peter I Island: Geochimica et Cosmochimica Acta, v. 59, p. 3379-3388.

Hole, M. J., and LeMasurier, W. E., 1994, Tectonic controls on the geochemical composition of Cenozoic mafic alkaline volcanic rocks from West Antarctica: Contributions to Mineralogy and Petrology, v. 117, p. 187-202.

Hollin, J. T., 1962, On the glacial history of Antarctica: Journal of Glaciology, v. 4, p. 173-195.

Honnorez, J., and Kirst, P., 1975, Submarine basaltic volcanism: morphometric parameters for discriminating hyaloclastites from hyalotuffs: Bulletin of Volcanology, v. 39, p. 1-25.

Houghton, B. F., and Schmincke, H.-U., 1986, Mixed depositions of simultaneous strombolian and phreatomagmatic volcanism: Rothenberg volcano, East Eifel volcanic field: Journal of Volcanology and Geothermal Research, v. 30, p. 117-130.

Hu, Q., Smith, P. E., Evensen, N. M., and York, D., 1994, Lasing in the Holocene: extending the ^{40}Ar-^{39}Ar laser probe method into the ^{14}C age range: Earth and Planetary Science Letters, v. 123, p. 331-336.

Hughes, T. J., 1973, Is the West Antarctic Ice Sheet disintegrating?: Journal of Geophysical Research, v. 78, p. 7884-7910.

Hughes, T. J., 1987, Ice dynamics and deglaciation models when ice sheets collapsed, *in* Jr., W. F. Ruddiman and H. E. Wright, ed., The Geology of North America: Boulder, Geological Society of America, p. 183-220.

Huybrechts, P., 1993, Glaciological modelling of the late Cenozoic East Antarctic Ice Sheet: stability or dynamism?: Geografiska Annaler, v. 75A, p. 221-238.

Jones, J. G., 1969, Intraglacial volcanoes of the Laugarvatn Region, south-west Iceland, I: Geological Society of London Quarterly Journal, v. 124, p. 197-211.

Jones, J. G., 1970, Intraglacial volcanoes of the Laugarvatn Region, south-west Iceland, II: Journal of Geology, v. 78, p. 127-140.

Jones, J. G., and Nelson, P. H. H., 1970, The flow of basalt lava from air into water- its structural expression and stratigraphic significance: Geological Magazine, v. 107, p. 13-19.

Jouzel, J., Raisbeck, G., Benoist, J. P., Yiou, F., Lorius, C., Raynaud, D., Petit, J. R., Barkov, N. I., Korotkevitch, Y. S., and Kotlyakov, V. M., 1989, A comparison of deep Antarctic ice cores and their implications for climate between 65,000 and 15,000 years ago: Quaternary Research, v. 31, p. 135-150.

Karlen, W., and Melander, O., 1978, Reconnaissance of the glacial geology of Hobbs Coast and Ruppert Coast, Marie Byrd Land: Antarctic Journal of the U.S., v. 13, p. 46-47.

Kellogg, D. E., and Kellogg, T. B., 1996, Diatoms in South Pole ice: Implications for eolian contamination of Sirius Group deposits: Geology, v. 24, p. 115-118.

Kellogg, T. B., and Kellogg, D. E., 1987, Recent glacial history and rapid ice-stream retreat in the Amundsen Sea: Journal of Geophysical Research.

Kellogg, T. B., Truesdale, R. S., and Osterman, L. E., 1979, Late Quaternary extent of the West Antarctic ice sheet: New evidence from Ross Sea cores: Geology, v. 7, p. 249-253.

Kennett, J. P., 1977, Cenozoic evolution of Antarctic glaciation, the Circum-Antarctic Ocean, and their impact global paleo-oceanography: Journal of Geophysical Research, v. 82, p. 3843-3860.

Kennett, J. P., 1995, A review of polar climatic evolution during the Neogene, based on the marine sediment record, *in* Vrba, E. S., Denton, G. H., Partridge, T. C., and Burckle, L. H., eds., Paleoclimate and evolution, with emphasis on human origins: New Haven and London, Yale University Press, p. 49-64.

Kennett, J. P., and Barker, P. F., 1990, Latest Cretaceous to Cenozoic climate and oceanographic developments in the Weddell Sea, Antarctica: an ocean-drilling perspective, *in* Barker, P. F., and Kennett, J. P. e. a., eds., Proceedings of the Ocean Drilling Program, scientific results, vol. 113: Washington, U.S. Government Printing Office, p. 937-958.

Kokelaar, B. P., 1983, The mechanism of surtseyan volcanism: Journal of the Geological Society of London, v. 140, p. 939-944.

Kokelaar, B. P., 1986, Magma-water interactions in subaqueous and emergent basaltic volcanism: Bulletin of Volcanology, v. 48, p. 275-289.

Kyle, P. R., 1990, McMurdo Volcanic Group- western Ross Embayment, *in* Thomson, W. E. L. a. J. W., ed., Volcanoes of the Antarctic Plate and Southern Oceans: Washington, D.C., AGU, p. 19-25.

Kyle, P. R., McIntosh, W. C., Panter, K. S., and Smellie, J. L., 1991, Is volcanism in Marie Byrd Land related to a mantle plume?, *in* Sixth International Symposium on Antarctic Earth Sciences, Saitama, Japan, p. 337.

LeBas, M. J., LeMaitre, R. W., Streckeisen, A., and Zanettin, B., 1986, A chemical classification volcanic rocks based on the total alkali-silica diagram: Journal of Petrology, v. 27, p. 745-750.

LeMasurier, W. E., 1972a, Volcanic record of Antarctic glacial history: Implications with regard to Cenozoic sea levels, *in* Price, R. J., and Sugden, D. E., eds., Polar Geomorphology, Special Publication 4: London, Institute of British Geographers, p. 59-74.

LeMasurier, W. E., 1972b, Volcanic record of Cenozoic glacial history in Marie Byrd Land, *in* Adie, R. J., ed., Antarctic Geology and Geophysics: Oslo, Universitetsforlaget, p. 251-260.

LeMasurier, W. E., 1976, Intraglacial volcanoes in Marie Byrd Land: Antarctic Journal of the United States, v. 11, no. 4, p. 269-270.

LeMasurier, W. E., 1976, Intraglacial volcanoes in Marie Byrd Land: Antarctic Journal of the United States, v. 11, p. 269-270.

LeMasurier, W. E., and Landis, C. A., 1996, Mantle-plume activity recorded by low-relief erosion surfaces in West Antarctica and New Zealand: Geological Society of America Bulletin, v. 108, p. 1450-1466.

LeMasurier, W. E., and Rex, D. C., 1982, Volcanic record of Cenozoic glacial history in Marie Byrd Land and western Ellsworth Land: Revised chronology and evaluation of tectonic factors., *in* Craddock, C., ed., Antarctic Geoscience: Madison, University of Wisconsin Press, p. 725-734.

LeMasurier, W. E., and Rex, D. C., 1983, Rates of uplift and the scale of ice level instabilities recorded by volcanic rocks in Marie Byrd Land, West Antarctica, *in* Oliver, R. L., James, P. R., and Jago, J. B., eds., Antarctic Earth Sciences: Canberra, Australian Academy of Science, p. 660-673.

LeMasurier, W. E., and Rex, D. C., 1989, Evolution of linear volcanic ranges in Marie Byrd Land, West Antarctica: Journal of Geophysical Research, v. 94, p. 7223-7236.

LeMasurier, W. E., and Rex, D. R., 1991, The Marie Byrd Land Volcanic Province and its relation to the Cainozoic West Antarctic rift system, *in* Tingey, R. J., ed., The geology of Antarctica: Oxford, Clarendon Press, p. 249-284.

LeMasurier, W. E., and Thomson, J. E., 1990, Volcanoes of the Antarctic Plate and Southern Oceans, Antarctic Research Series: Washington, D.C., AGU, p. 146-163.

LeMasurier, W. E., Harwood, D. M., and Rex, D. C., 1994, Geology of Mount Murphy Volcano: An 8-m.y. history of interaction between a rift volcano and the West Antarctic ice sheet: Geological Society of America Bulletin, v. 106, p. 265-280.

LeMasurier, W. E., Melander, O., Grindley, G. W., and McIntosh, W. C., 1979, Tillite, glacial striae and hyaloclastite associations on Hobbs Coast, Marie Byrd Land: Antarctic Journal of the United States, v. 14, p. 48-50.

MacAyeal, D., 1992, Irregular oscillations of the West Antarctic ice sheet: Nature, v. 27, p. 321-325.

Major, J. J., and Newhall, C. G., 1989, Snow and ice perturbation during historical eruptions and the formation of lahars and floods: Bulletin of Volcanology, v. 52, p. 1-27.

Mathews, W. H., "Tuyas," flat-topped volcanoes in northern British Columbia: American Journal of Science, v. 245, p. 560-570.

McDougall, I., and Harrison, T. M., 1988, Geochronology and thermochronology by the $^{40}Ar/^{39}Ar$ method: New York, Oxford University Press.

McIntosh, W. C., and Gamble, J.A., 1991, A subaerial eruptive environment for the Hallett Coast volcanoes, *in* Thomson, M. R. A., Crame, J. A., and Thomson, J. W., eds., Geological evolution of Antarctica: Cambridge, England, Cambridge University Press, p. 657-661.

McIntosh, W. C., LeMasurier, W. E., Ellerman, P. J., and Dunbar, N. W., 1985, A reinterpretation of glaciovolcanic interaction at Mount Takake and Mount Murphy, Marie Byrd Land, Antarctica: Antarctic Journal of the United States, v. 19, p. 57-59.

McIntosh, W. C., Smellie, J. L., and Panter, K. S., 1991, Glaciovolcanic interaction in eastern Marie Byrd Land, Antarctica, *in* Sixth International Symposium on Antarctic Earth Sciences, Saitama, Japan, p. 402.

McPhie, J., Doyle, M., and Allen, R., 1993, Volcanic textures: a guide to the interpretation of textures in volcanic rocks: Hobart, Tasmania, Centre for Ore Deposit and Exploration Studies, University of Tasmania, 198 p.

Mercer, J. H., 1978, West Antarctic ice sheet and CO2 greenhouse effect: a threat of disaster: Nature, v. 271, p. 321-325.

Miller, K. G., 1985, Oligocene to Miocene carbon isotope cycles and abyssal circulation changes, *in* Sundquist, E. T., and Broecker, W. S., eds., The carbon cycle and atmospheric natural variations Archean to present, American Geophysical Union, p. 469-486.

Moore, J. G., 1975, Mechanism of formation of pillow lava: American Scientist, v. 63, p. 269-277.

Palais, J. M., Kyle, P. R., McIntosh, W. C., and Seward, D., 1988, Magmatic and phreatomagmatic volcanic activity at Mount Takahe, West Antarctica based on tephra layers in the Byrd ice core and field observations at Mt. Takahe: Journal of Volcanology and Geothermal Research, v. 35, p. 295-317.

Panter, K. S., McIntosh, W. C., and Smellie, J. L., 1994, Volcanic history of Mount Sidley, a major alkaline volcano in Marie Byrd Land, Antarctica: Bulletin of Volcanology, v. 56, p. 361-376.

Paterson, W. S. B., 1981, The physics of glaciers, 2nd edition: Oxford, Pergamon Press, 380 p.

Raymo, M. E., Ruddiman, W. F., Backman, J., Clement, B. M., and Martinson, D. G., 1989, Late Pliocene variation in Northern Hemisphere ice sheet and North Atlantic deep water circulation: Paleoceanography, v. 4, no. 4, p. 413-446.

Raynaud, D., and Whillans, I. M., 1982, Air content of the Byrd core and past changes in the West Antarctic Ice Sheet: Annals of Glaciology, v. 3, p. 269-273.

Samson, S. D., and Alexander, C. E., 1987, Calibration of the interlaboratory $^{40}Ar/^{39}Ar$ dating standard, Mmhb-1: Isotope Geoscience, v. 66, p. 27-34.

Savin, S. M., Douglas, R. G., and Stehli, F., 1975, Tertiary marine paleotemperatures: Bulletin of the Geological Society of America, v. 86, p. 1499-150.

Scherer, R. P., 1991, Quaternary and Tertiary microfossils from beneath Ice Stream B: Evidence for a dynamic West Antarctic Ice Sheet history: Palaeogeography, Palaeoclimatology, Palaeoecology, v. 90, p. 395-412.

Shackleton, N. J., and Kennett, J. P., 1975, Paleotemperature history of the Cenozoic and the initiation of Antarctic glaciation: oxygen and carbon isotope analyses in DSDP Sites 277, 279, and 281, *in* Kennett, J. P., and Houtz, R. E., eds., Initial Reports of the Deep Sea Drilling Project 29: Washington D.C., U.S. Government Printer, p. 743-755.

Sigvaldason, G. E., Annertz, K., and Nilsson, M., 1992, Effect of glacier loading/deloading on volcanism: postglacial volcanic production rate of the Dyngjufjoll area, central Iceland: Bulletin of Volcanology, v. 54, p. 385-392.

Singer, B. S., Thompson, R. A., Dungan, M. A., Teeley, T. C., Nelson, S. T., Pickens, J. C., Brown, L. L., Wulff, A. W., Davidson, J. P., and Metzger, J., 1997, Volcanism and erosion during the past 930 k.y. at the Tatara-San Pedro complex, Chilean Andes: Geological Society of America Bulletin, v. 109, p. 127-142.

Skilling, I. P., 1994, Evolution of an englacial volcano: Brown Bluff, Antarctica: Bulletin of Volcanology, v. 56, p. 573-591.

Smellie, J. L., and Hole, M. J., 1997, Products and processes in Pliocene-Recent, subaqueous to emergent volcanism in the Antarctic Peninsula: example of englacial Surtseyan volcano construction: Bulletin of Volcanology, v. 58, p. 628-646.

Smellie, J. L., and Skilling, I. P., 1994, Products of subglacial volcanic eruptions under different ice thicknesses two examples form Antarctica: Sedimentary Geology, v. 91, p. 115-129.

Smellie, J. L., Hole, M. J., and Nell, P. A. R., 1993, Late Miocene valley-confined subglacial volcanism in northern Alexander Island, Antarctic Peninsula: Bulletin of Volcanology, v. 55, p. 273-288.

Smellie, J. L., McIntosh, W. C., Gamble, J. A., and Panter, K. S., 1990, Preliminary stratigraphy of volcanoes in the Executive Committee Range, central Marie Byrd Land: Antarctic Science, v. 2, p. 353-354.

Sohn, Y. K., 1995, Geology of Tok Island, Korea: eruptive and depositional processes of a shoaling to emergent island volcano: Bulletin of Volcanology, v. 56, p. 660-674.

Sohn, Y. K., 1996, Hydrovolcanic processes forming basaltic tuff rings and cones on Cheju Island, Korea: Geological Society of America Bulletin, v. 108, p. 1199-1211.

Sohn, Y. K., and Chough, S. K., 1989, Depositional processes of the Suwolbong tuff ring, Cheju Island (Korea): Sedimentology, v. 36, p. 837-855.

Sohn, Y. K., and Chough, S. K., 1990, Depositional mechanics and sequences of base surges, Songaksan tuff ring, Cheju Island, Korea: Sedimentology, v. 37, p. 1115-1135.

Sohn, Y. K., and Chough, S. K., 1992, The Ilchulbong tuff cone, Cheju Island, South, Korea: depositional processes and evolution of an emergent Sursetyan-type tuff cone: Sedimentology, v. 39, p. 523-544.

Sohn, Y. K., and Chough, S. K., 1992, The Ilchulbong tuff cone, Cheju Island, South, Korea: depositional processes and evolution of an emergent Sursetyan-type tuff cone: Sedimentology, v. 39, p. 523-544.

Sohn, Y. K., and Chough, S. K., 1993, The Duo tuff cone, Cheju Island, South Korea: transformation of pyroclastic fall into debris fall and grain flow on a steep volcanic cone slope: Sedimentology, v. 40, p. 769-786.Baker, P. E., 1969, A volcano erupts beneath the Antarctic ice: Geographical Magazine, v. 41, p. 115-126.

Steiger, R. H., and Jaeger, E., 1977, Subcommission on Geochronology: Convention of the use of decay constants in geo- and cosmochronology: Earth and Planetary Science Letters, v. 36, p. 359-362.

Stroeven, A. P., and Prentice, M. L., 1997, A case for Sirius Group alpine glaciation at Mount Fleming, South Victoria Land, Antarctica: A case against Pliocene East Antarctic Ice Sheet reduction: Geological Society of America Bulletin, v. 109, p. 825-840.

Stuiver, M., Denton, G. H., Hughes, T. J., and Fastook, J. L., 1981, History of the marine ice sheet in West Antarctica during the last glaciation: A working hypothesis, *in* Denton, G. H., and Hughes, T. J., eds., The Last Great Ice Sheets: New York, Wiley-Interscience, p. 319-349.

Sugden, D. E., Marchant, D. R., and Denton, G. H., 1993, The case for a stable East Antarctic Ice Sheet: the background: Geografiska Annaler, v. 75A, p. 151-154.

Thomas, R. H., and Bentley, C. R., 1978, A model for Holocene retreat of the West Antarctic Ice Sheet: Quaternary Research, v. 10, p. 150-170.

Tribble, G. W., 1991, Underwater observation of active lava flows from Kilauea Volcano, Hawaii: Geology, v. 19, p. 633-636.

van den Bogaard, P., 1995, $^{40}Ar/^{39}Ar$ ages of sanidine phenocrysts from Laacher See Tephra (12,900 yr BP): Chronostratigraphic and petrological significance: Earth and Planetary Science Letters, v. 133, p. 163-174.

Walker, G. P. L., 1992, Morphometric study of pillow-size spectrum among pillow lavas: Bulletin of Volcanology, v. 54, p. 459-474.

Walker, G. P. L., and Blake, D.H., B., 1966, The formation of a palagonite breccia mass beneath a valley glacier in Iceland: Quarterly Journal of the Royal Society of London, v. 122, p. 45-61.

Walker, G. P. L., and Croasdale, R., 1972, Characteristics of some basaltic pyroclastics: Bulletin of Volcanology, v. 35, p. 303-317.

Webb, P.-N., and Harwood, D. M., 1991, Late Cenozoic glacial history of the Ross Embayment, Antarctica: Quaternary Science Reviews, v. 10, p. 215-224.

Wilch, T. I., Lux, D. R., Denton, G. H., and McIntosh, W. C., 1993, Minimal Pliocene-Pleistocene uplift of the dry valleys sector of the Transantarctic Mountains: A key parameter in ice-sheet reconstructions: Geology, v. 21, no. 9, p. 841-844.

Wilson, G. S., 1995, The Neogene East Antarctic Ice Sheet: a dynamic or stable feature?: Quaternary Science Reviews, v. 14, p. 101-123.

Wohletz, K. H., 1983, Mechanisms of hydrovolcanic pyroclast formation: grain-size, scanning electron microscopy, and experimental studies: Journal of Volcanology and Geothermal Research, v. 16, p. 31-63.

Wohletz, K. H., and Sheridan, M. F., 1983, Hydrovolcanic explosions II. Evolution of basaltic tuff rings and tuff cones: American Journal of Science, v. 283, p. 385-413.

Wörner, G., and Viereck, L., 1987, Subglacial to emergent volcanism at Shield Nunatak, Mt. Melbourne Volcanic Field, Antarctica: Polarforschung, v. 57, p. 27-41.

Yamagishi, H., 1991, Morphological and sedimentological characteristics of the Neogene submarine coherent lavas and hyaloclastites in Southwest Hokkaido, Japan, In: R.Cas and C. Busby-Spera (Editors), Volcaniclastic Sedimentation: Sedimentary Geology, v. 74, p. 5-23.

Appendix I: $^{40}Ar/^{39}Ar$ Analytical Data

Analytical data are organized in the following manner:

First, furnace step-heating data are presented in the order that they appear in Table 1.

Second, laser data are presented in the order that they appear in Table 1.

Appendix I. $^{40}Ar/^{39}Ar$ Analytical Data

ID	Temp (°C)	$^{40}Ar/^{39}Ar$	$^{37}Ar/^{39}Ar$	$^{36}Ar/^{39}Ar$ (x 10^{-3})	$^{39}Ar_K$ (x 10^{-15} mol)	K/Ca	Cl/K (x 10^{-3})	$^{40}Ar^*$ (%)	^{39}Ar (%)	Age (Ma)	±2s (Ma)
WCM90-69, U3:17, whole rock, 51.0 mg, J=0.0007939±0.13%, nm-17, Lab#=1860-01											
Mt. Murphy, Sechrist Peak											
C	750	1.574	1.775	4.372	11.2	0.29	34.3	25.4	20.0	0.572	0.054
D	850	1.865	2.823	5.574	16.0	0.18	23.7	22.3	48.7	0.596	0.049
E	950	1.132	2.381	2.971	9.69	0.21	20.3	36.9	66.0	0.600	0.065
F	*1050*	*2.435*	*4.869*	*7.557*	*3.61*	*0.10*	*11.3*	*22.9*	*72.5*	*0.80*	*0.14*
G	*1150*	*2.184*	*5.415*	*6.507*	*3.18*	*0.094*	*12.3*	*30.1*	*78.2*	*0.95*	*0.16*
H	*1250*	*1.436*	*7.841*	*5.261*	*7.37*	*0.065*	*17.0*	*32.4*	*91.4*	*0.669*	*0.079*
I	*1400*	*3.473*	*37.64*	*20.21*	*4.10*	*0.014*	*12.6*	*10.8*	*98.7*	*0.55*	*0.19*
J	*1650*	*17.58*	*42.16*	*63.99*	*0.719*	*0.012*	*2.1*	*10.8*	*100.0*	*2.79*	*0.95*
total gas age			n=8		55.9	0.17				0.66	0.15
natural plateau			n=3	steps C-E	36.9	0.22			66.0	0.587	0.043
WCM93-139B, WR 54.5 MG, J=0.0007902±0.13%, NM-17, Lab#=1866-01											
Mt. Murphy, Sechrist Peak											
A	*500*	*143.4*	*3.039*	*465.8*	*0.046*	*0.17*	*65.4*	*4.1*	*0.1*	*8.4*	*12.7*
B	600	26.29	2.783	88.84	0.574	0.18	64.4	0.9	0.8	0.34	0.92
C	700	4.501	1.934	14.40	5.78	0.26	48.3	8.3	8.0	0.54	0.11
D	800	1.274	2.354	3.464	18.5	0.22	29.4	32.3	31.0	0.588	0.030
E	900	1.527	2.250	4.292	14.7	0.23	35.5	27.0	49.3	0.59	0.38
F	1000	1.770	2.315	5.109	11.6	0.22	32.5	23.7	63.7	0.599	0.050
G	1100	1.942	2.888	5.830	7.75	0.18	14.2	21.7	73.3	0.603	0.075
H	1200	3.443	3.984	10.96	3.32	0.13	13.3	14.2	77.4	0.70	0.15
I	1300	2.753	11.04	10.82	15.3	0.046	16.9	14.0	96.4	0.552	0.060
J	*1400*	*4.638*	*18.94*	*18.41*	*2.88*	*0.027*	*14.7*	*13.6*	*100.0*	*0.91*	*0.21*
total gas age			n=10		80.4	0.18				0.60	0.18
natural plateau			n=8	steps B-I	77.5	0.18			96.4	0.592	0.040

Appendix I. $^{40}Ar/^{39}Ar$ Analytical Data

ID	Temp (°C)	$^{40}Ar/^{39}Ar$	$^{37}Ar/^{39}Ar$	$^{36}Ar/^{39}Ar$ (x 10^{-3})	$^{39}Ar_K$ (x 10^{-15} mol)	K/Ca	Cl/K (x 10^{-3})	$^{40}Ar^*$ (%)	^{39}Ar (%)	Age (Ma)	±2s (Ma)
WCM90-37a:w3:NM-1, whole rock 8.3 mg, J=0.004339884, NMUM-1, Lab#=704-01											
Mt. Murphy basal section of main shield, 1820'											
A	*550*	*56.58*	*1.025*	*190.5*	*0.885*	*0.50*	*5.0*	*0.6*	*0.9*	*2.8*	*8.2*
B	*625*	*14.61*	*1.305*	*45.88*	*4.48*	*0.39*	*3.0*	*7.8*	*5.2*	*8.9*	*1.5*
C	*700*	*6.033*	*1.228*	*16.57*	*11.2*	*0.42*	*1.0*	*20.1*	*16.1*	*9.48*	*0.63*
D	775	2.138	0.9924	3.501	26.4	0.51	0.38	54.3	42.0	9.08	0.15
E	800	1.585	0.9373	1.790	13.3	0.54	0.43	70.0	55.0	8.67	0.17
F	1000	1.466	1.183	1.418	27.8	0.43	0.44	76.4	82.1	8.755	0.089
G	1200	1.925	14.05	6.453	14.3	0.036	4.9	56.1	96.0	8.51	0.29
H	*1700*	*3.158*	*22.55*	*12.39*	*4.06*	*0.023*	*4.0*	*38.4*	*100.0*	*9.61*	*0.78*
total gas age			n=8		102	0.39				8.86	0.37
selected mean			n=4	steps D-G	81.9	0.41			79.9	8.80	0.20
WCM90-37,w4:nmum-1, Thom's whole rock, J=0.004401057±0.23%, NMUM-1, Lab#=61-01											
Mt. Murphy basal section of main shield, 1820'											
B	*590*	*88.42*	*0.7342*	*294.5*	*0.040*	*0.69*	*2.7*	*1.6*	*0.03*	*11*	*33*
C	*690*	*8.285*	*0.9319*	*24.71*	*2.22*	*0.55*	*1.5*	*12.5*	*1.7*	*8.23*	*0.87*
D	800	2.792	1.108	5.862	30.4	0.46	0.57	40.4	25.0	8.93	0.12
E	198	1.477	1.185	1.508	36.1	0.43	0.26	74.8	52.5	8.756	0.056
F	495	1.622	1.377	2.013	15.7	0.37	0.43	68.7	64.5	8.840	0.097
G	244	2.344	1.542	4.441	10.1	0.33	1.5	48.3	72.3	8.98	0.14
H	304	1.924	2.934	3.312	14.3	0.17	3.6	59.9	83.2	9.14	0.11
I	*268*	*2.285*	*28.02*	*10.46*	*13.3*	*0.018*	*7.8*	*58.1*	*93.3*	*10.71*	*0.23*
J	*1450*	*2.829*	*14.46*	*6.418*	*7.74*	*0.035*	*2.4*	*71.6*	*99.2*	*16.17*	*0.18*
K	*1737*	*7.605*	*2.173*	*13.81*	*1.00*	*0.23*	*0.087*	*48.3*	*100.0*	*29.0*	*1.2*
total gas age			n=10		131	0.33				9.65	0.16
plateau			n=5	steps D-H	107	0.39			81.5	8.86	0.15
WCM90-39:w5:NM-1, whole rock 8.8 mg, J=0.004327609, NMUM-1, Lab#=705-01											
Mt. Murphy basal section of main shield, 1320'											
B	625	5.795	1.808	15.81	18.1	0.28	0.082	21.5	19.3	9.71	0.49
C	700	1.458	1.912	1.347	40.8	0.27	-0.205	81.5	62.9	9.272	0.093
D	775	1.268	2.569	0.8971	21.0	0.20	-0.025	93.2	85.3	9.22	0.12
E	*800*	*1.316*	*2.900*	*0.9345*	*3.44*	*0.18*	*0.036*	*94.6*	*88.9*	*9.71*	*0.43*
F	*1000*	*1.489*	*3.387*	*1.576*	*6.70*	*0.15*	*0.52*	*85.0*	*96.1*	*9.88*	*0.30*
G	*1200*	*1.569*	*67.05*	*19.04*	*2.80*	*0.008*	*3.1*	*68.7*	*99.1*	*8.8*	*1.1*
H	*1700*	*7.725*	*82.50*	*39.66*	*0.872*	*0.006*	*3.1*	*30.1*	*100.0*	*19.1*	*2.6*
total gas age			n=7		93.7	0.23				9.48	0.26
natural plateau			n=3	steps B-D	79.9	0.25			85.3	9.26	0.14
WCM90-39,w6:nmum-1, Thom's whole rock, J=0.004390248±0.23%, NMUM-1, Lab#=63-01											
Mt. Murphy basal section of main shield, 1320'											
B	620	2.009	2.970	3.802	2.30	0.17	-0.215	54.5	2.7	8.68	0.47
C	711	1.438	3.260	1.820	9.30	0.16	-0.158	78.8	13.6	8.97	0.18
D	752	1.247	3.293	1.152	26.6	0.15	-0.085	91.5	44.9	9.040	0.055
E	800	1.257	3.006	1.061	22.9	0.17	-0.056	92.0	71.8	9.158	0.073
F	850	1.305	3.192	1.380	10.8	0.16	0.081	86.2	84.5	8.90	0.12
G	900	1.327	3.205	1.537	6.45	0.16	0.41	83.0	92.0	8.72	0.18
I	*1732*	*14.92*	*18.99*	*39.18*	*0.484*	*0.027*	*-0.382*	*32.0*	*92.6*	*38.0*	*2.6*
K	*1250*	*1.373*	*85.43*	*23.75*	*4.92*	*0.006*	*3.5*	*65.7*	*98.4*	*7.56*	*0.71*

Appendix I. $^{40}Ar/^{39}Ar$ Analytical Data

ID	Temp (°C)	$^{40}Ar/^{39}Ar$	$^{37}Ar/^{39}Ar$	$^{36}Ar/^{39}Ar$ (x 10^{-3})	$^{39}Ar_K$ (x 10^{-15} mol)	K/Ca	Cl/K (x 10^{-3})	$^{40}Ar^*$ (%)	^{39}Ar (%)	Age (Ma)	±2s (Ma)
J	*1450*	*2.941*	*115.0*	*33.18*	*1.36*	*0.004*	*3.4*	*66.5*	*100.0*	*16.7*	*1.7*
total gas age			n=9		85.1	0.15				9.21	0.21
selected mean			n=6	steps B-G	78.3	0.16			92.0	9.03	0.12
WCM90-33, w2:nmum-1, Thom's whole rock, J=0.004408342±0.23%, NMUM-1, Lab#=62-01											
Mt. Murphy basal section of main shield, 1210'											
A	*623*	*2.597*	*1.400*	*5.377*	*8.19*	*0.36*	*2.1*	*42.3*	*4.4*	*8.72*	*0.23*
B	*715*	*1.471*	*1.113*	*1.186*	*36.5*	*0.46*	*0.29*	*80.8*	*23.8*	*9.430*	*0.067*
C	800	1.294	1.407	0.8037	70.9	0.36	-0.022	88.6	61.4	9.107	0.099
D	850	1.327	2.549	1.226	25.4	0.20	0.27	86.1	74.9	9.077	0.063
E	900	1.419	3.475	1.816	13.4	0.15	0.93	79.7	82.1	8.99	0.11
F	*1000*	*1.549*	*4.490*	*2.665*	*14.7*	*0.11*	*2.3*	*70.3*	*89.9*	*8.66*	*0.13*
G	*1250*	*1.815*	*27.66*	*9.713*	*17.4*	*0.018*	*15.4*	*58.0*	*99.1*	*8.50*	*0.17*
H	*1450*	*3.410*	*19.13*	*12.44*	*1.18*	*0.027*	*9.8*	*34.8*	*99.8*	*9.53*	*0.90*
I	*1737*	*11.60*	*3.904*	*30.41*	*0.450*	*0.13*	*2.5*	*25.0*	*100.0*	*22.9*	*2.8*
total gas age			n=9		188	0.29				9.09	0.13
natural plateau			n=3	steps C-E	110	0.30			58.3	9.07	0.09
WCM90-33:w1:NM-1, whole rock 10.0 mg, J=0.004347777, NMUM-1, Lab#=703-01											
Mt. Murphy basal section of main shield, 1210'											
A	650	1.855	1.226	2.469	18.1	0.42	0.30	64.8	21.9	9.40	0.15
B	725	1.508	1.476	1.384	28.1	0.35	0.057	79.2	55.9	9.36	0.12
C	800	1.677	2.354	2.135	14.3	0.22	0.39	72.1	73.1	9.48	0.19
D	900	2.189	3.543	4.131	7.69	0.14	1.7	55.9	82.4	9.59	0.39
E	1000	2.305	4.626	5.076	4.81	0.11	4.1	49.6	88.2	8.97	0.50
F	1200	2.463	31.22	12.40	8.81	0.016	20.5	47.9	98.9	9.42	0.62
G	*1400*	*29.59*	*16.06*	*97.01*	*0.864*	*0.032*	*8.6*	*7.2*	*99.9*	*16.9*	*4.6*
H	*1700*	*177.8*	*19.69*	*521.7*	*0.043*	*0.026*	*15.4*	*14.1*	*100.0*	*189*	*90*
total gas age			n=8		82.7	0.27				9.57	0.34
natural plateau			n=6	steps A-F	81.8	0.27			98.9	9.39	0.12
WCM90-50:w8:NM-1, whole rock 45.7 mg, J=0.00438209, NMUM-1, Lab#=706-01											
Mt. Murphy basal section of main shield, stratigraphically lower than 1210'											
B	625	6.260	1.586	17.64	22.3	0.32	21.2	18.4	7.1	9.09	0.63
C	700	2.068	1.963	3.380	76.7	0.26	4.9	58.1	31.7	9.49	0.11
D	775	1.319	3.313	1.305	96.1	0.15	0.33	88.7	62.5	9.249	0.066
E	900	1.465	3.454	1.791	48.4	0.15	1.0	80.8	78.0	9.348	0.094
F	*1000*	*1.705*	*3.526*	*2.920*	*19.7*	*0.14*	*2.0*	*64.2*	*84.3*	*8.66*	*0.19*
G	*1200*	*1.722*	*22.91*	*8.292*	*38.2*	*0.022*	*1.9*	*58.9*	*96.5*	*8.12*	*0.27*
H	*1700*	*2.225*	*26.42*	*10.58*	*10.9*	*0.019*	*2.6*	*49.9*	*100.0*	*8.92*	*0.42*
total gas age			n=7		312	0.17				9.13	0.18
selected mean			n=4	steps B-E	244	0.20			78.0	9.32	0.13

Appendix I. $^{40}Ar/^{39}Ar$ Analytical Data

ID	Temp (°C)	$^{40}Ar/^{39}Ar$	$^{37}Ar/^{39}Ar$	$^{36}Ar/^{39}Ar$ (x 10^{-3})	$^{39}Ar_K$ (x 10^{-15} mol)	K/Ca	Cl/K (x 10^{-3})	$^{40}Ar^*$ (%)	^{39}Ar (%)	Age (Ma)	±2s (Ma)
WCM90-50:w10:NM-1, whole rock 40.5 mg, J=0.004303745, NMUM-1, Lab#=707-01											
Mt. Murphy basal section of main shield, stratigraphically lower than 1210'											
B	625	5.135	0.8707	13.28	53.6	0.59	39.2	24.5	17.9	9.75	0.37
C	675	2.155	1.755	3.526	54.3	0.29	7.7	57.1	36.0	9.54	0.14
D	725	1.354	2.837	1.159	64.4	0.18	0.75	89.5	57.5	9.402	0.074
E	750	1.312	3.616	1.293	39.6	0.14	0.23	90.7	70.8	9.236	0.093
F	800	1.391	3.643	1.510	28.6	0.14	0.18	86.7	80.3	9.36	0.11
G	900	1.665	3.711	2.563	20.2	0.14	0.51	70.6	87.0	9.12	0.16
H	*1000*	*1.815*	*4.422*	*3.380*	*11.3*	*0.12*	*0.85*	*62.7*	*90.8*	*8.84*	*0.27*
I	*1200*	*1.953*	*36.67*	*12.85*	*21.6*	*0.014*	*3.3*	*48.9*	*98.0*	*7.59*	*0.45*
J	*1700*	*2.912*	*40.95*	*16.14*	*5.95*	*0.012*	*4.3*	*43.7*	*100.0*	*10.12*	*0.72*
total gas age			n=9		299	0.24				9.31	0.21
selected mean			n=6	steps B-G	261	0.27			87.0	9.35	0.13
WCM90-110, V1:17, whole rock, 45.4 mg, J=0.0007997±0.13%, nm-17, Lab#=1862-01											
Mt. Murphy, Hedin Nunatak											
B	600	15362.4	2.168	51072.4	0.160	0.24	53.2	1.8	0.2	354	1421
BB	0	891.9	1.394	2914.6	5.06	0.37	39.4	3.4	7.8	43.9	14.4
C	750	301.8	0.7893	961.2	1.14	0.65	44.7	5.9	9.5	25.5	5.1
D	850	61.69	1.703	184.9	10.2	0.30	31.7	11.6	24.7	10.31	0.93
E	950	41.07	1.887	116.7	8.71	0.27	26.7	16.3	37.7	9.66	0.63
F	1050	23.45	2.289	60.92	8.22	0.22	19.5	23.9	49.9	8.08	0.35
G	1150	13.40	2.358	29.38	9.56	0.22	13.4	36.4	64.2	7.04	0.18
H	1250	10.93	4.113	21.95	13.3	0.12	21.2	43.4	84.0	6.84	0.13
I	1400	19.31	18.21	52.01	9.54	0.028	35.5	27.5	98.2	7.76	0.29
J	1650	58.23	18.41	179.5	1.18	0.028	13.8	11.3	100.0	9.6	1.3
total gas age			n=10		67.1	0.21				12.0	5.0
no plateau			n=10	steps B-J	67.1	0.21			100.0	7.22	0.57
WCM90-47, U1:17, whole rock, 44.1 mg, J=0.0007995±0.13%, nm-17, Lab#=1859-01											
Mt. Murphy, Icefall Nunatak											
B	600	50.79	0.8697	154.4	1.02	0.59	76.0	10.3	1.9	7.5	1.3
C	750	13.92	1.159	31.71	8.32	0.44	42.6	33.2	17.2	6.66	0.28
D	850	6.975	2.471	8.956	12.4	0.21	16.1	64.5	39.9	6.49	0.11
E	950	7.695	2.681	11.23	7.06	0.19	14.0	59.3	52.9	6.58	0.12
F	1050	7.543	3.515	11.51	3.23	0.15	15.3	58.2	58.8	6.34	0.20
G	*1150*	*7.728*	*4.113*	*14.76*	*1.65*	*0.12*	*19.6*	*47.4*	*61.9*	*5.29*	*0.35*
H	*1250*	*8.772*	*7.355*	*17.20*	*16.9*	*0.069*	*43.5*	*48.3*	*92.9*	*6.13*	*0.19*
I	*1400*	*13.33*	*22.98*	*34.73*	*2.96*	*0.022*	*23.5*	*36.1*	*98.4*	*7.04*	*0.28*
J	*1650*	*29.47*	*19.54*	*84.33*	*0.892*	*0.026*	*9.7*	*20.5*	*100.0*	*8.79*	*0.99*
total gas age			n=9		54.4	0.19				6.46	0.25
natural plateau			n=5	steps B-F	32.0	0.27			58.8	6.52	0.13

Appendix I. $^{40}Ar/^{39}Ar$ Analytical Data

ID	Temp (°C)	$^{40}Ar/^{39}Ar$	$^{37}Ar/^{39}Ar$	$^{36}Ar/^{39}Ar$ (x 10^{-3})	$^{39}Ar_K$ (x 10^{-15} mol)	K/Ca	Cl/K (x 10^{-3})	$^{40}Ar^*$ (%)	^{39}Ar (%)	Age (Ma)	±2s (Ma)
WCM90-48, S1:17, whole rock, 42.8 mg, J=0.0008017±0.12%, nm-17, Lab#=1853-01											
Mt. Murphy, Icefall Nunatak											
A	*500*	*4220.2*	*1.617*	*13980*	*1.03*	*0.32*	*36.4*	*2.1*	*2.1*	*124.9*	*169.8*
B	*600*	*398.7*	*1.611*	*1302.7*	*2.59*	*0.32*	*31.9*	*3.5*	*7.4*	*20.0*	*6.1*
C	*750*	*131.6*	*1.809*	*420.6*	*9.46*	*0.28*	*21.3*	*5.7*	*26.9*	*10.8*	*2.1*
D	*850*	*21.08*	*3.635*	*54.49*	*8.22*	*0.14*	*13.7*	*24.9*	*43.8*	*7.59*	*0.30*
E	950	18.53	2.741	47.30	5.82	0.19	10.5	25.6	55.8	6.86	0.27
F	1050	16.07	2.627	38.48	4.29	0.19	9.7	30.4	64.6	7.06	0.30
G	1150	13.92	3.430	30.97	3.93	0.15	9.9	36.0	72.7	7.25	0.23
H	1250	28.22	10.68	81.11	11.2	0.048	18.0	17.9	95.7	7.34	0.50
I	*1400*	*43.97*	*53.76*	*138.0*	*1.66*	*0.009*	*15.5*	*16.6*	*99.2*	*10.92*	*0.88*
J	*1650*	*53.82*	*29.11*	*146.1*	*0.408*	*0.018*	*8.0*	*23.9*	*100.0*	*18.9*	*1.9*
total gas age			n=10		48.6	0.17				11.3	4.6
natural plateau			n=4	steps E-H	25.2	0.12			51.9	7.10	0.25
WCM90-94, T3:17, whole rock, 46.8 mg, J=0.0007952±0.13%, nm-17, Lab#=1857-01											
Mt. Murphy, Turtle Peak, top											
C	750	121.9	1.295	399.7	9.53	0.39	71.3	3.2	15.3	5.6	2.0
D	850	6.871	1.595	12.64	23.1	0.32	65.7	47.1	52.4	4.645	0.080
E	950	12.69	1.561	31.83	14.3	0.33	57.6	26.7	75.3	4.86	0.20
F	1050	23.98	2.981	69.91	4.29	0.17	46.1	14.7	82.2	5.06	0.45
G	1150	34.01	3.855	103.8	4.32	0.13	48.8	10.6	89.1	5.20	0.66
H	1250	28.16	18.96	87.75	4.64	0.027	49.5	13.0	96.6	5.33	0.54
I	*1400*	*20.98*	*75.35*	*72.74*	*1.99*	*0.007*	*36.6*	*25.1*	*99.8*	*7.95*	*0.58*
J	*1650*	*116.8*	*88.24*	*296.0*	*0.135*	*0.006*	*-6.076*	*30.9*	*100.0*	*54.3*	*6.1*
total gas age			n=8		62.3	0.28				5.17	0.58
natural plateau			n=6	steps C-H	60.1	0.29			96.6	4.70	0.15
WCM90-92, U5:17, whole rock, 41.8 mg, J=0.0008153±0.12%, nm-17, Lab#=1861-01											
Mt. Murphy, Turtle Peak, middle											
B	0	12.49	1.796	28.86	2.83	0.28	50.2	32.7	6.5	6.00	0.25
C	0	6.526	3.387	9.590	8.24	0.15	30.4	60.3	25.2	5.79	0.10
D	0	6.487	4.551	9.680	4.74	0.11	28.2	61.0	36.1	5.83	0.13
E	0	6.866	2.855	10.80	6.06	0.18	25.7	56.4	49.9	5.70	0.13
F	0	5.967	4.963	9.336	2.57	0.10	19.7	59.8	55.7	5.26	0.21
G	0	6.102	4.690	10.13	3.11	0.11	24.0	56.6	62.8	5.09	0.22
H	0	9.929	10.97	24.49	12.2	0.047	35.1	35.4	90.6	5.20	0.15
I	*0*	*9.669*	*18.46*	*21.70*	*3.29*	*0.028*	*19.0*	*48.1*	*98.1*	*6.92*	*0.25*
J	*0*	*18.01*	*20.92*	*47.29*	*0.852*	*0.024*	*6.0*	*31.2*	*100.0*	*8.37*	*0.84*
total gas age			n=9		43.8	0.11				5.69	0.22
selected mean			n=7	steps B-H	39.7	0.12			90.6	5.65	0.23

Appendix I. $^{40}Ar/^{39}Ar$ Analytical Data

ID	Temp (°C)	$^{40}Ar/^{39}Ar$	$^{37}Ar/^{39}Ar$	$^{36}Ar/^{39}Ar$ (x 10^{-3})	$^{39}Ar_K$ (x 10^{-15} mol)	K/Ca	Cl/K (x 10^{-3})	$^{40}Ar^*$ (%)	^{39}Ar (%)	Age (Ma)	±2s (Ma)
WCM90-87, Q1:43, 46.28 mg WR, J=0.0006314912, NM-43, Lab#=6064-01											
Mt. Murphy, Turtle Peak, middle											
A	*625*	*8614.9*	*0.8805*	*26418*	*0.105*	*0.58*	*70*	*9.4*	*0.5*	*744.5*	*263.3*
B	*700*	*522.1*	*1.215*	*1636.7*	*2.33*	*0.42*	*4.8*	*7.4*	*11.7*	*43.4*	*7.8*
C	*750*	*128.9*	*1.144*	*392.8*	*0.601*	*0.45*	*2.1*	*10.0*	*14.6*	*14.7*	*2.0*
D	800	52.92	1.483	152.2	7.99	0.34	0.86	15.2	53.2	9.18	0.70
E	875	45.15	2.524	126.3	3.72	0.20	0.60	17.8	71.2	9.13	0.61
F	975	49.43	4.038	139.1	1.70	0.13	0.88	17.5	79.4	9.85	0.70
G	*1075*	*34.17*	*5.159*	*92.46*	*1.09*	*0.099*	*0.88*	*21.2*	*84.6*	*8.26*	*0.59*
H	*1250*	*38.93*	*22.03*	*114.1*	*2.50*	*0.023*	*1.5*	*17.8*	*96.7*	*7.98*	*0.56*
I	*1650*	*59.97*	*10.52*	*173.8*	*0.689*	*0.049*	*1.4*	*15.7*	*100.0*	*10.8*	*1.1*
total gas age			n=9		20.7	0.25				16.8	2.8
plateau			n=3	steps D-F	13.4	0.28			64.7	9.36	0.60
Mt. Takahe (see Part A of dissertation for summit crater data)											
MT-85-1, D1,D2:37, 149 mg, WR , J=0.000219088, NM-37, Lab#=5386-01											
Mt. Takahe, Gill Bluff, pillow interior											
B	*600*	*108.0*	*0.1452*	*373.3*	*5.74*	*3.5*	*0.61*	*-2.1*	*4.2*	*-0.92*	*0.63*
C	700	26.43	0.1306	89.52	23.7	3.9	0.29	-0.1	21.4	-0.01	0.16
D	800	8.367	0.1073	28.08	31.4	4.8	0.23	0.9	44.2	0.030	0.050
E	900	4.957	0.1033	16.63	24.8	4.9	0.22	1.0	62.2	0.020	0.032
F	1000	10.84	0.1640	36.73	16.4	3.1	0.29	0.0	74.1	-0.001	0.069
G	1100	13.01	0.3914	43.74	20.6	1.3	0.34	0.9	89.2	0.047	0.079
H	*1200*	*8.169*	*0.4312*	*26.98*	*11.3*	*1.2*	*0.26*	*2.8*	*97.4*	*0.090*	*0.053*
I	*1300*	*5.733*	*0.3037*	*19.24*	*3.15*	*1.7*	*0.074*	*1.2*	*99.7*	*0.027*	*0.068*
J	*1450*	*5.362*	*0.2264*	*20.23*	*0.436*	*2.3*	*0.63*	*-11.2*	*100.0*	*-0.24*	*0.26*
total gas age			n=9		137.6	3.5				-0.01	0.10
natural plateau			n=5	steps C-G	116.9	3.8			85.0	0.022	0.026
MT-85-2, D3,D4:37, 145.2 mg, WR , J=0.000219093, NM-37, Lab#=5387-01											
Mt. Takahe, Gill Bluff, lava											
B	*600*	*22.85*	*0.0797*	*78.89*	*10.1*	*6.4*	*0.23*	*-2.0*	*7.9*	*-0.18*	*0.14*
C	700	11.30	0.0665	38.24	34.2	7.7	0.26	0.0	34.6	0.002	0.066
D	800	4.315	0.0502	14.35	30.2	10.2	0.30	1.8	58.2	0.031	0.028
E	900	2.912	0.0516	9.575	22.5	9.9	0.22	3.0	75.8	0.034	0.022
F	1000	3.134	0.1284	10.45	13.2	4.0	0.087	1.8	86.1	0.022	0.024
G	1100	3.394	0.5063	11.51	7.80	1.0	0.22	0.9	92.2	0.012	0.030
H	1200	4.104	1.795	14.04	7.33	0.28	0.15	2.3	97.9	0.037	0.032
I	1300	3.537	0.3476	11.67	2.67	1.5	0.23	3.2	100.0	0.045	0.060
total gas age			n=8		127.9	7.2				0.006	0.047
natural plateau			n=7	steps C-I	117.8	7.3			92.1	0.028	0.014
W-85-85, F3-4:36, 135.8 mg, WR , J=0.000212989, NM-36, Lab#=5340-01											
Mt. Takahe, Gill Bluff, pillow interior											
B	*600*	*18.6988*	*0.6238*	*62.3391*	*2.926*	*0.82*	*0.53*	*1.7*	*3.4*	*0.12*	*0.13*

Appendix I. $^{40}Ar/^{39}Ar$ Analytical Data

ID	Temp (°C)	$^{40}Ar/^{39}Ar$	$^{37}Ar/^{39}Ar$	$^{36}Ar/^{39}Ar$ (x 10^{-3})	$^{39}Ar_K$ (x 10^{-15} mol)	K/Ca	Cl/K (x 10^{-3})	$^{40}Ar^*$ (%)	^{39}Ar (%)	Age (Ma)	±2s (Ma)
C	700	6.3106	0.4661	21.0651	10.702	1.09	0.31	1.9	15.9	0.047	0.039
D	800	3.3662	0.2965	11.1266	16.573	1.72	0.30	3.0	35.3	0.039	0.024
E	900	2.8904	0.2487	9.6465	17.429	2.05	0.23	2.0	55.7	0.023	0.019
F	1000	9.0090	0.2639	30.0389	15.019	1.93	0.42	1.7	73.3	0.058	0.053
G	1100	7.4604	0.3803	24.9037	14.394	1.34	0.41	1.7	90.1	0.050	0.046
H	*1200*	*9.0404*	*4.5165*	*30.2078*	*7.646*	*0.11*	*0.10*	*5.1*	*99.1*	*0.178*	*0.061*
I	*1300*	*11.6459*	*5.2690*	*34.6936*	*0.780*	*0.10*	*-0.43*	*15.4*	*100.0*	*0.69*	*0.15*
total gas age			n=8		85.468	1.49				0.063	0.042
natural plateau			n=5	steps C-G	74.117	1.68			86.7	0.034	0.018
W-85-31, E5.E6:37, 139.2 mg, WR , J=0.0002199715, NM-37, Lab#=5392-01											
Mt. Takahe, Moll Spur lava											
A	500	1771	0.0590	6046	0.971	8.6	5.9	-0.9	1.0	-6.1	12.5
B	600	38.06	0.0693	130.1	12.6	7.4	0.27	-1.0	13.6	-0.15	0.23
C	700	6.063	0.0639	20.80	33.7	8.0	0.25	-1.3	47.5	-0.031	0.038
D	800	6.113	0.0558	20.72	21.8	9.1	0.17	-0.1	69.5	-0.003	0.038
E	900	5.875	0.0668	19.26	10.2	7.6	0.30	3.2	79.7	0.075	0.042
F	1000	9.087	0.1578	30.57	5.53	3.2	0.36	0.7	85.3	0.026	0.072
G	1100	11.39	0.4146	38.63	5.54	1.2	0.36	0.0	90.9	0.001	0.080
H	1200	11.54	1.726	38.82	5.54	0.30	0.19	1.8	96.5	0.081	0.090
I	1300	7.218	0.9737	23.84	3.51	0.52	0.32	3.4	100.0	0.098	0.064
total gas age			n=9		99.3	6.8				-0.07	0.19
no plateau			n=9	steps A-I	99.3	6.8			100.0	0.021	0.040
MT-85-10, E3.E4:37, 133.3 mg, WR , J=0.0002199709, NM-37, Lab#=5391-01											
Mt. Takahe, Oeschger Bluff, basanite pahoehoe											
B	*600*	*8.831*	*0.4779*	*30.35*	*7.78*	*1.1*	*0.25*	*-1.1*	*13.8*	*-0.040*	*0.065*
C	700	2.016	0.4543	6.911	20.4	1.1	0.24	0.4	50.0	0.003	0.016
D	800	2.443	0.4463	8.246	12.1	1.1	0.13	1.7	71.6	0.016	0.020
E	900	2.674	0.6378	9.169	5.95	0.80	0.36	0.5	82.2	0.005	0.030
F	1000	3.712	0.9706	12.72	3.93	0.53	0.17	0.8	89.1	0.011	0.045
G	1100	7.591	1.314	26.18	2.68	0.39	0.65	-0.6	93.9	-0.017	0.074
H	*1200*	*12.79*	*10.92*	*44.91*	*2.32*	*0.047*	*0.70*	*2.8*	*98.0*	*0.14*	*0.12*
I	*1300*	*14.00*	*14.05*	*49.79*	*0.934*	*0.036*	*-0.540*	*2.6*	*99.7*	*0.15*	*0.17*
J	*1450*	*18.25*	*5.979*	*61.22*	*0.170*	*0.085*	*0.68*	*3.4*	*100.0*	*0.25*	*0.55*
total gas age			n=9		56.2	0.94				0.009	0.039
natural plateau			n=5	steps C-G	45.0	0.99			80.1	0.007	0.013
MT-85-3, D5:37, 85.3 mg, WR , J=0.0002190971, NM-37, Lab#=5388-01											
Mt. Takahe, Roper Point, basanite lava											
B	600	10.95	0.5988	36.53	5.02	0.85	0.012	1.8	17.2	0.080	0.075
C	700	5.012	0.6628	16.15	8.08	0.77	0.12	5.8	44.8	0.115	0.041
D	800	5.309	0.6900	17.33	4.55	0.74	0.25	4.5	60.3	0.095	0.054

Appendix I. $^{40}Ar/^{39}Ar$ Analytical Data

ID	Temp (°C)	$^{40}Ar/^{39}Ar$	$^{37}Ar/^{39}Ar$	$^{36}Ar/^{39}Ar$ (x 10^{-3})	$^{39}Ar_K$ (x 10^{-15} mol)	K/Ca	Cl/K (x 10^{-3})	$^{40}Ar^*$ (%)	^{39}Ar (%)	Age (Ma)	±2s (Ma)
E	900	5.554	0.9080	18.13	2.94	0.56	0.20	4.8	70.4	0.106	0.058
F	1000	8.001	1.414	26.54	2.00	0.36	0.72	3.3	77.2	0.105	0.089
G	*1100*	*25.24*	*1.703*	*83.72*	*1.58*	*0.30*	*0.67*	*2.5*	*82.6*	*0.25*	*0.21*
H	*1200*	*42.37*	*6.417*	*142.3*	*5.09*	*0.080*	*1.2*	*1.9*	*100.0*	*0.32*	*0.27*
total gas age			n=7		29.2	0.58				0.15	0.10
natural plateau			n=5	steps B-F	22.6	0.72			77.2	0.104	0.028

W-85-35, F1-2:36, 150.1 mg, WR , J=0.000212952, NM-36, Lab#=5339-01

Mt. Takahe, Stauffer Bluff, pillow lava

A	*500*	*242.3*	*0.5761*	*805.6*	*1.04*	*0.89*	*1.6*	*1.7*	*1.9*	*1.6*	*1.5*
B	600	11.34	0.6942	38.02	6.34	0.73	0.22	1.4	13.3	0.059	0.072
C	700	5.966	0.7668	19.69	12.2	0.67	0.12	3.5	35.3	0.079	0.038
D	800	5.322	0.5738	17.85	9.46	0.89	0.18	1.7	52.4	0.036	0.037
E	900	6.002	0.6408	20.17	7.53	0.80	0.12	1.5	66.0	0.035	0.045
F	1000	10.87	0.8336	36.75	6.52	0.61	0.40	0.7	77.8	0.027	0.071
G	*1100*	*23.54*	*1.319*	*77.75*	*7.03*	*0.39*	*0.44*	*2.8*	*90.5*	*0.26*	*0.14*
H	*1200*	*41.87*	*8.991*	*142.3*	*4.77*	*0.057*	*0.48*	*1.2*	*99.1*	*0.20*	*0.26*
I	*1300*	*47.71*	*4.765*	*155.0*	*0.519*	*0.11*	*1.3*	*4.8*	*100.0*	*0.88*	*0.41*
total gas age			n=9		55.4	0.63				0.13	0.11
selected mean			n=5	steps B-F	42.1	0.74			75.9	0.050	0.029

MT85-009, Q5,Q6:36, Takahe, 117 mg, anorthoclase J=0.0002129827, nm-36, Lab#=5368-01

Mt. Takahe, Steuri Glacier cone trachyte

B	*700*	*2.402*	*0.0118*	*5.284*	*7.58*	*43.2*	*0.13*	*35.0*	*3.3*	*0.323*	*0.016*
C	*800*	*0.7245*	*0.0098*	*1.468*	*19.9*	*52.1*	*0.17*	*40.2*	*11.8*	*0.112*	*0.005*
D	900	0.4037	0.0100	0.9008	35.4	50.9	0.22	34.2	27.0	0.053	0.003
E	1000	0.2629	0.0095	0.5357	45.9	53.6	0.18	40.0	46.7	0.040	0.002
F	1100	0.3692	0.0095	0.8521	48.5	53.4	0.14	31.9	67.6	0.045	0.003
G	*1200*	*0.5806*	*0.0097*	*1.369*	*27.6*	*52.8*	*0.20*	*30.4*	*79.4*	*0.068*	*0.004*
H	*1250*	*0.6791*	*0.0104*	*1.728*	*16.2*	*49.2*	*0.29*	*24.9*	*86.4*	*0.065*	*0.006*
I	*1300*	*0.3058*	*0.0108*	*0.6953*	*14.0*	*47.3*	*0.31*	*33.0*	*92.4*	*0.039*	*0.006*
J	*1350*	*1.971*	*0.0134*	*0.8394*	*5.78*	*38.2*	*0.13*	*87.5*	*94.9*	*0.662*	*0.014*
K	*1400*	*3.008*	*0.0159*	*4.640*	*1.40*	*32.0*	*0.56*	*54.4*	*95.5*	*0.629*	*0.055*
L	*1500*	*2.481*	*0.0301*	*4.346*	*1.68*	*16.9*	*-0.297*	*48.3*	*96.2*	*0.461*	*0.047*
M	*1750*	*1.158*	*0.0552*	*3.492*	*8.84*	*9.2*	*-0.043*	*11.3*	*100.0*	*0.050*	*0.012*
total gas age			n=12		232.9	49.5				0.086	0.005
selected mean			n=3	steps D-F	129.8	52.8			55.7	0.045	0.007

Appendix I. $^{40}Ar/^{39}Ar$ Analytical Data

Crary Mountains, Marie Byrd Land (1992-93 Field Season)

ID	Temp (°C)	$^{40}Ar/^{39}Ar$	$^{37}Ar/^{39}Ar$	$^{36}Ar/^{39}Ar$ (x 10^{-3})	$^{39}Ar_K$ (x 10^{-15} mol)	K/Ca	Cl/K (x 10^{-3})	$^{40}Ar^*$ (%)	^{39}Ar (%)	Age (Ma)	±2s (Ma)
TW92-001, T1:13, J=0.0006485, nm-13, Lab#=1421-01											
hyaloclastite at Trabucco Cliff, Mt. Rees, Crary Mtns											
A	600	23.13	0.9819	48.65	32.0	0.52	119	38.1	42.2	10.28	0.17
B	700	10.84	2.999	10.39	17.2	0.17	75.8	73.6	64.9	9.335	0.068
C	800	12.12	3.629	15.39	8.05	0.14	64.0	64.6	75.5	9.16	0.11
D	875	12.31	3.687	15.53	2.96	0.14	57.5	64.8	79.4	9.34	0.16
E	1000	10.88	4.826	15.80	1.89	0.11	40.2	60.3	81.9	7.68	0.26
F	1100	9.393	4.450	10.69	2.36	0.11	69.5	69.8	85.0	7.67	0.18
G	1200	9.178	17.37	13.02	10.2	0.029	62.6	72.4	98.5	7.85	0.11
H	1400	12.52	29.66	24.39	1.13	0.017	13.5	60.4	100.0	9.02	0.43
total gas age			n=8		75.8	0.29				9.42	0.17
no plateau			n=8	steps A-H	75.8	0.29			100.0	9.13	0.53
TW92-41, I5:21, 56.6 mg, J=0.00073991, nm-21, Lab#=2538-01											
hyaloclastite at Tasch Peak ridge, Mt. Rees, Crary Mtns											
A	*500*	*30.07*	*0.5268*	*77.56*	*5.04*	*0.97*	*185*	*23.7*	*4.6*	*9.49*	*0.75*
B	600	9.700	0.5752	11.19	10.3	0.89	80.7	65.7	14.0	8.49	0.23
C	700	7.684	0.6267	4.497	21.9	0.81	35.2	82.5	33.8	8.44	0.11
D	800	8.369	0.5859	6.272	15.5	0.87	39.6	77.6	47.8	8.65	0.13
E	875	8.267	0.5691	6.716	7.34	0.90	22.2	75.8	54.5	8.34	0.19
F	*1000*	*7.674*	*0.8375*	*3.513*	*5.82*	*0.61*	*11.8*	*86.2*	*59.7*	*8.811*	*0.082*
G	*1150*	*10.77*	*1.866*	*3.744*	*19.1*	*0.27*	*25.5*	*89.6*	*77.0*	*12.829*	*0.068*
H	*1300*	*7.036*	*3.201*	*3.338*	*25.3*	*0.16*	*17.2*	*85.7*	*100.0*	*8.033*	*0.043*
total gas age			n=8		110.2	0.59				9.20	0.14
selected mean			n=4	steps B-E	55.0	0.85			49.9	8.50	0.16
TW92-38, T13:13, J=0.0006579, NM-13, Lab#=1534-01											
hyaloclastite at Tasch Peak ridge, Mt. Rees, Crary Mtns											
C	*675*	*15.45*	*0.5923*	*24.72*	*6.13*	*0.86*	*165.3*	*52.9*	*3.7*	*9.67*	*0.15*
D	750	7.795	0.5386	2.645	40.6	0.95	50.3	90.2	28.2	8.331	0.031
E	825	7.569	0.6169	2.164	53.3	0.83	16.3	91.9	60.5	8.239	0.031
F	900	8.164	0.6334	4.228	16.8	0.81	11.2	85.0	70.6	8.224	0.048
G	1050	7.681	0.7022	2.845	19.5	0.73	6.2	89.5	82.4	8.142	0.042
H	1250	7.179	3.185	2.625	25.4	0.16	8.5	92.3	97.8	7.864	0.038
I	1650	9.907	3.942	11.71	3.70	0.13	10.1	67.9	100.0	7.99	0.12
total gas age			n=7		165.5	0.73				8.239	0.046
selected mean			n=6	steps D-I	159.3	0.72			96.3	8.21	0.13

Appendix I. $^{40}Ar/^{39}Ar$ Analytical Data

Crary Mountains, Marie Byrd Land (1992-93 Field Season)

ID	Temp (°C)	$^{40}Ar/^{39}Ar$	$^{37}Ar/^{39}Ar$	$^{36}Ar/^{39}Ar$ (x 10^{-3})	$^{39}Ar_K$ (x 10^{-15} mol)	K/Ca	Cl/K (x 10^{-3})	$^{40}Ar^*$ (%)	^{39}Ar (%)	Age (Ma)	±2s (Ma)
TW92-34, T11:13, J=0.0006564, nm-13, Lab#=1424-01											
hyaloclastite at Tasch Peak ridge, Mt. Rees, Crary Mtns											
A	*600*	*15.35*	*0.5492*	*24.90*	*45.0*	*0.93*	*31.7*	*52.2*	*15.3*	*9.468*	*0.100*
B	700	7.772	0.4925	2.709	81.9	1.0	15.0	89.9	43.3	8.259	0.033
C	800	8.242	0.5728	4.306	66.4	0.89	10.5	84.8	65.9	8.264	0.037
D	875	8.645	0.5862	5.464	27.8	0.87	7.7	81.6	75.4	8.336	0.052
E	1000	7.495	0.6019	1.934	27.8	0.85	4.9	92.7	84.9	8.212	0.041
F	1200	7.231	3.052	2.139	30.8	0.17	8.5	94.2	95.4	8.065	0.035
G	1300	7.358	3.778	2.645	11.9	0.14	10.6	93.0	99.5	8.109	0.050
H	*1400*	*8.761*	*3.177*	*6.585*	*1.59*	*0.16*	*8.6*	*80.3*	*100.0*	*8.33*	*0.28*
total gas age			n=8		293.3	0.82				8.422	0.053
selected mean			n=6	steps B-G	246.7	0.80			84.1	8.230	0.087
TW92-31, T9:13, J=0.0006544, nm-13, Lab#=1418-01											
hyaloclastite at Tasch Peak ridge, Mt. Rees, Crary Mtns											
A	600	26.73	0.3811	60.18	50.5	1.3	81.1	33.5	14.7	10.54	0.20
B	700	9.005	0.3844	4.278	66.7	1.3	96.0	86.0	34.0	9.127	0.038
C	800	8.294	0.4552	1.451	56.3	1.1	91.9	95.0	50.4	9.280	0.033
D	875	8.250	0.3915	1.204	30.7	1.3	50.0	95.8	59.3	9.308	0.040
E	1000	7.900	0.5135	1.323	29.5	0.99	18.3	95.3	67.9	8.867	0.041
F	1100	7.672	0.8254	1.736	17.0	0.62	8.5	93.9	72.8	8.486	0.051
G	1300	8.125	1.976	3.806	86.3	0.26	27.2	87.8	97.8	8.410	0.033
H	1400	8.632	2.826	5.227	7.42	0.18	18.2	84.4	100.0	8.594	0.083
total gas age			n=8		344.4	0.94				9.130	0.064
no plateau			n=8	steps A-H	344.4	0.94			100.0	8.98	0.28
TW92-028, T7:13, J=0.0006518, nm-13, Lab#=1417-01											
dry lava at Tasch Peak ridge, Mt. Rees, Crary Mtns											
AA	*600*	*39.82*	*0.2800*	*100.8*	*32.2*	*1.8*	*34.3*	*25.2*	*10.7*	*11.76*	*0.33*
AB	700	10.96	0.1634	10.81	59.0	3.1	32.5	70.8	30.3	9.095	0.051
AC	800	9.134	0.1557	4.740	66.4	3.3	39.7	84.6	52.3	9.060	0.037
AD	875	8.658	0.1938	3.088	37.8	2.6	41.1	89.4	64.8	9.078	0.038
AE	*1000*	*8.258*	*0.2696*	*2.172*	*33.6*	*1.9*	*57.8*	*92.2*	*76.0*	*8.934*	*0.045*
AF	*1100*	*7.742*	*0.6673*	*1.379*	*17.8*	*0.76*	*19.5*	*95.1*	*81.9*	*8.642*	*0.045*
AG	*1300*	*8.103*	*2.313*	*3.299*	*45.0*	*0.22*	*16.6*	*89.9*	*96.8*	*8.558*	*0.039*
AH	*1400*	*8.593*	*2.550*	*4.604*	*8.31*	*0.20*	*9.7*	*86.2*	*99.6*	*8.704*	*0.079*
AI	*1750*	*22.88*	*2.984*	*53.51*	*1.31*	*0.17*	*4.0*	*31.8*	*100.0*	*8.55*	*0.78*
total gas age			n=9		301.5	2.2				9.232	0.079
natural plateau			n=3	steps AB-AD	163.2	3.1			54.1	9.075	0.064

Appendix I. $^{40}Ar/^{39}Ar$ Analytical Data

Crary Mountains, Marie Byrd Land (1992-93 Field Season)

ID	Temp (°C)	$^{40}Ar/^{39}Ar$	$^{37}Ar/^{39}Ar$	$^{36}Ar/^{39}Ar$ (x 10^{-3})	$^{39}Ar_K$ (x 10^{-15} mol)	K/Ca	Cl/K (x 10^{-3})	$^{40}Ar^*$ (%)	^{39}Ar (%)	Age (Ma)	±2s (Ma)
TW92-023, T5:13, J=0.0006508, nm-13, Lab#=1416-01											
hyaloclastite at Tasch Peak ridge, Mt. Rees, Crary Mtns											
A	600	15.48	0.3486	25.76	45.8	1.5	150.4	50.9	19.2	9.220	0.099
B	700	8.468	0.4275	2.754	45.5	1.2	60.5	90.5	38.4	8.980	0.034
C	800	8.588	0.4689	3.052	30.2	1.1	54.4	89.7	51.1	9.021	0.046
D	875	8.528	0.4213	2.647	15.3	1.2	55.7	91.0	57.5	9.086	0.065
E	1000	8.132	0.4848	2.304	14.4	1.1	42.1	91.8	63.5	8.748	0.064
F	1200	8.239	0.9700	2.795	73.7	0.53	54.1	90.6	94.5	8.750	0.033
G	1300	8.007	1.702	2.040	11.3	0.30	13.2	93.8	99.2	8.810	0.066
H	1400	8.891	2.520	5.650	1.84	0.20	10.6	83.2	100.0	8.67	0.20
total gas age			n=8		238.1	0.97				8.943	0.056
no plateau			n=8	steps A-H	238.1	0.97			100.0	8.91	0.12
TW92-59, T15:13, J=0.0006599, nm-13, Lab#=1420-01											
hyaloclastite at Tasch Peak ridge, Mt. Rees, Crary Mtns											
A	*600*	*166.1*	*2.921*	*534.5*	*6.07*	*0.17*	*86.2*	*5.0*	*8.3*	*10.0*	*1.8*
B	*700*	*40.22*	*2.498*	*107.8*	*5.53*	*0.20*	*76.3*	*21.2*	*15.9*	*10.14*	*0.41*
C	*800*	*40.36*	*2.798*	*110.1*	*5.73*	*0.18*	*59.9*	*19.8*	*23.8*	*9.53*	*0.42*
D	*875*	*27.05*	*2.094*	*63.80*	*6.73*	*0.24*	*50.9*	*30.8*	*33.0*	*9.91*	*0.28*
E	1000	14.11	2.141	21.33	11.6	0.24	16.1	56.4	49.0	9.46	0.12
F	1100	12.09	2.231	14.97	5.46	0.23	7.5	64.6	56.5	9.29	0.16
G	1300	11.98	14.14	18.64	30.2	0.036	14.6	62.9	98.0	9.039	0.082
H	*1400*	*20.11*	*27.89*	*45.55*	*1.45*	*0.018*	*7.6*	*43.6*	*100.0*	*10.62*	*0.50*
total gas age			n=8		72.8	0.14				9.44	0.38
selected mean			n=3	steps E-G	47.3	0.11			65.0	9.34	0.24
TW92-117, T31:13, J=0.0006716, nm-13, Lab#=1402-01											
lava, southwest of Tasch Peak Mt. Rees, Crary Mtns											
A	*600*	*306.0*	*0.9218*	*995.7*	*1.81*	*0.55*	*78.7*	*3.9*	*1.6*	*14.3*	*4.4*
B	700	12.32	1.316	21.60	13.9	0.39	24.9	48.8	13.7	7.28	0.11
C	800	7.174	1.562	5.257	28.9	0.33	11.3	79.7	38.9	6.922	0.040
D	875	7.172	1.416	5.363	17.9	0.36	13.6	79.1	54.5	6.868	0.047
E	1000	8.870	1.691	11.41	13.9	0.30	32.5	63.2	66.6	6.787	0.079
F	1100	13.30	1.613	27.63	12.6	0.32	58.2	39.4	77.6	6.35	0.11
G	1200	12.60	6.422	28.17	21.2	0.079	45.1	37.7	96.1	5.77	0.10
H	*1400*	*17.20*	*32.66*	*47.75*	*4.12*	*0.016*	*21.5*	*32.4*	*99.7*	*6.90*	*0.27*
I	*1650*	*48.44*	*9.355*	*145.8*	*0.352*	*0.055*	*33.1*	*12.5*	*100.0*	*7.4*	*1.6*
total gas age			n=9		114.6	0.28				6.78	0.18
selected mean			n=6	steps B-G	108.3	0.29			94.5	6.82	0.26

Appendix I. $^{40}Ar/^{39}Ar$ Analytical Data

Crary Mountains, Marie Byrd Land (1992-93 Field Season)

ID	Temp (°C)	$^{40}Ar/^{39}Ar$	$^{37}Ar/^{39}Ar$	$^{36}Ar/^{39}Ar$ (x 10^{-3})	$^{39}Ar_K$ (x 10^{-15} mol)	K/Ca	Cl/K (x 10^{-3})	$^{40}Ar^*$ (%)	^{39}Ar (%)	Age (Ma)	±2s (Ma)
TW92-114, T29:13, J=0.0006705, nm-13, Lab#=1401-01											
lava, southwest of Tasch Peak Mt. Rees, Crary Mtns											
A	*600*	*233.6*	*1.678*	*756.5*	*0.842*	*0.30*	*53.5*	*4.3*	*0.7*	*12.2*	*3.9*
B	700	16.08	1.556	34.92	7.60	0.33	15.8	36.4	7.0	7.08	0.17
C	800	8.961	1.351	10.44	8.81	0.38	9.8	66.5	14.4	7.198	0.080
D	875	7.458	1.004	5.760	18.7	0.51	10.6	77.9	30.0	7.021	0.052
E	1000	9.045	1.098	11.81	14.8	0.46	31.1	62.1	42.4	6.787	0.065
F	1200	14.02	1.402	29.70	50.2	0.36	63.1	38.0	84.3	6.44	0.10
G	1400	17.31	12.45	43.71	18.8	0.041	54.1	30.8	100.0	6.49	0.16
total gas age			n=7		119.7	0.35				6.72	0.14
selected mean			n=6	steps B-G	118.9	0.35			99.3	6.92	0.21
TW92-112,H1:21, 41.9 mg, J=0.00074269, nm-21, Lab#=2486-01											
lava, north end, Mt. Rees, Crary Mtns											
A	*500*	*130.7*	*0.2315*	*392.9*	*0.921*	*2.2*	*174*	*11.2*	*0.3*	*19.4*	*2.7*
B	*600*	*13.16*	*0.1205*	*17.37*	*3.69*	*4.2*	*115*	*60.9*	*1.6*	*10.70*	*0.20*
C	700	7.441	0.0755	2.301	30.2	6.8	38.3	90.6	12.4	9.011	0.042
D	800	7.222	0.0641	1.723	51.0	8.0	29.6	92.7	30.6	8.946	0.037
E	875	7.172	0.0865	1.745	30.2	5.9	45.3	92.5	41.4	8.871	0.043
F	1000	7.716	0.1271	2.453	32.7	4.0	56.4	90.4	53.1	9.317	0.047
G	*1150*	*16.21*	*0.6118*	*3.061*	*63.4*	*0.83*	*25.7*	*94.3*	*75.7*	*20.370*	*0.091*
H	*1300*	*11.33*	*0.8836*	*4.313*	*54.6*	*0.58*	*8.8*	*88.6*	*95.2*	*13.398*	*0.065*
I	*1400*	*8.920*	*0.2998*	*6.530*	*12.2*	*1.7*	*8.5*	*78.2*	*99.5*	*9.316*	*0.084*
J	*1700*	*85.65*	*0.3581*	*264.4*	*1.34*	*1.4*	*1.8*	*8.8*	*100.0*	*10.0*	*1.5*
total gas age			n=10		280.3	3.7				12.517	0.077
selected mean			n=4	steps C-F	144.2	6.4			51.5	9.02	0.19

Appendix I. $^{40}Ar/^{39}Ar$ Analytical Data

Crary Mountains, Marie Byrd Land (1992-93 Field Season)

ID	Temp (°C)	$^{40}Ar/^{39}Ar$	$^{37}Ar/^{39}Ar$	$^{36}Ar/^{39}Ar$ (x 10^{-3})	$^{39}Ar_K$ (x 10^{-15} mol)	K/Ca	Cl/K (x 10^{-3})	$^{40}Ar^*$ (%)	^{39}Ar (%)	Age (Ma)	±2s (Ma)
TW92-109, H3:21, 31.8 mg, J=0.000742637, nm-21, Lab#=2487-01											
lava, north end, Mt. Rees, Crary Mtns											
A	*500*	*112.2*	*0.1788*	*340.2*	*1.27*	*2.9*	*134*	*10.4*	*0.8*	*15.6*	*1.9*
B	*600*	*12.29*	*0.1240*	*18.10*	*6.21*	*4.1*	*65.4*	*56.3*	*4.5*	*9.24*	*0.14*
C	650	7.732	0.0944	3.633	13.4	5.4	37.4	85.9	12.6	8.874	0.079
D	700	7.088	0.0864	1.845	19.9	5.9	28.9	92.0	24.6	8.720	0.044
E	750	7.042	0.1086	1.542	20.0	4.7	27.4	93.3	36.7	8.778	0.062
F	800	7.019	0.1296	1.703	18.2	3.9	26.9	92.6	47.7	8.683	0.047
G	850	7.323	0.1495	2.546	11.0	3.4	32.6	89.5	54.3	8.757	0.090
H	900	7.784	0.1499	4.149	8.20	3.4	34.7	84.0	59.3	8.740	0.096
I	950	8.161	0.1474	5.902	7.14	3.5	27.3	78.4	63.6	8.55	0.11
J	1000	8.410	0.1590	6.415	7.45	3.2	19.6	77.2	68.1	8.681	0.084
K	1075	8.462	0.2096	7.038	14.1	2.4	13.5	75.2	76.6	8.505	0.090
L	1150	8.261	0.4731	6.113	16.6	1.1	9.5	77.9	86.7	8.60	0.11
M	1300	9.494	1.181	10.26	19.8	0.43	9.9	67.9	98.7	8.612	0.075
N	*1350*	*13.09*	*0.5567*	*21.68*	*1.97*	*0.92*	*11.8*	*50.9*	*99.8*	*8.91*	*0.25*
O	*1450*	*47.81*	*1.196*	*139.0*	*0.263*	*0.43*	*14.0*	*14.0*	*100.0*	*9.0*	*2.1*
total gas age			n=15		165.5	3.4				8.761	0.097
selected mean			n=11	steps C-M	155.8	3.4			94.1	8.699	0.075
TW92-95, K1:21, 56.6 mg, J=0.00074329, nm-21, Lab#=2493-01											
foliated lava, north side, Mt. Steere, Crary Mtns											
A	*500*	*45.42*	*0.5879*	*128.7*	*1.73*	*0.87*	*78*	*16.2*	*0.9*	*9.87*	*0.78*
B	*600*	*7.419*	*0.5527*	*9.528*	*6.46*	*0.92*	*18*	*61.8*	*4.4*	*6.14*	*0.10*
C	700	4.930	0.3416	2.107	35.4	1.5	3.9	87.0	23.1	5.741	0.029
D	800	4.698	0.3130	1.337	48.0	1.6	1.2	91.2	48.6	5.735	0.039
E	875	4.816	0.3450	1.752	30.7	1.5	1.5	88.9	64.9	5.729	0.029
F	*1000*	*5.699*	*0.5100*	*3.986*	*19.0*	*1.0*	*4.5*	*79.0*	*75.0*	*6.027*	*0.041*
G	*1150*	*13.54*	*1.138*	*6.246*	*16.7*	*0.45*	*12*	*86.2*	*83.9*	*15.586*	*0.082*
H	*1300*	*8.643*	*3.518*	*12.04*	*26.1*	*0.15*	*18*	*58.6*	*97.8*	*6.781*	*0.073*
I	*1400*	*38.57*	*5.036*	*115.8*	*3.26*	*0.10*	*14*	*11.3*	*99.5*	*5.82*	*0.60*
J	*1700*	*13.48*	*5.994*	*33.75*	*0.944*	*0.085*	*7.3*	*25.9*	*100.0*	*4.67*	*0.39*
total gas age			n=10		188.3	1.1				6.832	0.065
natural plateau			n=3	steps C-E	114.1	1.5			60.6	5.735	0.042

Appendix I. $^{40}Ar/^{39}Ar$ Analytical Data

Crary Mountains, Marie Byrd Land (1992-93 Field Season)

ID	Temp (°C)	$^{40}Ar/^{39}Ar$	$^{37}Ar/^{39}Ar$	$^{36}Ar/^{39}Ar$ (x 10^{-3})	$^{39}Ar_K$ (x 10^{-15} mol)	K/Ca	Cl/K (x 10^{-3})	$^{40}Ar^*$ (%)	^{39}Ar (%)	Age (Ma)	±2s (Ma)
TW92-64, T17:13, J=0.0006618, NM-13, Lab#=1535-01											
dike, Mt. Steere, Crary Mtns											
A	*500*	*43.89*	*0.0768*	*123.3*	*3.48*	*6.6*	*38.5*	*17.0*	*1.1*	*8.86*	*0.49*
B	600	13.31	0.0531	22.31	14.7	9.6	33.1	50.3	5.9	7.98	0.10
C	675	10.61	0.2833	18.42	0.081	1.8	88.2	48.7	5.9	6.2	3.4
D	750	8.940	0.0434	7.113	6.49	11.7	37.9	76.3	8.0	8.124	0.082
E	825	8.760	0.0486	6.330	33.6	10.5	89.2	78.4	18.9	8.185	0.041
F	900	7.527	0.0679	2.349	29.1	7.5	98.1	90.6	28.4	8.120	0.037
G	1050	7.471	0.0858	2.526	46.0	5.9	28.4	89.8	43.3	7.992	0.031
H	1250	7.417	0.1036	2.321	142.8	4.9	90.9	90.6	89.6	8.002	0.028
I	1650	7.736	0.0871	3.104	32.0	5.9	29.5	87.9	100.0	8.105	0.050
total gas age			n=9		308.2	6.4				8.053	0.044
selected mean			n=8	steps B-I	304.8	6.4			98.9	8.058	0.076
TW92-169, T57:13, J=0.0006747, nm-13, Lab#=1415-01											
lava, ridge southeast of Lie Cliff, Mt. Steere, Crary Mtns											
A	600	7.846	0.7912	7.099	44.4	0.64	9.1	73.8	35.3	7.034	0.045
B	700	5.540	1.367	1.871	24.6	0.37	7.8	91.5	54.9	6.166	0.038
C	800	5.655	1.432	2.152	16.7	0.36	9.0	90.3	68.2	6.211	0.041
D	875	5.618	1.469	2.142	9.83	0.35	11.1	90.3	76.0	6.174	0.053
E	*1000*	*5.370*	*1.876*	*2.636*	*9.80*	*0.27*	*11.3*	*87.8*	*83.8*	*5.736*	*0.054*
F	*1200*	*6.095*	*8.211*	*8.896*	*19.7*	*0.062*	*60.4*	*66.9*	*99.5*	*4.982*	*0.056*
G	*1300*	*11.30*	*29.88*	*30.84*	*0.674*	*0.017*	*48.9*	*39.5*	*100.0*	*5.54*	*0.67*
total gas age			n=7		125.7	0.41				6.257	0.065
selected mean			n=4	steps B-D	95.5	0.49			76.0	6.41	0.43
TW92-165, T55:13, J=0.0006726, nm-13, Lab#=1414-01											
lava, ridge southeast of Lie Cliff, Mt. Steere, Crary Mtns											
A	*600*	*24.65*	*2.046*	*59.08*	*10.2*	*0.25*	*35.8*	*29.7*	*12.6*	*8.89*	*0.27*
B	700	6.944	1.541	3.156	20.5	0.33	14.3	88.0	38.0	7.404	0.047
C	800	7.096	1.652	3.854	17.0	0.31	8.6	85.4	59.1	7.349	0.055
D	875	7.574	1.634	5.524	7.77	0.31	8.1	79.8	68.7	7.329	0.076
E	1000	8.049	2.205	6.933	7.44	0.23	11.4	76.4	77.9	7.46	0.10
F	*1200*	*8.659*	*4.285*	*11.94*	*8.22*	*0.12*	*11.5*	*62.8*	*88.1*	*6.608*	*0.093*
G	*1300*	*10.95*	*27.27*	*25.86*	*8.60*	*0.019*	*23.9*	*49.2*	*98.8*	*6.65*	*0.15*
H	*1400*	*13.54*	*39.37*	*34.93*	*0.979*	*0.013*	*13.1*	*46.0*	*100.0*	*7.75*	*0.40*
total gas age			n=8		80.6	0.25				7.42	0.14
natural plateau			n=4	steps B-E	52.7	0.31			65.3	7.378	0.072

Appendix I. $^{40}Ar/^{39}Ar$ Analytical Data

Crary Mountains, Marie Byrd Land (1992-93 Field Season)

ID	Temp (°C)	$^{40}Ar/^{39}Ar$	$^{37}Ar/^{39}Ar$	$^{36}Ar/^{39}Ar$ (x 10^{-3})	$^{39}Ar_K$ (x 10^{-15} mol)	K/Ca	Cl/K (x 10^{-3})	$^{40}Ar^*$ (%)	^{39}Ar (%)	Age (Ma)	±2s (Ma)
TW92-162, 113:17, 23.3 mg, J=0.0009609, nm-17*, Lab#=1883-01											
lava, ridge southeast of Lie Cliff, Mt. Steere, Crary Mtns											
B	750	3.415	1.392	-1.3175	1.15	0.37	1.0	114.0	2.5	6.74	0.34
C	1000	3.879	1.462	0.3877	14.1	0.35	0.081	99.5	32.8	6.683	0.041
D	1150	3.841	1.464	0.2565	7.59	0.35	0.15	100.5	49.1	6.683	0.062
E	1250	3.897	1.484	0.3249	5.40	0.34	0.072	100.0	60.7	6.749	0.083
F	*1349*	*4.817*	*1.642*	*2.793*	*3.24*	*0.31*	*0.32*	*85.1*	*67.7*	*7.10*	*0.12*
G	*1450*	*4.464*	*1.519*	*2.099*	*5.90*	*0.34*	*0.33*	*88.3*	*80.4*	*6.827*	*0.080*
H	*1550*	*4.853*	*2.056*	*4.350*	*4.59*	*0.25*	*0.97*	*76.4*	*90.3*	*6.42*	*0.10*
I	*1750*	*5.679*	*2.304*	*8.033*	*4.53*	*0.22*	*0.18*	*61.0*	*100.0*	*6.00*	*0.11*
total gas age			n=8		46.5	0.32				6.65	0.09
natural plateau			n=4	steps B-E	28.2	0.35			60.7	6.695	0.048
TW92-85, T25:13, J=0.0006681, nm-13, Lab#=1412-01											
lava, Lie Cliff, Mt. Steere, Crary Mtns											
A	*600*	*53.44*	*1.168*	*152.0*	*12.9*	*0.44*	*83.5*	*16.1*	*9.3*	*10.33*	*0.53*
B	700	10.01	1.275	9.838	16.2	0.40	55.0	71.7	21.1	8.64	0.10
C	800	8.748	1.385	5.414	17.5	0.37	34.6	82.7	33.8	8.705	0.099
D	875	9.216	1.427	6.864	8.61	0.36	25.4	78.9	40.1	8.757	0.097
E	1000	9.400	1.627	8.543	9.87	0.31	21.6	74.2	47.2	8.40	0.11
F	1200	9.286	2.664	10.09	15.9	0.19	16.6	69.9	58.8	7.817	0.080
G	1400	10.91	5.060	15.32	56.6	0.10	27.0	61.9	99.8	8.150	0.062
H	*1750*	*56.46*	*51.82*	*182.2*	*0.233*	*0.010*	*4.5*	*11.6*	*100.0*	*8.2*	*2.6*
total gas age			n=8		137.8	0.24				8.50	0.14
selected mean			n=6	steps B-G	124.7	0.22			90.5	8.38	0.33
TW92-82, T23:13, J=0.0006657, nm-13, Lab#=1411-01											
pillow lava, Lie Cliff, Mt. Steere, Crary Mtns											
A	*600*	*34.60*	*0.4586*	*94.22*	*2.25*	*1.1*	*8.7*	*19.6*	*1.1*	*8.12*	*0.78*
BB	*700*	*40.28*	*0.5698*	*99.92*	*33.6*	*0.90*	*6.5*	*26.7*	*17.7*	*12.90*	*0.31*
CC	800	8.878	0.5856	6.265	61.9	0.87	2.3	79.4	48.4	8.450	0.039
D	875	7.678	0.7481	2.421	30.9	0.68	1.6	91.1	63.7	8.390	0.040
E	1000	7.532	0.9688	2.673	22.4	0.53	3.1	90.2	74.8	8.147	0.050
F	1200	7.913	2.455	5.270	13.8	0.21	14.9	82.4	81.7	7.830	0.063
G	1400	7.708	6.103	5.121	36.7	0.084	12.3	86.2	99.9	7.992	0.047
H	*1650*	*50.14*	*7.116*	*149.6*	*0.284*	*0.072*	*14.3*	*12.9*	*100.0*	*7.8*	*2.0*
total gas age			n=8		201.8	0.62				9.02	0.11
selected mean			n=5	steps CC-G	165.7	0.56			82.1	8.28	0.21

Appendix I. $^{40}Ar/^{39}Ar$ Analytical Data

Crary Mountains, Marie Byrd Land (1992-93 Field Season)

ID	Temp (°C)	$^{40}Ar/^{39}Ar$	$^{37}Ar/^{39}Ar$	$^{36}Ar/^{39}Ar$ (x 10^{-3})	$^{39}Ar_K$ (x 10^{-15} mol)	K/Ca	Cl/K (x 10^{-3})	$^{40}Ar^*$ (%)	^{39}Ar (%)	Age (Ma)	±2s (Ma)
TW92-079, T19:1:13, 45.3 mg, J=0.000663295, nm-13, Lab#=2095-01											
Lie Cliff, Mt. Steere, Crary Mtns											
B	*600*	*45.79*	*0.5643*	*119.1*	*3.81*	*0.90*	*12.0*	*23.2*	*2.3*	*12.66*	*0.51*
C	750	8.161	0.3285	3.704	35.6	1.6	2.9	86.6	24.0	8.442	0.043
D	850	7.544	0.2499	1.575	34.6	2.0	2.1	93.8	45.0	8.449	0.038
E	950	7.621	0.2497	1.948	22.9	2.0	4.5	92.4	58.9	8.409	0.045
F	*1050*	*7.835*	*0.3358*	*3.163*	*20.8*	*1.5*	*7.4*	*88.1*	*71.5*	*8.244*	*0.046*
G	*1150*	*7.976*	*0.6383*	*4.217*	*14.1*	*0.80*	*7.2*	*84.7*	*80.1*	*8.071*	*0.052*
H	*1250*	*8.851*	*3.053*	*7.931*	*8.05*	*0.17*	*7.5*	*75.9*	*85.0*	*8.041*	*0.072*
I	*1400*	*7.852*	*2.033*	*4.143*	*23.3*	*0.25*	*8.5*	*86.1*	*99.1*	*8.085*	*0.046*
J	*1750*	*25.99*	*4.850*	*65.13*	*1.43*	*0.11*	*9.1*	*27.3*	*100.0*	*8.50*	*0.43*
total gas age			n=9		164.7	1.4				8.410	0.062
natural plateau			n=3	steps C-E	93.1	1.9			56.6	8.435	0.061
TW92-86, T27:13, J=0.0006691, nm-13, Lab#=1413-01											
lava, Lie Cliff, Mt. Steere, Crary Mtns											
A	*600*	*140.0*	*1.731*	*445.5*	*6.33*	*0.29*	*38.2*	*6.0*	*5.6*	*10.2*	*1.5*
B	700	40.16	1.188	111.2	8.32	0.43	38.6	18.4	12.9	8.90	0.39
C	800	37.07	1.291	100.5	8.55	0.40	34.5	20.1	20.5	8.98	0.38
D	875	26.27	1.432	64.51	8.04	0.36	36.4	27.8	27.5	8.80	0.29
E	1000	17.83	1.601	36.02	12.1	0.32	18.8	40.9	38.2	8.78	0.16
F	1200	14.26	3.958	25.87	53.3	0.13	17.0	48.4	85.2	8.333	0.092
G	1300	15.61	12.28	32.74	15.6	0.042	13.0	43.9	99.0	8.33	0.14
H	*1400*	*21.55*	*14.30*	*50.55*	*1.17*	*0.036*	*7.9*	*35.7*	*100.0*	*9.35*	*0.55*
total gas age			n=8		113.4	0.20				8.62	0.27
selected mean			n=6	steps B-G	105.9	0.20			93.4	8.52	0.23
TW92-193, T63:13, J=0.0006785, nm-13, Lab#=1406-01											
dike, ridge northwest of Lie Cliff, Mt. Steere, Crary Mtns											
A	*800*	*33.48*	*0.5123*	*87.50*	*41.9*	*1.00*	*64.6*	*22.8*	*16.6*	*9.33*	*0.29*
B	800	10.46	0.3655	11.76	13.1	1.4	75.3	66.8	21.7	8.536	0.087
C	800	10.06	0.3711	10.68	16.6	1.4	75.2	68.7	28.2	8.441	0.091
D	875	14.29	0.5052	25.01	38.3	1.0	64.1	48.4	43.4	8.448	0.094
E	1000	11.34	0.6001	15.48	36.6	0.85	42.3	59.9	57.8	8.298	0.068
F	1200	7.356	1.880	3.233	49.2	0.27	20.0	88.7	77.3	7.978	0.035
G	1400	7.651	2.024	3.830	57.6	0.25	38.7	87.0	100.0	8.137	0.035
total gas age			n=7		253.3	0.71				8.41	0.10
selected mean			n=6	steps B-G	211.4	0.66			83.4	8.19	0.18

Appendix I. $^{40}Ar/^{39}Ar$ Analytical Data

Crary Mountains, Marie Byrd Land (1992-93 Field Season)

ID	Temp (°C)	$^{40}Ar/^{39}Ar$	$^{37}Ar/^{39}Ar$	$^{36}Ar/^{39}Ar$ (x 10^{-3})	$^{39}Ar_K$ (x 10^{-15} mol)	K/Ca	Cl/K (x 10^{-3})	$^{40}Ar^*$ (%)	^{39}Ar (%)	Age (Ma)	±2s (Ma)
TW92-194, T66:13, J=0.000679, nm-13, Lab#=1407-01											
pillow lava, ridge northwest of Lie Cliff, Mt. Steere, Crary Mtns											
B	*700*	*140.9*	*0.8518*	*434.8*	*2.90*	*0.60*	*46.7*	*8.8*	*1.4*	*15.2*	*1.5*
C	800	18.19	0.4473	37.04	47.9	1.1	70.4	39.9	24.3	8.86	0.13
D	875	14.13	0.4836	24.47	38.3	1.1	68.3	48.9	42.6	8.456	0.095
E	1000	11.54	0.5944	15.87	30.1	0.86	46.0	59.6	57.0	8.400	0.073
F	1200	7.240	1.885	2.720	41.3	0.27	23.2	90.6	76.7	8.027	0.037
G	1400	7.530	1.947	3.470	48.7	0.26	41.8	88.1	100.0	8.117	0.035
total gas age			n=6		209.1	0.70				8.47	0.10
selected mean			n=5	steps C-G	206.2	0.70			98.6	8.19	0.22
TW92-189, T61:13, J=0.0006763, nm-13, Lab#=1404-01											
pillow lava, ridge northwest of Lie Cliff, Mt. Steere, Crary Mtns											
A	600	225.5	1.318	737.7	1.24	0.39	53.2	3.4	0.9	9.3	3.4
B	700	65.39	0.9341	192.7	21.7	0.55	86.3	13.0	16.8	10.33	0.60
C	800	22.16	0.7251	50.14	40.7	0.70	63.2	33.3	46.7	8.98	0.17
D	875	33.25	0.7315	85.89	14.1	0.70	17.2	23.8	57.0	9.62	0.32
E	1000	16.00	0.9852	29.61	12.9	0.52	7.8	45.7	66.5	8.90	0.16
F	1200	10.78	5.509	15.67	20.9	0.093	11.1	60.7	81.9	7.999	0.087
G	1400	10.94	8.613	17.02	24.7	0.059	12.3	59.9	100.0	8.027	0.079
total gas age			n=7		136.3	0.45				8.93	0.27
no plateau			n=7	steps A-G	136.3	0.45			100.0	8.45	0.46
TW92-190, T63:13, J=0.0006769, nm-13, Lab#=1405-02											
pillow lava, ridge northwest of Lie Cliff, Mt. Steere, Crary Mtns											
A	600	84.55	0.9608	253.2	19.8	0.53	96.8	11.6	21.2	11.93	0.82
B	700	31.98	1.443	82.51	13.4	0.35	85.2	24.0	35.6	9.37	0.30
C	800	19.39	2.744	42.28	30.8	0.19	48.9	36.6	68.6	8.65	0.14
D	875	25.57	3.196	62.89	8.97	0.16	28.9	28.2	78.3	8.80	0.25
E	1000	12.45	3.767	21.82	5.54	0.14	18.8	50.4	84.2	7.66	0.15
F	1200	8.084	17.89	12.70	11.9	0.029	27.6	70.3	96.9	7.02	0.11
G	1400	9.767	24.25	17.93	2.85	0.021	4.5	64.6	100.0	7.82	0.17
total gas age			n=7		93.3	0.25				9.17	0.35
no plateau			n=7	steps A-G	93.3	0.25			100.0	8.27	0.64

Appendix I. $^{40}Ar/^{39}Ar$ Analytical Data

Crary Mountains, Marie Byrd Land (1992-93 Field Season)

ID	Temp (°C)	$^{40}Ar/^{39}Ar$	$^{37}Ar/^{39}Ar$	$^{36}Ar/^{39}Ar$ (x 10^{-3})	$^{39}Ar_K$ (x 10^{-15} mol)	K/Ca	Cl/K (x 10^{-3})	$^{40}Ar^*$ (%)	^{39}Ar (%)	Age (Ma)	±2s (Ma)
TW92-186, T59:13, J=0.0006754, nm-13, Lab#=1403-01											
lava, ridge northwest of Lie Cliff, Mt. Steere, Crary Mtns											
A	*600*	*2111.2*	*2.525*	*6965.9*	*0.238*	*0.20*	*102.3*	*2.5*	*0.2*	*63.5*	*61.7*
B	*700*	*408.2*	*2.232*	*1331.8*	*1.04*	*0.23*	*111.5*	*3.6*	*1.0*	*18.0*	*6.0*
C	*800*	*58.79*	*1.785*	*170.5*	*12.2*	*0.29*	*152.1*	*14.5*	*10.1*	*10.35*	*0.59*
D	*875*	*26.52*	*1.316*	*64.40*	*15.3*	*0.39*	*72.7*	*28.6*	*21.6*	*9.21*	*0.25*
E	*1000*	*20.07*	*1.354*	*43.33*	*22.6*	*0.38*	*28.3*	*36.6*	*38.5*	*8.95*	*0.18*
F	1100	10.69	1.286	13.04	11.3	0.40	12.2	64.6	47.0	8.405	0.098
G	1200	21.59	5.249	51.04	59.4	0.097	16.9	31.9	91.4	8.40	0.16
H	1400	34.06	8.925	94.55	11.4	0.057	17.3	19.9	100.0	8.30	0.35
total gas age			n=8		133.6	0.22				8.93	0.39
natural plateau			n=3	steps F-H	82.2	0.13			61.5	8.40	0.11
TW92-145, T44:13, J=0.0006649, nm-13, Lab#=1398-01											
lava, Morrison Rocks, Mt. Frakes, Crary Mtns											
B	*625*	*54.79*	*1.521*	*167.9*	*0.329*	*0.34*	*49.2*	*9.6*	*0.2*	*6.3*	*1.7*
C	725	2.841	1.218	4.336	46.2	0.42	29.9	57.4	35.0	1.957	0.024
D	800	2.253	1.564	2.734	23.8	0.33	34.7	68.5	53.0	1.852	0.026
E	850	2.350	2.042	3.342	8.70	0.25	37.0	63.7	59.6	1.798	0.040
F	900	2.461	2.215	4.218	5.79	0.23	37.8	55.4	63.9	1.636	0.057
G	1000	2.540	2.546	4.415	5.96	0.20	37.5	55.5	68.4	1.692	0.063
H	1200	3.241	5.568	7.911	40.2	0.092	42.8	40.4	98.8	1.576	0.033
I	*1400*	*24.51*	*82.81*	*55.18*	*1.65*	*0.006*	*29.7*	*59.3*	*100.0*	*18.43*	*0.45*
total gas age			n=8		132.7	0.27				2.001	0.073
selected mean			n=6	steps C-H	130.7	0.27			98.5	1.85	0.11
TW92-142, T43:13, J=0.0006638, nm-13, Lab#=1397-01											
lava, Morrison Rocks, Mt. Frakes, Crary Mtns											
A	*550*	*52.98*	*1.317*	*168.6*	*0.232*	*0.39*	*88.3*	*6.1*	*0.3*	*3.9*	*2.6*
B	*625*	*10.86*	*0.8368*	*30.97*	*8.66*	*0.61*	*66.9*	*16.1*	*11.3*	*2.10*	*0.15*
C	725	2.738	1.268	4.486	24.6	0.40	47.4	54.3	42.5	1.782	0.031
D	800	2.448	1.909	3.523	16.5	0.27	48.9	62.6	63.3	1.836	0.026
E	850	2.858	2.397	4.972	6.19	0.21	43.6	54.3	71.2	1.859	0.054
F	*900*	*3.306*	*2.587*	*7.010*	*3.62*	*0.20*	*37.7*	*42.7*	*75.8*	*1.693*	*0.094*
G	*1000*	*3.395*	*2.877*	*7.822*	*3.91*	*0.18*	*34.7*	*37.8*	*80.7*	*1.538*	*0.090*
H	*1100*	*3.868*	*4.224*	*9.919*	*2.21*	*0.12*	*39.9*	*32.0*	*83.5*	*1.49*	*0.14*
I	*1200*	*4.775*	*7.284*	*13.90*	*10.9*	*0.070*	*53.2*	*25.2*	*97.4*	*1.449*	*0.077*
J	*1400*	*19.05*	*85.01*	*56.26*	*2.07*	*0.006*	*37.2*	*46.9*	*100.0*	*11.35*	*0.36*
total gas age			n=10		78.9	0.30				2.02	0.11
selected mean			n=3	steps C-E	47.3	0.33			59.9	1.815	0.051

Appendix I. $^{40}Ar/^{39}Ar$ Analytical Data

Crary Mountains, Marie Byrd Land (1992-93 Field Season)

ID	Temp (°C)	$^{40}Ar/^{39}Ar$	$^{37}Ar/^{39}Ar$	$^{36}Ar/^{39}Ar$ (x 10^{-3})	$^{39}Ar_K$ (x 10^{-15} mol)	K/Ca	Cl/K (x 10^{-3})	$^{40}Ar^*$ (%)	^{39}Ar (%)	Age (Ma)	±2s (Ma)
TW92-128, T37:13, whole rk, J=0.0006765, nm-13, Lab#=1395-01											
lava, Morrison Rocks, Mt. Frakes, Crary Mtns											
C	*725*	*41.77*	*1.448*	*131.5*	*2.29*	*0.35*	*30.2*	*7.2*	*2.2*	*3.68*	*0.69*
D	800	4.187	1.460	7.278	17.9	0.35	7.9	50.8	19.0	2.596	0.045
E	850	2.822	1.221	2.928	22.9	0.42	3.7	71.9	40.6	2.477	0.026
F	900	3.026	1.296	3.429	12.0	0.39	4.1	69.1	51.9	2.551	0.040
G	1000	3.419	1.602	4.977	18.7	0.32	6.1	59.9	69.6	2.502	0.034
H	*1100*	*6.228*	*2.211*	*14.94*	*7.34*	*0.23*	*18.7*	*31.5*	*76.5*	*2.395*	*0.093*
I	*1200*	*12.65*	*3.169*	*37.44*	*6.30*	*0.16*	*27.2*	*14.3*	*82.5*	*2.20*	*0.17*
J	*1400*	*12.71*	*12.54*	*39.99*	*18.2*	*0.041*	*28.9*	*14.4*	*99.7*	*2.25*	*0.16*
K	*1650*	*52.28*	*15.07*	*173.3*	*0.356*	*0.034*	*34.5*	*4.2*	*100.0*	*2.7*	*1.9*
total gas age			n=9		105.9	0.29				2.48	0.11
selected mean			n=4	steps D-G	71.4	0.37			67.4	2.517	0.057
TW92-125, T33:13, J=0.0006742, nm-13, Lab#=1394-01											
lava, Morrison Rocks, Mt. Frakes, Crary Mtns											
B	*625*	*459.9*	*1.639*	*1519.9*	*0.489*	*0.31*	*52.4*	*2.4*	*0.4*	*13.2*	*9.0*
C	*725*	*19.16*	*1.394*	*57.47*	*8.66*	*0.37*	*21.3*	*11.8*	*7.9*	*2.75*	*0.21*
D	800	6.197	1.077	13.98	12.2	0.47	13.6	34.3	18.5	2.585	0.074
E	850	5.172	0.8766	10.59	7.85	0.58	16.5	40.3	25.3	2.538	0.083
F	900	5.794	1.055	12.71	5.86	0.48	22.1	36.2	30.4	2.55	0.11
G	1000	10.14	1.627	27.88	7.06	0.31	39.1	19.8	36.5	2.44	0.15
H	1100	25.09	1.551	79.66	7.56	0.33	55.5	6.6	43.0	2.01	0.32
I	1200	31.41	1.724	99.99	19.9	0.30	53.0	6.3	60.3	2.41	0.32
J	*1650*	*26.78*	*6.237*	*84.19*	*45.9*	*0.082*	*62.2*	*8.8*	*100.0*	*2.89*	*0.25*
total gas age			n=9		115.5	0.27				2.68	0.27
selected mean			n=6	steps D-I	60.5	0.39			52.3	2.535	0.093
TW92-130, T35:13, J=0.0006751, nm-13, Lab#=1396-01											
lava, Morrison Rocks, Mt. Frakes, Crary Mtns											
C	*725*	*16.10*	*1.361*	*41.09*	*5.49*	*0.37*	*16.0*	*25.1*	*4.8*	*4.92*	*0.20*
D	*800*	*4.347*	*1.361*	*3.973*	*18.2*	*0.37*	*4.4*	*74.9*	*20.7*	*3.965*	*0.033*
E	850	3.933	1.068	2.753	20.7	0.48	2.5	80.8	38.9	3.871	0.030
F	900	4.119	0.8986	3.329	11.3	0.57	3.7	77.3	48.8	3.874	0.038
G	1000	4.504	1.010	4.612	17.0	0.51	8.0	71.0	63.6	3.891	0.031
H	1100	6.401	1.189	11.24	9.86	0.43	17.6	49.2	72.3	3.834	0.074
I	*1200*	*8.205*	*2.729*	*18.88*	*13.1*	*0.19*	*31.9*	*34.3*	*83.7*	*3.430*	*0.090*
J	*1400*	*8.986*	*14.38*	*25.18*	*18.6*	*0.035*	*32.2*	*29.3*	*100.0*	*3.23*	*0.10*
total gas age			n=8		114.3	0.36				3.782	0.087
natural plateau			n=4	steps E-H	58.9	0.49			51.5	3.876	0.034

Appendix I. $^{40}Ar/^{39}Ar$ Analytical Data

Crary Mountains, Marie Byrd Land (1992-93 Field Season)

ID	Temp (°C)	$^{40}Ar/^{39}Ar$	$^{37}Ar/^{39}Ar$	$^{36}Ar/^{39}Ar$ (x 10^{-3})	$^{39}Ar_K$ (x 10^{-15} mol)	K/Ca	Cl/K (x 10^{-3})	$^{40}Ar^*$ (%)	^{39}Ar (%)	Age (Ma)	±2s (Ma)
TW94-151, M1:39, 147.7 mg, J=0.0000460528, NM-39, Lab#=5621-01											
cinder cone, English Rock, Mt. Frakes, Crary Mtns											
A	*500*	*15.90*	*1.483*	*55.65*	*0.107*	*0.34*	*94.3*	*-2.8*	*2.0*	*-0.04*	*0.13*
B	600	20.37	1.062	67.95	0.620	0.48	84.6	1.7	13.4	0.029	0.047
C	700	4.965	0.7326	15.53	1.28	0.70	94.2	8.2	37.0	0.034	0.013
D	800	6.617	0.8094	21.29	1.44	0.63	86.4	5.5	63.5	0.030	0.016
E	900	9.834	1.365	32.45	0.708	0.37	79.1	3.3	76.6	0.027	0.026
F	1000	16.77	2.235	56.14	0.208	0.23	68.2	2.0	80.4	0.027	0.067
G	*1100*	*26.44*	*3.449*	*85.54*	*0.164*	*0.15*	*65.7*	*5.3*	*83.4*	*0.12*	*0.10*
H	*1200*	*22.10*	*10.29*	*70.34*	*0.782*	*0.050*	*73.5*	*9.4*	*97.9*	*0.174*	*0.037*
I	*1300*	*200.0*	*19.79*	*313.1*	*0.043*	*0.026*	*78.9*	*54.5*	*98.7*	*9.16*	*0.54*
J	*1450*	*124.7*	*8.750*	*272.5*	*0.039*	*0.058*	*75.5*	*35.9*	*99.4*	*3.74*	*0.41*
K	*1650*	*66.67*	*7.609*	*179.4*	*0.034*	*0.067*	*60.4*	*21.3*	*100.0*	*1.19*	*0.41*
total gas age			n=11		5.42	0.46				0.158	0.039
selected mean			n=5	steps B-F	4.25	0.57			78.4	0.032	0.010
natural plateau			n=7	steps A-G	4.521	0.55			83.4	0.032	0.012
TW92-151, T49:13, J=0.0006688, nm-13, Lab#=1391-01											
cinder cone, English Rock, Mt. Frakes, Crary Mtns											
A	*550*	*7.007*	*0.6844*	*24.47*	*2.73*	*0.75*	*94.7*	*-2.7*	*1.8*	*-0.23*	*0.24*
B	625	1.033	0.5386	3.431	8.98	0.95	77.8	3.8	7.7	0.047	0.037
C	725	0.4265	0.8165	1.478	46.3	0.62	64.2	7.2	38.3	0.037	0.010
D	800	0.3131	0.8271	1.116	29.6	0.62	63.9	7.9	57.9	0.030	0.011
E	850	0.3523	0.9179	1.258	21.2	0.56	60.5	8.3	71.9	0.035	0.014
F	900	0.4440	1.320	1.702	13.7	0.39	54.9	4.6	80.9	0.025	0.028
G	1000	0.8016	2.094	3.051	10.5	0.24	46.9	4.8	87.9	0.047	0.034
H	*1100*	*1.609*	*3.544*	*5.907*	*3.98*	*0.14*	*34.5*	*7.1*	*90.5*	*0.137*	*0.076*
I	*1200*	*3.185*	*10.79*	*13.43*	*12.8*	*0.047*	*48.2*	*0.8*	*99.0*	*0.029*	*0.072*
J	*1400*	*15.58*	*52.01*	*42.53*	*1.55*	*0.010*	*42.4*	*44.9*	*100.0*	*8.73*	*0.36*
total gas age			n=10		151.4	0.52				0.122	0.049
natural plateau			n=6	steps B-G	130.3	0.58			86.1	0.035	0.010

Appendix I. $^{40}Ar/^{39}Ar$ Analytical Data

Crary Mountains, Marie Byrd Land (1992-93 Field Season)

ID	Temp (°C)	$^{40}Ar/^{39}Ar$	$^{37}Ar/^{39}Ar$	$^{36}Ar/^{39}Ar$ (x 10^{-3})	$^{39}Ar_K$ (x 10^{-15} mol)	K/Ca	Cl/K (x 10^{-3})	$^{40}Ar^*$ (%)	^{39}Ar (%)	Age (Ma)	±2s (Ma)
TW92-157, 109:17, 31.3 mg, J=0.0009519, nm-17*, Lab#=1877-01											
cinder cone, English Rock, Mt. Frakes, Crary Mtns											
B	*0*	*20.96*	*2.604*	*67.77*	*0.324*	*0.20*	*1.2*	*5.3*	*0.8*	*1.9*	*1.4*
C	0	0.8982	2.761	2.104	4.72	0.18	0.042	52.3	12.9	0.808	0.083
D	0	0.8665	2.749	1.819	5.99	0.19	0.11	60.2	28.3	0.897	0.064
E	0	0.8916	2.794	1.924	6.71	0.18	-0.047	58.2	45.5	0.892	0.061
FF	0	0.8573	2.751	2.175	6.94	0.19	-0.063	47.5	63.3	0.700	0.055
GG	0	0.8237	2.705	1.778	12.0	0.19	-0.089	59.2	94.2	0.838	0.032
HH	*0*	*6.167*	*1.308*	*22.79*	*1.08*	*0.39*	*-4.000*	*-7.9*	*97.0*	*-0.84*	*0.41*
I	*0*	*6.619*	*0.6589*	*21.30*	*1.18*	*0.77*	*-0.011*	*5.4*	*100.0*	*0.61*	*0.37*
total gas age			n=8		39.0	0.21				0.78	0.11
selected mean			n=5	steps C-GG	36.4	0.19			93.4	0.826	0.079
TW92157, T51:13, J=0.0006701, nm-13, Lab#=1392-01											
cinder cone, English Rock, Mt. Frakes, Crary Mtns											
A	*550*	*1092.8*	*0.0000*	*5082.7*	*0.001*	*-*	*285.1*	*-37.4*	*0.0*	*-578*	*3293*
B	*625*	*134.1*	*4.736*	*543.2*	*0.024*	*0.11*	*200.1*	*-19.4*	*0.0*	*-32*	*26*
C	*725*	*4.122*	*0.9875*	*11.62*	*11.2*	*0.52*	*161.3*	*18.0*	*6.3*	*0.896*	*0.077*
D	800	1.217	1.166	1.950	31.1	0.44	134.9	58.2	23.6	0.857	0.017
E	850	1.323	1.104	2.236	25.9	0.46	137.9	54.8	38.0	0.877	0.019
F	900	2.259	1.291	5.667	20.4	0.40	131.6	29.3	49.4	0.800	0.037
G	1000	1.278	1.553	2.250	21.7	0.33	126.3	55.6	61.4	0.860	0.025
H	1200	1.994	3.809	5.556	65.9	0.13	112.6	31.2	98.1	0.754	0.021
I	*1650*	*10.51*	*13.68*	*29.69*	*3.38*	*0.037*	*98.6*	*26.3*	*100.0*	*3.37*	*0.17*
total gas age			n=9		179.7	0.31				0.858	0.072
selected mean			n=5	steps D-H	165.1	0.30			91.8	0.851	0.036
TW92-159, T53:13, J=0.0006714, nm-13, Lab#=1393-01											
cinder cone, English Rock, Mt. Frakes, Crary Mtns											
B	*625*	*24.20*	*0.6481*	*71.49*	*0.633*	*0.79*	*13.9*	*12.8*	*0.2*	*3.75*	*0.82*
C	*725*	*9.562*	*0.5148*	*26.36*	*16.3*	*0.99*	*14.2*	*18.7*	*6.2*	*2.17*	*0.11*
D	800	1.946	0.5515	2.234	71.9	0.93	7.6	67.1	32.6	1.582	0.015
E	850	1.761	0.5929	1.569	58.0	0.86	6.3	75.0	54.0	1.600	0.013
F	900	1.748	0.8128	1.517	19.9	0.63	8.9	76.7	61.3	1.624	0.019
G	1000	1.662	1.039	1.357	45.8	0.49	7.0	79.4	78.1	1.597	0.013
H	*1100*	*1.692*	*1.552*	*1.965*	*24.3*	*0.33*	*8.7*	*71.4*	*87.0*	*1.465*	*0.025*
I	*1200*	*1.749*	*3.637*	*3.138*	*27.6*	*0.14*	*37.3*	*61.7*	*97.1*	*1.310*	*0.023*
J	*1650*	*6.342*	*19.75*	*19.19*	*7.77*	*0.026*	*18.9*	*34.2*	*100.0*	*2.66*	*0.12*
total gas age			n=9		272.3	0.66				1.624	0.039
selected mean			n=4	steps D-G	195.7	0.77			71.9	1.598	0.021

Appendix I. $^{40}Ar/^{39}Ar$ Analytical Data

Crary Mountains, Marie Byrd Land (1992-93 Field Season)

ID	Temp (°C)	$^{40}Ar/^{39}Ar$	$^{37}Ar/^{39}Ar$	$^{36}Ar/^{39}Ar$ (x 10^{-3})	$^{39}Ar_K$ (x 10^{-15} mol)	K/Ca	Cl/K (x 10^{-3})	$^{40}Ar^*$ (%)	^{39}Ar (%)	Age (Ma)	±2s (Ma)
TW92-140b, L3:21, 56.7 mg, plag, J=0.00074, nm-21, Lab#=2963-01											
pyroclast Boyd Ridge, Crary Mtns											
A	*500*	*857.7*	*0.7548*	*2458.1*	*0.385*	*0.68*	*6.5*	*15.3*	*1.0*	*167*	*16*
B	*700*	*31.52*	*4.144*	*95.57*	*0.472*	*0.12*	*13.2*	*10.3*	*2.3*	*4.3*	*1.3*
C	850	1.254	4.225	1.294	3.10	0.12	0.94	68.0	10.8	1.14	0.14
D	1000	1.146	4.168	1.294	5.91	0.12	0.38	65.0	26.8	0.993	0.071
E	1100	1.190	4.219	1.310	4.55	0.12	0.36	65.9	39.2	1.046	0.098
F	*1200*	*2.187*	*4.120*	*1.915*	*3.89*	*0.12*	*0.24*	*73.3*	*49.8*	*2.14*	*0.12*
G	*1300*	*1.967*	*4.255*	*2.411*	*2.83*	*0.12*	*0.43*	*62.8*	*57.5*	*1.65*	*0.15*
H	*1450*	*1.480*	*4.253*	*1.812*	*12.7*	*0.12*	*0.44*	*62.5*	*91.9*	*1.235*	*0.037*
I	*1750*	*25.04*	*3.945*	*4.616*	*2.97*	*0.13*	*0.21*	*94.5*	*100.0*	*31.30*	*0.21*
total gas age			n=9		36.8	0.13				5.50	0.28
selected mean			n=3	steps C-E	13.6	0.12			36.9	1.029	0.093
TW92-140a, K5:21, 47.8 mg, plag, J=0.0007402605, nm-21, Lab#=2962-01											
pyroclast Boyd Ridge, Crary Mtns											
A	*700*	*926.4*	*6.503*	*3120.9*	*0.301*	*0.078*	*14.3*	*0.5*	*1.2*	*5.6*	*35.3*
B	*850*	*4.099*	*5.947*	*10.36*	*1.53*	*0.086*	*0.88*	*24.8*	*7.0*	*1.36*	*0.28*
C	950	1.348	5.881	2.180	2.94	0.087	0.14	50.8	18.3	0.91	0.12
D	1050	1.548	5.949	3.069	3.62	0.086	0.28	40.2	32.3	0.83	0.11
E	1150	1.950	5.981	3.814	3.56	0.085	1.1	41.2	46.0	1.07	0.12
F	1200	1.773	6.009	3.108	2.46	0.085	1.8	47.1	55.5	1.11	0.15
G	*1300*	*2.679*	*6.118*	*5.305*	*2.61*	*0.083*	*4.9*	*40.8*	*65.5*	*1.46*	*0.16*
H	*1450*	*3.675*	*6.155*	*10.12*	*7.60*	*0.083*	*7.0*	*18.1*	*94.7*	*0.888*	*0.088*
I	*1750*	*11.52*	*5.729*	*7.396*	*1.37*	*0.089*	*17.0*	*80.9*	*100.0*	*12.40*	*0.28*
total gas age			n=9		26.0	0.085				1.68	0.54
selected mean			n=4	steps C-F	12.6	0.086			48.4	0.96	0.15
TW92-139, T42:13, J=0.0006709, nm-13, Lab#=1409-01											
pyroclast Boyd Ridge, Crary Mtns											
B	*700*	*15.55*	*0.7157*	*46.08*	*1.27*	*0.71*	*194.4*	*12.6*	*0.5*	*2.38*	*0.50*
C	*800*	*2.591*	*0.8356*	*4.960*	*27.2*	*0.61*	*140.3*	*45.1*	*11.0*	*1.413*	*0.028*
D	*875*	*1.538*	*0.8966*	*1.676*	*38.0*	*0.57*	*136.7*	*70.9*	*25.6*	*1.320*	*0.021*
E	1000	2.632	1.002	5.528	49.2	0.51	132.4	40.0	44.6	1.275	0.024
F	1200	3.976	1.982	10.37	142.6	0.26	129.0	26.2	99.6	1.264	0.035
G	1400	5.752	6.084	17.31	1.08	0.084	108.0	18.8	100.0	1.31	0.26
total gas age			n=6		259.4	0.39				1.295	0.040
natural plateau			n=3	steps E-G	192.9	0.32			74.4	1.272	0.027

Appendix I. $^{40}Ar/^{39}Ar$ Analytical Data

Crary Mountains, Marie Byrd Land (1992-93 Field Season)

ID	Temp (°C)	$^{40}Ar/^{39}Ar$	$^{37}Ar/^{39}Ar$	$^{36}Ar/^{39}Ar$ (x 10^{-3})	$^{39}Ar_K$ (x 10^{-15} mol)	K/Ca	Cl/K (x 10^{-3})	$^{40}Ar^*$ (%)	^{39}Ar (%)	Age (Ma)	±2s (Ma)
TW92-135, T39:13, J=0.0006774, nm-13, Lab#=1400-01											
hyaloclasite, Runyon Rock, Boyd Ridge, Crary Mtns											
A	600	162.4	0.8724	538.2	2.15	0.58	201.2	2.1	3.7	4.2	2.1
B	700	17.55	0.9076	53.07	5.51	0.56	160.0	10.9	13.2	2.35	0.25
C	800	12.80	1.640	36.96	37.7	0.31	105.9	15.5	78.5	2.42	0.13
D	*875*	*31.38*	*1.949*	*97.96*	*12.4*	*0.26*	*90.8*	*8.2*	*100.0*	*3.13*	*0.37*
total gas age			n=4		57.8	0.33				2.63	0.26
natural plateau			n=3	steps A-C	45.4	0.35			78.5	2.41	0.19
TW92-135, T40:13, J=0.0006722, nm-13, Lab#=1408-01											
hyaloclasite, Runyon Rock, Boyd Ridge, Crary Mtns											
A	*600*	*284.4*	*0.8527*	*945.7*	*2.63*	*0.60*	*196.8*	*1.8*	*1.8*	*6.1*	*3.6*
B	700	18.32	1.349	55.45	35.1	0.38	116.2	11.0	25.8	2.45	0.17
C	800	50.20	2.011	161.5	30.4	0.25	91.4	5.2	46.5	3.16	0.49
D	875	45.10	2.326	145.0	11.1	0.22	89.9	5.3	54.1	2.93	0.53
E	1000	36.18	2.333	112.9	12.6	0.22	90.3	8.3	62.7	3.63	0.39
F	1200	23.07	4.352	71.97	53.7	0.12	100.3	9.2	99.4	2.57	0.22
G	*1400*	*20.12*	*32.41*	*62.13*	*0.918*	*0.016*	*26.1*	*21.0*	*100.0*	*5.24*	*0.73*
total gas age			n=7		146.5	0.23				2.86	0.37
selected mean			n=5	steps B-F	143.0	0.23			97.6	2.67	0.39

Appendix I. $^{40}Ar/^{39}Ar$ Analytical Data

$^{40}Ar/^{39}Ar$ Furnace Data: Central and Western Marie Byrd Land (1993-94 Field Season)

ID	Temp (°C)	$^{40}Ar/^{39}Ar$	$^{37}Ar/^{39}Ar$	$^{36}Ar/^{39}Ar$ ($x10^{-3}$)	$^{39}Ar_K$ ($x10^{-15}$ mol)	K/Ca	Cl/K (x 10-3)	$^{40}Ar^*$ (%)	^{39}Ar (%)	Age (Ma)	±2s (Ma)
WCM93-199 wr, L3:33, 49.6 mg, J=0.001494377, nm-33, Lab#=5152-01											
Coleman Nunatak, Hobbs Coast, southend moat top of upper lava											
A	*500*	*126.6*	*0.5719*	*425.8*	*2.84*	*0.89*	*1.00*	*0.6*	*2.4*	*2.1*	*3.9*
B	*600*	*5.049*	*0.6321*	*14.66*	*17.2*	*0.81*	*0.29*	*15.2*	*16.8*	*2.07*	*0.15*
C	650	2.625	1.164	6.054	16.8	0.44	0.22	35.2	30.8	2.494	0.092
D	750	2.352	1.348	5.030	22.8	0.38	0.11	41.2	49.9	2.614	0.069
E	850	2.750	1.221	6.498	14.2	0.42	0.097	33.6	61.9	2.490	0.099
F	925	3.389	1.493	8.692	6.86	0.34	0.21	27.6	67.6	2.52	0.22
G	1000	3.608	1.773	9.438	3.93	0.29	0.61	26.5	70.9	2.58	0.20
H	1100	6.821	5.634	21.81	3.95	0.091	0.72	11.9	74.2	2.19	0.31
I	1250	7.898	10.92	26.51	30.8	0.047	0.59	11.4	100.0	2.45	0.22
total gas age			n=9		119.3	0.37				2.43	0.30
plateau			n=7	steps C-I	99.3	0.27			83.2	2.54	0.08
WCM93-185 wr, K3:33, 51.9 mg, whole rock hawaiite, J=0.00149676, nm-33, Lab#=5146-01											
Coleman Nunatak, Hobbs Coast, southend moat middle of upper lava											
A	*500*	*273.7*	*0.6132*	*916.1*	*4.67*	*0.83*	*0.51*	*1.1*	*4.2*	*8.2*	*8.3*
B	600	29.42	0.7002	96.61	12.8	0.73	0.34	3.2	15.9	2.51	0.81
C	700	14.17	1.288	45.10	27.4	0.40	0.21	6.6	40.8	2.53	0.38
D	800	16.41	1.247	52.37	16.5	0.41	0.31	6.3	55.8	2.79	0.47
E	900	18.81	1.654	60.95	8.98	0.31	0.34	5.0	64.0	2.52	0.53
F	*1100*	*43.80*	*3.670*	*143.2*	*17.5*	*0.14*	*0.99*	*4.0*	*79.9*	*4.7*	*1.2*
G	*1200*	*19.83*	*13.77*	*66.89*	*22.2*	*0.037*	*0.92*	*5.7*	*100.0*	*3.06*	*0.52*
total gas age			n=7		110.1	0.33				3.27	0.98
natural plateau			n=4	steps B-E	65.8	0.45			59.7	2.60	0.28
WCM93-184 wr, K1:33, 55 mg, whole rock basanite, J=0.00149676, nm-33, Lab#=5144-01											
Coleman Nunatak, Hobbs Coast, southend moat middle of upper lava											
B	600	32.05	0.8366	105.2	11.6	0.61	0.47	3.2	8.8	2.73	0.87
C	700	7.645	1.160	22.85	30.1	0.44	0.29	12.8	31.5	2.65	0.22
D	800	7.441	1.020	22.08	25.4	0.50	0.30	13.4	50.7	2.69	0.20
E	900	8.845	1.351	26.97	13.8	0.38	0.42	11.0	61.1	2.64	0.25
F	*1000*	*8.467*	*1.736*	*26.54*	*5.97*	*0.29*	*0.70*	*8.9*	*65.6*	*2.04*	*0.34*
G	*1100*	*13.82*	*3.388*	*45.48*	*11.2*	*0.15*	*0.71*	*4.6*	*74.1*	*1.73*	*0.43*
H	*1200*	*18.98*	*10.12*	*63.58*	*34.1*	*0.050*	*0.81*	*5.1*	*99.8*	*2.64*	*0.59*
I	*1300*	*45.19*	*60.87*	*161.7*	*0.201*	*0.008*	*1.3*	*4.6*	*100.0*	*5.9*	*6.0*
total gas age			n=8		132.4	0.33				2.56	0.43
natural plateau			n=4	steps B-E	80.9	0.47			61.1	2.66	0.13

Appendix I. $^{40}Ar/^{39}Ar$ Analytical Data

$^{40}Ar/^{39}Ar$ Furnace Data: Central and Western Marie Byrd Land (1993-94 Field Season)

ID	Temp (°C)	$^{40}Ar/^{39}Ar$	$^{37}Ar/^{39}Ar$	$^{36}Ar/^{39}Ar$ (x10^{-3})	$^{39}Ar_K$ (x10^{-15} mol)	K/Ca	Cl/K (x 10-3)	$^{40}Ar^*$ (%)	^{39}Ar (%)	Age (Ma)	±2s (Ma)
WCM93-192 wr, K6:33, 51.9 mg, J=0.00149676, nm-33, Lab#=5149-01											
Coleman Nunatak, Hobbs Coast, southend moat base of upper lava											
A	*500*	*143.3*	*0.5838*	*483.2*	*1.64*	*0.87*	*0.37*	*0.4*	*0.9*	*1.5*	*4.3*
B	600	37.53	0.3893	123.8	15.4	1.3	0.14	2.6	9.1	2.6	1.1
C	700	17.74	0.4237	57.13	37.6	1.2	0.16	5.0	29.1	2.41	0.49
D	800	13.20	0.5651	41.59	31.4	0.90	0.23	7.2	45.9	2.58	0.35
E	900	12.84	0.6700	40.19	24.1	0.76	0.24	7.9	58.7	2.74	0.35
F	1000	11.35	1.099	35.45	20.0	0.46	0.24	8.5	69.4	2.60	0.30
G	*1100*	*31.92*	*2.109*	*106.4*	*15.3*	*0.24*	*0.35*	*2.0*	*77.5*	*1.75*	*0.85*
H	*1200*	*37.97*	*7.817*	*126.1*	*42.2*	*0.065*	*0.62*	*3.5*	*100.0*	*3.6*	*1.2*
total gas age			n=8		187.5	0.69				2.72	0.70
natural plateau			n=5	steps B-F	128.4	0.94			68.5	2.61	0.20
WCM93-190 wr, K5:33, 46.4 mg, J=0.00149676, nm-33, Lab#=5148-01											
Coleman Nunatak, Hobbs Coast, southend moat base of upper lava											
A	*500*	*210.2*	*0.5043*	*703.3*	*2.05*	*1.0*	*0.64*	*1.2*	*1.4*	*6.5*	*7.6*
B	*675*	*17.15*	*0.7397*	*55.37*	*28.2*	*0.69*	*0.13*	*4.9*	*20.3*	*2.29*	*0.46*
C	750	10.77	1.205	32.88	18.4	0.42	0.065	10.6	32.6	3.09	0.29
D	850	10.16	0.6796	30.47	20.6	0.75	0.099	11.9	46.4	3.25	0.28
E	925	9.033	0.7625	26.24	14.2	0.67	0.11	14.8	55.9	3.61	0.26
F	1050	19.23	1.084	61.15	15.4	0.47	0.28	6.5	66.3	3.36	0.54
G	*1250*	*33.33*	*6.588*	*108.5*	*48.7*	*0.077*	*0.63*	*5.4*	*98.9*	*4.83*	*0.88*
GG	*1450*	*12.69*	*0.8801*	*9.363*	*1.58*	*0.58*	*0.20*	*78.7*	*100.0*	*26.80*	*0.66*
total gas age			n=8		149.2	0.44				3.91	0.65
selected mean			n=4	steps C-F	68.6	0.58			46.0	3.34	0.29
WCM93-195 wr, L1:33, 49.4 mg, J=0.001494377, nm-33, Lab#=5150-01											
Coleman Nunatak, Hobbs Coast, bomb from lower surge beds											
A	500	1475.3	1.682	4839.6	0.856	0.30	2.1	3.1	2.2	118.5	49.4
B	600	597.7	1.678	1905.2	5.63	0.30	0.23	5.8	17.0	91.7	19.6
C	700	198.2	1.327	610.1	16.6	0.38	0.057	9.1	60.4	47.9	5.6
D	800	159.2	1.565	493.0	15.2	0.33	-0.084	8.6	100.0	36.5	4.6
total gas age			n=4		38.3	0.35				51.4	8.3
no plateau											

Appendix I. $^{40}Ar/^{39}Ar$ Analytical Data

$^{40}Ar/^{39}Ar$ Furnace Data: Central and Western Marie Byrd Land (1993-94 Field Season)

ID	Temp (°C)	$^{40}Ar/^{39}Ar$	$^{37}Ar/^{39}Ar$	$^{36}Ar/^{39}Ar$ ($x10^{-3}$)	$^{39}Ar_K$ ($x10^{-15}$ mol)	K/Ca	Cl/K (x 10-3)	$^{40}Ar^*$ (%)	^{39}Ar (%)	Age (Ma)	±2s (Ma)
WCM93-198 wr, L2:33, 46.7 mg, J=0.001494377, nm-33, Lab#=5151-01											
Coleman Nunatak, Hobbs Coast, bomb from lower surge beds											
B	*600*	*75.47*	*0.8604*	*233.8*	*5.97*	*0.59*	*0.012*	*8.5*	*3.9*	*17.3*	*2.1*
C	*650*	*26.27*	*0.8675*	*76.60*	*10.2*	*0.59*	*0.29*	*14.1*	*10.6*	*9.95*	*0.70*
D	750	18.47	0.9094	53.94	24.4	0.56	0.28	14.1	26.5	7.00	0.51
E	850	22.51	1.009	66.39	24.7	0.51	0.29	13.2	42.5	7.98	0.55
F	925	23.10	1.081	69.95	14.0	0.47	0.31	10.9	51.6	6.77	0.63
G	*1000*	*82.40*	*1.552*	*263.1*	*8.46*	*0.33*	*0.51*	*5.8*	*57.1*	*12.9*	*2.2*
H	*1100*	*28.19*	*2.368*	*87.10*	*61.1*	*0.22*	*0.69*	*9.3*	*96.9*	*7.09*	*0.80*
I	*1250*	*17.85*	*40.73*	*61.51*	*4.72*	*0.013*	*2.0*	*15.7*	*100.0*	*7.8*	*1.1*
total gas age			n=8		153.5	0.38				8.12	0.85
selected mean			n=3	steps D-F	63.0	0.52			41.1	7.28	0.79
WCM93-188 wr, K4:33, 55.4 mg, J=0.00149676, nm-33, Lab#=5147-01											
Coleman Nunatak, Hobbs Coast, southend moat lower lava											
A	*500*	*106.8*	*0.2633*	*359.0*	*4.86*	*1.9*	*0.76*	*0.7*	*2.7*	*2.0*	*3.4*
B	675	6.117	0.6207	17.72	32.3	0.82	0.18	15.2	20.3	2.51	0.17
C	750	5.281	1.087	14.97	23.6	0.47	0.21	17.8	33.3	2.54	0.16
D	850	5.755	0.6078	16.37	28.4	0.84	0.12	16.7	48.8	2.60	0.15
E	925	4.513	0.7445	12.52	19.3	0.69	0.091	19.3	59.3	2.35	0.15
F	1050	4.964	1.198	14.23	17.2	0.43	0.30	17.1	68.7	2.30	0.15
G	*1250*	*14.85*	*6.989*	*48.51*	*57.1*	*0.073*	*0.50*	*7.1*	*100.0*	*2.86*	*0.40*
total gas age			n=7		182.8	0.52				2.58	0.34
natural plateau			n=5	steps B-F	120.8	0.68			66.1	2.46	0.14
WCM93-208 wr, H1:33, 50.0 mg, J=0.00149927, nm-33, Lab#=5132-01											
Coleman Nunatak, Hobbs Coast, north peak scoriaceous dike											
A	*500*	*215.4*	*0.4104*	*721.5*	*2.42*	*1.2*	*0.20*	*1.0*	*1.6*	*6.1*	*6.4*
B	600	7.326	0.3390	21.88	17.9	1.5	0.082	12.1	13.0	2.39	0.19
C	700	2.895	0.4831	6.821	31.8	1.1	0.022	31.7	33.4	2.478	0.075
D	800	3.114	0.7033	7.350	24.2	0.73	0.037	32.0	48.9	2.694	0.081
E	900	2.947	0.7142	6.879	18.9	0.71	0.080	32.9	61.0	2.621	0.099
F	1000	2.670	1.391	6.426	11.6	0.37	0.18	32.9	68.4	2.38	0.12
G	*1100*	*8.044*	*2.120*	*25.12*	*15.7*	*0.24*	*0.43*	*9.7*	*78.4*	*2.12*	*0.25*
H	*1200*	*10.19*	*10.56*	*33.78*	*33.7*	*0.048*	*0.60*	*10.0*	*100.0*	*2.78*	*0.30*
total gas age			n=8		156.1	0.67				2.60	0.30
selected mean			n=5	steps B-F	104.3	0.92			66.8	2.55	0.13

Appendix I. $^{40}Ar/^{39}Ar$ Analytical Data

$^{40}Ar/^{39}Ar$ Furnace Data: Central and Western Marie Byrd Land (1993-94 Field Season)

ID	Temp (°C)	$^{40}Ar/^{39}Ar$	$^{37}Ar/^{39}Ar$	$^{36}Ar/^{39}Ar$ ($x10^{-3}$)	$^{39}Ar_K$ ($x10^{-15}$ mol)	K/Ca	Cl/K (x 10-3)	$^{40}Ar^*$ (%)	^{39}Ar (%)	Age (Ma)	±2s (Ma)
WCM93-207 wr, L6:33, 48.2 mg, J=0.001494377, nm-33, Lab#=5155-01											
Coleman Nunatak, Hobbs Coast, north peak, dike in lapilli tuff											
A	*500*	*252.8*	*0.5219*	*845.1*	*2.14*	*0.98*	*0.96*	*1.2*	*1.7*	*8.5*	*7.3*
B	*600*	*5.571*	*0.5401*	*16.32*	*14.0*	*0.94*	*0.18*	*14.2*	*12.6*	*2.13*	*0.19*
C	650	3.102	0.9373	7.612	13.2	0.54	0.20	29.8	22.9	2.49	0.12
D	750	2.378	1.495	5.124	21.2	0.34	0.10	41.1	39.4	2.639	0.070
E	850	2.587	0.8217	5.608	18.1	0.62	0.057	38.4	53.5	2.676	0.089
F	925	2.622	0.9697	6.075	9.02	0.53	0.053	34.4	60.6	2.43	0.14
G	1000	3.778	1.354	10.02	6.55	0.38	0.16	24.4	65.7	2.48	0.18
H	*1100*	*8.852*	*4.818*	*28.61*	*4.44*	*0.11*	*0.73*	*8.7*	*69.2*	*2.08*	*0.37*
I	*1250*	*9.642*	*8.256*	*31.01*	*39.5*	*0.062*	*0.50*	*11.5*	*100.0*	*3.01*	*0.29*
total gas age			n=9		128.1	0.40				2.74	0.34
selected mean			n=5	steps C-G	68.0	0.48			53.1	2.59	0.11
WCM93-205 wr, L5:33, 47.8 mg, J=0.001494377, nm-33, Lab#=5154-01											
Coleman Nunatak, Hobbs Coast, north peak, dike in lapilli tuff											
B	600	65.12	0.6592	216.7	7.04	0.77	0.53	1.8	5.4	3.1	1.9
C	650	30.45	0.5711	98.98	10.4	0.89	0.49	4.1	13.4	3.36	0.98
D	750	23.02	0.5914	74.57	23.1	0.86	0.31	4.5	31.1	2.77	0.76
E	850	16.11	0.7161	51.49	26.9	0.71	0.32	5.9	51.7	2.57	0.48
F	925	18.53	0.9239	59.55	15.9	0.55	0.22	5.4	63.8	2.72	0.52
G	1000	19.94	1.244	64.52	10.9	0.41	0.28	4.9	72.2	2.61	0.58
H	1100	22.02	3.017	71.51	8.23	0.17	0.54	5.1	78.5	3.04	0.66
I	*1250*	*43.68*	*11.25*	*142.3*	*28.1*	*0.045*	*0.90*	*5.7*	*100.0*	*6.8*	*1.5*
total gas age			n=8		130.6	0.53				3.6	0.9
natural plateau			n=7	steps B-H	102.5	0.67			78.5	2.75	0.31
WCM93-202 wr, L4:33, 53.1 mg, J=0.001494377, nm-33, Lab#=5153-01											
Coleman Nunatak, Hobbs Coast, north peak, dike in lapilli tuff											
B	600	24.51	0.9975	80.25	11.1	0.51	0.27	3.6	10.5	2.36	0.73
C	650	8.660	1.698	26.01	12.8	0.30	0.32	12.8	22.7	2.98	0.26
D	750	7.591	2.155	22.95	18.1	0.24	0.24	12.8	39.9	2.63	0.22
E	850	10.05	1.848	30.75	11.9	0.28	0.28	11.0	51.1	2.99	0.30
F	*925*	*12.75*	*1.741*	*40.79*	*6.27*	*0.29*	*0.33*	*6.6*	*57.1*	*2.25*	*0.41*
G	*1000*	*13.22*	*1.892*	*42.87*	*5.02*	*0.27*	*0.53*	*5.3*	*61.9*	*1.89*	*0.47*
H	*1100*	*18.53*	*2.832*	*59.37*	*16.1*	*0.18*	*0.55*	*6.5*	*77.1*	*3.26*	*0.51*
I	*1250*	*19.89*	*11.56*	*67.18*	*24.1*	*0.044*	*0.74*	*4.6*	*100.0*	*2.51*	*0.59*
total gas age			n=8		105.3	0.23				2.69	0.47
natural plateau			n=4	steps B-E	53.9	0.32			51.1	2.81	0.27

Appendix I. $^{40}Ar/^{39}Ar$ Analytical Data

$^{40}Ar/^{39}Ar$ Furnace Data: Central and Western Marie Byrd Land (1993-94 Field Season)

ID	Temp (°C)	$^{40}Ar/^{39}Ar$	$^{37}Ar/^{39}Ar$	$^{36}Ar/^{39}Ar$ ($x10^{-3}$)	$^{39}Ar_K$ ($x10^{-15}$ mol)	K/Ca	Cl/K (x 10-3)	$^{40}Ar^*$ (%)	^{39}Ar (%)	Age (Ma)	±2s (Ma)
WCM93-218 wr, H2:33, 46.8 mg, J=0.00149927, nm-33, Lab#=5133-01											
Cousins Rock, Hobbs Coast, strombolian bomb											
A	*500*	*90.89*	*0.5807*	*303.0*	*4.11*	*0.88*	*0.74*	*1.5*	*2.3*	*3.8*	*2.7*
B	*600*	*5.785*	*0.6552*	*14.48*	*18.0*	*0.78*	*0.16*	*26.9*	*12.6*	*4.21*	*0.17*
C	700	3.599	0.9987	6.416	42.2	0.51	0.28	49.4	36.6	4.810	0.088
D	800	4.206	1.026	8.243	28.5	0.50	0.16	44.0	52.8	4.997	0.094
E	900	5.069	1.215	11.39	11.1	0.42	0.43	35.4	59.1	4.86	0.15
F	1000	3.926	1.623	7.923	5.41	0.31	0.46	43.5	62.1	4.62	0.19
G	1100	7.428	1.838	19.64	22.0	0.28	0.60	23.8	74.6	4.78	0.18
H	1200	6.906	2.628	17.88	43.9	0.19	0.64	26.4	99.6	4.93	0.17
I	*1300*	*13.13*	*6.692*	*37.58*	*0.760*	*0.076*	*0.36*	*19.3*	*100.0*	*6.9*	*1.3*
total gas age			n=9		176.0	0.42				4.79	0.21
natural plateau			n=6	steps C-H	153.1	0.37			87.0	4.87	0.11
WCM93-219 wr, H3:33, 48.9 mg, J=0.00149927, nm-33, Lab#=5134-01											
Cousins Rock, Hobbs Coast, strombolian lava											
A	*500*	*69.95*	*0.4292*	*228.1*	*3.35*	*1.2*	*0.088*	*3.7*	*1.8*	*6.9*	*2.2*
B	*600*	*3.489*	*0.4089*	*5.892*	*15.8*	*1.2*	*-0.037*	*51.0*	*10.4*	*4.808*	*0.087*
C	700	2.252	0.5611	1.588	49.7	0.91	0.10	81.1	37.4	4.933	0.035
D	800	2.503	0.8552	2.446	35.5	0.60	0.19	73.7	56.6	4.988	0.045
E	900	2.693	1.037	3.146	19.6	0.49	0.21	68.4	67.2	4.981	0.068
F	*1000*	*2.454*	*1.565*	*2.815*	*13.3*	*0.33*	*0.27*	*71.0*	*74.5*	*4.711*	*0.070*
G	*1100*	*2.781*	*2.119*	*4.461*	*7.45*	*0.24*	*0.45*	*58.5*	*78.5*	*4.40*	*0.13*
H	*1200*	*4.282*	*3.092*	*9.312*	*37.2*	*0.17*	*0.52*	*41.3*	*98.7*	*4.784*	*0.090*
I	*1300*	*6.074*	*5.103*	*14.91*	*2.37*	*0.100*	*0.30*	*33.9*	*100.0*	*5.58*	*0.43*
total gas age			n=9		184.1	0.61				4.91	0.12
natural plateau			n=3	steps C-E	104.7	0.73			56.9	4.956	0.049
WCM93-221 wr, H4:33, 51.1 mg, J=0.00149927, nm-33, Lab#=5135-01											
Shibuya Peak, Hobbs Coast, small east outcrop, bomb											
A	*500*	*134.4*	*1.111*	*452.0*	*2.43*	*0.46*	*0.73*	*0.7*	*1.8*	*2.5*	*4.2*
B	*600*	*25.38*	*0.9221*	*81.23*	*9.55*	*0.55*	*-0.024*	*5.7*	*8.9*	*3.91*	*0.76*
C	700	6.665	0.9792	16.57	27.4	0.52	0.15	27.7	29.2	4.99	0.17
D	800	7.070	1.360	17.94	25.2	0.38	0.12	26.5	47.9	5.06	0.17
E	900	8.938	1.827	24.22	19.5	0.28	0.14	21.5	62.3	5.20	0.23
F	*1000*	*6.399*	*2.162*	*16.20*	*8.53*	*0.24*	*0.26*	*27.8*	*68.6*	*4.81*	*0.22*
G	*1100*	*8.615*	*2.918*	*24.90*	*5.03*	*0.17*	*0.43*	*17.2*	*72.4*	*4.01*	*0.38*
H	*1200*	*16.70*	*6.903*	*51.87*	*35.9*	*0.074*	*0.70*	*11.4*	*99.0*	*5.18*	*0.41*
I	*1300*	*13.99*	*9.704*	*35.34*	*1.41*	*0.053*	*0.48*	*30.7*	*100.0*	*11.66*	*0.89*
total gas age			n=9		135.0	0.31				4.98	0.40
natural plateau			n=3	steps C-E	72.1	0.40			53.4	5.06	0.16

Appendix I. $^{40}Ar/^{39}Ar$ Analytical Data

$^{40}Ar/^{39}Ar$ Furnace Data: Central and Western Marie Byrd Land (1993-94 Field Season)

ID	Temp (°C)	$^{40}Ar/^{39}Ar$	$^{37}Ar/^{39}Ar$	$^{36}Ar/^{39}Ar$ (x10^{-3})	$^{39}Ar_K$ (x10^{-15} mol)	K/Ca	Cl/K (x 10-3)	$^{40}Ar^*$ (%)	^{39}Ar (%)	Age (Ma)	±2s (Ma)
WCM93-223 wr, H5:33, 50.2 mg, J=0.00149927, nm-33, Lab#=5136-01											
Shibuya Peak, Hobbs Coast, lava crust on block											
A	*500*	*533.6*	*0.8883*	*1802*	*2.51*	*0.57*	*0.37*	*0.2*	*2.0*	*3.4*	*15.1*
B	*600*	*49.37*	*1.048*	*163.6*	*7.06*	*0.49*	*0.26*	*2.2*	*7.8*	*3.0*	*1.4*
C	700	17.14	1.922	52.14	16.6	0.27	0.060	11.0	21.3	5.09	0.53
D	800	12.32	1.889	35.09	20.6	0.27	0.047	17.0	38.1	5.67	0.32
E	900	9.117	1.287	24.52	20.5	0.40	0.12	21.6	54.7	5.32	0.24
F	1000	8.155	1.222	21.47	14.3	0.42	0.11	23.3	66.4	5.15	0.21
G	1100	11.44	1.920	32.87	16.9	0.27	0.40	16.4	80.1	5.08	0.29
H	*1200*	*27.13*	*11.61*	*76.16*	*18.8*	*0.044*	*1.1*	*20.3*	*95.4*	*14.97*	*0.65*
I	*1300*	*39.99*	*9.354*	*60.92*	*5.63*	*0.055*	*0.55*	*56.8*	*100.0*	*60.80*	*0.68*
total gas age			n=9		122.8	0.28				9.14	0.77
selected mean			n=5	steps C-G	88.9	0.32			72.3	5.26	0.24
WCM93-229, H6:33, 52.4 mg, J=0.00149927, nm-33, Lab#=5137-01											
Shibuya Peak, Hobbs Coast, dike near strombolian lava											
B	*625*	*4.035*	*0.9046*	*9.110*	*32.8*	*0.56*	*0.38*	*35.0*	*30.9*	*3.82*	*0.11*
C	700	3.189	1.334	5.285	34.9	0.38	0.35	54.2	63.8	4.677	0.078
D	775	3.585	1.833	6.518	17.1	0.28	0.28	50.2	79.9	4.87	0.11
E	850	4.244	3.176	9.264	5.98	0.16	0.23	41.2	85.5	4.74	0.19
F	925	3.993	4.562	8.532	2.43	0.11	0.51	45.6	87.8	4.94	0.41
G	*1050*	*3.715*	*5.921*	*8.691*	*1.82*	*0.086*	*0.40*	*43.1*	*89.5*	*4.34*	*0.45*
H	*1125*	*9.002*	*14.24*	*29.54*	*9.42*	*0.036*	*1.2*	*15.2*	*98.4*	*3.73*	*0.36*
I	*1200*	*8.783*	*52.27*	*37.44*	*1.68*	*0.010*	*1.2*	*19.7*	*100.0*	*4.86*	*0.79*
total gas age			n=8		106.1	0.36				4.36	0.20
selected mean			n=4	steps C-F	60.4	0.32			56.9	4.75	0.12
WCM93-307, N1:33, 47.7 mg, J=0.00147295±0.14%, nm-33, Lab#=5162-01											
Patton Bluff, Hobbs Coast, 15 m thick lava											
A	*500*	*346.7*	*1.129*	*1164*	*1.07*	*0.45*	*-0.184*	*0.8*	*1.8*	*7.6*	*12.0*
B	*625*	*7.627*	*1.422*	*14.15*	*10.7*	*0.36*	*0.061*	*46.6*	*20.2*	*9.43*	*0.21*
C	*700*	*5.412*	*2.925*	*5.248*	*14.0*	*0.17*	*0.14*	*75.5*	*44.3*	*10.85*	*0.10*
D	775	5.837	3.534	6.120	11.1	0.14	0.25	73.7	63.3	11.42	0.12
E	850	7.068	3.031	10.22	6.66	0.17	-0.068	60.6	74.8	11.36	0.19
F	925	10.03	3.438	20.26	4.78	0.15	0.43	42.9	83.0	11.43	0.33
G	1050	6.802	4.491	10.34	4.38	0.11	0.54	60.1	90.5	10.87	0.25
H	*1125*	*7.631*	*12.81*	*16.22*	*2.46*	*0.040*	*1.2*	*50.1*	*94.7*	*10.22*	*0.38*
I	*1200*	*14.01*	*74.66*	*55.94*	*2.36*	*0.007*	*1.7*	*23.0*	*98.7*	*8.99*	*0.78*
J	*1450*	*21.38*	*37.26*	*59.64*	*0.732*	*0.014*	*0.86*	*30.9*	*100.0*	*18.0*	*1.4*
total gas age			n=10		58.3	0.19				10.73	0.55
selected mean			n=4	steps D-G	26.9	0.15			46.2	11.32	0.25

Appendix I. $^{40}Ar/^{39}Ar$ Analytical Data

$^{40}Ar/^{39}Ar$ Furnace Data: Central and Western Marie Byrd Land (1993-94 Field Season)

ID	Temp (°C)	$^{40}Ar/^{39}Ar$	$^{37}Ar/^{39}Ar$	$^{36}Ar/^{39}Ar$ ($x10^{-3}$)	$^{39}Ar_K$ ($x10^{-15}$ mol)	K/Ca	Cl/K (x 10-3)	$^{40}Ar^*$ (%)	^{39}Ar (%)	Age (Ma)	±2s (Ma)
WCM93-303 wr, F3:34, 47.6 mg, J=0.0015077, nm-34, Lab#=5212-01											
Kouperov Peak, Hobbs Coast, south end lava on unconformity											
A	*500*	*2090*	*1.144*	*7012*	*0.629*	*0.45*	*-0.544*	*0.9*	*0.5*	*48.5*	*106.6*
B	*600*	*370.1*	*0.8187*	*1223*	*2.68*	*0.62*	*0.54*	*2.4*	*2.5*	*23.8*	*12.2*
C	*700*	*220.1*	*0.6611*	*724.4*	*8.63*	*0.77*	*0.48*	*2.8*	*9.2*	*16.5*	*8.2*
D	*800*	*102.1*	*0.7181*	*326.0*	*22.0*	*0.71*	*0.53*	*5.8*	*26.0*	*15.9*	*3.2*
E	*900*	*70.56*	*1.328*	*220.7*	*26.8*	*0.38*	*0.53*	*7.7*	*46.6*	*14.8*	*2.4*
F	1000	31.43	1.441	94.13	19.5	0.35	0.34	11.8	61.5	10.11	0.94
G	1100	15.10	1.967	39.66	8.62	0.26	0.17	23.4	68.1	9.58	0.45
H	1200	25.96	6.086	75.97	37.0	0.084	0.43	15.3	96.5	10.83	0.77
I	1300	39.54	11.16	123.8	2.97	0.046	0.34	9.6	98.8	10.4	1.4
J	1400	29.24	10.55	89.35	1.05	0.048	-0.058	12.5	99.6	10.0	1.5
K	*1750*	*36.17*	*11.64*	*109.1*	*0.541*	*0.044*	*-1.395*	*13.3*	*100.0*	*13.2*	*4.1*
total gas age			n=11		130.4	0.36				13.1	2.8
selected mean			n=5	steps F-J	69.2	0.18			53.0	9.96	0.60
WCM93-303 plag, F4:34, 62.8 mg, J=0.0015077, nm-34, Lab#=5213-01											
Kouperov Peak, Hobbs Coast, south end lava on unconformity											
A	*550*	*64.60*	*13.07*	*213.3*	*0.183*	*0.039*	*-1.363*	*4.0*	*0.4*	*7.0*	*6.4*
B	700	7.221	13.61	16.09	1.49	0.037	0.49	48.6	3.8	9.62	0.72
C	800	6.948	12.62	15.41	4.23	0.040	0.40	48.4	13.3	9.21	0.45
D	900	9.924	11.91	24.43	2.48	0.043	0.43	36.5	18.9	9.91	0.72
E	1000	5.171	10.98	7.360	1.02	0.046	0.32	74.2	21.2	10.49	0.83
F	1150	4.600	11.84	7.103	2.27	0.043	0.62	74.1	26.3	9.33	0.33
G	1300	6.078	13.22	10.71	1.56	0.039	0.28	64.6	29.8	10.75	0.48
H	1450	3.869	10.23	4.151	13.3	0.050	0.34	88.6	59.7	9.366	0.097
I	1750	4.107	15.32	6.525	17.9	0.033	0.39	81.7	100.0	9.20	0.12
total gas age			n=9		44.4	0.041				9.39	0.54
selected mean			n=8	steps B-I	44.2	0.041			99.6	9.55	0.42

Appendix I. $^{40}Ar/^{39}Ar$ Analytical Data

$^{40}Ar/^{39}Ar$ Furnace Data: Central and Western Marie Byrd Land (1993-94 Field Season)

ID	Temp (°C)	$^{40}Ar/^{39}Ar$	$^{37}Ar/^{39}Ar$	$^{36}Ar/^{39}Ar$ ($x10^{-3}$)	$^{39}Ar_K$ ($x10^{-15}$ mol)	K/Ca	Cl/K (x 10-3)	$^{40}Ar^*$ (%)	^{39}Ar (%)	Age (Ma)	±2s (Ma)
WCM93-304, F5:34, copper, J=0.001507713±0.13%, NM-34, Lab#=5214-01											
Kouperov Peak, Hobbs Coast, lava											
A	*500*	*4804*	*1.878*	*15955*	*0.917*	*0.27*	*16.9*	*1.9*	*0.8*	*228*	*309*
B	*600*	*107.1*	*0.6730*	*348.0*	*5.68*	*0.76*	*0.51*	*4.0*	*5.4*	*11.7*	*4.4*
C	700	12.94	0.6105	32.59	19.2	0.84	0.30	25.9	21.3	9.10	0.47
D	800	18.84	1.332	51.57	13.8	0.38	0.16	19.7	32.7	10.05	0.69
E	900	27.74	1.303	81.26	19.0	0.39	0.17	13.8	48.4	10.4	1.0
F	1000	13.51	1.351	34.23	15.7	0.38	0.56	25.9	61.4	9.51	0.52
G	1100	14.08	2.460	36.71	26.9	0.21	0.28	24.3	83.6	9.28	0.50
H	1200	25.25	10.52	76.47	17.7	0.049	0.87	13.7	98.2	9.47	0.99
I	*1300*	*46.87*	*16.73*	*152.1*	*1.22*	*0.030*	*-0.902*	*6.8*	*99.2*	*8.8*	*3.3*
J	*1450*	*32.60*	*18.53*	*108.8*	*0.541*	*0.028*	*1.6*	*5.7*	*99.7*	*5.1*	*4.1*
K	*1650*	*38.97*	*27.95*	*122.3*	*0.397*	*0.018*	*-1.823*	*12.8*	*100.0*	*13.8*	*5.0*
total gas age			n=11		121.1	0.38				11.3	3.3
selected mean			n=6	steps C-H	112.3	0.37			92.8	9.46	0.42
natural plateau			n=6	steps D-I	94.4	0.27			77.9	9.60	0.44
WCM93-304p, F6:34, 60.6, J=0.001507713±0.13%, NM-34, Lab#=5215-01											
Kouperov Peak, Hobbs Coast, lava											
A	*550*	*113.2*	*8.048*	*383.0*	*0.402*	*0.063*	*2.5*	*0.6*	*0.8*	*1.8*	*10.2*
B	*650*	*19.26*	*8.051*	*61.01*	*1.39*	*0.063*	*0.17*	*9.6*	*3.5*	*5.1*	*1.7*
C	*750*	*11.69*	*11.89*	*33.36*	*5.03*	*0.043*	*0.55*	*23.5*	*13.5*	*7.52*	*0.70*
D	825	6.552	12.69	14.46	8.24	0.040	0.15	49.7	29.8	8.91	0.36
E	900	6.360	11.54	14.03	4.35	0.044	-0.217	48.8	38.4	8.48	0.45
F	1000	4.768	10.91	7.470	4.54	0.047	0.10	71.3	47.4	9.29	0.38
G	1100	3.733	11.86	4.929	6.82	0.043	0.46	85.4	60.9	8.72	0.27
H	1250	5.369	11.13	9.583	6.26	0.046	0.17	63.2	73.2	9.27	0.38
I	*1450*	*6.077*	*13.90*	*10.13*	*3.48*	*0.037*	*0.37*	*68.3*	*80.1*	*11.36*	*0.57*
J	*1650*	*4.894*	*13.42*	*8.750*	*10.1*	*0.038*	*0.22*	*68.2*	*100.0*	*9.14*	*0.27*
total gas age			n=10		50.6	0.043				8.84	0.67
selected mean			n=5	steps D-H	30.2	0.044			59.8	8.95	0.39

Appendix I. $^{40}Ar/^{39}Ar$ Analytical Data

$^{40}Ar/^{39}Ar$ Furnace Data: Central and Western Marie Byrd Land (1993-94 Field Season)

ID	Temp (°C)	$^{40}Ar/^{39}Ar$	$^{37}Ar/^{39}Ar$	$^{36}Ar/^{39}Ar$ ($x10^{-3}$)	$^{39}Ar_K$ ($x10^{-15}$ mol)	K/Ca	Cl/K (x 10-3)	$^{40}Ar^*$ (%)	^{39}Ar (%)	Age (Ma)	±2s (Ma)
WCM93-299, J6:34, 52.6 mg, J=0.00144608, nm-34, Lab#=5239-01											
Kennel Peak, Hobbs Coast, pillow lava											
A	*500*	*390.5*	*0.5331*	*1287*	*6.31*	*0.96*	*2.9*	*2.6*	*2.3*	*26.5*	*17.1*
B	600	9.052	0.6317	22.84	45.9	0.81	0.57	26.0	19.3	6.13	0.29
C	700	6.356	1.422	11.16	99.2	0.36	0.44	49.8	56.1	8.25	0.19
D	800	8.801	1.763	17.85	48.9	0.29	0.40	41.6	74.2	9.54	0.22
E	900	9.656	2.535	21.82	20.3	0.20	0.49	35.2	81.7	8.87	0.29
F	1000	6.357	3.288	12.92	12.6	0.16	0.86	43.9	86.4	7.29	0.23
G	1100	5.675	6.118	11.70	14.8	0.083	1.3	47.4	91.8	7.03	0.20
H	1200	8.308	17.13	22.79	17.0	0.030	1.2	34.8	98.1	7.61	0.28
I	*1300*	*17.40*	*19.44*	*48.48*	*2.21*	*0.026*	*2.4*	*26.2*	*98.9*	*12.0*	*1.1*
J	*1450*	*16.54*	*5.445*	*30.42*	*2.85*	*0.094*	*0.31*	*48.2*	*100.0*	*20.76*	*0.76*
total gas age			n=10		270.0	0.37				8.61	0.67
selected mean			n=7	steps B-H	258.6	0.37			95.8	7.99	0.89
WCM93-292, Holmes, M5:33, 53.5 mg, J=0.00148968, nm-33, Lab#=5160-01											
Holmes Bluff, Hobbs Coast, strombolian lava above valley-fill lava											
A	*500*	*90.75*	*0.5687*	*304.2*	*3.45*	*0.90*	*0.52*	*1.0*	*1.9*	*2.4*	*3.1*
B	625	6.960	0.5370	15.92	36.6	0.95	0.038	33.0	21.7	6.17	0.18
C	700	3.950	0.7275	5.620	52.4	0.70	0.13	59.4	50.1	6.294	0.085
D	775	5.503	0.7636	10.96	38.7	0.67	0.13	42.2	71.2	6.24	0.15
E	850	6.326	0.8650	13.62	21.2	0.59	0.17	37.4	82.7	6.36	0.18
F	925	7.012	1.152	16.06	8.86	0.44	0.085	33.6	87.5	6.32	0.25
G	*1050*	*4.516*	*1.562*	*8.064*	*9.70*	*0.33*	*0.24*	*49.9*	*92.7*	*6.05*	*0.14*
H	*1125*	*5.416*	*5.877*	*12.76*	*5.39*	*0.087*	*0.72*	*38.7*	*95.7*	*5.65*	*0.24*
I	*1200*	*12.78*	*30.77*	*44.44*	*7.05*	*0.017*	*0.83*	*15.8*	*99.5*	*5.52*	*0.53*
J	*1450*	*13.69*	*36.49*	*48.12*	*0.946*	*0.014*	*0.74*	*16.6*	*100.0*	*6.3*	*1.1*
total gas age			n=10		184.3	0.65				6.13	0.25
natural plateau			n=5	steps B-F	157.8	0.72			85.6	6.28	0.08

Appendix I. $^{40}Ar/^{39}Ar$ Analytical Data

$^{40}Ar/^{39}Ar$ Furnace Data: Central and Western Marie Byrd Land (1993-94 Field Season)

ID	Temp (°C)	$^{40}Ar/^{39}Ar$	$^{37}Ar/^{39}Ar$	$^{36}Ar/^{39}Ar$ ($x10^{-3}$)	$^{39}Ar_K$ ($x10^{-15}$ mol)	K/Ca	Cl/K (x 10-3)	$^{40}Ar^*$ (%)	^{39}Ar (%)	Age (Ma)	±2s (Ma)
WCM93-270 wr, F1:34, 77.7 mg, J=0.0015077, nm-34, Lab#=5210-01											
Mt. Siple, mid-flank outcrop, lithic clasts in lapilli tuff											
A	*500*	*143.3*	*1.014*	*477.8*	*1.33*	*0.50*	*1.0*	*1.5*	*0.7*	*6.0*	*5.0*
B	600	2.959	0.9370	9.343	12.2	0.54	0.002	9.1	7.1	0.73	0.13
C	700	0.7594	1.120	1.951	51.3	0.46	0.14	35.4	33.9	0.732	0.030
D	800	0.7105	1.238	1.825	52.1	0.41	0.16	37.5	61.1	0.724	0.029
E	900	1.106	1.466	3.140	24.3	0.35	0.19	26.3	73.8	0.792	0.051
F	1000	1.182	2.176	3.702	16.6	0.23	0.20	21.6	82.5	0.694	0.067
G	1100	1.392	2.325	4.388	13.1	0.22	0.34	19.7	89.3	0.746	0.088
H	1200	2.730	17.24	13.07	17.5	0.030	0.71	7.0	98.5	0.53	0.15
I	*1300*	*5.085*	*15.01*	*19.41*	*2.25*	*0.034*	*0.62*	*9.9*	*99.7*	*1.38*	*0.47*
J	*1450*	*4.915*	*15.81*	*19.33*	*0.643*	*0.032*	*0.43*	*8.5*	*100.0*	*1.2*	*1.0*
total gas age			n=10		191.4	0.36				0.76	0.16
natural plateau			n=7	steps B-H	187.2	0.36			97.8	0.736	0.036
WCM93-270 plag, F2:34, 68.2 mg, J=0.0015077, nm-34, Lab#=5211-01											
Mt. Siple, mid-flank outcrop, lithic clasts in lapilli tuff											
A	550	22.25	14.05	73.29	0.238	0.036	2.1	7.5	0.6	4.6	3.3
B	700	4.148	15.78	17.34	1.93	0.032	0.57	5.7	5.2	0.65	0.45
C	800	0.4988	15.47	5.131	3.38	0.033	0.51	34.3	13.3	0.47	0.21
D	900	0.5946	14.28	4.935	3.59	0.036	0.44	39.3	21.8	0.64	0.19
E	1000	0.5919	13.69	4.966	3.97	0.037	0.31	29.7	31.3	0.48	0.18
F	1150	1.679	13.85	6.105	7.25	0.037	0.24	55.9	48.6	2.58	0.14
G	1300	4.167	14.12	16.01	3.58	0.036	0.39	12.5	57.2	1.43	0.63
H	1450	2.236	15.31	9.434	2.04	0.033	0.026	27.9	62.1	1.72	0.35
I	1750	1.509	15.25	8.339	15.8	0.033	0.24	14.3	99.8	0.59	0.10
J	*1750*	*19.61*	*16.98*	*93.55*	*0.074*	*0.030*	*-1.974*	*-34.3*	*100.0*	*-18.6*	*10.3*
total gas age			n=10		41.9	0.035				1.04	0.57
no plateau			n=9	steps A-I	41.8	0.035			99.8	1.09	0.60

Appendix I. $^{40}Ar/^{39}Ar$ Analytical Data

$^{40}Ar/^{39}Ar$ Furnace Data: Central and Western Marie Byrd Land (1993-94 Field Season)

ID	Temp (°C)	$^{40}Ar/^{39}Ar$	$^{37}Ar/^{39}Ar$	$^{36}Ar/^{39}Ar$ ($x10^{-3}$)	$^{39}Ar_K$ ($x10^{-15}$ mol)	K/Ca	Cl/K (x 10-3)	$^{40}Ar^*$ (%)	^{39}Ar (%)	Age (Ma)	±2s (Ma)
WCM93-275, M1:33, 51.3 mg, J=0.00148968, nm-33, Lab#=5156-01											
Mt. Siple, sea side outcrop, lithic clasts in lapilli tuff											
A	500	266.2	0.9401	891.1	2.31	0.54	0.67	1.1	2.0	7.9	9.3
B	625	3.641	1.099	12.57	16.5	0.46	0.058	0.3	15.9	0.03	0.15
C	700	1.521	1.465	5.512	23.1	0.35	0.17	0.3	35.5	0.011	0.078
D	775	1.321	1.687	4.916	18.6	0.30	0.13	-0.1	51.2	-0.005	0.085
E	*850*	*1.507*	*1.731*	*5.316*	*10.9*	*0.29*	*0.11*	*4.6*	*60.4*	*0.19*	*0.10*
F	*925*	*1.965*	*2.074*	*6.951*	*5.20*	*0.25*	*0.17*	*3.6*	*64.8*	*0.19*	*0.20*
G	*1050*	*1.735*	*2.906*	*6.366*	*7.98*	*0.18*	*0.28*	*4.4*	*71.5*	*0.21*	*0.18*
H	*1125*	*4.996*	*5.238*	*18.20*	*12.1*	*0.097*	*0.61*	*0.4*	*81.8*	*0.06*	*0.22*
I	*1200*	*4.304*	*7.070*	*16.25*	*19.3*	*0.072*	*0.62*	*1.1*	*98.1*	*0.12*	*0.19*
J	*1450*	*6.784*	*9.736*	*25.28*	*2.24*	*0.052*	*0.25*	*0.9*	*100.0*	*0.17*	*0.50*
total gas age			n=10		118.1	0.26				0.23	0.36
natural plateau			n=4	steps A-D	60.4	0.37			51.2	0.008	0.088
WCM93-275, Y5:37, 113.5 mg, WR , J=0.000221419±0.90%, NM-37, Lab#=5399-01											
Mt. Siple, sea side outcrop, lithic clasts in lapilli tuff											
A	*500*	*1464*	*1.191*	*4979*	*1.06*	*0.43*	*4.9*	*-0.5*	*1.9*	*-3*	*11*
B	600	45.33	1.305	155.6	5.35	0.39	0.064	-1.2	11.5	-0.22	0.30
C	700	14.57	1.404	49.96	11.6	0.36	0.28	-0.6	32.3	-0.03	0.10
D	800	11.39	1.474	39.36	9.60	0.35	0.090	-1.1	49.5	-0.051	0.088
E	900	13.32	1.679	45.49	5.59	0.30	-0.107	0.1	59.5	0.00	0.13
F	*1000*	*17.11*	*2.465*	*60.38*	*2.92*	*0.21*	*0.67*	*-3.2*	*64.7*	*-0.22*	*0.17*
G	*1100*	*21.54*	*2.958*	*75.67*	*3.64*	*0.17*	*0.64*	*-2.8*	*71.3*	*-0.24*	*0.20*
H	*1200*	*47.82*	*6.555*	*161.0*	*14.9*	*0.078*	*1.0*	*1.6*	*97.9*	*0.30*	*0.29*
I	*1300*	*61.92*	*9.333*	*207.5*	*1.16*	*0.055*	*1.7*	*2.1*	*100.0*	*0.53*	*0.57*
total gas age			n=9		55.8	0.26				-0.025	0.395
selected mean			n=4	steps B-E	32.2	0.35			57.6	-0.041	0.076
natural plateau			n=5	steps A-E	33.214	0.35			59.5	-0.041	0.074

Appendix I. $^{40}Ar/^{39}Ar$ Analytical Data

$^{40}Ar/^{39}Ar$ Furnace Data: Central and Western Marie Byrd Land (1993-94 Field Season)

ID	Temp (°C)	$^{40}Ar/^{39}Ar$	$^{37}Ar/^{39}Ar$	$^{36}Ar/^{39}Ar$ (x10^{-3})	$^{39}Ar_K$ (x10^{-15} mol)	K/Ca	Cl/K (x 10-3)	$^{40}Ar^*$ (%)	^{39}Ar (%)	Age (Ma)	±2s (Ma)
WCM93-255 wr, E1:34, 58.5 mg, J=0.0015147, nm-34, Lab#=5204-01											
Mathewson Pt., Shepard Island, lava ponded in tuff cone											
B	600	4.600	1.036	15.24	8.42	0.49	-0.046	3.8	6.6	0.48	0.22
C	700	1.018	1.143	3.184	37.2	0.45	0.11	16.2	35.6	0.451	0.044
D	800	1.149	1.333	3.626	35.4	0.38	0.14	15.7	63.2	0.493	0.051
E	900	1.850	1.533	6.022	14.3	0.33	0.16	10.2	74.4	0.52	0.11
F	*1000*	*0.7945*	*2.095*	*2.813*	*8.28*	*0.24*	*0.22*	*15.6*	*80.9*	*0.34*	*0.11*
G	*1100*	*0.8727*	*3.244*	*3.382*	*6.51*	*0.16*	*0.49*	*14.0*	*85.9*	*0.34*	*0.13*
H	*1200*	*1.626*	*11.00*	*8.018*	*15.7*	*0.046*	*0.89*	*6.2*	*98.2*	*0.28*	*0.12*
I	*1300*	*1.980*	*10.60*	*9.195*	*2.37*	*0.048*	*0.30*	*3.9*	*100.0*	*0.21*	*0.40*
total gas age			n=8		128.1	0.34				0.43	0.14
natural plateau			n=4	steps B-E	95.3	0.41			74.4	0.475	0.049
WCM93-255 plag, E2:34, 58.6 mg, J=0.0015147, nm-34, Lab#=5205-01											
Mathewson Pt., Shepard Island, lava ponded in tuff cone											
A	550	70.04	13.77	245.6	0.104	0.037	5.4	-2.1	0.4	-4.1	9.6
B	700	4.255	17.57	19.49	1.21	0.029	0.54	-3.6	4.5	-0.42	0.65
C	800	1.006	17.54	7.846	4.73	0.029	0.21	3.5	20.8	0.10	0.18
D	900	1.334	15.59	9.040	3.09	0.033	0.40	-10.5	31.4	-0.39	0.25
E	1000	1.106	15.46	8.152	1.41	0.033	0.51	-10.4	36.2	-0.32	0.42
F	1150	0.8536	16.41	6.434	5.08	0.031	0.35	24.9	53.7	0.59	0.18
G	1300	3.695	16.76	11.42	1.40	0.030	0.51	43.5	58.5	4.44	0.44
H	1450	2.903	16.69	12.16	1.14	0.031	0.31	20.4	62.4	1.63	0.63
I	1550	1.077	17.00	7.491	10.6	0.030	0.19	15.7	99.0	0.47	0.12
J	1750	9.591	17.49	38.64	0.291	0.029	0.60	-5.0	100.0	-1.3	2.3
total gas age			n=10		29.1	0.031				0.47	0.66
no plateau			n=10	steps A-J	29.1	0.031			100.0	0.62	0.97
WCM93-258 wr, E3:34, 53.8 mg, J=0.0015147, nm-34, Lab#=5206-01											
Mathewson Pt., Shepard Island, clast in tuff cone beds											
A	*500*	*760.0*	*0.8729*	*2544.6*	*0.912*	*0.58*	*1.2*	*1.1*	*0.8*	*22.2*	*27.2*
B	600	29.31	0.9749	98.60	4.92	0.52	0.36	0.8	5.1	0.7	1.1
C	700	12.05	1.446	40.30	16.0	0.35	0.34	2.1	19.2	0.70	0.42
D	800	10.87	1.395	36.37	16.9	0.37	0.15	2.1	34.0	0.63	0.37
E	900	8.716	1.202	28.91	14.4	0.42	0.22	3.1	46.6	0.73	0.31
F	1000	3.996	1.343	13.18	13.5	0.38	0.096	5.1	58.4	0.56	0.18
G	1100	3.131	2.119	10.59	12.5	0.24	0.39	5.2	69.3	0.45	0.15
H	*1200*	*19.06*	*6.871*	*64.63*	*34.1*	*0.074*	*0.64*	*2.6*	*99.1*	*1.34*	*0.63*
I	*1300*	*15.67*	*9.109*	*57.02*	*0.997*	*0.056*	*0.65*	*-3.1*	*100.0*	*-1.3*	*1.4*
total gas age			n=9		114.2	0.28				0.99	0.67
natural plateau			n=6	steps B-G	78.2	0.37			68.5	0.55	0.14

Appendix I. $^{40}Ar/^{39}Ar$ Analytical Data

$^{40}Ar/^{39}Ar$ Furnace Data: Central and Western Marie Byrd Land (1993-94 Field Season)

ID	Temp (°C)	$^{40}Ar/^{39}Ar$	$^{37}Ar/^{39}Ar$	$^{36}Ar/^{39}Ar$ (x10^{-3})	$^{39}Ar_K$ (x10^{-15} mol)	K/Ca	Cl/K (x 10-3)	$^{40}Ar^*$ (%)	^{39}Ar (%)	Age (Ma)	±2s (Ma)
WCM93-258 plag, E4:34, 60.7 mg, J=0.0015147, nm-34, Lab#=5207-01											
Mathewson Pt., Shepard Island, clast in tuff cone beds											
A	650	0.8690	16.30	5.791	0.778	0.031	0.057	47.2	2.3	1.1	1.0
B	800	0.4782	15.13	5.109	5.25	0.034	0.48	27.3	18.1	0.36	0.17
C	1000	0.6164	16.07	6.069	7.02	0.032	0.33	9.4	39.2	0.16	0.14
D	1150	0.2709	15.80	4.737	6.25	0.032	0.27	31.3	58.0	0.23	0.13
E	1500	0.7490	15.91	6.294	13.8	0.032	0.25	14.9	99.4	0.308	0.092
F	*1650*	*4.931*	*16.51*	*19.93*	*0.192*	*0.031*	*-1.857*	*6.3*	*100.0*	*0.9*	*3.8*
total gas age			n=6		33.3	0.032				0.29	0.56
natural plateau			n=5	steps A-E	33.1	0.032			99.4	0.31	0.33
WCM93-265, E5:34, 89.5 mg, J=0.001514706, NM-34, Lab#=5208-01											
Mt. Petinos, Shepard Island, clast in tuff cone beds											
A	500	77.96	0.9480	261.1	3.91	0.54	0.47	1.1	1.3	2.4	3.5
B	600	4.232	1.404	14.08	29.9	0.36	0.23	4.2	11.6	0.49	0.22
C	700	2.003	1.682	6.760	76.4	0.30	0.14	6.7	37.6	0.37	0.10
D	800	1.788	1.451	5.928	51.5	0.35	0.24	8.3	55.2	0.404	0.098
E	900	4.503	2.173	15.23	23.6	0.23	0.31	3.7	63.3	0.46	0.23
F	*1000*	*2.690*	*2.739*	*8.644*	*12.9*	*0.19*	*0.64*	*12.8*	*67.7*	*0.95*	*0.21*
G	*1100*	*3.478*	*3.005*	*11.94*	*24.5*	*0.17*	*0.69*	*5.2*	*76.0*	*0.49*	*0.21*
H	*1200*	*4.409*	*8.122*	*16.08*	*70.2*	*0.063*	*0.81*	*6.4*	*100.0*	*0.77*	*0.21*
total gas age			n=8		292.9	0.24				0.55	0.25
natural plateau			n=5	steps A-E	185.4	0.32			63.3	0.40	0.09
WCM93-265p, E6:34, 101 mg, J=0.001514706, NM-34, Lab#=5209-01											
Mt. Petinos, Shepard Island, clast in tuff cone beds											
A	550	18.42	24.53	56.20	0.174	0.021	-3.030	20.1	0.4	10.2	9.6
B	650	3.176	20.77	6.495	1.03	0.025	-0.236	89.8	2.8	7.9	1.3
C	750	0.6042	24.33	6.424	1.39	0.021	0.64	95.1	6.1	1.6	1.0
D	825	0.2086	24.70	7.923	1.58	0.021	-0.662	-113	9.8	-0.65	0.89
E	900	0.3392	23.86	7.647	2.10	0.021	0.33	-25.9	14.7	-0.24	0.72
F	1000	0.3932	23.63	7.249	4.67	0.022	0.46	17.0	25.7	0.19	0.38
G	1100	0.5331	23.68	6.781	6.79	0.022	0.13	65.3	41.6	0.97	0.29
H	1250	1.248	23.57	7.305	9.64	0.022	0.19	72.1	64.3	2.50	0.25
I	1450	3.123	22.79	7.817	3.89	0.022	0.48	82.1	73.4	7.10	0.41
J	1650	0.8975	22.78	7.855	11.3	0.022	0.38	36.3	100.0	0.91	0.19
total gas age			n=10		42.6	0.022				1.88	0.91
no plateau											

Appendix I. $^{40}Ar/^{39}Ar$ Analytical Data

$^{40}Ar/^{39}Ar$ Furnace Data: Central and Western Marie Byrd Land (1993-94 Field Season)

ID	Temp (°C)	$^{40}Ar/^{39}Ar$	$^{37}Ar/^{39}Ar$	$^{36}Ar/^{39}Ar$ ($x10^{-3}$)	$^{39}Ar_K$ ($x10^{-15}$ mol)	K/Ca	Cl/K (x 10-3)	$^{40}Ar^*$ (%)	^{39}Ar (%)	Age (Ma)	±2s (Ma)
WCM93-308, N2:33, 53.5 mg, J=0.00147295, nm-33, Lab#=5163-01											
Mt. Andrus, eroded cinder cone											
A	*500*	*74.69*	*0.0000*	*240.1*	*1.41*	-	*0.49*	*5.0*	*0.9*	*9.9*	*2.7*
B	*625*	*6.725*	*0.7846*	*11.48*	*10.8*	*0.65*	*0.16*	*50.5*	*8.2*	*9.00*	*0.19*
C	700	4.314	0.7635	3.089	22.3	0.67	0.16	80.2	23.2	9.174	0.083
D	775	3.989	0.9034	2.042	28.5	0.56	0.095	86.6	42.3	9.163	0.059
E	850	4.067	0.9191	2.368	26.0	0.56	0.18	84.5	59.8	9.118	0.068
F	925	4.599	1.108	4.067	15.3	0.46	0.25	75.7	70.0	9.236	0.096
G	*1050*	*10.81*	*1.632*	*25.63*	*12.0*	*0.31*	*0.37*	*31.1*	*78.1*	*8.93*	*0.30*
H	*1125*	*19.98*	*2.476*	*57.68*	*4.20*	*0.21*	*0.62*	*15.6*	*80.9*	*8.29*	*0.70*
I	*1200*	*13.64*	*5.726*	*36.31*	*20.1*	*0.089*	*0.61*	*24.6*	*94.4*	*8.92*	*0.40*
J	*1450*	*18.52*	*7.530*	*52.58*	*8.35*	*0.068*	*0.42*	*19.2*	*100.0*	*9.49*	*0.57*
total gas age			n=10		149.1	0.45				9.10	0.23
natural plateau			n=4	steps C-F	92.2	0.57			61.8	9.163	0.063
WCM93-161 wr, K2:33, 53 mg, J=0.00149676, nm-33, Lab#=5145-01											
Koerner Bluff, Mt. Bursey, dense bomb											
A	*500*	*114.3*	*0.4902*	*376.6*	*3.32*	*1.0*	*0.64*	*2.7*	*1.9*	*8.2*	*3.4*
B	*600*	*7.916*	*0.6041*	*16.12*	*18.3*	*0.84*	*0.084*	*40.4*	*12.1*	*8.62*	*0.18*
C	700	5.421	1.061	6.207	38.8	0.48	0.18	67.7	33.7	9.886	0.094
D	800	5.883	1.185	7.111	29.3	0.43	0.19	65.8	50.0	10.435	0.099
E	900	6.286	1.463	9.092	14.4	0.35	0.18	59.0	58.1	10.00	0.15
F	1000	5.616	2.240	7.803	6.49	0.23	0.25	62.0	61.7	9.39	0.17
G	1100	12.12	1.884	30.11	17.8	0.27	0.46	27.8	71.6	9.09	0.29
H	1200	10.82	2.945	24.99	49.9	0.17	0.55	33.8	99.5	9.88	0.22
I	*1300*	*16.56*	*8.597*	*45.03*	*0.977*	*0.059*	*0.030*	*23.6*	*100.0*	*10.6*	*1.1*
total gas age			n=9		179.3	0.39				9.73	0.24
selected mean			n=6	steps C-H	156.7	0.33			87.4	9.99	0.33

Appendix I. $^{40}Ar/^{39}Ar$ Analytical Data

$^{40}Ar/^{39}Ar$ Furnace Data: Central and Western Marie Byrd Land (1993-94 Field Season)

ID	Temp (°C)	$^{40}Ar/^{39}Ar$	$^{37}Ar/^{39}Ar$	$^{36}Ar/^{39}Ar$ ($x10^{-3}$)	$^{39}Ar_K$ ($x10^{-15}$ mol)	K/Ca	Cl/K (x 10-3)	$^{40}Ar^*$ (%)	^{39}Ar (%)	Age (Ma)	±2s (Ma)
WCM93-146, Z5-6:37, 140.9 mg, J=0.000221355, NM-37, Lab#=5402-01											
Gawne Nunatak, Mt. Moulton, cinder cone bomb											
A	*500*	*3718*	*1.947*	*12618*	*0.487*	*0.26*	*-6.258*	*-0.3*	*0.5*	*-4*	*46*
B	600	139.2	1.339	463.9	4.50	0.38	0.34	1.6	5.3	0.89	0.89
C	700	46.05	1.273	146.6	12.8	0.40	0.33	6.2	18.9	1.13	0.26
D	800	29.28	1.185	90.09	11.8	0.43	0.38	9.4	31.5	1.10	0.16
E	900	37.45	1.471	117.8	8.79	0.35	0.30	7.4	40.9	1.10	0.22
F	1000	108.0	1.439	355.5	6.36	0.35	0.59	2.8	47.6	1.22	0.65
G	*1100*	*245.8*	*1.188*	*823.8*	*7.69*	*0.43*	*0.28*	*1.0*	*55.8*	*1.0*	*1.5*
H	*1200*	*341.3*	*3.075*	*1130*	*20.6*	*0.17*	*1.2*	*2.3*	*77.7*	*3.1*	*2.1*
I	*1300*	*370.7*	*6.569*	*1220*	*20.5*	*0.078*	*2.5*	*2.9*	*99.6*	*4.3*	*2.3*
J	*1450*	*561.7*	*13.21*	*1810*	*0.312*	*0.039*	*-0.360*	*5.0*	*99.9*	*11.2*	*6.8*
K	*1650*	*354.0*	*15.77*	*1225*	*0.081*	*0.032*	*6.2*	*-1.9*	*100.0*	*-3*	*11*
total gas age			n=11		93.9	0.27				2.2	1.5
selected mean			n=5	steps B-F	44.2	0.39			47.1	1.11	0.13
natural plateau			n=8	steps A-H	72.967	0.33			77.7	1.11	0.15
WCM93-146, J6:33, 78.2 mg, J=0.001500713, nm-33, Lab#=5143-01											
Gawne Nunatak, Mt. Moulton, cinder cone bomb											
A	*500*	*161.8*	*1.227*	*553.2*	*2.51*	*0.42*	*0.68*	*-1.0*	*1.3*	*-4.2*	*6.0*
B	625	15.15	1.027	50.36	18.1	0.50	0.16	2.3	10.5	0.93	0.54
C	700	5.189	1.163	16.60	26.3	0.44	0.16	7.2	24.0	1.01	0.19
D	775	3.640	1.384	11.47	24.7	0.37	0.13	9.8	36.7	0.96	0.13
E	850	4.431	1.477	14.13	18.2	0.35	0.23	8.3	46.0	1.00	0.16
F	*925*	*8.319*	*1.619*	*27.79*	*11.5*	*0.32*	*0.28*	*2.8*	*51.9*	*0.63*	*0.33*
G	*1050*	*22.49*	*1.241*	*76.41*	*18.7*	*0.41*	*0.32*	*0.0*	*61.4*	*0.02*	*0.82*
H	*1125*	*33.51*	*1.624*	*114.0*	*12.2*	*0.31*	*0.41*	*-0.1*	*67.7*	*-0.1*	*1.2*
I	*1200*	*35.60*	*4.381*	*119.9*	*46.7*	*0.12*	*0.77*	*1.4*	*91.6*	*1.4*	*1.2*
J	*1450*	*40.32*	*8.499*	*134.9*	*16.4*	*0.060*	*1.0*	*2.8*	*100.0*	*3.0*	*1.5*
total gas age			n=10		195.4	0.30				0.99	0.79
selected mean			n=4	steps B-E	87.4	0.41			44.7	0.99	0.10

Appendix I. $^{40}Ar/^{39}Ar$ Analytical Data

$^{40}Ar/^{39}Ar$ Furnace Data: Central and Western Marie Byrd Land (1993-94 Field Season)

ID	Temp (°C)	$^{40}Ar/^{39}Ar$	$^{37}Ar/^{39}Ar$	$^{36}Ar/^{39}Ar$ ($x10^{-3}$)	$^{39}Ar_K$ ($x10^{-15}$ mol)	K/Ca	Cl/K (x 10-3)	$^{40}Ar^*$ (%)	^{39}Ar (%)	Age (Ma)	±2s (Ma)
WCM93-279, M2:33, 51.3 mg, J=0.00148968, nm-33, Lab#=5157-01											
Mt. Flint, south rim, strombolian lava											
A	*500*	*128.1*	*0.5873*	*424.1*	*2.72*	*0.87*	*0.69*	*2.2*	*2.7*	*7.7*	*4.6*
B	625	6.155	0.6948	9.448	13.7	0.73	0.28	55.5	16.2	9.16	0.15
C	700	4.522	0.8318	3.406	20.4	0.61	0.28	79.2	36.4	9.599	0.080
D	775	4.460	1.120	3.178	15.6	0.46	0.23	80.9	51.8	9.676	0.093
E	850	4.631	1.464	3.806	11.1	0.35	0.27	78.1	62.7	9.71	0.12
F	925	5.299	1.800	6.755	6.48	0.28	0.35	64.9	69.1	9.24	0.15
G	*1050*	*8.282*	*1.960*	*17.35*	*7.61*	*0.26*	*0.34*	*39.9*	*76.6*	*8.87*	*0.27*
H	*1125*	*11.77*	*3.570*	*30.45*	*5.15*	*0.14*	*0.67*	*25.9*	*81.7*	*8.19*	*0.42*
I	*1200*	*11.80*	*13.28*	*32.38*	*15.8*	*0.038*	*0.85*	*27.5*	*97.3*	*8.79*	*0.34*
J	*1450*	*15.04*	*19.60*	*41.85*	*2.75*	*0.026*	*0.80*	*27.8*	*100.0*	*11.36*	*0.63*
total gas age			n=10		101.4	0.41				9.28	0.35
selected mean			n=5	steps B-F	67.3	0.53			66.4	9.55	0.20
WCM93-281, M3:33, 54.6 mg, J=0.00148968, nm-33, Lab#=5158-01											
Mt. Flint, south rim, strombolian lava											
B	625	4.397	0.7372	10.52	16.7	0.69	0.13	30.6	14.2	3.61	0.15
C	700	2.246	0.8203	3.123	20.4	0.62	0.17	61.7	31.5	3.723	0.055
D	775	2.048	1.091	2.567	15.0	0.47	0.16	67.0	44.2	3.688	0.070
E	850	2.093	1.303	2.694	9.24	0.39	0.25	66.7	52.0	3.75	0.11
F	925	2.606	1.640	4.742	4.84	0.31	0.29	51.1	56.1	3.58	0.16
G	*1050*	*4.277*	*1.875*	*10.62*	*6.12*	*0.27*	*0.29*	*30.0*	*61.3*	*3.45*	*0.21*
H	*1125*	*6.432*	*3.628*	*18.21*	*37.1*	*0.14*	*0.44*	*20.7*	*92.8*	*3.58*	*0.19*
I	*1200*	*9.464*	*22.50*	*32.54*	*8.54*	*0.023*	*1.0*	*16.7*	*100.0*	*4.30*	*0.38*
total gas age			n=8		118.0	0.37				3.68	0.20
natural plateau			n=5	steps B-F	66.2	0.55			56.1	3.700	0.063
WCM93-284, M4:33, 50 mg, J=0.00148968, nm-33, Lab#=5159-01											
Mt. Flint, lower cinder cone											
A	*500*	*68.36*	*0.4950*	*223.2*	*2.41*	*1.0*	*0.19*	*3.6*	*1.7*	*6.6*	*2.3*
B	*625*	*10.81*	*0.4450*	*24.48*	*18.8*	*1.1*	*-0.098*	*33.4*	*14.8*	*9.68*	*0.29*
C	*700*	*10.13*	*0.6740*	*22.52*	*19.0*	*0.76*	*0.017*	*34.8*	*28.0*	*9.47*	*0.29*
D	*775*	*7.735*	*1.139*	*15.03*	*12.8*	*0.45*	*0.079*	*43.7*	*36.9*	*9.07*	*0.23*
E	*850*	*9.072*	*1.227*	*19.59*	*8.63*	*0.42*	*0.15*	*37.2*	*42.9*	*9.06*	*0.26*
F	925	6.664	1.099	11.91	6.31	0.46	0.005	48.4	47.3	8.66	0.22
G	1050	8.992	1.019	20.07	16.9	0.50	0.15	34.9	59.1	8.43	0.24
H	1125	25.85	2.090	77.46	49.9	0.24	0.50	12.1	93.8	8.37	0.78
I	*1200*	*19.68*	*26.14*	*53.22*	*7.33*	*0.020*	*1.3*	*30.3*	*98.9*	*16.24*	*0.61*
J	*1450*	*30.61*	*33.76*	*63.53*	*1.58*	*0.015*	*1.2*	*47.1*	*100.0*	*39.3*	*1.0*
total gas age			n=10		143.8	0.50				9.52	0.53
natural plateau			n=3	steps F-H	73.2	0.32			50.9	8.55	0.24

Appendix I. $^{40}Ar/^{39}Ar$ Analytical Data

$^{40}Ar/^{39}Ar$ Laser Fusion Data: Crary Mountains, Marie Byrd Land (1992-93 Field Season)

ID	$^{40}Ar/^{39}Ar$	$^{37}Ar/^{39}Ar$	$^{36}Ar/^{39}Ar$ (x 10^{-3})	$^{39}Ar_K$ (x 10^{-15} mol)	K/Ca	%^{40}Ar*	Age (Ma)	±2s (Ma)
TW92-174, anorth multi-xals, J=0.0002399, NMUM-4, Lab#=235								
Trabucco Cliff, Mt. Rees, Crary Mtns.								
02	20.81	0.0226	0.9750	2.38	22.6	98.5	8.850	0.098
06	20.78	0.0272	0.7823	4.55	18.8	98.8	8.861	0.053
05	20.90	0.0364	0.8398	3.18	14.0	98.7	8.907	0.073
04	21.01	0.0311	0.9513	2.32	16.4	98.6	8.942	0.097
03	20.97	0.0264	0.7042	3.61	19.3	98.9	8.957	0.065
07	21.02	0.0278	0.7666	8.13	18.3	98.8	8.968	0.051
08	21.20	0.0278	0.8671	5.88	18.3	98.7	9.033	0.057
01	21.18	0.0314	0.7657	1.77	16.2	98.8	9.04	0.14
mean ± sdev			n=8		18.0	±5.1	8.94	0.14
mean ± SEM			n=8		18.0	±5.1	8.944	0.054
weighted mean ± Taylor err			n=8		18.0	±5.1	8.943	0.033
weighted mean ± S & A err			n=8		18.0	±5.1	8.943	0.057
TW92-175, anorth multi-xals, J=0.0002402, NMUM-4, Lab#=234								
Trabucco Cliff, Mt. Rees, Crary Mtns.								
03	21.09	0.0109	2.184	2.77	46.7	96.8	8.829	0.088
08	21.23	0.0217	2.092	1.39	23.5	97.0	8.90	0.16
07	21.36	0.0205	2.337	1.86	24.9	96.7	8.93	0.12
05	21.47	0.0196	2.519	1.89	26.0	96.4	8.95	0.13
04	21.41	0.0189	2.267	1.90	27.0	96.8	8.95	0.11
02	21.43	0.0115	2.232	3.59	44.3	96.8	8.969	0.070
06	21.41	0.0210	1.992	1.80	24.3	97.2	8.99	0.13
01	21.20	0.0067	1.219	2.40	75.9	98.2	8.997	0.094
09	21.47	0.0133	1.983	2.15	38.3	97.2	9.02	0.11
mean ± sdev			n=9		36.8	±34.4	8.95	0.12
mean ± SEM			n=9		36.8	±34.4	8.948	0.044
weighted mean ± Taylor err			n=9		36.8	±34.4	8.948	0.041
weighted mean ± S & A err			n=9		36.8	±34.4	8.948	0.058

Appendix I. $^{40}Ar/^{39}Ar$ Analytical Data

$^{40}Ar/^{39}Ar$ Laser Fusion Data: Crary Mountains, Marie Byrd Land (1992-93 Field Season)

ID	$^{40}Ar/^{39}Ar$	$^{37}Ar/^{39}Ar$	$^{36}Ar/^{39}Ar$ (x 10^{-3})	$^{39}Ar_K$ (x 10^{-15} mol)	K/Ca	$\%^{40}Ar^*$	Age (Ma)	±2s (Ma)
TW92-006, Tray C 1, north multi-xals, J=0.000729882, nm-21, Lab#=2152								
Trabucco Cliff, Mt. Rees, Crary Mtns.								
01A	7.934	0.0117	3.959	3.38	43.7	85.0	8.860	0.083
04	7.623	0.0077	2.825	3.51	66.2	88.8	8.892	0.073
03	7.208	0.0095	1.328	3.98	53.5	94.3	8.927	0.051
02	7.305	0.0089	1.618	9.53	57.2	93.2	8.941	0.053
06	8.040	0.0120	4.104	2.73	42.7	84.7	8.942	0.093
09	7.469	0.0110	2.093	7.26	46.4	91.5	8.973	0.052
05	7.834	0.0112	3.217	5.88	45.7	87.6	9.017	0.064
08	8.034	0.0112	3.846	3.07	45.5	85.6	9.034	0.088
07	7.085	0.0089	0.6179	3.87	57.2	97.2	9.041	0.056
10	7.376	0.0113	1.474	3.56	45.0	93.8	9.091	0.065
mean ± sdev			n=10	50.3	±15.6		8.97	0.15
mean ± SEM			n=10	50.3	±15.6		8.972	0.067
weighted mean ± Taylor err			n=10	50.3	±15.6		8.975	0.053
weighted mean ± S & A err			n=10	50.3	±15.6		8.975	0.068
TW92-015, anorth multi-xals, J=0.0002394, NMUM-4, Lab#=236								
Trabucco Cliff, Mt. Rees, Crary Mtns.								
08	21.26	0.0098	1.390	6.85	51.9	98.0	8.971	0.047
06	21.24	0.0107	1.310	2.96	47.5	98.1	8.975	0.065
05	21.07	0.0111	0.7284	7.01	46.0	98.9	8.975	0.048
04	21.15	0.0105	0.9177	5.26	48.7	98.6	8.986	0.050
07	21.28	0.0105	1.079	4.49	48.4	98.4	9.020	0.066
03	21.30	0.0107	0.8203	4.14	47.5	98.8	9.061	0.059
02	21.34	0.0105	0.9635	4.59	48.5	98.6	9.062	0.052
01	21.51	0.0046	1.147	2.48	111.2	98.3	9.11	0.11
mean ± sdev			n=8		56.2	±44.5	9.02	0.11
mean ± SEM			n=8		56.2	±44.5	9.020	0.043
weighted mean ± Taylor err			n=8		56.2	±44.5	9.007	0.030
weighted mean ± S & A err			n=8		56.2	±44.5	9.007	0.044

Appendix I. $^{40}Ar/^{39}Ar$ Analytical Data

$^{40}Ar/^{39}Ar$ Laser Fusion Data: Crary Mountains, Marie Byrd Land (1992-93 Field Season)

ID	$^{40}Ar/^{39}Ar$	$^{37}Ar/^{39}Ar$	$^{36}Ar/^{39}Ar$ (x 10^{-3})	$^{39}Ar_K$ (x 10^{-15} mol)	K/Ca	$\%^{40}Ar^*$	Age (Ma)	±2s (Ma)
TW92-036, anorth multi-xals, J=0.000731493, nm-21, Lab#=2154								
Tasch Peak Ridge, Mt. Rees, Crary Mtns.								
03	6.586	0.4014	3.255	2.45	1.3	85.1	7.382	0.087
04	6.454	0.0923	2.640	6.46	5.5	87.6	7.447	0.049
01	6.524	0.0837	2.740	3.20	6.1	87.3	7.500	0.074
08	6.089	0.0326	1.202	6.13	15.6	93.9	7.526	0.049
02	6.114	0.1144	1.276	4.31	4.5	93.5	7.530	0.052
10	6.352	0.0385	2.050	6.54	13.3	90.2	7.542	0.060
05	7.523	0.2467	5.959	4.58	2.1	76.3	7.563	0.082
09	6.467	0.1860	2.344	3.81	2.7	89.0	7.579	0.067
06	6.378	0.1264	2.040	2.68	4.0	90.3	7.580	0.076
07	7.296	0.1771	5.112	4.00	2.9	79.0	7.593	0.077
mean ± sdev			n=10	5.8	±9.7		7.52	0.14
mean ± SEM			n=10	5.8	±9.7		7.524	0.059
weighted mean ± Taylor err			n=10	5.8	±9.7		7.521	0.046
weighted mean ± S & A err			n=10	5.8	±9.7		7.521	0.059
TW92-118, anorthclase, J=0.000729938±0.27%, nm-21, Lab#=2165								
West of Mt. Steere caldera								
03	6.282	0.0721	1.849	0.029	7.1	91.0	7.512	0.067
10	5.984	0.0236	0.8415	0.014	21.6	95.5	7.512	0.074
09	5.939	0.0373	0.6681	0.012	13.7	96.4	7.521	0.071
06	6.531	0.0321	2.653	0.024	15.9	87.7	7.528	0.071
01	6.424	0.0543	2.272	0.013	9.4	89.3	7.535	0.075
02	5.903	0.0559	0.4708	0.020	9.1	97.3	7.550	0.057
08	5.959	0.0412	0.6249	0.016	12.4	96.6	7.563	0.076
07	6.212	0.0563	1.432	0.011	9.1	92.9	7.582	0.083
05	5.921	0.0212	0.3342	0.015	24.0	98.0	7.626	0.068
04	*7.795*	*1.120*	*4.122*	*0.002*	*0.46*	*84.1*	*8.62*	*0.43*
mean ± sdev			n=9		13.6	±11.8	7.548	0.086
mean ± SEM			n=9		13.6	±11.8	7.548	0.048
weighted mean ± Taylor err			n=9		13.6	±11.8	7.547	0.048
weighted mean ± S & A err			n=9		13.6	±11.8	7.547	0.054

Appendix I. $^{40}Ar/^{39}Ar$ Analytical Data

$^{40}Ar/^{39}Ar$ Laser Fusion Data: Crary Mountains, Marie Byrd Land (1992-93 Field Season)

ID	$^{40}Ar/^{39}Ar$	$^{37}Ar/^{39}Ar$	$^{36}Ar/^{39}Ar$ (x 10^{-3})	$^{39}Ar_K$ (x 10^{-15} mol)	K/Ca	$\%^{40}Ar^*$	Age (Ma)	±2s (Ma)
TW92-053:TRAY C 7, Sing xal anorth, J=0.000729678, nm-21, Lab#=2156								
Mt. Steere interior								
10AA	6.629	0.0345	1.830	2.68	14.8	91.6	7.972	0.076
07	6.450	0.0393	0.8252	3.57	13.0	95.9	8.127	0.056
09A	6.405	0.0275	0.5176	2.97	18.5	97.3	8.186	0.070
04	6.724	0.0232	1.572	3.64	22.0	92.8	8.196	0.059
03	6.701	0.0256	1.449	4.94	20.0	93.3	8.214	0.050
05	6.530	0.0579	0.8711	3.44	8.8	95.8	8.214	0.060
06	6.872	0.0271	1.958	2.57	18.8	91.3	8.241	0.074
09B	6.446	0.0214	0.2615	4.48	23.8	98.5	8.339	0.053
01	6.455	0.0174	0.2825	3.52	29.3	98.4	8.343	0.057
02	6.580	0.0209	0.6793	4.27	24.4	96.7	8.353	0.052
mean ± sdev			n=10	19.3	±12.0		8.22	0.23
mean ± SEM			n=10	19.3	±12.0		8.22	0.09
weighted mean ± Taylor err			n=10	19.3	±12.0		8.235	0.049
weighted mean ± S & A err			n=10	19.3	±12.0		8.235	0.083
TW92-093:TRAY D1, sing xal anorth, J=0.000729982, nm-21, Lab#=2160								
Mt. Steere interior								
05	6.848	0.0536	2.360	2.44	9.5	89.5	8.057	0.090
08	6.840	0.0695	2.107	3.19	7.3	90.6	8.145	0.068
04	6.659	0.0510	1.328	3.20	10.0	93.8	8.209	0.058
09	6.651	0.0628	1.236	2.54	8.1	94.2	8.234	0.079
03	7.274	0.0590	3.327	4.96	8.7	86.2	8.241	0.069
06	6.764	0.0466	1.578	5.06	10.9	92.8	8.250	0.056
07	6.941	0.0404	2.023	5.67	12.6	91.1	8.309	0.056
10	7.114	0.1182	2.457	3.09	4.3	89.5	8.368	0.086
01	7.042	0.0572	2.033	2.16	8.9	91.2	8.438	0.095
mean ± sdev			n=9	8.9	±4.7		8.25	0.23
mean ± SEM			n=9	8.9	±4.7		8.250	0.088
weighted mean ± Taylor err			n=9	8.9	±4.7		8.246	0.051
weighted mean ± S & A err			n=9	8.9	±4.7		8.246	0.080

Appendix I. $^{40}Ar/^{39}Ar$ Analytical Data

$^{40}Ar/^{39}Ar$ Laser Fusion Data: Crary Mountains, Marie Byrd Land (1992-93 Field Season)

ID	$^{40}Ar/^{39}Ar$	$^{37}Ar/^{39}Ar$	$^{36}Ar/^{39}Ar$ (x 10^{-3})	$^{39}Ar_K$ (x 10^{-15} mol)	K/Ca	$\%^{40}Ar^*$	Age (Ma)	±2s (Ma)
TW92-063:TRAY C 8, 2 xal anorth, J=0.000728835, nm-21, Lab#=2157								
Mt. Steere interior								
04	6.432	0.0436	0.6992	2.49	11.7	96.5	8.143	0.074
02	6.492	0.0187	0.8304	4.66	27.3	95.9	8.170	0.049
03	6.411	0.0206	0.4305	3.91	24.8	97.7	8.218	0.052
01	7.196	0.0320	3.044	4.00	15.9	87.2	8.235	0.063
06	6.383	0.0234	0.2889	4.77	21.8	98.4	8.237	0.046
05	6.355	0.0377	0.1099	3.37	13.5	99.2	8.269	0.058
09A	6.402	0.0195	0.2462	4.31	26.2	98.6	8.278	0.046
08	6.623	0.0297	0.9361	3.50	17.2	95.5	8.301	0.059
07	6.530	0.0278	0.4643	3.78	18.3	97.6	8.362	0.054
10A	6.520	0.0397	0.1272	3.77	12.9	99.1	8.479	0.056
09	*6.764*	*0.0138*	*0.5085*	*0.145*	*37.0*	*97.5*	*8.65*	*0.94*
mean ± sdev			n=10	19.0	±11.5		8.27	0.20
mean ± SEM			n=10	19.0	±11.5		8.269	0.076
weighted mean ± Taylor err			n=10	19.0	±11.5		8.271	0.049
weighted mean ± S & A err			n=10	19.0	±11.5		8.271	0.076
TW92-051:TRAY C 5, MULT XST ANORTH, J=0.000731212, nm-21, Lab#=2155								
Mt. Steere interior								
07	7.217	0.0136	3.076	4.68	37.6	87.1	8.277	0.071
09	7.183	0.0287	2.927	6.40	17.8	87.7	8.290	0.052
04	8.666	0.2961	7.931	2.90	1.7	72.7	8.30	0.11
05	8.435	0.0350	7.104	6.33	14.6	74.9	8.314	0.075
02	7.166	0.0107	2.782	7.65	47.8	88.3	8.325	0.058
10	6.617	0.0143	0.9156	2.90	35.8	95.6	8.327	0.065
03	6.830	0.0179	1.556	7.81	28.5	93.0	8.359	0.046
08	6.983	0.0682	1.590	1.54	7.5	93.0	8.55	0.16
06	7.225	0.0326	2.113	0.345	15.6	91.1	8.66	0.51
01	*711.9*	*0.0000*	*2320.1*	*0.006*	-	*3.7*	*34.4*	*190.7*
mean ± sdev			n=9	23.0	±30.6		8.38	0.27
mean ± SEM			n=9	23.0	±30.6		8.38	0.10
weighted mean ± Taylor err			n=9	23.0	±30.6		8.325	0.051
weighted mean ± S & A err			n=9	23.0	±30.6		8.325	0.061

Appendix I. $^{40}Ar/^{39}Ar$ Analytical Data

$^{40}Ar/^{39}Ar$ Laser Fusion Data: Crary Mountains, Marie Byrd Land (1992-93 Field Season)

ID	$^{40}Ar/^{39}Ar$	$^{37}Ar/^{39}Ar$	$^{36}Ar/^{39}Ar$ (x 10^{-3})	$^{39}Ar_K$ (x 10^{-15} mol)	K/Ca	$\%^{40}Ar^*$	Age (Ma)	±2s (Ma)
TW92-107:TRAY D 4, sing xal anorth, J=0.000731463, nm-21, Lab#=2162								
Mt. Steere arete								
9	*6.517*	*0.0288*	*4.789*	*0.088*	*17.7*	*78.0*	*6.7*	*1.7*
02A	6.370	0.0348	0.1940	4.84	14.6	98.8	8.286	0.051
5	6.666	0.0282	1.142	5.67	18.1	94.7	8.307	0.050
7	6.878	0.0334	1.839	5.88	15.3	91.8	8.315	0.051
8	6.941	0.0295	1.983	5.49	17.3	91.3	8.341	0.056
6	6.548	0.0297	0.6115	3.97	17.2	97.0	8.358	0.053
3	7.217	0.0742	2.800	3.02	6.9	88.3	8.387	0.079
01A	6.402	0.0476	0.0124	3.42	10.7	99.6	8.398	0.063
4	6.889	0.0873	1.547	3.08	5.8	93.1	8.443	0.074
mean ± sdev			n=8	13.2	±9.6		8.4	0.1
mean ± SEM			n=8	13.2	±9.6		8.4	0.1
weighted mean ± Taylor err			n=8	13.2	±9.6		8.342	0.050
weighted mean ± S & A err			n=8	13.2	±9.6		8.342	0.061
TW92-104:TRAY D 2, sing xal anorth, J=0.000730731, nm-21, Lab#=2161								
Mt. Steere arete								
02	6.502	0.0518	0.7562	3.74	9.9	96.3	8.233	0.062
04	7.387	0.0668	3.693	4.62	7.6	85.0	8.255	0.065
07	7.155	0.0725	2.883	3.44	7.0	87.8	8.265	0.070
06	6.815	0.0584	1.715	2.56	8.7	92.3	8.272	0.087
09	6.449	0.0614	0.1451	5.66	8.3	99.0	8.401	0.053
10	6.808	0.0657	1.297	4.10	7.8	94.1	8.425	0.060
08	6.717	0.0576	0.9889	3.62	8.9	95.4	8.425	0.064
03A	7.065	0.0807	2.064	3.86	6.3	91.1	8.465	0.070
03	*6.536*	*0.0451*	*-0.3251*	*0.117*	*11.3*	*101.2*	*8.7*	*1.1*
01	*6.363*	*0.1541*	*-1.9246*	*0.029*	*3.3*	*108.6*	*9.1*	*5.4*
mean ± sdev			n=8	8.1	±2.2		8.34	0.19
mean ± SEM			n=8	8.1	±2.2		8.34	0.08
weighted mean ± Taylor err			n=8	8.1	±2.2		8.350	0.051
weighted mean ± S & A err			n=8	8.1	±2.2		8.350	0.083

Appendix I. $^{40}Ar/^{39}Ar$ Analytical Data

$^{40}Ar/^{39}Ar$ Laser Fusion Data: Crary Mountains, Marie Byrd Land (1992-93 Field Season)

ID	$^{40}Ar/^{39}Ar$	$^{37}Ar/^{39}Ar$	$^{36}Ar/^{39}Ar$ (x 10^{-3})	$^{39}Ar_K$ (x 10^{-15} mol)	K/Ca	$\%^{40}Ar^*$	Age (Ma)	±2s (Ma)
TW92-108, anorthclase, J=0.00073125±0.27%, nm-21, Lab#=2164								
Mt. Steere arete								
04	7.100	0.0933	2.553	0.038	5.5	89.1	8.327	0.073
05	6.580	0.0399	0.7632	0.043	12.8	96.3	8.339	0.052
10	6.571	0.0741	0.7056	0.019	6.9	96.5	8.349	0.055
03	6.987	0.0435	2.099	0.040	11.7	90.8	8.354	0.059
02	7.050	0.0547	2.286	0.016	9.3	90.1	8.36	0.11
07	7.059	0.0725	2.315	0.023	7.0	90.0	8.366	0.073
08	7.277	0.0513	3.015	0.042	10.0	87.5	8.380	0.062
01	6.759	0.0510	1.223	0.026	10.0	94.4	8.396	0.070
09	8.150	0.0516	5.795	0.027	9.9	78.8	8.448	0.085
06	8.680	0.0533	7.584	0.022	9.6	74.0	8.449	0.093
mean ± sdev			n=10		9.3 ±4.5		8.377	0.096
mean ± SEM			n=10		9.3 ±4.5		8.377	0.053
weighted mean ± Taylor err			n=10		9.3 ±4.5		8.368	0.051
weighted mean ± S & A err			n=10		9.3 ±4.5		8.368	0.056
TW92-091:TRAY C 11, sing xal anorth, J=0.000728348, nm-21, Lab#=2159								
Mt. Steere east side								
04	6.680	0.0459	1.223	3.07	11.1	94.3	8.259	0.054
07	6.718	0.0598	0.8913	3.25	8.5	95.8	8.436	0.066
03	6.838	0.0556	1.247	4.18	9.2	94.3	8.457	0.055
01	6.524	0.0519	0.1615	3.00	9.8	99.0	8.464	0.057
02	6.611	0.0410	0.4517	2.74	12.4	97.7	8.466	0.064
06	6.678	0.0549	0.4883	4.34	9.3	97.6	8.540	0.063
05	6.644	0.0518	0.3744	3.69	9.9	98.0	8.540	0.058
08	6.942	0.0460	1.248	2.90	11.1	94.4	8.592	0.078
09	*10.46*	*0.0504*	*11.47*	*0.509*	*10.1*	*67.4*	*9.24*	*0.40*
mean ± sdev			n=8	10.2	±2.6		8.47	0.21
mean ± SEM			n=8	10.2	±2.6		8.47	0.08
weighted mean ± Taylor err			n=8	10.2	±2.6		8.457	0.051
weighted mean ± S & A err			n=8	10.2	±2.6		8.457	0.089

Appendix I. $^{40}Ar/^{39}Ar$ Analytical Data

$^{40}Ar/^{39}Ar$ Laser Fusion Data: Crary Mountains, Marie Byrd Land (1992-93 Field Season)

ID	$^{40}Ar/^{39}Ar$	$^{37}Ar/^{39}Ar$	$^{36}Ar/^{39}Ar$ (x 10^{-3})	$^{39}Ar_K$ (x 10^{-15} mol)	K/Ca	$\%^{40}Ar^*$	Age (Ma)	±2s (Ma)
TW92-181, D11:21, anorthoclase, J=0.00072867±0.27%, nm-21, Lab#=2172								
Mt. Steere, east side								
06	6.226	0.0838	1.223	0.002	6.1	93.9	7.67	0.34
01	6.887	0.0874	3.276	0.002	5.8	85.7	7.74	0.31
09	6.412	0.0760	1.454	0.002	6.7	93.0	7.82	0.40
03	6.611	0.0861	1.798	0.004	5.9	91.7	7.95	0.18
10	6.361	0.0665	0.4001	0.003	7.7	97.8	8.16	0.27
07	*9.698*	*0.3186*	*11.17*	*0.001*	*1.6*	*65.8*	*8.37*	*0.52*
04	*41.00*	*0.2142*	*117*	*0.003*	*2.4*	*15.9*	*8.53*	*0.82*
02	*70.45*	*0.4343*	*216*	*0.003*	*1.2*	*9.3*	*8.6*	*1.5*
05	*96.13*	*0.2695*	*301*	*0.003*	*1.9*	*7.4*	*9.3*	*2.1*
08	*366*	*2.704*	*1195*	*0.001*	*0.19*	*3.4*	*16.3*	*30.7*
mean ± sdev			n=5		6.4 ±1.5		7.87	0.39
mean ± SEM			n=5		6.4 ±1.5		7.87	0.18
weighted mean ± Taylor err			n=5		6.4 ±1.5		7.91	0.13
weighted mean ± S & A err			n=5		6.4 ±1.5		7.91	0.20
TW92-182, E1:21, Anorthoclase 2 xals, J=0.000736366±0.27%, nm-21, Lab#=2196								
Mt. Steere, east side								
05	9.538	0.0053	10.67	0.016	95.9	66.8	8.44	0.11
04	6.497	0.0041	0.3715	0.016	123.9	98.0	8.440	0.053
10	6.772	0.0045	1.209	0.017	114.2	94.4	8.477	0.051
06	6.639	0.0053	0.7319	0.023	96.8	96.5	8.487	0.042
09	6.823	0.0051	1.314	0.018	100.8	94.0	8.503	0.053
08	6.593	0.0043	0.5058	0.019	119.3	97.4	8.514	0.047
07	6.620	0.0062	0.4688	0.024	81.8	97.6	8.565	0.047
01	6.586	0.0051	0.3379	0.017	99.2	98.2	8.572	0.053
02	6.596	0.0045	0.3357	0.023	113.0	98.2	8.585	0.044
03	6.663	0.0046	0.5317	0.016	111.4	97.4	8.597	0.064
mean ± sdev			n=10		105.6	±25.7	8.52	0.13
mean ± SEM			n=10		105.6	±25.7	8.518	0.059
weighted mean ± Taylor err			n=10		105.6	±25.7	8.523	0.049
weighted mean ± S & A err			n=10		105.6	±25.7	8.523	0.060

Appendix I. $^{40}Ar/^{39}Ar$ Analytical Data

$^{40}Ar/^{39}Ar$ Laser Fusion Data: Crary Mountains, Marie Byrd Land (1992-93 Field Season)

ID	$^{40}Ar/^{39}Ar$	$^{37}Ar/^{39}Ar$	$^{36}Ar/^{39}Ar$ (x 10^{-3})	$^{39}Ar_K$ (x 10^{-15} mol)	K/Ca	$\%^{40}Ar^*$	Age (Ma)	±2s (Ma)
TW92-183, E2:21, Anorthoclase 2 xals, J=0.000736655±0.27%, nm-21, Lab#=2197								
Mt. Steere, east side								
03	6.578	0.0052	0.5813	0.024	97.9	97.1	8.468	0.044
10	6.598	0.0040	0.6089	0.014	128.1	97.0	8.484	0.065
02	6.495	0.0056	0.2511	0.018	90.8	98.6	8.488	0.050
07	7.191	0.0045	2.558	0.019	112.6	89.2	8.507	0.058
01	6.540	0.0049	0.3551	0.017	103.5	98.1	8.507	0.055
09	6.652	0.0048	0.7236	0.018	105.6	96.5	8.511	0.050
05	6.495	0.0045	0.0925	0.015	114.4	99.3	8.550	0.056
08	6.518	0.0059	0.1646	0.009	86.3	99.0	8.552	0.077
04	6.605	0.0048	0.4404	0.016	105.5	97.7	8.559	0.049
06	6.558	0.0047	0.1166	0.017	109.0	99.2	8.624	0.052
mean ± sdev			n=10		105.4	±24.0	8.52	0.10
mean ± SEM			n=10		105.4	±24.0	8.525	0.055
weighted mean ± Taylor err			n=10		105.4	±24.0	8.523	0.049
weighted mean ± S & A err			n=10		105.4	±24.0	8.523	0.058
TW92-178, Mt. Steere, Crary Mtns., anorth multi-xals, J=0.0002385, NMUM-4, Lab#=238								
Mt. Steere, east side								
06	20.41	0.0522	2.093	7.16	9.8	96.9	8.490	0.044
08	20.74	0.0572	2.969	9.20	8.9	95.7	8.518	0.048
07	20.17	0.0536	0.9994	8.91	9.5	98.4	8.525	0.048
02	20.12	0.0531	0.7834	4.92	9.6	98.8	8.532	0.052
01	20.22	0.0558	0.9449	5.29	9.1	98.5	8.550	0.060
05	20.45	0.0652	1.523	7.56	7.8	97.7	8.579	0.042
04	20.36	0.0541	1.086	7.41	9.4	98.3	8.594	0.044
03	20.52	0.0547	1.373	7.90	9.3	97.9	8.626	0.042
mean ± sdev			n=8		9.2	±1.2	8.552	0.093
mean ± SEM			n=8		9.2	±1.2	8.552	0.038
weighted mean ± Taylor err			n=8		9.2	±1.2	8.555	0.027
weighted mean ± S & A err			n=8		9.2	±1.2	8.555	0.043

Appendix I. $^{40}Ar/^{39}Ar$ Analytical Data

$^{40}Ar/^{39}Ar$ Laser Fusion Data: Crary Mountains, Marie Byrd Land (1992-93 Field Season)

ID	$^{40}Ar/^{39}Ar$	$^{37}Ar/^{39}Ar$	$^{36}Ar/^{39}Ar$ (x 10^{-3})	$^{39}Ar_K$ (x 10^{-15} mol)	K/Ca	$\%^{40}Ar^*$	Age (Ma)	±2s (Ma)
TW92-080:TRAY C 10, sing xal anorth, J=0.000728067, nm-21, Lab#=2158								
Lie Cliff, Mt. Steere, Crary Mountains								
03	6.261	0.0301	1.208	3.78	17.0	94.0	7.714	0.078
09	6.044	0.0207	0.3594	2.14	24.7	97.9	7.757	0.087
06	6.147	0.0288	0.6089	5.27	17.7	96.8	7.796	0.043
04	6.120	0.0417	0.4955	4.11	12.2	97.3	7.804	0.048
08	6.109	0.0245	0.4577	4.14	20.8	97.5	7.804	0.053
07	6.381	0.0290	1.331	2.42	17.6	93.5	7.823	0.082
05	6.146	0.0266	0.4389	4.02	19.2	97.6	7.860	0.051
02A	6.170	0.0292	0.4994	3.51	17.5	97.3	7.868	0.057
01A	6.065	0.0302	0.1291	3.25	16.9	99.1	7.874	0.061
10	*6.626*	*0.0585*	*0.2760*	*3.39*	*8.7*	*98.5*	*8.550*	*0.054*
mean ± sdev			n=9	18.2	±6.7		7.81	0.11
mean ± SEM			n=9	18.2	±6.7		7.811	0.056
weighted mean ± Taylor err			n=9	18.2	±6.7		7.818	0.047
weighted mean ± S & A err			n=9	18.2	±6.7		7.818	0.056
TW92-89, B11:21, anorthoclase, J=0.0007318±0.27%, nm-21, Lab#=2175								
Ridge northwest of Lie Cliff, Mt. Steere, Crary Mountains								
08	7.835	0.0126	6.899	0.043	40.5	73.7	7.611	0.070
09	7.225	0.0167	4.763	0.025	30.5	80.3	7.640	0.066
05	9.384	0.0481	12.06	0.010	10.6	61.8	7.64	0.16
04	10.46	0.0190	15.63	0.053	26.9	55.6	7.668	0.092
06	7.570	0.0142	5.814	0.057	35.8	77.1	7.684	0.057
10	8.746	0.0177	9.742	0.014	28.8	66.9	7.70	0.12
03	9.905	0.0489	13.58	0.025	10.4	59.3	7.74	0.10
07	11.67	0.0873	19.55	0.014	5.8	50.4	7.74	0.17
02	10.14	0.0366	14.26	0.025	13.9	58.2	7.78	0.12
01	10.10	0.0683	14.09	0.007	7.5	58.6	7.79	0.17
mean ± sdev			n=10		21.1	±25.6	7.70	0.13
mean ± SEM			n=10		21.1	±25.6	7.700	0.057
weighted mean ± Taylor err			n=10		21.1	±25.6	7.676	0.051
weighted mean ± S & A err			n=10		21.1	±25.6	7.676	0.061

Appendix I. $^{40}Ar/^{39}Ar$ Analytical Data

$^{40}Ar/^{39}Ar$ Laser Fusion Data: Crary Mountains, Marie Byrd Land (1992-93 Field Season)

ID	$^{40}Ar/^{39}Ar$	$^{37}Ar/^{39}Ar$	$^{36}Ar/^{39}Ar$ (x 10^{-3})	$^{39}Ar_K$ (x 10^{-15} mol)	K/Ca	$\%^{40}Ar^*$	Age (Ma)	±2s (Ma)
TW92-192, B8:21, anorthoclase, J=0.000731337±0.27%, nm-21, Lab#=2174								
Ridge northwest of Lie Cliff, Mt. Steere, Crary Mountains								
06	6.470	0.1523	1.026	0.006	3.3	95.0	8.09	0.13
08	6.514	0.1300	1.067	0.007	3.9	94.9	8.14	0.13
07	6.744	0.0940	1.825	0.009	5.4	91.7	8.14	0.10
10	6.647	0.0895	1.406	0.010	5.7	93.5	8.178	0.097
01	6.833	0.1022	1.967	0.009	5.0	91.2	8.21	0.12
09	6.429	0.0790	0.5688	0.011	6.5	97.1	8.216	0.076
04	6.445	0.1439	0.5309	0.013	3.5	97.3	8.253	0.061
03	6.543	0.1487	0.8135	0.009	3.4	96.0	8.272	0.087
02	6.868	0.1443	1.893	0.011	3.5	91.6	8.279	0.096
05	6.405	0.1173	0.2928	0.007	4.3	98.4	8.29	0.11
mean ± sdev			n=10		4.5 ±2.2		8.21	0.14
mean ± SEM			n=10		4.5 ±2.2		8.207	0.062
weighted mean ± Taylor err			n=10		4.5 ±2.2		8.222	0.054
weighted mean ± S & A err			n=10		4.5 ±2.2		8.222	0.065
TW92-122, anorth multi-xals, J=0.0002388, NMUM-4, Lab#=237								
Morrison Rocks, Mt. Frakes, Crary Mountains,								
03	10.58	0.0899	3.411	3.56	5.7	90.3	4.111	0.065
07	10.72	0.1217	3.892	2.51	4.2	89.2	4.114	0.083
04	10.97	0.1321	4.540	2.21	3.9	87.7	4.138	0.089
06	10.49	0.1278	2.788	2.83	4.0	92.0	4.153	0.069
01	11.50	0.1143	6.190	3.48	4.5	84.0	4.156	0.077
02	10.89	0.0664	3.761	4.10	7.7	89.6	4.202	0.046
05	11.30	0.1050	4.968	3.42	4.9	86.9	4.224	0.089
08	11.41	0.1046	4.960	2.13	4.9	87.0	4.28	0.10
mean ± sdev			n=8		5.0 ±2.5		4.17	0.12
mean ± SEM			n=8		5.0 ±2.5		4.172	0.042
weighted mean ± Taylor err			n=8		5.0 ±2.5		4.170	0.027
weighted mean ± S & A err			n=8		5.0 ±2.5		4.170	0.045

Appendix I. $^{40}Ar/^{39}Ar$ Analytical Data

$^{40}Ar/^{39}Ar$ Laser Fusion Data: Crary Mountains, Marie Byrd Land (1992-93 Field Season)

ID	$^{40}Ar/^{39}Ar$	$^{37}Ar/^{39}Ar$	$^{36}Ar/^{39}Ar$ (x 10^{-3})	$^{39}Ar_K$ (x 10^{-15} mol)	K/Ca	$\%^{40}Ar^*$	Age (Ma)	±2s (Ma)
TW92-121, A2:21, phonolite, anorthoclase phono., J=0.000730367±0.27%, nm-21, Lab#=2188								
Morrison Rocks, Mt. Frakes, Crary Mountains,								
01	*1.081*	*0.0089*	*0.5429*	*0.064*	*57.1*	*83.4*	*1.188*	*0.028*
03	*1.644*	*0.0101*	*2.439*	*0.020*	*50.4*	*55.0*	*1.192*	*0.042*
02	*1.137*	*0.0085*	*0.6373*	*0.029*	*60.0*	*81.8*	*1.224*	*0.030*
07	3.289	0.0586	0.3584	0.029	8.7	96.2	4.165	0.031
08	3.319	0.0914	0.4539	0.030	5.6	95.4	4.167	0.037
06	3.299	0.0809	0.3675	0.017	6.3	96.1	4.174	0.057
04	3.389	0.1065	0.6384	0.031	4.8	93.9	4.187	0.031
05	3.748	0.0772	1.741	0.040	6.6	85.8	4.231	0.041
mean ± sdev			n=5		6.4 ±2.9		4.185	0.059
mean ± SEM			n=5		6.4 ±2.9		4.185	0.034
weighted mean ± Taylor err			n=5		6.4 ±2.9		4.183	0.028
weighted mean ± S & A err			n=5		6.4 ±2.9		4.183	0.036
TW92-127, B2:21, anorthoclase, J=0.00074±0.27%, nm-21, Lab#=2173								
Morrison Rocks, Mt. Frakes, Crary Mountains,								
04	4.413	0.0955	4.232	0.028	5.3	71.2	4.191	0.062
06	3.621	0.0872	1.466	0.032	5.8	87.5	4.226	0.039
01	3.471	0.0697	0.9423	0.023	7.3	91.4	4.232	0.045
03	3.695	0.0751	1.691	0.038	6.8	86.0	4.236	0.035
07	3.988	0.0963	2.613	0.034	5.3	80.2	4.262	0.051
08	3.434	0.0749	0.7285	0.028	6.8	93.2	4.266	0.038
05	3.588	0.0989	1.243	0.028	5.2	89.2	4.269	0.038
09	3.756	0.0952	1.790	0.026	5.4	85.4	4.279	0.052
02	3.545	0.0853	1.055	0.024	6.0	90.7	4.286	0.045
mean ± sdev			n=9		6.0 ±1.6		4.250	0.065
mean ± SEM			n=9		6.0 ±1.6		4.250	0.031
weighted mean ± Taylor err			n=9		6.0 ±1.6		4.251	0.027
weighted mean ± S & A err			n=9		6.0 ±1.6		4.251	0.032

Appendix I. $^{40}Ar/^{39}Ar$ Analytical Data

$^{40}Ar/^{39}Ar$ Laser Fusion Data: Crary Mountains, Marie Byrd Land (1992-93 Field Season)

ID	$^{40}Ar/^{39}Ar$	$^{37}Ar/^{39}Ar$	$^{36}Ar/^{39}Ar$ (x 10^{-3})	$^{39}Ar_K$ (x 10^{-15} mol)	K/Ca	$\%^{40}Ar^*$	Age (Ma)	±2s (Ma)
TW92-134, anorthoclase, J=0.000730433±0.27%, nm-21, Lab#=2189								
Debris flow deposit at base of Runyon Rock, Boyd Ridge, Crary Mountains								
08	2.497	0.0455	3.345	0.023	11.2	59.6	1.961	0.038
03	2.157	0.0583	2.125	0.025	8.8	70.0	1.989	0.038
02	2.605	0.0525	3.629	0.022	9.7	58.1	1.994	0.044
04	3.117	0.0507	5.297	0.019	10.1	49.2	2.019	0.063
07	2.708	0.0727	3.836	0.018	7.0	57.4	2.048	0.062
05	3.474	0.0434	6.377	0.019	11.7	45.2	2.068	0.063
09	4.129	0.1691	8.437	0.022	3.0	39.2	2.129	0.075
01	6.555	0.0469	16.59	0.038	10.9	24.9	2.15	0.11
06	12.67	0.0768	37.25	0.022	6.6	12.9	2.16	0.21
10	8.010	0.0711	21.17	0.020	7.2	21.7	2.28	0.12
mean ± sdev			n=10		8.6 ±5.4		2.08	0.20
mean ± SEM			n=10		8.6 ±5.4		2.080	0.064
weighted mean ± Taylor err			n=10		8.6 ±5.4		2.019	0.022
weighted mean ± S & A err			n=10		8.6 ±5.4		2.019	0.049

Appendix I. $^{40}Ar/^{39}Ar$ Analytical Data

$^{40}Ar/^{39}Ar$ Laser Fusion Data: Central and Western Marie Byrd Land (1993-94 Field Season)

ID	$^{40}Ar/^{39}Ar$	$^{37}Ar/^{39}Ar$	$^{36}Ar/^{39}Ar$ (x 10^{-3})	$^{39}Ar_K$ (x 10^{-15} mol)	K/Ca		$\%^{40}Ar^*$	Age (Ma)	±2s.d. (Ma)
WCM-93-309, C16:34, multiple crystals, J=0.001475288, nm-34, Lab#=5197									
Lind Ridge, Mt. Andrus, clastogenic lava									
03	4.899	0.0236	0.6764	14.7	21.6		96.0	12.47	0.10
04	4.731	0.0127	0.0910	22.0	40.2		99.4	12.480	0.082
02	4.745	0.0046	0.1063	24.6	110.7		99.3	12.503	0.082
06	4.753	0.0192	0.1344	15.0	26.6		99.2	12.51	0.10
08	4.755	0.0161	0.0759	13.1	31.6		99.6	12.55	0.11
10	4.848	0.0190	0.3781	11.7	26.9		97.7	12.57	0.12
01	4.750	0.0418	0.0028	12.2	12.2		100.0	12.60	0.11
09	4.789	0.0222	0.1168	24.9	23.0		99.3	12.615	0.076
07	4.749	0.0162	-0.0376	15.3	31.6		100.3	12.628	0.098
05	4.823	0.0189	0.1820	9.66	27.0		98.9	12.65	0.13
mean ± sdev			n=10		35.1	±55.1		12.56	0.14
mean ± SEM			n=10		35.1	±55.1		12.558	0.054
weighted mean ± Taylor err			n=10		35.1	±55.1		12.552	0.046
weighted mean ± S & A err			n=10		35.1	±55.1		12.552	0.062
WCM-93-311, H4:34, single crystal, J=0.001508486, nm-34, Lab#=5225									
Lind Ridge, Mt. Andrus, clastogenic lava									
09	4.070	0.0045	0.1149	5.15	114.6		99.2	10.952	0.074
05	4.072	0.0063	0.1196	6.43	81.4		99.1	10.953	0.065
08	4.085	0.0055	0.1368	5.39	93.1		99.0	10.974	0.073
03	4.078	0.0058	0.1061	2.97	88.6		99.2	10.98	0.11
01	4.081	0.0058	0.0051	3.10	87.9		100.0	11.07	0.11
02	4.097	0.0056	0.0406	4.21	90.4		99.7	11.085	0.081
07	4.155	0.0051	0.1172	4.19	100.4		99.2	11.178	0.090
04	4.133	0.0048	-0.0010	1.34	105.7		100.0	11.21	0.23
10	4.122	0.0049	-0.0700	2.86	103.4		100.5	11.24	0.12
06	4.130	0.0053	-0.0581	3.10	97.1		100.4	11.25	0.11
mean ± sdev			n=10		96.3	±19.9		11.09	0.25
mean ± SEM			n=10		96.3	±19.9		11.089	0.083
weighted mean ± Taylor err			n=10		96.3	±19.9		11.045	0.041
weighted mean ± S & A err			n=10		96.3	±19.9		11.045	0.082

Appendix I. $^{40}Ar/^{39}Ar$ Analytical Data

$^{40}Ar/^{39}Ar$ Laser Fusion Data: Central and Western Marie Byrd Land (1993-94 Field Season)

ID	$^{40}Ar/^{39}Ar$	$^{37}Ar/^{39}Ar$	$^{36}Ar/^{39}Ar$ (x 10^{-3})	$^{39}Ar_K$ (x 10^{-15} mol)	K/Ca	%^{40}Ar*	Age (Ma)	±2s.d. (Ma)
WCM-93-312, H5:34, single crystal, J=0.001508486, nm-34, Lab#=5226								
Lind Ridge, Mt. Andrus, clastogenic lava								
06	2.184	0.0034	0.4264	2.11	149.5	94.2	5.59	0.13
01	2.233	0.0004	0.3640	5.79	1338.6	95.2	5.776	0.055
02	2.242	0.0006	0.3432	3.93	803.0	95.5	5.815	0.073
05	2.171	0.0016	0.0492	3.79	324.8	99.3	5.860	0.073
03	4.113	0.0070	0.3692	4.77	73.0	97.4	10.864	0.068
04	4.111	0.0049	0.2607	2.30	104.1	98.1	10.94	0.12
08	4.081	0.0067	-0.0502	2.85	76.3	100.4	11.11	0.10
07	4.082	0.0062	-0.0830	2.25	81.8	100.6	11.14	0.13
10	4.186	0.0049	-0.0354	1.59	103.2	100.3	11.39	0.17
09	4.092	0.0061	-0.3961	2.18	84.2	102.9	11.42	0.13
mean ± sdev			n=10		313.9	±850.1	9.0	5.6
mean ± SEM			n=10		313.9	±850.1	9.0	1.8
weighted mean ± Taylor err			n=10		313.9	±850.1	7.957	0.037
weighted mean ± S & A err			n=10		313.9	±850.1	8.0	1.7
WCM-93-156, C10:34, single crystal, J=0.001475288, nm-34, Lab#=5191								
Starbuck Crater, Mt. Bursey, lava								
06	3.167	0.0371	0.1260	30.6	13.8	98.9	8.317	0.050
03	3.156	0.0395	-0.0499	24.9	12.9	100.6	8.426	0.057
05	3.116	0.0680	-0.1987	13.8	7.5	102.0	8.443	0.078
07	3.214	0.0361	0.1150	19.0	14.2	99.0	8.452	0.068
04	3.200	0.0112	0.0462	12.4	45.7	99.6	8.463	0.089
01	3.314	0.0535	0.4133	16.8	9.5	96.4	8.486	0.078
08	3.159	0.0462	-0.1175	16.3	11.0	101.2	8.489	0.074
09	3.244	0.0387	0.1531	13.2	13.2	98.7	8.501	0.095
02	3.158	0.0127	-0.1542	22.6	40.3	101.5	8.508	0.062
10	3.167	0.0657	-0.1460	17.2	7.8	101.5	8.538	0.069
mean ± sdev			n=10		17.6	±27.3	8.46	0.12
mean ± SEM			n=10		17.6	±27.3	8.462	0.045
weighted mean ± Taylor err			n=10		17.6	±27.3	8.447	0.032
weighted mean ± S & A err			n=10		17.6	±27.3	8.447	0.056

Appendix I. $^{40}Ar/^{39}Ar$ Analytical Data

$^{40}Ar/^{39}Ar$ Laser Fusion Data: Central and Western Marie Byrd Land (1993-94 Field Season)

ID	$^{40}Ar/^{39}Ar$	$^{37}Ar/^{39}Ar$	$^{36}Ar/^{39}Ar$ (x 10^{-3})	$^{39}Ar_K$ (x 10^{-15} mol)	K/Ca	$\%^{40}Ar^*$	Age (Ma)	±2s.d. (Ma)
WCM-93-158, C11:34, single crystal, J=0.001475288, nm-34, Lab#=5192								
Syrstad Rock, Mt. Bursey, bomb								
10	0.1197	0.0187	0.2176	10.7	27.3	47.3	0.151	0.097
04	0.1161	0.0116	0.1898	12.8	44.1	52.3	0.162	0.072
07	0.0873	0.0146	0.0642	13.0	34.8	79.3	0.185	0.069
08	0.1277	0.0150	0.1835	10.8	34.1	58.3	0.198	0.092
06	0.1086	0.0140	0.0803	23.6	36.4	79.0	0.228	0.034
03	0.0862	0.0110	-0.0131	19.5	46.6	105.2	0.241	0.039
05	0.1176	0.0106	0.0704	29.7	48.0	82.8	0.259	0.040
01	0.1305	0.0084	0.0896	15.9	60.8	80.0	0.278	0.058
02	0.1012	0.0226	-0.0373	14.7	22.6	112.4	0.303	0.053
09	0.1133	0.0177	-0.0313	13.6	28.9	109.2	0.329	0.068
mean ± sdev			n=10		38.4 ±23.0		0.23	0.12
mean ± SEM			n=10		38.4 ±23.0		0.233	0.038
weighted mean ± Taylor err			n=10		38.4 ±23.0		0.244	0.017
weighted mean ± S & A err			n=10		38.4 ±23.0		0.244	0.033
WCM-93-160, C12:34, single crystal, J=0.001475288, nm-34, Lab#=5193								
Koerner Bluff, Mt. Bursey, lava								
07	3.735	0.0313	0.0798	17.6	16.3	99.4	9.858	0.075
04	3.731	0.0259	0.0177	46.3	19.7	99.9	9.893	0.049
02	3.741	0.0312	0.0330	27.6	16.4	99.8	9.910	0.059
08	3.737	0.0155	-0.0133	13.7	33.0	100.1	9.933	0.094
01	3.742	0.0255	-0.0053	12.1	20.0	100.1	9.940	0.095
09	3.762	0.0342	0.0438	24.5	14.9	99.7	9.957	0.062
03	3.741	0.0304	-0.0635	20.0	16.8	100.6	9.985	0.068
05	3.736	0.0233	-0.0946	17.8	21.9	100.8	9.993	0.080
10	3.736	0.0169	-0.1765	16.6	30.3	101.4	10.057	0.077
06	3.776	0.0178	-0.1786	11.2	28.7	101.4	10.164	0.098
mean ± sdev			n=10		21.8 ±13.1		9.97	0.18
mean ± SEM			n=10		21.8 ±13.1		9.969	0.062
weighted mean ± Taylor err			n=10		21.8 ±13.1		9.951	0.035
weighted mean ± S & A err			n=10		21.8 ±13.1		9.951	0.060

Appendix I. $^{40}Ar/^{39}Ar$ Analytical Data

$^{40}Ar/^{39}Ar$ Laser Fusion Data: Central and Western Marie Byrd Land (1993-94 Field Season)

ID	$^{40}Ar/^{39}Ar$	$^{37}Ar/^{39}Ar$	$^{36}Ar/^{39}Ar$ (x 10^{-3})	$^{39}Ar_K$ (x 10^{-15} mol)	K/Ca	%^{40}Ar*	Age (Ma)	±2s.d. (Ma)
WCM-93-288, C13:34, single crystal, J=0.001475288, nm-34, Lab#=5194								
Reynolds Ridge, Mt. Flint, hypabbyssal lava								
06	9.683	0.1917	7.192	29.4	2.7	78.2	20.05	0.15
04	9.808	0.1827	7.499	39.6	2.8	77.5	20.13	0.14
08	7.817	0.2418	0.7763	19.8	2.1	97.3	20.13	0.11
05	11.05	0.0848	11.65	47.8	6.0	68.9	20.14	0.19
01	9.054	0.1240	4.798	31.5	4.1	84.4	20.24	0.14
02	12.03	0.2042	14.88	38.4	2.5	63.6	20.24	0.21
09	10.72	0.0439	10.39	18.7	11.6	71.4	20.25	0.20
03	9.258	0.2411	5.496	17.6	2.1	82.7	20.26	0.15
07	13.35	0.1801	19.27	26.1	2.8	57.5	20.31	0.28
10	9.099	0.4540	4.858	14.4	1.1	84.6	20.38	0.17
mean ± sdev			n=10		3.8 ±6.1		20.21	0.20
mean ± SEM			n=10		3.8 ±6.1		20.213	0.083
weighted mean ± Taylor err			n=10		3.8 ±6.1		20.192	0.075
weighted mean ± S & A err			n=10		3.8 ±6.1		20.192	0.096
WCM-93-291, C14:34, single crystal, J=0.001475288, nm-34, Lab#=5195								
Reynolds Ridge, Mt. Flint, lava								
5	8.090	0.0204	1.722	25.7	25.0	93.7	20.07	0.14
4	7.929	0.0180	1.132	42.9	28.3	95.8	20.10	0.12
1	8.598	0.0220	3.257	46.6	23.1	88.8	20.21	0.12
2	13.96	0.0206	21.33	8.28	24.8	54.8	20.26	0.39
10	9.641	0.0166	6.673	24.0	30.7	79.6	20.30	0.17
6	10.94	0.0222	11.05	31.3	22.9	70.2	20.31	0.19
7	17.89	0.0150	34.55	31.9	34.0	42.9	20.33	0.39
9	9.520	0.0155	6.116	19.5	33.0	81.0	20.41	0.17
8	11.37	0.0152	12.27	16.9	33.6	68.1	20.50	0.24
3	*10.59*	*0.0063*	*0.1359*	*53.2*	*80.6*	*99.6*	*27.87*	*0.13*
mean ± sdev			n=9		28.4 ±9.1		20.28	0.28
mean ± SEM			n=9		28.4 ±9.1		20.28	0.11
weighted mean ± Taylor err			n=9		28.4 ±9.1		20.224	0.078
weighted mean ± S & A err			n=9		28.4 ±9.1		20.22	0.12

Appendix II. XRF Geochemical Data

Volcano	Mt. Rees	Mt. Rees	Mt. Rees	Mt. Rees	Mt. Rees	Mt. Rees	Mt. Rees	Mt. Rees
Outcrop	Trabucco north lava	Trabucco north lava	Trabucco north lava	Trabucco north lava	Trabucco central pillow	Trabucco central lava	Trabucco central dike	Trabucco south lava
Rock Type	trach	trach	trach	trach	mug	basn	haw	trach
TW92-	174	175	177	6	41	45	14	15
Lab.	UK	UK	UK	UK	UK	UK	UK	UK
Age (Ma)	8.94	8.95	~8.95	8.98	9.01			9.13
SiO_2	62.73	64.81	63.63	65.81	52.67	42.22	44.7	65.82
TiO_2	0.49	0.41	0.43	0.35	1.78	2.8	3.49	0.34
Al_2O_3	14.69	14.37	14.34	13.86	16.85	16.37	15.85	14.2
Fe_2O_3	8.23	7.24	7.65	6.6	11.42	14.5	15.34	6.34
MnO	0.24	0.2	0.22	0.17	0.27	0.19	0.23	0.16
MgO	0.01	0	0	0	1.96	6.81	4.8	0
CaO	1.52	1.21	1.36	0.79	5.27	11.64	9.29	0.8
Na_2O	6.82	6.94	7.2	7.06	6.13	2.55	3.98	7.2
K_2O	4.96	4.94	4.91	4.79	2.2	0.59	1.03	4.86
P_2O_5	0.03	0.02	0.03	0	0.59	0.25	0.45	0
LOI	-0.04	0.01	0.32	0.15	1	1.62	1.1	0.23
Total	99.68	100.14	100.1	99.57	100.14	99.53	100.27	99.96
Ba	95	48	82	17	854	174	309	18
La	77	116	98	146	64	11	36	157
Ce	202	252	239	376	150	33	76	335
Nd	68	78	78	118	52	16	31	111
Cl	17	95	184	91	201	112	185	0
S	47	99	61	54	131	197	476	51
Cr	1	1	1	5	0	35	1	2
Cu	7	10	5	7	19	80	26	4
Ga	30	36	33	37	22	20	21	33
Nb	96	132	115	186	92	28	48	160
Ni	4	4	3	3	4	59	9	4
Pb	20	24	21	33	13	11	10	28
Rb	113	167	146	227	37	15	25	191
Sr	4	2	3	1	513	605	686	4
Th	16	30	19	34	10	4	2	42
V	3	0	0	0	0	349	211	0
Y	65	55	76	114	50	22	31	78
Zn	166	180	177	221	118	87	108	207
Zr	465	737	553	883	341	115	191	986

Appendix II. XRF Geochemical Data

Volcano	Mt. Rees	Mt. Rees	Mt. Rees	Mt. Rees	Mt. Rees	Mt. Rees	Mt. Rees	Mt. Rees
Outcrop	Trabucco north pillow	Trabucco central dike	Trabucco central lava	Trabucco central lava	Tasch Ridge dike	Tasch Ridge lava	Tasch Ridge pillow	Tasch Ridge lava
Rock Type	haw	mug	haw	mug	phono	mug	mug	ben
TW92-	1	9	72	78	36	33	31	25
Lab.	UK	UK	UK	UK	UK	UK	UK	UK
Age (Ma)					7.52	8.23	8.98	9.08
SiO_2	44.36	52.26	48.83	48.85	60.01	49.61	51.19	52.13
TiO_2	3.44	1.82	2.92	2.66	0.2	1.91	1.71	1.61
Al_2O_3	15.66	16.02	16.81	16.91	18.69	18.57	18.91	17.81
Fe_2O_3	15.33	12.79	12.63	12.7	5.3	9.83	9.33	9.81
MnO	0.23	0.23	0.21	0.21	0.15	0.19	0.18	0.23
MgO	4.54	2.12	3.23	2.98	0.07	2.17	1.75	2.01
CaO	9.15	5.41	7.89	7.32	1.25	6.88	6.32	5.35
Na_2O	4.09	5.25	4.25	4.85	8.72	5.53	6.06	6.43
K_2O	0.99	2.77	1.96	1.56	5.04	2.36	2.49	2.79
P_2O_5	0.46	0.71	0.63	0.55	0.03	0.75	0.59	0.54
LOI	1.33	0.95	1.02	1.7	0.44	2.13	1.11	1.49
Total	99.6	100.34	100.38	100.3	99.9	99.92	99.64	100.21
Ba	302	678	523	592	717	668	746	738
La	25	64	48	51	113	54	60	90
Ce	70	139	98	104	185	110	103	149
Nd	26	50	44	35	39	37	40	53
Cl	170	57	207	165	2042	400	507	795
S	128	59	135	144	58	88	59	81
Cr	2	0	1	0	3	6	0	1
Cu	30	17	33	34	13	27	23	23
Ga	22	22	21	21	25	19	20	23
Nb	48	72	66	67	161	82	93	112
Ni	7	5	8	6	4	5	4	6
Pb	9	14	13	11	17	11	12	12
Rb	24	64	49	28	164	55	63	77
Sr	670	509	741	699	47	838	727	572
Th	4	12	5	6	28	3	6	10
V	253	10	107	134	9	56	31	12
Y	31	48	37	37	39	35	36	44
Zn	110	119	91	94	98	75	77	79
Zr	203	308	242	267	679	308	356	402

Appendix II. XRF Geochemical Data

Volcano	Mt. Rees	Mt. Rees	Mt. Rees	Mt. Rees	Mt. Rees	Mt. Rees	Mt. Steere	Mt. Steere
Outcrop	Tasch Ridge pillow	Tasch Ridge lava	Tasch Ridge dike	Tasch Ridge lava	north end lava	north end lava	west side lava	northeast lava
Rock Type	ben	haw	mug	basn	trach	trach	phono	mug
TW92-	23	55	56	59	112	109	118	95
Lab.	UK	UK	UK	UK	UK	UK	UK	UK
Age (Ma)	8.91			9.34	9.02	8.7	7.57	5.74
SiO_2	54.54	48.29	48.5	43	59.47	58.88	60.17	52.81
TiO_2	1.14	2.04	1.9	2.96	0.44	0.47	0.08	1.52
Al_2O_3	18.53	20.86	18.41	16.31	17.37	17.26	18.6	16.33
Fe_2O_3	8.4	9.08	11.09	15.17	8.06	8.21	4.99	13.18
MnO	0.22	0.16	0.16	0.19	0.24	0.24	0.17	0.26
MgO	1.24	2.53	2.46	5.92	0.29	0.35	0	2.09
CaO	4.1	9.46	7.48	11.39	2.57	2.63	0.76	5.21
Na_2O	6.68	4.21	4.59	2.79	7.08	6.93	9.69	5.65
K_2O	2.69	1.31	1.7	0.64	4.4	4.27	4.95	2.36
P_2O_5	0.31	0.64	0.7	0.29	0.09	0.1	0.01	0.93
LOI	1.7	1.13	3.34	0.93	0	0.18	0.51	-0.61
Total	99.56	99.7	100.33	99.58	99.99	99.51	99.93	99.73
Ba	860	391	552	186	2151	2080	194	685
La	90	40	63	22	101	95	136	75
Ce	190	63	117	44	214	194	227	132
Nd	67	32	50	26	66	66	46	45
Cl	389	165	34	43	605	334	2401	33
S	86	50	56	62	50	52	49	56
Cr	0	5	8	24	4	4	8	0
Cu	15	25	32	78	11	12	8	26
Ga	22	20	18	21	32	29	25	23
Nb	136	50	65	28	137	139	154	79
Ni	3	3	18	49	3	4	1	8
Pb	12	12	8	9	19	18	23	13
Rb	55	30	38	16	96	92	189	62
Sr	469	996	844	598	220	229	8	641
Th	15	2	3	0	16	16	37	12
V	12	97	68	359	2	1	2	16
Y	46	26	34	22	68	66	39	49
Zn	87	56	67	82	103	123	134	78
Zr	476	177	267	131	551	538	834	352

Appendix II. XRF Geochemical Data

Volcano	Mt. Steere	Mt. Steere	Mt. Steere	Mt. Steere	Mt. Steere	Mt. Steere	Mt. Steere	Mt. Steere
Outcrop	northeast dike	northeast dike	northeast lava	northeast dike	northeast dike	northeast lava	east side dike	east side dike
Rock Type	phono	ben	trach	rhyo	trach	trach	trach	phono
TW92-	64	52	53	93	63	51	91	181
Lab.	UK	UK	UK	UK	UK	UK	UK	UK
Age (Ma)	8.06		8.24	8.25	8.27	8.24	8.46	7.91
SiO_2	58.69	49.84	58.64	68.15	60.1	59.83	65.28	58.52
TiO_2	0.15	1.4	0.69	0.23	0.31	0.67	0.34	0.19
Al_2O_3	19.01	15.73	16.75	14.2	16.87	16.64	14.91	17.84
Fe_2O_3	5.83	10.76	7.12	3.85	7.3	6.95	6.1	6.52
MnO	0.17	0.28	0.2	0.14	0.2	0.19	0.19	0.22
MgO	0	1.37	0.49	0	0.13	0.34	0.1	0
CaO	1	5.54	2.29	1.65	1.42	2.02	1.49	0.97
Na_2O	9.39	5.7	6.66	5.37	6.46	6.52	6.12	8.37
K_2O	4.99	3.11	4.34	5.19	5.38	4.38	5.26	4.72
P_2O_5	0.01	0.38	0.12	0	0.02	0.11	0.03	0.01
LOI	1.02	6.04	2.41	0.89	1.92	1.87	-0.01	2.39
Total	100.26	100.15	99.71	99.67	100.11	99.53	99.79	99.76
Ba	16	840	1119	670	269	1039	367	394
La	140	69	66	93	128	81	84	129
Ce	316	134	133	212	281	132	173	285
Nd	94	56	46	72	79	46	55	78
Cl	1524	67	3	0	56	5	0	0
S	65	504	85	50	71	57	49	65
Cr	2	0	0	5	3	0	5	0
Cu	6	14	10	4	8	9	8	3
Ga	39	21	27	29	37	28	29	35
Nb	221	106	9	107	176	92	79	195
Ni	6	3	5	3	5	3	5	3
Pb	19	11	15	25	28	14	20	18
Rb	143	93	121	195	172	110	133	123
Sr	5	396	137	39	31	133	25	15
Th	25	10	14	25	28	13	16	20
V	11	12	19	7	12	20	10	5
Y	101	49	47	72	100	51	62	84
Zn	193	127	80	143	142	78	120	165
Zr	874	337	361	518	863	405	382	688

Appendix II. XRF Geochemical Data

Volcano	Mt. Steere	Mt. Steere	Mt. Steere	Mt. Steere	Mt. Steere	Mt. Steere	Mt. Steere	Mt. Steere
Outcrop	east side lava	east side lava	east side erratic	east side lava	Lie Cliff, SE ridge lava	Lie Cliff, SE ridge lava	Lie Cliff, SE ridge lava	Lie Cliff, SE ridge lava
Rock Type	rhyo	rhyo	tph-ph	trach	basn	bas	bas	ben
TW92-	182	183	179	178	169	165	162	160
Lab.	UK	UK	UK	UK	UK	UK	UK	UK
Age (Ma)	8.52	8.52		8.55	6.41	7.38	6.7	
SiO_2	73.45	72.65	55.23	65.54	44.92	45.77	45.31	56.69
TiO_2	0.21	0.2	0.84	0.32	3.43	2.11	1.99	0.85
Al_2O_3	11.86	12.06	18.59	15.18	16.39	15.12	14.72	17.03
Fe_2O_3	3.77	3.91	8.37	5.9	14.8	12.91	13.33	9.38
MnO	0.05	0.08	0.23	0.17	0.22	0.18	0.2	0.27
MgO	0	0	1.02	0	5.14	9.52	10.86	0.73
CaO	0.44	0.18	3.23	0.9	8.17	9.58	8.94	3.04
Na_2O	4.42	5.51	7.71	6.1	5.02	3.42	3.68	7.11
K_2O	5.03	4.62	3.55	5.47	1.64	0.8	0.98	3.73
P_2O_5	0	0	0.3	0.02	0.85	0.4	0.38	0.25
LOI	0.79	0.37	0.68	0.21	-0.67	0.03	-0.49	0.76
Total	100.01	99.59	99.76	99.81	99.91	99.86	99.9	99.85
Ba	15	6	1145	358	472	249	344	1319
La	184	294	83	96	51	25	28	93
Ce	385	463	188	195	103	55	53	193
Nd	128	206	55	61	46	39	17	59
Cl	2	168	572	2	371	248	129	376
S	58	163	80	49	79	58	78	98
Cr	7	1	4	2	16	427	425	2
Cu	2	2	19	8	48	77	71	18
Ga	36	38	24	31	17	17	18	26
Nb	172	185	138	96	73	34	45	126
Ni	5	5	3	3	29	224	281	7
Pb	56	27	18	12	11	8	9	15
Rb	276	271	95	135	35	18	25	76
Sr	1	2	345	21	884	525	532	245
Th	38	39	17	16	6	0	1	15
V	9	5	6	5	141	203	178	3
Y	126	115	55	65	38	25	26	62
Zn	202	237	104	132	83	77	83	130
Zr	779	766	482	419	232	147	159	476

Appendix II. XRF Geochemical Data

Volcano	Mt. Steere	Mt. Steere	Mt. Steere	Mt. Steere	Mt. Steere	Mt. Steere	Mt. Steere	Mt. Steere
Outcrop	Lie Cliff, SE ridge erratic	Lie Cliff dike	Lie Cliff lava	Lie Cliff dike	Lie Cliff pillow	Lie Cliff lava	Lie Cliff, NW ridge dike	Lie Cliff, NW ridge dike
Rock Type	phono	trach	haw	bas	mug	haw	phono	mug
TW92-	173	80	85	81	82	86	89	193
Lab.	UK	UK	UK	UK	UK	UK	UK	UK
Age (Ma)		7.82	8.38		8.28	8.52	7.68	8.19
SiO_2	59.28	60.65	46.93	42.25	49.21	45.83	55.91	51.8
TiO_2	0.25	0.39	2.48	1.95	2.48	2.74	0.08	1.47
Al_2O_3	19.35	16.07	18.33	14.43	15.59	15.97	18.9	17.21
Fe_2O_3	5.65	8.35	12.73	12.23	13.97	14.73	5.27	11.86
MnO	0.18	0.31	0.21	0.17	0.27	0.24	0.19	0.25
MgO	0.19	0.08	3.03	8.6	2.78	4.59	0	1.92
CaO	1.66	1.26	9.91	9.81	7.1	9.26	0.69	5.62
Na_2O	9.02	6.71	4.11	3.38	4.82	4.42	9.62	6.43
K_2O	4.54	5.3	1.15	0.75	1.93	1.03	4.86	2.06
P_2O_5	0.05	0.02	0.48	0.28	0.87	0.4	0.01	0.63
LOI	0.18	0.77	0.97	6.21	0.99	0.85	4.4	1.16
Total	100.36	99.92	100.32	100.07	100.01	100.06	99.93	100.41
Ba	1119	167	313	258	573	312	44	592
La	105	143	17	13	61	26	187	58
Ce	191	291	61	49	121	58	332	124
Nd	51	71	25	33	50	20	87	46
Cl	1343	4	126	352	22	67	148	461
S	57	52	75	155	59	99	51	52
Cr	7	0	6	392	0	6	2	0
Cu	14	14	25	89	18	35	14	16
Ga	27	32	20	15	20	19	35	23
Nb	164	188	45	33	79	45	245	78
Ni	3	4	10	152	7	15	4	7
Pb	17	20	13	8	12	9	23	10
Rb	131	141	29	20	43	24	202	48
Sr	132	11	678	431	528	590	2	604
Th	23	28	2	2	10	4	29	9
V	8	13	129	194	0	234	14	0
Y	54	81	30	24	49	31	74	45
Zn	110	202	94	79	128	104	172	114
Zr	658	454	162	134	254	164	1075	281

Appendix II. XRF Geochemical Data

Volcano	Mt. Steere	Mt. Steere	Mt. Steere	Mt. Steere	Mt. Steere	Mt. Steere	Mt. Frakes	Mt. Frakes
Outcrop	Lie Cliff, NW ridge pillow	Lie Cliff, NW ridge pillow	Lie Cliff, NW ridge pillow	Lie Cliff, NW ridge lava	Lie Cliff, NW ridge	Lie Cliff, NW ridge	Mor. Rk east lava	Mor. Rk east lava
Rock Type	phono	haw	haw	haw	haw	haw	bas	bas
TW92-	192	189	190	186	184	88	145	142
Lab.	UK	UK	UK	UK	UK	UK	UK	UK
Age (Ma)	8.22	8.45	8.27	8.4			1.81	1.82
SiO_2	59.01	45.72	45.69	46.18	45.36	45.61	47.43	46.23
TiO_2	0.4	2.86	2.85	2.84	2.74	2.91	1.77	1.78
Al_2O_3	17.26	15.75	15.62	15.86	15.94	15.45	14.83	14.49
Fe_2O_3	7.5	15.24	15.24	15.47	15.22	15.73	11.62	11.69
MnO	0.24	0.24	0.25	0.25	0.24	0.25	0.2	0.2
MgO	0.23	4.12	4	4.5	4.1	3.89	9.75	10.42
CaO	1.49	8.82	8.73	9.01	9.3	8.52	9.93	10.65
Na_2O	7.79	4.36	4.17	4.26	4.09	4.53	3.63	3.26
K_2O	4.95	1.33	1.01	1.03	0.96	1.23	1.2	1.04
P_2O_5	0.04	0.5	0.52	0.41	0.39	0.42	0.31	0.31
LOI	0.89	1.17	1.69	0.58	1.51	1.55	-0.46	-0.29
Total	99.79	100.1	99.76	100.38	99.86	100.09	100.21	99.77
Ba	494	389	383	319	319	336	291	254
La	105	34	36	23	27	33	33	27
Ce	228	79	85	55	60	69	69	51
Nd	76	39	32	23	20	25	34	25
Cl	1147	288	92	122	122	173	136	149
S	60	81	115	175	202	64	84	70
Cr	0	0	6	4	2	0	498	545
Cu	10	42	36	30	33	22	75	80
Ga	31	21	22	20	21	20	19	17
Nb	174	53	56	48	43	49	55	44
Ni	3	13	9	13	13	8	219	228
Pb	18	10	10	10	10	10	11	13
Rb	135	32	26	26	25	34	35	28
Sr	13	569	568	589	617	596	386	397
Th	23	5	7	6	4	5	5	4
V	0	233	207	224	240	210	192	212
Y	73	32	35	31	30	33	33	30
Zn	146	99	109	108	104	112	92	82
Zr	575	196	197	167	171	177	207	171

Appendix II. XRF Geochemical Data

Volcano	Mt. Frakes	Mt. Frakes	Mt. Frakes	Mt. Frakes	Mt. Frakes	Mt. Frakes	Mt. Frakes
Outcrop	Mor. Rk lava	Mor. Rk lava	Mor. Rk lava	Mor. Rk lava	Mor. Rk lava	Mor. Rk lava	Mor. Rk lava
Rock Type	haw	haw	bas	bas	phono	phono	phono
TW92-	128	125	130	148	121	122	127
Lab.	UK	UK	UK	UK	UK	UK	UK
Age (Ma)	2.52	2.54	3.88		4.17	4.18	4.25
SiO_2	46.45	47.08	46.75	47.04	55.62	55.88	55.71
TiO_2	2.29	2.33	2.33	1.77	0.41	0.42	0.39
Al_2O_3	16.13	15.9	15.92	14.89	19.54	19.65	19.61
Fe_2O_3	12.69	12.57	12.76	11.49	6.8	6.76	6.73
MnO	0.19	0.19	0.19	0.2	0.24	0.24	0.24
MgO	7.22	7.32	7.76	9.37	0.33	0.33	0.36
CaO	9.18	9.35	9.24	10.1	1.3	1.34	1.29
Na_2O	4.05	3.78	3.82	3.69	9.92	10.7	9.46
K_2O	1.22	1.29	1.12	1.22	4.77	4.77	4.89
P_2O_5	0.5	0.46	0.46	0.31	0.1	0.1	0.09
LOI	-0.01	0.1	-0.48	-0.26	0.6	0.05	0.85
Total	99.92	100.37	99.87	99.81	99.63	100.23	99.63
Ba	340	337	320	304	393	426	371
La	30	27	30	30	137	131	131
Ce	61	61	63	68	248	243	258
Nd	25	34	28	25	68	64	69
Cl	161	217	262	27	1190	1042	487
S	101	73	68	292	85	94	162
Cr	245	260	265	482	6	5	6
Cu	61	64	53	76	9	9	9
Ga	17	18	19	18	35	34	34
Nb	46	49	44	55	276	273	279
Ni	104	111	112	199	6	3	5
Pb	12	12	11	12	17	16	16
Rb	30	32	27	32	157	153	158
Sr	586	556	594	388	61	69	55
Th	2	6	4	4	34	32	34
V	174	188	180	191	7	10	10
Y	31	32	30	33	86	87	88
Zn	80	86	82	89	144	141	146
Zr	191	191	177	206	860	852	866

Appendix II. XRF Geochemical Data

Volcano	Mt. Frakes	Mt. Frakes	Mt. Frakes	Boyd R.	Boyd R.	Boyd R.
Outcrop	English Rk lowest lava	English Rk lava	English Rk lava	east end lava	Runyon Rk NW clast	Runyon Rk NE clast
Rock Type	basn	basn	basn	ph-tph	haw	phono
TW92-	151	157	159	139	135	134
Lab.	UK	UK	UK	UK	UK	UK
Age (Ma)	0.032	0.826	1.6	1.27	2.41	2.02
SiO_2	46.44	46.54	48.28	48.62	47.53	60.25
TiO_2	2.55	2.43	2.14	2.1	1.9	0.09
Al_2O_3	15.94	16.49	16.55	17.76	16.91	19.45
Fe_2O_3	12.34	13.23	12.04	11.68	12.15	3.76
MnO	0.19	0.21	0.19	0.21	0.22	0.15
MgO	7.4	6.16	5.5	4.63	5.9	0.01
CaO	8.79	8.24	7.23	6.88	8.69	0.89
Na_2O	4.48	4.88	5.34	6.12	4.86	9.58
K_2O	1.66	1.54	1.85	2	1.47	4.8
P_2O_5	0.6	0.74	0.75	0.54	0.47	0.03
LOI	-0.51	-0.64	-0.44	-0.43	0.05	1.07
Total	99.89	99.8	99.42	100.12	100.14	100.07
Ba	367	438	411	544	484	338
La	42	40	45	61	48	128
Ce	73	83	97	122	94	226
Nd	33	32	44	45	34	53
Cl	229	436	399	676	435	775
S	87	111	72	78	142	77
Cr	255	146	173	12	158	6
Cu	59	58	46	40	58	6
Ga	20	18	17	19	17	30
Nb	63	63	67	88	70	150
Ni	105	67	66	24	75	3
Pb	10	10	11	12	11	24
Rb	40	37	42	62	39	214
Sr	663	868	779	751	573	94
Th	5	5	8	11	7	55
V	192	156	101	116	147	0
Y	33	32	32	34	31	50
Zn	80	79	83	81	86	139
Zr	272	264	298	308	207	919

Appendix II. XRF Geochemical Data

Volcano outcrop	Hobbs Coleman south	Hobbs Coleman south	Hobbs Coleman south	Hobbs Coleman south	Hobbs Coleman south	Hobbs Coleman south	Hobbs Coleman south	Hobbs Coleman south
Rock Type	basn	basn	basn	basn	basn	basn	basn	basn
WCM93-	199	185	184	192	190	195	198	188
Lab.	UK	UK	UK	UK	UK	UK	UK	NM
Age (Ma)	2.54	2.6	2.66	2.61	3.34?	51.4?	7.28?	2.46
SiO_2	42.86	42.31	42.41	42.89	42.42	40.91	42.68	40.47
TiO_2	3.75	3.73	3.77	3.84	3.80	3.91	4.00	3.62
Al_2O_3	15.09	14.85	14.82	15.15	14.96	14.18	14.95	15.70
Fe_2O_3	14.77	14.64	14.82	14.81	14.75	15.03	15.28	14.09
MnO	0.22	0.22	0.22	0.22	0.21	0.21	0.22	0.21
MgO	6.73	6.68	6.74	6.70	6.75	7.30	6.86	6.93
CaO	9.84	9.75	9.84	9.92	9.90	9.49	9.91	9.26
Na_2O	4.41	4.52	4.29	4.59	4.44	3.72	4.35	4.04
K_2O	1.77	1.70	1.81	1.77	1.74	1.43	1.61	1.31
P_2O_5	0.86	0.85	0.86	0.87	0.86	0.77	0.84	0.82
LOI	0.00	0.64	0.29	0.00	0.22	2.81	0.00	0.00
Total	100.29	99.89	99.86	100.52	100.05	99.76	100.36	96.45
Cl	71	188	113	181	155	212	227	
S	137	157	181	599	200	289	180	
V	200	206	203	200	196	199	210	217
Cr	99	99	96	91	99	91	98	121
Ni	68	64	66	68	70	79	68	72
Cu	48	49	50	50	50	44	45	41
Zn	97	101	100	92	93	100	98	100
Ga	20	20	18	19	17	16	20	20
As								0
Rb	36	40	40	42	40	31	35	39
Sr	1078	1062	1063	1078	1068	988	1040	1133
Y	38	38	39	39	39	35	39	35
Zr	300	300	301	298	299	255	285	320
Nb	85	86	86	84	85	70	79	92
Mo								3
Ba	532	521	529	523	517	426	464	469
La	60	70	60	63	60	42	45	
Ce	127	123	115	118	126	95	109	
Nd	48	51	38	50	57	43	47	
Pb	11	10	10	11	11	10	11	0
Th	9	8	7	6	9	5	8	0
U								0

Appendix II. XRF Geochemical Data

Volcano outcrop	Hobbs Coleman north	Hobbs Coleman north	Hobbs Coleman north	Hobbs Coleman north	Hobbs Coleman north	Hobbs Cousins Bomb	Hobbs Cousins lava
Rock Type	basn	basn	basn	basn	basn	ph-teph	ph-teph
WCM93-	208	207	207	205	202	218	219
Lab.	UK	UK	NM	UK	UK	UK	UK
Age (Ma)	2.55	2.59	2.59	2.75	2.81	4.87	4.96
SiO_2	42.60	42.55	42.41	42.35	43.28	48.76	49.06
TiO_2	3.84	3.93	3.87	3.93	3.69	2.28	2.28
Al_2O_3	15.02	14.91	14.52	14.84	15.11	16.91	17.02
Fe_2O_3	14.78	15.06	14.71	15.05	15.25	13.36	13.37
MnO	0.21	0.21	0.21	0.22	0.21	0.22	0.23
MgO	6.78	6.96	7.16	6.78	6.83	3.32	3.29
CaO	9.96	9.99	9.90	10.03	9.88	6.25	6.28
Na_2O	4.38	4.40	4.17	4.40	4.01	5.47	5.37
K_2O	1.71	1.67	1.68	1.71	1.39	1.90	2.01
P_2O_5	0.87	0.87	0.85	0.87	0.85	1.11	1.11
LOI	0.00	0.00	0.16	0.00	0.00	0.33	0.00
Total	99.87	100.38	99.65	99.67	99.98	99.92	99.72
Cl	313	189		160	164	123	79
S	390	423		165	236	93	82
V	199	207	214	211	180	46	44
Cr	95	98	115	92	105	0	0
Ni	72	73	70	72	79	8	9
Cu	50	55	46	56	66	29	30
Zn	95	97	108	94	95	102	94
Ga	18	19	19	18	19	20	20
As			0				
Rb	37	36	36	40	28	33	39
Sr	1069	1053	1101	1069	1059	945	961
Y	39	39	34	39	35	36	38
Zr	296	295	311	296	250	368	368
Nb	84	82	89	82	64	84	83
Mo			2				
Ba	521	490	419	516	396	509	524
La	54	51		54	48	73	67
Ce	115	121		124	99	152	130
Nd	55	54		53	41	60	53
Pb	11	10	6	11	11	11	10
Th	5	5	7	6	6	9	9
U			0				

Appendix II. XRF Geochemical Data

Volcano outcrop	Hobbs Patton B. lava	Hobbs Shibuya bomb	Hobbs Shibuya dike	Hobbs Kouperov south lava	Hobbs Kouperov lava	Hobbs Kouperov lava	Hobbs Kouperov
Rock Type	bas	haw	haw	basalt	basalt	basalt	trach
WCM93-	307	221	229	303	304	304	305
Lab.	UK	UK	UK	UK	NM	UK	NM
Age (Ma)	11.32	5.06	4.75	9.18	8.95	8.95	
SiO_2	45.10	46.10	45.57	45.72	45.49	45.87	58.27
TiO_2	2.82	2.89	2.91	2.82	2.79	2.81	0.53
Al_2O_3	15.99	16.40	15.63	16.70	16.02	16.54	18.26
Fe_2O_3	13.42	13.74	13.57	13.42	13.13	13.45	6.77
MnO	0.18	0.19	0.20	0.20	0.19	0.20	0.18
MgO	7.38	5.22	6.73	6.13	6.07	6.16	1.09
CaO	10.91	8.60	9.62	9.31	9.29	9.49	2.32
Na_2O	2.88	4.26	4.00	3.62	3.24	3.39	6.91
K_2O	0.85	1.26	1.36	1.30	1.41	1.39	4.43
P_2O_5	0.54	0.66	0.76	0.74	0.74	0.74	0.17
LOI	0.10	0.72	0.00	0.53	1.22	0.42	1.63
Total	100.17	100.04	99.94	100.49	99.59	100.46	100.57
Cl	24	118	146	151		110	
S	92	134	113	97		115	
V	201	183	165	147	174	155	0
Cr	195	65	206	96	116	93	11
Ni	101	38	96	62	60	58	0
Cu	65	40	62	54	45	54	9
Zn	85	100	91	86	100	92	119
Ga	22	23	18	21	21	20	26
As					0		0
Rb	12	27	27	23	25	25	81
Sr	717	732	848	848	858	848	264
Y	28	31	32	33	30	32	43
Zr	187	233	240	231	251	239	712
Nb	28	50	59	44	50	48	146
Mo					2		4
Ba	197	335	378	340	346	348	1280
La	17	33	33	33		36	
Ce	52	73	86	74		70	
Nd	27	22	34	32		38	
Pb	14	10	12	9	0	12	7
Th	3	4	5	2	0	2	14
U					0		4

Appendix II. XRF Geochemical Data

Volcano outcrop	Hobbs Kouperov	Hobbs Kennel pillow	Hobbs Kennel pillow	Hobbs Holmes upper lava	Hobbs Holmes valley lava	Siple mid-flank	Siple Lovitt Bluff
Rock Type	trach	haw	haw	basn	basn	basalt	haw
WCM93-	305	296	299	292	294	270	275
Lab.	UK	UK	UK	UK	UK	UK	UK
Age (Ma)		7.99	7.99	6.28		0.736	0
SiO_2	58.10	46.68	46.00	45.45	45.23	48.37	45.87
TiO_2	0.56	2.30	2.22	2.24	2.44	2.36	3.32
Al_2O_3	18.66	16.81	16.50	15.52	15.57	16.77	16.26
Fe_2O_3	6.85	11.85	11.40	13.01	13.39	12.34	14.44
MnO	0.18	0.20	0.20	0.18	0.19	0.17	0.19
MgO	0.54	2.95	4.14	7.05	7.46	5.85	5.82
CaO	2.36	8.07	7.98	8.75	9.24	9.53	8.25
Na_2O	7.44	4.45	4.47	4.64	4.21	3.65	3.47
K_2O	4.36	1.90	1.84	1.69	1.57	1.23	1.51
P_2O_5	0.15	0.73	0.71	0.86	0.81	0.76	0.73
LOI	0.73	3.71	4.35	0.52	0.46	0.00	0.19
Total	99.93	99.64	99.80	99.90	100.56	100.48	100.05
Cl	591	905	343	85	260	0	135
S	52	214	112	76	124	58	376
V	0	138	159	145	164	138	160
Cr	1	58	63	171	195	129	61
Ni	1	40	43	99	108	58	57
Cu	11	46	43	62	61	45	45
Zn	116	95	94	82	86	91	111
Ga	26	19	19	20	17	20	23
As							
Rb	81	40	40	32	30	22	27
Sr	257	856	839	986	979	658	571
Y	44	31	32	34	32	29	37
Zr	668	327	315	257	219	185	262
Nb	125	74	72	64	63	41	52
Mo							
Ba	1255	494	500	520	492	343	341
La	77	54	58	51	48	39	45
Ce	165	92	100	99	97	80	79
Nd	55	34	41	41	44	36	36
Pb	14	12	11	11	10	11	10
Th	13	6	6	5	3	3	0
U							

Appendix II. XRF Geochemical Data

Volcano outcrop	Shepard I. Mat. Pt. lava	Shepard I. Mat. Pt. tuff clast	Shepard I. Mt. Colburn	Shepard I.	Shepard I. Mt. Petinos lava	Bursey Starbuck Crater	Bursey Syrstad Rock
Rock Type	basn	basn	trach	trach	haw	trach	mug
WCM93-	255	258	262	264	265	156	158A
Lab.	UK	UK	UK	UK	UK	NM	NM
Age (Ma)	0.475	0.55			0.4	8.45	
SiO_2	44.59	44.40	60.52	60.02	47.54	60.84	49.02
TiO_2	3.37	3.37	0.42	0.51	2.90	0.38	2.57
Al_2O_3	14.38	14.35	15.66	14.77	18.37	15.86	16.38
Fe_2O_3	16.70	16.67	9.29	10.34	11.69	8.33	13.06
MnO	0.25	0.25	0.29	0.32	0.16	0.23	0.21
MgO	4.62	4.54	0.07	0.03	3.89	0.10	3.65
CaO	8.77	8.82	2.67	2.60	9.40	2.11	6.46
Na_2O	4.31	4.08	5.95	6.29	4.25	6.26	5.11
K_2O	1.24	1.34	4.91	4.70	0.94	5.21	1.90
P_2O_5	2.24	2.30	0.06	0.10	0.53	0.10	1.36
LOI	0.00	0.00	0.65	0.62	0.05	0.15	0.03
Total	99.96	100.02	100.47	100.29	99.73	99.57	99.75
Cl	455	455	295	361	194		
S	187	229	691	142	142		
V	95	88	4	5	152	0	49
Cr	5	0	1	0	24	0	15
Ni	21	17	4	3	25	7	5
Cu	43	37	10	13	31	0	7
Zn	139	153	187	189	93	187	92
Ga	23	24	32	31	21	37	22
As						0	0
Rb	21	13	88	80	18	95	30
Sr	859	884	57	38	901	23	1230
Y	51	51	75	69	25	78	37
Zr	245	246	640	564	153	816	363
Nb	54	55	102	86	30	128	72
Mo						5	2
Ba	512	527	1148	851	304	429	590
La	42	48	98	86	20		
Ce	107	126	231	216	39		
Nd	45	59	75	70	28		
Pb	9	8	17	16	11	17	6
Th	4	2	14	13	1	15	8
U						4	0

Appendix II. XRF Geochemical Data

Volcano outcrop	Bursey Syrstad Rock	Bursey Syrstad Rock	Bursey Koerner Bluff	Bursey Koerner Bluff	Moulton Gawne Nun. cone	Moulton Prahl Crag welded fall	Moulton Prahl Crag welded fall	Moulton Edward's Spur
Rock Type	mug	basn	phono	haw	haw	rhyo	rhyo	trach
WCM93-	158B	159	160	161	146	318	318	345
Lab.	NM	NM	NM	NM	UK	UK	NM	NM
Age (Ma)			9.95	9.99	0.99	5.87	5.87	3.98
SiO_2	49.32	47.69	61.32	47.96	46.13	71.40	71.62	58.76
TiO_2	2.61	2.49	0.09	2.76	2.87	0.30	0.29	0.22
Al_2O_3	16.48	15.74	18.26	16.25	15.38	7.68	7.71	16.72
Fe_2O_3	13.10	13.91	5.03	13.60	13.41	8.64	8.46	7.32
MnO	0.22	0.23	0.21	0.22	0.19	0.24	0.23	0.21
MgO	3.94	3.71	0.19	3.95	7.54	0.00	0.49	0.12
CaO	6.47	6.38	0.73	6.70	8.84	0.28	0.30	0.76
Na_2O	5.07	5.13	8.86	4.97	3.87	7.03	6.56	8.95
K_2O	1.89	1.79	5.07	1.66	1.28	4.29	4.30	4.65
P_2O_5	1.36	1.86	0.04	1.33	0.57	0.00	0.03	0.05
LOI	0.03	0.03	0.69	0.00	0.32	0.00	0.00	1.57
Total	100.48	98.95	100.49	99.10	100.41	99.77	99.93	99.32
Cl					461	923		
S					294	100		
V	54	46	0	66	193	4	0	0
Cr	0	0	10	10	196	0	11	15
Ni	0	0	0	0	115	5	0	0
Cu	9	8	0	9	60	7	0	0
Zn	92	97	222	114	99	399	419	227
Ga	22	23	43	21	20	37	40	43
As	0	0	0	0			0	0
Rb	30	33	153	27	25	203	208	133
Sr	1223	1338	9	1197	755	5	5	0
Y	38	39	87	38	31	187	183	116
Zr	360	360	1815	369	266	1952	2103	1996
Nb	73	69	231	73	50	261	299	302
Mo	2	3	17	2			19	18
Ba	606	784	23	471	297	9	23	0
La					36	219		
Ce					70	581		
Nd					32	171		
Pb	5	3	22	0	11	32	35	16
Th	8	0	33	0	5	41	39	32
U	0	0	7	0			9	6

Appendix II. XRF Geochemical Data

Volcano outcrop	Andrus Lind R. cone	Andrus Lind R. lava	Andrus Lind R. lava	Andrus Lind R. lava	Flint lower cone	Flint Reynolds Ridge	Flint Reynolds Ridge
Rock Type	basn	trach	trach	trach	basn	trach	trach
WCM93-	308	309	311	312	284	288	289A
Lab.	UK	NM	NM	NM	UK	NM	NM
Age (Ma)							
SiO_2	46.40	62.15	66.97	66.85	43.33	59.79	60.91
TiO_2	3.66	0.66	0.45	0.45	3.65	0.62	0.42
Al_2O_3	16.00	13.48	12.51	12.41	15.01	16.98	14.91
Fe_2O_3	14.96	9.48	7.18	7.17	13.75	5.92	8.72
MnO	0.22	0.28	0.18	0.19	0.18	0.21	0.27
MgO	4.71	0.08	0.06	0.11	7.96	0.40	0.13
CaO	7.52	1.57	0.69	0.67	9.43	2.07	0.82
Na_2O	4.53	6.16	6.40	6.58	4.08	6.83	7.92
K_2O	1.49	4.72	4.72	4.71	1.41	4.47	3.99
P_2O_5	0.88	0.07	0.03	0.03	1.36	0.18	0.04
LOI	0.00	0.97	0.42	0.42	0.00	1.79	1.21
Total	100.23	99.62	99.61	99.59	99.59	99.24	99.32
Cl	44				121		
S	53				104		
V	139	0	0	0	197	0	0
Cr	3	12	0	12	169	16	0
Ni	7	0	0	0	115	0	0
Cu	26	0	0	0	57	0	0
Zn	119	252	286	281	80	88	202
Ga	23	43	41	41	17	31	44
As		0	0	0		0	0
Rb	26	84	260	214	26	68	69
Sr	864	0	3	3	1300	539	22
Y	42	84	130	129	32	45	106
Zr	274	806	1510	1486	197	536	1347
Nb	53	141	236	234	50	97	273
Mo		5	13	15		6	5
Ba	481	24	15	11	478	1090	20
La	42				36		
Ce	86				85		
Nd	45				42		
Pb	10	0	78	33	11	3	16
Th	4	0	37	36	4	7	30
U		0	9	10		0	6

Appendix II. XRF Geochemical Data

Volcano outcrop	Flint Reynolds Ridge	Flint Reynolds Ridge	Flint Reynolds Ridge
Rock Type	trach	trach	trach
WCM93-	289B	290	291
Lab.	NM	NM	NM
Age (Ma)			
SiO_2	60.68	60.84	60.65
TiO_2	0.42	0.41	0.54
Al_2O_3	14.85	14.99	15.34
Fe_2O_3	8.76	8.45	8.61
MnO	0.26	0.28	0.26
MgO	0.13	0.16	0.23
CaO	0.77	0.83	1.44
Na_2O	7.75	7.15	7.08
K_2O	4.06	5.21	4.84
P_2O_5	0.04	0.02	0.07
LOI	1.21	1.15	0.65
Total	98.93	99.49	99.72
Cl			
S			
V	0	0	0
Cr	0	12	11
Ni	4	0	0
Cu	0	0	0
Zn	201	229	201
Ga	44	45	40
As	0	0	0
Rb	70	133	117
Sr	22	21	123
Y	106	115	92
Zr	1341	1392	1177
Nb	273	264	219
Mo	6	5	11
Ba	23	17	300
La			
Ce			
Nd			
Pb	15	14	15
Th	29	27	24
U	6	6	6